Characteristics of striae and clast shape in glacial and non-glacial environments

Clifford Barrie Atkins

A thesis

submitted to Victoria University of Wellington

in fulfilment of the

requirements for the degree of

Doctor of Philosophy

in Geology

Victoria University of Wellington

2003

Frontispiece: View from Mueller Ridge, looking northeast toward Aoraki/Mt Cook and the Hooker Valley. The lower part of the Mueller Glacier is visible in the foreground. Photograph by Barrie Atkins.

ABSTRACT

Linear abrasion features on rock surfaces are produced by interacting rock particles in relative motion. The most common examples are striae produced by temperate glaciers, and as a consequence, striae have long been used as a means of identifying the passage of past glaciers. However, there are many non-glacial processes that can produce striae. These have been sporadically documented in the geological literature but have failed to make a lasting impression on the wider Earth Sciences community. These non-glacial processes include tectonic deformation, meltwater flow, non-glacial ice, wind action, volcanic blasting, mass movements of rock debris, among many others. Many produce coarse-grained deposits similar in character to glacial tills and there are several instances where non-glacial deposits and striae have been misinterpreted as glacial in origin.

This thesis examines linear abrasion features (mostly striae) from five different environments, three glacial (temperate, polythermal and cold) and two non-glacial environments (mass movement and tectonic) to characterise the striae from different origins. The aim was to assess if there are readily observable and measurable differences in striae character between environments and to develop field-based criteria that allow a sound judgement of their origin in the geological record. Over 760 measurements of individual striae were made (orientation and size) on around 20 representative clasts and characteristic features of about 50 striated clasts from the various environments are illustrated in an "Atlas of linear abrasion features". In addition clast shape and striae occurrence were measured on 1260 clasts from deposits and about 100 bedrock linear abrasions from a cold-based glacier were recorded.

The results show that some striae are diagnostic of certain environments but a combination of clast shape and striae characteristics is the most reliable method of correctly interpreting coarse-grained deposits with striated clasts. Results also highlight

the wide range of striae characteristics within each environment and the importance of lithology in striae generation. This is evident even within the well-known temperate glacial environment where there is a marked contrast between striae formed within a thick debris layer and those formed in thin debris-rich basal ice. There appears to be little difference in striae formed by temperate and polythermal glaciers, but glacial striae are readily distinguishable from striae found in various mass movement deposits or tectonically deformed conglomerates.

Glacial striae tend to be sub-parallel to the clast long axes and show a high density on individual surfaces, whereas those in non-glacial origin typically show a lower density of slightly shorter, wider striae and show either no preferred orientation or weak grouping.

The survivability of glacial abrasion features of clasts once they have entered a fluvial system has been assessed in a small South Island glacier fed river. This has provided a basis for estimating the proximity of a glaciofluvial deposit to the glacier front. Striae are found to survive only 1 to 2 km and glacial facets are mostly removed within 6 km.

The study has also documented previously undescribed linear abrasion features from a cold-based glacier in Antarctica. This discovery is a significant advance in understanding cold glacial processes, and has provided new criteria for recognising the passage of cold-based glaciers in polar areas or regions where cold-based ice may have existed in the past.

ACKNOWLEDGEMENTS

Many people have influenced me and helped to produce this thesis over the last few years. Firstly is my supervisor, Professor Peter Barrett who suggested the project, convinced me to do it, and has guided me through. I am immensely grateful to him for his guidance and the Antarctic opportunities he has provided.

From an academic and technical point of view I would like to thank Drs. Andrew Mackintosh, Vanessa Thorn, Mike Hannah and Warren Dickinson. In particular, thanks are due to Alex Pyne for showing me everything Antarctic, and always having the time to problem solve. Also, a special thank you to Dr. John Patterson for his endless patience, good advice and skill in taking digital images.

Many friends helped with fieldwork in various places, so thanks to Jeremy Mitchell, Vanessa Thorn, Helen Ryrie, Phil Holme, Maria Calcott and Joe Prebble. In particular Phil for the many geological conversations and Maria for the hours of help with clast measuring and making sure I knew when to walk away occasionally.

Many other friends helped in various ways, so cheers to Alex Johansen, Nick Jackson, Ursula Cochran, Ed Butler, Jo Anderson, Nancy Bertler, Belinda Miller (special thanks for translating all the French papers), Dene Carroll and Sarah Halliday for editing parts of the text and Catherine Moger for keeping the flat together during my long absences.

Thanks to the Cape Roberts crew for their friendship, good humour and legendary times, especially Nick, Jo, Ed, Tim Paulsen, John Smellie, Terry Wilson, Tim Naish, Betty Trummel, and also Ross Powell, Mike Hambrey and Jeremy Rigden (who assisted in the field) and finally Japp van der Meer for passing on useful papers regarding striae. The staff at Scott Base staff over several seasons has always been exceptionally helpful. Thanks to Steve Brown and Brian Reid for helping build "Cliff's clast contraption".

I am also grateful to Mike Thomson, John Smellie and Mike Tabeski for making me welcome and providing everything I needed at the British Antarctic Survey.

Financial support was provided by a Victoria University of Wellington targeted Post-graduate scholarship. I thank Shona de Sain for being exceptionally helpful and understanding as the Dean of Students. I would also like to acknowledge the generous assistance from the Transantarctic Association for enabling me to travel overseas to present my work.

Last but certainly not least, thank you to my family who have always been supportive in every way throughout my endeavours at university over the years. You have allowed me to follow my dream and that is appreciated more than I can possibly say.

To anyone I've missed who should be here, my apologies, your help is appreciated and thank you.

TABLE OF CONTENTS

LIST OF FIGURES

LIST OF TABLES

LIST OF APPENDICIES

CHAPTER ONE

INTRODUCTION

1.1 BACKGROUND AND AIMS

Many types of surface abrasion features are found on rock surfaces. These are formed by the relative motion of rock surfaces or fragments and vary widely in shape and form. *Striations* or *striae* are perhaps the most well known surface features and the term *striation* is the most commonly used descriptor applied to linear abrasions of variable sizes and shapes.

By far the most prevalent reference to striae is in the glacial context. These abrasion marks are usually formed at the base of a glacier and are "among the most common features of glacial erosion" (Hambrey, 1994). These features were recognised early in the study of earth surface processes in association with the break-through "Glacial Theory" in the 19th Century (e.g. Agassiz, 1838; Geikie, 1863; Chamberlain, 1888). Analysis of striae quickly developed into a useful means of interpreting the passage of past glaciers. Characteristic shapes and orientation of striae on deglaciated bedrock were used to indicate ice-flow direction. The relationship between sets of cross-cutting striae allowed relative timing of glacial advance and retreat to be established. In addition, the presence of striated clasts in "boulder clays" was used to help map the distribution of glacial deposits. This enabled the reconstruction of complex patterns of past glacial activity and is still one of the most common uses of striae in Earth science (e.g. Kleman, 1990; Mattsson, 1997). The common reference to striae in a glacial context has resulted in striae becoming used as a supposedly unambiguous indicator of glacial influence, and one of the most widely recognised means of establishing a glacial origin (e.g. papers in Hambrey and Harland, 1981; Powell and Veevers, 1987; Aitken, 1991; Lewis and Iillgner, 2000; Spenceley; 2001).

This presents a central problem because "as indicators of glaciation, striae have certain limitations. They are insufficient in themselves since other non-glacial agencies can give rise to striae" (Hambrey, 1994). Several early works reported striae formed by non-glacial mechanisms, (e.g. Hovey, 1909; von Engeln, 1930; Wentworth, 1928; Dyson, 1937). This was followed by later reports of non-glacial striae (e.g. Nichols, 1961; McLennan, 1971; Dionne, 1973; Schermerhorn, 1974a; Zamoruev, 1974), all cautioning an immediate glacial interpretation. In a re-evaluation of the evidence for glaciation in Earth history, Schermerhorn (1974a) observed that these cautions did not leave much of an impression on the wider science community and the misconception that striae alone are evidence for glacial influence continued. Eyles (1993) again raised this in a further review of the evidence for past glacial conditions. He drew attention to non-glacial mechanisms of producing diamictites and also striated clasts including a long list (29 references) of examples where deposits originally identified as "glacial", actually formed by non-glacial processes in terrestrial, marine and volcanic environments. The importance of accurate identification of key criteria such as striae to the interpretation of the origin of deposits is highlighted by the statement made by Eyles (1993): "Explaining the timing and climatic origin of pre-Pleistocene ice ages in Earth history is one of the longest standing problems in geology".

The issue of striae origin is addressed in this thesis by asking the question: Are there readily observable and measurable differences in striae formed in different environments? This is achieved by characterising small-scale linear abrasion marks formed in modern environments where the origin is known. It focuses on striae found on clasts in coarse-grained deposits but also includes some on some bedrock surfaces. The aim is to develop field-based criteria for the reliable interpretation of striae in the geological record.

1.2 STRIAE - THE STORY SO FAR

The description and classification of striae as well as theory of striae formation has been almost exclusively generated in glaciological and glacial geology literature. Therefore, this literature review focuses initially on the glacial environment, reviewing theory,

models and classification of abrasion, and then considers the large number of non-glacial mechanisms that produce linear abrasion features on rock surfaces. Figure 1.1 displays a summary timeline of important milestones in the study of striae and linear abrasion on rock surfaces.

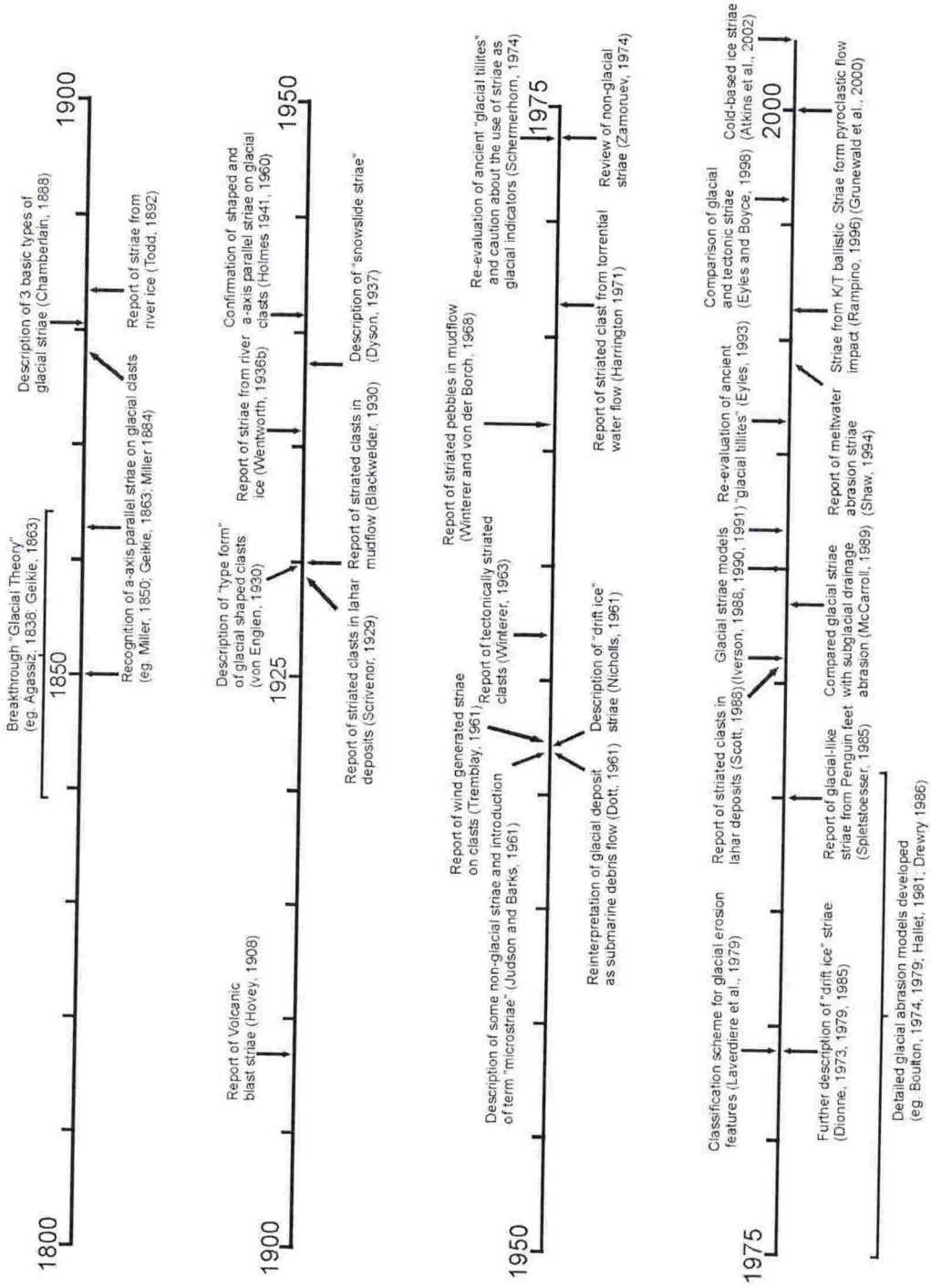

Figure 1.1 Timeline showing significant papers dealing with striae on rock surfaces.

1.2.1 Glacial abrasion

The mechanics of glacial erosion have long been the subject of study, but in more recent years, theoretical models have been produced (Boulton, 1974, 1979; Hallet, 1979, 1981; Drewry, 1986). The models have concentrated on understanding abrasion of bedrock beneath temperate wet-based glaciers, and have shown that striae are formed when asperities (striator) are dragged over subglacial bedrock or till surfaces. Temporary tensile stress is produced below the asperity leading to crack growth and brittle failure of the rock surface as the asperity moves forward (Figure 1.2). The culmination of many small brittle failure events produces an apparently continuous striation marking the passage of overriding particles. Factors that appear critical to the generation of striae are, relative hardness of rock surfaces and striating fragment, force pressing the striator against the bed, velocity of the striator relative to the bed and concentration of debris in ice at the abrading surface (Drewry, 1986).

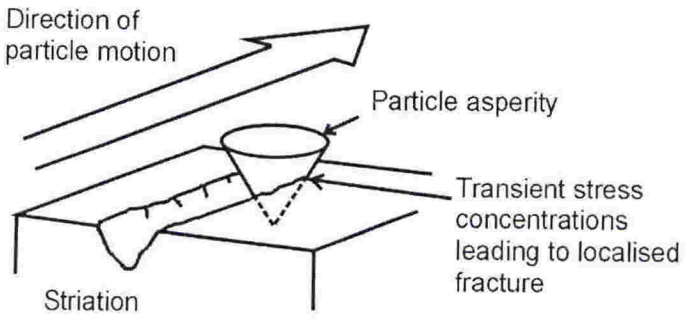

Figure 1.2 Simple model of the striation process (redrawn from Benn and Evans, 1998).

Others have furthered this by testing the theories in the laboratory and simulating glacial abrasion. For example, Matthews (1979) used a simple grindstone made of ice and crushed quartz between two stone plates in a domestic deep freeze. Following this, Iverson (1988, 1990, 1991) noted that large variation in the shape of natural glacial striae could not be easily explained by existing abrasion models. He suggested that the geometry of the striator and the zone of contact effects the magnitude of shear stress exerted on the bed, thus influencing striae shape. Using complex apparatus with striators

of different shapes he closely simulated abrasion of bedrock surfaces by a temperate glacier, measuring important variables and creating striae similar to those observed on glaciated bedrock. These results were compared with the pioneering work of Chamberlain (1888) who recognised three dominant striation shapes and classified them as Type 1, 2 or 3 (Figure 1.3).

Type 1: Striae become progressively wider and deeper down glacier until they end abruptly, often as deep, steep-walled gouges. These are commonly known as "nailhead" striae.

Type 2: The most common striae. These steadily broaden and deepen until a maximum width and depth is reached at the centres; then they terminate as they began.

Type 3: Striae begin abruptly as deep gouges and then become progressively narrower and shallower down glacier.

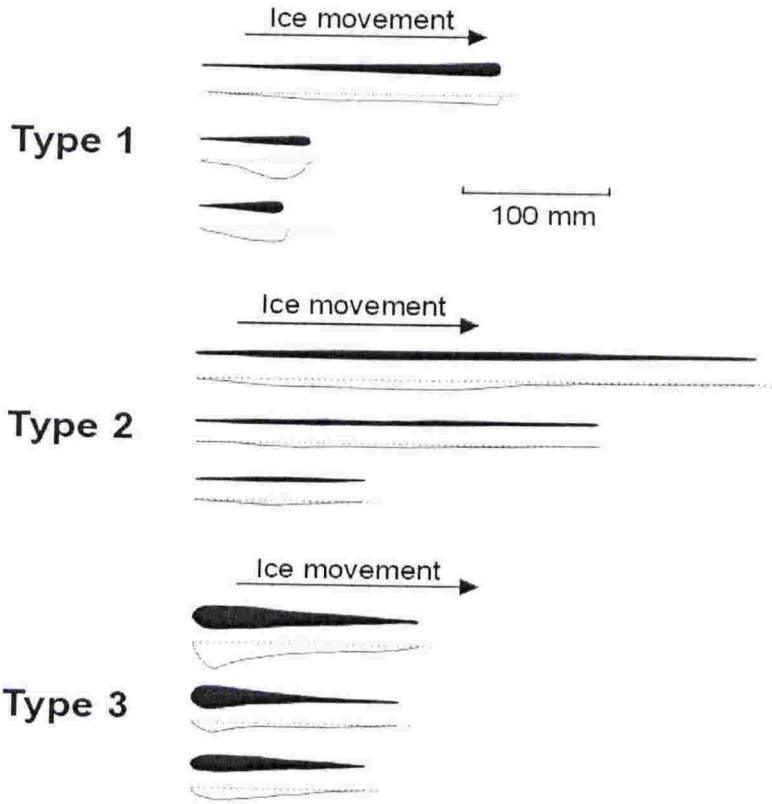

Figure 1.3 Examples of types of glacial striae in plan view and longitudinal cross section. Ice movement from left to right. Ten fold exaggeration in striation depth. Examples are redrawn from experimental results of Iverson (1991).

Iverson (1991) suggested that Type 1 striae result when a sharp striator makes contact with the bed and ploughs progressively deeper, decelerating as the shear stress increases until the striator point either breaks off or the torque on the clast is sufficient to rotate the clast out of the groove. Type 2 striae result from a sharp striator that rotates as it slides. The striator initially ploughs progressively deeper, resulting in more rapid rotation and possibly point comminution, then the striator accelerates and the depth of indentation decreases. For Type 3 striae, the striator initially indents the bed. Rotation with little displacement along the bed produces a small ploughing angle so that a gradual reduction in indentation occurs as the clast velocity increases. He concluded that glacial abrasion models should include the effect of rotation of striating rock fragments, which affect the amount of shear stress between the striator and the bed. He also noted that marks similar to glacial striae (particularly Type 1 striae) can form on fault surfaces, showing that some of the physical parameters beneath glaciers also apply to other situations where rock surfaces move relative to each other. This led to further refinement of abrasion models and glacial mechanics (Shoemaker, 1988; Hallet, 1996; Hindmarsh, 1996). Figure 1.4 shows a well-defined Type 3 striation on fine-grained bedrock.

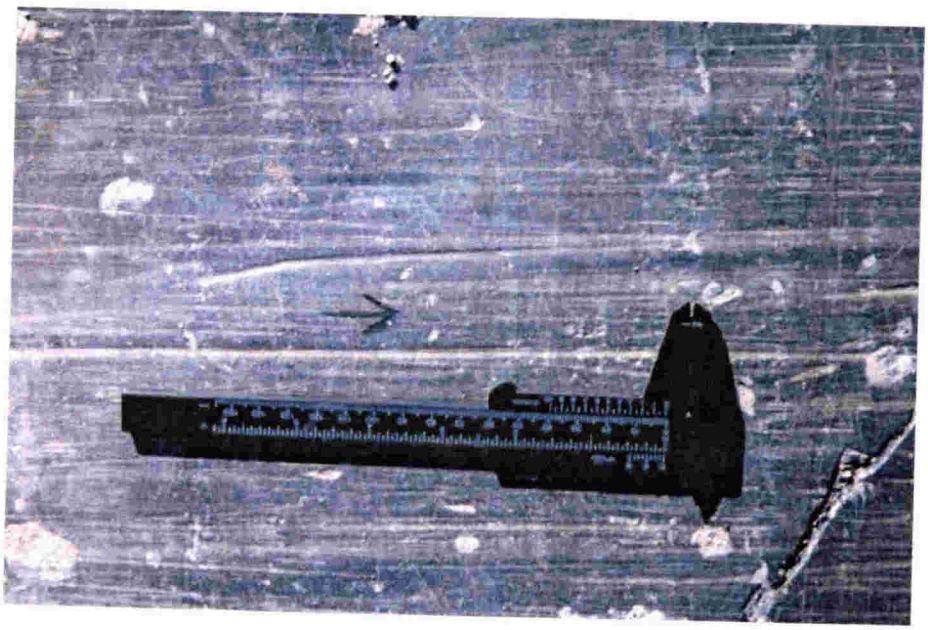

Figure 1.4 Recently exposed glacially abraded, fine-grained limestone bedrock showing a variety of striae. Ice movement was from left to right. A curved Type 3 striation is visible near the centre. Athabasca Glacier, Alberta, Canada. Photograph by Cliff Atkins.

1.2.2 Striae scale and definition

The term striation is defined as a "linear mark on a surface, slight ridge or furrow or score" (The Concise Oxford dictionary, sixth edition, 1976) and is not restricted to glacial literature and does not imply abrasion processes. The definitions provided in geological dictionaries often imply abrasion produced by glaciers. For example:

- "A marking on the surface of a pebble or bedrock produced by ice movement" (The New Penguin Dictionary of Geology, 1996).
- "Small grooves. The term is commonly applied to grooves formed by glacial action" (Penguin Dictionary of Geology, 1972).
- "A tiny groove or scratch on the surface of an ice-abraded rock, produced by the scoring action of rocks frozen into the base of a glacier" (Penguin Dictionary of Physical Geography, 1984).
- "One of multiple scratches or minute lines, generally parallel, inscribed on a rock surface by a geological agent, i.e. glaciers, streams or faulting" (Glossary of Geology, 1987).

Striae is simply the plural of striation, although the word striations is often used in the literature. Striae is the term used in this thesis

Despite insightful and detailed observations of earlier workers such as Chamberlain (1888), poorly constrained usage has resulted in loose meaning in terms of scale and characteristics, even within the glacial literature, often being interchanged with other terms such as *scratch* and *groove*.

Most references to striae are outcrop scale and are commonly millimetres to centimetres wide and deep and centimetres to metres long, although they can be found on much smaller sub-millimetre scales which are sometimes termed micro-striations (Judson and Barks, 1961). The wide range in scale highlights the problem of using the same terminology for abrasion features formed on bedrock surfaces (that may extend for several metres) and those formed on clast surfaces (tens of centimetres or less).

1.2.3 Bedrock striae

Laverdiere et al. (1979), Laverdiere and Guimont (1980) and Laverdiere et al. (1985), provided the most comprehensive terminology for bedrock striae (Table 1.1). These papers presented a qualitative and quantitative hierarchical classification of minor glacial erosion features, ranging from glacial "polish" to quarried walls and truncated planes several metres in dimension. This classification has not influenced mainstream glacial geological literature, possibly due to initial publication in French with some detail lost in translation.

Table 1.1 Features and sizes of linear marks of glacial origin (Laverdiere et al. 1979).

Term	*Definition*	*Size*
Polish	Smooth and brilliant surface.	
Graze	Superficial but wide scratch.	Width: 10-20 mm or more; length: short; depth: very shallow.
Striations/ striae	Group of fine scratches, parallel to one another, sometimes overlapping.	Width: up to 5 mm; length: variable; depth: shallow.
Small Groove	Group of large scratches, parallel to one another, sometimes overlapping.	Width: 5 mm, but may reach 100mm; length: variable; depth: may reach one-third of width.
Scores	Group of very superficial or weathered striations and small grooves.	(see those terms)
Scratches	A few short striations or small grooves somewhat arranged in a fan shape; rare.	(see those terms)
Large Groove	Elongate or canoe-shaped depression, generally occurring alone, or more or less open at both ends.	Width: 100 mm to 5 m; length: variable; depth: may reach one-third of width.
Grooved joint	Rather narrow and deep large groove dug out from a joint roughly parallel to the direction of ice flow	Width: decimetric rather than metric; length: decimetric to metric; depth: centimetric to decimetric.
Furrow	Long, narrow and shallow depression; may lead morphologically to a small valley.	Width: from 5 m to a few dozen metres; Length: up to 1.5 km; depth: may reach one-third of width.

Others have produced less detailed classifications for glacial textbooks. For example, Hambrey (1994) presented a classification scheme of glacial erosion features according to process of formation, relief and scale. Striae are recorded as being less than 5 mm in scale (presumably width or depth) and grooves ranging from 5 cm to 100 m. Benn and Evans (1998) classified striae generally as one of several "small-scale erosional forms" that include striae, rat tails, chattermarks, gouges, fractures and P-forms. Striae are recorded as ranging in length from less than 1 cm to several metres and grooves ranging from several metres to kilometres.

Orientation of bedrock striae is the most commonly measured feature. This has great value in determining the overall ice flow pattern in glacial reconstructions, but is of limited use in characterising the actual striae. The striae can be straight and extend for many metres, but may also be curved "tracks" or deviate markedly from the mean flow direction (Benn and Evans, 1996; Rastas and Seppala, 1981). On flat surfaces, the deviation may be due to the striating asperity rotating while still in contact with the surface. On irregular surfaces, deviation from the mean flow and curved striae may result from irregularities in basal flow of the glacier (Benn and Evans, 1996; Virkkala, 1960). For example, Rastas and Seppala (1981) documented striae on roches moutonnées in Finland. They suggested that rock surfaces dipping less than 30° have a small influence on striae deviation. A dip of more than 50° has a marked effect. On gently dipping surfaces, striae are longer and better formed than on steep surfaces. In addition, Gray (1982) described unweathered glaciated bedrock in Wales, noting that striae converge into trenches and grooves indicating the streaming of basal ice and debris into the trenches.

1.2.4 Glacial clasts

As already mentioned, the presence of striae on clasts in glacial deposits has been known for a long time and quickly became used as a means of establishing a glacial origin. This common assumption continues today. Schermerhorn (1974a) stated, "Striated and/or faceted stones in mixtites are often considered to furnish a prime

argument in favour of glacial deposition". Huggett and Kid (1983) reiterated this point, "Clasts in glacial environments are often striated and the presence of the striae and facets is probably the best evidence of glacial origin".

It has long been known that clasts in tills exhibit characteristic "flatiron" shapes with faceted faces, and that these have striae predominantly parallel to the clast long axis (e.g. Geikie 1863; von Englen, 1930; Holmes, 1941, 1960). There are many exceptions to these characteristics and in more recent years it has become clear that the factors controlling clast abrasion and therefore clast shape and surface features are complex. For example, the particular transport path that a clast has taken through a glacier (e.g. Boulton, 1978), particular subglacial conditions and the lithology of the clasts greatly affects the clast shape and striae characteristics. This results wide-ranging percentages of faceted and striated clasts in various glacial deposits. The characteristics of glacial clasts are discussed in detail in Chapter 3.

These complexities within the glacial environment are secondary in importance to the fact that non-glacial processes may striate clasts. Schermerhorn (1974a) cautioned, "Scratched stones in a mixtite do not by themselves prove the deposit to be a tillite. First it must be established that the striae are truly glacial". Dowdeswell et al. (1985) suggested that too little systematic work exists to establish whether the wide variations in the intensity of striation carry useful information concerning till even though several works have suggested striae orientation may hold clues to striae genesis. For example, Anderson (1983) suggested that the number of sets of sub-parallel striae on a clast may be significant and Frakes (1979) claimed striae on clasts in debris flows show a random pattern and those of tectonic origin may all be parallel.

1.2.5 Summary of glacial abrasion

Much effort has been directed at understanding the glacial environment, with many advances made in understanding the complex interaction between ice and substrate. Abrasion is one of the most common features of glacial influences on rock surfaces and has long been used as a means of inferring past glacial conditions. Despite this long history, only limited systematic work exists on the measurement of glacial striae on bedrock and clasts. This has limited the development of striae as a useful palaeoenvironmental tool and restricted their use to being simple glacial indicators, or at best, to delineate ice flow direction in glacial reconstructions.

The difficulty in definition and classification of linear abrasion marks is partly due to the loose historical usage of terms, but also because of the wide range in the variables in the glacial environment. These variables influence the formation, characteristics and preservation of abrasion and lead to a broad spectrum of features with variable scale, shape and appearance. The most important variable is the lithology, as this not only influences the character of the abrasion, but also the generation of abrasion marks in the first place. Finally, the common ignorance of non-glacial mechanisms of producing striae has meant that the presence of striae has sometimes been incorrectly used as evidence of past glacial conditions.

1.2.6 Non-glacial abrasion

Linear abrasion features have been documented from a wide variety of non-glacial environments. Despite many individual notes scattered widely through the literature and even several reviews of non-glacial striae (e.g. Judson and Barks, 1961; Dionne 1970, 1973; Zamoruev, 1974; Schermerhorn, 1974a; Eyles, 1993), the misconception that striae indicate glacial influence continues. Some non-glacial environments and processes mentioned in the literature are reviewed below.

1.2.7 Sub-glacial drainage

Abrasion features produced by catastrophic, sediment laden, turbulent sub-glacial drainage have a wide variety of forms. These include flutes, grooves, potholes, P-forms, rat-tails and hairpin erosional marks (see Shaw, 1987, 1994; Sharpe and Shaw, 1989 for review and references therein). However, many of these forms could also be produced by glacial or tectonic mechanisms (Eyles and Boyce, 1998). McCarroll et al. (1989), discussed "striae" produced by sub-glacial drainage of a glacier dammed lake in Southern Norway (Figure 1.5). Striae from rock surfaces within the area of sub-glacial drainage were measured and compared with striae from a glacially abraded "control" site. The results indicated that on the basis of length or width measurements alone, "striae" produced by the sub-glacial drainage are not consistently distinguishable from those produced by glacial abrasion. However, using a ratio of length to width, striae from the sub-glacial drainage sites often have a lower length to width ratio and more variable orientation than striae from the glacially abraded sites. The study advised caution when interpreting striae in an area where sub-glacial drainage is a possibility.

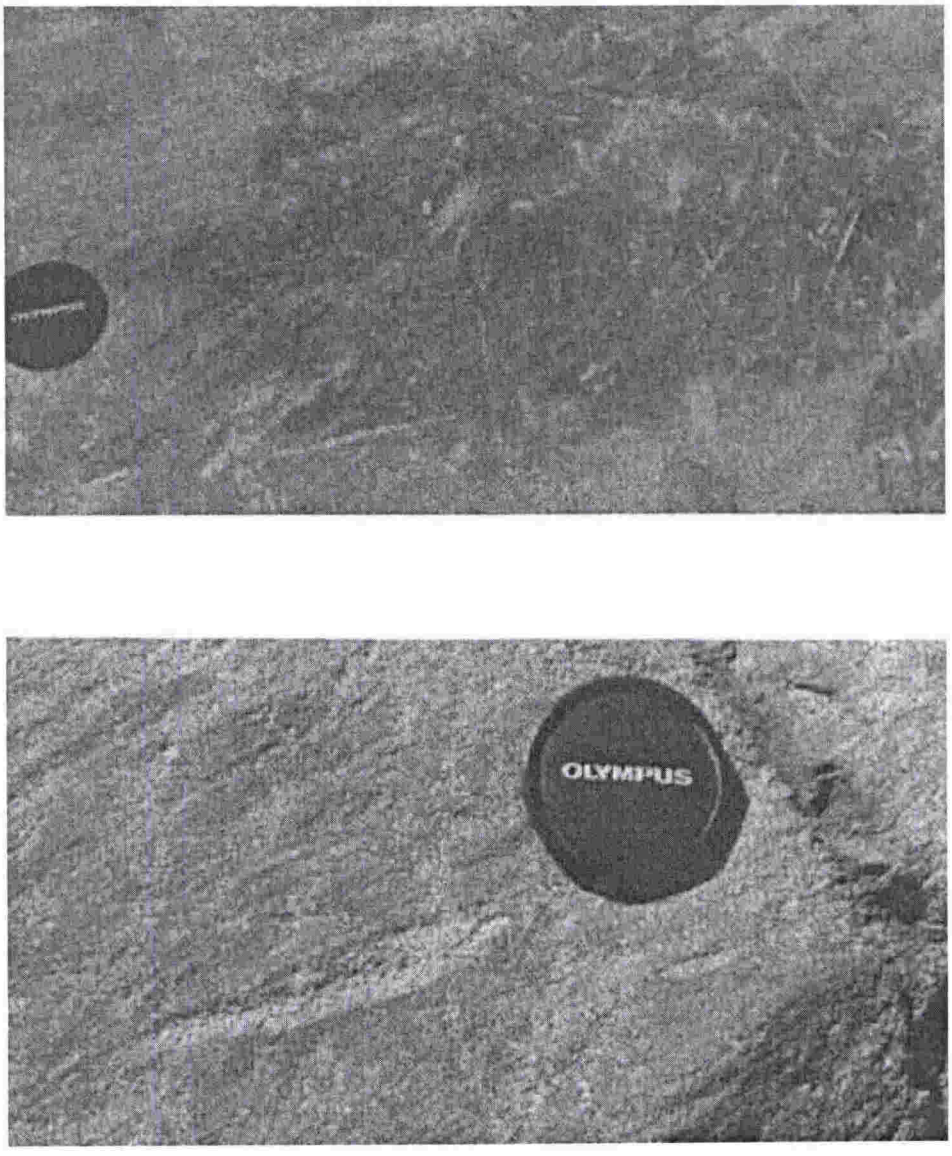

Figure 1.5 Example of catastrophic sub-glacial drainage striae. The top image shows variable oriented cross-cutting striae and the bottom image shows short, wide tapering striae from impact of boulders transported by saltation. (From McCarroll et al. 1989).

1.2.8 Tectonic abrasion

Abrasion forms of tectonic origin have become well known to structural geologists and widely employed as kinematic indicators of fault movement (Eyles and Boyce, 1998). These features have been described from both fault plane surfaces and less commonly on the surfaces of clasts that have been produced or abraded by tectonic forces. A separate terminology has developed in structural geology literature with discussion on processes and mechanism of formation. It includes terms such as striation, groove and tool mark (that are also widely used in glacial geology), but also terms such as slickenside or slickenline that are usually restricted to structural geology. The terminology has many inconsistencies in the meaning of specific terms even within structural geology literature (Fleuty, 1975). This is discussed in detail in Chapter 7 (Tectonic striae).

Judson and Barks (1961) reviewed a number of papers from the late 19th Century and 20th century, which refer to tectonically striated clasts. Even in these early reports it was noted that tectonic striae might be mistaken for glacial striae. Many subsequent reports extended these observations by reporting tectonic striae produced by deformation within conglomerates with a fine-grained matrix (Pettijohn, 1956; Winterer, 1963; Clifton, 1965 and Robertson, 1971). In particular, Winterer, (1963) showed that diamictites in France that had previously been interpreted as glacial in origin, were clearly the product of differential movement of clasts and matrix during tectonic deformation. Clifton (1965) described polished and striated pebbles from deformed conglomerates. The striae were parallel microstriae typically less than 0.5 mm long and 0.05 mm wide, parallel to the long axis of the clast. Frakes (1979) suggested striae of tectonic origin might all be parallel and that this may distinguish them from glacial striae, but offered no examples.

Iverson (1991) noted the similarity of some glacial striae to features found on fault surfaces and Eyles and Boyce (1998) reiterated this by stating: "the similarity of such abrasion forms with those in glaciated terrains is not widely appreciated by glacial geologists". Furthermore, they examined abrasion features on slip planes formed by moving sheets of gouge during repeated faulting and shearing, which they claimed were

identical to abrasion features found in glaciated terrain. The features included grooves cut into the fault plane by the dragging of coarse diamict over slip surfaces (Figure 1.6) and bullet-shaped clasts exhibiting unidirectional striae (Figure 1.7). In addition, larger features such as flute ridges and crescentic scours were also described from the slip plane and the similarity of these tectonic features to much larger flutes and drumlins in glacial terrains noted. Eyles and Boyce (1998) concluded that the conditions along faults and under glaciers are essentially similar, with that both generating cataclastites, which display morphologically identical, but differently scaled genetically related features.

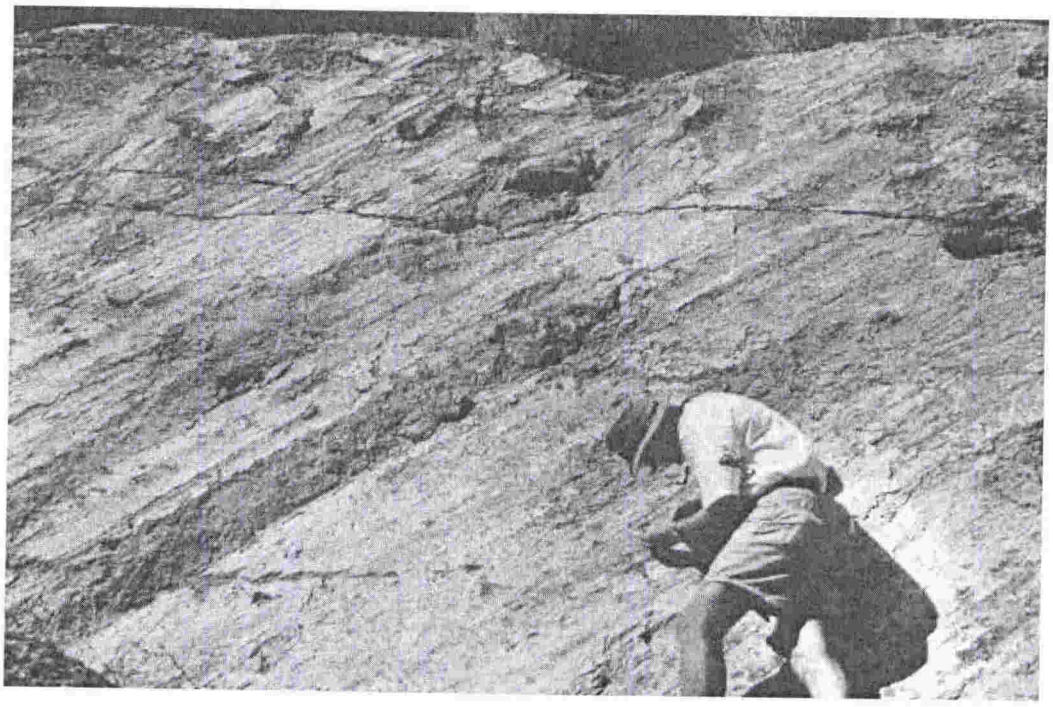

Figure 1.6 Example of striated fault surface near Phoenix, Arizona, USA (from Eyles and Boyce, 1998)

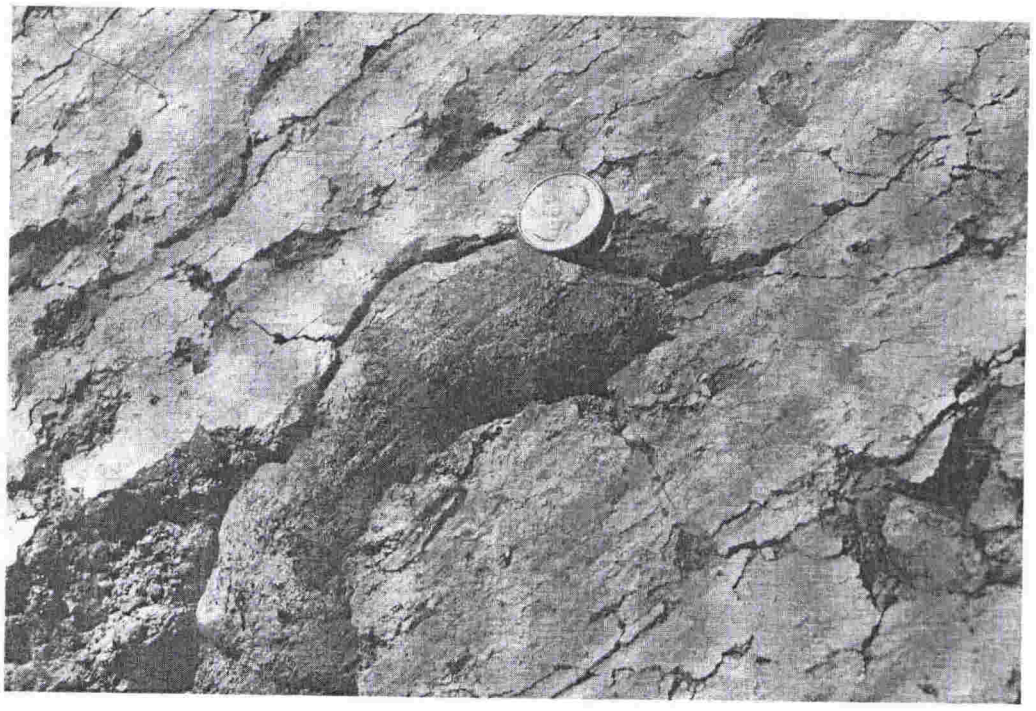

Figure 1.7 Example of a tectonically striated clast exposed on the fault surface (Eyles and Boyce).

1.2.9 Wind action abrasion

The effect of wind has been long known as an effective geological process (Greely and Iverson, 1985), and several papers have referred to pitted surfaces and glacial like striae on pebbles and ventifacts which are attributed to wind action (e.g. Judson and Barks, 1961). Whitney (1978) presented an extensive study of lineations developed by wind erosion that included features such as pits and grooves on several scales: flutes (1 cm to several metres wide), rills, (1 to 10 mm wide) striae, (less than 1 mm wide) and micro-lineations. These were observed on a number of surfaces including ventifacts, bedrock, snow and sand dunes. Recognition of wind-generated striae has forced reinterpretation of some supposedly glacial striae. For example, Tremblay (1961) reinterpreted supposed glacial striae from northern Alberta and Saskatchewan, Canada as products of wind action and sandblasting. These features occur on all surfaces of outcrops including under surfaces of low ledges, but not on the buried portion. Bedrock and clasts appeared

highly polished, more so than on common glacially polished surfaces. The striae were described as fine grooves, channels or funnel-shaped striae depending on size, depth and shape. They are generally shallow and closely spaced with an almost square cross-section and typically less than a foot long. Although appearing to cross an entire outcrop, they are actually a succession of short scoop-like depressions 1 inch to a few inches long, and slightly deeper near the back of the scoop and opening into the direction from which the wind came.

1.2.10 Volcanic Activity (volcanic blast and pyroclastic flow) abrasion

Hovey (1909) reported bedrock that had been smoothed, scored and grooved by volcanic sandblasting during the Mont Pelee eruptions in 1902 and 1903. "The surface of the ground here was completely denuded of soil and the tuff-agglomerate was scored with hundreds of parallel straight striae, many (10 to 15) metres long and several (2 to 10 or more) centimetres deep". These striae were noted on horizontal and vertical surfaces and the "direction of the striae depended on the position of the striated surface with relation to the radii drawn with the crater as the centre". Sparks et al. (1997) reported that spectacular erosion features on bedrock and boulders formed by the effect of pyroclastic flows generated by the April 1993 eruption of Lascar Volcano, Chile. The abrasions range from metre-scale furrows to striae several metres long and centimetres wide, sub-parallel in areas where flows were confined in narrow gorges. A glacial origin is discounted as the striated surfaces are below the current ice limit and unequivocally post-glacial in age (Figure 1.8). Grunewald et al. (2000) described striae and slickensided friction marks on blocks from pyroclastic flows from the 1995-1999 eruption of Soufriere Hills volcano in Montserrat, noting the similarity to tectonic abrasion.

Figure 1.8 Striae formed on ignimbrite by pyroclastic flow. Lascar Volcano, Chile (Sparks et al., 1997).

1.2.11 Mass movement abrasion

This has long been known as an effective process of striating both bedrock and clasts. Several studies refer to striae created by different types of mass-movements including debris-flows, debris-avalanches, mudflows, lahars and even solifluction and snowslide deposits. Several have also noted the superficial similarity with glacial striae and that this may create confusion in interpreting some deposits (e.g. Judson and Barks, 1961; Dott, 1961; Zamoruev, 1974; Schermerhorn, 1974a,b; Eyles, 1993; Jensen and Wulff-Pedersen, 1996). This is further complicated by the fact that debris-flows often involve glacial or tectonically derived sediments. In these circumstances, a single debris flow deposit may include clasts striated by several different mechanisms. Below are some examples of striae formed by various types of mass movements.

Subaerial debris-flow

Park (1926) described poorly sorted deposits with striated boulders on the slopes of Mt Ruapehu, an active volcano in New Zealand, as glacial deposits. The deposits were subsequently re-interpreted to be the result of debris-avalanche from a sector collapse of the volcano flank (Hackett and Houghton, 1989; Palmer and Neall, 1989). These deposits are investigated in detail in Chapter 6. Hancox et al. (1991) described a large rock-avalanche that occurred in 1991 on the flank of Mt Cook in the southern Alps of New Zealand. Some clasts show striae thought to be produced by clast collisions within the rock avalanche (McSaveney, personal communication). Furthermore, Hewitt (1999) reported that rock-avalanches have often been mistaken for glacial deposits in many mountainous areas of the world and cited fifteen individual rock-avalanches in the Baltistan region of the Himalaya that had been previously mapped as till.

Sundell (1985) described basal shearing with gouge and striae in medial and distal deposits of a gigantic debris-flow deposit in Wyoming, USA, and concluded that a combination of slide and flow processes were the mechanisms responsible for the debris deposit and associated striae. Bishop (1997) noted similar basal striae as indicative of rock-avalanche deposits in south-eastern California, USA.

Jensen and Wulff-Pedersen (1996) reinterpreted the Bigganjargga tillite in Northern Norway as the result of a debris-flow. The original interpretation as a tillite was based partly on the presence of a striated pavement beneath the deposit and striated clasts within the diamict.

Other examples include striated and slickensided fault and scarp surfaces on large landslides in Utah, USA (Flemming and Johnson, 1989). Shakesby and Matthews (1996) described angular clasts with only occasional indistinct striae as the product of landsliding in South Wales, UK.

Submarine debris-flow

Dott (1961) re-interpreted the Squantum Tillite in Massachusetts as the product of a subaqueous mass-movement and states "most of the criteria cited for the glacial origin, (including striated clasts) of this and many other tillites can be explained as well by other mechanisms". Furthermore, he advised that most examples of ancient tillites must be re-examined. Eyles and Eyles (1989) and Eyles (1990, 1993) re-interpreted many so-called tillites of various ages to be the result of submarine debris-flows.

Snow-slide

Dyson (1937) described striae from steeply inclined limestone surfaces in Glacier National Park, Montana, attributing them to snow-slide action. The unweathered striae occur on slopes that have not been glaciated for many years and range from "a mere trace to more than an inch in width and have depth up to ¼ inch". The grooves are parallel and oriented directly downslope and some extend for a distances over 10 metres, often becoming more prominent, particularly in width downslope and with boulders lodged at the end. The author states: "There is no essential difference in the striae produced by the scouring erosion of both snow-slides and glaciers. There is however, a profound difference in the rapidity of the action".

Mudflow

Harrington (1971) reported a block of striated tuff embedded in Holocene alluvium in the Atacama Desert. It displays sub-parallel grooves like glacial striae over several tens of centimetres and he stated: "Had the block been found in a glaciated area, it would have been dismissed outright as a commonplace feature". He concluded that the striae were actually caused by the rasping action of hard rocks in a debris-laden torrential mudflow (Figure 1.9). Blackwelder (1930) reported striated boulders in mudflow deposits in San Francisco and Death Valley where a glacial origin can be discounted.

Van Houten (1957) demonstrated that a Colorado conglomerate showing striated clasts was most likely a mudflow deposit rather than a glacial deposit as originally interpreted (see Judson and Barks, 1961; Schermerhorn, 1974a for reviews and references therein).

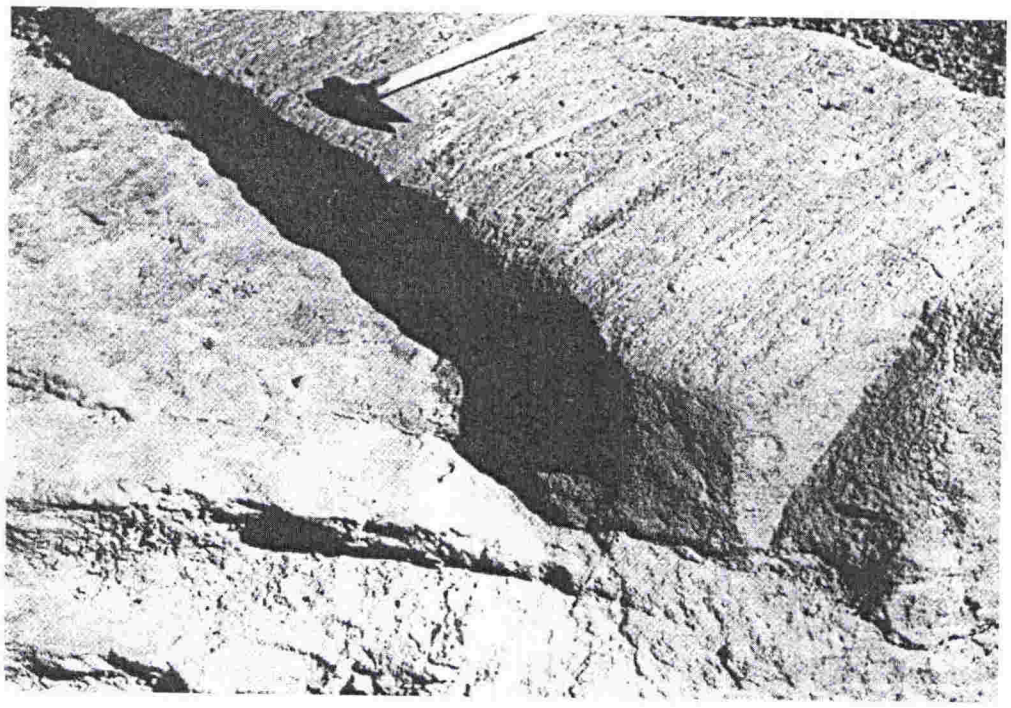

Figure 1.9 Mudflow striae on the surface on a rhyolite block, Atacama Desert. Direction of flow follows the hammer, from handle to head (From Harrington, 1971).

Winterer and von der Borch, (1968) investigated a mudflow deposit in South Australia that contained striated pebbles. Only about 1% of the deposit consists of clasts larger than sand size but approximately 50 % of these display shallow striae. The striae are best developed on finer grained and softer lithologies and generally run in many directions and on all surfaces of the clasts including ends and corners. Straight and curved striae are present with some curving around the corners. The semi-arid desert conditions rule out glacial influence but suit the formation of subaerial mudflows due to cloudburst events. They concluded that the striae were formed during the late "drying" stage of the mudflow when intergranular pressures are maximised. This contrasts with

observations by Zamoruev (1974) who described flatiron shaped boulders and clasts with predominantly straight striae from mudflow deposits in Russia.

Volcanic mudflows or lahars are known to produce striated clasts. For example, Scrivenor (1929) described polished and striated boulders from mudflow deposits on the slopes of a volcano in Indonesia, and Scott (1988) reported striae from lahars during the Mt. St Helens eruption. Eyles (1993) presented evidence of crudely striated boulders in modern lahar deposits from Costa Rica (Figure 1.10).

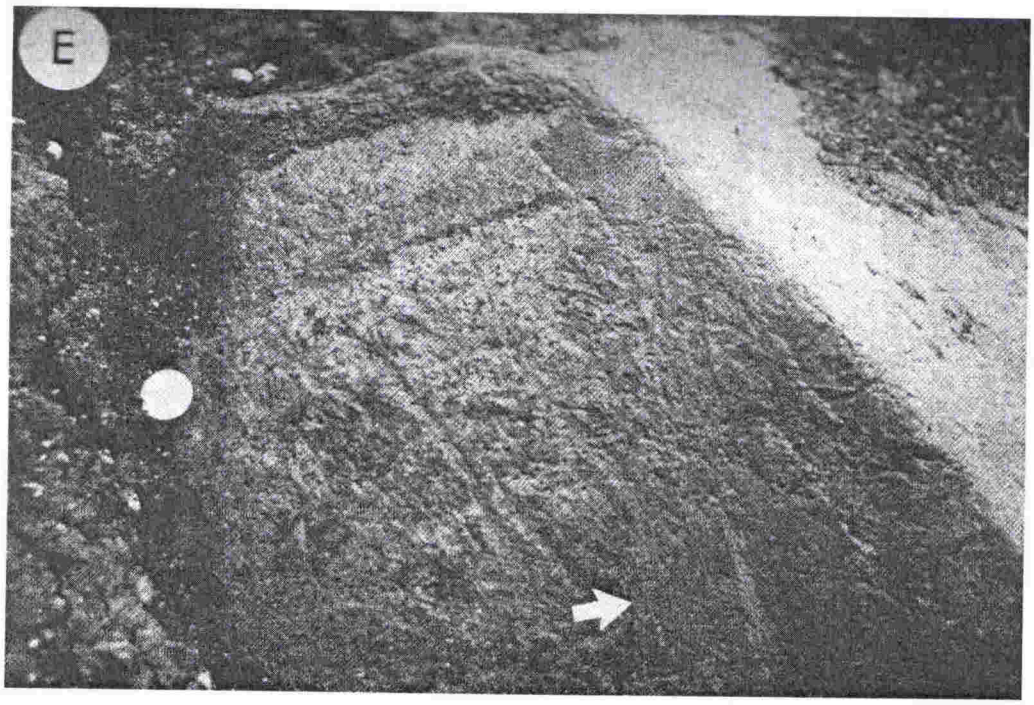

Figure 1.10 Striae on a boulder (arrow) from a modern lahar deposit, Costa Rica. (From Eyles, 1993).

Impact blast

Of a more unusual origin, Rampino et al. (1996) and Ocampo et al. (1996) reported striae from debris-flow diamictites near Belize, Mexico. These Cretaceous/Tertiary age deposits were interpreted to be the product of debris-flows resulting from the Chicxulub impact ejecta. The striae occur on clasts and boulders up to 8 m in diameter and have a range of shapes including nailhead striae. Rampino et al. (1996) suggest that the ballistic effect of high velocity impact and violent collisions combined with abrasion within the high-speed debris-flow are the main causes of striae formation. Also noted is that clast features including abrasions depend partly on lithology and that characterisation of these clast features may allow the identification and discrimination of debris-flows of various origins.

1.2.12 Non-glacial ice abrasion

Non-glacial ice has long been known as a method of striating both bedrock and clasts and there is a small literature base on the topic, mostly published in French, drawing attention to the distinction between striae created by glacial and non-glacial ice. There are many types of non-glacial ice, with floating marine and lake ice the most commonly referred to. Some examples are listed next.

Drift ice

The most important non-glacial striae are abrasion marks along shorelines by the action of debris-laden floating ice (McLennan, 1971). Dionne (1970, 1973) provided an exhaustive bibliography of the many early works that debated the importance of drift-ice and the distinction between drift-ice and glacial striae. Dionne (1985) pointed out that although these have been reported several times from many regions during the last century, their importance has only been realised recently.

Nichols (1961) recognised that ice-push and drift-ice striae can produce striae in polar regions. He suggests that these can be differentiated from glacial striae using the following criteria:

- They are not associated with well-planed and smoothed surfaces.
- They are not as deep, straight or as long as glacial striae.
- They are oriented in general at high angles to the strand line.
- Chattermarks, grooves, trenches and roches moutonnées are absent.
- They are not well developed on vertical and steeply inclined surfaces.

McLennan (1971) apparently unaware of previous reports, described "striae indistinguishable from glacial striae" formed near water bodies in Canada. These formed by drift-ice and ice-push in lakes during ice break-up in the spring. The striae appear to radiate from the centre of the widest adjacent stretch of water. He concluded "ambiguities may appear if one relies too heavily on striae evidence alone when interpreting glacial environments". Dionne (1973, 1979, 1985) criticised this strongly, and provided a set of criteria that he argued could easily discriminate between striae formed by glaciers from those formed by drift ice on bedrock surfaces (Figure 1.11). He separated abrasion into polish, scratches, striae, small grooves and friction cracks. The criteria offered included:

- Drift ice striae usually cover small surfaces of a large exposed bedrock surface.
- They commonly have an untidy distribution, sporadic nature and multi-directional orientations and show a criss-cross pattern unlike glacial striae, which are usually parallel over long distances.
- They are usually short, shallow, isolated, intermittent, divergent, discontinuous and irregular in width, length and depth and are often sinuous, curved and crooked.
- Finally, they are restricted to soft rocks in modern and former coastal areas.

Identification of drift-ice striae on pebbles is more difficult. Stones that have not moved, but which have been striated by floating ice may show the upper surface striated only. If the ice has moved the stones, they may have striae on several sides and the shape of the stone may be important in distinguishing the origin of the striae (Dionne, 1973). These two sets of criteria provide a convincing argument that drift-ice striae can be distinguished from glacial striae but are only applicable to striated bedrock or boulder surfaces.

Figure 1.11 Examples of drift-ice striae on fine-grained bedrock surfaces. Note pencil for scale (Dionne, 1985).

River-ice

Floating ice in rivers can also produce striae on rock fragments, boulders, cobbles and pebbles. Todd (1892) reported striation of rocks by river-ice and Barnett (1910) reported striae or furrows in river gravels, often with an uprooted tree at the downstream end. It is suggested that these features formed either by partly submerged trees dragging across the gravel bars, held down by debris and ice or ice-blocks beneath a load or ice jam. Wentworth (1936b) also reported river-ice striae in ice jams in Arctic rivers. Dionne (1985) concluded that it is usually difficult to distinguish between abrasion marks on erratics made by floating ice and those made by glacier ice, particularly when the rock fragments have been transported and redeposited.

Ice-berg scour

Ice-shelves, ice-bergs and sea-ice can produce scour marks on sea floor sediments. On modern shelves these features have been variously described as striations, plough marks, gouges, scores, grooves, furrows, scours and troughs. Scale varies considerably depending on the size of the ice mass, but some may be up to 250 m wide, and 20 metres deep and kilometres in length (Drewry, 1986). Some of these furrows have smaller centimetre scale striae superimposed on the surfaces. Woodworth-Lynas (1995) reviewed many examples where soft sediment scouring and related striated surfaces have been interpreted as indicating a direct glacial origin but suggested many of these are actually produced by floating ice-bergs (e.g. Savage, 1972; Aitchison et al., 1988) (Figure 1.12).

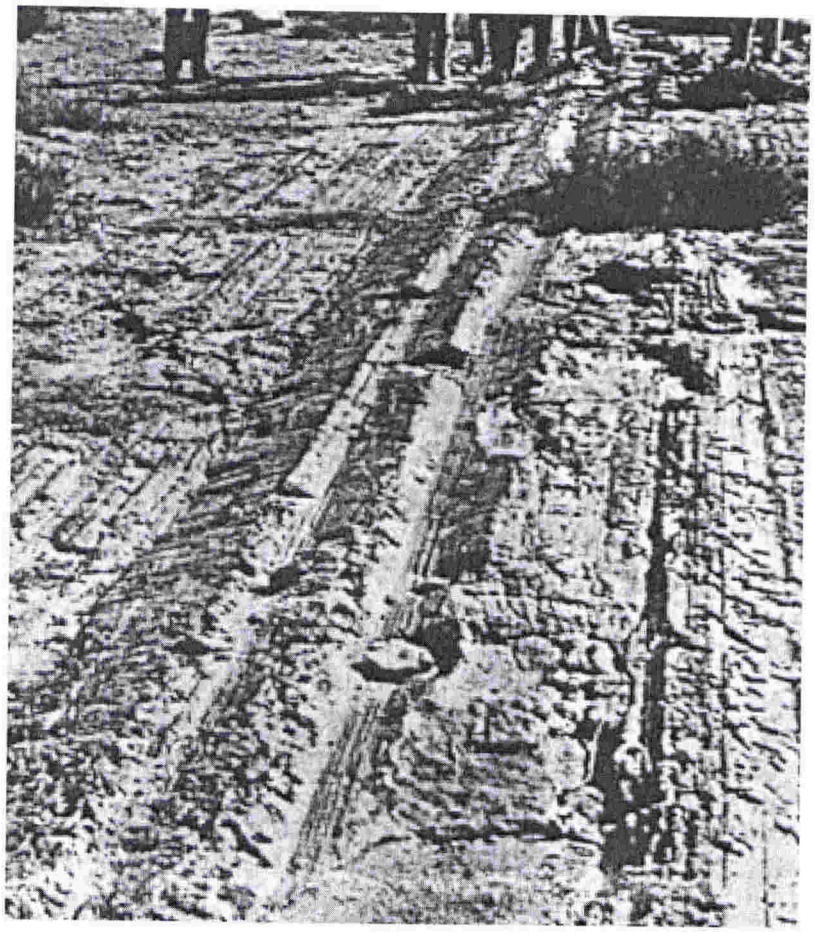

Figure 1.12 Example of furrows with striae in soft sediment, probably produced by iceberg scour, Dywka Formation, South Africa. From Savage (1972).

1.2.13 Other striae

Several other mechanisms of producing striae are found in the literature. While these examples are few, they illustrate the broad use of the term striae for a variety of features that have a superficial similarity to the better-known glacial striae.

Lava stretching

Fininger (1978, 1979) examined an unusual striated andesite outcrop in Peru which displays remarkably continuous grooves ranging in scale from millimetres to decimetres wide and up to 10 cm deep. Several previous explanations for the formation of these features included glacial abrasion and faulting (Schopf, 1979). However, Fininger (1979) suggested that the striae were actually formed by stretching of freshly extruded andesite, analogous to lineations seen on pulled taffy. While it is clear that these are not abrasion features, it illustrates the wide use of the term striation and the potential for misinterpretation.

Fluvial action

Wentworth (1928) described striae on clasts in fluvial deposits in the southern states of the USA, where it is impossible for the clasts to be redeposited glacial clasts. The striae are described as being predominantly straight and even in form.

Biogenic

Splettstoesser (1985) reported striae and gouges between 2 and 5 cm deep on indurated sandstone bedrock and clasts on the Falkland Islands. The explanation offered was that the striae were incised by the clawed feet of many generations of rockhopper penguins as they passed over the same site to and from the water. Furthermore, it was suggested that these might be confused with glacial striae or erosion by water. Chumakov (1998) reinterpreted supposed glacial striae on the surfaces of pebbles from Upper Cretaceous deposits in southern England as representing trace fossils of Cretaceous animals that scraped food from the pebble surface.

Periglacial features

Schubert (1973) reported unusual striae from high in the Venezuelan Andes. He described them as periglacial features which consist of aligned lumps of fine to coarse sand, separated by small discontinuous channels (1 to 3 cm wide). These features form by freezing and thawing of water in the sediment and needle ice was observed forming in the channels. The striae were found to be oriented in the same direction as the freezing wind, indicating that the wind was an important factor in the formation of the striae. Lliboutry (1973) suggested the features were actually a consequence of instability in the ablation process by the sun's rays in a cold atmosphere, and follows the direction of the sun's path, producing the linear "striae". Zotov (1940) described similar striae in the Kaimanawa Mountains of New Zealand. Again, these are obviously not abrasion features but again highlight the diverse use of the term striae.

1.3 SUMMARY

This review of striae reveals a modest body of literature spanning over 150 years. Early recognition of abrasion features in glacial environments quickly developed into a useful tool for delineating past glacier movements but also revealed a diverse list of non-glacial striae. Nevertheless, widespread ignorance of non-glacial origins of striae has persisted despite sporadic notes urging caution about the use of striae to establish glacial origin. Within glacial literature, poor definition and classification and a lack of systematic analyses have hindered the use of striae as a palaeoenvironmental tool. This possibly reflects the immense diversity in character of individual striae (in both size and shape), and the complex nature of the glacial environment. These difficulties are further exacerbated by the influence of lithology on striae formation and preservation making any classification difficult to apply universally.

The potential of using striae as a palaeoenvironmental tool is obvious and attractive, but faces widespread misconception and paucity of reliable data, not only within glacial geology, but also in the wider Earth science context.

Investigation of abrasion features on rock surfaces requires a systematic approach to document striae in known glacial and non-glacial environments to begin the task of establishing criteria to enable useful comparisons to be made.

This thesis begins this task.

CHAPTER TWO

METHODOLOGY

2.1 INTRODUCTION

This chapter presents the scientific methods and techniques employed in this study of abrasion features, as well as problems encountered and lessons learned.

The literature review of striae (Chapter One) reveals that little detailed work exists regarding the measurement and possible palaeoenvironmental use of striae. Therefore, there was no established tested method for recognising features that are diagnostic of striae from a particular environment or mode of origin.

The rationale behind this study of abrasion features (striae) is that particular aspects (e.g. size, shape and orientation) might hold clues about the processes that have acted on the rock, assisting in the interpretation of past environments. The motivation for the study was a wish to provide a sound basis for comparison and interpretation of Cenozoic strata recovered by the Cape Roberts Project in the Victoria Land Basin, Antarctica, (Barrett et al., 1995). To establish if there were observable and quantifiable differences in striae formed by different processes, studies of striae from known modern environments where their origin is unambiguous were needed. Of the many processes that produce striae identified in Chapter One, five major categories were selected for this study. They comprise three glacial examples (temperate, polythermal and polar), mass movement and tectonic processes.

This approach initially appeared to be a simple and attractive way of generating a useful tool for deciphering erosion processes that have influenced the rocks, and ultimately understanding the origin of a landscape or deposit. However, the task of actually

measuring striae has proven to be complex and difficult due to the lack of adequate nomenclature, paucity of published data and the many variables that influence the generation and preservation of striae.

2.2 MEASURING STRIAE

2.2.1 Field based approach

This study has been committed to a field-based approach for measuring striae. The concept was to produce a means of quickly describing and analysing the striae on the basis of readily observable and measurable characteristics in the field to establish the origin.

This required a method of description and measurement with simple field tools. Length, width and depth of individual striae were the obvious parameters that needed to be measured. This seductively simple approach soon proved inadequate. The reason is the large variation in scale between bedrock and clast striae, the variation in width and depth along a single striation and the variation in striae shape and character depending on the lithology.

2.2.2 The problem of scale and definition

The study initially planned to document striae on both bedrock and clast surfaces. This quickly highlighted a problem of scale. The term "striation" is used liberally in geological literature in reference to both bedrock and clasts, but with widely different meanings in terms of scale.

Striae on bedrock surfaces are generally decimetres to metres in length, and millimetres to centimetres in width, although this definition is often extended to include smaller scale "scratches" and larger scale "grooves". Striae on clasts are typically much smaller

and often controlled by the surface area of the clast. This is particularly true for clasts from drillcores, where clasts are often only a few centimetres in diameter. Striae on clasts are often sub-millimetre in width and depth and centimetres or less in length. Differences in scale make these difficult to compare. For example, a linear abrasion 5 mm wide and deep may be described as a small striation on a bedrock outcrop but constitutes a large groove on the surface of a pebble. Similarly, a sub-millimetre abrasion mark on a pebble is likely to be called a striation, but dismissed as a superficial scratch on a bedrock surface.

The problem of scale and terminology is partly overcome by treating bedrock and clast data separately, making clear what is meant in each context. For example, Judson and Barks (1961) introduced the term "microstriae" to describe millimetre-scale linear abrasions on pebbles. Having two orders of scale for striae has some merit from a practical viewpoint, although a "grey area" remains when dealing with surfaces of boulders, where bedrock scale is possibly more appropriate than clast-scale terminology.

This study has evolved to focus on striae on pebble to cobble-sized clasts in response to the availability of good examples of striated clasts in various environments, and also in recognising that the striae on clasts are more likely to be confused and misinterpreted than are bedrock striae.

2.2.3 The problem of lithology

Lithology plays an important role in the generation and preservation of abrasion features. This had been noted by several previous studies (e.g. Kuhn et al., 1993; Hambrey, 1994; Bennett et al., 1997). Coarse-grained rocks such as granite or strongly foliated rocks rarely show striae (Glasser et al., 1998). The grain-size and hardness of different rock types also influences the character of the striae. For example, fine-grained mudstones can display smaller striae than coarser grained sandstones. In a study aimed at characterising striae characteristics from different environments, the added

complication of lithology is critical because any variation in striae characteristics due to different mechanisms may be overshadowed by the differences caused by lithology. Therefore it is difficult to draw meaningful conclusions about striae genesis from rocks of distinctly different lithology and texture. Figure 2.1 shows an example of how lithology can influence the generation of striae. The clast contains a contact between medium-grained granite (light speckled) and fine-grained dolerite (dark). The clearly glacially faceted and striated clast shows sub–parallel striae on the dolerite but none on the granite of the same surface. Where possible, similar lithologies have been used in this study and specific note of the rock type, grain size and relative hardness have been made.

Figure 2.1 Glacially striated cobble from Cuff Cape, Antarctica. The cobble shows a contact between fine-grained dolerite (lower part) and medium-grained granite (light speckled upper part) on a well-developed glacial facet. Striae are clearly visible on the dolerite but absent on the granite.

2.3 METHODS FOR ANALYSING CLASTS

2.3.1 Multiple criteria approach

Recognition of the problems of scale, lithology and variation in the form of striae led to a focus on clasts in coarse-grained deposits and to a multiple criteria approach to document the occurrence and character of striae. This approach utilises clast shape as well as the actual surface features themselves. Fieldwork for the study involved three elements:

1) Recording the field context of the striae. For modern glaciers, this meant documenting the location of basal debris in the glacier itself. For other situations, outcrop descriptions of the deposits or exposures were made.

2) Random clast sample. This was achieved by taking a bulk sample of outcrop or basal glacial debris. This was designed to provide at least 100 randomly selected clasts for clast-shape analyses and to give an overall percentage of striated clasts from each example.

3) Selected pebbles or cobbles with obvious striae were collected to provide a suitable number of striae for detailed striae analysis.

The background and detail of methods involved in this multiple criteria approach discussed next.

2.3.2 Clast shape

Clasts attain characteristic shapes that reflect the transport processes that have influenced the clasts. Analysis of clast shape has been used in many studies of conglomerates and diamictites, both ancient and modern, to help distinguish those of glacial origin from those of non-glacial origin and to differentiate between different

glacial facies. In the glacial context, several early studies showed that clasts transported by glaciers attained characteristic shapes (see literature review, Chapter 1). Boulton (1978), showed that clast shape is largely a function of the various glacial transport mechanisms, and recognised a clear distinction between clasts transported in the active subglacial zone and clasts transported in the passive supraglacial/englacial zones. Lithology appears to have little effect on clast shape in active subglacial zone. For example, Kuhn et al. (1993) studied the shape of various clast lithologies in glaciomarine sediments in Antarctica and concluded, "the shape of clasts is independent of lithology". Others have also noted this (e.g. Dowdeswell et al., 1985; Bennett et al., 1997). In this study, clast lithology is not considered in the shape analyses.

Clast shape can be expressed in terms of three independent properties: form (overall shape), roundness and surface texture (Barrett, 1980). This approach is widely used in the analysis of clast-rich sediments and has commonly been regarded as a good indicator of transport mechanisms (Kuhn et al., 1993). Graphical displays and simple summary statistics are often used to describe clast data (e.g. Domack et al., 1980; Dowdeswell et al., 1985; Hall, 1989; Kuhn et al., 1993; Bennett et al., 1997). This approach is followed here.

Form

Form is the gross overall shape of a clast (Barrett, 1980). Clast form can be described in terms of three orthogonal axes, that is, the long (a), intermediate (b) and short (c) axes, which define three basic shapes: 1) Blocks (spheres), 2) Slabs (discs) and 3) Elongate (rods) (Benn and Ballantyne, 1993). Benn and Ballantyne (1994) introduced ternary diagrams that display these basic shapes by plotting the b/a and c/a axial ratios of clasts to describe clast form and to assist in the discrimination of different erosional "histories" of clasts (Figure 2.2). In a glacial context, they have shown that blocks are typical of "actively" transported clasts, whereas slabby or elongate forms reflect unmodified "passively" transported clasts. This technique is useful for plotting data from all clast-rich deposits and is adopted for all samples used in this study.

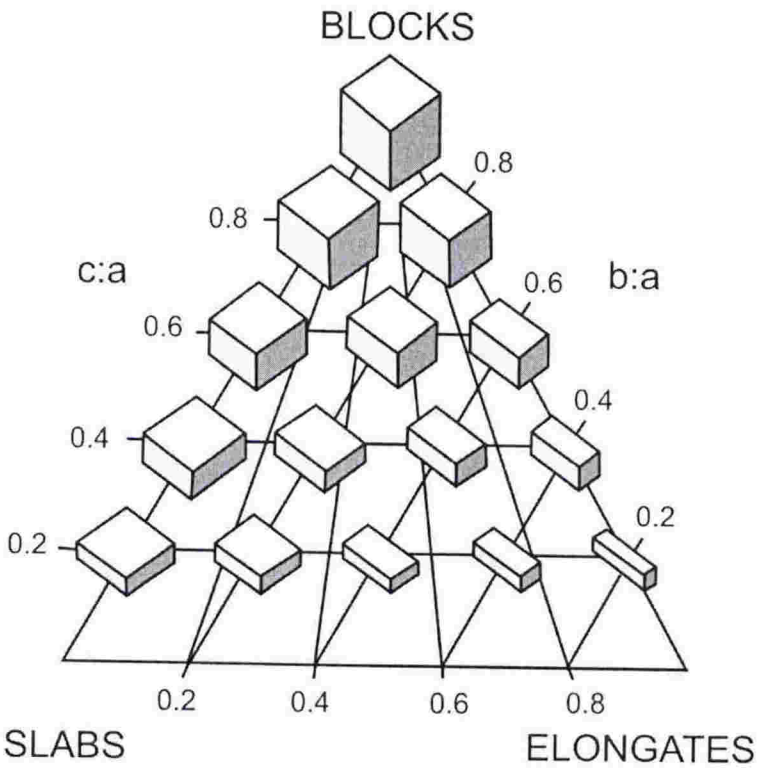

Figure 2.2 Clast form ternary diagram of Benn and Ballantyne (1993). Unmodified clasts (such as rock-fall or scree) tend to plot lower on the diagram toward "slab" or "elongate" forms. Clasts that have more equidimentional or "blocky" shapes (typical of active glacial transport) plot higher on the diagram above a c:a axial ratio of 0.4.

Roundness

Krumbein (1941) devised a visual comparison chart that consisted of a set of pebble images of pre-determined roundness according to the scheme devised by Wadell (1932) (Figure 2.3). The Krumbein chart divides clasts into one of nine roundness categories ranging from 0.1 (very-angular) to 0.9 (well-rounded) and provides an effective means of quantifying clast roundness (Barrett, 1980). The scheme is widely used and data are often displayed as histograms of percent frequency of clasts in each roundness category (Figure 2.4). Krumbein roundness values correspond to Powers (1953) roundness classes as follows: very angular 0.0–0.17; angular 0.17–0.25; subangular 0.25–0.35; subrounded 0.35–0.49; rounded 0.49–0.7; well rounded 0.7–1.0.

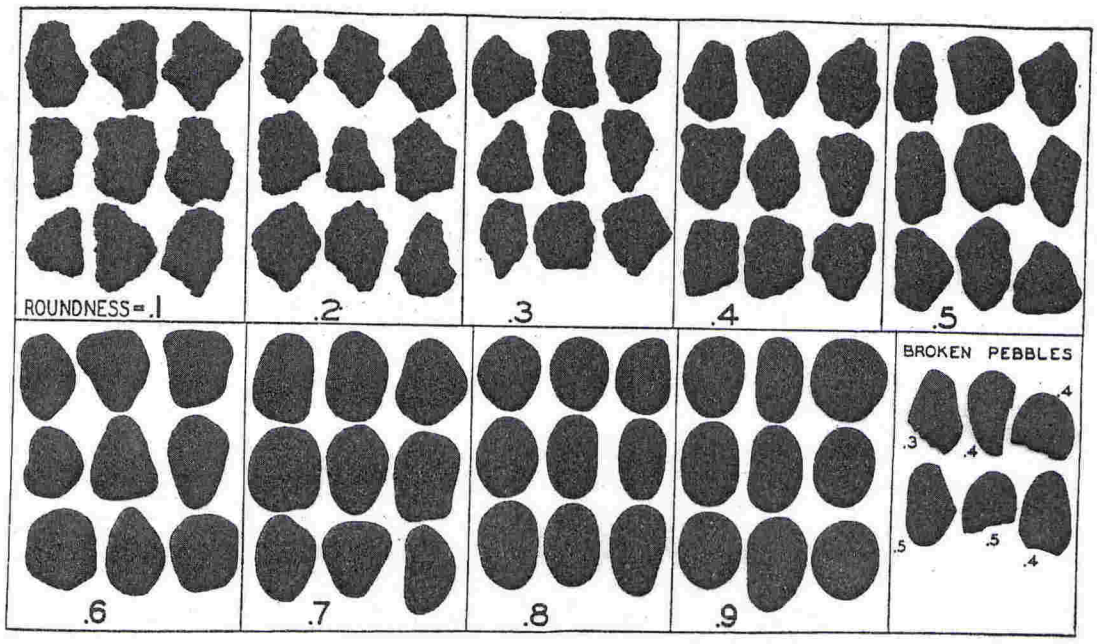

Figure 2.3 Visual roundness comparison chart of Krumbein (1941). This divides clasts into one of nine roundness categories.

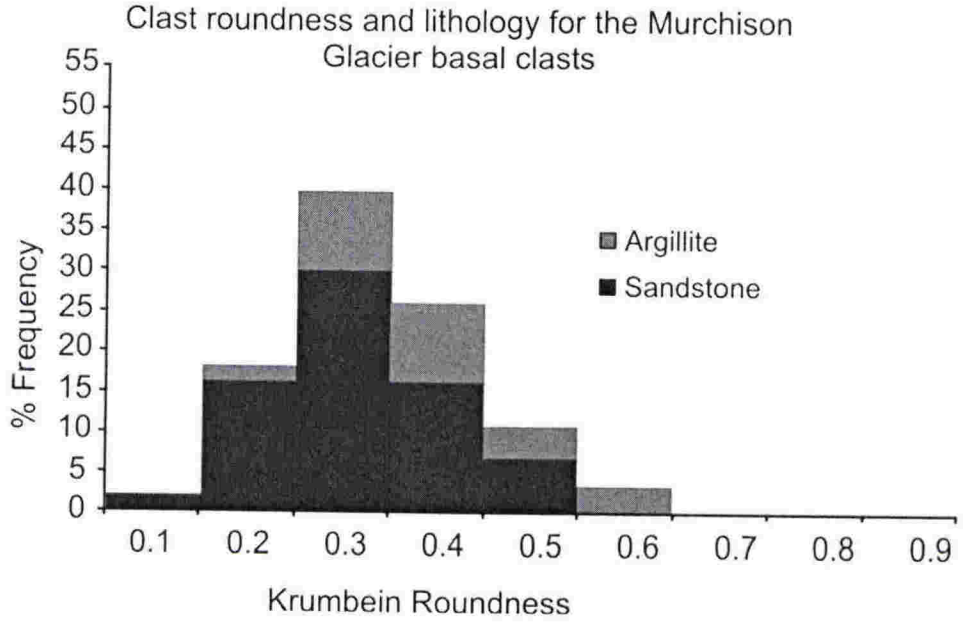

Figure 2.4 Frequency percent histogram of clast roundness and lithology. This example is from basal ice of the Murchison Glacier, New Zealand (see Chapter 3).

Clast form and roundness

Clast morphology can be further explored using plots of shape against roundness. Boulton (1978) introduced a simple biaxial diagram that plots clast roundness versus sphericity. These have been widely used in the analysis of glacial sediments (e.g. Domack et al., 1980; Dowdeswell et al., 1985; Hambrey, 1994). While the "Boulton" diagrams do show differences in roundness between samples, the shape data all have similar ranges in all samples. Therefore, plotting shape against roundness yields little more information than the use of roundness indices alone because the shape index is insensitive to the actual variation in the data (Benn and Evans, 1996).

Therefore, Benn and Ballantyne (1994) developed a new method that plots the C_{40} index (percentage of clasts with c/a axial ratio of ≤ 0.4) against the RA index (percentage of angular and very-angular clasts) (Figure 2.5). They argued that this provides excellent discrimination between different glacial facies (fields from published data from temperate and polythermal glaciers are shown). It clearly differentiates clasts with rounded edges and blocky shapes (high c/a axial ratios) that have experienced "active" glacial transport, from "passively" transported clasts that are more angular and have low c/a axial ratios. Bennett et al. (1997) supported this and concluded that covariant plots of the RA index and C_{40} index give superior data visualisation and should be adopted in preference to the more traditional sphericity and roundness plots of Boulton (1978). Although this was developed for analysis of glacial clasts, it is used to display clast shape from other deposits in this study.

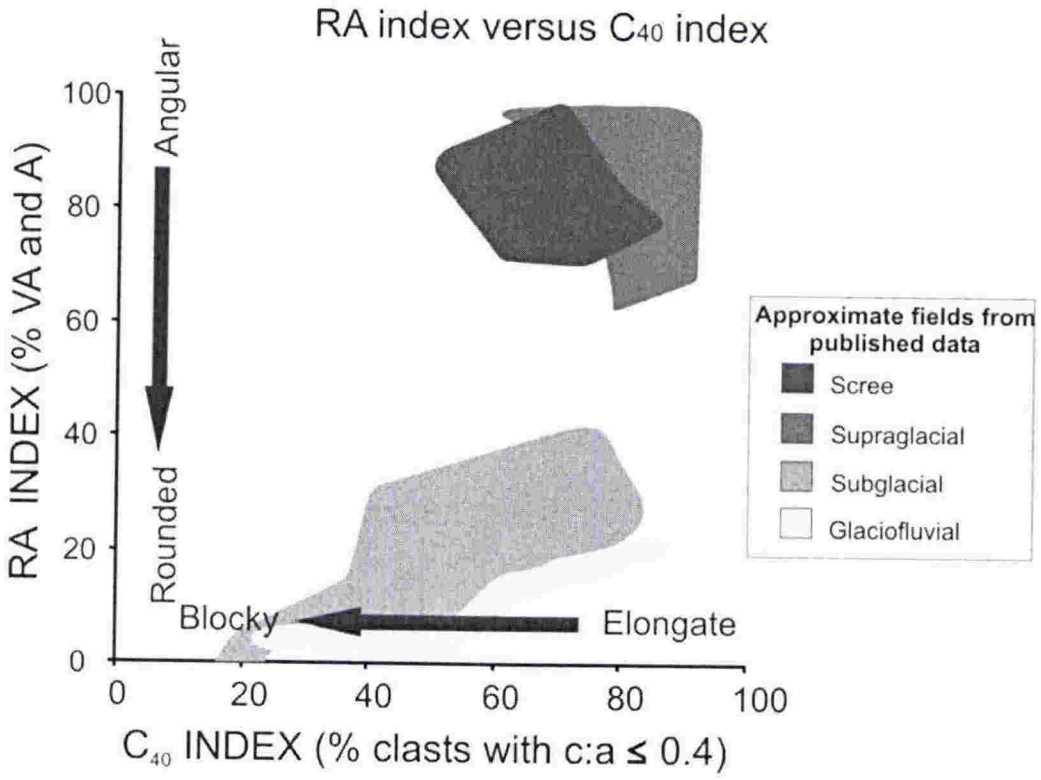

Figure 2.5 RA-C_{40} diagram of Benn and Ballantyne (1994). RA index is the percentage of angular and very-angular clasts and C_{40} index is the percentage of clasts with a c:a axial ratio of ≤ 0.4. Shaded fields are from data in Benn and Ballantyne (1994) and Bennett et al. (1997) for temperate and polythermal glaciers.

2.3.3 Clast fabric

Many researchers have used clast fabric to assist in the interpretation of clast-rich sediments, particularly those of glacial origin, specifically to infer the mode of deposition and to define glacial flow directions (e.g. Domack and Lawson, 1985; Dowdeswell et al., 1985). Clast fabric was measured for the drill core samples from the Cape Roberts Project, which is discussed briefly in Chapter 8. Fabric data are presented in Atkins (2001), included at the end of this thesis. Clast fabric analysis on drillcore is inherently difficult due to low numbers of clasts and because these are usually only seen on split core faces. This has prompted some to attempt two-dimensional fabric studies (e.g. Hambrey, 1989). Three-dimensional fabric analysis is preferable and this was

employed for the Cape Roberts drill core by sampling whole-round sections of core from the coarse grained units. A simple supporting apparatus was designed to allow the cores to be secured in an upright position (Figure 2.6). A horizontal stage was lowered over the core and chisels used to systematically disaggregate the core, exposing individual whole clasts (uncut by coring) in a manner similar to that outlined by Hicock (2000). The trend of the a-axis (long axis) of each clast was recorded on the stage with a protractor, and the plunge was measured with a standard geological compass clinometer, to provide three dimensional clast fabric data.

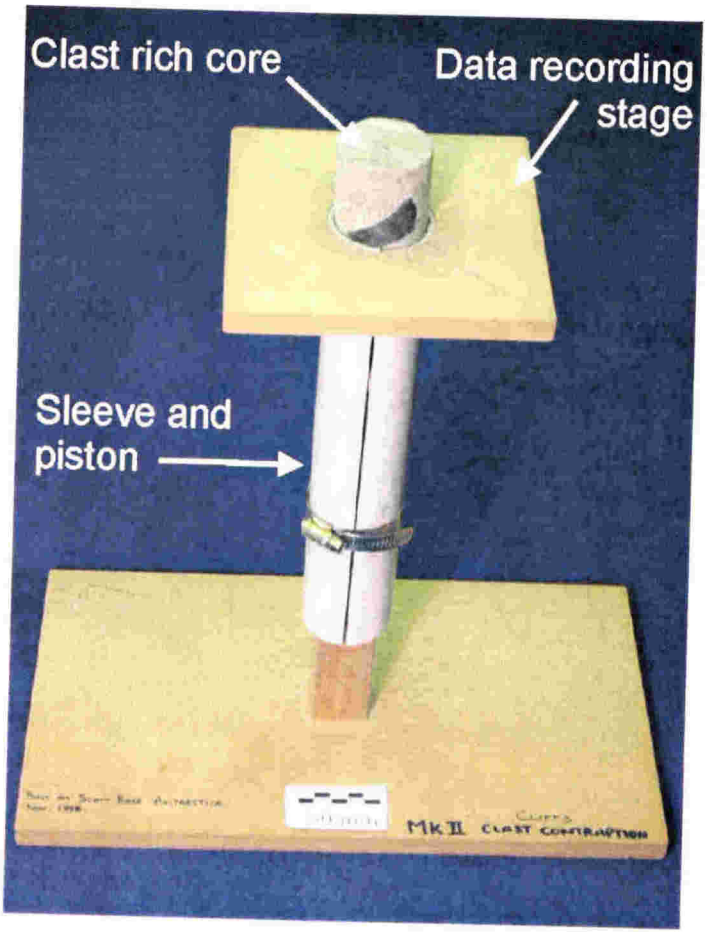

Figure 2.6 Simple supporting apparatus to allow systematic disaggregation of whole-round sections of drillcore for three-dimensional clast analysis.

2.3.4 Striae Analysis

Procedures were developed to describe both bedrock and clast striae. As this study progressed, various modifications were made as knowledge was gained. The initially simple concept of measuring striae proved to be difficult, particularly with the commitment to using only simple field instruments.

Bedrock striae

For bedrock striae, basic dimensions (length, width and depth) were measured on individual striae. This was a complicated task because the width and depth often vary along the length of a striation. For example, a nail-head or wedge striation will be wider and deeper at one end and taper toward the other. To more accurately describe the shape of bedrock striae, multiple measurements of width and depth at points along the length can be made. A schematic diagram of this concept is shown in Figure 2.7.

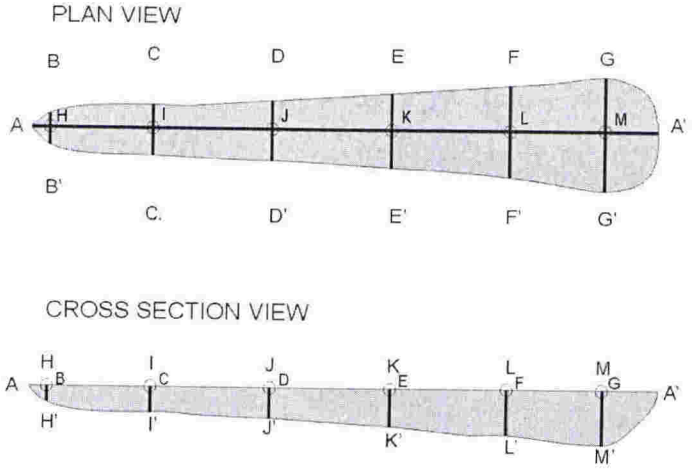

Figure 2.7 Schematic diagram of idealised linear abrasion and series of width and depth measurements at points along the abrasion length needed to define the shape.

This method for measuring bedrock striae proved to be a tedious and unpractical approach in the field, and the time involved in this technique limits its use as an effective field method. Dimensions were obtained using callipers and a tape measure. Other characteristics such as distinctive channel shape or texture, channel edge symmetry; channel levées or remnants of abrading tool were noted. The only bedrock abrasion mark measurements presented in this thesis are from cold-based glaciers in Antarctica. The three striae types defined by Chamberlain (1888) for temperate glacial striae were not used, as these did not adequately describe the shape of the cold-based glacial abrasion marks. In practice, these were described and classified by their general appearance and only maximum length, width and depth are presented, rather the multiple measurement scheme outlined above (see Chapter five).

Orientation of bedrock abrasion marks were measured as an azimuth with a standard geological compass and plotted onto a circle (orientation wheel), giving a visual representation of orientation and grouping. An average orientation for each site was also plotted on the orientation wheel and then plotted onto a map (Figure 2.8). Orientation data for abrasion marks were plotted with Stereonet (version 3.03).

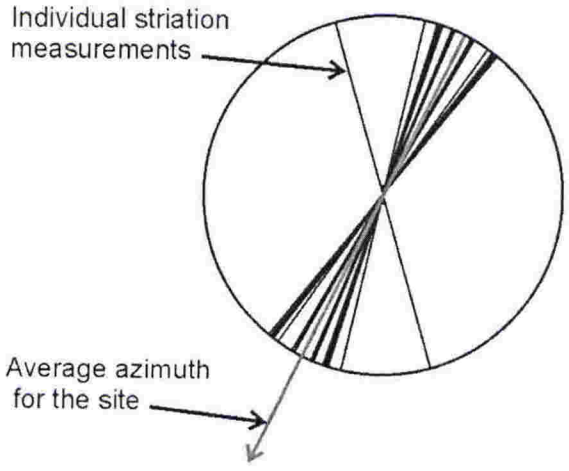

Figure 2.8 Bedrock abrasion mark orientation wheel. Individual abrasions are plotted and an average azimuth given.

Clast striae

For striae on clasts, a different approach was necessary. Striae on clasts are much smaller scale than on bedrock (commonly only millimetres to centimetres in length and millimetres or less in width and depth), and many surfaces show a pervasive covering of fine striae that are visible to the naked eye but impossible to measure individually with a standard ruler. These visible, but not measurable fine striae are here termed "background microstriae" (e.g. Image 5, Temperate glacial striae, Appendix 1). Collection of striae data was made in two ways. Firstly, for bulk clast samples from various environments, a range of observations was made to document the occurrence of striae. This involved recording the:

1. Total percentage of striated clasts in a sample
2. Percentage of striae on different lithologies
3. Roundness class of striated clasts
4. Overall shape of striated clasts
5. Relationship to clast surfaces such as on facets or flat faces

Secondly, clearly striated clasts were collected from each environment to provide suitable examples of striae for detailed analysis. This involved recording the:

1. Orientation of striae in regard to the long axis of clast
2. Length and width measurements of each striation (depth was not recorded, as this was not reliably measurable at this scale
3. Density and distribution of striae on a given surface, including the presence of fine "background" striae, termed "microstriae"
4. Curvature of striae

The measurements were made by taking high-resolution digital images of striated surfaces and printing them with a square grid overlay. The grid scale was usually 5 mm squares (25 mm^2) although two larger clasts had 10 mm squares (100 mm^2). For most clasts, either 50 squares (12.5 cm^2) or 100 squares (25 cm^2) over a representative section

of the clast were selected. Clearly visible and measurable striae (> 0.25 mm width and > 2 mm length) were marked on the image using the actual clast with wet surfaces under low angle lighting as a guide (Figure 2.9).

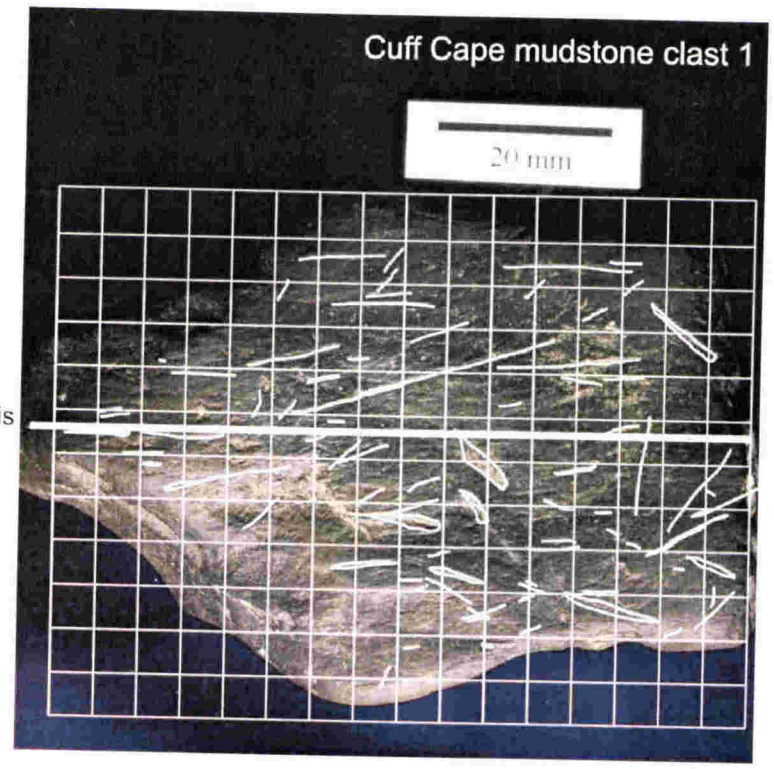

Figure 2.9 Diagram showing a striated clast and 25 mm^2 overlay grid with striae marked on the image. The percentage of squares with "background" microstriae and percentage of squares showing at least one striation were recorded. Also, the total number of striae for the measured area and orientation of striae relative to the long axis of the clast (180°) was recorded.

Striae orientation

The orientation of each striation was measured as a direction between 90° and 270° relative to a reference line along the long axis (a-axis) of the clast (180°), although no direction of striation is intended (Figure 2.9). The striae orientations were grouped into 5° degree segments and plotted on half rose diagrams (Figure 2.10). The length of each sector indicates the percentage of the total striae in each segment. All striae orientation

data was plotted with Stereonet (version 3.03). The range of orientations is recorded relative to the long axis and therefore has a maximum value of 90°. Standard deviation from the average orientation is given. Average orientation is indicated by an arrow and direction in degrees. The data were not analysed with further statistical techniques, as the graphical representation was considered sufficient to display striae orientation effectively.

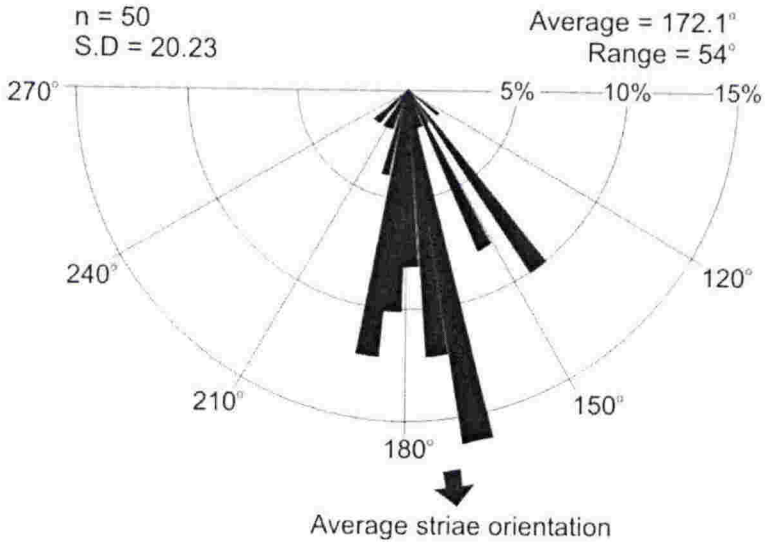

Figure 2.10 Half rose diagram shows the orientation of striae relative to the long axis of the clast (180°). Striae are grouped into 5° segments and length of segment indicates the percentage of striae. Average striae direction is indicated along with the range in values relative to the long axis and standard deviation from the mean orientation. No direction for striae is intended.

Length and width

The length and width of each striation was measured using a standard ruler. Width proved difficult to measure, as many are sub-mm scale. In practice, striae width was grouped to the nearest 0.25 mm. Striae less than 0.5 mm were assigned a value of 0.25 mm and striae less than 0.25 mm were considered "background" microstriae. Only the maximum width was recorded even though some striae showed a change in width along the length. Length and width data were plotted using a simple scatter plot of width and

length and also as range charts showing maximum, minimum and average values for each clast.

Width divided by length produces a ratio between 0 and 1. This allows an estimation of striae shape regardless of striae or clast size. The data are ranked lowest to highest and plotted against the striation number. Summary data are also plotted on a range chart. The striae shape data were not treated with statistical techniques because the number of clasts in each environment was considered too low for this approach to be useful.

Striae density

The percentage of squares that displayed "background" microstriae was recorded. In addition, the total number of measurable striae (larger than 0.25 mm wide) was counted and divided by the total measured area to provide a number of striae per cm^2. These data were plotted on a density chart that shows average measurable striae per cm^2 and the percent background microstriae for each clast. This background density is represented by a pie graph, with the black sector indicating the percentage of the measured surface showing background striae (Figure 2.11).

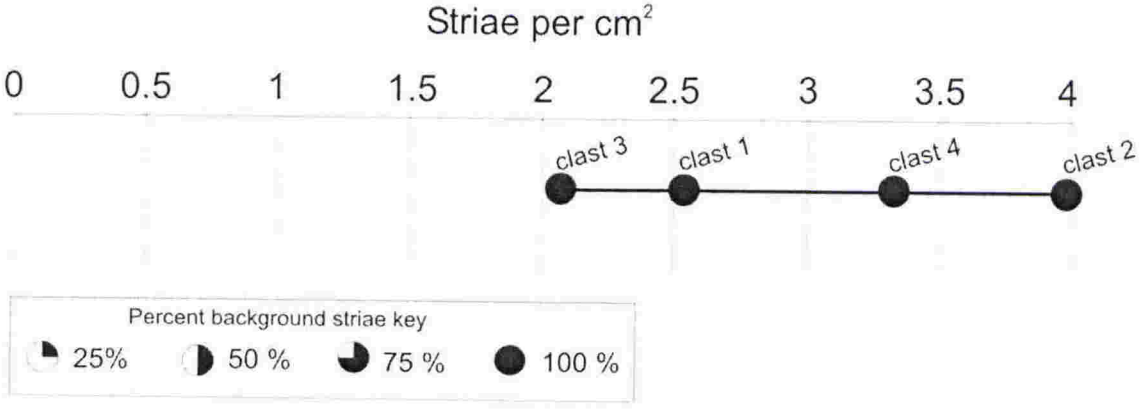

Figure 2.11 Density chart showing that number of striae per cm^2 and the percent of "background" microstriae on each clast. The example shown is for four clasts from a temperate till (Lake Pukaki moraine). The clasts all have at least 2 striae per cm^2 and 100 % background striae.

Striation curvature was noted as this probably represents clast rotation during the striation process. Also, other special features, such as compound striae, which are wider than average striae and commonly have finer parallel striae on the abrasion surface, were noted.

2.4 APPENDIX 1, LINEAR ABRASION PHOTOGRAPHIC ATLAS

Because only a limited number of clasts were used to analyse striae in detail, and many aspects of striae and the relationship to clast shape are difficult to describe quantitatively, a visual reference guide was established in the form of a photographic atlas (appendix 1). The atlas provides images of linear abrasion features (mostly striae) at a variety of scales from each of the environments investigated, accompanied by an explanation of important features. It aims to present a wide range of different striae characteristics seen on clasts in each environment to highlight the variability rather than focussing on the more common features. The atlas is divided into five parts representing different environments where linear abrasion marks were measured. These are:

Part One: **Temperate glacial striae**

Examples of striated clasts from debris layers from basal ice in the Mueller and Murchison Glaciers and also from the Lake Pukaki moraine, Mt. Cook region, New Zealand.

Part Two: **Polythermal glacial striae**

Striated clasts from debris layers in overturned icebergs on the Mackay Glacier tongue and also clasts from Cuff Cape, Granite Harbour, Victoria Land, Antarctica.

Part Three: **Polar, cold-based linear abrasion features**

Examples of abraded bedrock and clasts from Allan Hills, Victoria Land, Antarctica.

Part Four: **Mass movement striae**

Examples of striated clasts from a volcanic debris-avalanche, Mt Ruapehu, New Zealand and a rock-fall in the Murchison Valley, Mt. Cook, New Zealand.

Part Five: **Tectonic striae**

Examples of striated clasts from a tectonically sheared beach gravel, Ngapotiki Fault, New Zealand and a tectonically sheared fluvial deposit, Wellington Fault, New Zealand.

A full introduction and description of methods is given in appendix 1 "Linear Abrasion Atlas".

2.5 OTHER APPENDICES

This thesis contains six appendices. Appendix 1 consists of the linear abrasion atlas. Appendices 2, 3, 5 and 6 consist of spreadsheets of clast data from each environment. The spreadsheets include clast lithology, length of the three axes and averages, clast roundness, presence of glacial facets or flat surfaces, presence of striae, calculated axial ratios and values for RA index and C_{40} index. Also presented is the striae data for selected clasts from each environment. These include summary clast shape data, striae density measurements, striae orientation, length, width measurements, width/length ratios and presence of curved and compound striae. Appendix 4 is in two parts and contains measurements of cold-based glacier abrasion features from Allan Hills Antarctica. The first part includes location, type of abrasion, orientation, maximum length, width and depth of each linear bedrock abrasion mark. The second part contains orientation, length and width measurements of abrasion marks superimposed on wind-polished cobbles. Appendix 7 provides an overview of the Cape Roberts Project and how the results from this study relate to the clasts recovered from the drillcore in the Victoria Land Basin.

2.6 FIELDWORK LOCATIONS

Fieldwork locations are in New Zealand and Antarctica. Three different glacial environments were selected to investigate potential differences in abrasion character from ice in different thermal states. Temperate (wet-based) glacial conditions were investigated at the Murchison and Mueller Glaciers and also the Lake Pukaki moraine in the Mount Cook region of the Southern Alps, New Zealand. These results are discussed in Chapter 3. The Mackay Glacier and nearby Cuff Cape in Granite Harbour, Antarctica was used to investigate abrasion features from a polythermal glacier and these results are presented in Chapter 4. Chapter 5 presents bedrock abrasion features produced by a polar (cold-based glacier) at Allan Hills, South Victoria land, Antarctica.

Chapter 6 presents analyses of striated clasts from a Holocene debris-avalanche on the slopes of Mt Ruapehu volcano in the central North Island, New Zealand, and also from a small-scale rock-fall in the Murchison Valley, South Island, New Zealand.

Chapter 7 presents striae produced from recent faulting of conglomerate deposits at two locations in the southern North Island, New Zealand. The first is the Ngapotiki Fault where greywacke bedrock has been thrust over a modern beach. The second is a Quaternary fluvial conglomerate sheared by active faulting near Wellington. Finally, clasts recovered in cores from the Cape Roberts Drilling Project in Antarctica are summarised in Chapter 8.

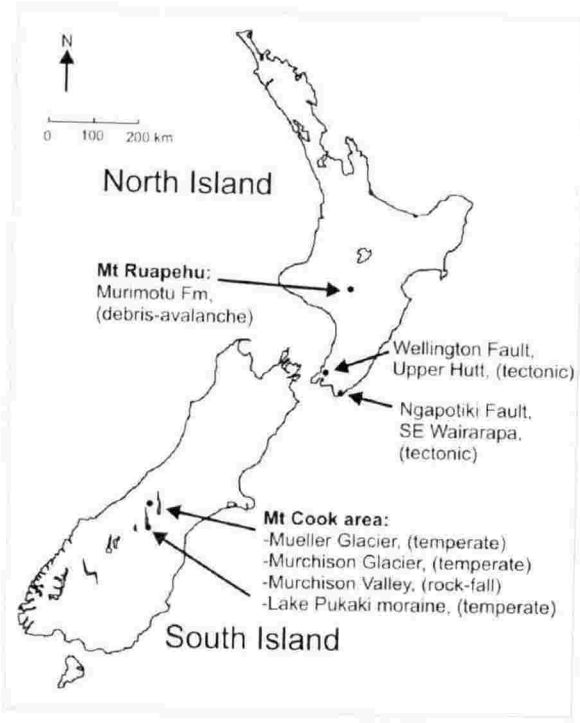

Figure 2.12 Location map showing New Zealand field sites.

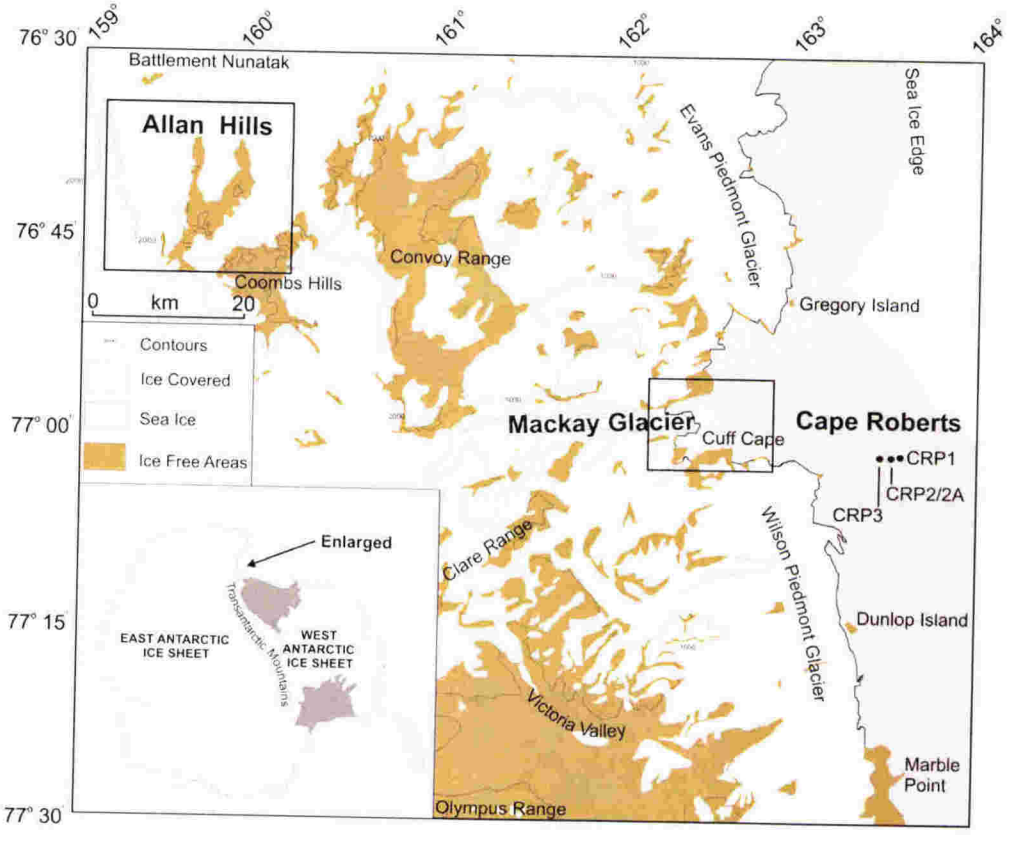

Figure 2.13 Location map showing Antarctic field sites, Allan Hills, Mackay Glacier and Cape Roberts Project drillsites.

2.7 OTHER SITES INVESTIGATED

Several other environments where abrasion was considered likely were investigated early in the study. However, none of these yielded striae. A brief description of these follows.

2.7.1 Coastal sea-ice abrasion

A survey of exposed coastal rock was carried out in the Granite Harbour area of the south Victoria Land coast, Antarctica, for evidence of sea-ice abrasion. Sea-ice forms annually along this coastline and extends approximately 10–20 kilometres offshore. The likelihood of abrasion caused by sea-ice movement on coastal headlands was considered high. Extensive areas of coast were explored from Gregory Island north of Granite Harbour, into Granite Harbour itself and further south past Cape Roberts and finally the southernmost location of Dunlop Island (Figure 2.13).

No abrasion marks were found on any of the coastal bedrock surfaces. However, a large amount of broken ice and sea-floor debris (clasts, sand, and shells) was found on the shoreline suggesting that significant sediment-laden ice is pushed onto the rocks in some areas (Figure 2.14). The absence of abrasion marks is probably due to the lithology of the bedrock. The entire area comprises coarse-grained granite bedrock. The weathered surfaces and large crystal size are not suitable for striae generation or preservation, as individual crystals tend to flake and chip from the surface rather than becoming scored.

Figure 2.14 Large blocks of sea-ice "piled" onto coastal headlands on Dunlop Island, Antarctica.

2.7.2 Alluvial fan

The Ngapotiki fan in southeastern Wairarapa, New Zealand is an active alluvial fan on the eastern side of the Aorangi ranges. The fan consists of poorly sorted angular clasts ranging from pebbles to boulders several metres in diameter that are composed of indurated sandstone and mudstone (Figure 2.15). Despite extensive searching, no abraded clasts were found. This is surprising considering the large volume of coarse sediment moved by high-energy fluvial and also gravity-driven processes on the fan, which produce impacts between rock surfaces. The reason that no abrasion was found is possibly because they are rare, or the collision force of interacting rock surfaces is too low to leave recognisable abrasion marks.

Figure 2.15 Ngapotiki Alluvial fan, southeastern Wairarapa, New Zealand. No striated clasts were found in this setting. Photo by Lloyd Homer (Homer and Moore, 1989).

2.7.3 Lahar deposits

Striated clasts in lahar deposits have been noted in geological literature (see Chapter 1). The central North Island of New Zealand has several composite andesite volcanoes in the Taupo Volcanic Zone. Extensive areas on the sloping ringplain have previously been mapped as lahar deposits. Several of these were examined for the presence of striated clasts. Despite examining many outcrops of several different formations, no abrasion marks were found. This is possibly due to the distance from the source area or particular flow characteristics of lahars in this region.

CHAPTER THREE

TEMPERATE GLACIAL STRIAE

3.1 INTRODUCTION

This chapter investigates striae on clasts transported by temperate glaciers. This is achieved by examining clasts from two modern temperate valley glaciers (Mueller and Murchison) and a Late Pleistocene till (Lake Pukaki moraine) in the Mt Cook region on the eastern side of the Southern Alps of New Zealand. These were selected to provide clasts that have undoubtedly experienced temperate (wet-based) glacial transport. I

below melting point and are entirely frozen to the bed with no basal sliding. These are referred to as "dry-based" or more commonly "cold-based" glaciers. In the past, it was generally accepted that glacier sliding and abrasion can only occur beneath temperate wet-based ice and that beneath cold-based glaciers erosion and deposition do not occur (cf. Sugden and John, 1976; Drewry, 1986).

It is now clear that this division is simplistic and defines end member conditions only. Thermal regime and associated basal conditions vary greatly both spatially and temporally and form a continuum between warm and cold-based ice. Glaciers with both warm and cold layers within the glacier or where there are patches of warm-based or cold-based conditions at the bed are termed polythermal glaciers (Blatter and Hutter, 1991). These polythermal glaciers often have wet-based inner regions but cold-based margins (Menzies, 1995a), (Figure 3.1).

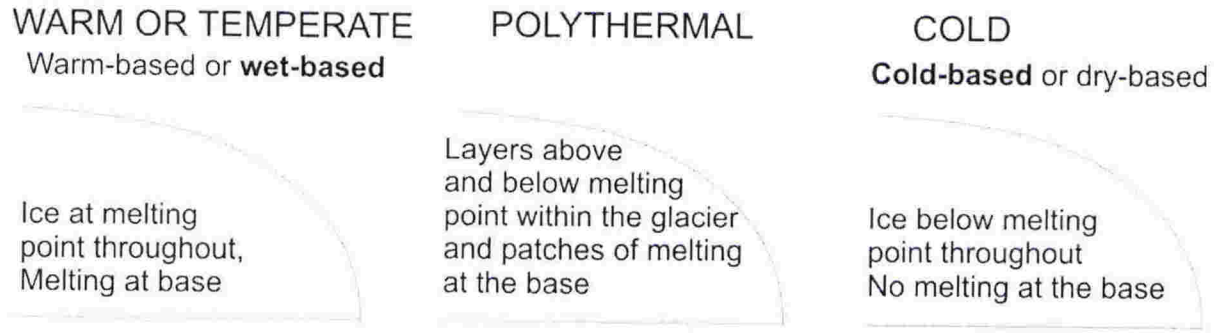

Figure 3.1 Simple schematic diagrams showing the main types of glacier thermal regime, emphasising the basal conditions.

In addition to the temperature character of glacier ice and bed contact, the nature of the substrate is also important for understanding the processes occurring beneath glaciers. The interplay between the thermal state of the glacier bed and the substrate at any one point beneath a glacier influences the way the glacier moves. Figure 3.2 shows how movement is achieved by glaciers of differing thermal states on various substrates.

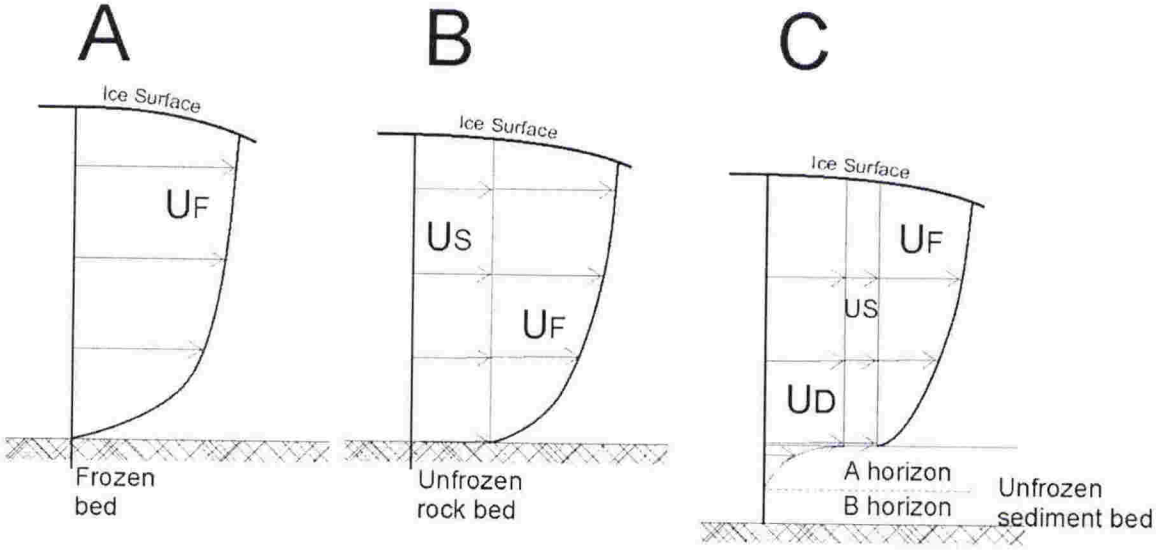

Figure 3.2 Schematic diagram of ice velocity for different thermal and substrate conditions. **A)** Cold-based ice, where glacier movement occurs by internal deformation of ice only (U_F). **B)** Wet-based ice, where glacier movement occurs by internal ice deformation (U_F) and basal sliding (U_S). **C)** Wet-based ice, where glacier movement occurs by internal deformation, (U_F), basal sliding, (U_S) and deformation of subglacial sediments, (U_D). Polythermal glaciers are represented by a combination of all three situations. Adapted from drawings in Drewry, (1986) and Benn and Evans, (1996).

Temperate "wet-based" glaciers and deposits are widespread in middle latitudes with most glaciological and glacial geology literature referring to processes and effects of temperate glaciers.

3.1.2 Striae from temperate glaciers

Abrasion marks such as striae are among the most common features of glacial erosion (Hambrey, 1994) and most literature refers to striae in the temperate glacial context (see Chapter 1 review). Striae shape and cross-cutting relationships on deglaciated bedrock have long been used to infer the direction of past temperate glacial events. Similarly, striae on clasts in diamicton deposits have been used as a means of establishing a glacial origin. The common reference to striae in a glacial context has resulted in striae becoming used as a supposedly unambiguous indicator of glacial influence (e.g. Schermerhorn, 1974a; papers in Hambrey and Harland, 1981; Huggett and Kid, 1983; Powell and Veevers, 1987; Aitken, 1991; Lewis and Iillgner, 2000; Spenceley; 2001).

However, a variety of non-glacial agencies that can produce striae are identified in Chapter 1. Therefore, the presence of striae alone does not imply glacial origin. Documenting striae (occurrence, distribution, shape, orientation) from modern environments can enable better interpretation of ancient deposits.

Previous attempts at classifying striae have considered only temperate glacial examples on bedrock (Chamberlain, 1888; Sugden and John, 1976; Laverdiere et al., 1979; Iverson, 1991; Hambrey, 1994; Benn and Evans 1998) (see Chapter 1). This is of limited use without some consideration of non-glacial striae or striae on clast surfaces in coarse-grained deposits.

3.1.3 Shape and surface features of glacial clasts

The approach used in this study utilises clast shape, clast form and surface features to characterise each deposit. Therefore, an understanding of clast shape (see Chapter 2) and its relationship to striae is important.

Several early papers noted that clasts in till exhibit particular shapes and that many exhibit striae often parallel to the long axis of the clast (Geikie, 1863; Miller, 1850;

Miller, 1884). Later studies confirmed this (e.g. Gregory, 1915) and Von Engeln (1930) provided the first rigorous confirmation that glacial abrasion produces faceted, triangular clasts that were termed "flatiron" shapes. This was supported by Wentworth (1936a) who concluded that the characteristic glacial clast produced by glacial abrasion was a "pentagonal wedge" and that these clasts carry more conspicuous striae. Holmes (1941, 1960) provided detailed studies of the evolution of clast shape in till and confirmed earlier suggestions that larger clasts show deeper striae. This was used to account for the fact that there was a higher percentage of striation reported for cobbles than for pebbles (Figure 3.3). He also noted that the more angular "wedge-form" clasts display strong striae parallel to each other or a prominent edge and that this tendency was much reduced with increased roundness, so that on well-rounded clasts, individual striae are less pronounced and traverse convex surfaces apparently at random.

Figure 3.3 An example of a glacially shaped clast showing many of the features "indicative" of active basal transport. Ice flow from left to right. The left side shows the smooth and rounded "stoss" end. The right side show the abrupt, jagged lee side produced by plucking. Striae are predominantly parallel or sub-parallel to the long axis (a-axis). Athabasca Glacier, Alberta, Canada. Pencil for scale. Photograph by Cliff Atkins.

Kuenen (1971, unpublished manuscript) recognised that the orientation of striae on glacial clasts had received little attention compared with the orientation of the clasts (clast fabric) in glacial studies. He measured the orientation of glacial striae and clast long-axes from glacial deposits in the Netherlands, Switzerland and India. The results confirmed earlier reports that the long axis is the median direction for striae orientation. Also, the more equidimensional the clast, the less preferred orientation of the striae, suggesting that rounded clasts rotate easily during transport. For oblong clasts, the tendency was for striae to form only on flat surfaces and not on ends. Subrounded clasts were the most intensely striated. Finally, this work also supported the observation that the larger the clast, the larger the striae (longer and deeper).

The use of clast shape and surface features has been extended in more recent years to distinguish clasts deposited from different glacial transport modes. For example, clasts transported as supraglacial debris are characterised by angular clasts that lack striae (Boulton, 1978; Domack et al., 1980), due to the lack of abrasion. Clasts transported in the basal debris zones commonly have faceted sides and random striation directions, whereas clasts deposited in lodgement till by actively flowing ice show sub-parallel striae on individual facets. More recent studies have suggested that the abrasion history of clasts can be more complex. Straight and parallel striae indicate relative stability of the clast relative to the striating medium. Often such striae are parallel to the long axis of the clast and typify the upper surfaces of clasts lodged beneath sliding ice (Sharp, 1982; Kruger, 1984; Benn, 1994). Curved and/or multiple orientations indicate clast rotation and realignment during the striating process or a clast that has experienced abrasion during several different glacial events. Many of the features common to clasts that have experienced active glacial transport are summarised in Table 3.1.

The percentage of striated clasts varies greatly within known glacial deposits and appears to be largely controlled by lithology. Dowdeswell et al. (1985), stated "too little systematic work exists to establish whether the wide variations in the intensity of striation carry useful information concerning till, or whether they are a function of lithology and operator definitions of striae". Table 3.2 lists some published examples of the percentage of striated clasts in glacial deposits.

Table 3.1. Summary characteristics of "glacial clasts" and striae on glacial clasts that have experienced active glacial transport.

Feature		Comment
Shape:		Triangular or flatiron or "bullet" shape, stoss and lee ends, Facets.
Roundness:		Subangular to subrounded.
Surface features:	**Striae percentage:**	See Table 3.2.
	Striae and facets:	Predominantly occur on facets, occurrence reduces with increased roundness.
	Striae orientation:	Commonly parallel to a-axis, parallel to other striae, less parallel on more rounded or equidimensional clasts.
	Striae and clast size:	Larger striae occur on larger clasts.
	Striae and clast roundness:	Predominantly occur on subrounded clasts; seldom occur on ends, more random orientation on more equidimensional clasts.
	Other features:	Curved and random striae indicate rotation and realignment of clast during transport.

Table 3.2. Examples of the percentage of striated clasts in various glacial deposits.

Environ -ment	Published example	Location	% striated clasts & (% faceted clasts)	Other comments
Glacio-terrestrial	Holmes (1941)	New York tills	28%	
	Flint (1971)		5-10%	
	Drake (1972)	New England till	3% (hard rocks) 0.1% (soft rocks)	Noted lithology influence
	Sharp (1982)	Icelandic lodgement till	65%	Noted lithology influence
	Humlum (1985)	Icelandic tills	20%	
	Dowdeswell et al (1985)	Sveanor Fm (Svalbard)	0 to 18%	Neoproterozoic tillite
	Bennett et al. (1997)	Pedersenbreen, Spitsbergen	56% (limestone) 2% (schist)	Noted lithology influence
	Atkins (this study)	Mueller and Murchison Glaciers and Lake Pukaki moraine (NZ)	11%, 16%, 33% striated 22%, 28% 41% faceted	Usually on argillite clasts
Glacio-marine	Barrett (1975b)	DSDP 270, Ross Sea, Antarctica	10%	
	Hall (1989)	CIROS -1 core, Antarctica	60%	
	Domack (1980)	George V continental shelf, Antarctica	57% striated 80% faceted	
	Kuhn et al. (1993))	Weddell and Lazarev seas, Antarctica	4% (igneous rocks) 43% (fine grained metabasic rocks	Noted lithology influence
	Atkins (2001)	Cape Roberts core, Antarctica	5% striated 15-50% faceted	Usually on mudstone clasts

3.1.4 Summary of temperate glacial striae characteristics

The overview of an extensive literature body indicates that clasts transported in the basal zones of temperate (wet-based) glaciers produce characteristic clast shapes and striae patterns. Clasts often become subangular to subrounded with facets on one or more sides making up 15 % to 80 % of clasts in the deposit. Some clasts show flatiron shapes with bullet noses (stoss ends) and jagged lee ends. Clasts commonly display striae, but the overall percentage of striated clasts in glacial deposits varies greatly (typically between 5 % and 60 %). The striae are predominantly sub-parallel to the long axis of oblong clasts and occur on faceted surfaces. Some clasts show striae that deviated from the long axis reflecting clast realignment or multiple glacial events. In addition, curved striae indicate clast rotation during the striation process. Lithology does not appear to influence clast shape noticeably but it does influence striae generation, with softer and finer-grained lithologies preserving striae better than hard, foliated or coarse-grained lithologies.

3.2 MURCHISON AND MUELLER GLACIERS, (TEMPERATE GLACIERS), MT COOK REGION, NEW ZEALAND

3.2.1 Background and setting

The Murchison and Mueller Glaciers are temperate valley glaciers located in the Mt Cook region on the eastern side of the Southern Alps, New Zealand (Figure 3.4). These glaciers are surrounded by steep topography consisting of sandstone "greywacke" and argillite with minor basic lavas of the Torlesse Group, thought to be of Jurassic and Triassic age (Gair, 1967). Both glaciers have shown progressive down-wasting during the last century but they have maintained stationary fronts over this period due to a characteristic thick (up to 2 m) mantle of insulating supraglacial debris (Chinn, 1996).

The Mueller Glacier flows from a main cirque area at 1900-2000 metres above sea level (m-asl) approximately 12 km, terminating at about 800 m-asl. Small ponds developed at the terminus of the Mueller Glacier by the mid 1980s and had formed a small (0.7 km long) proglacial lake by 1993 (Hochstein et al., 1995). The proglacial area of the Mueller Glacier shows a complex zone of stagnant ice and glacial debris forming hummocky topography with small streams and fluvial outwash fans draining into the lake.

The Murchison Glacier flows from its cirque area at 2000 m-asl, about 14 km to the terminus at 1000 m-asl. A small, but elongate (3 km) proglacial lake exists directly around the snout and eastern side of the glacier, but this has only developed in the last few years. Hochstein et al. (1995) noted a "preglacial lake" beginning to form by 1995. However, this was not listed as a proglacial lake by Chinn (1996). Much of the glacier presently terminates as ice cliffs (up to 15 m high) directly into the lake, but a complex zone of ice, glacial debris and small outwash fans similar to those at the Mueller Glacier is present on the eastern side of the Murchison Glacier.

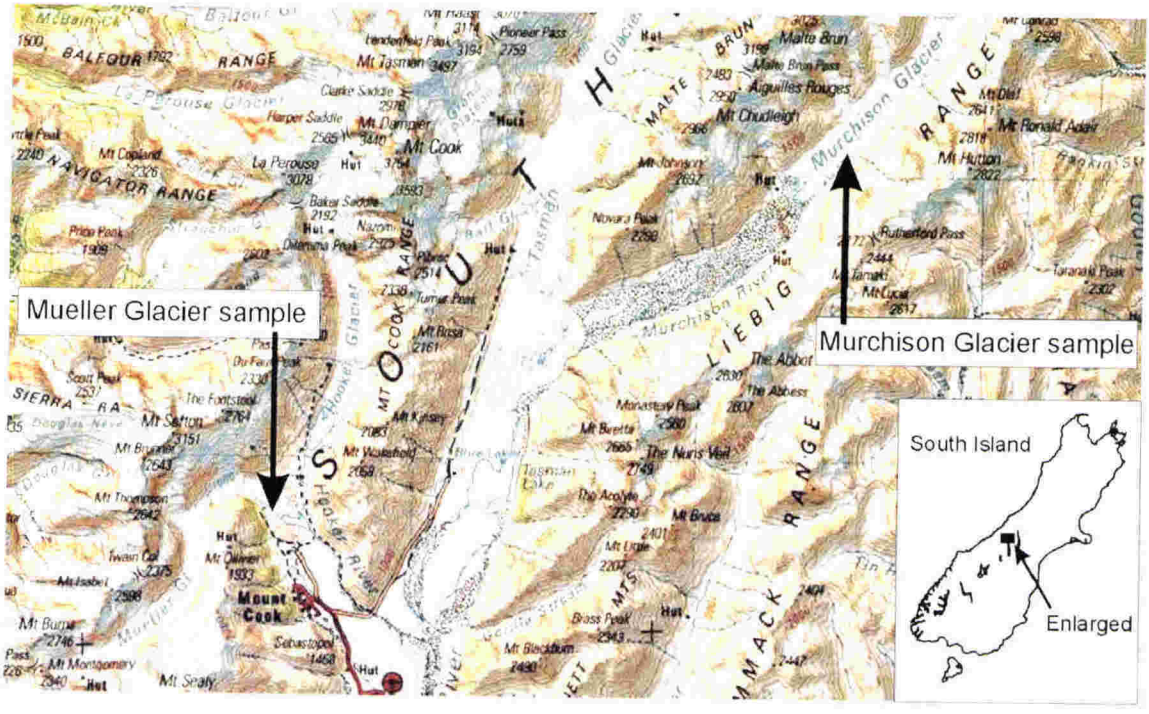

Figure 3.4 Map showing the location of the Mueller and Murchison Glaciers, Mt Cook region.

3.2.2 Fieldwork and sample collection

Fieldwork involved photographing and sampling englacial debris layers on the terminal face of the Mueller Glacier (170°05'00S, 43°42'20E) (Figure 3.5) and within a tunnel at the terminus of Murchison Glacier (170°20'00S, 43°36'10E) (Figure 3.6). The terminus areas are complex environments consisting of glacial debris from a variety of sources. Significant within-site variability exists in these settings and clasts may have a complex transport and erosion histories. However, the sampled debris layers contain facetted and striated clasts that have plainly experienced basal glacial transport. Therefore, the debris layers are interpreted to have been elevated from the base by faulting or folding.

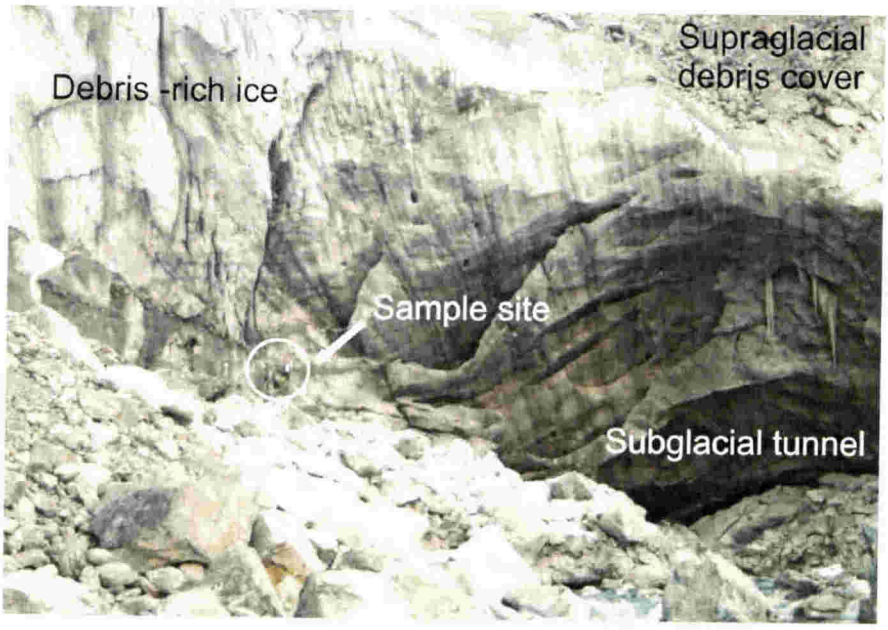

Figure 3.5 The terminal face and glacial tunnel of the Mueller Glacier with sample location indicated (arrow and circle). Debris bands have been deformed up from the base into steeply dipping layers. Note person for scale (circled).

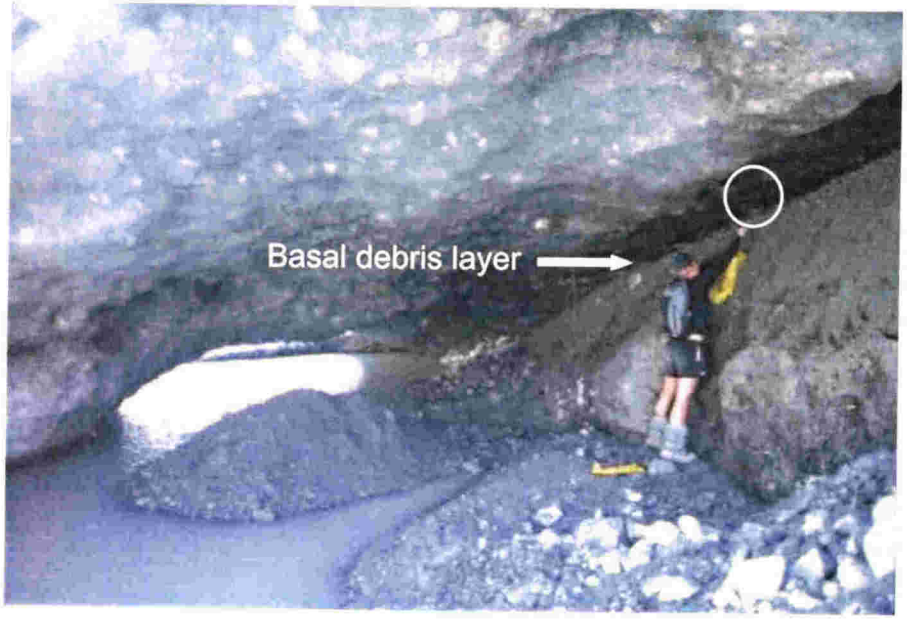

Figure 3.6 A tunnel within the terminus of the Murchison Glacier showing the sample location (circled) within a debris layer dipping toward the terminus (left). These debris layers contain clasts that have been basally transported.

3.2.3 Clast shape

One hundred clasts were measured from the bulk samples collected from *in situ* debris layers at each location. Shape analyses were performed using the method outlined in Chapter 2 and clast data are presented in appendix 2.

The Mueller and Murchison Glacier samples show similar proportions of clast lithologies. Both are dominated by sandstone clasts (72 % and 74 % respectively) with subordinate argillite (26% each) and 2% quartz clasts for the Muller Glacier sample.

Clast form is displayed in Figure 3.7 and shows that both samples have broad distributions with clast c:a axial ratios plotting from 0.15 to 0.95 for the Mueller Glacier and 0.12 to 0.76 for the Murchison Glacier. There is no tendency toward one particular clast shape and the average values for c:a and b:a axial ratios are very similar, plotting in central positions on the form diagrams (large dot).

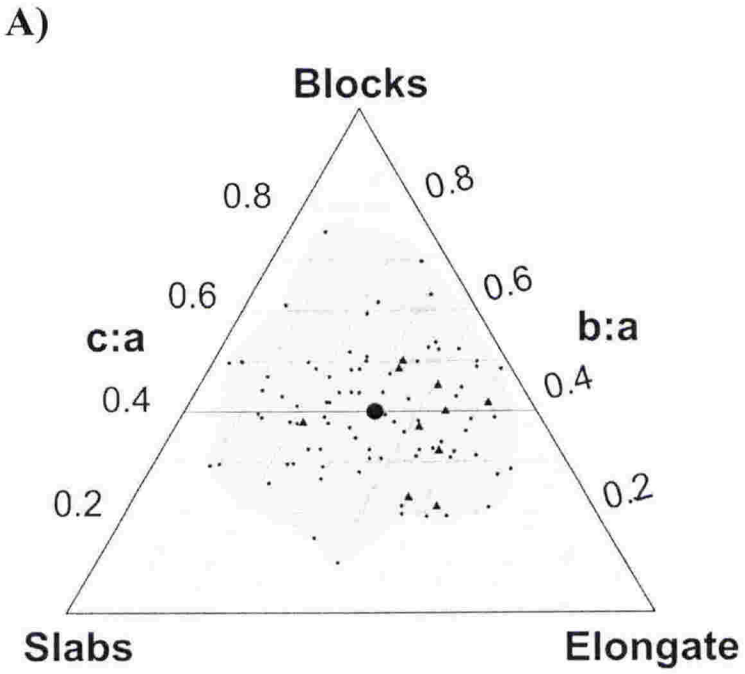

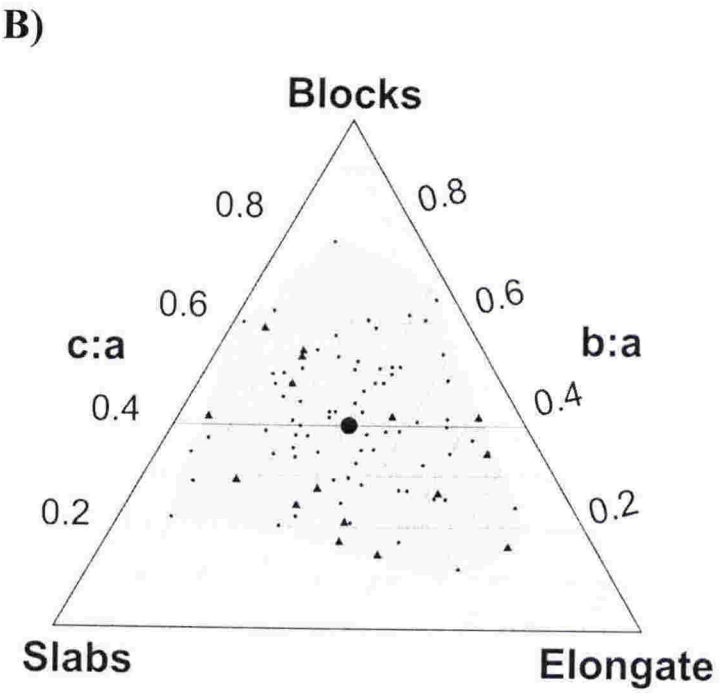

Figure 3.7 Clast form diagrams for: (A) Muller Glacier. (B) Murchison Glacier. Both show broad clast form distributions. Larger black dots indicate average c:a and b:a axial ratios occupying central positions. Triangles represent striated clasts.

Clast roundness and lithology is displayed in frequency percent histograms in Figure 3.8. The distribution for the Mueller Glacier data is broad with all roundness classes up to 0.6 represented. The sample has an average roundness of 0.32 (subangular). There is no apparent relationship between lithology (sandstone or argillite) and roundness class. Twenty two percent of the clasts show flat surfaces that are interpreted as glacially formed facets and these occur on clasts in all roundness classes. Argillite clasts are almost twice as likely to display facets than sandstone clasts (35 % of total argillite clasts, compared with 18% of total sandstone clasts).

The Murchison Glacier data shows a more normally shaped distribution than the Mueller Glacier, but is still broad with all roundness classes up to 0.6 represented. It has a similar average roundness value (0.34 subangular), but displays a strong modal peak in the 0.3 roundness class. No argillite clasts occur in the very angular roundness class (0.1) or in the 0.6 roundness class. Twenty eight percent of clasts show facets

interpreted to be glacially formed. These occur only on clasts in the 0.3, 0.4 and 0.5 roundness classes. Again, argillite clasts are more likely to display facets (50 % of all argillite clasts) than are sandstone clasts (20 % of all sandstone clasts).

A)

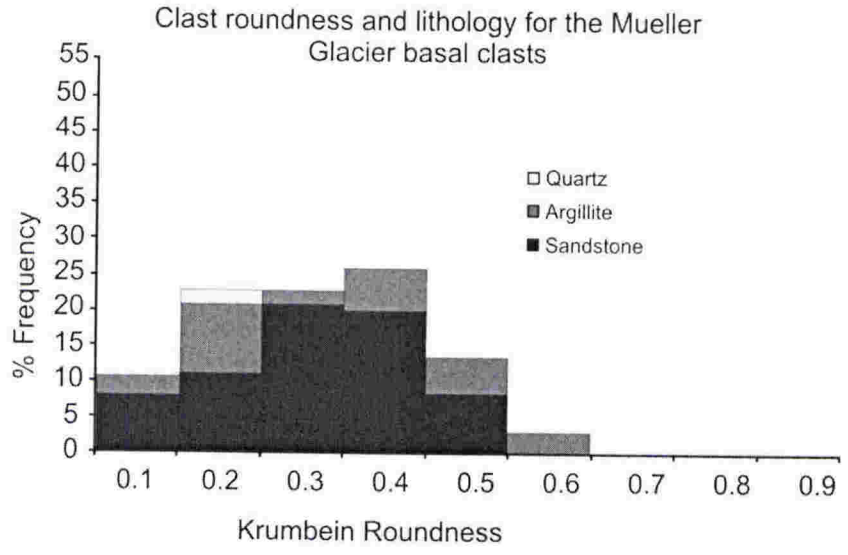

B)

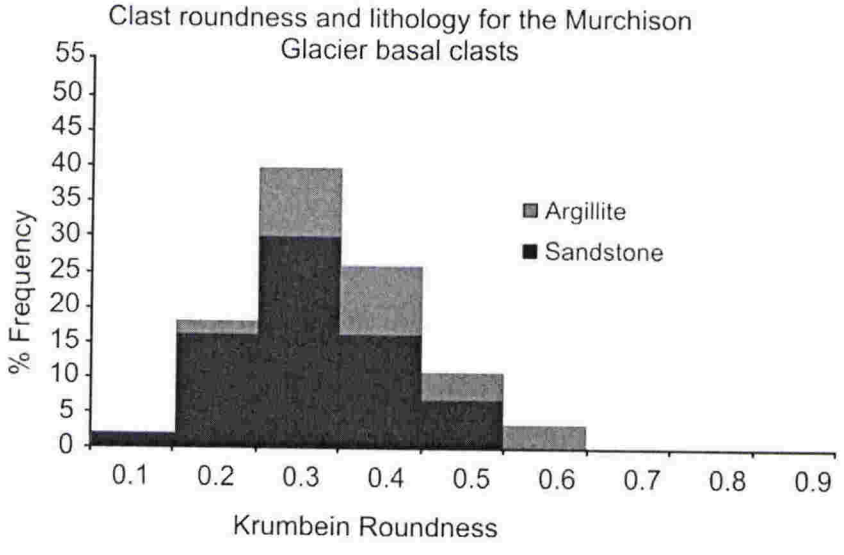

Figure 3.8 Roundness and lithology histograms for the Mueller and Murchison Glaciers samples. Average roundness values are similar (0.32 for the Mueller and 0.34 for the Murchison).

Shape characteristics are highlighted in the covariant plot of RA index (% of angular and very angular clasts) versus C_{40} index (% of clasts with a c:a axial ratio of ≤ 0.4), (Figure 3.9). The Mueller Glacier sample has an RA index of 34 and a C_{40} index of 52 compared with the Murchison Glacier sample that displays a lower RA index of 20 but similar C_{40} index of 53. These results plot within the "subglacial field" determined from published data of Benn and Ballantyne (1994) and Bennett et al. (1997).

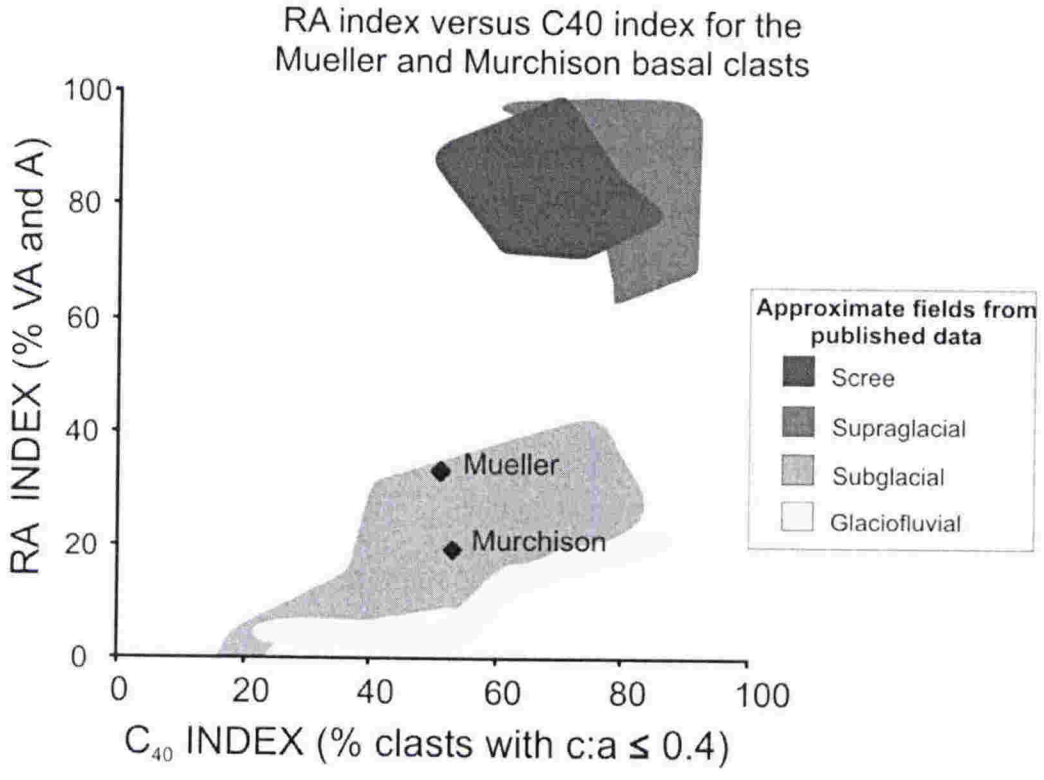

Figure 3.9 RA-C_{40} index diagram for clasts from the Mueller and Murchison Glaciers, Mt Cook area. These samples fall within the subglacial field. Shaded fields are from published data in Benn and Ballantyne (1994) and Bennett et al. (1997).

3.2.4 Clast striae

Striae occur on 11% of clasts from the Mueller Glacier. These are found in all Krumbein roundness classes except 0.1 and are most frequent in the 0.5 class. They

occur preferentially on argillite clasts (38 % of all argillite) compared with sandstone clasts (14 % of all sandstone), and form preferentially on faceted clasts.

The Murchison Glacier data show striae on 16% of clasts, and only in the 0.3, 0.4 and 0.5 classes, again most frequently in the 0.5 roundness class. They occur preferentially on argillite clasts (50% of all argillite clasts) although a few occur on sandstone clasts (4 % of all sandstone clasts). Striae preferentially occur on clasts with facets.

The striae are generally rare, small and faintly inscribed (Figure 3.10). Many clasts show striae parallel or sub-parallel to the long axis although exceptions occur. Lithology influences the preservation of striae. Figure 3.10, B shows a clearly faceted sandstone clast with faint striae parallel to the clast long axis. These are only visible under low angle lighting. Their subtlety is due to the coarser grain-size of the clast and this could result in them not being recognised on many sandstones, giving a lithologic bias against the occurrence of striae on sandstone clasts.

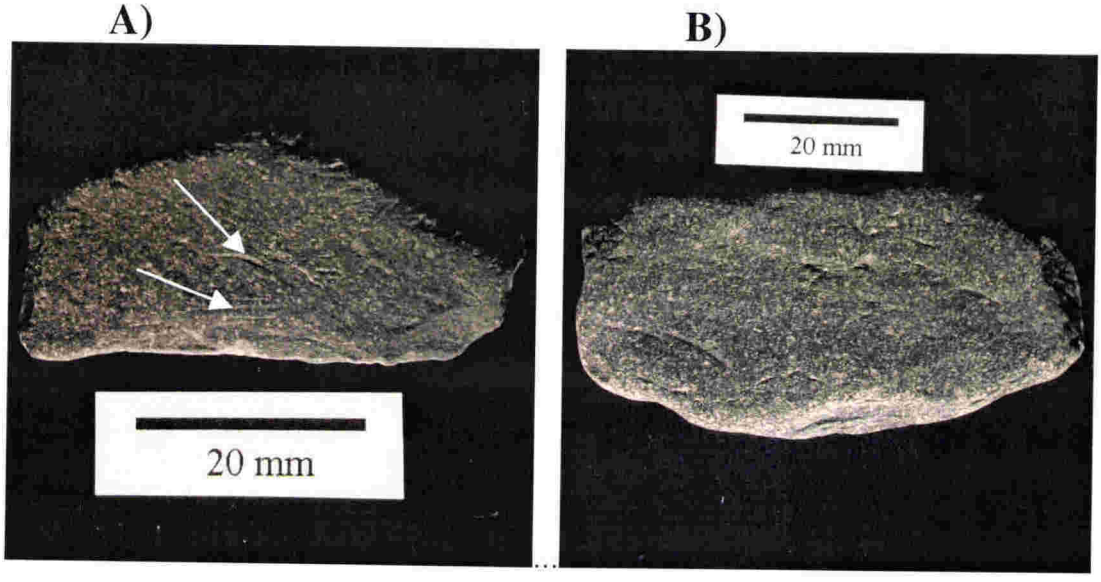

Figure 3.10 A) Striated argillite clast from the Mueller Glacier showing a clear facet with one isolated, curved striae and three short parallel striae on the surface (arrows). B) A faceted sandstone clast from the Murchison Glacier. This surface has long axis parallel striae that are very faint and plainly visible by eye only under low angle lighting but they are also exceptionally difficult to photograph.

Because these samples have relatively few striated clasts and the striae themselves are rare, numbers were considered insufficient for detailed striae analysis. Instead, clearly striated clasts were collected from a compacted diamicton termed the Lake Pukaki moraine, formed during the last glacial by the Palaeo-Tasman Glacier which included ice from the Mueller and Murchison catchments. The results of detailed striae analysis on these clasts are discussed in section 3.3.5.

3.2.5 Summary of Mueller and Murchison clasts

Samples from the Mueller and Murchison Glaciers represent clasts that have experience basal glacial transport within discrete debris layers beneath temperate glaciers. Overall, the samples show very similar clast characteristics. The percentage of various lithologies is close and the clast form distributions show central clustering with few clasts plotting toward blocky, elongate or slabby forms. Average form values are almost identical with c:a axial ratios just below 0.4. The two samples have similar average roundness values but the Murchison sample has a lower percentage of angular and very angular clasts causing it to plot lower on the RA-C_{40} diagram. However, both samples plot within the sub-glacial field on the diagram, consistent with the field context of the samples.

Glacial shapes are rare with few obvious examples of bullet-shaped or stoss and lee-end clasts. However, both samples contain clasts with distinctive flat faces and rounded edges, considered to be glacially produced facets. The percentage of faceted clasts is again consistent with published data from known glacial deposits.

Both samples contain striated clasts, 11 % for the Mueller sample compared with 16 % for the Murchison sample. Striae occur preferentially on argillite clasts and are more common on subrounded and rounded clasts (0.35-0.7). This is also consistent with published data from basal glacial deposits. The relationship between striae and facets is less clear, with striae occurring preferentially on smooth, flattish surfaces although

many of these surfaces are not recognised as facets. Few striated clasts show well-developed long axis parallel striae on clear glacial facets that is "characteristic" of glacial deposits. The striae from the Mueller and Murchison samples are rare, often solitary, faint and lack the pervasive "background" of microstriae seen on other glacially abraded clasts (section 3.3.5). The striae percentage is similar to other known glacial deposits, but the character of the striae is less consistent.

3.3 LAKE PUKAKI MORAINE, (TEMPERATE GLACIAL DEPOSIT), MT COOK REGION, NEW ZEALAND

3.3.1 Background and setting

The Lake Pukaki moraine is located on the southern shore of Lake Pukaki in the McKenzie Basin, New Zealand (Figure 3.11). The westward flowing palaeo-Tasman glacier deposited the moraines during the last glacial maximum (Otiran Glaciation) (Gair, 1967, Porter, 1975). This glacier was a temperate valley glacier that flowed approximately 80 km from the present Tasman, Mueller, Murchison and Hooker Valleys, terminating at about 600 metres above sea-level several km south of the present southern margin of Lake Pukaki (Porter, 1975). The lake itself occupies the lower part of the glacially scoured valley. Glacial deposits including subglacial till, glaciolacustrine sediments and glaciofluvial gravel are exposed in vertical bluffs on the southern margin of the lake (Hart, 1996).

3.3.2 Fieldwork and sample collection

An excellent exposure of glacial moraine on the southern margin of the Lake Pukaki was selected and a section was measured ($170^0$10'00 S, $44^0$10'30E) (Grid reference 838 665 on NZMS 260, Ohau, H38) (Figure 3.11). A bulk sample was collected from a diamicton unit interpreted as a till deposited either subglacially or by rainout of basal debris in a lake. This provided 100 clasts for shape analysis to compare with the results

from debris layers in the modern temperate Mueller and Murchison Glaciers. In addition, several clearly striated clasts were collected from the diamictite to provide suitable examples of temperate striae for detailed analysis. This was needed because the striated clasts from the modern glaciers were relatively few and often poorly striated, making characterisation on these clasts impractical.

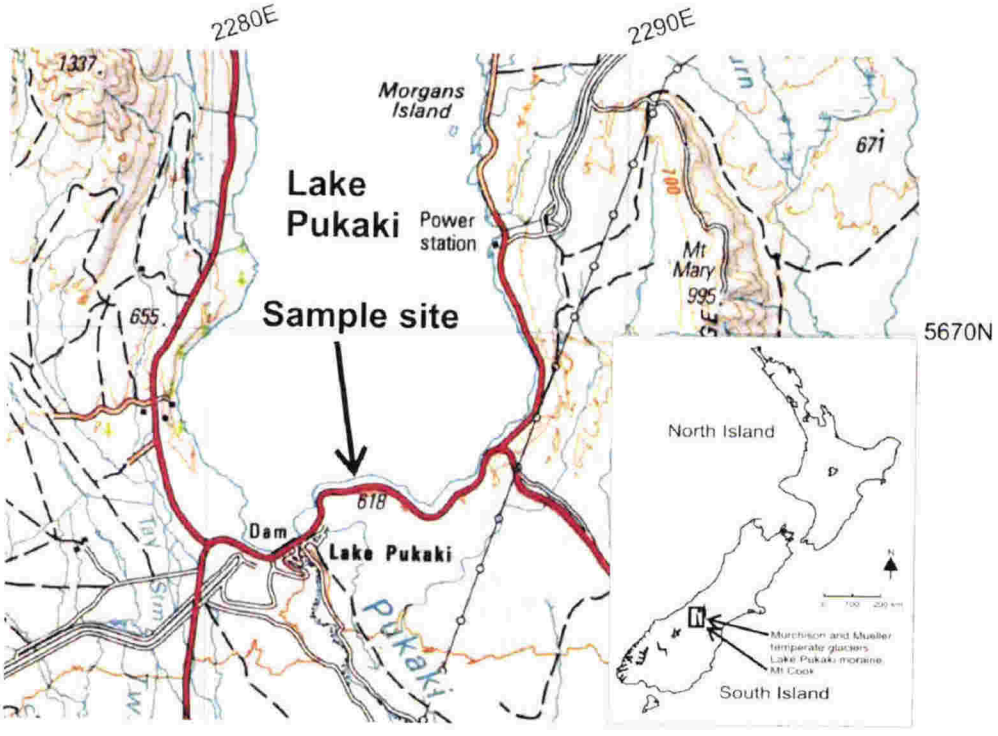

Figure 3.11 Map showing the location of the Lake Pukaki moraine sampled in this study. Map is NZMS 260, sheet H38, 1:50000, Edition 1.

Outcrop description for Lake Pukaki moraine

UNIT 1 DIAMICTON

Lower contact obscured by lake beach. Compacted matrix-supported yellow-grey diamicton. Clasts range from boulders up to 40 cm a-axis to granules. Average clast size is 5-10 cm. Clasts are subangular to rounded. Very poorly sorted to unsorted. Lithologies are sandstone and argillite. Many clast surfaces (especially argillite) show fine striae predominantly oriented parallel to the clast long axis. Some show clear facets and stoss-lee form. Matrix is sandy silt

with granules. Vague bedding apparent in places marked by gravel lenses up to 30 cm thick and 2 m long and clast poor laminated silt layers up to 20 cm thick. The unit has maximum thickness of 3 m above beach to base of UNIT 2.

UNIT 2 GRAVEL

Lower contact with UNIT 1 is sharp and wavy with up to 40 cm relief. UNIT 2 is a clast-supported gravel. Clasts range from boulders up to 1.0 m long axis to pebbles. Average clast size is approximately 5-10 cm. Clasts are subangular to well-rounded and consist of sandstone and argillite lithologies. Poorly sorted with no obvious bedding. UNIT 2 has variable thickness up to 2.0 m thick, but mostly about 1.5 m thick.

UNIT 3 DIAMICTON

Lower contact with UNIT 2 is sharp and wavy with up to 30 cm relief. UNIT 3 is a clast poor matrix supported diamicton. Clasts range from 30 cm long axis to pebbles with average clasts size of 5 cm. Clasts are angular to rounded and is comprised of sandstone and argillite. Some show glacial shapes and striated surfaces. Matrix is sandy silt. Faintly bedded with irregular lenses of laminated siltstone and some glaciotectonic deformation apparent. UNIT 3 is up to 3 m thick to the top of exposure.

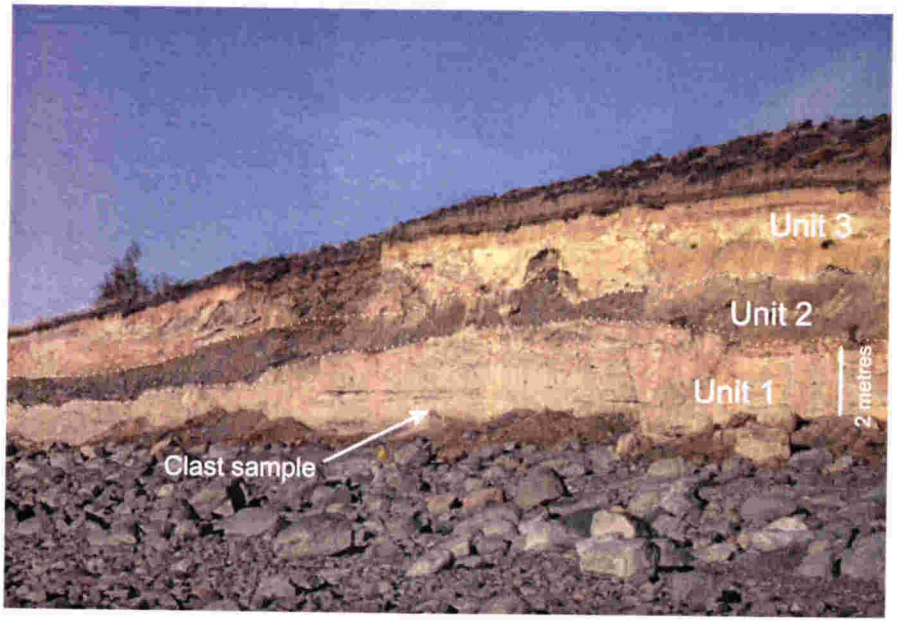

Figure 3.12 Outcrop of glacial moraine at the southern margin of Lake Pukaki. Three units are present. The clast samples were taken from the clast-rich diamicton of UNIT 1 (arrow).

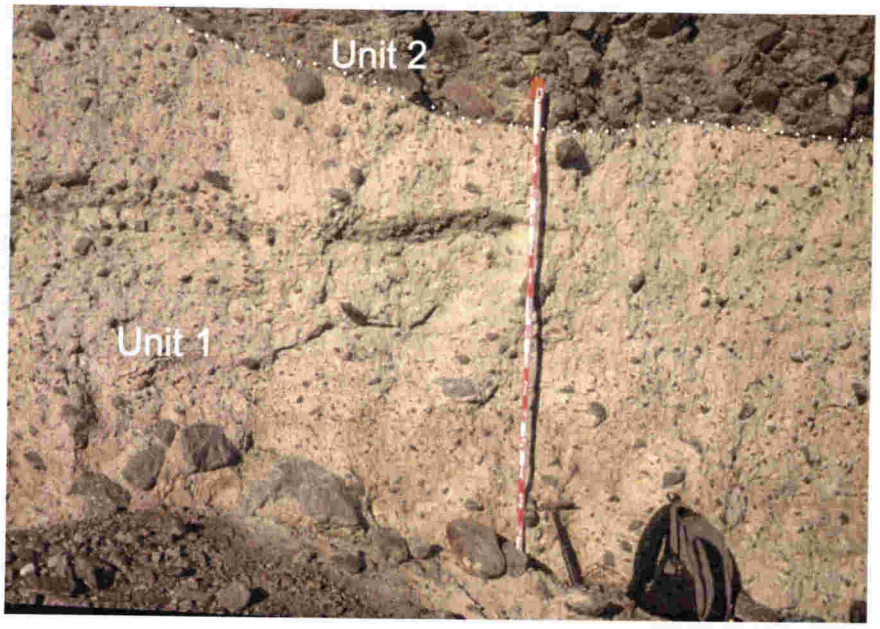

Figure 3.13 Close-up of the diamicton of UNIT 1. Abundant striated clasts are present in this unit. Tape measure is 2 metres long.

3.3.3 Clast shape

The sample collected from Unit 1 provided 100 clasts for shape analyses. Clast shape data are presented in appendix 2.

The Lake Pukaki sample is dominated by sandstone clasts (82%) with subordinate argillite (18%). Clast form analysis shows that the sample has a broad distribution with clast c:a axial ratios plotting from 0.16 to 0.88 and an average of 0.45 (Figure 3.14).

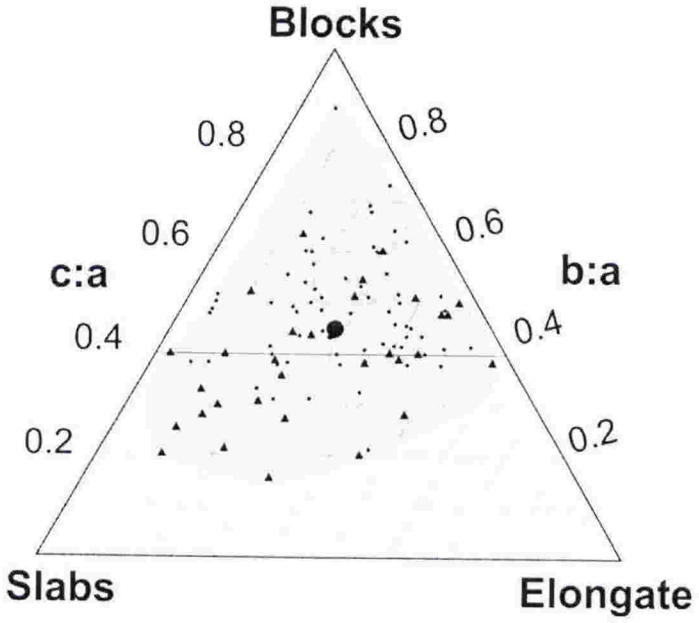

Figure 3.14 Clast form diagram for the Lake Pukaki moraine. Large black dot indicates average c:a and b:a axial ratio. Small black triangles represent striated clasts.

Roundness and lithology are displayed in frequency percent histograms in Figure 3.15. The distribution is broad and bimodal with all roundness with modal peaks in the 0.3 and 0.6 classes, reflecting a mix of pre-existing fluvially rounded gravel (rounded) and glacially modified clasts (subangular). The sample contains no very angular clasts (0.1) and has an average roundness of 0.43 (subrounded), which is higher than the Mueller and Murchison Glaciers. There is no relationship between lithology (sandstone or argillite) and roundness class, although no argillite occurs in the 0.7 class. Forty-one percent of the clasts show flat surfaces (glacially formed facets) and these occur on clasts in the 0.2, 0.3, 0.4 and 0.5 roundness classes. Eighty-nine percent of the argillite clasts show facets, compared with only 30 % of sandstone clasts. The percentage of faceted clasts is higher than for the Mueller and Murchison Glacier samples.

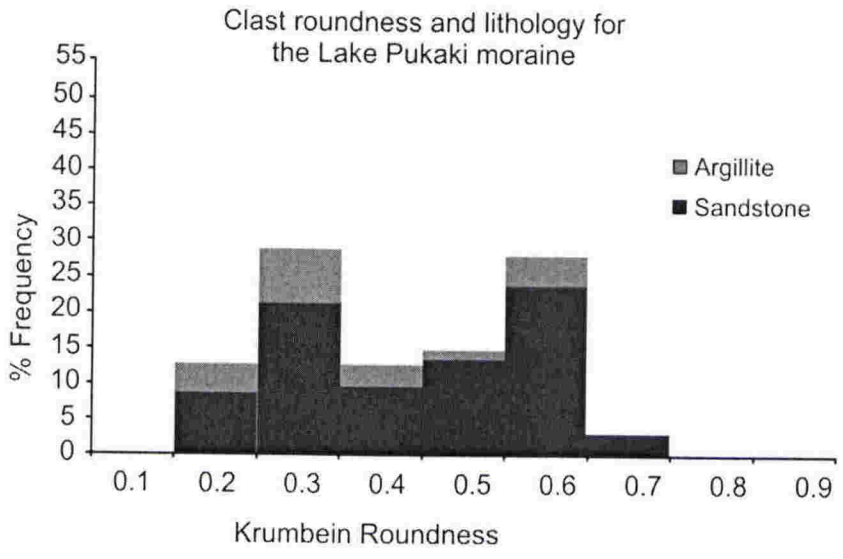

Figure 3.15 Roundness and lithology histograms for clasts from the Lake Pukaki moraine. The distribution is bimodal reflecting the mix of pre-existing fluvially rounded clasts and glacial modification of some clasts providing a subangular component. Average roundness (0.43, subrounded) is greater than for the Mueller and Murchison Glaciers.

Figure 3.16 displays a covariant plot of RA index (% of angular and very angular clasts) versus C_{40} index (% of clasts with a c:a axial ratio of ≤ 0.4). The data show an RA index of 13 and a C_{40} index of 34. These results plot within the "subglacial field" determined from published data of Benn and Ballantyne (1994) and Bennett et al. (1997), but lower and to the left of the samples from the Mueller and Murchison Glaciers, highlighting the more rounded and more equidimensional clasts in the Lake Pukaki moraine.

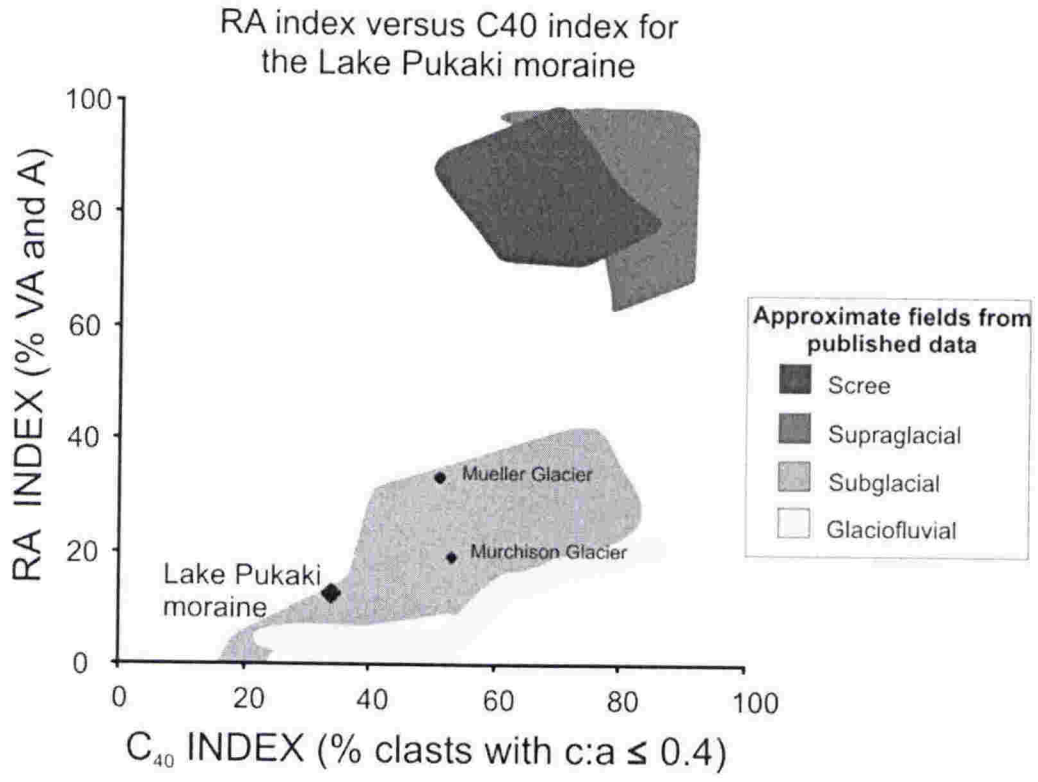

Figure 3.16 RA-C_{40} index diagram for clasts from the Lake Pukaki moraine, Mt Cook. The sample plots within the subglacial field. Also shown are samples from Mueller and Murchison Glaciers. Shaded fields are from published data in Benn and Ballantyne (1994) and Bennett et al. (1997).

3.3.4 Clast striae

Small-scale striae occur on 33% of clasts from the Lake Pukaki moraine. This is significantly higher than the percentage from either the Mueller (11%) or the Murchison (16%) Glaciers. The striae in the Lake Pukaki sample occur on clasts in all Krumbein roundness classes except 0.7. They occur preferentially on argillite clasts (94 % of all argillite) compared with sandstone clasts (19.5 % of all sandstone) and form preferentially (but not exclusively) on faceted clasts. Striae occur on clasts of all forms (Figure 3.14) although preferentially on clasts with slabby forms (clasts that plot to the left and below the 0.4 c:a axial ratio line of the form triangle.

3.3.5 Character of striae

General characteristics of striae are highlighted in the "Linear Abrasion Atlas" presented in appendix 1. The atlas aims to present a range of features observed on temperate glacially striated clasts from the modern Mueller and Murchison Glaciers and the Lake Pukaki moraine.

A common characteristic is that many clasts display surfaces (both faceted and non-faceted) with a pervasive "background" of microstriae (< 0.25 mm width and < 2 mm length), with larger striae superimposed on top. Many elongate clasts show striae parallel or sub-parallel to the long axis, some with larger striae occasionally oblique to the long axis. (Figure 3.17). This occurs on flat glacial facets and also on curved clast surfaces.

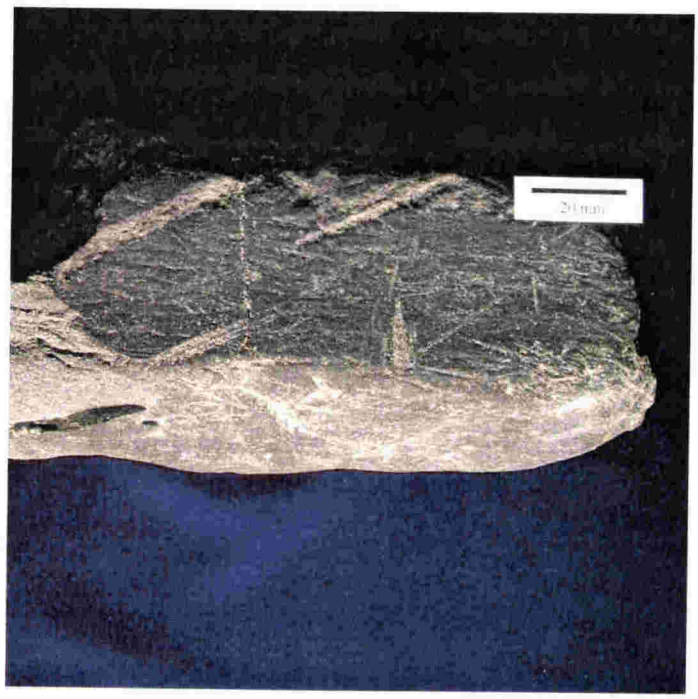

Figure 3.17 An elongate (b:a axial ratio of 0.40) fine-grained sandstone clast from the Lake Pukaki moraine showing a pervasively striated surface. This consists of a "background" of microstriae with larger striae superimposed. These range up to 5 mm wide and cut obliquely across the clast. Most striae are parallel to the long axis of the clast. This clast is also shown in appendix 1, (Linear abrasion Atlas – Temperate striae, Image 2).

However, there are many exceptions to this generalisation. For example, some clasts show apparently random striae orientations, particularly if the clast is close to equidimensional. These clasts also commonly display curved striae indicative of clast rotation during the striation process (Figure 3.18).

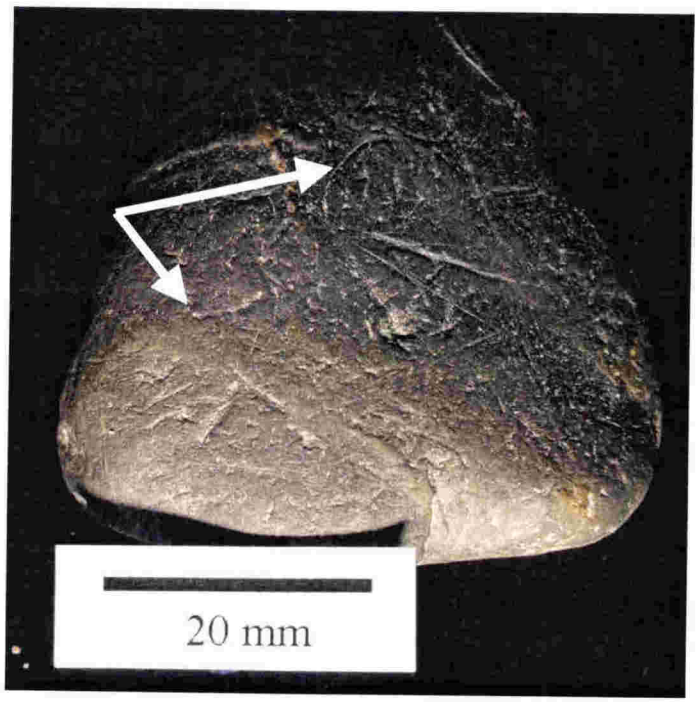

Figure 3.18 An equidimensional argillite clast (b:a axial ratio of 0.98) from the Lake Pukaki moraine showing multiple striae directions (clast 2 in Figure 3.19). Two curved striae (arrows) are also visible suggesting rotation during the striation process.

Striae orientation

Orientations of striae on four clasts from the Lake Pukaki moraine were measured with reference to the long axis of the clast as described in Chapter 2. This produced a direction with reference to the long axis (180°) of between 90° and 270° for each striation. These were grouped into 5° segments and displayed on half rose diagrams

(Figure 3.19). Additional high-resolution images of these and other clasts are provided in Appendix 1.

Lake Pukaki moraine clast 1 is a clearly striated fine-grained sandstone clast. It has a distinctly elongate shape with a b:a axial ratio of 0.4. The striae are preferentially oriented parallel to the long axis (180°) with 38 % falling within 5° and 84 % within 30° of the long axis giving an average orientation of 181°. A small percentage of striae are oriented oblique to the long axis giving an overall range of 70° and standard deviation of 24°. This pattern is also displayed by clasts 3 and 4 from the Lake Pukaki moraine, which also have distinct long axes (b:a ratios of 0.41 and 0.63 respectively) and show striae that are preferentially oriented parallel to the long axis. Clast 3 shows a strong clustering with 80 % of striae within 30° of the long axis, giving a low range (54°) and a low standard deviation of 20°. Clast 4 has 75% of striae within 30° of the long axis with a similar range of 58° (standard deviation of 26°). Clasts 3 and 4 have 4 % curved striae suggesting some rotation during the striation process despite the overall dominance of long axis parallel striae.

These data contrast markedly with clast 2, which is a smaller (45 mm-long axis) argillite clast (Figure 3.18) that has almost equal long and intermediate axes (b:a axial ratio of 0.98). The striae have no preferred orientation with only 30 % of striae within 30° of the long axis. The striae have a wide range of 89° and high standard deviation of 48°. This clast has 6% curved striae.

Although only four clasts are considered, these data illustrate the wide range in striae orientations within the temperate glacial environment. It also indicates a strong association between than striae orientation and the shape of the clast. Striae parallel to the long axis are more common on elongate clasts and less common on more equidimensional clasts. This is ascribed to clast alignment during basal glacial transport with elongate clasts less likely to rotate once they have established a stable position (long axis parallel to flow) than equidimensional clasts, which are more likely to be rotated.

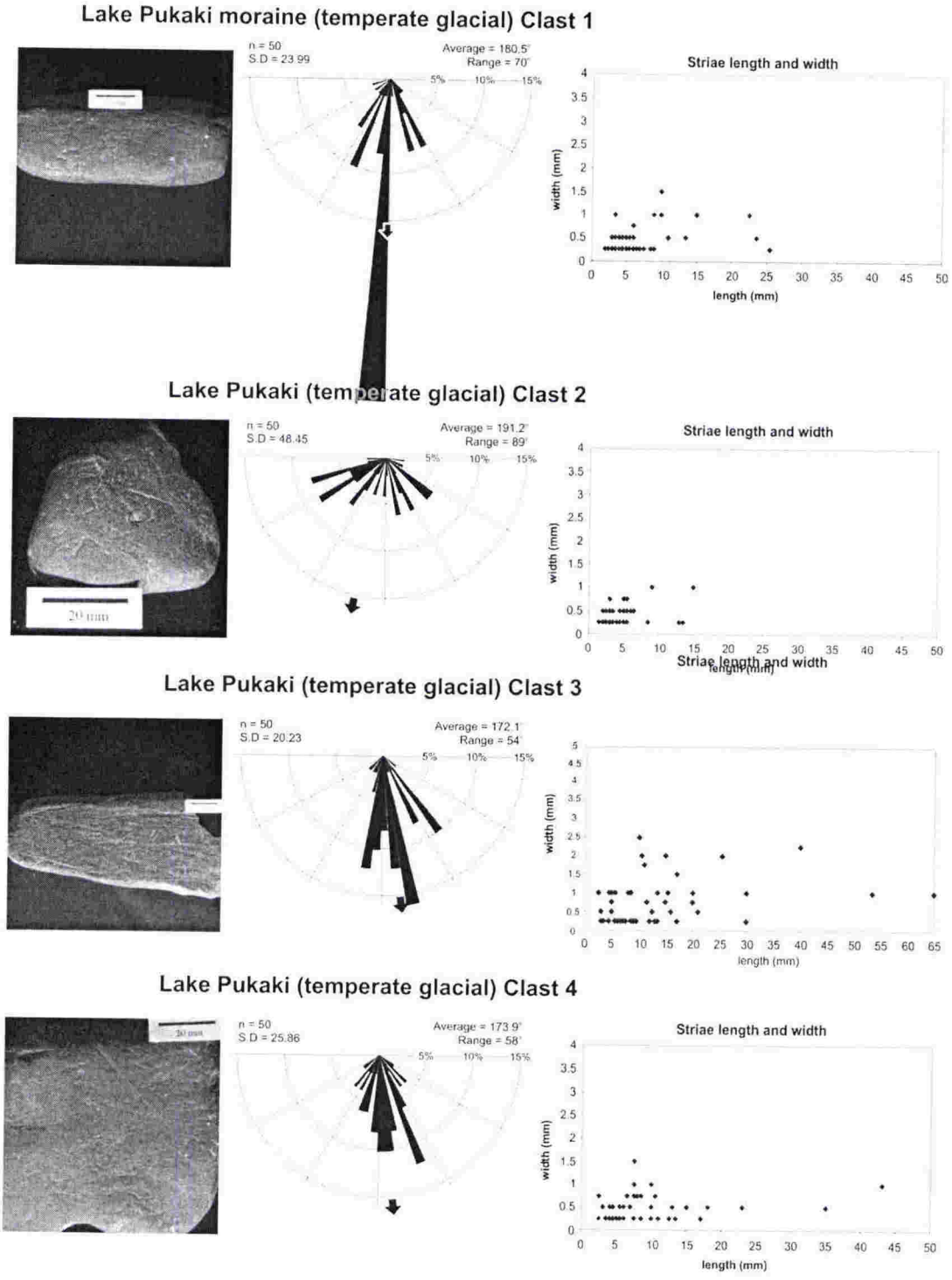

Figure 3.19 Striated clasts from the Lake Pukaki moraine. The half-rose diagrams represent orientation of striae relative to the long axis of the clast (180°). Striae are grouped into 5° segments. The black arrows indicate average striae orientation. Also shown is a plot of striae length and width.

Striae length

Striae length was measured for more than 40 striae on each clast and the results shown in Figure 3.19 and Figure 3.20. These data show that there is a wide range in striae length on individual clasts and that striae length is influenced by the size and shape of the clast. For example, the smallest and most equidimensional clast (clast 2 which is 45 mm long), has a maximum striae length of only 15 mm, the lowest average striae length (4.5 mm) and least range and standard deviation (2.9 mm). The largest, elongate clast (clast 3 which is 196 mm long) has a maximum striation length of 65 mm, average striation length of 13.2 mm and much higher range and standard deviation of 12.4 mm (Figure 3.20).

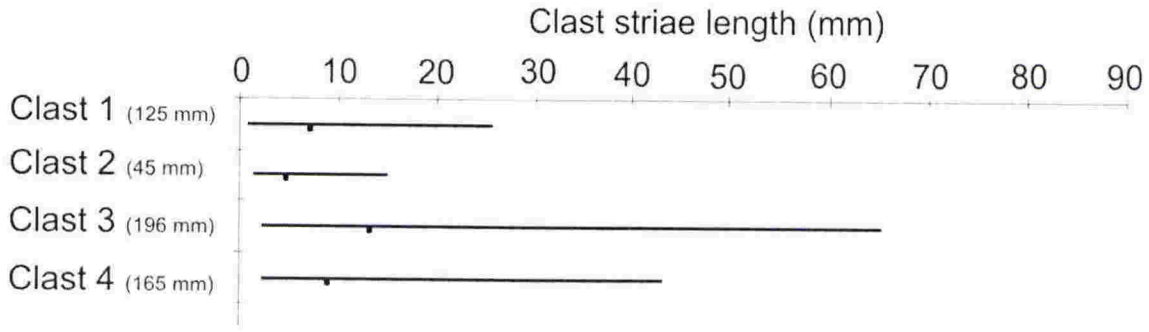

Figure 3.20 Striae length ranges and averages for the four clasts from the Lake Pukaki moraine. The longest striae, greatest range and highest average occur on the longest clast (clast 3) and the smallest range and lowest average occur on the smallest clast (clast 2). Clast length is shown in brackets.

Striae width

Striae width is displayed in Figure 3.19 and Figure 3.21. A wide variation in striae width occurs even on individual clasts, but width is also related to clast size and shape. The widest striae (2.5 mm), highest average width (0.7 mm) and greatest standard deviation (0.61mm) occur on the largest elongate clast, whereas the smallest maximum

striae width (1 mm), lowest average (0.25 mm) and smallest standard deviation (0.20 mm) occur on the smallest, equidimensional clast.

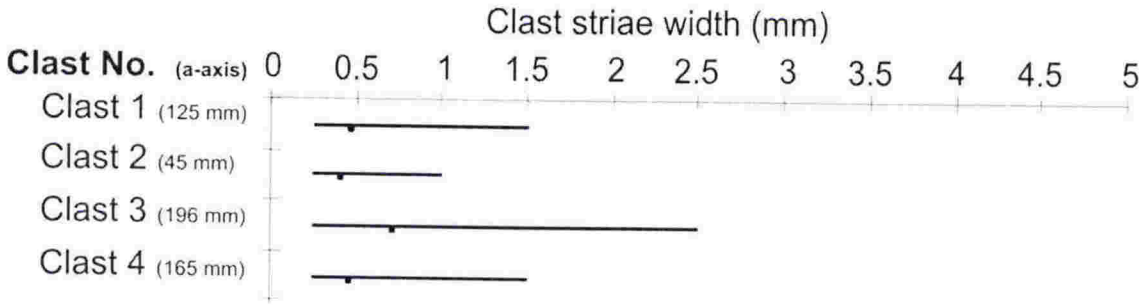

Figure 3.21 Striae width ranges and averages. The widest striae (2.5 mm), highest average width and greatest width range occur on the largest clast (clast 3) and the lowest average and range occur on the smallest clast (clast 2). Clast lengths are shown in brackets.

Width and length ratios

Length and width of striae are not closely linked. Some longer striae are wider than average, but other long striae have average and less than average widths. Width divided by length of each striation was calculated to produce a ratio between 0 and 1. These are displayed in Figure 3.22. The results are interesting because although the range of values for each clast appears to reflect the size of the clast (greatest range on the longest clast and smallest range on the smallest clast), the average width/length ratios do not. These average values are all close but the highest average ratio (0.102) occurs on the smallest and most equidimensional clast. This indicates that it has slightly wider and shorter striae relative to the more elongate clasts.

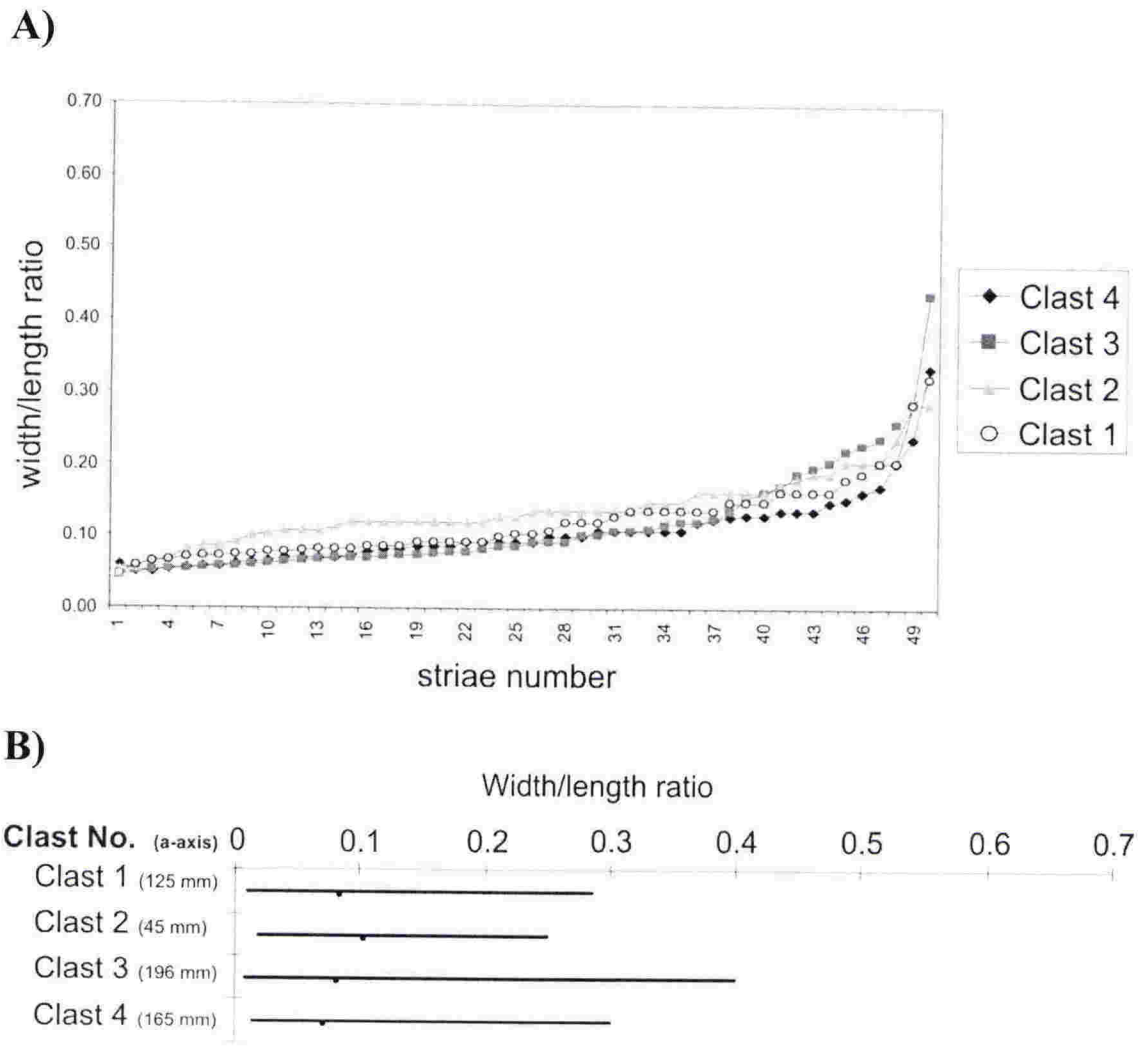

Figure 3.22 A) Width/length ratios for the four Lake Pukaki clasts ranked lowest to highest. B) Width/length ratio ranges and averages. The largest clast (clast 3) shows the highest range in width/length ratio up to 0.40. The smallest clast (clast 2) has the least range in values but has the highest average width/length ratio, indicating that it has the relatively shortest and widest striae.

Striae density

The density of striae was measured using the technique outlined in Chapter 2. This provided an average number of striae per cm^2 and also a percentage of the measured surface that contains "background" striae. These results are displayed in Figure 3.23. In

addition, indication of striae distribution was obtained by calculating the percentage of 25 mm^2 squares over the measured area that have at least one striation.

All of the Lake Pukaki moraine clasts are pervasively striated with 100 % background microstriae on the measured surfaces. The number of striae per cm^2 ranges from a low of 2.1 on the largest clast (fine sandstone) to a maximum of 4.0 striae per cm^2 on the smallest clast (argillite). The clasts have a minimum of 74 % of squares with at least 1 striation showing that striae are widely distributed across the surface.

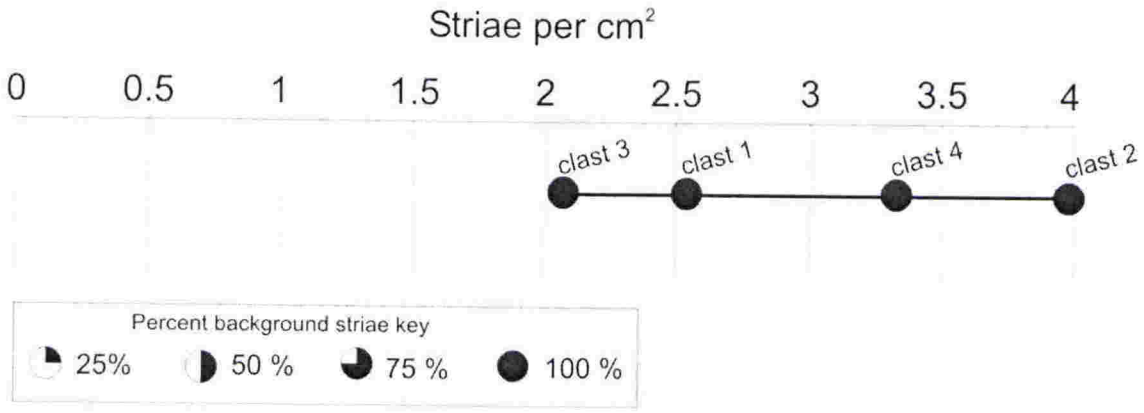

Figure 3.23 Striae density diagram showing the number of striae per cm^2 for each clast and the percentage of "background" striae. The clasts have at least 2 striae per cm^2 and 100% background striae.

3.3.6 Discussion and conclusion

The Lake Pukaki moraine is undoubtedly a temperate glacial deposit from the palaeo-Tasman Glacier. However, clast shape and striae characteristics differ considerably from the clasts recovered from basal debris layers of the modern Mueller and Murchison Glaciers.

The deposit has identical lithologies represented but shows a slightly higher percentage of sandstone clasts compared with the modern glacier samples. It shows a more variable

clasts shape distribution but has a slightly higher average clast form indices of 0.45 compared with values just under 0.4 for the glacier samples. This indicates that the Lake Pukaki moraine sample is on average slightly more equidimensional or blocky than the modern glacier samples. This is seen also in the roundness, with the Lake Pukaki moraine sample showing a broader and better-rounded distribution. When plotted on the RA-C_{40} diagram, all three samples plot within the known subglacial field but the greater blockiness and roundness of the Lake Pukaki samples is evident. This most likely reflects entrainment of pre-existing fluvially rounded clasts from the floor of the Pukaki valley into the basal debris layer of the advancing palaeo-Tasman glacier, which were then abraded and deposited as till at the terminal moraine. Most clasts have retained their fluvial shape, despite subsequent basal glacial abrasion. The glaciers in the region have generally been retreating since the last glacial that deposited the Lake Pukaki moraine. They are presently at their minimum extent and therefore the debris within the modern glaciers will not have experienced previous fluvial abrasion, though they may have been affected by subglacial water flow.

The clasts from the Mueller and Murchison Glaciers display fewer obvious glacially formed facets (22 % and 28 % respectively) compared with the Lake Pukaki moraine, although in all samples, facets preferentially occur on argillite clasts. Also, the percentage of striated clasts is considerably lower, 11 % and 16 % for the modern glaciers compared with 33 % for the Lake Pukaki moraine. Although striae preferentially occur on argillite clasts in all samples, the striae on the clasts from the modern glaciers are rare, often solitary and generally faintly inscribed and lack the pervasive "background" of microstriae. Abrasion is certainly occurring within the basal layers but is of a much lower intensity than that which produced the pervasively striated and commonly faceted clasts in the Lake Pukaki moraine.

Striae on the Lake Pukaki clasts conform with the long-standing idea that striae occur predominantly parallel to the long axis of elongate clasts. The striae preferentially occur on facets but are also seen on curved surfaces. The data also suggest that striae show less preferred orientations on more equidimensional clasts and that these clasts show more curved striae, reflecting the greater ability of equidimensional clasts to rotate

within basal glacial layers. Striae length displays great variation and is clearly related to clast size with longer striae forming on longer clasts. Width is less variable, showing consistently lower ranges in values than most other environments studied, but still related to clast size (widest striae occur on largest clasts). Overall, striae on temperate clasts tend to be long and narrow and lack the wide compound striae seen on clasts from other environments.

Clasts from the Lake Pukaki moraine show a pervasive "background" of microstriae on fine-grained lithologies. Clasts typically have at least 2 striae per cm^2 and are widespread over the clast surface. Striae density is much lower for clasts from the modern Mueller and Murchison Glaciers. This probably reflects the difference between abrasion that occurred in relatively thin debris layers (Mueller and Murchison examples), and abrasion that occurred within a thicker basal glacial zone (Lake Pukaki example) where there was more rock debris and a fine-grained matrix around clasts producing a high density of striae and pervasive background microstriae.

3.4 STRIAE "SURVIVABILITY" CASE STUDY - MURCHISON VALLEY

3.4.1 Introduction

The aim of this study is to investigate the "survivability" of glacial features of clasts during fluvial transport to allow an estimate of how far recognisable glacial clast features persist downstream from a glacier terminus. This was achieved by measuring clast shape and surface features from sites progressively further downstream from the terminus of the Murchison Glacier. This location was chosen because it is the most accessible glacier in the region that was not listed as having a proglacial lake (Chinn 1996), therefore providing a continuous fluvial transport path downstream from the glacier. However, a small proglacial lake had developed between 1996 and the date of fieldwork in April 2001. The lake had formed around the front and along the eastern margin of the glacier, in part occupying the old fluvial channel draining the glacier (evident on topographic maps). The lake presently blocks the fluvial transport path from the glacier snout to the fluvial braid plain. Because the development of the lake is recent, the samples used in this study are still considered to represent increasing fluvial transport distance downstream (Figure 3.24).

3.4.2 Background

As discussed in Chapter 2, clasts attain characteristic shapes that reflect the transport processes the clasts have undergone. In the glacial context, Boulton (1978) showed that clast shape is largely a function of the various glacial transport mechanisms and recognised a clear distinction between clasts transported in the active subglacial zone and clasts transported in the passive supraglacial/englacial zones. Many subsequent workers have replicated and extended this to use shape analysis to interpret glacial sediment and landforms of uncertain origin (cf. Bennett et al., 1997).

In the wider context, it has long been established that parameters such as particle size, shape, and roundness change progressively downstream in coarse-grained alluvial systems as a consequence of sorting, mechanical abrasion and chemical weathering during sediment transport (e.g. Mills, 1979; Huddart, 1994). Most temperate glaciers are drained by fluvial systems, but it appears that there has been little study on the effect of downstream change on the features specific to glacially derived clasts such as faceted surfaces and striae. The value of such a study is that it provides criteria for estimating fluvial transport distance for ancient glaciofluvial deposits, and proximity of the ice front for gravels with striated clasts.

3.4.3 Fieldwork

Ten sites (numbered MH 1 to MH 10) were selected ranging from a glacial tunnel (MH 1) at the glacier terminus, to 11 km downstream on the Murchison River braid plain (MH 10). The sites were chosen to reflect increasing fluvial transport distance from the glacier (Figure 3.24).

At each site, an area of riverbed covered with pebble to cobble sized clasts was selected and 50 clasts were measured, except at site one (MH 1, glacial tunnel) where 100 clasts within an englacial debris layer were measured. Shape analysis was performed using the method outlined in Chapter 2.

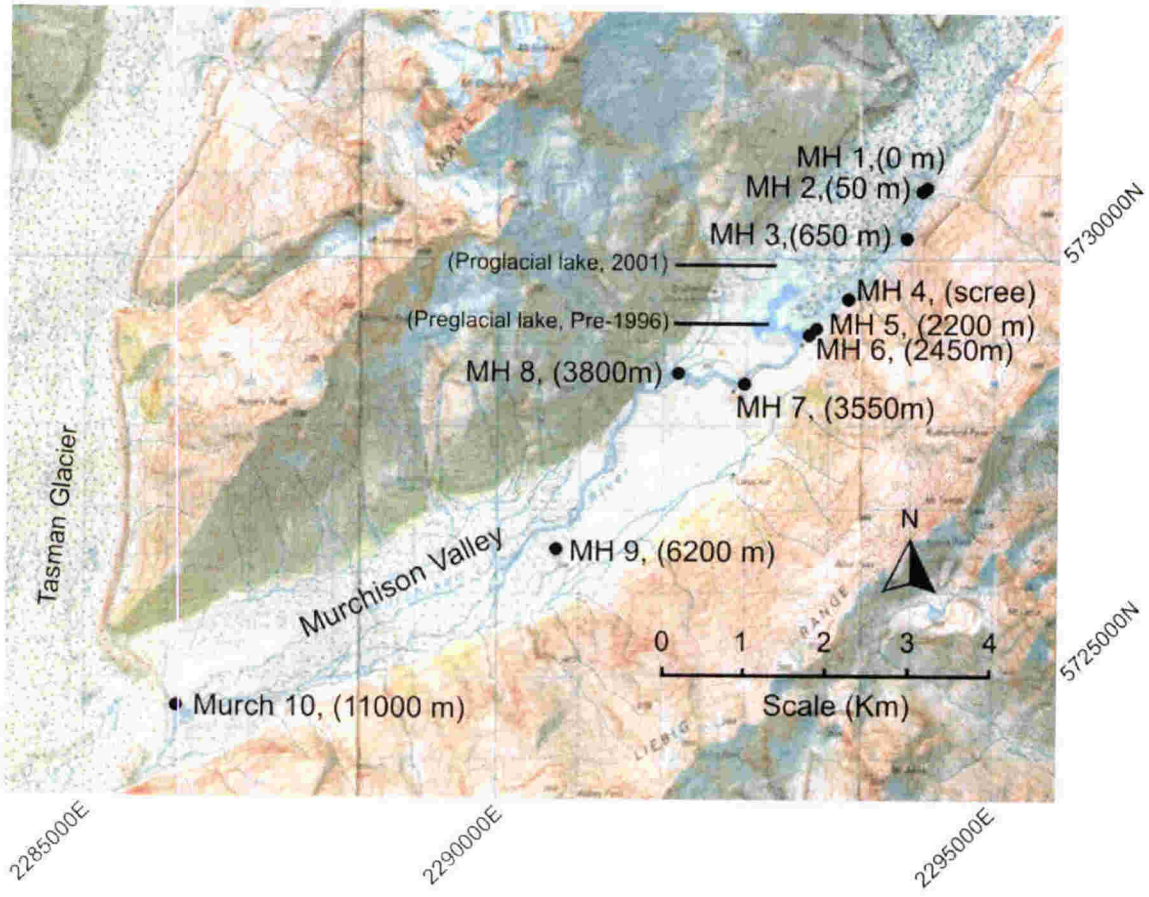

Figure 3.24 Map showing the ten sample sites with distance downstream from the Murchison Glacier terminus. The original map is Terralink Aoraki/Mt Cook alpine area 1;50000, (1999). A preglacial lake began forming in front of the glacier about 1995 (Hochstein et al., 1995), represented here by dark blue shading. This has since become a proglacial lake around the front and eastern margin of the glacier snout (indicated by transparent light blue shading).

3.4.4 Site descriptions

Site MH 1

Site MH 1 was located within a natural glacial tunnel on the eastern side of the glacier. This tunnel was the closest accessible grounded ice to the proglacial lake but did not terminate in the lake itself (Figure 3.6 and Figure 3.25). The sample was collected from an englacial debris-rich ice layer. However, the clasts had plainly experienced basal

transport and are likely to have been elevated to the englacial position by thrusting along shear planes within the glacier. This site was chosen to represent basally transported glacial clasts, which had not experienced fluvial transport (other than possible subglacial fluvial).

Site MH 2

MH 2 was located approximately 50 metres downstream from MH 1 on an active fluvial outwash fan formed by a meltwater stream draining from the glacial tunnel. The site was selected to reflect very limited amount of fluvial influence on glacially derived clasts.

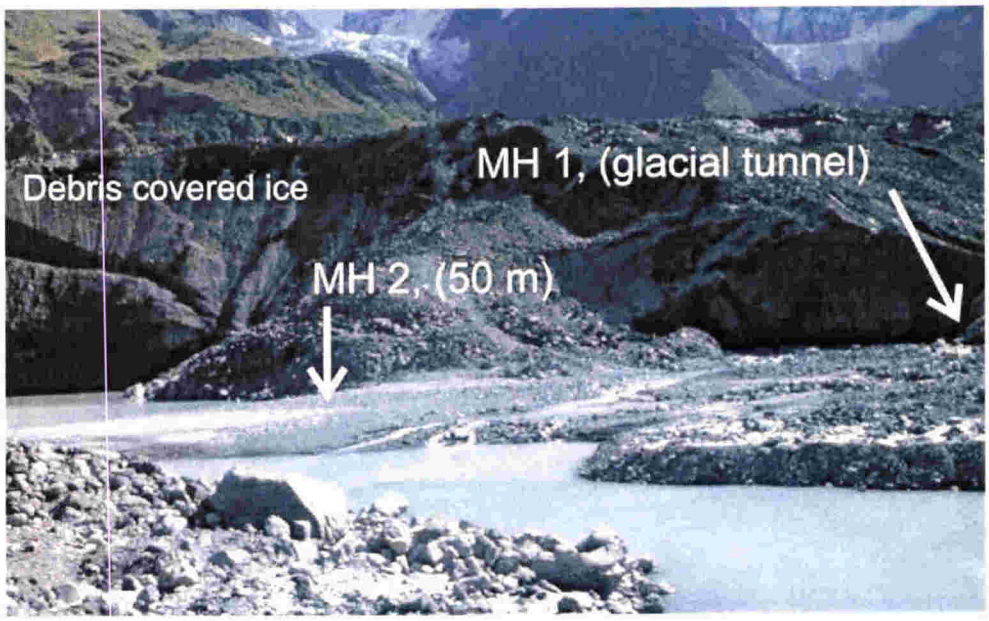

Figure 3.25 Sites MH 1 (glacial tunnel) and MH 2 (50 m downstream) on a fluvial outwash fan. Streamflow is from right to left. Stagnant debris-covered ice is visible in the background.

Site MH 3

Site MH 3 was located about 650 m down-stream from MH 2 on the bank of the main fluvial channel that has been partially inundated by the growth of the lake (Figure 3.26). The lake has formed a small beach at the site; however, the pebble-sized clasts at MH 3 are considered to represent sediment that has been fluvially transported from the glacier prior to lake formation.

Site MH 4

MH 4 was located 1900 m down-valley of MH 1 (Figure 3.26). This site was chosen to contrast with the fluvially transported debris. Site MH 4 was situated at the base of a steep, unstable active scree slope that today encroaches on the modern lake and is not representative of the fluvial transport pathway. The site comprised mostly shattered, angular rock-fall debris. This site is of particular interest as it contained many freshly broken clasts showing striae produced by the process of rock-fall and is investigated in detail in Chapter 6.

Site MH 5

MH 5 was also located on the lake edge but immediately down-valley from where the scree slopes enters the lake and does not contain rock-fall debris (Figure 3.26). Beaches have formed at this site but it appears to also be the bank of the pre-lake fluvial system similar to MH 3. MH 5 is therefore considered to represent 2200 m of fluvial transport.

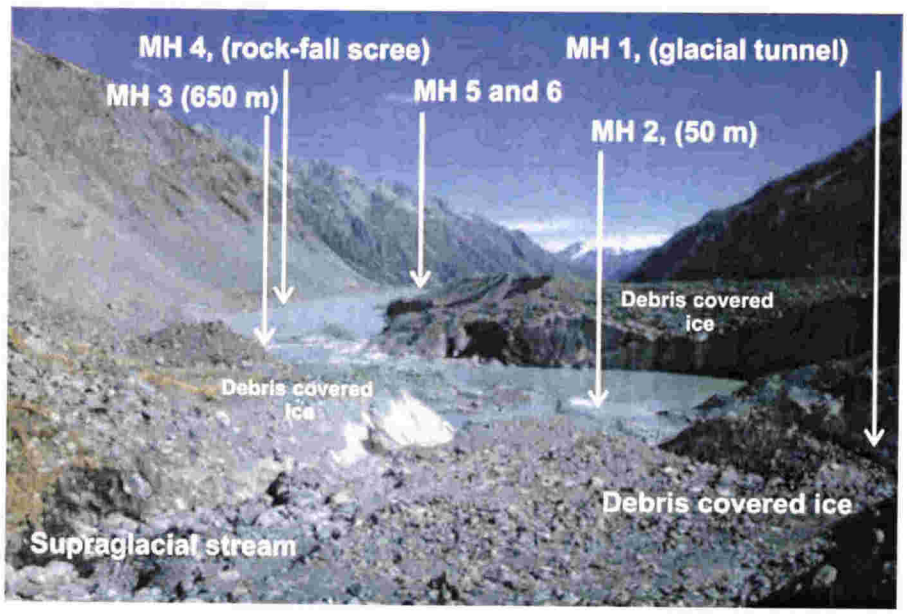

Figure 3.26 View looking down-valley from atop the Murchison Glacier. MH 1, (glacial tunnel) is located in the lower right. MH 2 (50 m downstream), MH 3 (650 m downstream) and MH 4 (rock-fall-scree), MH 5 (2200 m downstream) and MH 6 (2450 m downstream).

Site MH 6

MH 6 was located 250 m down-stream of site MH 5 (Figure 3.27). This was the last site before the lake outlet channel (cut in the end moraine) and represents 2450 m of fluvial transport distance from the glacial tunnel (MH 1).

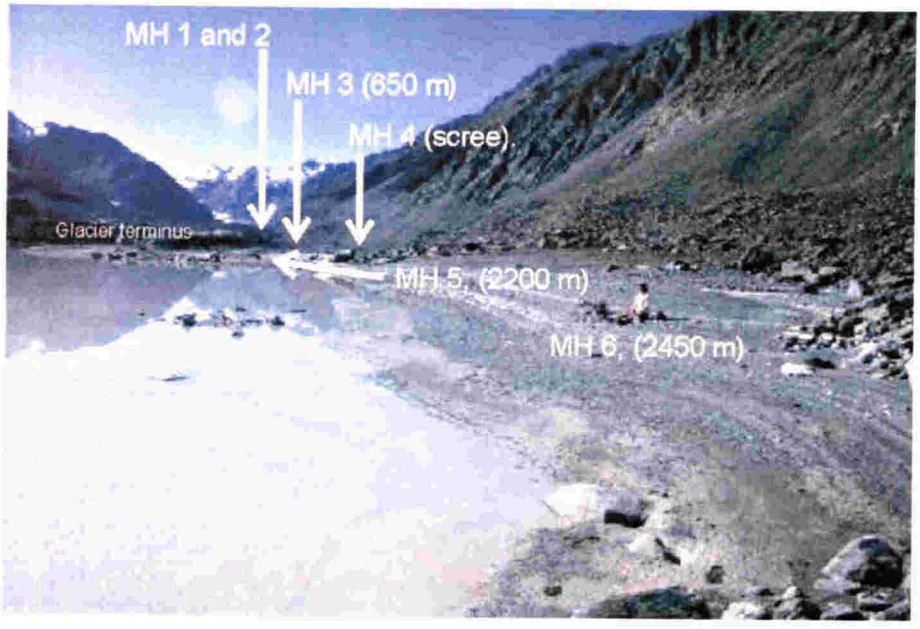

Figure 3.27 View from site MH 6, (2450 m) looking up valley to the Murchison Glacier and other sample sites.

Site MH 7

MH 7 was situated 3550 m down-stream of MH 1, where the Murchison River begins to braid and immediately in front of the end moraine of the Murchison Glacier. The sample was collected from a longitudinal bar in the main channel complex. The channel cutting the end moraine is stable with vegetated flanks. This indicates that the end moraine has not added debris into the fluvial system for a considerable time.

Site MH 8

MH 8 was located 3800 m down-stream of MH 1. The sample was again taken from a longitudinal bar within the active stream channel.

Site MH 9

MH 9 was located on the main channel bank 6200 m downstream of MH 1 (Figure 3.28).

Site MH 10

MH 10 was located 11000 m down-stream of MH 1 where the braid plain intersects the terminal moraine of the Murchison Glacier at the confluence with the Tasman Glacier (Figure 3.28).

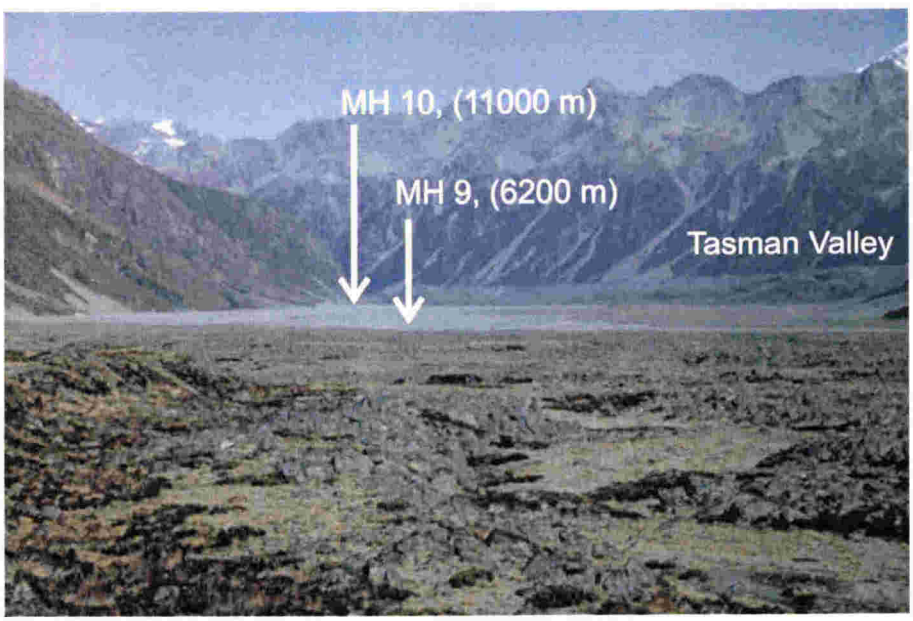

Figure 3.28 View down the Murchison Valley with sample sites MH 9 (6200 m downstream) and MH 10 (11000 m downstream) from the glacier terminus. Tasman Valley in background.

3.4.5 Clast Lithology

The clasts in the Murchison Valley samples were either indurated sandstone or argillite. These are derived from deformed beds of alternating sandstone (greywacke) and argillite of the Jurassic and Triassic age Torlesse Group sedimentary rocks that are widespread in the Southern Alps (Gair, 1967). All sites were dominated by sandstone clasts (at least 66%) (Figure 3.29). The percentage of argillite clasts decreases rapidly from 26 % in basal ice at site MH 1 to 6 % at MH 2, and shows an overall decrease in percentage of argillite clasts further downstream. MH 4 (rock-fall scree) shows a marked spike to 34 % argillite, reflecting the incorporation of unweathered rock-fall material. MH 5 and MH 6 both have 12 % argillite clasts, which decreases to 4 % at MH 7 and 8% at MH 8 (3800 m downstream). Sites MH 9 and MH 10 do not contain argillite clasts.

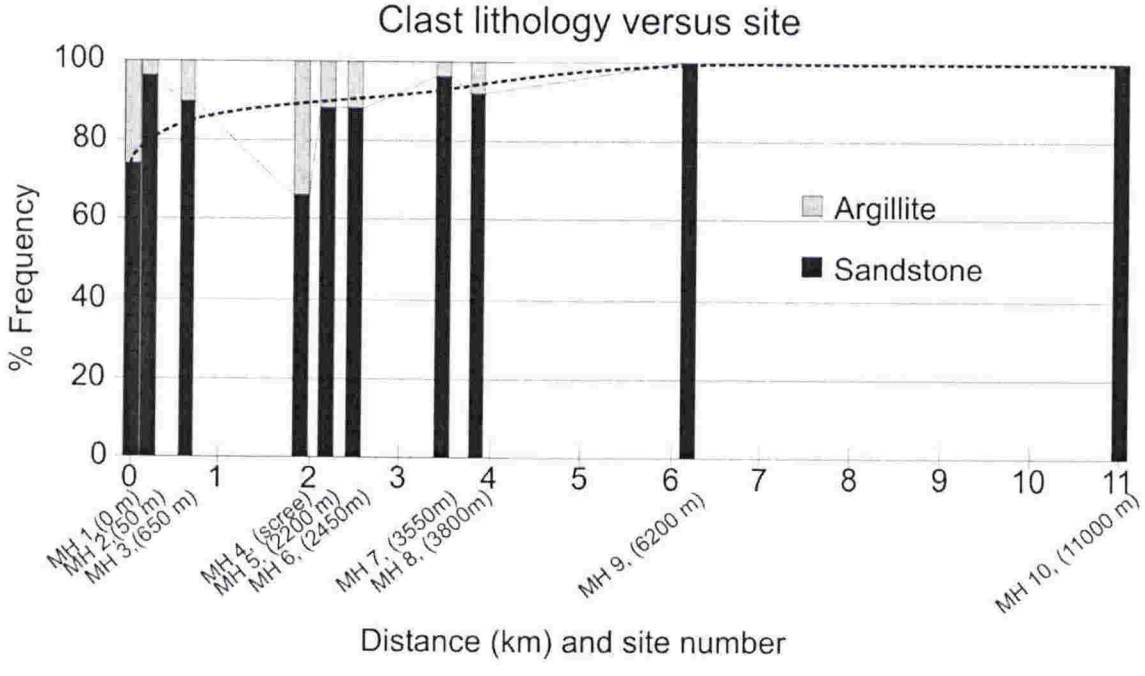

Figure 3.29 Clast lithology at each site. A sharp decrease in the percentage of argillite is evident from MH 1 to MH 2 and values fluctuate but overall decline for sites further downstream with none beyond MH 8. MH 4 (rock-fall scree) is a special case as this is where rock-fall clasts provide a "spike" in the percentage of argillite clasts, but is not part of the fluvial transport path.

3.4.6 Clast shape

Clast forms from the Murchison study are plotted on ternary diagrams in Figure 3.30. Clasts from MH 1 (debris-rich basal ice) shows a broad distribution in the central area, whereas MH 2 and MH 3 show a slight shift toward more equidimensional forms (c:a axial ratio of 0.39 for MH 1 to 0.43 shifts to 0.42 for MH 2 and MH 3 respectively.

MH 4 displays shows an obvious difference with more slabby and elongate clasts (average c:a axial ratio of 0.31), reflecting the character of fresh rock-fall material, that is not part of the fluvial transport pathway (see Chapter 6, mass movements deposits).

Clasts from MH 5 to MH 10 show increasing abundance of more equidimensional (blocky) shaped clasts (c:a axial ratios increasing from 0.43 for MH 5 to 0.49 for MH 9 and MH 10) with increasing downstream fluvial transport (Figure 3.31).

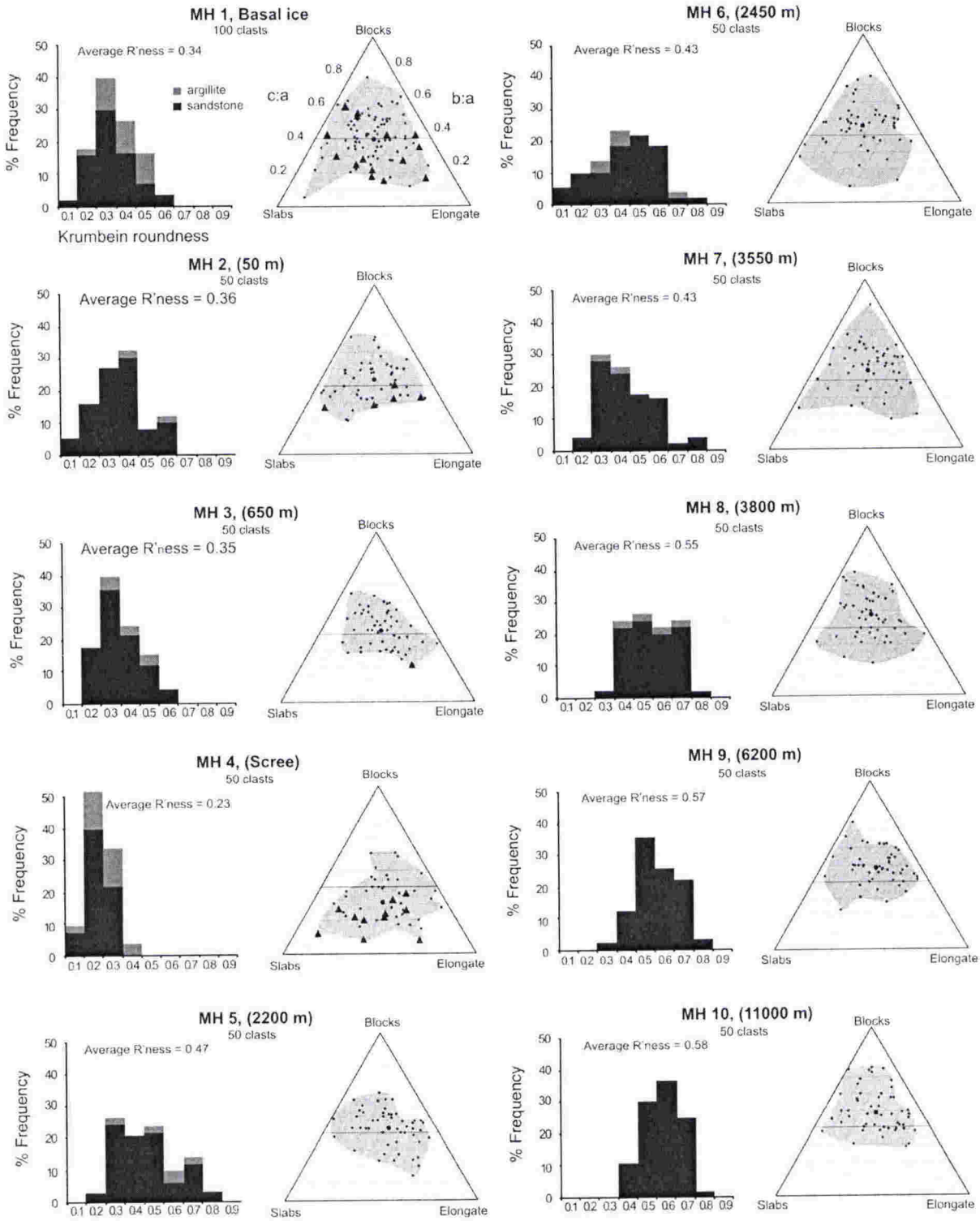

Figure 3.30 Clast form and clast roundness diagrams for the ten sample sites in the Murchison Valley, Mt Cook. Clasts become more equidimensional downstream. Average roundness increases with increasing fluvial transport distance. Small black triangles represent striated clasts.

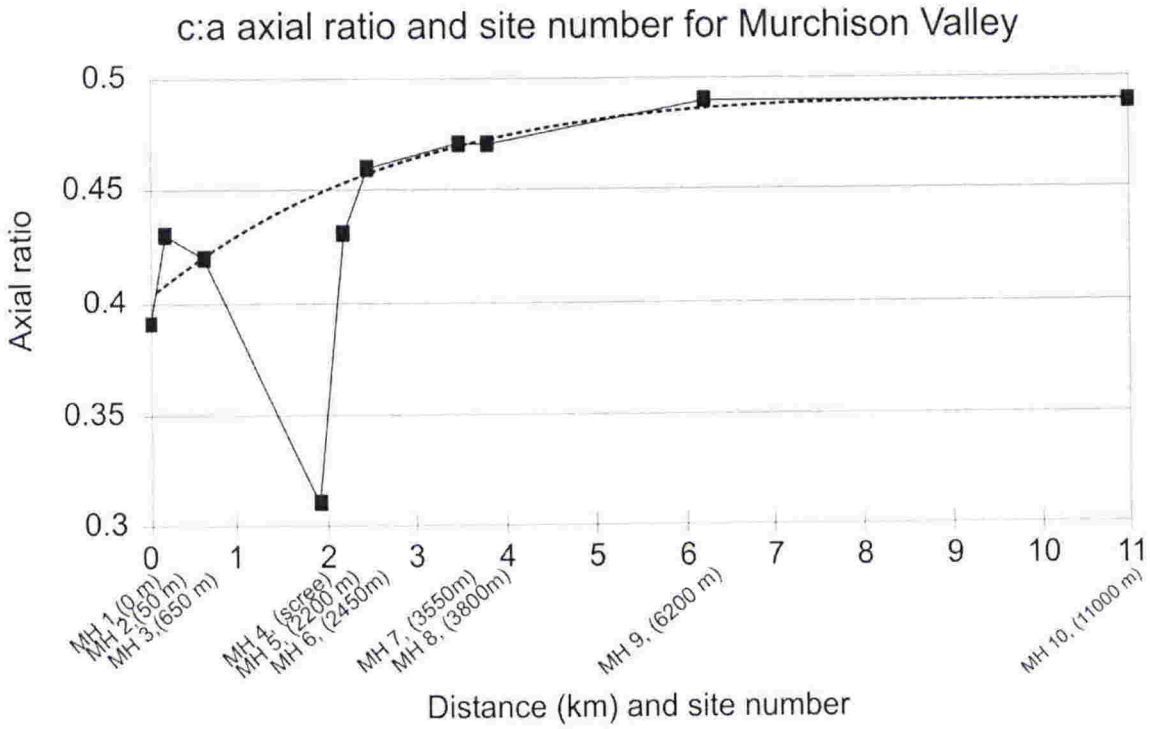

Figure 3.31 Graph showing the increase in average c:a axial ratio (trend toward more equidimensional clasts with distance downstream. The exception is Site MH 4 (rock-fall) with distinctly more slabby and elongate clasts (low c:a axial ratios). Dashed trend line is fitted by eye.

Krumbein roundness for each site is also shown in Figure 3.30 as percent frequency histograms. The data show generally broad distributions, but an overall increase in average roundness with distance downstream from 0.34 (subangular) for MH 1 to 0.58 (rounded) at MH 10 (Figure 3.32). The exception is again MH 4, which has a narrow distribution with 66% of clasts having roundness values of 0.1 and 0.2 and average roundness of 0.24 (angular). This again reflects the rock-fall debris at MH 4 (see Chapter 6). MH 6 is also anomalous, with 16 % of clasts having values of 0.1 and 0.2, contrasting with other samples downstream of the glacier terminus that do not have any clasts in the 0.1 class.

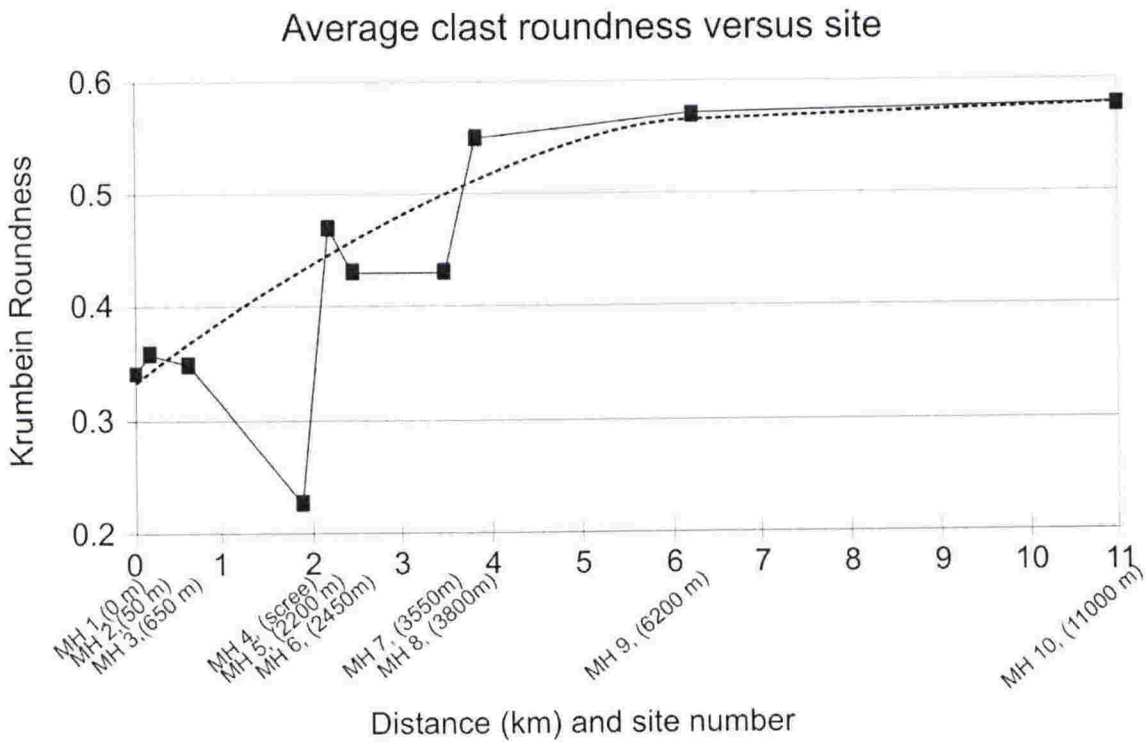

Figure 3.32 Average Krumbein roundness increases with increasing fluvial transport distance. The exception is site MH 4 (rock-fall) with distinctly more angular clasts. Dashed trend line is fitted by eye.

Clast form and roundness are also expressed on the covariant plot of RA versus C_{40} index (Figure 3.33). The most glacier proximal samples (MH 1, MH 2 and MH 3) all plot in the "subglacial" field. MH 4 (rock-fall) plots well away from all other samples in the "scree" field. MH 6 plots outside the defined fields with a notably high RA index of 16. The remaining samples have variable C_{40} index values, but all plot very low on the RA index.

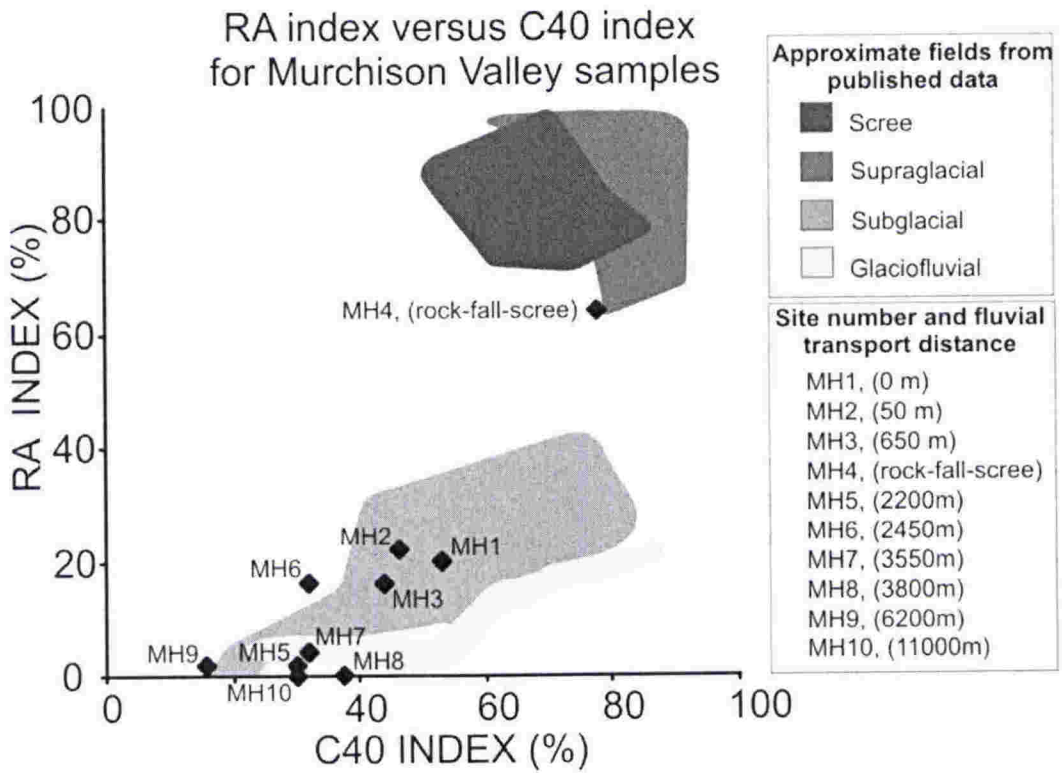

Figure 3.33 Covariant plot of RA index versus C_{40} index for Murchison samples. MH 1 (basal debris sample), MH 2 and MH 3 plot in the subglacial field. MH 4 plots away from the other samples in the "scree field. MH 5 to MH 10 show variable C_{40} values but are generally in the lower left. Shaded fields are from published data in Benn and Ballantyne (1994) and Bennett et al. (1997).

Clasts with flat faces and rounded edges are present in many of the samples. These surfaces are interpreted as glacially formed facets. The abundance of these glacially shaped clasts decreases downstream (Figure 3.34). However, the decrease is irregular and appears to be controlled in part by the lithology of the clasts. MH 1 has 28 % faceted clasts, with argillite being more likely to show facets (50 % of argillite clasts) compared with only 20 % of sandstone clasts. This suggests that argillite is more prone to faceting during basal glacial transport. MH 2 has only two argillite clasts, both faceted, but the sample has overall 38 % faceted clasts. The remaining samples show significantly less faceted clasts (maximum 18 % at MH 5) but persist downstream to MH 10 with 8 %. Numbers of faceted argillite clasts decrease more rapidly with none

found downstream of MH 5, although argillite clasts persist down to MH 8. This indicates that facets on argillite clasts are removed faster than on sandstone during fluvial transport (in this study 2200 m) and that this is not simply a reflection of the downstream decrease in argillite clasts.

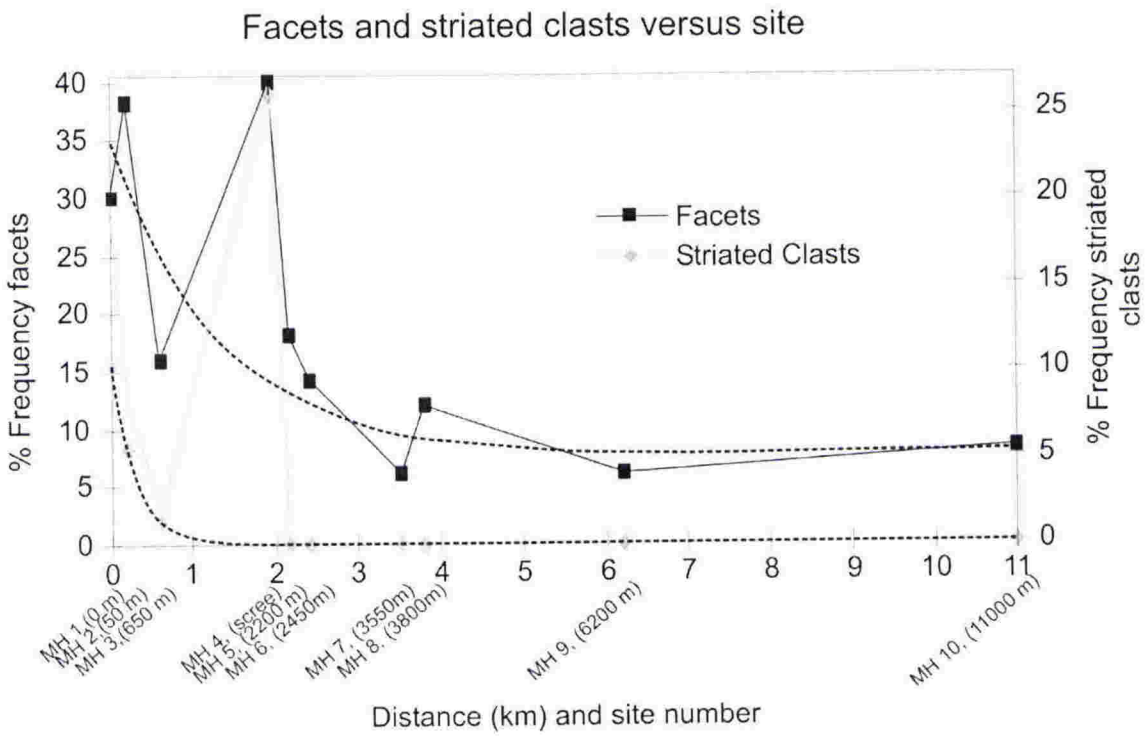

Figure 3.34 Graph showing the percentage of clasts with glacial facets and percentage of striated clasts with increasing fluvial transport distance. The percentage of flat faces decreases with transport distance but some are still evident even after 11000 m of fluvial transport. Striated clasts, however, decreased rapidly with few surviving more than 600 m fluvial transport and none more than 3350m.

The number of striated clasts decreases rapidly with fluvial transport distance. For basal debris sample MH 1, 16 % are striated (mostly argillite clasts). The striae occur on clasts in the 0.3, 0.4 and 0.5 roundness classes. The proportion of striated clasts decreases dramatically to MH 2, where only 8% are striated (6% of all sandstone and 1 of 2 argillite clasts). These occur on clasts in the 0.2 and 0.3 roundness classes. MH 3 has only one striated argillite clast (0.4 roundness class). MH 4 (rock-fall) has the

highest abundance of striated clasts, but the majority of these occur on freshly broken angular argillite clasts produced by rock-fall processes (discussed in Chapter 6). MH 5 (2200m) and samples further downstream had no striated clasts. Because site MH 4 (rock-fall) is not part of the fluvial transport path, MH 3 (650 m downstream) is actually the most distal sample from the glacier to contain striated clasts. The striae that form on sandstone clasts are weakly inscribed compared with striae on argillite clasts, even on well developed glacial facets.

3.4.7 Discussion and Conclusions

Many aspects of clast shape, in particular glacial features such as faceted clasts and striae, change progressively with increasing fluvial transport distance.

The Murchison Valley study confirms that lithology is an important variable influencing clast features in fluvial systems. Softer lithologies (in this case argillite) decrease in abundance downstream as they are more rapidly broken down into sand grains. This increases the relative percentage of harder, more resistant lithologies (sandstone) downstream from the glacier.

The form of clasts becomes progressively more equidimensional and clasts become better rounded during fluvial transport due to abrasion. This process of abrasion of removes the features specific to glacially sourced clasts. Facets become less distinct as edges are progressively rounded causing a decrease in the number of identifiably faceted clasts with increased fluvial transport distance. Facets on argillite clasts do not survive as well as those on sandstone clasts. Facets on some sandstone clasts are still recognisable even after 11 km of fluvial transport.

The generation of striae on clasts is highly dependent on the lithology and striae occur preferentially on the softer argillite clasts. Although some sandstone clasts in samples MH 1 and 2 carry very faint striae, these features are difficult to see on the clast surface and are not discernable at sites downstream, so have an extremely low "survivability"

(between 50 and 650 m fluvial transport). These striae are not well inscribed on the harder sandstone surfaces and are easily removed by weathering. The relatively soft and fine-grained argillite clasts allow clearly inscribed small-scale striae to form. Although better formed and clearer than striae on sandstone clasts, these striae are also removed quickly during fluvial transport. Most disappear within the first tens to hundreds of metres of transport with few surviving more 650 m (MH 3).

On the basis of this study, it appears that striae on glacial clasts are removed within 1 to 2 km of downstream fluvial transport. Glacial facets survive longer, but most become indistinguishable between 3 and 6 km of fluvial transport although some appear to survive at least 11 km. The further downstream the clasts have travelled, the more difficult it is to distinguish between glacial facets and other flat surfaces on clasts.

CHAPTER FOUR

POLYTHERMAL GLACIAL STRIAE

4.1 INTRODUCTION

Striae on clasts found in the basal layers of the polythermal Mackay Glacier on the Victoria Land coast in Antarctica are investigated in this chapter. The aim is to characterise the striae and identify differences, if any, between striae from polythermal glaciers and temperate glaciers.

4.1.1 Polythermal glaciers

Glacier thermal regime and classification is discussed in Chapter 3. Polythermal or sub-polar glaciers are those that have both warm and cold ice and associated patches of warm and cold-based bed conditions. This commonly means the interior is warm-based but the margins of the glacier are cold-based and frozen to the substrate.

Several of the larger glaciers in the Dry Valley region of Antarctica fall into this category. The Mackay Glacier is a well-studied example of an East Antarctic Ice Sheet outlet glacier that exists in a polar environment, but has polythermal basal conditions due to the thickness of the glacier allowing pressure melting of basal ice along its axis. This study describes the character of the glacial sediment it carries and in particular the occurrence of striae on clasts. This is especially relevant considering the close proximity of the Mackay Glacier to the Cape Roberts drill-sites and likelihood that the Mackay Valley has been the main sediment source for Granite Harbour and the Cape Roberts area for much of the Cenozoic epoch (Powell et al., 2000) (see Chapter 8).

4.2 MACKAY GLACIER, GRANITE HARBOUR

4.2.1 Background and setting

The Mackay Glacier is an outlet glacier draining from the East Antarctic ice sheet into Granite Harbour on the western side of McMurdo Sound, Antarctica (Figure 4.1). The glacier is approximately 65 km long and 5 km wide (Macpherson, 1987). Calkin (1974) used radio-echo soundings to show that it is about 500 m thick over much of its length. It terminates as a floating marine ice tongue approximately 3 km wide and 5 km long (Pyne et al., 1991). The glacier descends from a bedrock elevation of about 1200 m (65 km inland) to -400 m at the grounding-line, cutting through plutonic, sedimentary and intrusive and rocks of the Transantarctic Mountains.

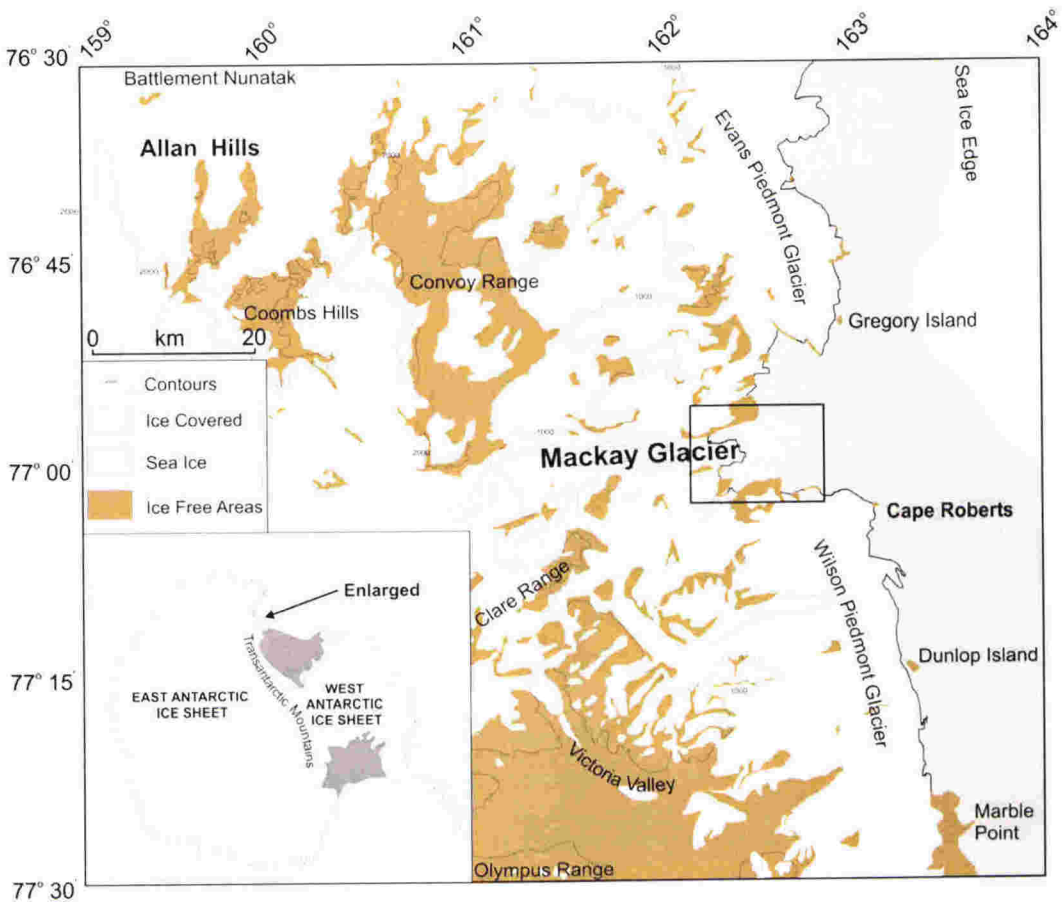

Figure 4.1 Location map of Mackay Glacier in Victoria Land, Antarctica. Black rectangle indicates area enlarged in Figure 4.2.

Macpherson (1987) used the relatively high geothermal gradient in the region calculated by Decker and Bucher (1977) and the equation of Weertman (1961) to show that the Mackay Glacier is wet-based due to pressure melting wherever the glacier exceeds 425 m thickness. Furthermore, the glacier moves at about 212 ma^{-1} (up glacier from the grounding-line) with a total discharge of 0.238 km^3 yr^{-1} (Macpherson, 1987). The floating tongue of the Mackay Glacier thins dramatically from over 400 m at the grounding-line to about 200 m at the glacier snout where it calves into Granite Harbour. However, the ice tongue is locked in sea-ice (up to 2.5 m thick) for approximately eleven months of the year.

In situ basal debris layers such as those at the terminus of the polythermal Taylor Glacier 80 km to the south, are not directly visible at the Mackay Glacier because of its floating terminus. However, Macpherson (1987) observed basal debris in an unusual way. Several small, (up to 42 m long) debris-charged icebergs with large grooves on the base were found close to the grounding-line within narrow canyons and along the ice tongue margins. The layers of debris-rich ice displayed coarse, subangular to sub rounded (average roundness 0.36), faceted and striated clasts (up to 51% striated). These bergs were considered to represent marginal portions of basal ice of the Mackay Glacier that had broken off and floated upside down to the surface as the glacier passed the grounding-line, exposing basally transported sediment. Similar overturned bergs displaying prominent englacial layers of debris were found in during reconnaissance fieldwork for this study. Clasts within the layers display faceted and striated clasts that have clearly experienced basal transport. Therefore, the layers are likely to have been elevated from the bed to an englacial position by glaciotectonic faulting or folding. The bergs remained intact and locked in sea-ice throughout three summer field seasons. In addition, glacial debris from the Mackay Glacier was found on a low bedrock ridge (Cuff Cape) at the margin of the glacier (Figure 4.2 and Figure 4.3).

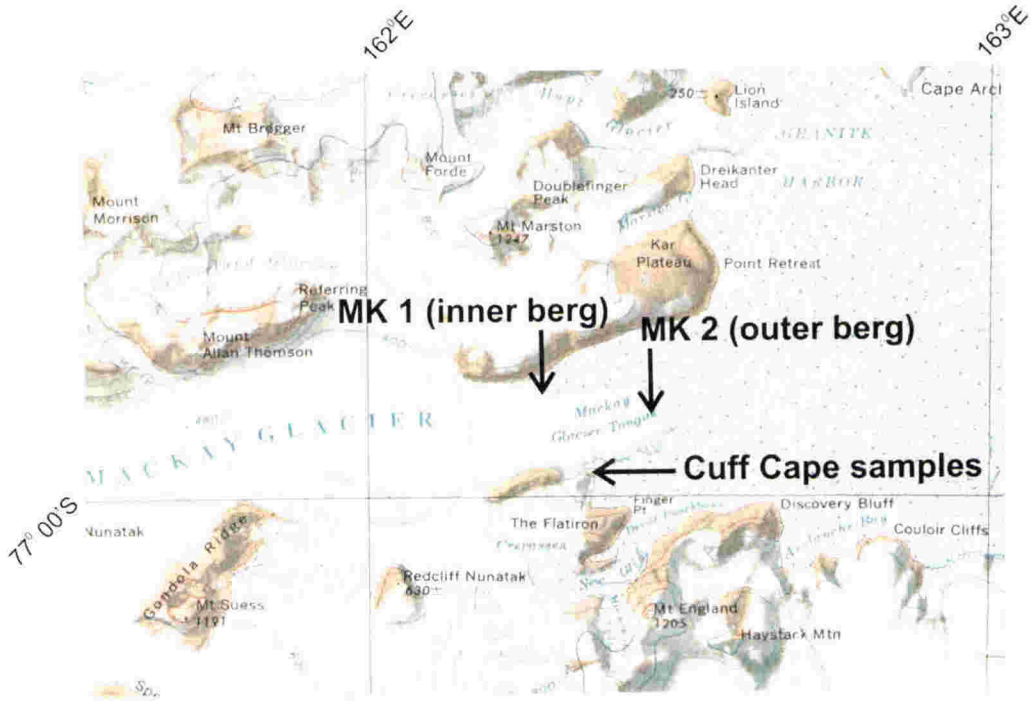

Figure 4.2 Map of Mackay Glacier and Granite Harbour, showing location overturned debris-bearing icebergs on the floating glacier tongue and Cuff Cape.

4.2.2 Fieldwork and sample collection

Bulk samples of well-exposed debris layers in overturned bergs were collected at two sites. The first was MK 1 located on the northern side of the floating tongue close to the grounding-line (Figure 4.2, Figure 4.3 and Figure 4.4) and the second was MK 2 near the present most seaward tip of the glacier tongue (Figure 4.2, Figure 4.3 and Figure 4.5). In addition, several clearly striated clasts were collected from Cuff Cape (Figure 4.2 and Figure 4.3). These all provided examples for characterisation of striae (see section 4.3).

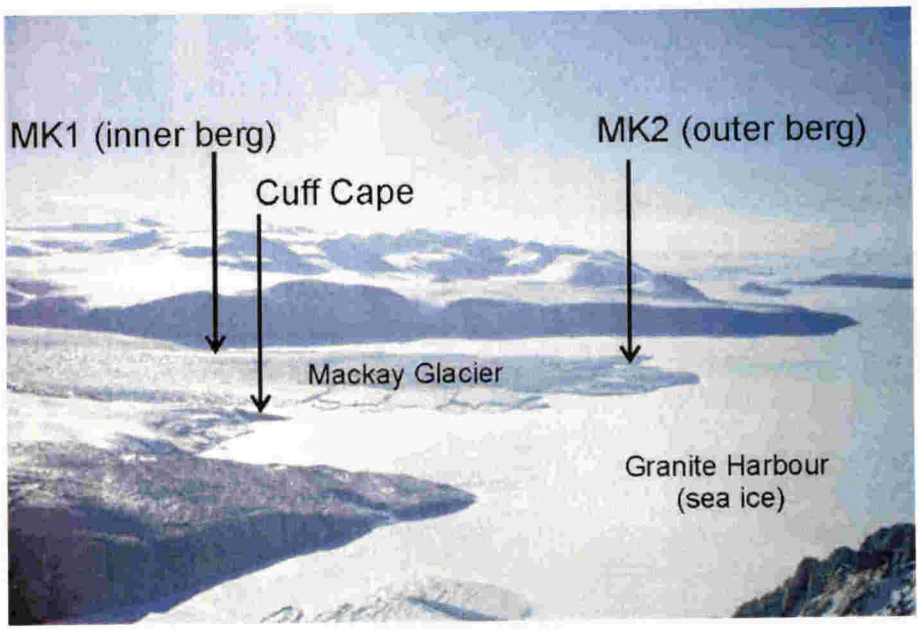

Figure 4.3 View of northern Granite Harbour (looking north from Mt. England) showing the floating ice-tongue of the Mackay Glacier with sample sites MK 1 (inner berg), MK 2 (outer berg) and Cuff Cape on the immediate southern margin of the Glacier.

Figure 4.4 Sample site MK 1 on an overturned glacier berg (inner-berg) near the present grounding-line of the Mackay Glacier. Note the bag and hammer (circle) for scale.

Figure 4.5 Sample site MK 2 on an overturned glacier berg (outer-berg), Rock hammer is 33 cm long.

4.2.3 Clast shape

The bulk samples collected from debris layers in the overturned bergs provided 100 clasts each for shape analyses. This was performed using the method outlined in Chapter 2, and clast data are presented in appendix 3.

The Mackay Glacier samples are dominated by dolerite and granitic clasts with minor siltstone and other lithologies. The proportions vary between the samples, with MK 1 (inner berg) consisting of 64% dolerite, 30% granite and 6 % other, whereas MK 2 (outer berg) contained only 24 % dolerite and 72% granite and 4 % other.

Clast form is displayed in Figure 4.6 and shows that both samples have broad distributions, but with the majority of clasts lying above the 0.4 c:a axial ratio line (toward blocky shaped clasts). Average axial ratios are similar but MK 2 (outer berg)

has a slightly higher c:a value of 0.53 compared with MK 1 with 0.50. These values are higher than those for the sandstone and argillite clasts from temperate glacial samples.

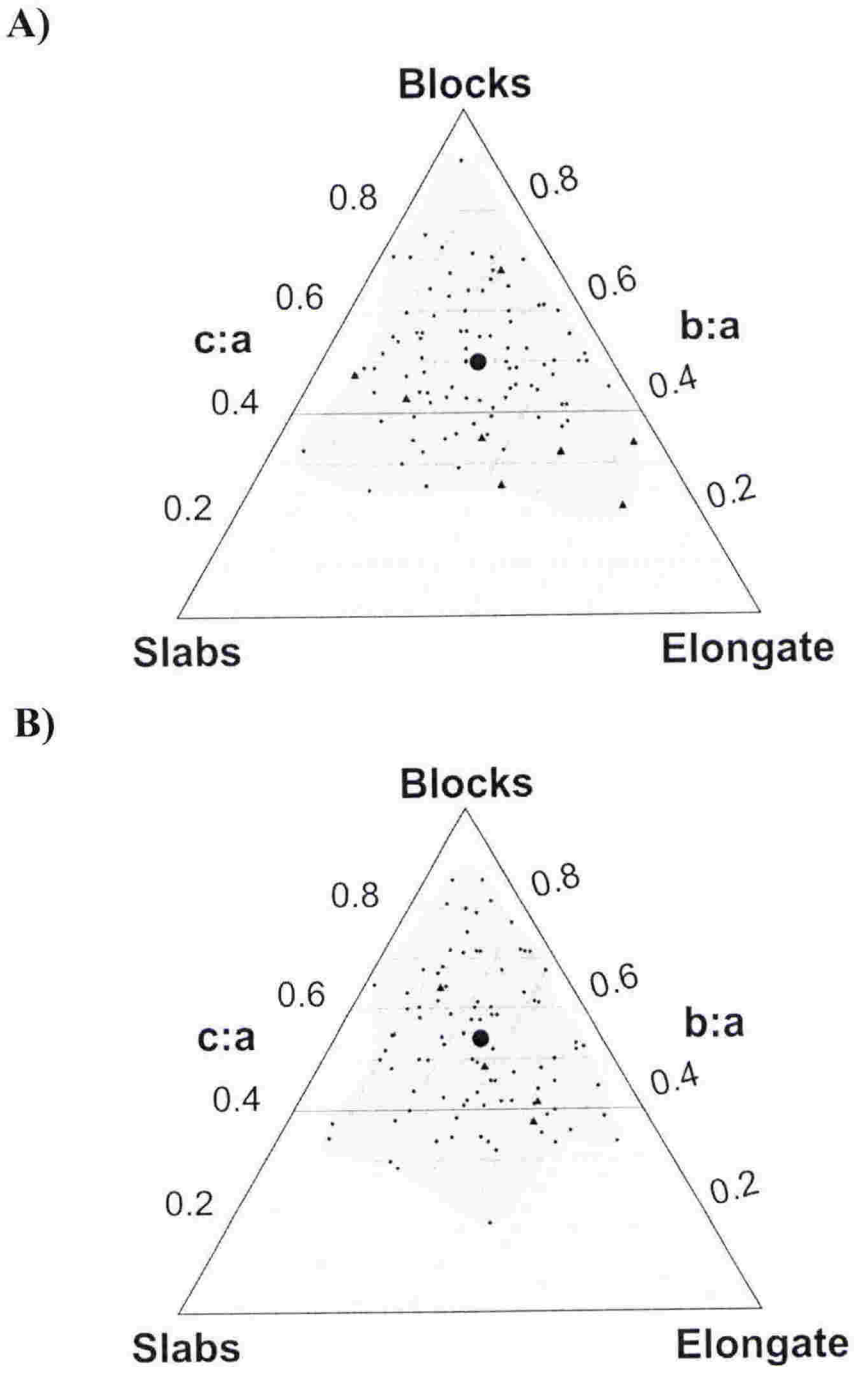

Figure 4.6 Clast form diagrams for: (A) (MK 1, inner berg), (B) (MK 2, outer berg). Both show broad distributions. Average c:a and b:a axial ratios (large black dots) are similar, although MK 2 has slightly higher c:a axial ratio of 53 compared with MK 1 with a c:a axial ratio of 50. Black triangles represent striated clasts.

Roundness and lithology are displayed in frequency percent histograms in Figure 4.7. The distribution for the MK 1 (inner berg) is broad with all roundness classes up to 0.5 represented, but 63% of clasts fall in the angular and very angular classes, giving an average roundness of 0.23 (angular). Dolerite dominates the 0.2 roundness class. Twenty two percent of the clasts display flat surfaces with rounded edges. These are interpreted as glacially formed facets and these occur on clasts in the 0.2, 0.3, 0.4 and 0.5 roundness classes and preferentially on dolerite clasts (27 % of all dolerite clasts), although the small number (5) of "other" lithologies (not dolerite or granite) clasts also display facets.

Sample MK 2 (outer berg) displays a more normally shaped distribution than MK 1, but with all roundness classes up to 0.6 represented and with a slightly higher average roundness of 0.28 (subangular). Granite dominates in all roundness classes. Facets occur on 12 % of clasts in the 0.2 to 0.4 roundness classes, usually on dolerite or "other" lithologies and less commonly on granitic clasts.

A)

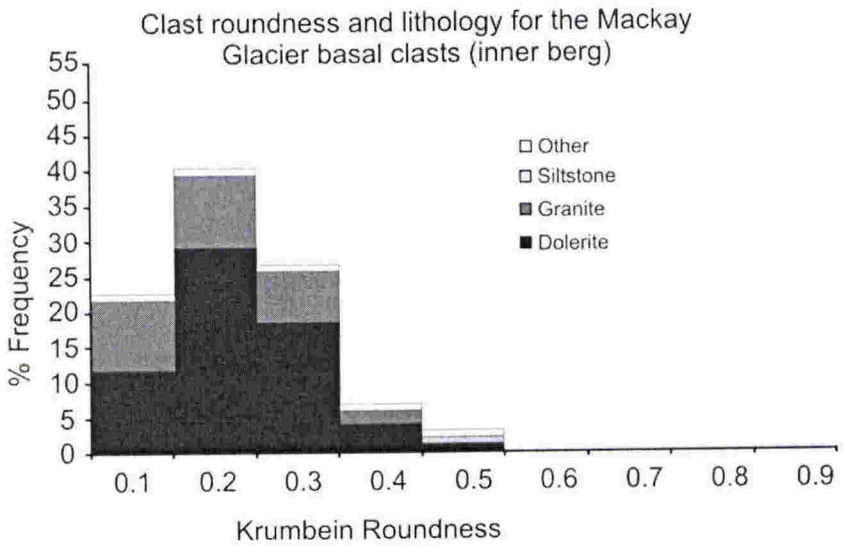

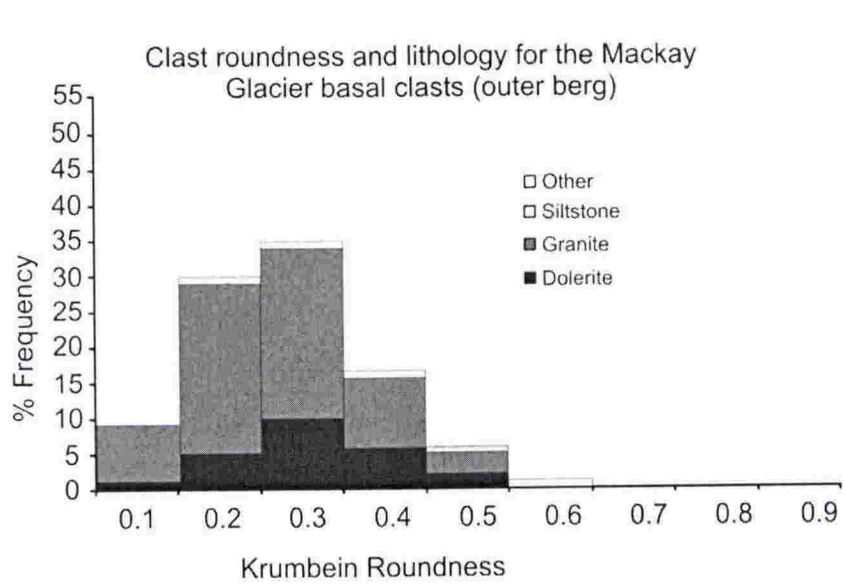

Figure 4.7 Roundness and lithology histograms for clasts from basal debris samples from the Mackay Glacier. A) MK 1 (inner berg) has a higher percentage of angular and very angular clasts (averages roundness of 0.23). B) MK 2 (outer berg) has average roundness of 0.28.

Shape characteristics are highlighted in the covariant plot of RA index (% of angular and very angular clasts) versus C_{40} index (% of clasts with a c:a axial ratio of ≤ 0.4) (Figure 4.8). The samples show similar C_{40} indices of 22 % for MK 1 (inner berg) and 21 % for MK 2 (outer berg) reflecting the dominance of blocky or equant shaped clasts in both samples. The main difference between the samples is the much higher RA index of 63 % for MK 1 compared with 40 % for MK 2, highlighting the higher percentage of very angular clasts in the MK 1 sample.

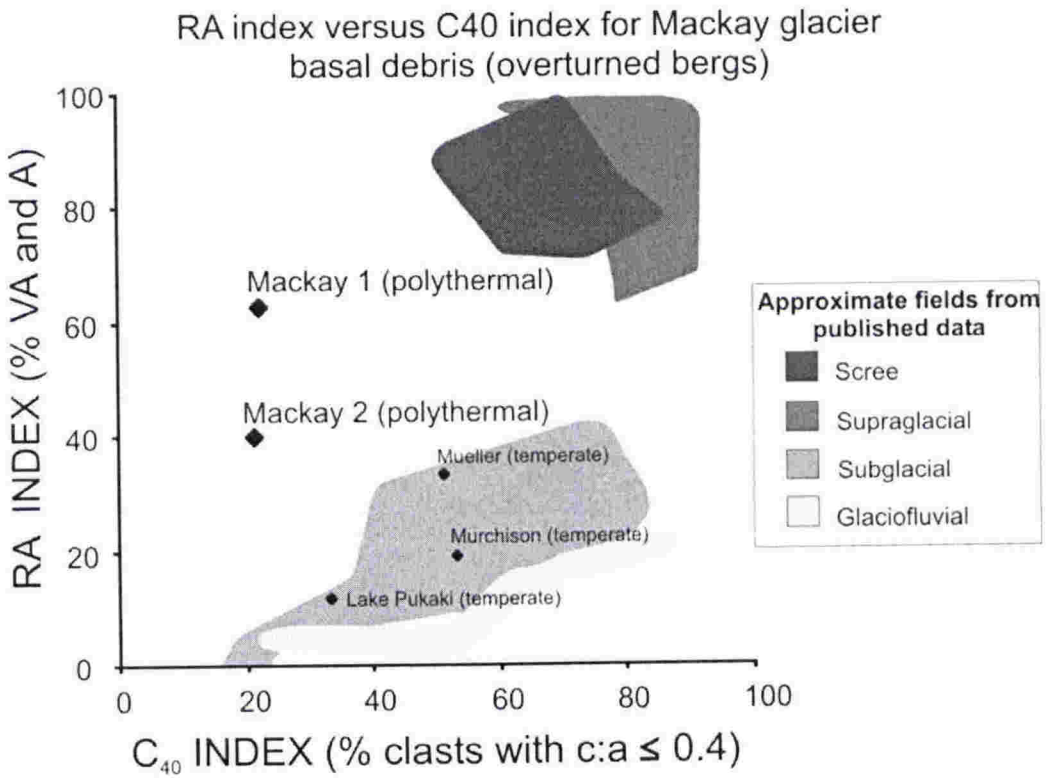

Figure 4.8 RA versus C_{40} index diagram for clasts from overturned bergs on the Mackay Glacier tongue. Both samples plot outside known fields with low C_{40} values and high RA values particularly for sample MK 1 (inner berg), reflecting the high percentage of angular and very angular clasts. Shaded fields are from published data in Benn and Ballantyne (1994) and Bennett et al. (1997).

4.2.4 Clast striae

Small-scale striae occur on 8% of MK 1 clasts, on all lithologies (but rare on granite) and in all size classes except 0.1. Striae only occur on clear faceted surfaces. For sample MK 2, only 5 % of the clasts carry striae. These occur on dolerite clasts (0.3 and 0.4 roundness classes), and on a single siltstone clast (0.5 roundness class) and a single mudstone clast (0.3 roundness class). As with MK 1, striae occur only on clearly faceted clasts. Striae features are discussed in detail in section 4.3.2.

4.3 CUFF CAPE, GRANITE HARBOUR

4.3.1 Background and setting

Cuff Cape is a partially ice covered granite bedrock ridge located on the southern margin of the Mackay glacier (Figure 4.2 and Figure 4.3). The ridge has clearly been overridden by the Mackay Glacier and displays striated bedrock surfaces and abundant glacial debris. Many dolerite clasts and boulders show obvious striae. Several of these striated clasts were collected for the purpose of characterising the striae formed by the polythermal Mackay Glacier. These provide clearer examples of striated clasts than the bulk samples from the overturned icebergs from the floating Mackay Glacier ice tongue.

4.3.2 Characteristics of clast striae

Appendix 1, "Linear Abrasion Atlas" presents images and notes highlighting the main features of the clasts from the Mackay Glacier and Cuff Cape. The more common features are discussed next with particular reference to striae on four striated clasts from Cuff Cape that were studied in detail.

The striae on clasts from the Mackay Glacier and Cuff Cape show a wide range in size and orientation. Fine-grained sedimentary clasts and dolerite clasts are the most commonly striated. On elongate clasts, striae are preferentially oriented parallel to the long axis of the clast. The surfaces tend to be pervasively striated with a "background" of microstriae (< 2 mm long and < 0.25 mm wide). Individual striae of this type are difficult to define or measure individually. Superimposed on this "background" are larger, distinct striae up to 4 mm wide and several 10's of mm long, occasionally deviating by up to 90° from the long axis (Figure 4.9). The background microstriae occur on both flat facets and on slightly curved surfaces. These characteristics are similar to those observed on temperate glacially striated clasts.

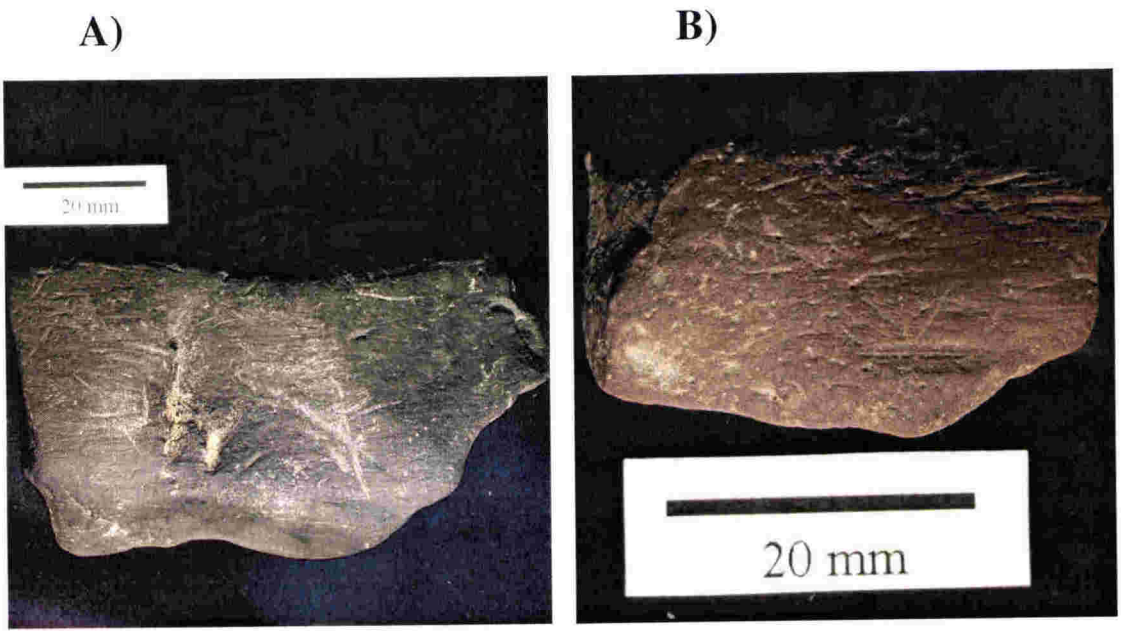

Figure 4.9 A) A mudstone clast from Cuff Cape shows a striated surface with most striae parallel to the long axis. It has a "background" of microstriae and some larger striae oriented oblique to the long axis. This clast is also shown in appendix 1, (Linear Abrasion Atlas – Polythermal Glacial striae, Images 1 and 2). B) A siltstone clast from an overturned iceberg on the Mackay Glacier tongue, showing similar features at a smaller scale.

There are exceptions to the characteristics described above. Some elongate clasts show wide variation in orientations of striae unrelated to the long axis (Figure 4.12, clast 3) and some almost equidimensional clasts have striae remarkably parallel to the long axis (Figure 4.12, clast 4).

Some larger clasts show large compound striae up to 20 mm wide that consist of several smaller, parallel striae. The most common compound striae were found on a large glacially shaped dolerite clast (Figure 4.10). One of these compound striae is curved and almost perpendicular to the long axis suggestive of clast rotation during the striation process.

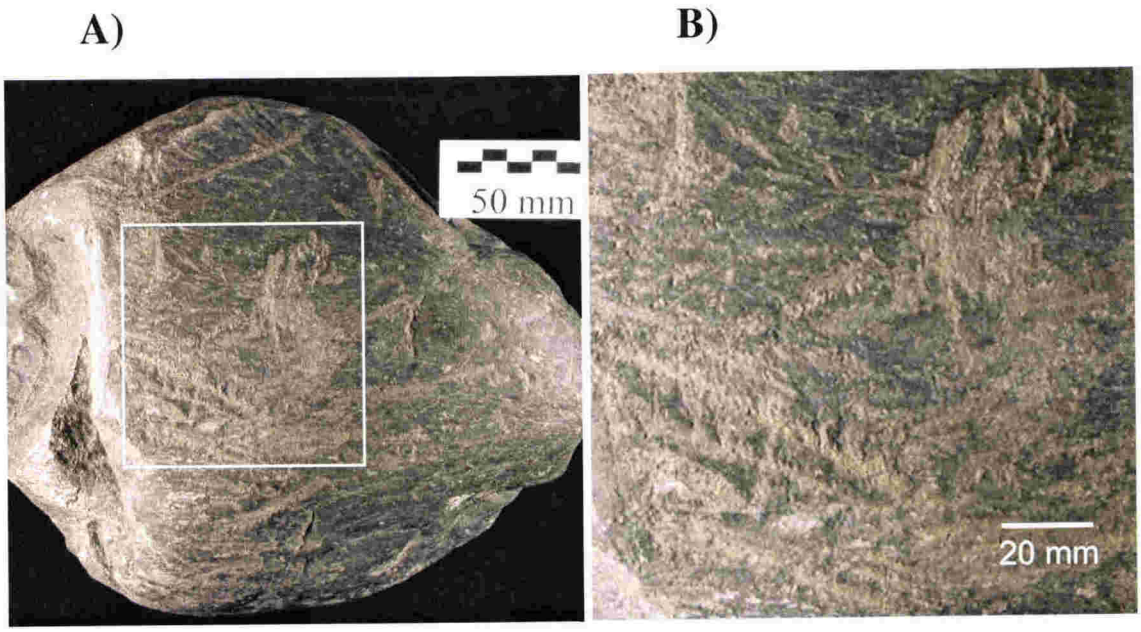

Figure 4.10 A) Large striated dolerite cobble showing a densely striated surface with large compound striae up to 20 mm wide. B) The compound striae consist of many smaller parallel striae and one is slightly curved and oriented perpendicular to the long axis. This clast is also shown in appendix 1, (Linear Abrasion Atlas – Polythermal Glacial striae, Images 11 and 12).

The generation of striae is influenced by the lithology of the clast. Striae rarely occur on coarse-grained dolerite or granite clasts. When they do, the striae are usually wide (> 2 mm) and on larger clasts. An example is displayed in Figure 4.11, which is a medium-fine grained granite clast from the Mackay Glacier. The facet is pervasively striated but the striae are poorly inscribed and only the largest striae are individually distinguishable.

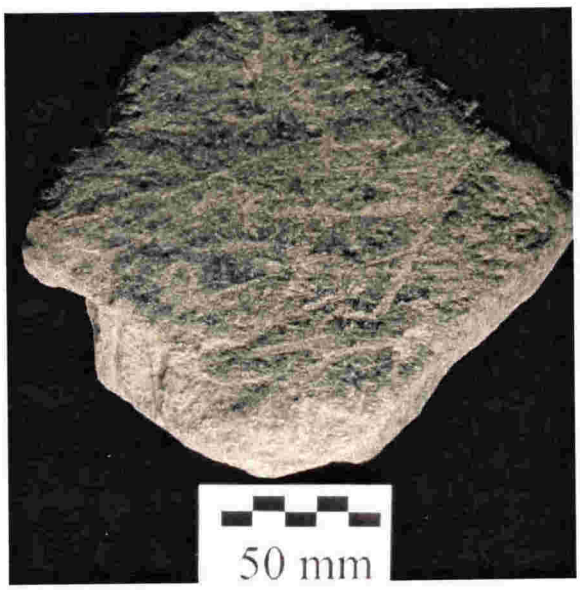

Figure 4.11 Striated dolerite clast from sample MK 1. The surface is intensely striated but only the largest striae are individually distinguishable. This clast is also shown in appendix 1, (Linear Abrasion Atlas – Polythermal Glacial striae, Image 7).

Striae orientation

Four of the Cuff Cape clasts showing a range of shapes and striae characteristics were selected for detailed analysis. Striae orientations are displayed in Figure 4.12. Clast 2 is an elongate (b:a axial ratio of 0.5) dolerite clast with a clear glacially faceted surface. The striae are oriented parallel to the long axis with 32 % within 5° and a smaller mode oriented at 165°. A small percentage of striae are oblique to the long axis giving an average striae orientation of 174° and range of 60° (standard deviation is 15.5°).

The other clasts show less defined long axis parallelism. Clast 1 is a mudstone clast with higher b:a ratio of 0.69. It shows a strong mode about the long axis, but a greater range of 90° (standard deviation 31°). Four percent of the striae are curved. Clast 3 has a less obvious long axis (b:a ratio of 0.75), weak clustering with several modes at various orientations and has a wide range of 76° and standard deviation (35.7). This clast has no curved striae.

Clast 4 is the most equidimensional clast in the collection (b:a ratio of 0.9). However, it shows moderate clustering with a strong mode parallel to the long axis and a slightly oblique mode at about 160°. It has 2 % curved striae. While the curved striae suggest clast rotation, the dominance of long axis sub-parallel striae indicate that equidimensional clasts do not necessarily show more variable orientations. These results highlight both similarities and differences when compared with temperate striae. Striae parallel to the long axis of elongate clasts is a common characteristic of both environments and reflect the process of clast alignment with the ice flow and movement of striating rock particles along the long axes of clasts. However, there are exceptions and a wide range of striae orientations are possible depending on the particular abrasion history of individual clasts.

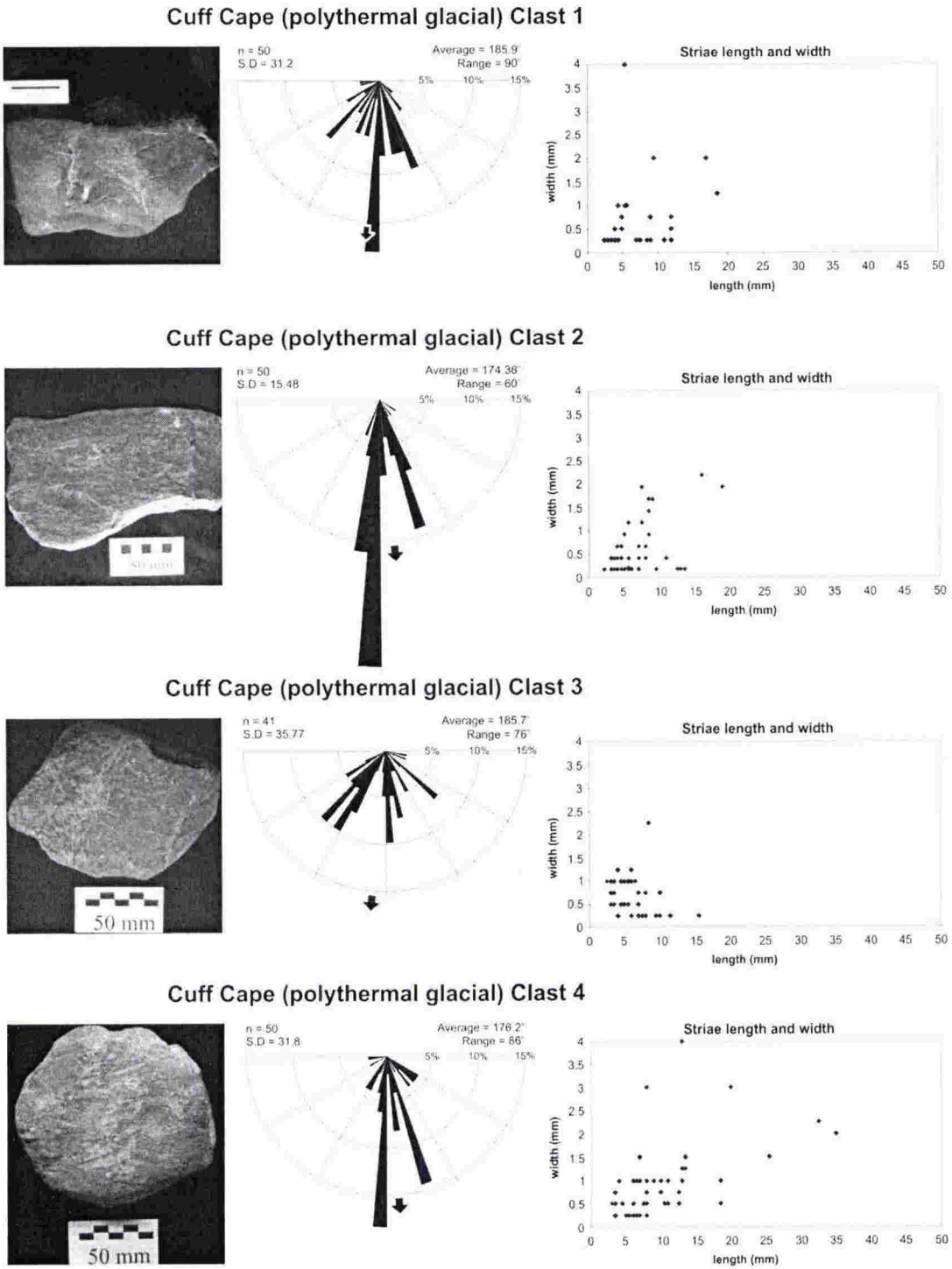

Figure 4.12 Striated clasts from Cuff Cape. The half-rose diagrams represent orientation of striae relative to the long axis of the clast (180°). Striae are grouped into 5° segments. The black arrows indicate average striae orientation. Also shown is a plot of striae length and width. Large colour images of clasts are presented in appendix 1, Linear abrasion Atlas – Polythermal Glacial striae.

Striae length

Striae length shows wide variation, but is generally shorter than striae on temperate striated clasts. Furthermore, striae length for the Cuff Cape clasts is not consistently linked to clast size (Figure 4.12 and Figure 4.13). For example the longest striae (35 mm), highest average striae length (9.97 mm) and greatest range occur on an intermediate sized and most equidimensional clast (clast 4). The smallest average length (5.96 mm) and smallest range occur on the other elongate clast that has the least preferred striae orientation (clast 3). The longest and most elongate clast (clast 2) has an intermediate range and average length (6.4 mm) similar to clasts 1 and 3.

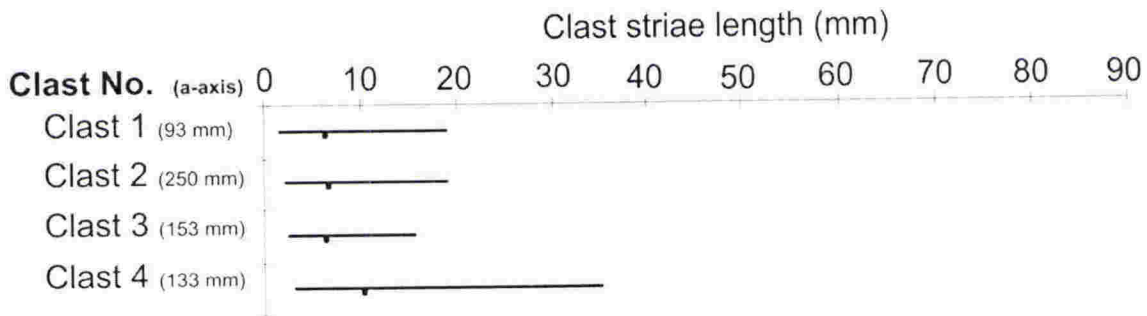

Figure 4.13 Striae length ranges and averages for the four clasts from the Cuff Cape. The greatest range and highest average length occur on an intermediate sized, equidimensional clast (clast 4).

Striae width

Striae width values also show mixed results (Figure 4.14). The two largest and most elongate clasts (clasts 2 and 3) show identical maximum striae widths of 2.25 mm and low ranges with standard deviations of 0.54 and 0.42 respectively, while the smaller clasts (1 and 4) have rare compound striae up to 4 mm wide giving higher ranges and standard deviations of 0.65 and 0.78 respectively. This is not mirrored in the average values. The smallest (clast 1, mudstone) has the lowest average width (0.54 mm) and largest (clast 2, dolerite) has only a slightly higher average of 0.62 mm. The intermediate sized clast 3 has an average width of 0.7 mm and the most equidimensional

clast has the widest average striae (0.9 mm). These results are different from the temperate striae measurements with the Cuff Cape clasts showing a higher number of wider striae, greater ranges of widths and higher averages that are not consistently related to clast size.

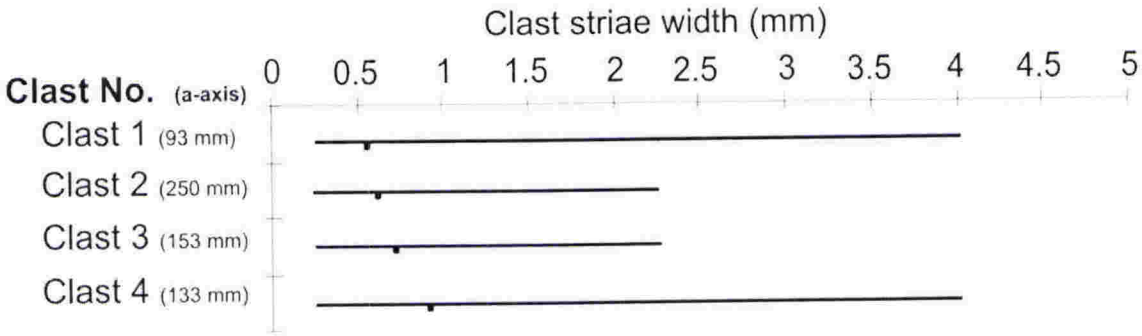

Figure 4.14 Striae width ranges and averages for polythermal striated clasts. Width ranges up to 4 mm. The highest average width occurs on the most equidimensional (but not the largest) clast 4.

Width and length ratios

Width and length is displayed in Figure 4.12, and width/length ratios displayed in Figure 4.15. Longer striae are generally wider than average but there are many exceptions. For example, Clast 1 displays one compound striation that is 4 mm wide but only 6 mm long. This influences the width/length ratio producing the highest width/length ratio (0.67) of all striae from all environments in this study (Figure 4.15). However, the average width/length ratios are generally similar, although clast 3 (intermediate size) has a slightly higher average than the other 3 clasts. These results are broadly similar to those on temperate striated clasts, but highlight the presence of a few short and wide (usually compound) striae on the polythermal striated clasts.

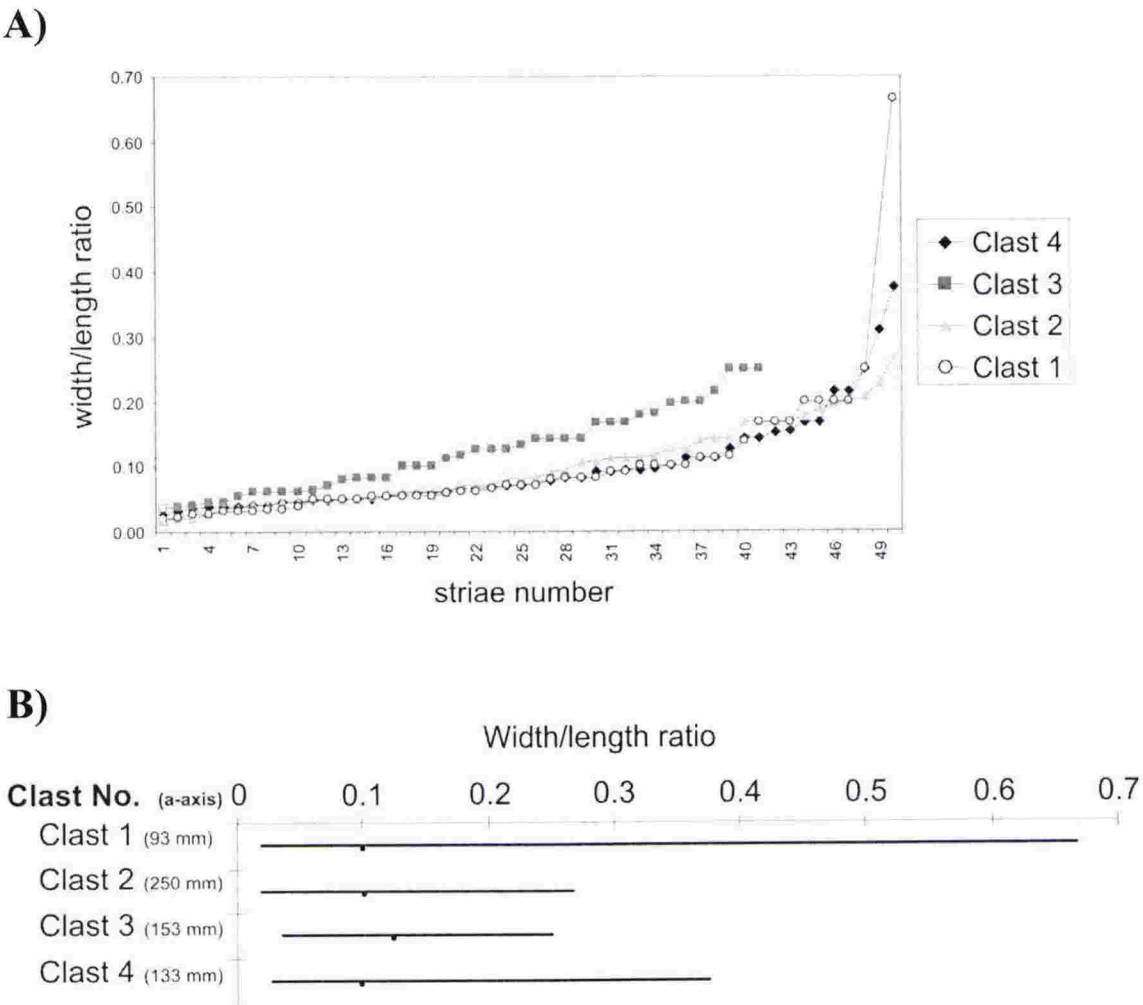

Figure 4.15 A) Width/length ratios for the four Cuff Cape clasts ranked lowest to highest. B) Width/length ratio ranges and averages. The smallest clast (clast 1) shows the highest range in width/length ratio up to 0.67.

Striae density

Striae density for the Cuff Cape clasts is high. Striae per square cm ranges from a low of 2.1 on the most equidimensional clast (clast 4) to 3.3 on the largest and most elongate clast (clast 2). The percentage of background striae is also high, with all showing 100% except the mudstone clast 1, which has a depression on the surface that has escaped abrasion resulting in 92 % background striae. The percentage of 25 mm^2 squares on the

measured surfaces with at least one striation ranges from 65% to 81%, indicating that the striae are broadly distributed across the clast surfaces. The striae density characteristics for Cuff Cape clasts are similar to those on temperate striated clasts (see Chapter 3), with both having a high density of background striae, at least 2 striae per cm^2 and broad distribution over the clast surface

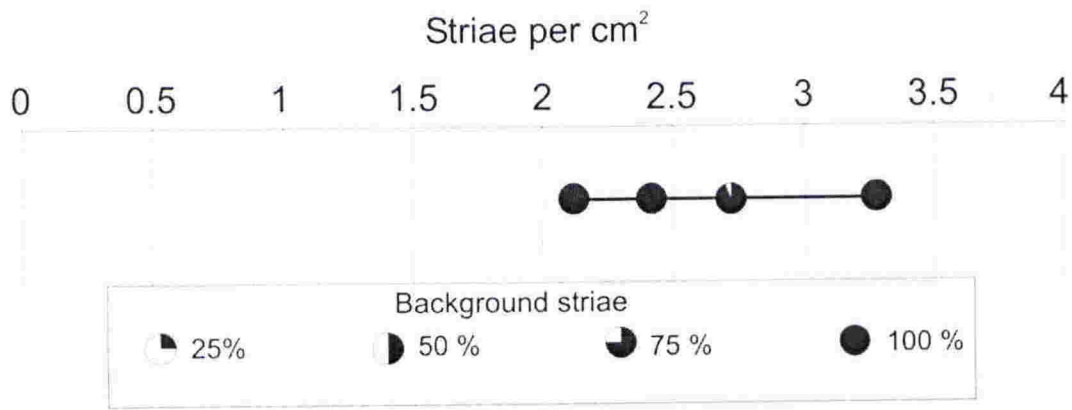

Figure 4.16 Striae density diagram showing the number of striae per cm^2 for each clast and the percentage of "background" striae. The Cuff Cape clasts have at least 2 striae per cm^2 and at least 92 % background striae. These results are similar to temperate clast striae density.

4.4 DISCUSSION AND CONCLUSIONS

Samples from the Mackay Glacier icebergs represent clasts that have been transported beneath a large polythermal glacier. The percentage of various lithologies is variable with MK 1 (inner berg) dominated by dolerite clasts and MK 2 (outer berg) dominated by granite. However, clast form is similar with both samples displaying broad distributions but with axial ratios trending toward more equidimensional or blocky shaped clasts (average c:a axial ratios of 0.53 for MK 2 (outer berg) and 0.50 for MK 1). These are higher than those recorded for temperate glacial clasts reflecting either the different lithologies between the samples or possibly a difference in the abrasion occurring beneath the glaciers.

The two Mackay Glacier samples have similar average roundness values but the MK 1 sample has a higher percentage of angular and very angular clasts compared with MK 2 causing it to plot significantly higher on the RA-C_{40} diagram showing there is local variability in clast shape between individual debris layers. Both samples plot well outside the subglacial field defined from temperate and polythermal clasts because of dominance of blockier and more angular clasts, consistent with the observations of Macpherson (1987). Despite this, both samples contain clasts with distinctive flat faces and rounded edges, considered to be facets produced by basal glacial abrasion. The percentage in MK 2 is similar to the modern temperate glaciers, but MK 1 is much lower. However, these values are still consistent with published data from known temperate glacial deposits.

Both samples contain low numbers of striated clasts, 8 % for the MK 1 (inner berg) compared with 5 % for the MK 2 (outer berg). This contrasts with the results of Macpherson (1987), who recorded 51 % striated clasts from the Mackay Glacier. This suggests that the debris sampled by Macpherson (1987) experienced significantly more basal transport and abrasion than the clasts in this study. Striae occur preferentially on subangular to subrounded, fine-grained sedimentary clasts and are oriented predominantly sub-parallel to the long axis. Dolerite clasts usually have indistinct weakly inscribed striae. The percentage of striated clasts is slightly lower than for modern temperate glacial clasts from the Mueller and Murchison Glaciers and significantly lower than the temperate Lake Pukaki moraine.

Striae from the nearby Cuff Cape also represent clasts abraded by the polythermal Mackay Glacier. They commonly show long axis parallel striae on elongate clasts, although there are exceptions. Surfaces of fine-grained sedimentary and dolerite clasts commonly show a "background" of microstriae and the number of larger striae superimposed on this background is similar to that of temperate glacially striated clasts, with the Cuff Cape clasts showing at least 2 striae per cm^2.

Striae size is not as clearly related to clast size as it is on temperate glacial clasts. While the largest striae seen on a clast from Cuff Cape, does occur on the largest clast (Figure 4.10), there are many exceptions. Average striae lengths are broadly similar to those on temperate clasts but there is a smaller range in lengths, even on large clasts. Average width and range in striae widths is generally higher than on temperate clasts, resulting is slightly higher width/length ratios. In other words, the striae on polythermal clasts from Cuff Cape are generally a little shorter and wider relative to temperate clast striae.

Despite these minor differences, the overall character of the striae on fine-grained clasts from Cuff Cape is not readily distinguishable from those produced beneath temperate glaciers, suggesting that conditions influencing striation processes beneath the polythermal Mackay Glacier are similar to those beneath temperate glaciers. Clast shape and roundness however are significantly different. This may reflect the markedly different lithologies in the two studies, or may indicate a difference in the conditions beneath the glaciers.

CHAPTER FIVE

COLD-BASED GLACIAL ABRASION FEATURES

5.1 INTRODUCTION

This chapter documents newly discovered abrasion features created beneath a cold-based glacier in Antarctica. This discovery is significant as it is commonly assumed that sliding and erosion cannot occur beneath cold-based ice and is the first documented geological evidence of cold-based ice advance. These features have been reported in Atkins and Barrett (2000) and Atkins et al. (2002) from work carried out for this study. A review of the current understanding of cold-based glaciers is provided, followed by a case study of cold-based bedrock abrasion features in the Allan Hills, south Victoria Land, Antarctica.

5.2 COLD-BASED ICE

5.2.1 Traditional view of cold-based ice movement

Cold-based ice is usually found in polar environments, but can also form at high altitudes in temperate latitudes (Hambrey, 1994). The generally accepted view is that the ice is frozen to the bed and all movement of the ice is due to internal deformation of the ice mass by slippage or "creep" within or between ice individual ice crystals (Menzies, 1995). Because the ice is frozen to the substrate, no basal sliding occurs, and therefore no erosion.

5.2.2 Landscape preservation by cold-based ice

The widely held opinion that cold-based ice is non-erosive has been used in many studies of landscape evolution and glacial reconstructions. A common theme is that cold-based ice can actually protect landforms and other features from weathering and erosion. For example, Goldthwait (1960) and Falconer (1966) observed vegetation such as lichens that had survived overriding by cold-based ice in Greenland and Arctic Canada. Others described landforms that have been preserved beneath cold-based ice. For example, England (1986) reported an alluvial fan passively overridden by ice on Ellesmere Island, Arctic Canada. Sugden (1978) observed "landscapes of selective linear erosion" where pre-existing valleys channelled ice flow creating a situation where there was warm-based ice in the valleys and cold-based ice over the intervening plateau. The plateaus show little or no sign of glacial erosion suggesting that cold-based ice protected the landscape. Another example is Kleman et al. (1994), who suggested that drift lineations and esker swarms previously interpreted to be the product of the Late Wisconsinian Laurentide Ice Sheet in the Quebec-Labrador region of Canada were in fact formed during the deglaciation of an older ice sheet and preserved in a cold-based central zone of the Laurentide Ice Sheet.

Similar observations of landscape preservation have been reported from Scandinavia (Kleman and Borgstrom, 1994; Kleman, 1990; Rea et al., 1996). In the Asgard Range, Antarctica, Sugden et al. (1991) reported unconsolidated sediments from subglacial meltwater channels thought to have been covered and preserved by cold-based ice. Holmlund and Näslund (1994) and Näslund (1997), detected large-scale landforms by radio-echo sounding beneath the present cold-based Amundsenisen Ice Sheet in Dronning Maud Land, East Antarctica. They claimed that glacially eroded and sediment-filled valleys have been covered and protected by the present ice sheet since at least mid-Pliocene (but probably Miocene) times.

5.2.3 Sliding and erosion at sub-freezing temperatures

Boulton (1972) suggested that in cold-based ice frozen to the bed, differential movement would occur along a smooth flowline approximating the shape of the bed, creating limited erosion. This flowline is the lowest level of debris transport and only reaches and erodes the bed at the summit of high protuberances. This concept was supported by Holdsworth (1974) who observed an "effective bed" forming a smooth curve over the bouldery surface allowing debris to abrade the boulder summits beneath the Meserve Glacier in the Wright Valley, Antarctica.

Shreve (1984) was the first to introduce the idea of basal sliding at subfreezing temperatures by regelation around small protrusions in the ice and concluded that basal sliding velocities would be extremely low, but total distance of sliding by a glacier during the lifetime of a large glacier can be of consequence and result in abrasion. Several other workers on both theoretical and experimental grounds extended this concept of a liquid layer around particles and sub-temperate sliding (e.g. Fowler, 1986; Cuffey et al., 1999). This was supported by direct observations of basal sliding and debris entrainment at sub-freezing temperatures of -5^0 C (Echelmeyer and Wang, 1987) and -17^0 C beneath the Meserve Glacier, Antarctica (Cuffey et al., 1999; Cuffey et al., 2000). These observations suggested that the entrainment has occurred at subfreezing temperatures due to local melt and refreeze of interfacial films between ice and immersed solids. Furthermore, Cuffey et al. (2000) suggest that the U-shaped trough beneath the Meserve Glacier is result of cold-based erosion implying that significant geomorphic work is possible by cold-based ice.

Drewry (1986) proposed that abrasion could occur beneath cold ice even if there is no sliding motion at the ice-rock interface *sensu stricto* by considering a situation where a clast resting on bedrock, but embedded in ice is rotated by shear in the lowermost layers of ice. The rotating motion produces torque, giving rise to an angular velocity (ω_c), and forward motion that causes dragging along the bed producing abrasion (Figure 5.1).

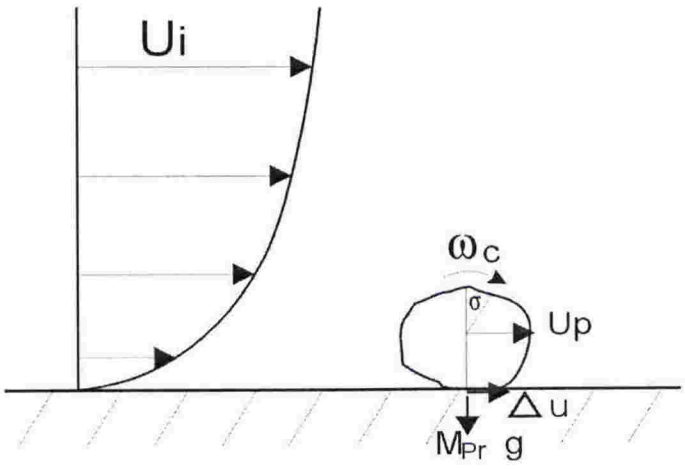

Figure 5.1 Diagram from Drewry (1986), showing rotation and net forward motion of a particle embedded in the basal layer of a cold glacier frozen to bedrock. The vertical velocity profile is shown (left) with zero forward movement at the bed but with finite horizontal flow, due to creep, increasing with distance above the bed (hence a shear zone). The clast experiences angular velocity (ω_c) and forward velocity (U_p). The net forward motion of the clast (U_p) by rolling is; $U_p = \omega_c r_c$.

None of these studies has reported ancient cold-based sub-glacial abrasion features that have survived to the present day. During this study, features of erosion and deposition interpreted to be the product of cold-based ice advance were identified at Allan Hills in South Victoria Land, Antarctica. These observations suggest that cold-based ice is an important but little recognised geomorphic agent.

5.3 ALLAN HILLS, VICTORIA LAND, ANTARCTICA

5.3.1 Introduction

The Allan Hills (76°42'S, 159°40'E) form a wishbone-shaped nunatak situated high (1600-2100 m above sea level) in the Transantarctic Mountains in south Victoria Land at the edge of the present East Antarctic Ice Sheet (EAIS). The 50 square kilometres

(km) of exposed rock is barely emergent with most of the area rising less than 300 m above the surrounding ice making the nunatak sensitive to fluctuations in the edge of the EAIS (Figure 5.2).

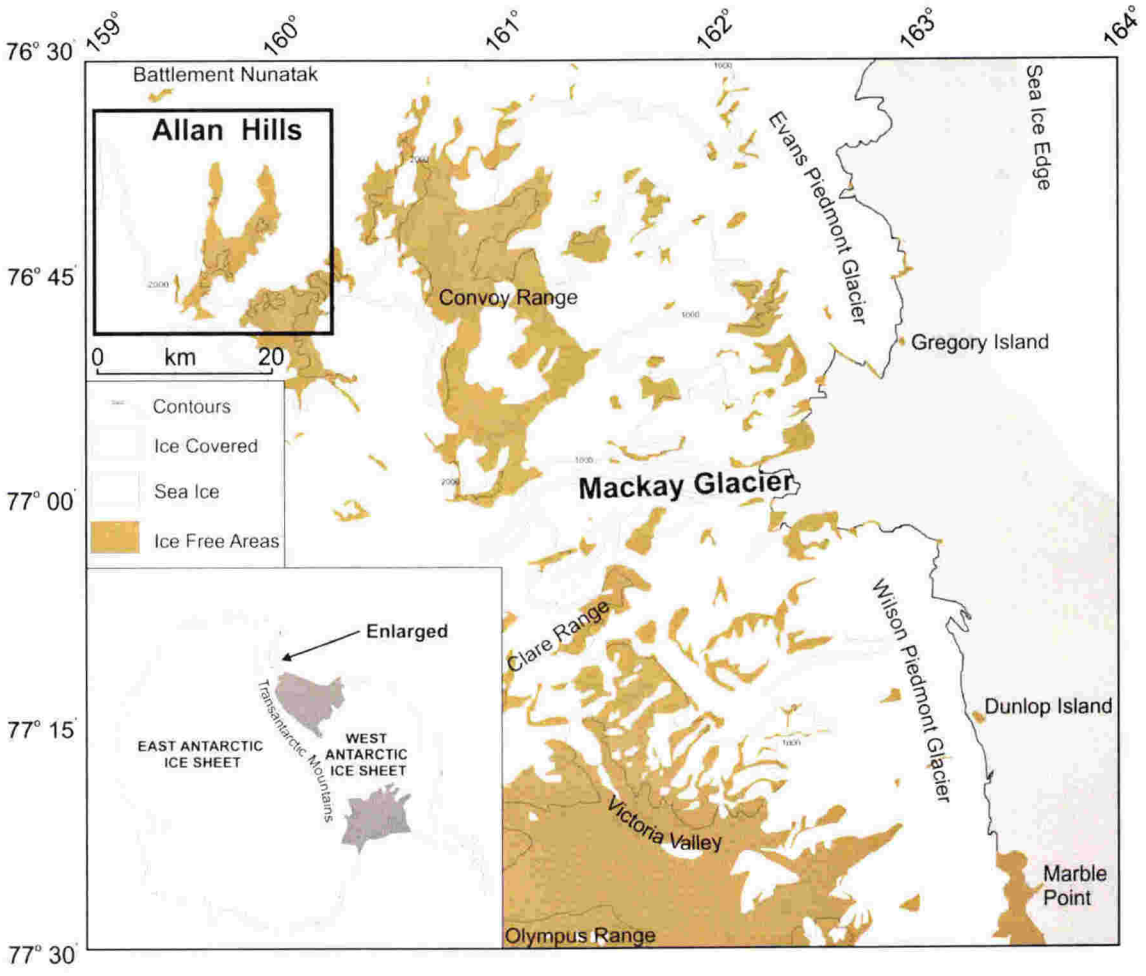

Figure 5.2 Location map of Allan Hills near the margin of the East Antarctic Ice Sheet (EAIS) in south Victoria Land.

The Polar Plateau bounds the southern and western sides of the nunatak. On the eastern side, the Odell Glacier separates Allan Hills from Coombs Hills. The centre of the wishbone is occupied by the Manhaul Bay Glacier (unofficial name) and is fed by ice flowing north on either side of the glacier turning south around the tips of the wishbone. The eastern part of Allan hills has a broad U-shaped valley named Trudge Valley and is partially occupied by a tongue of the Odell glacier (Figure 5.3).

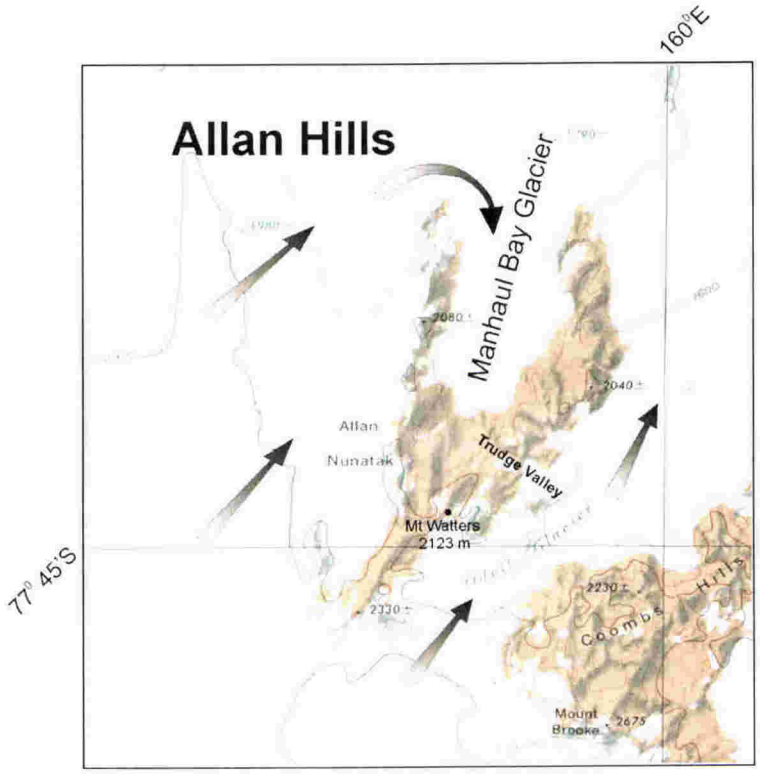

Figure 5.3 Allan Hills with estimated ice flow into the centre of the wishbone feeding the central Manhaul Bay Glacier.

5.3.2 Bedrock geology of Allan Hills

The bedrock of Allan Hills comprises near flat-lying Permian and Triassic sandstones, shales and coal measures of the Beacon Supergroup, intruded by extensive sills and occasionally thin dykes of Jurassic Ferrar Dolerite (Ballance and Watters, 1971). A patchy distribution of diamictite mantles the Beacon strata throughout the central area of Allan Hills and is considered to be part of the Sirius Group diamictite deposits.

The Sirius Group tills are thought to represent the last time the area was overridden by sliding warm-based advance of the EAIS. Although these deposits have not been dated directly, other Sirius deposits and rock surfaces in the Dry Valleys region south of Allan Hills have yielded ages as old as 10 Ma, with volcanic ash deposits as old as 15 Ma

(Summerfield et al., 1999). The nature of the surfaces and the preservation of the ashes indicate that the landscape has experienced persistent polar desert conditions dominated by wind erosion since those times.

5.3.3 Present climate and recent glacial activity

The mean annual temperature at Allan Hills is approximately -30^0C (Robin, 1983). The present Manhaul Bay Glacier is estimated at ~200 m thick in the middle, with basal temperatures of ~-24 °C (estimated from the MAT of –30°C and the graph of Robin, 1955, Fig. 3). The ice fronts of the Manhaul Bay and Odell Glaciers are wind-sculpted "blue ice" typical of ablation that has been measured at 5 cm/yr in ice fields several kilometres west (Faure and Buchanan, 1987). Retreat of these glaciers, presumably from Last Glacial Maximum (LGM) advance, has exposed abrasional and depositional features on rock platforms and ridges beyond the margin of the glaciers (Figure 5.4 and Figure 5.5). These features must have formed beneath ice that is here estimated to be of similar thickness and low basal temperature to that of today.

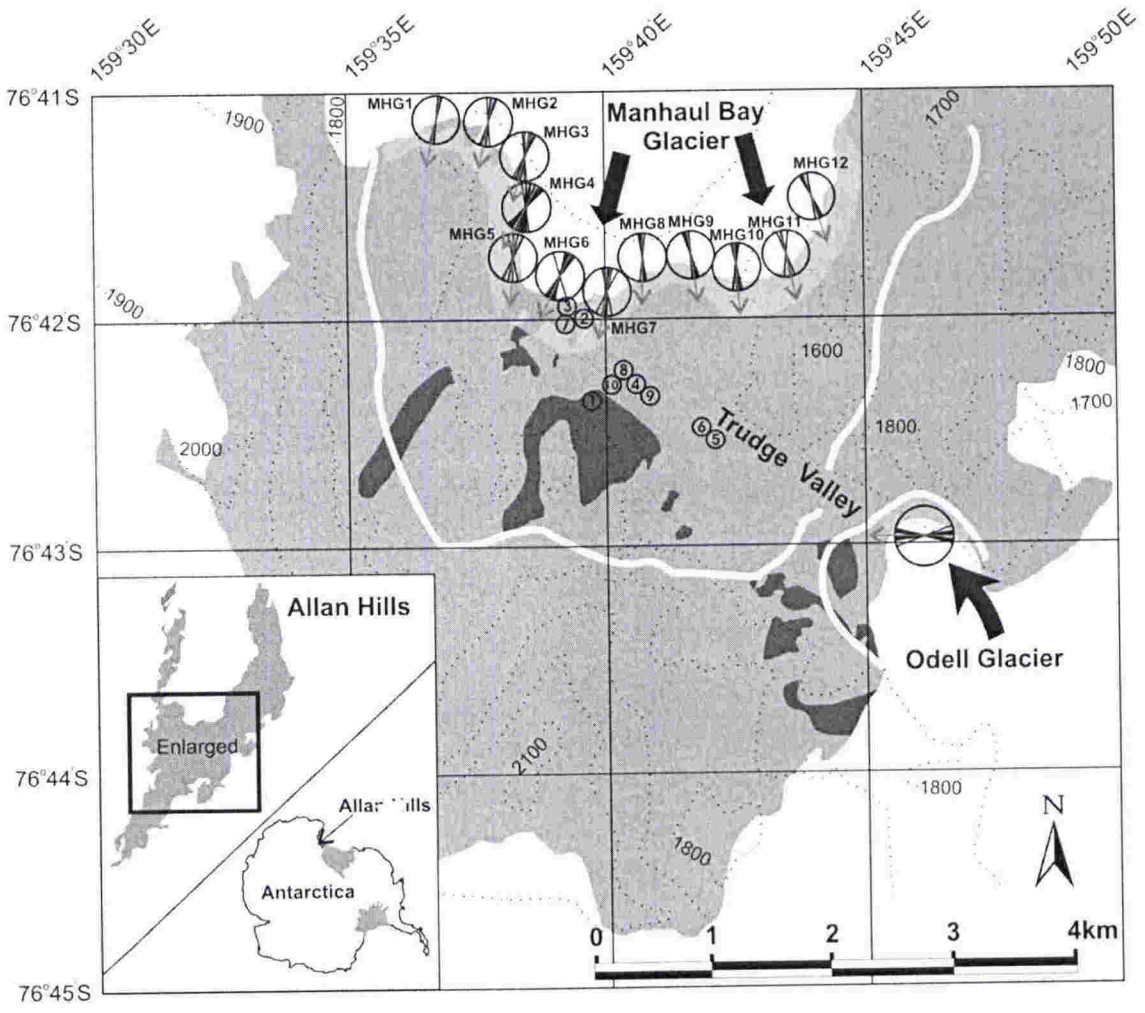

Figure 5.4 Map of central Allan Hills, Antarctica showing distribution of abrasion features recording former extent of Manhaul Bay and Odell Glaciers. Dark shading shows distribution of much older Sirius diamictite. The light shading indicates the distribution of abrasion marks around the ice margins, and circles around the ice margins show linear abrasion orientations and average azimuth at each site (small grey arrows). Small circles with numbers refer to cobbles with cold-based abrasion marks. Large dark arrows on the glaciers indicate the ice-advance direction, and white lines indicate maximum advance limit of cold-based Manhaul Bay and Odell Glaciers. Contours in metres above sea level.

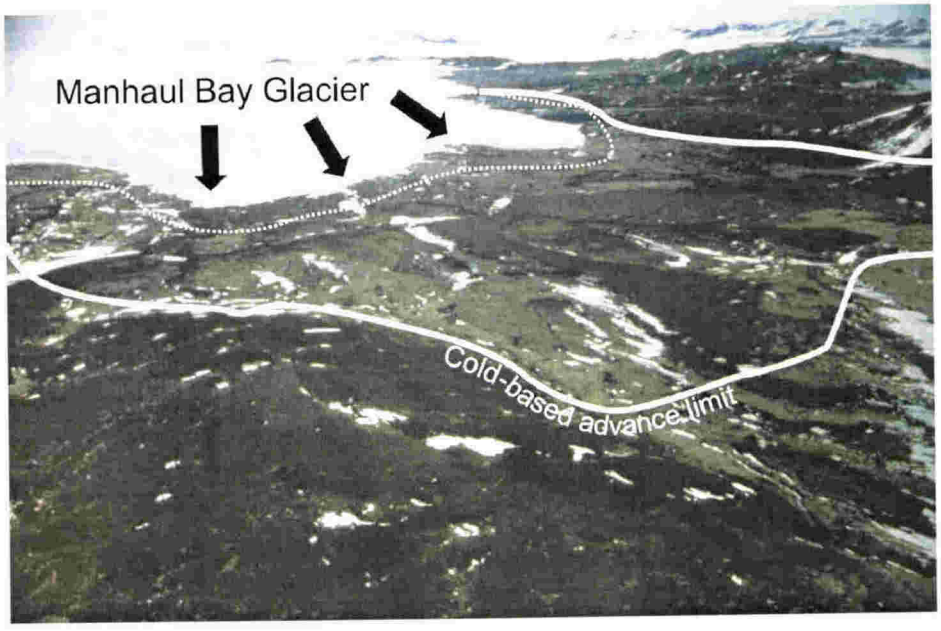

Figure 5.5 Aerial photograph of central Allan Hills looking north east, showing the

Type 1: Broad Scrapes

Broad unweathered scrapes (up to 500 mm width, 40 mm depth, 1200 mm length), but defined as (width >75 mm, depth > 15 mm, length >340 mm), typically consist of many smaller striae or grooves centimetres or millimetres in width. Some examples (Figure 5.6) show progressive increase in depth and width with an abrupt terminus. Typically the abrasion mark has crushed sandstone remnants of the abrading tool smeared onto the surface, particularly at the deepest terminal wall. Occasionally, small centimetre-scale "levées" occur along the sides of the abrasion mark. These marks are close to the present margin of the Manhaul Bay Glacier and indicate ice movement from north to south.

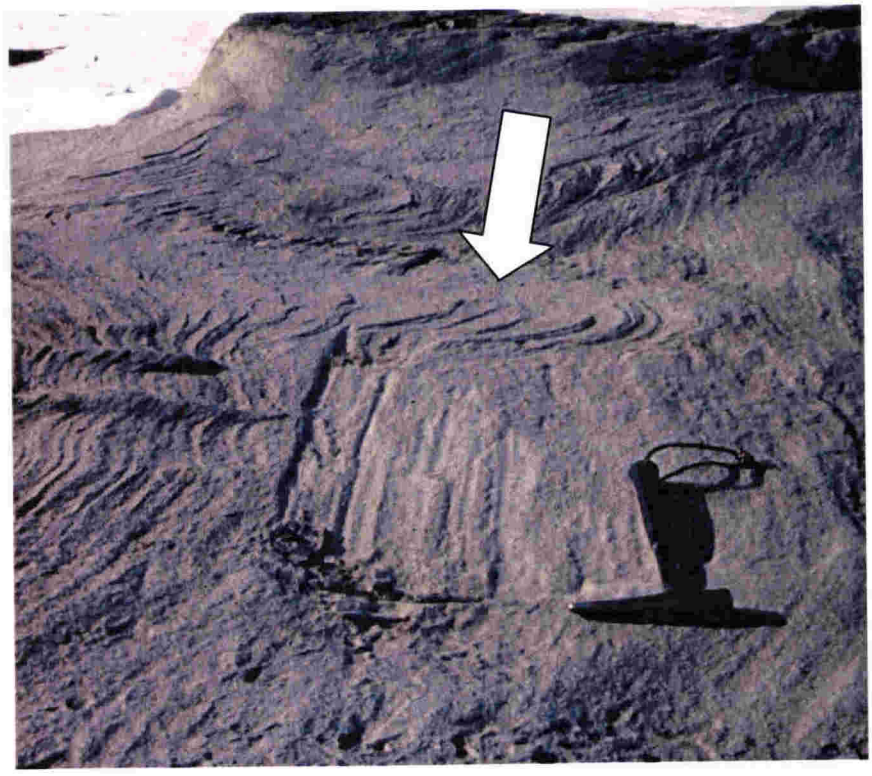

Figure 5.6 Type 1 abrasion. Large broad scrape consisting of multiple grooves cut in well-developed foresets of Beacon sandstone. Example becomes deeper and wider with an abrupt terminus and has remnants of abrading tool on surface. Arrow indicates ice-movement direction. Hammer is 33 cm long.

Type 2: Individual striae and grooves

Variably shaped, unweathered individual linear abrasions (scrapes, striae, and grooves) make up a wide variety of discrete abrasion marks (defined as: length unlimited, width < 75 mm, depth <15 mm). Where several marks occur in one location, they are generally sub-parallel. Some show a progressive increase in depth and width (nail-head) whereas others have more symmetrical, tapered ends. Occasionally, individual marks occur "in line" to form a trail of marks up to 2 m in length (Figure 5.7). Some marks have crushed sandstone remnants of the abrading tool smeared onto the surface and are sometimes bordered by small centimetre-scale "levées." These abrasion features are common near the present margins of Manhaul Bay and Odell Glaciers and rare farther inland from the ice, protected beneath brecciated sandstone debris.

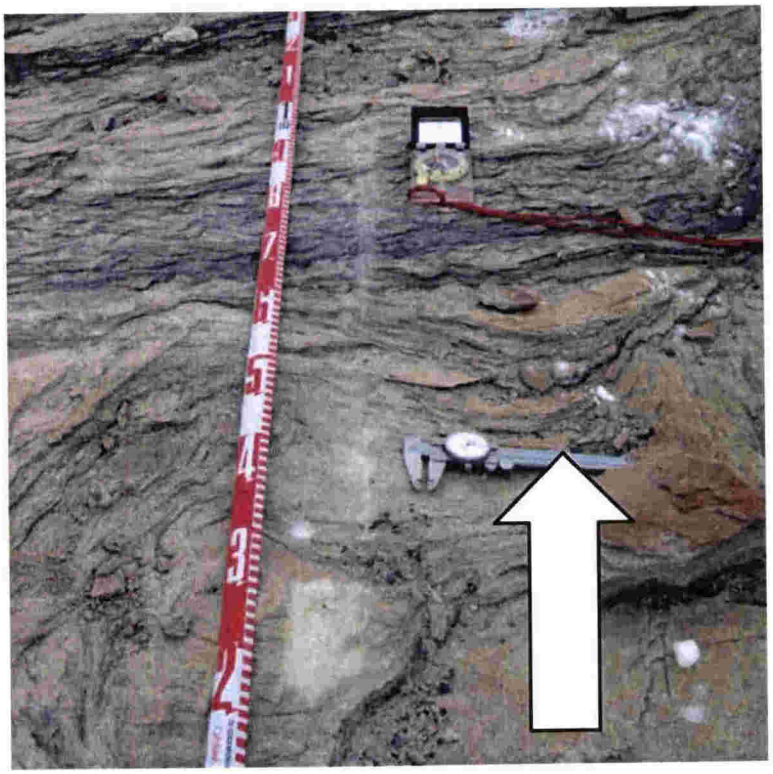

Figure 5.7 Type 2 abrasion. Variably shaped, individual unweathered abrasion marks on Beacon sandstone. Arrow indicates ice-flow direction.

Type 3: Scraped boulders and cobbles

Variably shaped, unweathered scrapes up to several centimetres wide (and related striae) occur on the stoss side of some weathered dolerite boulders and cobbles lodged within, or resting on, Sirius diamictite. Abrasion has removed the characteristic dark brown desert varnish from the surfaces of the boulders, making the marks clearly visible (Figure 5.8). Some boulders have been overturned, exposing a surface that lacks the wind polish typical on exposed surfaces. These distinctive overturned and abraded boulders and cobbles were found over a wide area in central the Allan Hills, and up to 1800 m south (inland) of the present Manhaul Bay Glacier margin (Figure 5.4).

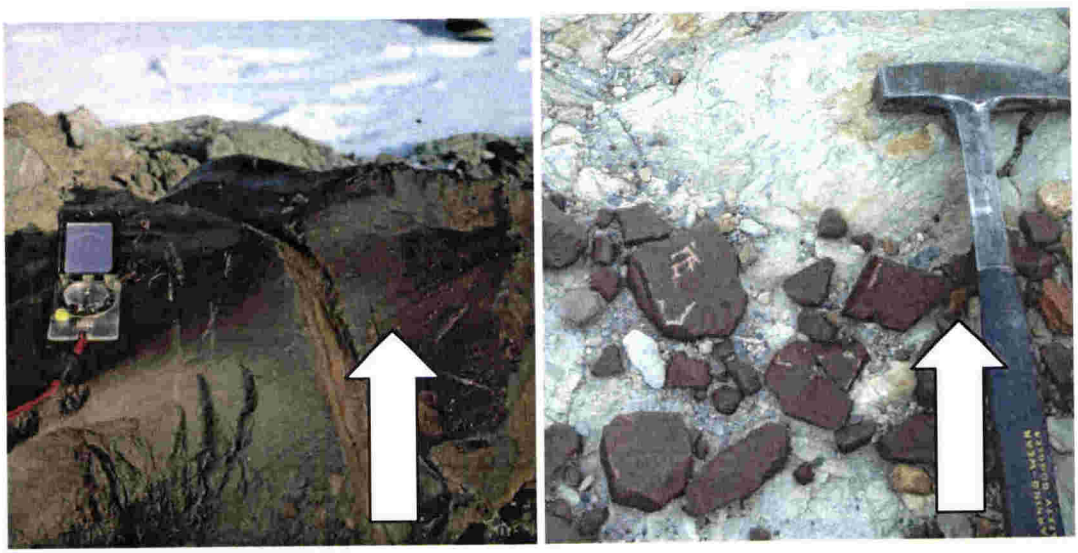

Figure 5.8 Type 3 abrasion. Unweathered scrapes. A) On weathered, wind-polished dolerite boulder in Sirius diamictite. Some scraped boulders have been overturned. B) Abrasions on wind-polished clasts. Associated abrasion mark on the bedrock surface is visible (centre-top of photograph). Hammer is 33 cm long. Arrows indicate direction of ice-movement.

Type 4: Ridge-and-Groove lineations

Localised surfaces display abraded patches with many parallel fine lineations (millimetre scale width and depth), described here as ridge-and-groove lineations. The surfaces are typically dark and have a platy appearance and sheen similar to slickensides (Figure 5.9). These abraded patches occur within thin carbonaceous layers beneath brecciated sandstone debris and indicate north to south glacier movement. These patches occur over a wide area in the central Allan Hills within the Manhaul Bay Glacier advance limit shown in Figure 5.5.

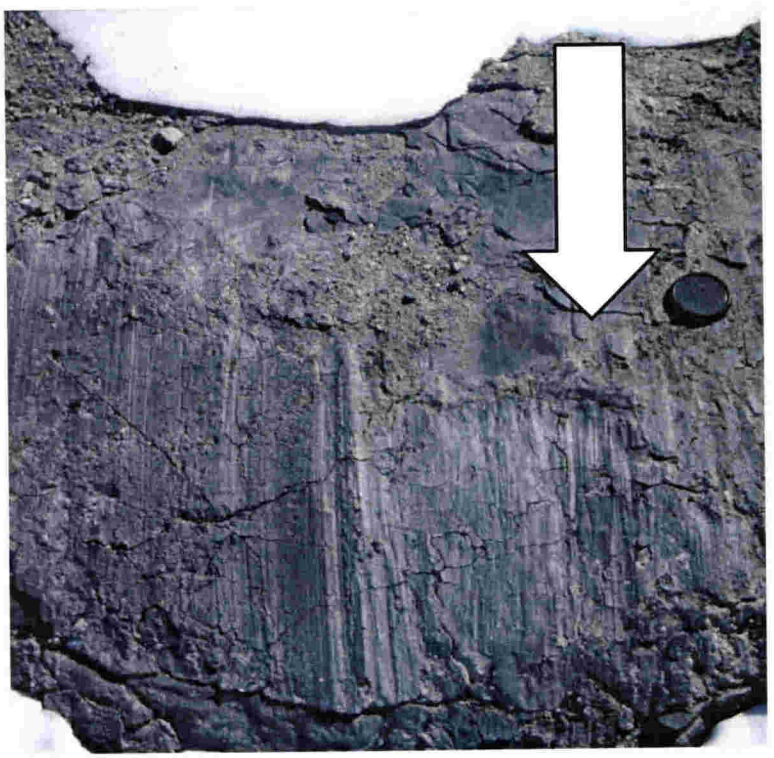

Figure 5.9 Type 4 abrasion. Ridge-and-Groove lineations on thin carbonaceous layers in Beacon strata. Surfaces have a sheen similar to slickensides. Ice movement was from top to bottom. This surface is within 5 m of the Manhaul Bay Glacier margin.

5.3.5 Characteristics and orientation of bedrock linear abrasions

Basic dimensions of type 1 and type 2 linear abrasion marks from around the margins of the Manhaul Bay and Odell glaciers were measured. Measurement of abrasion marks proved difficult due to the range in shape and size, with many showing significant change in width and depth along the same striation. Data presented here are length, maximum width and maximum depth only.

Length and width of cold-based bedrock abrasion marks are shown in Figure 5.10 and Figure 5.11. The measurements separate the cold-based abrasion marks into 2 types. Type 1 is generally longer and wider and deeper than type 2. The maximum length for type 1 abrasion marks is 1130 mm and maximum width is 470 mm (average length is 682 mm and average width is 200 mm). Depth is the least reliable measurement because of the difficulty measuring in the field but ranged from 18 mm to 40 mm (average is 26 mm). For type 2 abrasion marks, maximum length is 1780 mm and maximum width is 160 mm (average length is 324 mm and average width is 29 mm). Maximum measured depth of type 2 abrasion marks is 15 mm and average is 3.7 mm. Some overlap between the two types occurs because a few type 2 abrasion marks are long (especially if several occur in line) giving a wide range and a few are wider than the 75 mm lower width limit of type 1 abrasion marks. These are still classified as type 2 because they are shallow (< 15 mm).

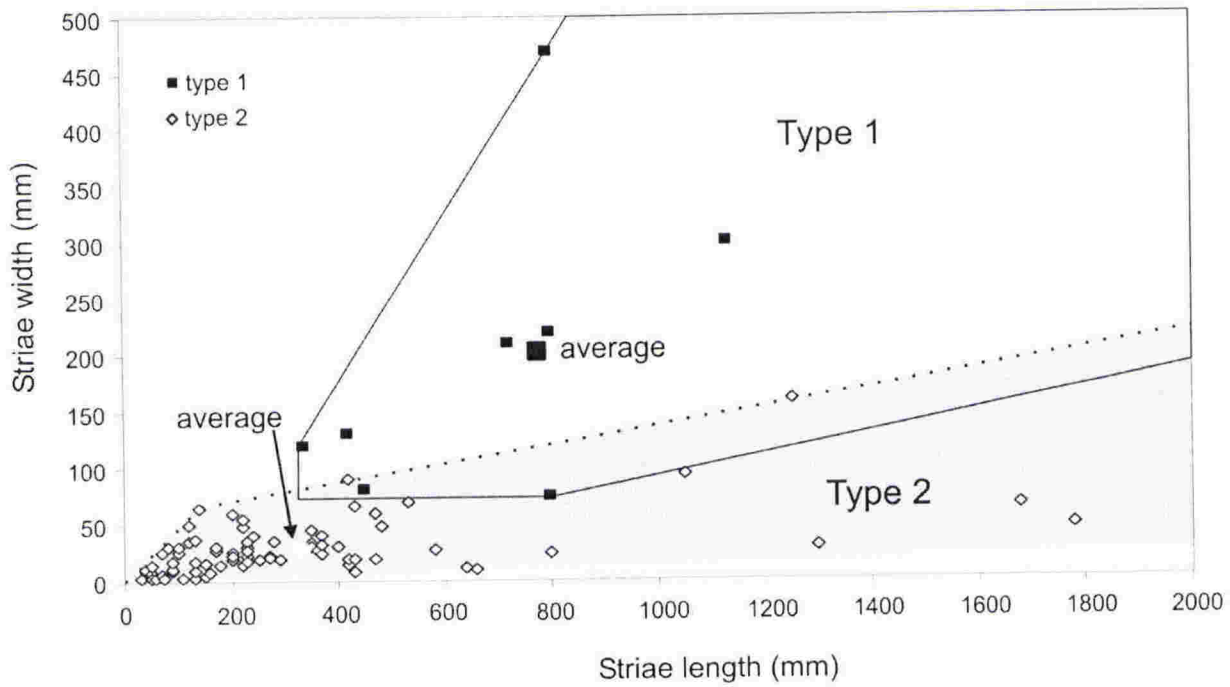

Figure 5.10 Length and width of cold-based bedrock abrasion marks. Boxed field indicates type 1 abrasion marks. Light shading is type 2 abrasion mark field.

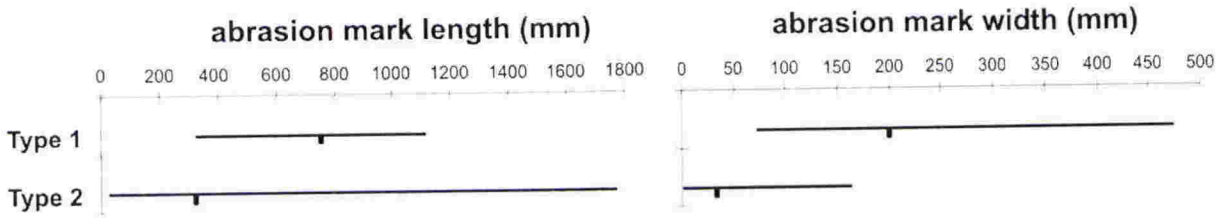

Figure 5.11 Length and width ranges and averages for cold-based bedrock abrasion marks.

Width divided by length produces a ratio between 0 and 1. The range and average width/length ratios for the bedrock abrasion marks are shown in Figure 5.12. Despite type 1 abrasion marks having a higher average length than type 2, their even greater average width means the type 1 striae have a distinctly higher width/length ratio than type 2.

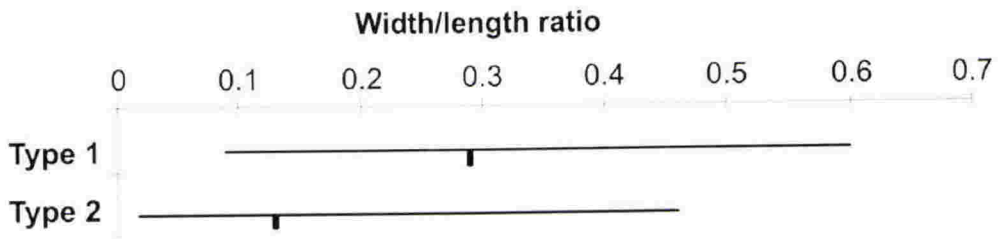

Figure 5.12 Width/length ratio range and average for the cold-based bedrock abrasions showing that the Type 1 have a much higher average than type 2 abrasion marks.

Figure 5.13 clearly shows fresh, short, discontinuous type 2 cold-based abrasion mark on a weathered Beacon sandstone surface. These contrast with the older, weathered, long and continuous wet-based striae extending under a cover of Sirius till.

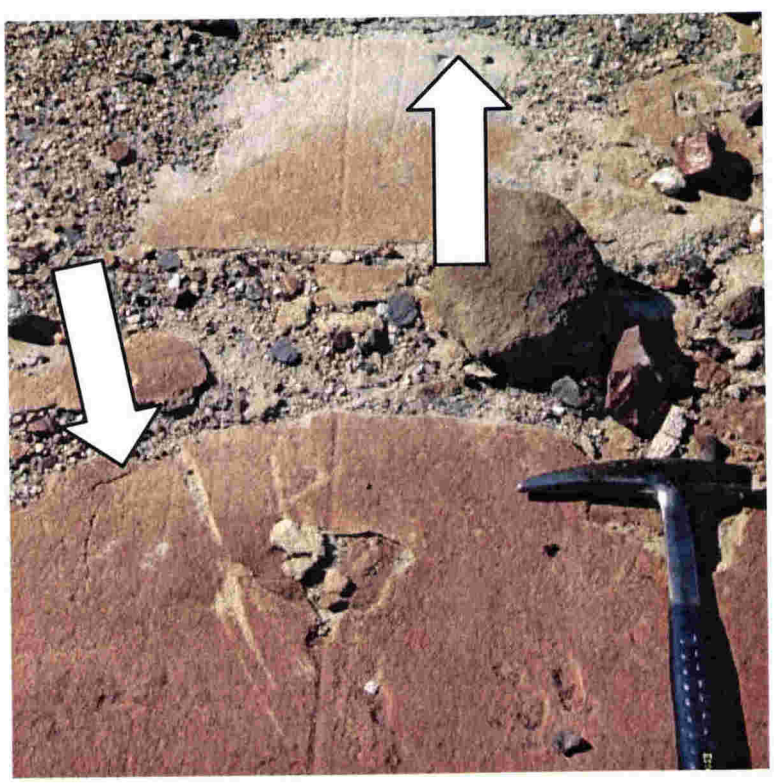

Figure 5.13 Linear abrasion marks on a Beacon sandstone surface with Sirius till on top. Surface shows two clear sets of linear abrasion marks. Weathered striae are long and narrow. Recent cold-based abrasion marks are shorter, wider and less regular than older wet-based "Sirius striae". Arrows indicate ice flow directions that generated the abrasion marks. Hammer is 33 cm long.

Orientation of bedrock abrasion marks (Type 1 and 2 abrasion) was measured around the perimeter of the Manhaul Bay Glacier. Between 3 and 15 individual measurements were made from at each location from an area of several hundred metres. All indicate movement from north to south (inland). The measurements are displayed as orientation wheel diagrams in Figure 5.5, with small grey arrows showing the mean orientation for each site. These show a generally splayed pattern radiating from beneath the glacier confirming that these have been produced by the Manhaul Bay Glacier. Measurements of Type 2 abrasion marks were also made on the northern edge of the Odell Glacier and indicate a westerly ice movement into Trudge Valley.

5.3.6 Characteristics and orientation of clast abrasion marks

Ten weathered, wind-polished dolerite cobbles showing fresh cold-based abrasions were collected from within the cold-based advance limit in central Allan Hills (Fig 5.4). On these clasts, abrasion has removed the characteristic brown weathered surface leaving distinctive abrasion mark (Figure 5.14). Additional images of these and other clasts are presented in appendix 1, Linear Abrasion Atlas, Cold-based glacial abrasion.

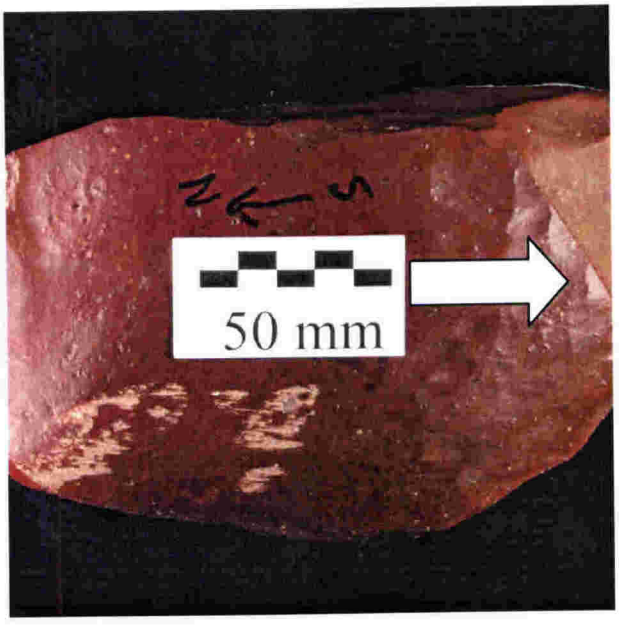

Figure 5.14 Example of a cold-based abrasion mark on wind-polished dolerite clast. Abrasion has removed the weathered surface. Arrow indicates ice-flow direction.

Measurements of these abrasions are presented in appendix 4. The linear abrasion marks show great variation in length, ranging from 17 mm to 80 mm (average of 51 mm) and width ranging from 3 mm to 30 mm (average of 9 mm). No consistent relationship is evident between the length and width (Figure 5.15). Depth was not measured, but all are less than 1mm.

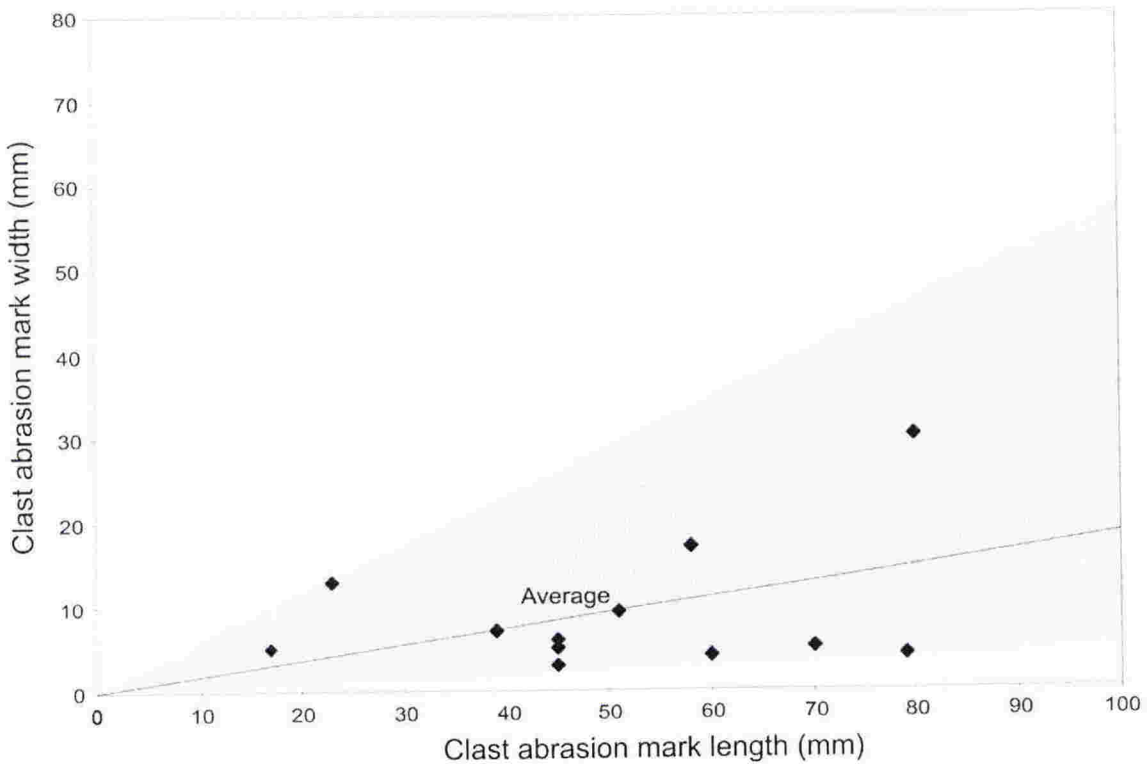

Figure 5.15 Comparison of length and width of cold-based abrasion marks on desert varnished dolerite clasts from central Allan Hills. Maximum abrasion mark length is 80 mm and maximum width is 30 mm. Average is 51 mm length and 9 mm width. Grey shading indicates field of cold-based linear abrasion mark dimensions on clasts from the Allan Hills data.

The abrasion marks occur on the top surface or on the northern side of clasts. For the latter, this is the side of the clast facing the Manhaul Bay Glacier and is therefore interpreted as the stoss side. Some abrasions preferentially occur on raised portions of the clast such as ridges between faces and appear to influence the orientation and

curvature of the abrasion. Also, the length and width of the abrasion marks are often controlled by the surface on which the abrasion has occurred. If the surface is not planar, the abrasions may appear "intermittent" with several individual abrasions "in-line" as the striator has made contact with the raised parts of the surface.

The orientation of abrasion marks on clasts was measured relative to the long axis of the clast and also relative to the north-south azimuth in the field (Figure 5.16). There is a preference for abrasion marks to be aligned sub-parallel to the long axis of the clast. Variation from the long axis varied up to 75 degrees. This may be due to a preference for clast long-axes to be oriented north/south, although the reason for this is not clear.

The abrasion marks are preferentially oriented sub-parallel to the north-south azimuth. This is the expected direction of flow from the Manhaul Bay Glacier over the clasts. Variation from the north-south line ranged up to 34 degrees but 5 of the 11 measured abrasion marks were aligned exactly parallel to the north/south line.

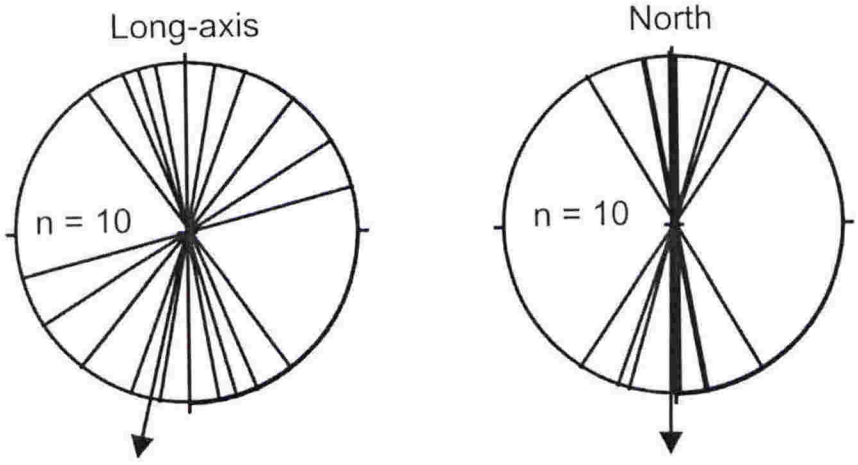

Figure 5.16 Orientation wheels for abrasion marks on ten weathered, wind-polished clasts from central Allan Hills (Figure 5.4). On the left, orientation is relative to the long axis of the clast. On the right, orientation is relative to north. Arrows indicate average orientation for the abrasion marks.

5.3.7 Interpretation of erosional features

Broad scrapes (type 1 abrasion marks) and individual striae and grooves (type 2 abrasion marks) are interpreted to be the result of debris within the ice being dragged along the bedrock by either basal slip or forward rotational movement created by the striator projecting into the deforming ice mass as suggested by Drewry (1986). Because the abrading particles were most likely to be the same lithology as the bedrock, there was little hardness contrast, and abrasions tend to be broad and shallow and commonly have remnants of the sandstone striator on the abraded surface or as low levées on the sides. This is particularly noticeable on abrasions that progressively deepen and then terminate abruptly, indicating that the striator disintegrated under dry simple shear with no melt water to wash away the levées. Examples that have more symmetrical tapered ends suggest that the striator made contact with the bed briefly, but lifted off again. Occasionally, several of these abrasions occur in line over 1-2 m where the striator touched the bedrock surface several times on its journey (Figure 5.7).

A similar process is inferred for the short irregular abrasional marks on wind-polished boulders and cobbles (type 3 abrasion marks) (Figure 5.8). Differential ice movement close to the glacier bed has initially dragged the striating tool over the boulders and cobbles abrading the northern (stoss) face or the top surface and in some cases overturned them.

Type 4 abrasion (Figure 5.9) is interpreted as a glaciotectonic structure formed by differential slip on thin, weak carbonaceous shale layers within the Beacon strata in response to increased shear stress from loading as cold ice moved over bedrock promontories.

These processes are depicted in a schematic model of cold-based glacial processes at Allan Hills (Figure 5.17).

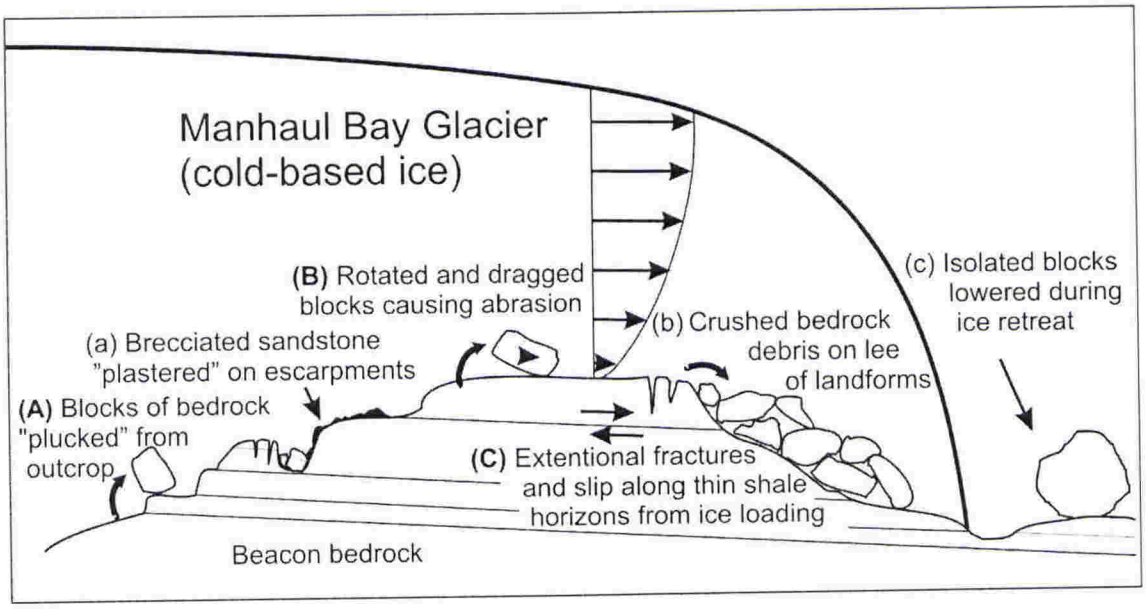

Figure 5.17 Schematic model of processes beneath cold-based ice at Allan Hills. Vertical profile indicates assumed ice velocity within glacier. Erosion followed by entrainment occur by (A) plucking stoss sides of outcrops, (B) dragging blocks along bedrock surface either by sliding or rotation of clast by velocity gradient above bed, and (C) glaciotectonic extension producing fractures and differential slip along weak layers producing abraded, slickenside surfaces. Depositional processes are shown also but not discussed here. For an explanation of depositional processes see Atkins et al. (2002).

5.3.8 Interpretation of cold-based glacier movement at Allan Hills

The solid white lines in Figure 5.4 represent the maximum advance positions for the margins of the Manhaul and Odell Glaciers, delineated by the most inland positions of overturned and abraded boulders and cobbles (type 2 abrasion) and sandstone breccia deposits (not discussed here). Reconstruction of the longitudinal profile of the Manhaul Bay Glacier, following the modern profile to the limit shown, indicates that a maximum ice thickness of ~200 m was attained at the present southern ice margin.

On the basis of fresh abrasion marks cutting through desert varnish on boulders and cobbles, the unweathered appearance of glacial scrapes, grooves, and striae on rock

ledges close to the ice margins, the features described here are interpreted to have formed during the Last Glacial Maximum (LGM). This was the last time the East Antarctic Ice Sheet was more extensive in this region (Hughes, 1998; Siegert, 2001; Denton and Hughes, 2002). A more extensive Manhaul Bay Glacier most likely produced many abrasion features over the extensive bedrock platforms it once covered, but these have been removed by wind erosion apart from those most recently exposed by ice ablation or still protected by debris.

5.4 CONCLUSIONS AND IMPLICATIONS

The recent advance of the Manhaul Bay Glacier, whose limit has been reasonably well defined, must have been entirely cold-based. This has produced a range of glacial abrasion features indicating that cold-based ice is capable of erosion.

The abrasion features show a wide variety in size and shape but are distinctly different from those produced by wet-based sliding ice. The development of these abrasions is likely to be influenced by the character of the bedrock, forming mostly on relatively soft lithologies such as Beacon sandstone. In the case of cold-based abrasion features on wind-polished dolerite clasts these are likely to have formed by contact with equally hard clasts. In addition, there appears to be a low preservation potential on soft bedrock due to erosion by wind. The preservation potential of abrasion features is significantly higher on harder wind-polished boulders and cobbles, where it takes longer to weather the surface and remove abrasion marks.

These features have been used to define the limit of the southward advance of cold ice 2 km into the present ice-free area of the central Allan Hills during the LGM. This advance overtopped landforms up to 100 m above the present ice limit. Such an ice advance requires that the adjacent outlet glaciers flowing north past Allan Hills were higher by a similar amount. These newly recognised cold-based glacier features provide criteria for mapping the former LGM extent of ice throughout the TAM and elsewhere in Antarctica where similar bedrock lithologies are present.

CHAPTER SIX

MASS MOVEMENT STRIAE

6.1 INTRODUCTION

This chapter draws attention to the generation of striae in gravity-driven movements of rock debris by examining two mass movement deposits of very different character. The first example is a debris-avalanche deposit of Holocene age on the lower slopes of Mt. Ruapehu in the North Island of New Zealand, and the second is a modern rock-fall from the central Southern Alps in the South Island of New Zealand. Characterising striae formed by mass movement is important because mass movement deposits can have similar texture and appearance to glacial deposits.

"Mass movement" is the down-slope movement of soil and rock material under the influence of gravity (Selby, 1993). This encompasses a wide variety of movements that differ depending on material, slope and water content. Several classification schemes have been developed, but considerable confusion exists in the application of terms. One of the most widely used classifications is that of Varnes (1958), which provides a simple depiction of the main types of mass movement (Figure 6.1) and is used in this study.

As the name implies, rock-falls are the result of falling particles of resistant rock. This contrasts with debris-avalanches that occur near the opposite end of the mass-movement spectrum and result from the process of flow involving variably wet soils and unconsolidated rock.

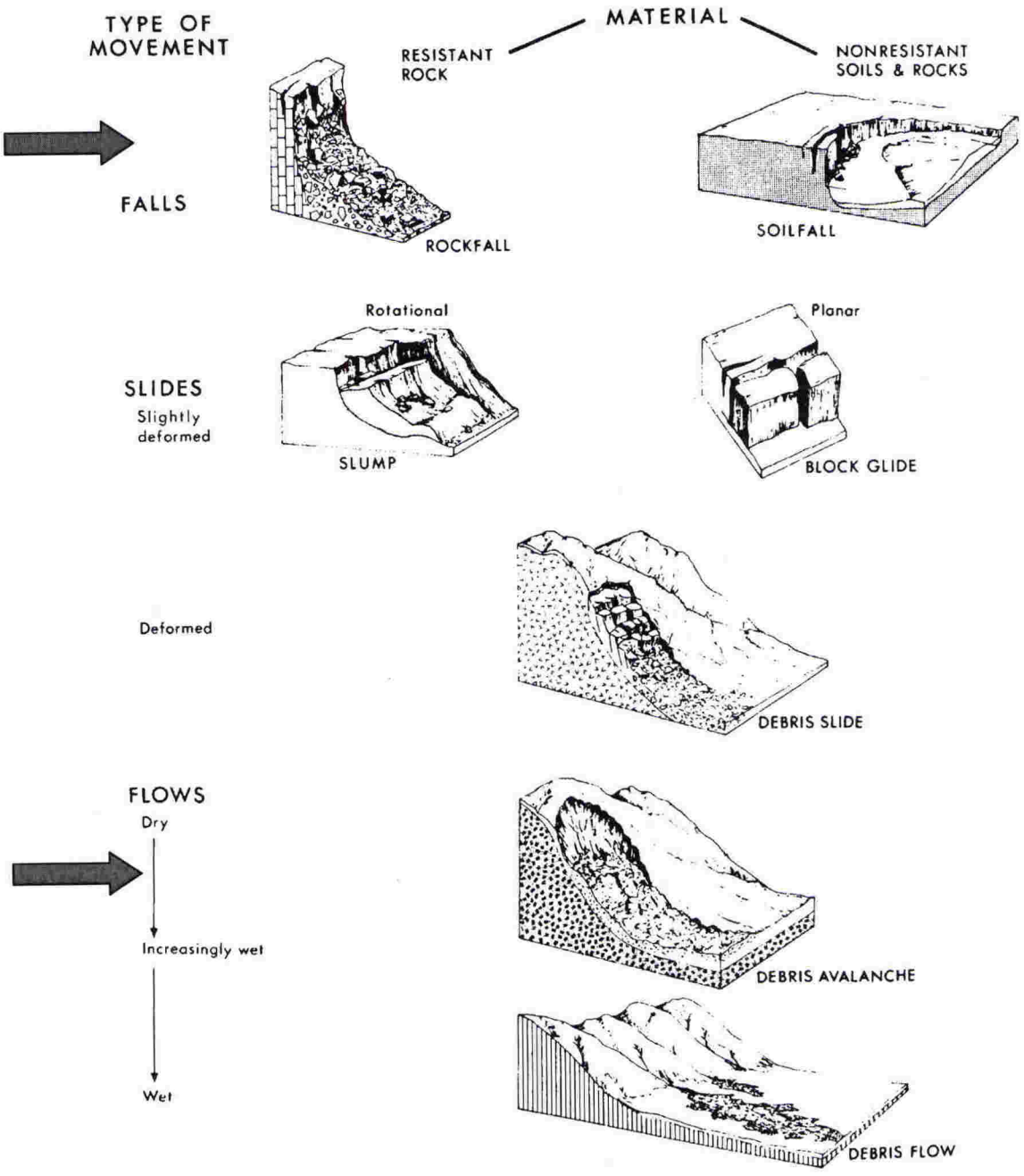

Figure 6.1 Classification of mass movement types according to Varnes (1958). Rock-fall and debris-avalanche are positioned at opposite ends of the mass movement spectrum (large arrows), (modified from Selby, 1993).

Rock-falls produce talus at the base of steep slopes and generate clasts ranging in size from pebbles to large boulders. The deposits are typically poorly-sorted and have often been misinterpreted as glacial deposits (Hewitt, 1999). Individual rock particles move by rolling, bouncing and sliding until they reach a lower slope and an area comprising similar-sized particles. Larger rocks will roll and bounce over the smaller ones and tend to accumulate lower on the talus slope (Selby, 1993). Grain-to-grain interactions are frequent, but impact forces will vary depending on the size and movement of each rock particle. However, these are often great enough to produce abrasion marks on rock surfaces.

Debris-avalanches have been defined as "rapid movements of an incoherent unsorted mass of rock and soil mobilised by gravity" (Schuster and Crandell, 1984). These are separated from debris-slides and debris-flows on the basis of water content and degree of deformation of the soil material (Figure 6.1). Therefore, a debris-avalanche contains more water and shows greater deformation than a debris-slide, but less water and deformation than a debris-flow (Selby, 1993). Inter-particle contact forces and deformation are significant and can produce both large shattered blocks that still preserve the original bedrock stratigraphy and also discrete clasts and matrix (Palmer and Neall, 1989). Debris-avalanches typically produce hummocky, poorly-sorted and chaotic deposits that are similar to glacial tills.

Several studies have noted the superficial similarity between mass-movement and glacial striae. This has led to confusion in the distinction between glacial and non-glacial poorly-sorted deposits (e.g. Judson and Barks, 1961; Dott, 1961; Zamoruev, 1974; Schermerhorn, 1974a; Eyles, 1993; Jensen and Wulff-Pedersen, 1996, Hewitt, 1999), (see "Literature Review", Chapter One). This is further complicated by the fact that debris-flows often involve glacial or tectonically derived sediments. In these circumstances, a single mass movement deposit may include clasts striated by several different mechanisms. Thus, a better understanding of striae characteristics in mass movement deposits should help in correctly interpreting poorly-sorted deposits of unknown origin.

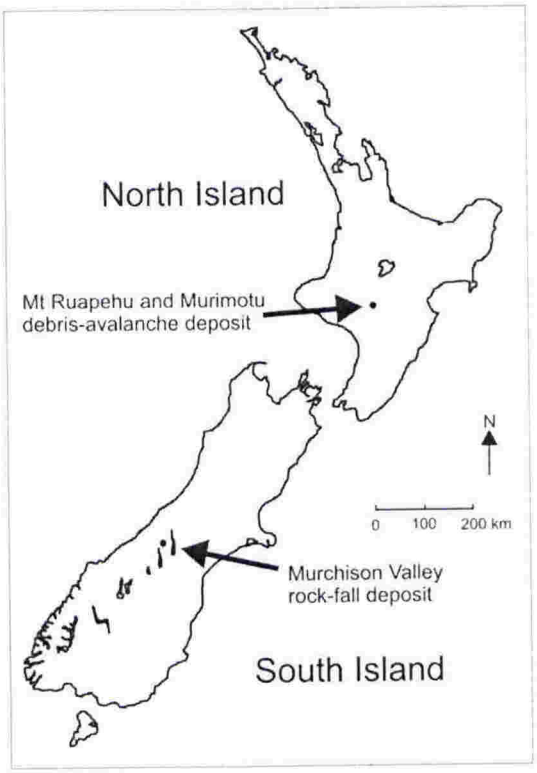

Figure 6.2 Map of New Zealand showing the location of the mass movement study sites

6.2 MURIMOTU FORMATION, (DEBRIS-AVALANCHE), MT RUAPEHU, NEW ZEALAND

6.2.1 Background

Mt Ruapehu (2797 m) is the highest mountain in the North Island, New Zealand. It is an active andesitic stratovolcano in the southern part of the Tongariro volcanic centre of the Taupo Volcanic Zone (Hackett and Houghton, 1989). A distinctive area of hummocky topography is present on the northwestern lower flank of the mountain near Highway 48 and the Chateau Tongariro (Figure 6.3 and Figure 6.4). This is part of the Murimotu Formation, which has been identified as a debris-avalanche deposit (Palmer and Neall, 1989). Striated clasts are present in the deposit and provide a clear example of non-glacial striae in a diamicton deposit.

The mounds were originally interpreted to be blisters on the surface of lava that had flowed over water-saturated ground (Hill, 1891; Bossard, 1928, both referenced in Gregg, 1960). Park (1926) described them as conical hills and interpreted them to be glacial moraines on the basis of their similarity to poorly-sorted deposits in glacial terrain. These and other "dome-shaped hills" found on the western slopes of Mt Egmont in Taranaki were later interpreted by Grange (1931) to be the result of "mudflows caused either by eruption from a crater lake, collapse of a sector of the volcano, or by the action of rain and volcanic ash on the sides of the volcano during or following an eruption". Interestingly, rare striated and faceted boulders were noted in the deposits. These were suggested to be either scratches formed in the mudflow or glacial striae on boulders incorporated into the mudflow.

The mounds have subsequently been interpreted to be the result of a debris-avalanche (Hackett and Houghton, 1989; Palmer and Neall, 1989). Palmer and Neall (1989) restricted the use of the term "Murimotu" to diamictons and breccias exposed in the area of the Whakapapanui and Whakapapaiti streams and formally named them the Murimotu Formation. The Formation covers c. 23 km^2 and contains 0.2 km^3 of material forming an irregular lobe that pinches out onto older deposits (Figure 6.3). The Formation is divided into three facies. Facies 1 and 2 are characterised by the presence of debris-avalanche blocks and hummocky surface topography. Facies 1 occupies the central axis of the formation and Facies 2 occurs along the lateral margins. Facies 3 contains few blocks and either overlies Facies 2 or occurs beyond the lateral margins of Facies 2. The deposit was interpreted as a single debris-avalanche from a gravity-driven sector collapse high on the western flank of Mt Ruapehu (Figure 6.4). The flow was initially confined in the Whakapapanui Valley before becoming unconfined in the vacinity of the Chateau Tongariro (Palmer and Neall, 1989). Timing of the event was c. 9540 years B.P from wood found within the formation (Topping, 1973).

The sampled outcrop in this study is located in the central axis of the deposit, within Facies 1 of Palmer and Neall (1989). They described Facies 1 as containing >50% debris-avalanche blocks up to 36 m long that constitute completely shattered masses of clasts and matrix-supported breccia. The deposit also contains fragments of lithified

volcaniclastic rock and subangular to angular clasts of andesite and dacite up to 4 m in length. The upper surface is hummocky with up to 10 m relief (Figure 6.4). Interestingly, Palmer and Neall (1989) make no mention of striated clasts or boulders within the deposit. Finally, it is possible that some glacially striated bedrock or moraine debris from higher parts of Mt Ruapehu was incorporated in the debris avalanche.

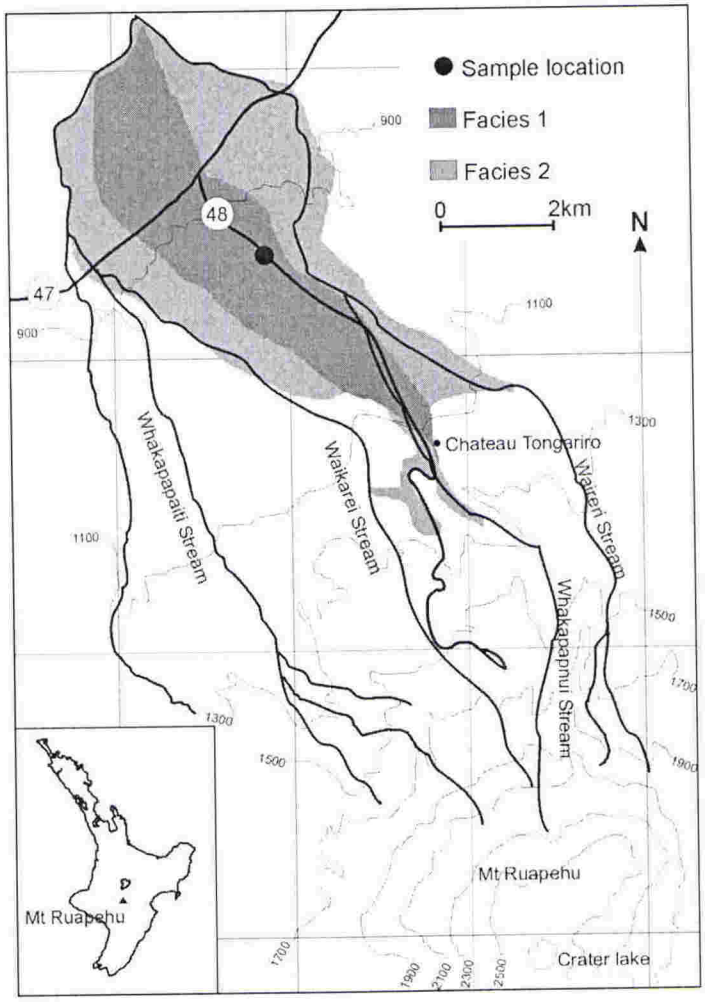

Figure 6.3 Map showing the distribution of the Murimotu Formation and sample location (modified from Palmer and Neall (1989).

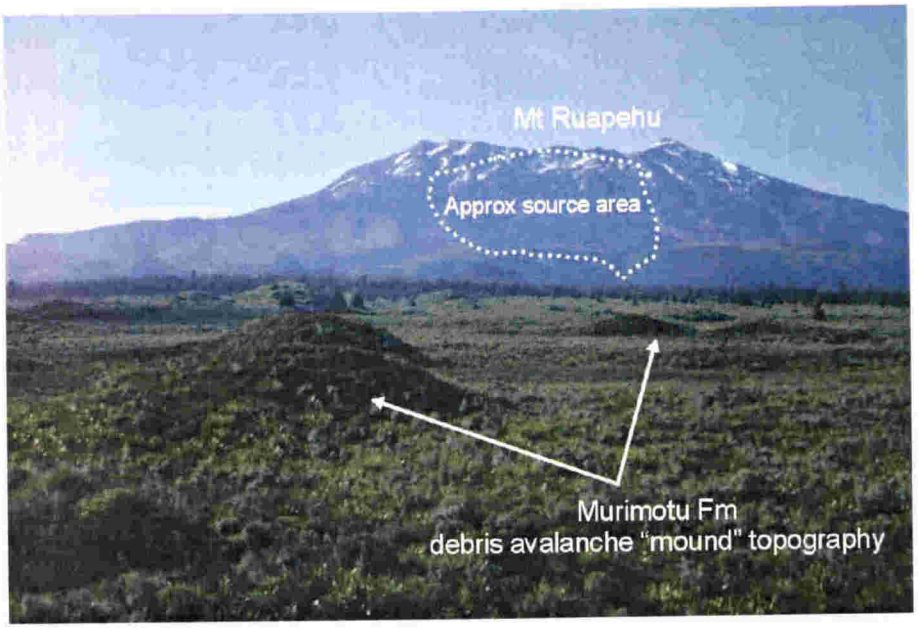

Figure 6.4 View looking southeast showing Mt Ruapehu and the Murimotu debris-avalanche mound topography in the foreground. The approximate source area of the debris is marked.

6.2.2 Fieldwork

Highway 48 dissects one of the distinctive debris-avalanche mounds of the Murimotu Formation, approximately 4.5 km by road from the Chateau Tongariro (175°30'30" 39°10'10") or 265229 NZMS 260, S19, Raurimu. (Figure 6.3). A section was measured and three units were defined (Figure 6.5). Units 1 and 2 occur within the Murimotu Formation and are mantled by the overlying air-fall deposits of the Papakai Tephra Formation (Unit 3) (Topping, 1973; Palmer and Neall, 1989). Two collections of clasts were taken from Unit 1 (Figure 6.6), one being a bulk sample of predominantly pebble-sized clasts for the purpose of clast-shape analyses, and the other being several clearly striated larger clasts were selected from the outcrop for striae characterisation.

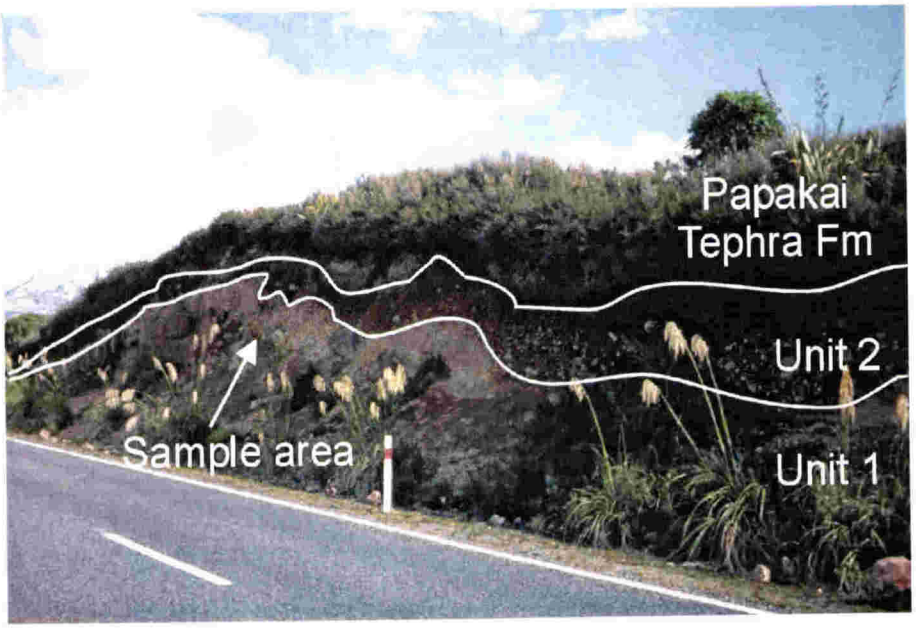

Figure 6.5 An outcrop of one of the debris-avalanche mounds showing Unit 1 and Unit 2 of the Murimotu Formation and overlying Papkai Tephra Formation. Clast sample location also shown.

Outcrop description for Murimotu Formation, Highway 48, Mt Ruapehu

UNIT 1 DIAMICTON

Lower contact obscured by scree. Matrix-supported (locally-clast supported) diamicton. Red-brown oxidised colour (particularly in centre of outcrop). Clasts range from boulders up to 1.3 m diameter to granules. Average clast size is large pebble to cobble size. Clasts are angular to subangular, some show striae. No obvious imbrication. Very poorly sorted to unsorted. Lithologies include pumice, light and dark-coloured andesite and altered andesite. Some clast surfaces show an orange/pink weathering colour and show many small striae. Matrix is coarse sand and granules. Thickness is maximum 2.3 m above scree slope to base of UNIT 2.

UNIT 2 DIAMICTON

Lower contact with UNIT 1 is distinct but gradational over 15 cm, irregular and wavy with 30-40 cm relief. UNIT 2 fines up (normal grading). Basal 50 cm is matrix to clast-supported diamicton. Red-brown colour. Clasts range from 30 cm a-axis to granules. Average clast size is approximately 5 cm. Clasts are angular to sub angular. Some show striae. No obvious

imbrication. Very poorly sorted. Matrix is sand and granules. Lithologies as in UNIT 1. Above basal 50 cm, significantly lower clast concentration. Matrix-supported. Clast size is unchanged from below and angular to subangular. Matrix is sand and silt. Upper 30 cm clast poor, dark brown paleosol horizon. Thickness of UNIT 2 is variable up to 2.0 m.

UNIT 3 LAPILLI (PAPAKAI TEPHRA FORMATION)

Lower contact with UNIT 2 is sharp and wavy with up to 50 cm relief, but mostly 20 cm. The unit is poorly sorted pumiceous lapilli. The deposit appears to drape UNIT 2 and has soil developed on the top with abundant vegetation. UNIT 3 is up to 1 m thick.

Figure 6.6 Detail of UNIT 1 (Facies 1 of Palmer and Neall, 1989) showing angular, poorly sorted diamicton with striated clasts. The bulk clast sample was taken from the area around the hammer, which is 33 cm long.

6.2.3 Clast shape

One hundred clasts were measured from the bulk sample taken from Unit 1 (Figure 6.6). Shape analyses were performed using the method outlined in Chapter 2 and clast shape data are presented in Appendix 5.

The clast sample comprises light-coloured andesite/dacite clasts (54 %), dark-coloured andesite clasts (34 %) and deeply oxidised clasts (12 %). The dark andesite clasts are slightly harder than the lighter andesite/dacite clasts and the oxidised clasts. Clast form is displayed in Figure 6.7 and shows a broad distribution with clast c:a axial ratios plotting from 0.26 to 0.83. The majority of clasts falling above 0.4 and show the highest average c:a ratio (0.54) of all environments in this study. This indicates a marked tendency toward blocky shapes and the absence of elongate or slabby clasts.

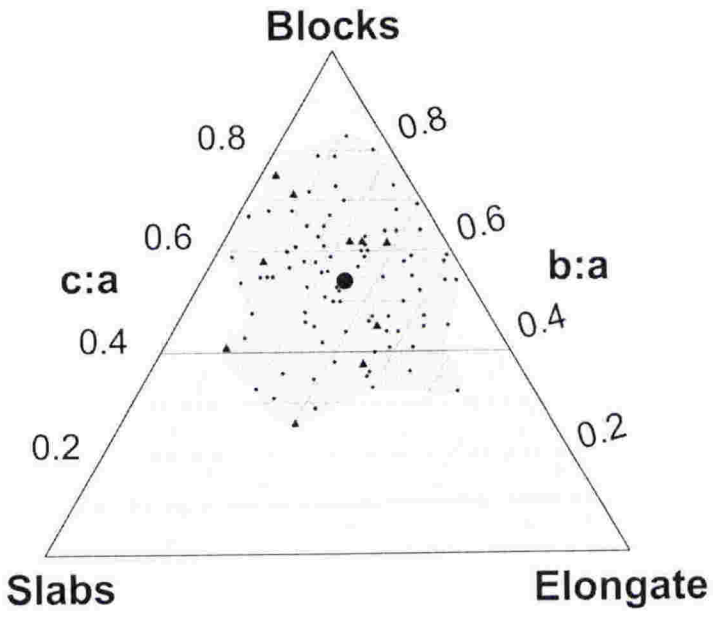

Figure 6.7 Clast form diagram showing the dominance of blocky clasts and highest average c:a axial ratio of all environments studied. Small black triangles represent striated clasts.

Clast roundness is displayed in frequency percent histograms in Figure 6.8. The distribution shows a dominance of very angular and angular clasts, with 47% in the 0.1 category, 50% in the 0.2 category and no clasts with roundness greater than 0.3. Average roundness shows the lowest value (0.16) of all environments in this study. The 0.1 class is dominated by dark-coloured andesite clasts, the 0.2 class is dominated by slightly softer light-coloured andesite/dacite clasts and the 0.3 class contains only light andesite/dacite, suggesting that lithology influences roundness.

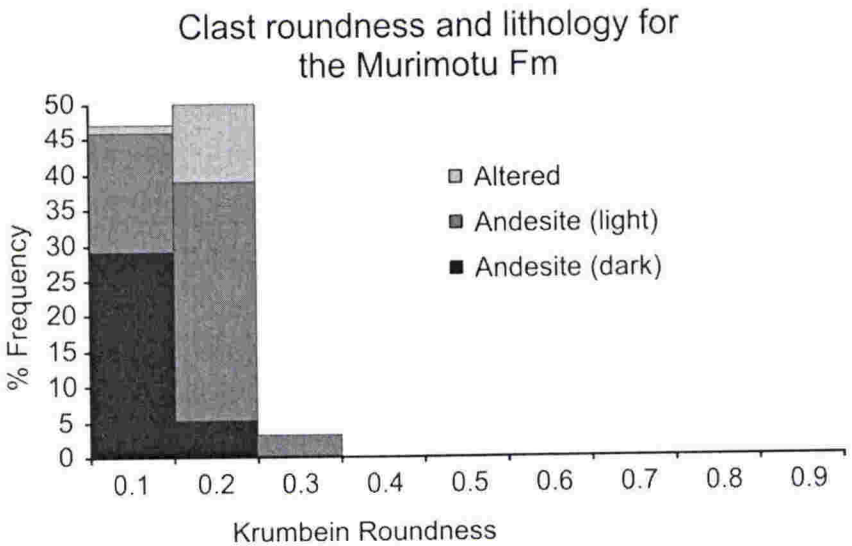

Figure 6.8 Roundness and lithology histogram for clasts from Unit 1 (Facies 1) of the Murimotu Formation debris-avalanche deposit. The sample is the most angular of all samples in this study (average roundness of 0.16).

The shape characteristics are highlighted in the covariant plot of RA index versus C_{40} index (Figure 6.9). Clasts from the sample show a low C_{40} index of only 14% and a remarkably high RA index (97%) This unusual combination of extreme angularity with blocky clast form means the debris-avalanche sample plots in a unique field on the diagram, well away from glacial, scree and tectonically influenced deposits (see summary diagram in Chapter 8 for comparison).

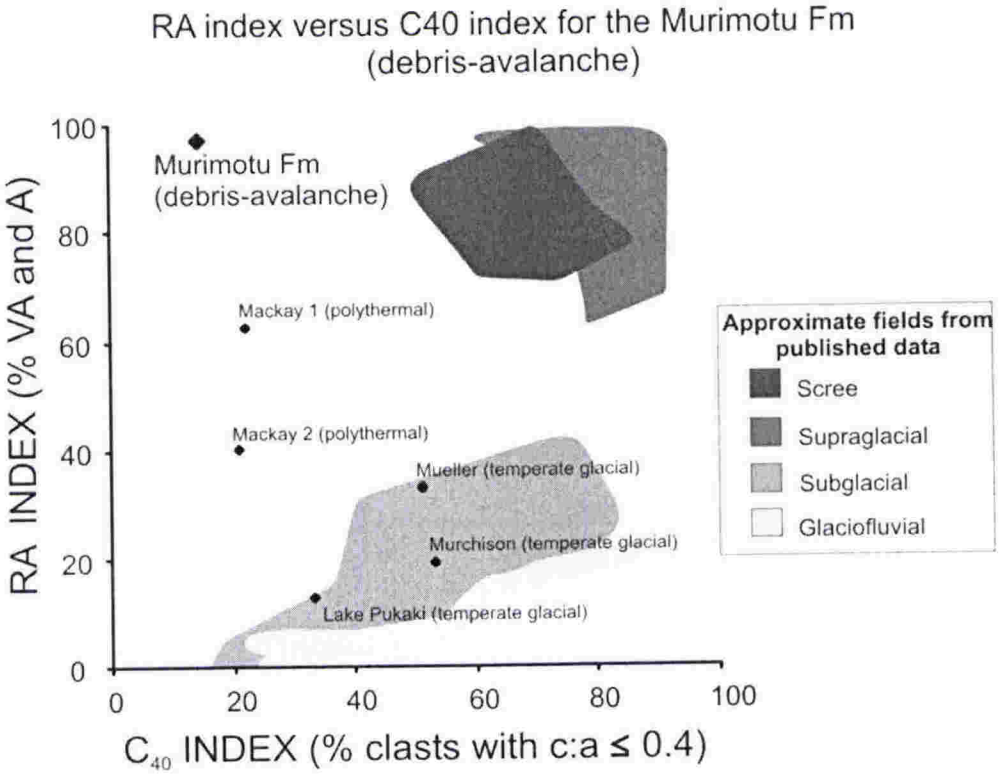

Figure 6.9 RA versus C_{40} index diagram for clasts from Unit 1 of the Murimotu Formation, which plots in a distinct part of the diagram, well away from all other samples and known fields. This reflects the very angular and blocky character of the clasts. Shaded fields are from published data in Benn and Ballantyne (1994) and Bennett et al. (1997).

Distinct planar fracture surfaces occur on 40 % of the clasts. These surfaces typically have a slightly oxidised pink and orange weathered appearance. Small-scale striae occur on 10 % of the clasts, mostly on the weathered surfaces and all of which are dark-coloured andesite clasts in the 0.1 Krumbein class. Striae occur on clasts of all shapes (Figure 6.7).

6.2.4 Character of debris-avalanche striae

Several clasts showing obvious striated surfaces were selected from the outcrop for detailed striae analyses. General observations are discussed below and additional large colour images and comments are presented in Appendix 1, "Linear Abrasion Atlas-Mass movement striae - (debris-avalanche)" and striae data are presented in appendix 5.

Although striae were recorded only on dark-coloured andesite clasts in the bulk sample, the larger clasts selected from the outcrop show striae on both dark-coloured andesite and light-coloured andesite/dacite. The striae are best preserved on weathered fracture (often flat) surfaces. The surfaces have no consistent relationship with the long axis of the clast. Parts of some surfaces show a "background" of microstriae (< 0.25 mm width and <2 mm length). Larger striae are superimposed on this background and range up to broad compound striae (4 mm wide) that have fine parallel striae on the surfaces.

Some clasts display striae with no preferred orientation and wide range in shape and size on a single surface (Figure 6.10, A and B). However, others show sets of more regular parallel striae on an individual face, occasionally sub-parallel to the long axis (Figure 6.10, C and D).

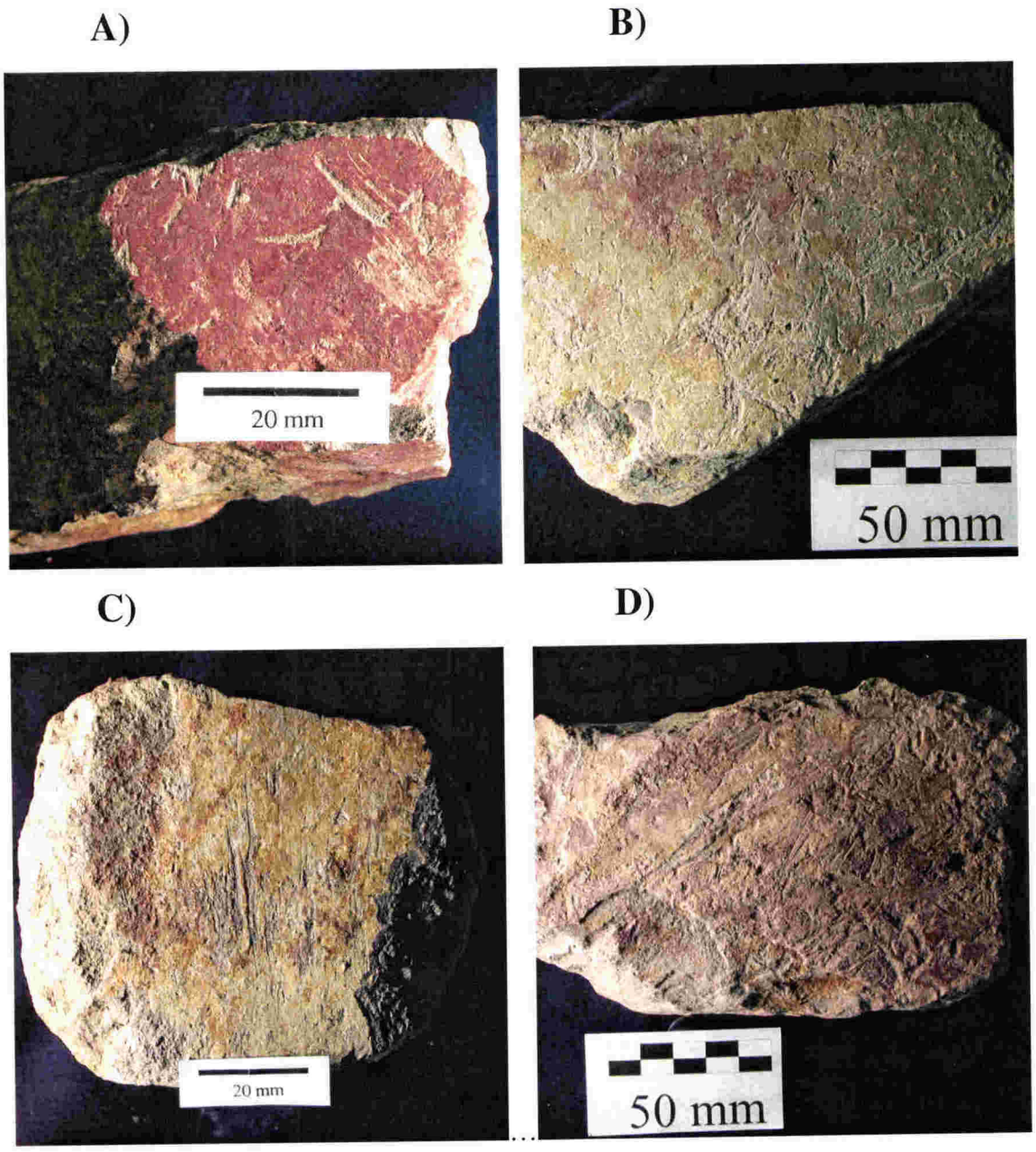

Figure 6.10 Examples of striae on weathered fracture surfaces of clasts from the Murimotu Formation. A) Well-defined striae on a weathered flat face showing weakly grouped striae, but many others at multiple orientations. B) A flat face showing a high density of small striae with only weak clustering of striae (clast 1 in Fig. 6.12). C) Parallel striae on the flat face at the end of a clast (clast 2 in Fig 6.12). D) A surface showing high density of striae, some of which are large compound striae sub-parallel to the long axis of the clast. Larger images of these and other clasts with additional comments are presented in appendix 1, Linear abrasion Atlas – Mass movements striae (debris-avalanche).

One unusual example displayed fine sub-mm width striae that appear to radiate from the centre of the clast (Figure 6.11). The surface has several larger striae superimposed on the finer striae. The process producing these splayed striae is not clear.

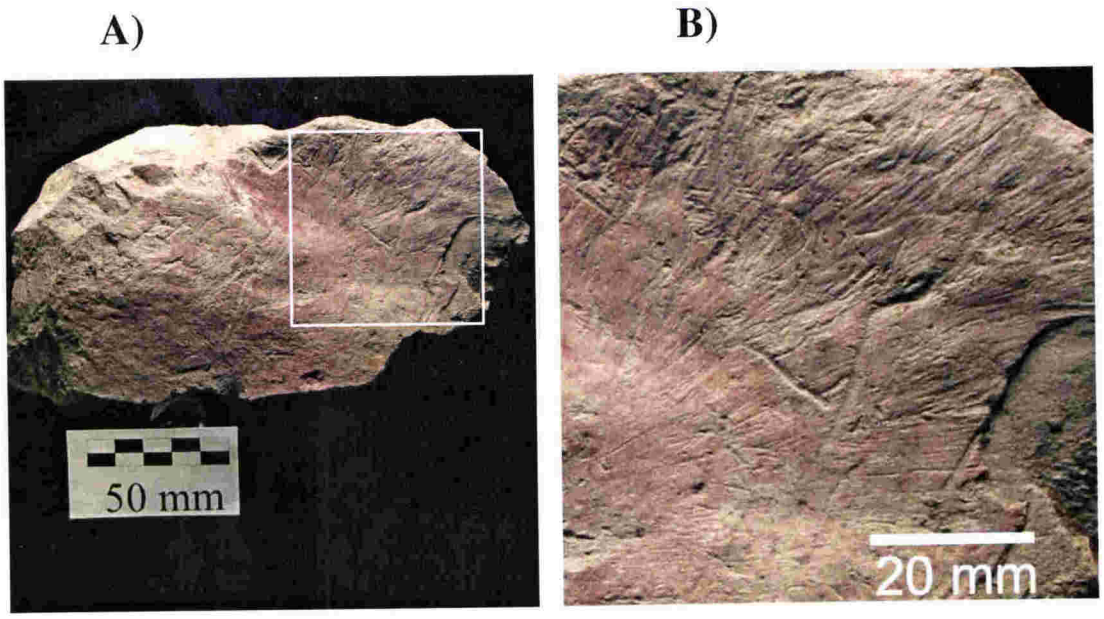

Figure 6.11 A) A striated andesite/dacite clast showing part of the surface where thin striae radiate outward from the centre of the clast. B) Closeup of the splayed striae with one striation cutting across the others. This clast is also shown in appendix 1, Linear abrasion Atlas – Mass movements striae (debris-avalanche), Images 5 and 6.

Striae orientation

Wide-ranging orientation patterns are evident on the Murimotu debris-avalanche clasts. These are displayed in Figure 6.12. Clast 1 is a large light-coloured andesite/dacite clast, which is very angular and elongate (b:a ratio of 0.65), with a flat face showing an exceptionally wide range in orientations. There are two weak clusters in orientation but it also shows the highest standard deviation (46.96) of the three clasts.

This contrasts with clast 2, which is a blocky (b:a ratio of 0.86) andesite clast. It has a flat face showing remarkably parallel striae. The face occurs on the clast end and

therefore the striae were not measured relative to the long axis of the clast. Rather, they were measured relative to an arbitrary axis that coincided with the main trend of the striae. Eighty five percent of striae occur within 30° of the arbitrary axis (180°), indicating a well-defined mode and low range (58°) and standard deviation (21°). The striae are clearly not related to the long axis of the clast indicating that parallel striae can occur on flat faces of any orientation in debris-avalanches.

Clast 3 is an elongate (b:a ratio of 0.61), light-coloured andesite/dacite clast with an undulating fracture surface showing abundant striae. The striae are moderately well grouped (standard deviation 36°) with a range of 66°, and a well-developed mode occurring between 120° and 150°, but still shows a wide range in striae orientation ranging up to 66° from the long axis, with a standard deviation of 36°.

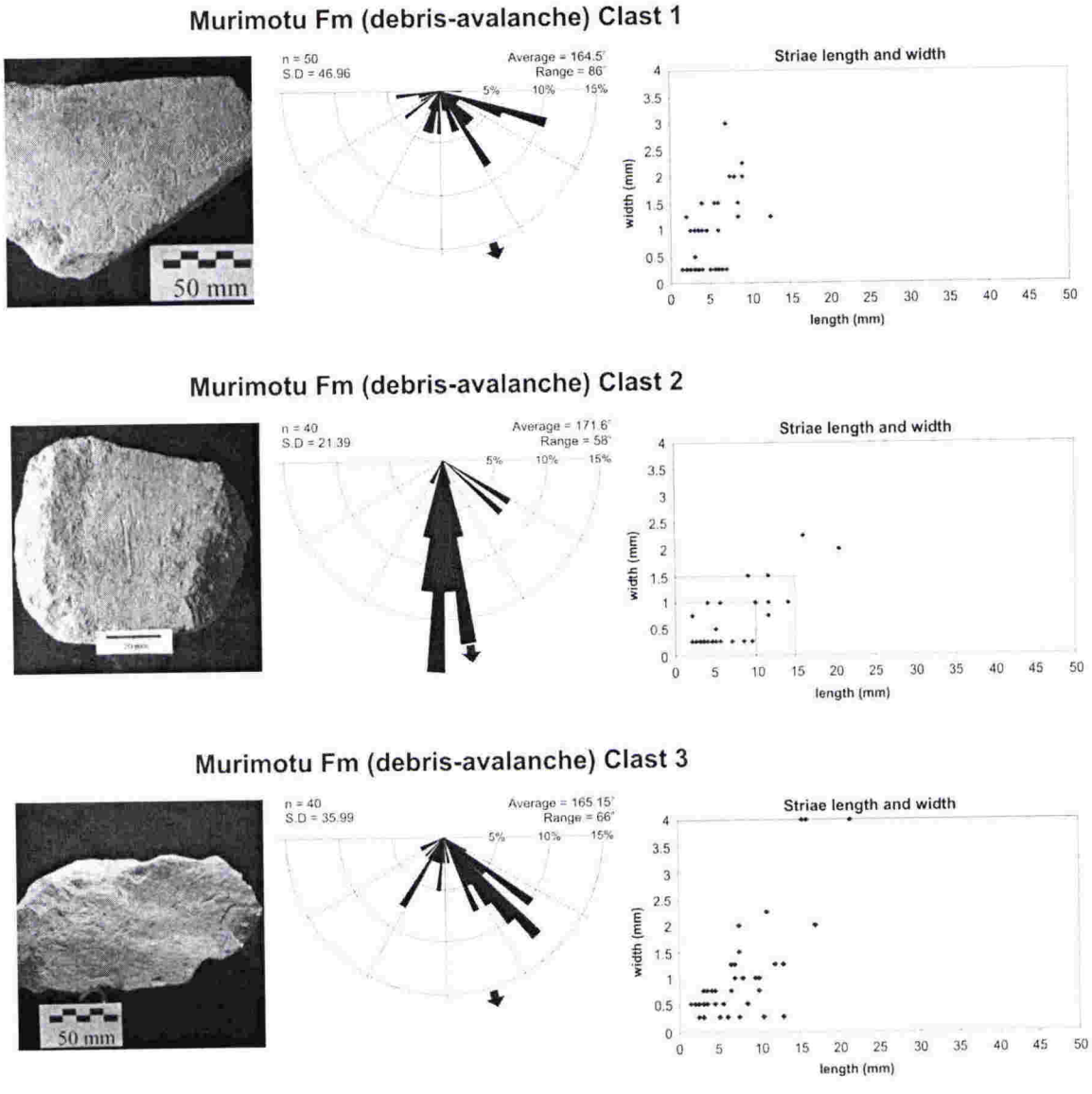

Figure 6.12 Striated clasts from the Murimotu debris-avalanche deposit. The half-rose diagrams represent the orientation of striae relative to the long axis of the clast (180°), except clast 2 (see text). Striae are grouped into 5° segments. The black arrows indicate average striae orientation. Also shown is a plot of striae length and width. Additional large colour images of these and other clasts are presented in appendix 1, Linear Abrasion Atlas-(Mass movement striae).

Striae length

Striae length is represented in Figure 6.12 and Figure 6.13. The clasts show the shortest maximum lengths and least range in striae length of all environments studied. Clast 1 shows the shortest maximum length of 12 mm, lowest average length (4.5 mm) and lowest range, despite not being the smallest clast. Clast 3 (longest clast) shows only a slightly longer maximum striae length than the smallest clast (21.5 mm and 20.5 mm respectively), as well as a slightly longer average striae length (7.3 mm and 5.6 mm respectively). These data suggest there is no obvious relationship between striae length and clast size or shape.

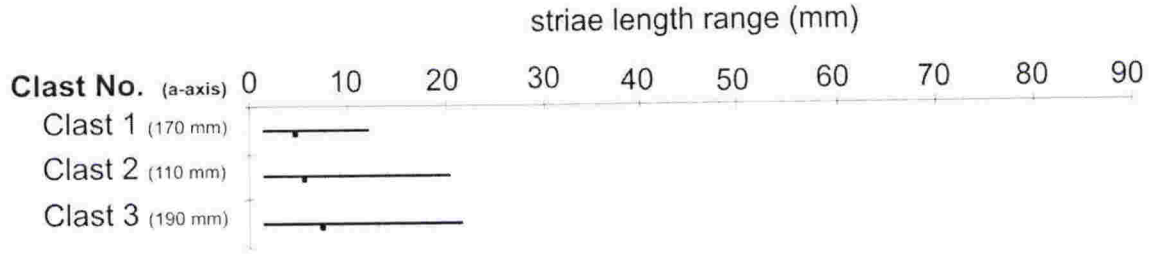

Figure 6.13 Striae length ranges and averages for the three clasts from the Murimotu Fm debris-avalanche deposit. The striae show the shortest maximum lengths and smallest range of all clasts in all the environments in this study.

Striae width

Striae width is shown in Figure 6.12 and Figure 6.14. Clast 3 is the largest clast and shows the widest striation (4 mm) and widest average (1.0 mm). The widest striae are compound striae that constitute broad scrapes, most of which have fine parallel striae on the surface. These are probably the result of a single striating rock fragment. Clast 2 is the smallest clast with the most equidimensional shape and a striated surface on one end. It shows the smallest range and average striae width. While only three clasts are

considered here, the data suggest that wider striae occur on larger and more elongate clasts.

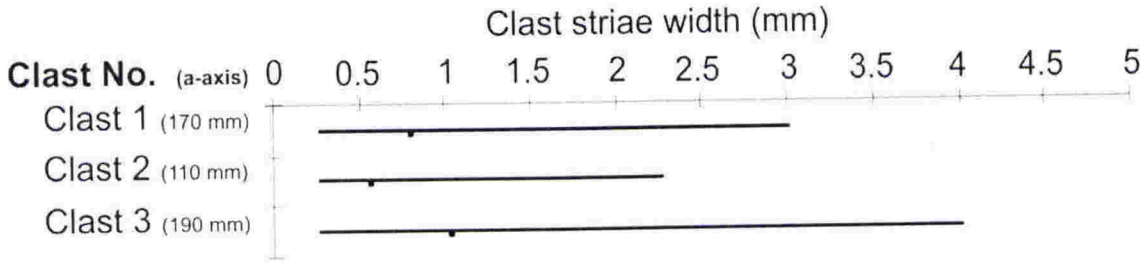

Figure 6.14 Striae width for the Murimotu Fm debris-avalanche clasts. Clast 3 (largest clast) has the widest striae and highest average width, whereas clast 2 (smallest clast) has the lowest range and average width.

Striae width and length ratios

Despite the overall shortness of the striae on the Murimotu Fm debris-avalanche clasts, the striae are relatively wide. Width divided by length ratios show that clast 1 has the highest width/length ratio (0.625) of the three clasts and is the second highest value from all environments studied (Figure 6.15). Only one polythermal glacially striated clast has a higher width/length ratio. Furthermore, clast 1 has the highest average width/length ratio of all clasts in all environments studied. This indicates that the striae are generally shorter and wider compared with striae on other clasts. Clast 2 (the smallest and blockiest clast) has the lowest average width/length ratio of the three clasts indicating that most of its striae are relatively longer and thinner than the striae on the other two clasts.

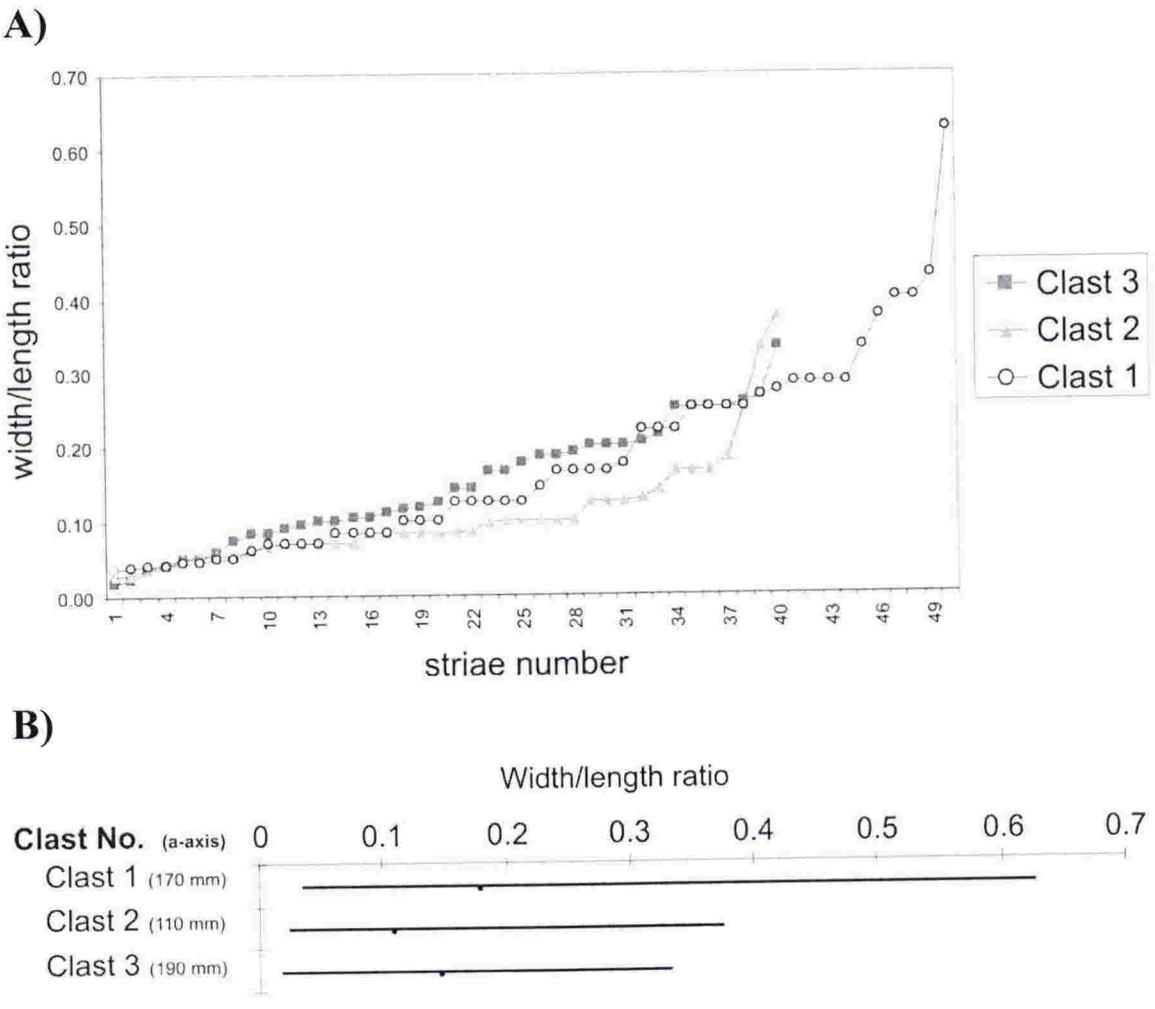

Figure 6.15 A) Width/length ratios for the Murimotu Fm debris-avalanche clasts ranked from lowest to highest. B) Width/length ratio ranges and averages show that the smallest clast (clast 2) displays the lowest average ratio (i.e. longest and thinnest striae) and the largest clast (clast 3) has the highest average ratio of all clasts in all of the environments studied.

Striae density

Striae density for the Murimotu Fm debris-avalanche shows the lowest variability in striae per cm^2 of all the environments studied, ranging from a low of 1.2 on clast 1 to a high of 1.7 on clast 2 (Figure 6.16). However, background striae density is more variable with a low of 28 % on clast 2 and higher on the more elongate clasts 1 and 3, which have values of 59 % and 56% respectively. The percentage of squares with at

least 1 striation is also variable with a low of 48 % on clast 2 due to the striae being closely grouped, whereas clasts 1 and 3 show higher values of 78 % and 79 % respectively indicating the striae are distributed widely across the clast surface. These results indicate that overall, the density of striae is lower than on glacial clasts but variable, with many combinations of individual striae, background density and distribution possible.

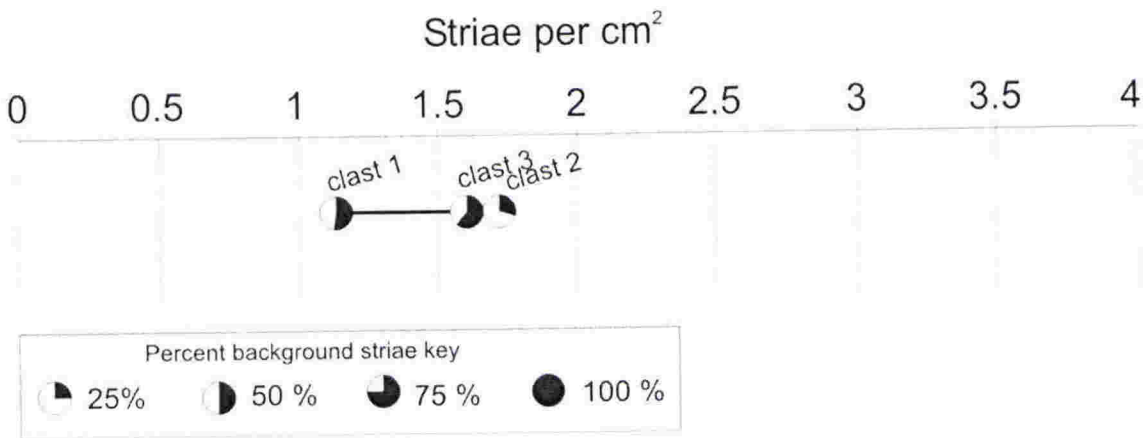

Figure 6.16 Striae density diagram showing the number of striae per cm^2 and the percentage of background striae for each clast. The clasts have the lowest range in striae per cm^2 of all environments studied.

6.2.5 Summary of the Murimotu Fm debris-avalanche deposit

The Murimotu Formation is a volcanic debris-avalanche deposit that contains clasts striated by particle collisions during the avalanche process. The deposit has distinctive clast shape characteristics. It is dominated by blocky clast form (c:a axial ratios > 0.6) with the highest average c:a axial ratio (0.54) of all environments in this study, reflecting the massive crystalline character of the source rocks that have few natural planes of weakness. The clasts are distinctly angular (0.1-0.3 Krumbein roundness) with the lowest average Krumbein value (0.16) of all environments and common flat fracture faces with sharp irregular edges. This means the clast sample plots in a unique position on the RA-C_{40} diagram, separate from glacial, rock-fall and tectonic samples. Lithology

appears to influence the roundness of the clasts with dark-coloured andesite clasts dominating the 0.1 class, and softer light-coloured andesite/dacite clasts tending to become slightly more rounded. These features are interpreted to reflect turbulent transport within the debris-avalanche, which generates frequent clast breakage and only minor edge rounding on clasts.

Striae occur on 10 % of the clasts and exclusively on very angular clasts but are not influenced by the shape of clasts. Striae occur only on the dark-coloured andesite clasts in the sample of 100 clasts, but are also present on larger light-coloured andesite/dacite clasts selected from the outcrop.

Striae occur mostly on flat, weathered faces but are also found on curved and irregular surfaces. Striae orientation ranges from random or weakly grouped, to parallel striae in exceptional cases, but these are not aligned with the long axis. A few curved striae occur on some clasts. Striae occasionally form on clast ends. This particular characteristic was also found on the tectonic clasts.

Striae length shows the lowest overall range of all environments, but striae width varies markedly reflecting the occurrence of wide compound striae on most clasts. The debris-avalanche clasts show lower striae density than glacial clasts and smallest range in striae per cm^2 of all environments. However, the density of background striae varies markedly.

6.3 MURCHISON VALLEY, (ROCK-FALL DEPOSIT), NEW ZEALAND

6.3.1 Background

The Murchison Valley is situated in the Mt Cook region of the central South Island of New Zealand (Figure 6.2). The valley contains the Murchison Glacier and an extensive gravel outwash system downstream from the glacier terminus. The valley is surrounded by steep mountain topography consisting of Mesozoic sandstone "greywacke" and argillite. The location has been used as a case study on the "survivability" of glacially striated clasts after they enter a fluvial environment. This case study, a full introduction to the area and a location map are included in Chapter 3, "Temperate glacial striae". Modern scree slopes are present on the eastern side of the Murchison Valley. These comprise largely rock-fall debris and display many angular broken clasts with striated surfaces. One site was selected to provide examples for characterisation of striae produced by the rock-fall process.

6.3.2 Fieldwork and site description

The rock-fall site is one of eleven used for the case study focussing on striae survivability. For consistency with this case study the site is named "MH 4". It is located on the eastern side of the Murchison Valley approximately 1900 m downstream from the glacier terminus. At this site, a steep scree slope encroaches the modern proglacial lake. The site consists of angular, poorly sorted, unlithified debris with clasts ranging from boulders several metres in diameter to pebbles (Figure 6.17)

Figure 6.17 Site MH 4 on the eastern side of the Murchison Valley. Active scree slopes extend into the modern proglacial lake. Note the large range in clast size and angular shape.

6.3.3 Clast shape

Fifty clasts were randomly selected from site MH 4, and clast-shape analysis was performed using the method outlined in Chapter 2. The clast data are presented in appendix 5.

The lithology of the scree clasts is dominated by indurated sandstone (66%), with the remainder being argillite (34%). Clast form is displayed in Figure 6.18. Most clasts plot lower on the diagram (low c:a axial ratios with average 0.31) toward slabs and particularly elongate forms (low b:a axial ratios).

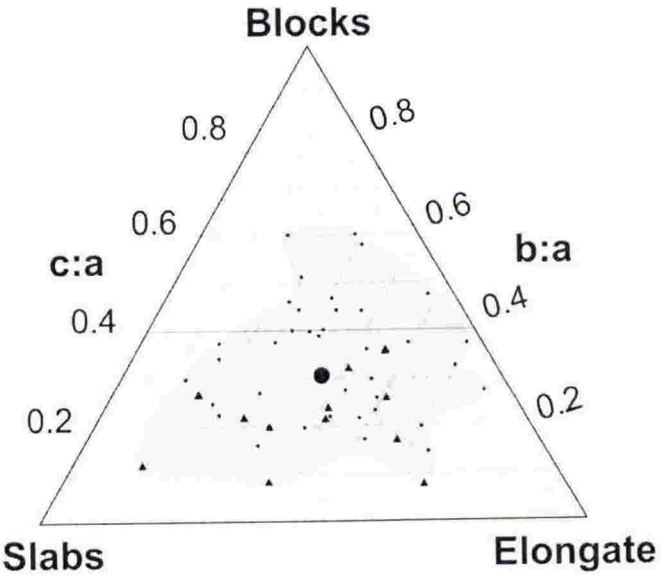

Figure 6.18 Clast form diagram for Site MH 4, rock-fall deposit. The sample shows the lowest c:a axial ratio (0.31) of all environments studied. Small black triangles represent striated clasts.

Figure 6.19 displays frequency percent histograms of clast roundness and lithology. The distribution shows roundness classes up to with 0.4 represented. Only 10% of clasts occur in the 0.1 roundness category, but a distinct modal peak in the 0.2 category (56%) and 30% in the 0.3 category, give an average roundness of 0.23 (angular).

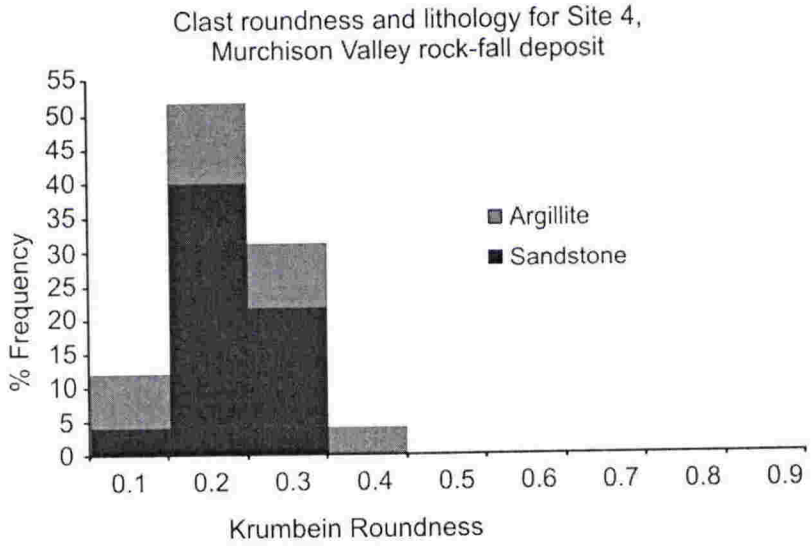

Figure 6.19 Roundness and lithology histogram for clasts from Site MH 4, rock-fall deposit. The sample has an average roundness of 0.23 (angular).

Form and roundness results are also displayed in a covariant plot of RA index versus C_{40} index (Figure 6.20). The high to moderate number of very angular and angular clasts (66%), and high percentage (78%) of clasts with c:a axial ratios below 0.4 means the sample plots high and to the right on the diagram close to the supraglacial and scree fields.

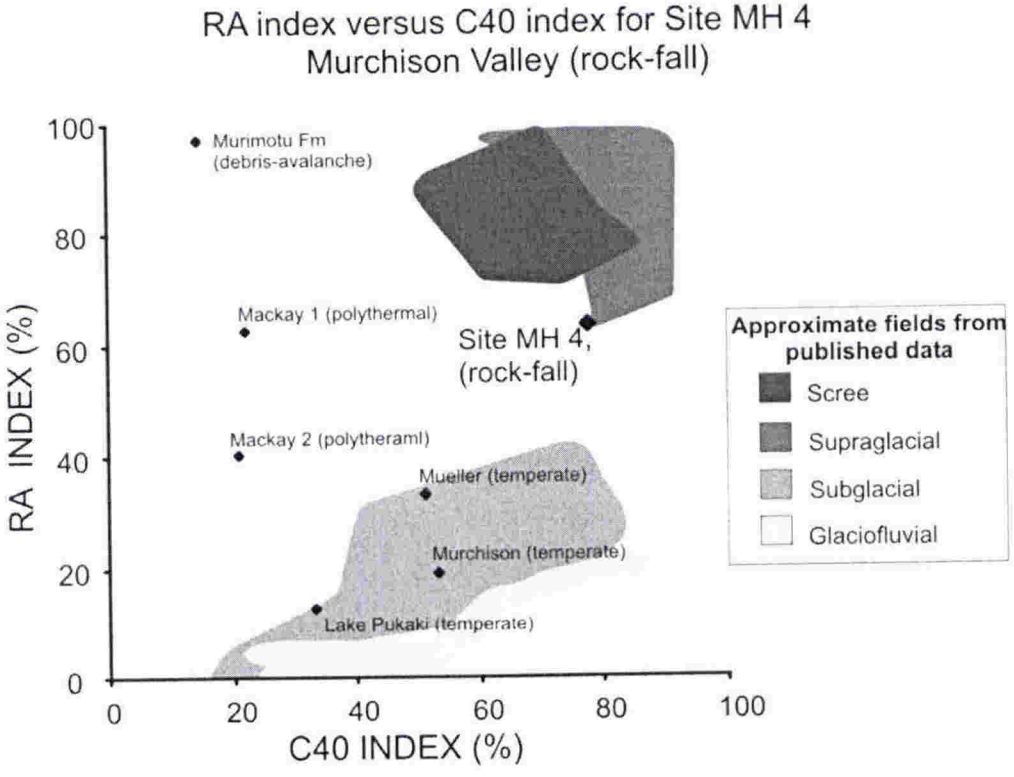

Figure 6.20 RA versus C_{40} index diagram for clasts from site MH 4, rock-fall deposit. The sample plots high and to the right on the diagram just outside the supraglacial field. The supraglacial and scree fields have a significant overlap. Shaded fields are from published data in Benn and Ballantyne (1994) and Bennett et al. (1997).

6.3.4 Character of rock-fall striae

Striae occur on 26 % of the 50 clasts samples and in all roundness categories from 0.1 to 0.4. Preservation of striae is highly dependant on lithology with only argillite clasts showing striae. This may be true only for small-scale striae on pebble-sized clasts,

because larger abrasion marks are seen on sandstone boulders. Flat surfaces are common and usually represent fracturing along bedding planes within the argillite. These surfaces are present in all roundness categories, and striae generally occur on the flat fracture surfaces. The striae range from microstriae to wide compound striae (up to 4 mm wide) (Figure 6.21). Striae orientation ranges from random to sub-parallel but there appears to be no consistent relationship between striae and long axis of the clast.

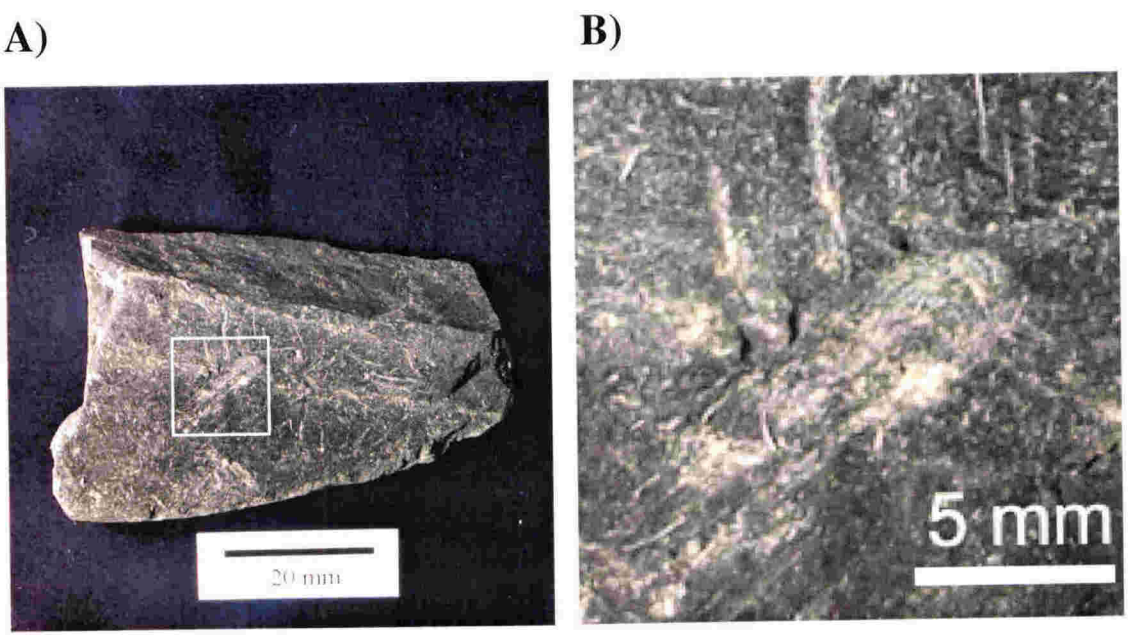

Figure 6.21 Example of an angular striated argillite clast from the rock-fall deposit. A) Randomly oriented striae on a fresh fracture surface. Striae range from microstriae to the 11 mm long, 5 mm wide compound striation (inset square). B) Closeup image of the surface showing the broad compound striation with other individual striae oriented perpendicular to the long axis (centre top of the image). This is MH 4 clast 1 in Figure 6.23.

Striae on clast surfaces at Murchison Site MH 4 vary widely in scale. On large boulders with fresh fractured surfaces, abrasion marks range from superficial scrapes to centimetre deep gouges. These were not studied in detail but nevertheless show that abrasion marks occur on clasts of all sizes (Figure 6.22).

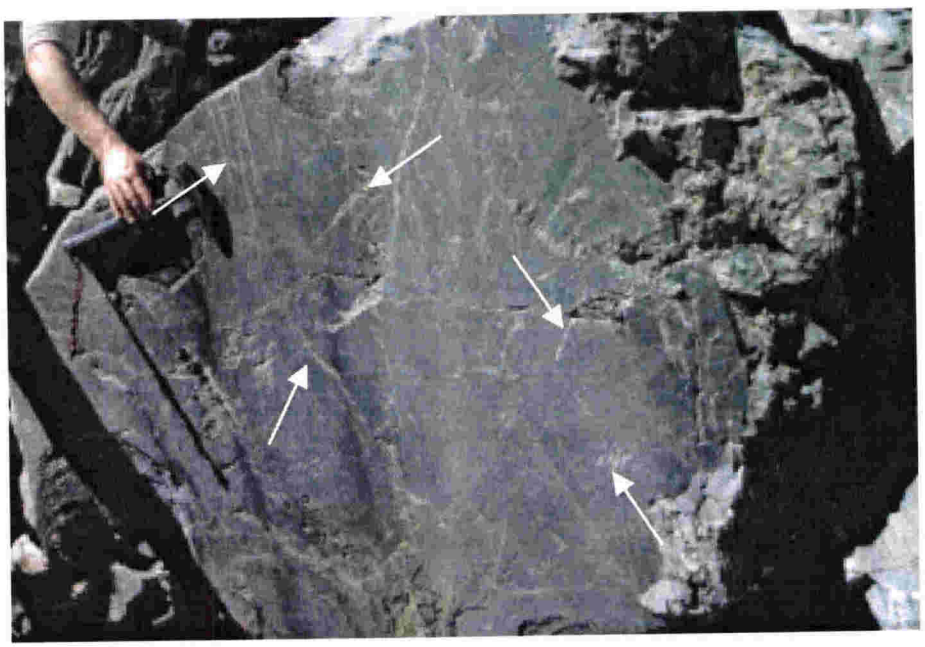

Figure 6.22 A large sandstone boulder showing a freshly broken surface and common variable abrasion marks interpreted as the product of clast collision during rock-fall on scree slopes. The most prominent abrasion marks are arrowed.

Several pebble-sized clasts showing obvious striae were selected for detailed analyses. Large colour images and notes on the main features are presented in appendix 1, "Linear Abrasion Atlas, Mass movement - rock-fall". Striae data are presented in appendix 5. Details of the striae are discussed below.

Striae orientation

Striae orientation on clasts from the rock-fall deposit was measured relative to the clast long axis as outlined in Chapter 2. The results are shown in Figure 6.23. The striae are not preferentially oriented parallel to the long axis of the clasts. Striae on clast 1 have no obvious preferred orientation and show a high standard deviation of 54°. Several of these striae are curved. Striae on clast 2 also show a high standard deviation of 62.5°. However, 54.5 % of striae are clustered between 240° and 270°, showing that some striae are oriented parallel to each other, although they are almost perpendicular to the long axis of the clast. This clast has no curved striae. Striae on clast 3 also show a similar high standard deviation of 55°. However, some striae are clustered about a mode at 240°. This clast shows one curved striation.

Although only three clasts are considered, the data show that striae on rock-fall clasts are not related to the long axis of the clast. Striae show very wide ranges in orientations on all three clasts, although two clasts show some weakly clustered striae. These results suggest that the striae are inscribed by multiple striating events, with the clasts changing orientation many times during transport. This is consistent with them having fallen, bounced and rolled down the scree slope incurring many impacts with other rock particles.

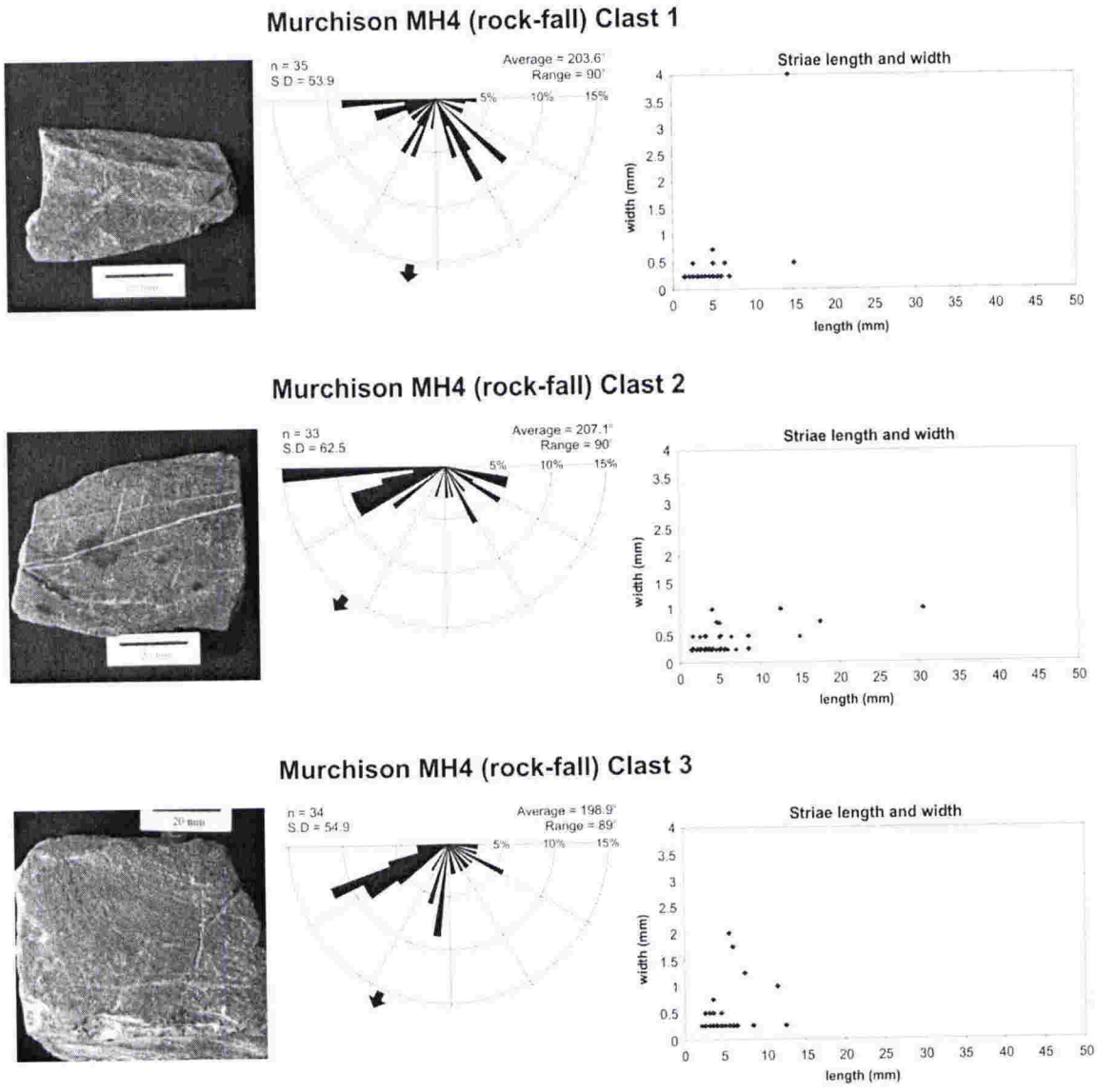

Figure 6.23 Striated clasts from MH 4 rock-fall deposit. The half-rose diagrams represent orientation of striae relative to the long axis of the clast (180°). Striae are grouped into 5° segments. The black arrows indicate average striae orientation. Also shown is a plot of striae length and width.

Striae length

Striae length does not appear to be clearly related to clast size or shape (Figure 6.23 and Figure 6.24). The shortest striae and lowest average length do occur on the smallest clast (clast 1), but the intermediate sized clast 2, has the longest striae (30.5 mm). These

two clasts have identical b:a axial ratios (0.62). Average lengths are very close although clast 3 (the largest clast) has a slightly higher average length (5.7 mm) compared with clast 1 (4.1 mm) and clast 2 (5.3 mm).

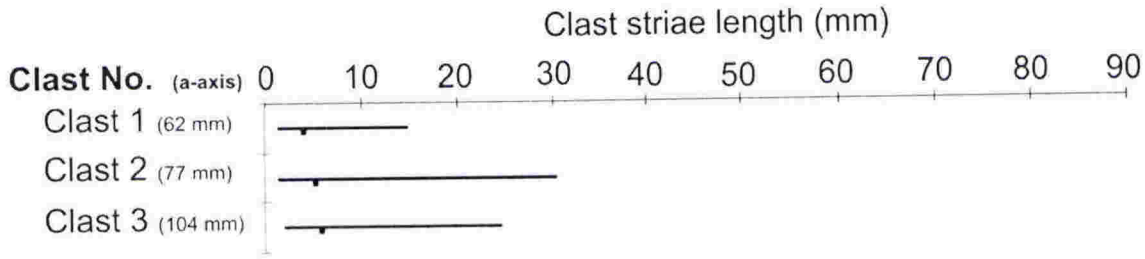

Figure 6.24 Striae length ranges and averages for the three clasts from Site MH 4 rock-fall deposit. The shortest striae and lowest average length occur on the smallest clast (clast 1) but the longest striae occur on the intermediate size clast (clast 2).

Striae width

Striae width is highly variable and is not related to clast size or shape. The widest striation (4 mm) is a compound striation and occurs on the smallest clast (clast 1). The shortest maximum striae width and smallest range occurs on the intermediate size clast (clast 2). Average widths are all low and very close. Clasts 1 and 2 have almost identical average widths of 0.41 mm and 0.4 mm respectively while the largest clast has an average width of 0.5 mm (Figure 6.23 and Figure 6.25).

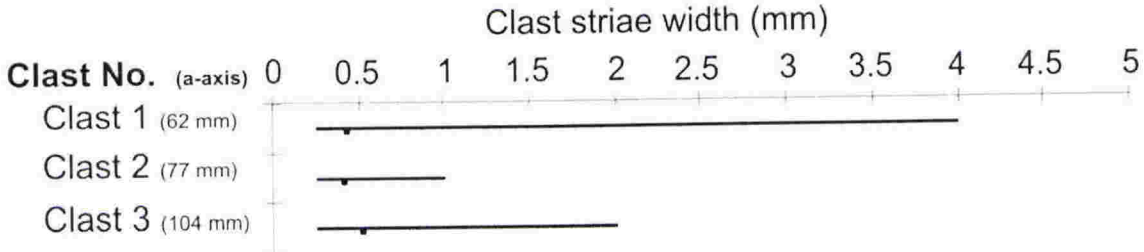

Figure 6.25 Striae widths range up to 4 mm. The widest is a broad compound striation on the smallest clast (clast 1). Average widths are all low and very close (between 0.4 mm and 0.5 mm).

Striae width and length ratios

Width/length ratios are shown in Figure 6.26. The largest clast (clast 3) shows the highest range in width/length ratio, and the smallest clast (clast 1) has the lowest range, however, average width/length ratios are similar for all three clasts indicating that striae are generally the same regardless of the clast size.

A)

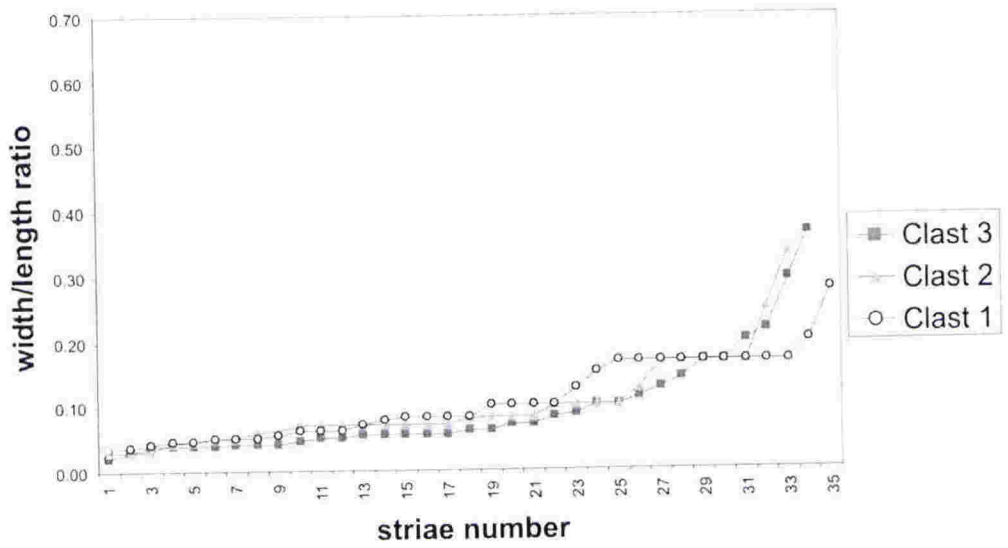

B)

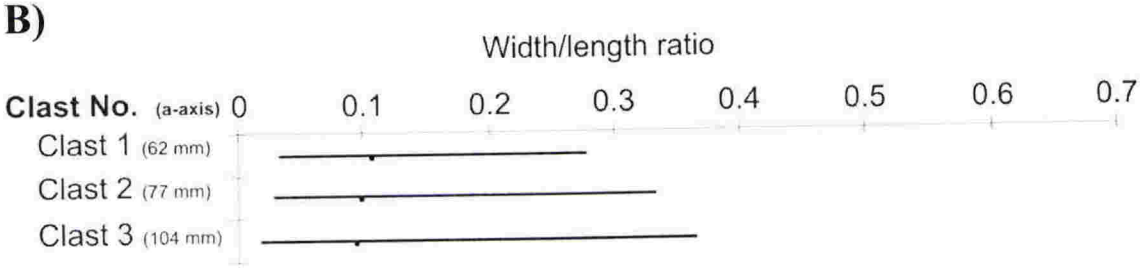

Figure 6.26 A) Width/length ratios for the three MH 4 rock-fall clasts ranked lowest to highest. B) Width/length ratio ranges and averages. The largest clast (clast 3) shows the highest range in width/length ratio, and the smallest clast (clast 1) has the lowest range in values. Average width/lengths ratios are all similar.

Striae density

The rock-fall clasts show a wide range in density (Figure 6.27). Clast 1 has the highest number of striae per cm^2 of 2.8, compared with the much lower values of 1.4 and 1.5 striae per cm^2 for clasts 1 and 2 respectively. These clasts show the widest range in percent background striae of all the environments studied. Clast 1 has 100 % background striae, whereas clast 2 has 60 % and clast 3 only 20 %, which is the lowest for all the environments studied. The percentage of counted squares showing at least 1 striation also varies widely. Clast 1 has a high of 72 % indicating striae are widely distributed whereas clasts 2 and 3 have 48% and 49 % respectively, but this reflects the scarcity of striae rather than limited distribution.

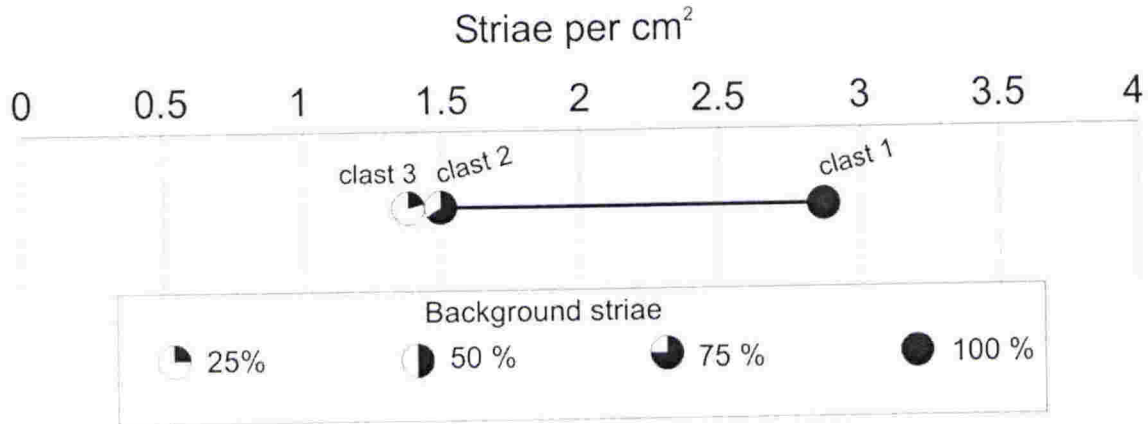

Figure 6.27 Striae density diagram showing the number of striae per cm^2 for each clast, as well as the percentage of "background" striae. This environment shows the widest range in background striae.

6.3.5 Summary of MH 4 rock-fall deposit

Clasts from Site MH 4 are the result of rock-fall. Form and roundness of pebble-sized clasts highlight the elongate, slabby and angular character of the clasts. This sample shows the lowest average c:a axial ratio of all the environments studied. This reflects

the character of the well-bedded source bedrock that breaks along bedding planes and also the limited edge rounding during the short, rapid downslope transport. These shape characteristics cause the sample to plot high and to the right on the RA-C_{40} diagram close to the unmodified "supraglacial" and "scree" fields.

Striae occur on about a quarter of clasts and are dependant on lithology, with striae occurring only on argillite clasts and most commonly on fresh, planar fracture surfaces. Striae orientation ranges from random to weakly grouped, but are not related to the clast long axes. Curved striae occur on some clasts. Average striae lengths and widths are low. However, maximum striae widths are large, despite the small size of the clasts, reflecting the presence of rare but characteristic compound striae on the clasts. The clasts show a wide range in striae density and have the largest range in background striae of all the environments studied.

6.4 COMPARISON, DISCUSSION AND CONCLUSIONS

The two forms of mass movement studied here show remarkably different shape characteristics, reflecting the character of the source rock. For the Murimotu sample, the source rock is massive volcanic andesite with few planes of natural weakness, producing blocky and extremely angular clasts that were transported by turbulent conditions within a large debris-avalanche. The Murchison clasts are derived from well-bedded and extensively fractured fine-grained sedimentary rock with a natural tendency to break along weak bedding planes, producing angular slabby shaped clasts during small-scale rock-fall. The clast shape characteristics are highlighted on the RA-C_{40} diagram with the samples plotting on different sides, but both higher than all other samples from all the environments studied.

Both samples have striated clasts (10% for Murimotu debris-avalanche sample and 26 % for Murchison rock-fall sample) and these are preferentially preserved on flat fracture surfaces. Striae occur on the ends of some blocky debris-avalanche clasts. The only other clasts that show striae on the ends are found in tectonic deposits.

Rock-fall striae have the lowest average widths of all environments studied, which reflect the smaller clast sizes. However, both samples have wide range in width measurements reflecting the occasional compound striae that occur on most clasts.

Both deposits display variable striae orientations. The Murimotu debris-avalanche shows the greatest variability, with striae ranging from multiple orientations with only weak clustering to markedly parallel but unrelated to the long axis. The Murchison rock-fall clasts either show no preferred orientation or weak clustering, again unrelated to the long axis.

For debris-avalanche clasts, the overall short, but occasionally very wide striae with common weakly clustered orientations unrelated to the clast long axis, and variable striation densities reflect the nature of clast interactions during the mass movement. These are dominated by brief, multiple collisions within a chaotic, turbulent movement of variably coherent rock fragments to produce a wide variety of abrasion possibilities on a single clast.

For rock-falls, clasts move by falling, bouncing and rolling, unconstrained by other debris. This generates numerous and frequent clast impacts varying in force depending on the size of the falling clast, producing short but occasionally wide, variably oriented striae. Density of striae depends on the number of individual impact events during down-slope movement.

The examples studied here suggest that the combined analysis of shape, roundness and surface features of clasts allow the clear distinction of between different types of mass-movement deposits. It provides a basis for distinguishing mass-movement from glacial deposits, which generally show better-rounded clasts and a higher density of long, thin striae parallel to the clast long axis that reflects the continual traction of striating rock fragments over the clast surface.

CHAPTER SEVEN

TECTONIC STRIAE

7.1 INTRODUCTION

This chapter documents striae formed by tectonic movements by examining two locations where conglomerate clasts and boulders have been incorporated into shear planes of major active faults. The study sites are located in the southern North Island, New Zealand. The first site is the Ngapotiki Fault, where Mesozoic greywacke bedrock contacts modern beach gravels and the second site has Mesozoic greywacke in contact with Holocene fluvial conglomerate along the Wellington Fault (Figure 7.1). These provide examples of tectonically striated clasts for comparison with glacial and non-glacial striae.

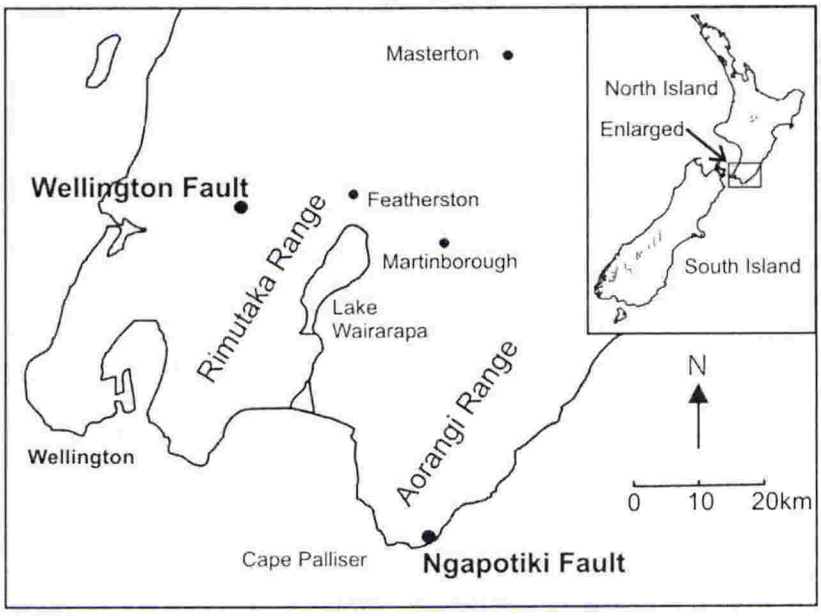

Figure 7.1 Map of lower North Island, New Zealand showing location of active faults where tectonically striated clasts were collected.

7.1.1 Tectonic abrasion nomenclature

Structural geologists have long recognised shiny, polished surfaces and linear features on fault plane slip surfaces and used them as kinematic indicators of fault movement (e.g. Tija, 1964, 1971; Petit, 1987; Lundin, 1989; Fry, 1992). These features are formed during frictional sliding by removal of material by abrasion and by "plastering" on of material through adhesion. A variety of terms have been used to describe various tectonic features formed in these ways. These include terms such as *striation*, *groove*, and *tool mark*, which are widely used in glacial geology (e.g. Eyles and Boyce, 1998; also see literature review, Chapter 1) but also include terms such as *slickenside* and *slickenline* that are usually restricted to structural geology. The terminology has many inconsistencies in the meaning of specific terms even within structural geology literature (Fleuty, 1975).

Slickensides have been defined as "polished and smoothly striated surfaces that result from friction along the fault plane" (Gary et al., 1977). However, the term slickenside appears to be used liberally and is often interchanged with "striation", slip lineation and slickenline. This not only confuses the distinction between planar and linear features, but also the distinction between abrasive, adhesive and fibrous growth features. Fleuty (1975) recognised the widespread confusion concerning the term slickenside, noting that it had become common practice to use slickenside to describe linear features such as striae or grooves as well as the "polished surface" (see Fleuty, 1975 and references therein). He stated that "Such confusing usage for a simple, common term seem quite unnecessary, leads to misunderstanding and poor communication of information". To remedy this, the following terms and definition were proposed.

- *Slickenside*: "A polished and commonly, though not invariably, striated shear surface in rocks".
- *Slickenline*: "A linear structure, either striation or grooving, resulting from friction on a slickenside".

- *Slickenstep* (Slickenside step):"A minute step feature on a slickenside, usually approximately perpendicular to slickenlines".

Finally, Fleuty (1975) also acknowledged that other features variably described as slickensides, slickenside striations and slickenside steps are not produced by friction and abrasion, but are in fact "bundles of overlapping quartz or calcite fibres.

Despite this attempt to clarify the terminology, many workers persisted with the liberal use of such terms. Means (1987) recognised this broad usage and extended the term slickenside to cover a wide range of linear features on fault planes. This included "classical slickensides", which refers to smooth or shiny fault surfaces (slickensides of Fleuty, 1975) that are commonly striated in the slip direction, to less shiny types where the lineation dominates, such as mats of parallel crystal fibres, vein bearing, non fibrous surfaces with parallel slip lineation and surfaces of lineated gouge.

Means (1987) described six types of slip-parallel linear features on slickensides.

1. *Grooves or scratches resulting from asperity ploughing* - Produced by a proturbance that is part of one sliding surface, or as a piece of debris between the surfaces, with excavation accomplished by a variety of brittle or ductile deformation processes. Terms such as "wear grooves", "wear tracks" or "tool tracks" are used.
2. *Debris streaks* -Slip parallel elongate bodies of gouge formed either by the wearing down of a soft asperity leaving a streak on the other surface or by the "piling" up of debris fore and aft of the asperity, as in a manner claimed for some glacial drumlins.
3. *Erosional sheltering* - Tails of erosion-sheltered material on the down slip side of hard asperities in the same manner as "crag-and-tails".
4. *Fibre growth* - Fibres and rods of vein material (commonly quartz and calcite) that fill potential voids behind steps or asperities.
5. *Slickolite formation* - Dissolution surfaces with spikes and columns pointing in the displacement direction. These are the inverse of crystal fibre slickenside lineations.

6. *Nested ridge-in-groove lineations* - Corrugated surfaces of nested ridges and grooves that match each other on both sides of the fault plane.

7.1.2 Tectonic abrasion on fault surfaces

Hancock and Barka (1987) presented a detailed description of linear structures on slip planes from normal faults in western Turkey. They recognised a hierarchy of linear abrasion features listed in Table 7.1.

Table 7.1. Average dimensions of slip-parallel lineations on fault surfaces (Hancock and Barka, 1987).

Lineation type	Width or wavelength (mm)	Depth or amplitude (mm)	Length (mm)
Scratch-like striae	1	0.5	<200
Groove-like striae	20	5	<300
Tool tracks	30	15	>1140
Gutters	45	25	ca 2500
Minor corrugations	50	20	ca 3000
Major corrugations	450	60	ca 10000
Mega corrugations	4500	250	ca 15000

Striae are described as ranging from *scratches* to *minor grooves*, with scratches being most characteristic of the polished areas of slip planes, often superimposed on larger forms such as *tool tracks*, *gutters* and *corrugations*. Tool tracks are described as isolated *score marks* (abrasive), and some are deeper at the up-slope end and others deeper at the downslope end. Levee-like ridges, a few millimetres wide and high flank the edges of some tool tracks. These tool tracks have been variously described as "*prod marks*" (Tija, 1971), "*wear tracks*" or "*wear grooves*" (Means, 1987). Striae, grooves and tool tracks are all abrasion features produced by "asperity ploughing" described by Means (1987). Gutters are described as rectilinear, steep sided, flat-floored channels a few centimetres wide but do not, unlike striae, define a pervasive lineation on slip planes.

Iverson (1991) noted the similarity of some glacial striae to features found on fault surfaces, and Eyles and Boyce (1998) documented grooves ranging from a few millimetres wide and less than 20 cm long, up to 4 cm wide and 30 cm long on tectonic slip planes. Other features included crescentic fractures and positive relief features such as ridge-in-groove marks (less than 1 cm high and 2 cm wide) similar to "rat-tail" glacial structures that form as a ridge in the lee of a hard asperity and taper away. Eyles and Boyce (1998) concluded that the gouge (diamict) produced by low grade shearing along fault planes is directly comparable to deformation till (diamict) formed by pervasive shearing beneath soft-bedded ice sheets. In their view, both diamict facies are tectonically generated cataclasites, which display morphologically identical, but differently scaled, genetically related features.

7.1.3 Tectonic striae on clasts

Reports that refer to tectonically striated clasts are much fewer (e.g. Judson and Barks, 1961; Pettijohn, 1956; Clifton, 1965; Robertson, 1971; Schermerhorn, 1974a; Winterer, 1963; Rattenbury and Sporli, 1985, Eyles and Boyce, 1998; see literature review in Chapter 1). Perhaps the most detailed is that by Clifton (1965). He described polished and striated pebbles from deformed conglomerates of various ages in the United States. The striae are parallel microstriae typically between 0.1 and 0.5 mm long and 0.01 and 0.05 mm wide on polished pebble surfaces although larger "gouges" several mm long and up to 1.0 mm across showing internal striae were also noted. Striae on opposite faces of the same clast were generally parallel and over 50% of clasts showed striae parallel to the long axis of the clast. Finally, he also noted that the striae commonly were parallel to fracture planes in the clasts and oriented normal to the overall structural trend of the area. More recently, Eyles and Boyce (1998) reported that some clasts on tectonic slip surfaces have flat-iron or bullet shapes and exhibit unidirectional striae parallel to the ridges. They also noted the similarity between these and glacially striated clasts. In the next section, two new occurrences of tectonically striated clasts are reported.

7.2 NGAPOTIKI FAULT, WAIRARAPA, NEW ZEALAND

7.2.1 Background and setting

The Ngapotiki Fault is located in the southeast Wairarapa region on the East Coast of the North Island, New Zealand. It lies on the eastern side of coastal ranges on the leading edge of the Australian plate within the "Hikurangi forearc", a fold-thrust belt/ subduction complex (Lewis and Pettinga, 1993). The fault is active and juxtaposes the Late Jurassic-Early Cretaceous greywackes of the rapidly rising Aorangi range with Late Miocene marine strata (Figure 7.2). The fault contact strikes approximately north-south and dips west at about 45° (Grapes et al., 1997). Raised beach ridges and tilted Quaternary terraces indicate an uplift rate of 0.8 m/ka.

Te Rakauwhakamataku Point is a prominent boulder bank extending several hundred metres offshore from the present sea-cliff near where the Ngapotiki fault intersects the coast. It is considered to have formed within the last few hundred years and may record the last coseismic displacement of the Ngapotiki Fault (Grapes et al., 1997). The inferred position of the Ngapotiki Fault contact between greywacke and Miocene mudstone lies east and seaward of the modern beach. However, a secondary low-angle pug-lined thrust plane has formed within a wide zone of sheared greywacke that forms the hanging wall of the Ngapotiki Fault and is exposed in the present sea-cliff at the base of the headland. This has created a situation where crushed greywacke is thrust over the modern beach (Figure 7.3). Several rounded beach boulders and associated beach gravel is partly enclosed and overlain by greywacke cataclasite in the thrust plane. The upper surfaces of the larger boulders display obvious abrasional striae. The striae trend 094°, which is identical to the trend of slickenlines developed on the thrust plane of the Ngapotiki Fault further inland, confirming a tectonic origin for the striae and the close relationship between the main and secondary thrusts (Grapes et al., 1997).

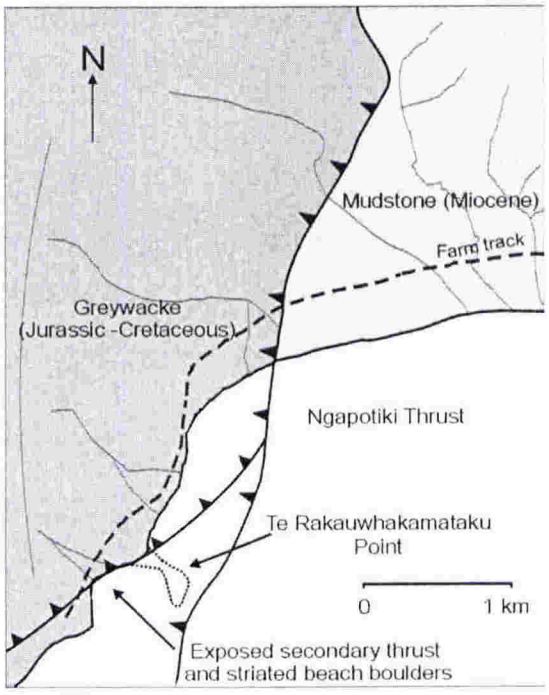

Figure 7.2 Location map showing the Ngapotiki Fault separating Jurassic–Cretaceous age greywacke and Miocene mudstone. A secondary thrust plane has developed east of the main fault at the base of Te Rakauwhakamataku Point (modified from Grapes et al., 1997)

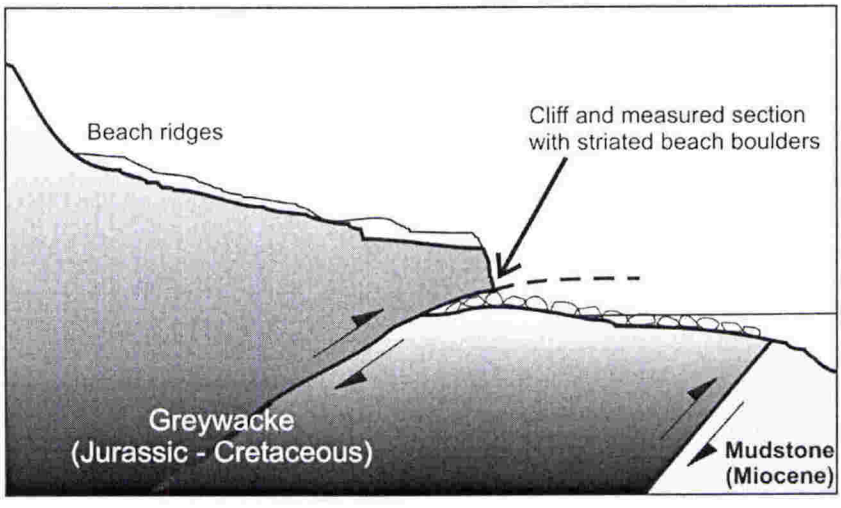

Figure 7.3 Schematic cross-section showing the Ngapotiki Fault and secondary fault, thrusting crushed greywacke over beach boulders at Te Rakauwhakamataku Point (modified from Grapes et al., 1997).

7.2.2 Fieldwork

Fieldwork consisted of describing and measuring the sea-cliff outcrop of the secondary thrust plane at Te Rakauwhakamataku Point. A bulk clast sample was collected from the sheared conglomerate layer immediately surrounding one of several large, *in situ* striated boulders at the base of the outcrop at the modern beach level. The sample site is located at (175°22'10"E 41°35'05"S).

Outcrop description of secondary Ngapotiki Fault (south to north) at Te Rakauwhakamataku Point

UNIT 1 GREYWACKE BRECCIA

Indurated sandstone and argillite (greywacke). Variably brecciated with abundant deformed quartz veins, but some original bedding present. UNIT 1 becomes increasingly brecciated along outcrop (northward) toward UNIT 2. A vertical shear zone about 1 m wide occurs 17 m before the contact. The shear zone shows fine, grey fault gouge with broken quartz veins. UNIT 1 is 30 m wide.

UNIT 2 GREYWACKE CATACLASITE

Contact with Unit 1 is gradational and marked by an increase in deformation. Pervasively deformed greywacke with abundant broken quartz veins and multiple shear planes at various angles showing fault pug (gouge) texture. One dominant shear plane cuts across the outcrop from south to north at 40°. The shear plane consists of fine grey fault pug (gouge) with abundant fractured greywacke clasts up to 10 cm in diameter. UNIT 2 is 23 m wide.

UNIT 3 SHEARED CATACLASITE WITH STRIATED BOULDERS

Contact with UNIT 2 is gradational, marked by the presence of striated boulders along the base of the outcrop. UNIT 3 is similar to UNIT 2 but overlies and partially encloses beach boulders. The boulders occur at beach level and are up to 1.5 m diameter. The boulders are greywacke sandstone and subrounded. Several display parallel striae on the upper surfaces. Irregular layers and pockets of tectonically sheared clasts and rounded beach clasts occur around the boulders.

Some of these clasts show striae. This is where the bulk clast sample was collected. UNIT 3 is 53 m wide.

UNIT 4 GREYWACKE BRECCIA

Contact with UNIT 3 is gradational and marked by a lack of obvious shear planes. UNIT 4 is similar to UNIT 1 and consists of variably brecciated greywacke with abundant quartz veins and remnants of original bedding are present.

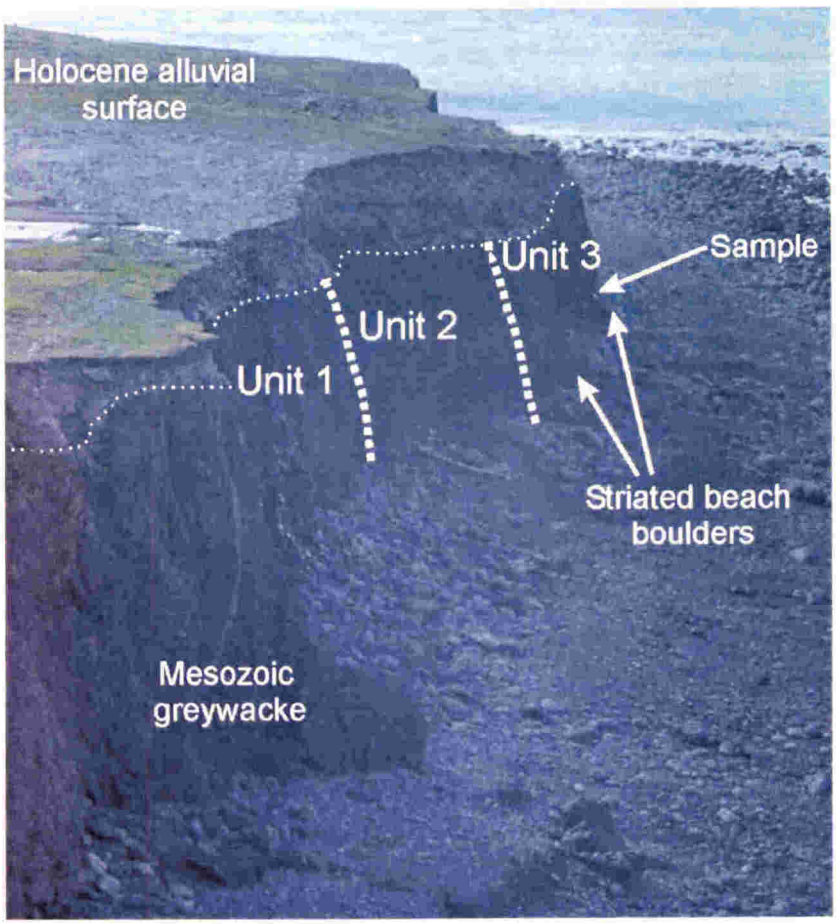

Figure 7.4 Exposure of the shear zone associated with the secondary Ngapotiki Fault, Te Rakauwhakamataku Point. UNITS 1 to 3 and sample location are shown. The general direction of thrust movement is from left to right over the beach. The sea cliff subsequently erodes back to expose the tectonically striated clasts.

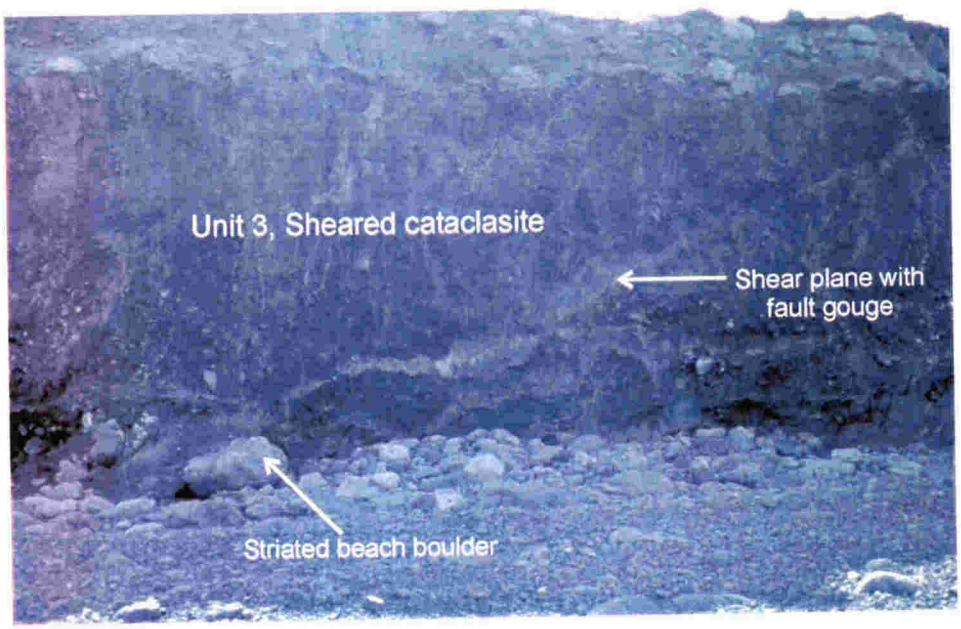

Figure 7.5 The sea cliff exposing sheared cataclasite of UNIT 3 and *in situ* overthrust striated beach boulders. Discrete shear planes occur within the cataclasite.

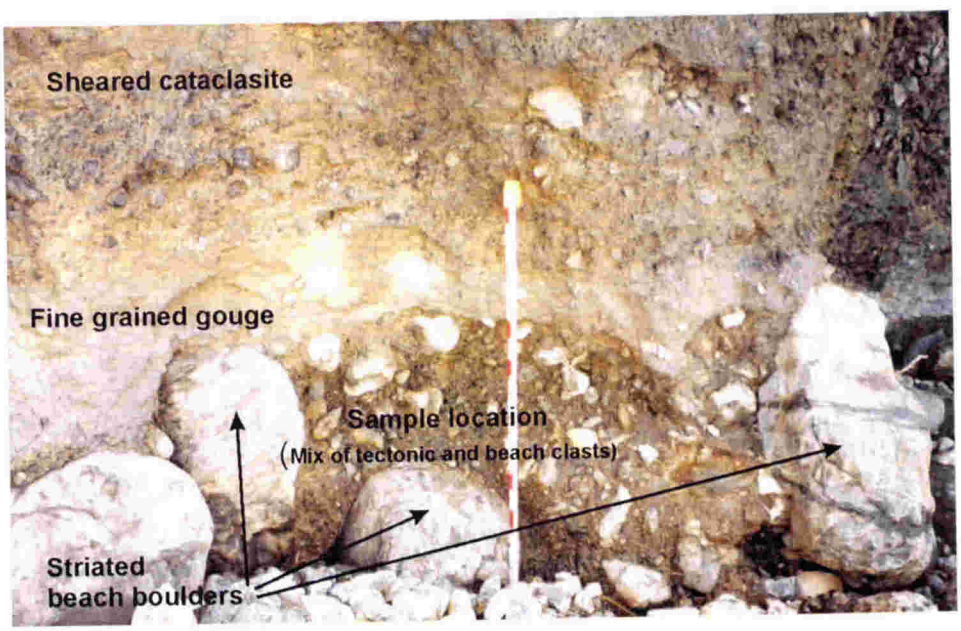

Figure 7.6 Closeup of *in situ* striated beach boulders within UNIT 3. A shear plane with fine-grained fault gouge is visible above the boulders. The sample was taken from the deformed layers and pockets of clasts comprising a mix of tectonic and beach clasts around the larger beach boulders. This outcrop is approximately 10 m to the left of the outcrop shown in Figure 7.5.

7.2.3 Clast shape

The bulk sample collected from the sheared conglomerate in Unit 3, provided 100 clasts for shape analysis that was performed using the method outlined in Chapter 2. The clast data are presented in Appendix 6 -Tectonic clast data.

The clast sample contains more sandstone (54%) than argillite clasts (46%), derived from the local "greywacke" terrain. Clast form is displayed in Figure 7.7 and shows a broad distribution with clast c:a axial ratios plotting from 0.16 to 0.7 (average is 0.45), indicating a slight tendency toward blocky shapes. This is similar to the average c:a axial ratios measured for temperate glacier clasts.

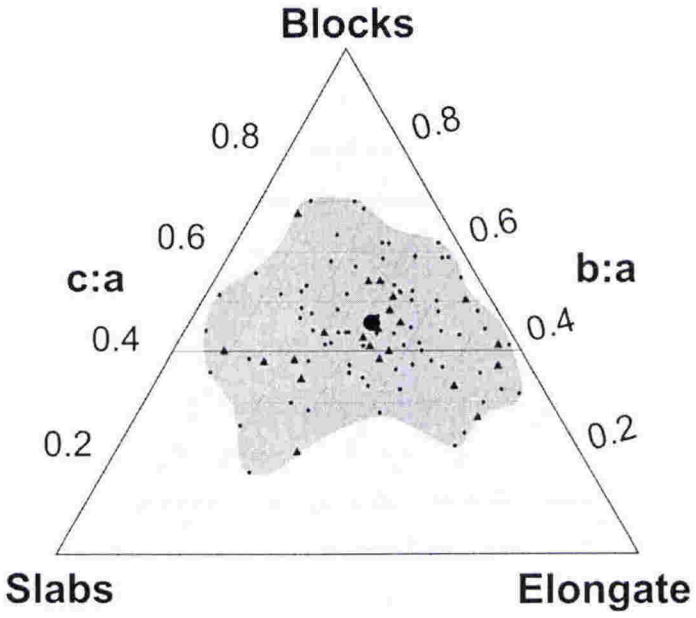

Figure 7.7 Clast form diagram showing a dominance of blocky clasts from a shear zone (Unit 3) of the secondary Ngapotiki Fault. The average c:a axial ratio is 0.45 (large black dot). Small black triangles represent striated clasts.

Roundness and lithology are displayed in frequency percent histograms in Figure 7.8. The distribution again shows a broad distribution, with all Krumbein roundness classes up to 0.7 represented, reflecting the mix of angular tectonically fractured or tectonically generated clasts with the better rounded beach clasts. The average roundness is 0.33

(subangular), which is similar to average roundness for temperate glacial clasts. There is no significant trend of one particular lithology (sandstone or argillite) in any roundness class. Twenty one percent of the clasts showed evidence of tectonic fracturing. Slightly more sandstone clasts (24 % of total sandstone clasts) showed this as compared with 17 % of argillite clasts and these occur on clasts in all roundness classes except 0.7 (well rounded).

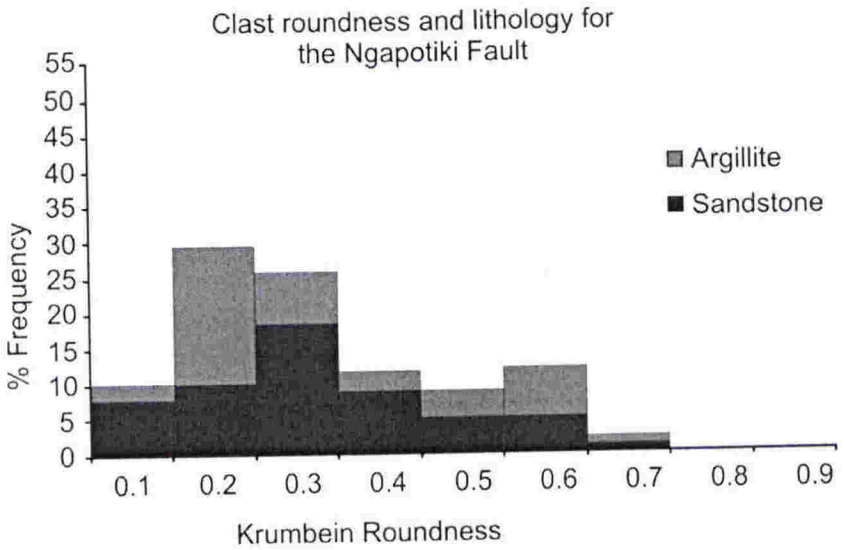

Figure 7.8 Roundness and lithology histogram for clasts from the shear zone (Unit 3) from the Ngapotiki Fault. The average roundness is 0.33 (subangular).

Shape characteristics are highlighted in the covariant plot of RA index versus C_{40} index (Figure 7.9). The sample has an RA index of 39 and C_{40} index of 32, reflecting the wide range in roundness and intermediate clast form.

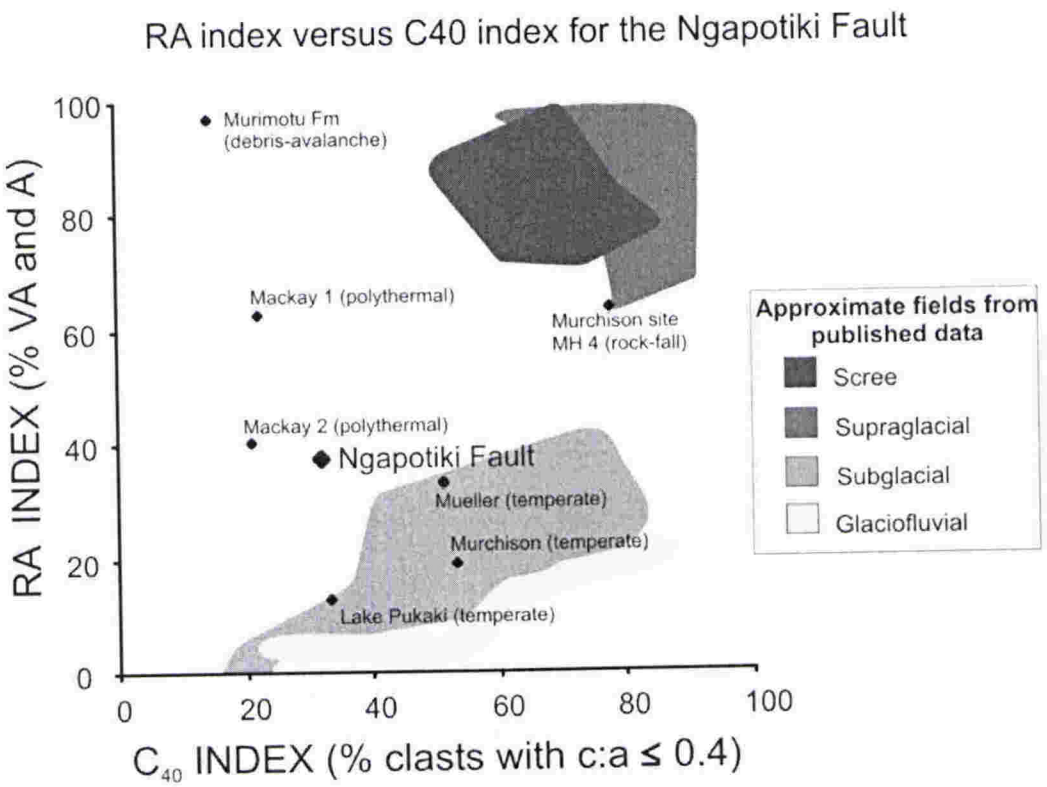

Figure 7.9 RA versus C_{40} index diagram for clasts from the Ngapotiki Fault. The sample plots outside known glacial fields and reflects moderate number of angular and very angular clasts combined with an intermediate clast form. Data from other environments are included for comparison. Shaded fields are from published data in Benn and Ballantyne (1994) and Bennett et al. (1997).

7.2.4 Clast striae

Striae occur on 22% of the clasts, and in all Krumbein roundness classes except the most angular (0.1) and the most rounded (0.7), with a slight tendency to occur on clasts in the 0.6 roundness class. Slightly more argillite clasts carry striae (34 % of all argillite clasts) compared with 20 % of sandstone clasts. The striae occur on both the fractured clasts as well as on whole, non-fractured clasts, and clast form does not appear to influence the presence of striae (Figure 7.7).

Tectonic striae are discussed in detail in section 7.3.6. However, striae on the large boulders at the base of the Ngapotiki outcrop are briefly discussed below.

At the base of the outcrop in Unit 3, the cataclasite has eroded to expose *in situ* beach boulders that show striae on the upper surfaces. These striae are parallel to each other in the direction of fault movement. The striae are difficult to distinguish individually, but are continuous over curved boulder surfaces, but not on the lee ends. This suggests the striating fragments were held firmly in the enclosing fault gouge as it deformed around the boulder, but then ceased to striate the boulder once in the pressure shadow that would occur on the lee side (Figure 7.10).

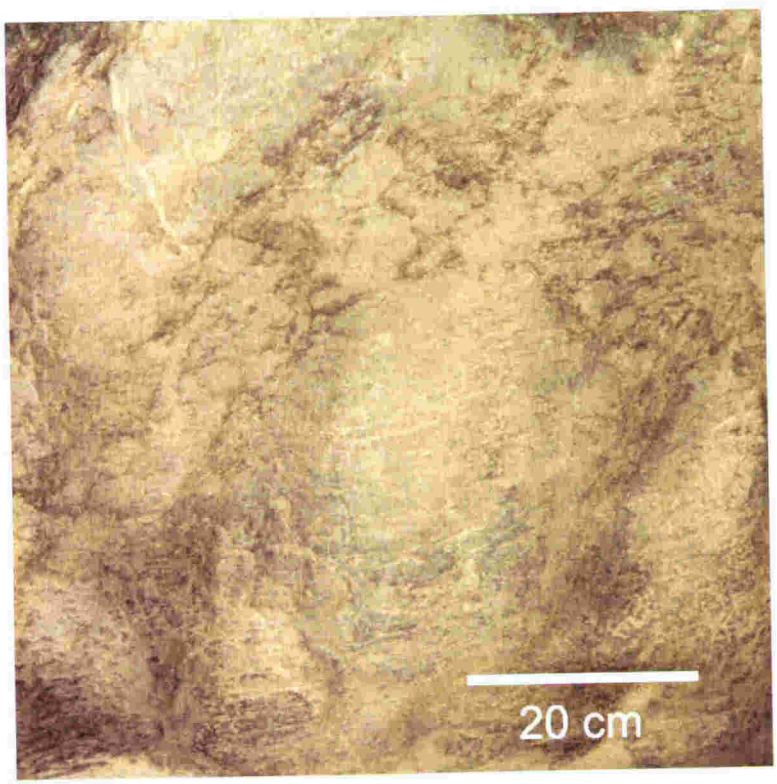

Figure 7.10 The surface of a striated, *in situ* beach boulder. The top surface shows parallel striae produced as the cataclasite of Unit 3 was thrust over the top of the beach. Individual striae are difficult to distinguish, but form pervasively striated surfaces.

7.2.5 Summary of the Ngapotiki Fault clasts

The tectonically sheared outcrop at Te Rakauwhakamataku Point contains sandstone and argillite clasts that have been rounded on a high-energy beach, subsequently overthrust, and incorporated into a low-angle thrust plane associated with the Ngapotiki Fault. This tectonic movement has caused differential movement between greywacke cataclasite and the beach, producing striae on the upper surfaces of large, *in situ* boulders and on surfaces of clasts.

The clast form and roundness distributions represent both the rounded high-energy beach clasts (blocky and subrounded to well-rounded), and also tectonically fractured or possible tectonically generated clasts (variable form and more angular). Therefore, the sample plots in an intermediate zone on the RA-C_{40} diagram. Argillite clasts are slightly more prone to tectonic fracturing than sandstone clasts, but this is not obvious in the form and roundness distributions. Clast form and roundness do not appear to be associated with the occurrence of tectonic striae, although it is noted that no striae occur on very angular (0.1) clasts. Argillite clasts are slightly more likely to carry striae than sandstone clasts.

The percentage of striated clasts in this outcrop (22 %) is similar to the percentage in temperate glacial deposits. The striae show a wide range in character. These features are discussed in detail in section 7.3.6. Striae on overthrust, *in situ* boulders that have not been displaced by fault movement, are remarkably parallel to direction of fault movement.

7.3 WELLINGTON FAULT, HARCOURT PARK, NEW ZEALAND

7.3.1 Background and setting

The Wellington Fault is one of the longest and more laterally persistent of New Zealand's on-shore active faults (Begg et al., 1997). It is a predominantly dextral reverse fault with a near vertical dipping fault plane upthrown on the western side. Along the Wellington-Hutt section of the fault, the downthrown side has produced several basins that are filled with Quaternary fluvial sediments. An average horizontal slip rate estimated from offset terraces is 6.6 mm/yr and vertical movement is <0.5 mm/yr. The calculated average recurrence interval is 485-783 years (Berryman, 1990).

At Harcourt Park in Upper Hutt, the fault offsets a series of Quaternary alluvial terraces and the fault plane is clearly exposed in the true right bank of the Hutt River (Figure 7.11). The fault dips at 65° to the southeast and cuts Holocene age (< 15000 yrs) fluvial terrace gravels (Berryman, 1990).

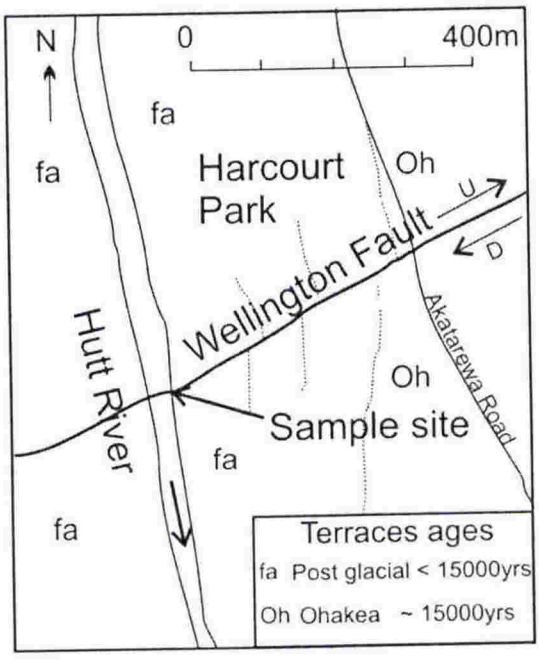

Figure 7.11 Map of Harcourt Park and Quaternary fluvial terraces offset by the active Wellington Fault. Outcrop and sample site are indicated.

Crushed greywacke bedrock is exposed in the riverbed and lower stream bank on the upstream side of the fault. Fault gouge is visible close to the fault zone and contacts compacted fluvial conglomerate. The compacted conglomerate forms a unit approximately 11 metres wide that stands out in the riverbank profile. Near vertical shear planes on both the up and downstream sides of the unit contain fault pug (gouge) and fractured and striated clasts. On the downstream side, the compacted conglomerate contacts undeformed, horizontally bedded fluvial terrace conglomerate (Figure 7.12). The conglomerate unit has moved as a coherent block in response to movement on the Wellington Fault with slip occurring on both margins (upstream and downstream).

7.3.2 Fieldwork

Fieldwork consisted of describing and measuring the riverbank outcrop of the Wellington Fault at Harcourt Park (175°05'00"E 41°07'00"S) or NZMS 260, R27, 856094). Two clast samples were collected. The first was a bulk sample providing a random collection of pebble-sized clasts from the downstream sheared margin of the compacted conglomerate unit for clast-shape analysis. The second consisted of several clearly striated clasts (up to 30 cm diameter) for characterising the striae. These striated clasts were collected from the shear planes on both sides of the compacted conglomerate unit (Figure 7.13).

Outcrop description of the Wellington Fault at Harcourt Park

UNIT 1 GREYWACKE CATACLASITE

Dark grey, fine grained sandstone and argillite with abundant quartz veins. Extensively deformed with original bedding almost obliterated. Brecciated into angular, slabby slivers of greywacke. Some greenish mineralised surfaces. Occasional near-vertical shear planes up to 20 cm wide with angular greywacke chips on margins and sticky, grey pug with occasional clasts. Deformed greywacke with shear zones extends at least 50 m upstream from fault.

UNIT 2 FAULT GOUGE

Contact with greywacke cataclasite (UNIT 1) is gradational as deformation becomes more pervasive closer to the fault plane. UNIT 2 is soft, dark-grey, sticky gouge with variable abundance of coarse grit and angular greywacke clast up to 4 cm diameter. Near vertical lineations obvious in the finer grained gouge zone. UNIT 2 is 2-4 m wide with distinct weathering back of bank profile.

UNIT 3 COMPACTED CONGLOMERATE

Near vertical distinct fault contact between fault gouge (UNIT 2) and pug-lined margin of compacted conglomerate (UNIT 3). Unit consists of clast-supported conglomerate. Clasts are up to 30 cm diameter. Average is 5-10 cm. Clasts are greywacke and generally well-rounded but many are fractured. Some show striae. No apparent orientation. Matrix is sand. Clasts are tightly packed forming a compacted unit that stands out in weathering profile. Pug-lined shear zones (30-50 cm wide) with common striated rounded clasts occur on both sides of the compacted conglomerate unit. Pug is grey, fine and sticky. Some elongate clasts are aligned near vertical in the shear zone. UNIT 3 (including shear zones on both sides) is 11.4 m wide.

UNIT 4 UNDEFORMED CONGLOMERATE

Contact with UNIT 3 is distinct. Conglomerate is matrix supported with largest clasts up to 50 cm diameter. Average clast size is 5-20 cm. Clasts are greywacke and rounded to well rounded. Matrix is sand and grit. Crude horizontal bedding is marked by slight clast size changes. Vague clast imbrication is evident.

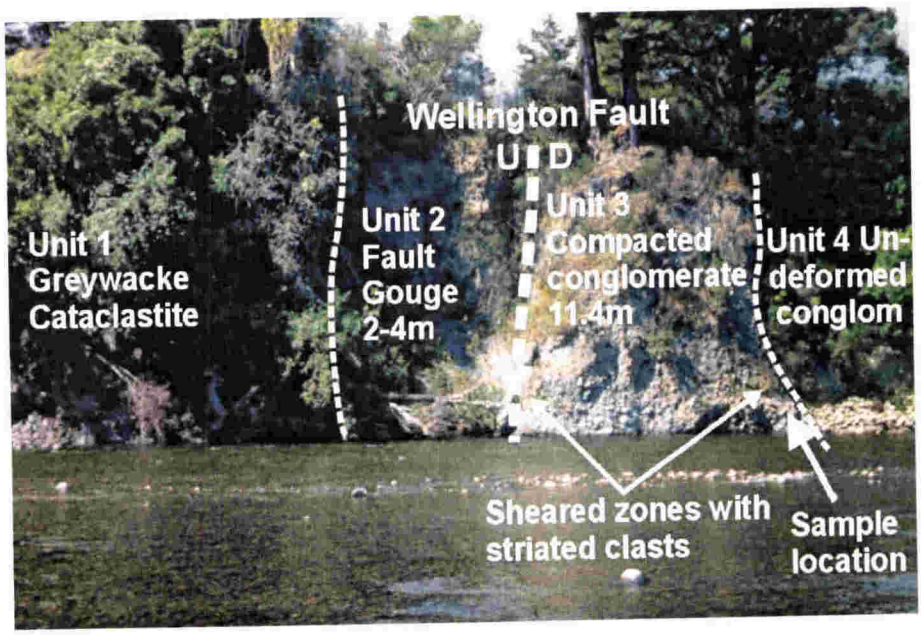

Figure 7.12 Exposure of the Wellington Fault in the bank of the Hutt River, Harcourt Park. The four units described above and sample locations are shown. Two shear planes occur, one on each side of the compacted conglomerate (UNIT 3).

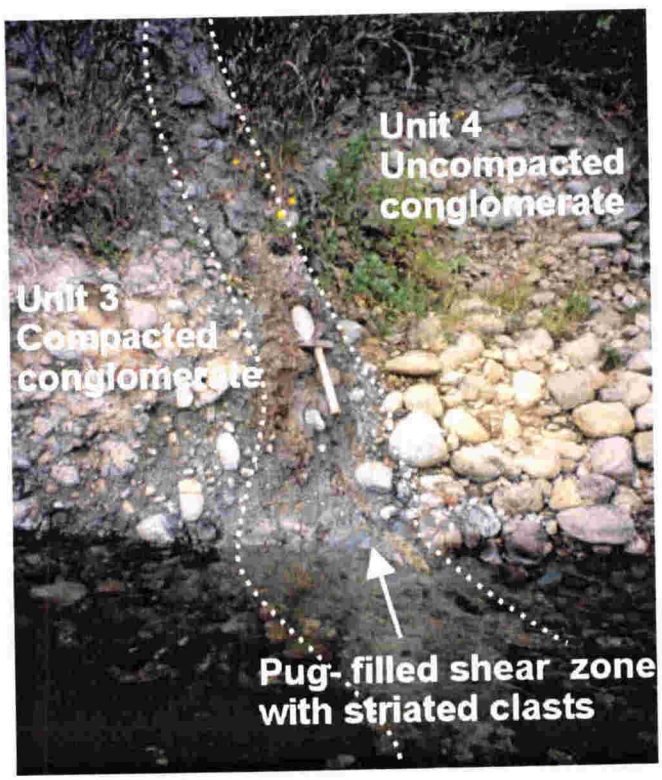

Figure 7.13 Close up of pug-filled shear plane separating Unit 3 and Unit 4. Some striated clasts are aligned with the long axes parallel to the shear plane. Hammer is 35 cm long.

7.3.3 Clast shape

A bulk clast sample was collected from the sheared margin of Unit 3. Shape analysis was performed on 100 clasts using the method outlined in Chapter 2 and clast data are presented in Appendix 6.

The sample is dominated by sandstone clasts (74%) with the remainder being argillite clasts (26%). Clast form is displayed in Figure 7.14 and shows that the sample has a broad scatter with c:a axial ratios ranging from 0.23 to 0.74, but the majority of clasts falling above the 0.4 line (average is 0.49) meaning the sample trends slightly toward blocky (equidimensional) shapes. This is only slightly higher than for the Ngapotiki Fault (0.45) and similar to values for temperate glacial clasts.

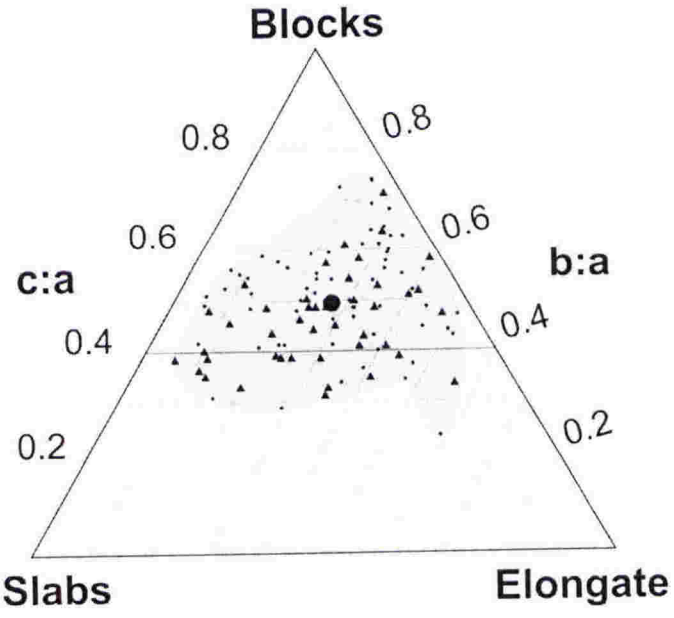

Figure 7.14 Clast form diagram showing a central clustering, but slight trend toward blocky clast form in the sheared margin of UNIT 3 (compacted conglomerate), Wellington Fault. Average c:a axial ratio is 0.49. Small black triangles represent striated clasts.

Roundness and lithology are displayed in the frequency percent histogram in Figure 7.15. This shows a broad bimodal distribution with clasts in all Krumbein roundness classes up to 0.7 (well-rounded) and modal peaks in the 0.3 (subangular) and 0.7 roundness classes. The sample has 61% of clasts in the 0.5-0.7 classes (rounded and well-rounded) producing an average roundness of 0.47 (subrounded). This is the highest average roundness value for all environments studied. Clast lithology does not appear to influence roundness, although it is noted that no argillite clasts occur in the 0.1 class and 0.4 classes.

Fifteen percent of the clasts are fractured indicating that fracturing due to fault movement is common. This influences the roundness distribution, with fractured clasts making up 76% of clasts in the 0.1 and 0.2 roundness classes. Both sandstone and argillite clasts show fractures and these are usually normal to the long axis.

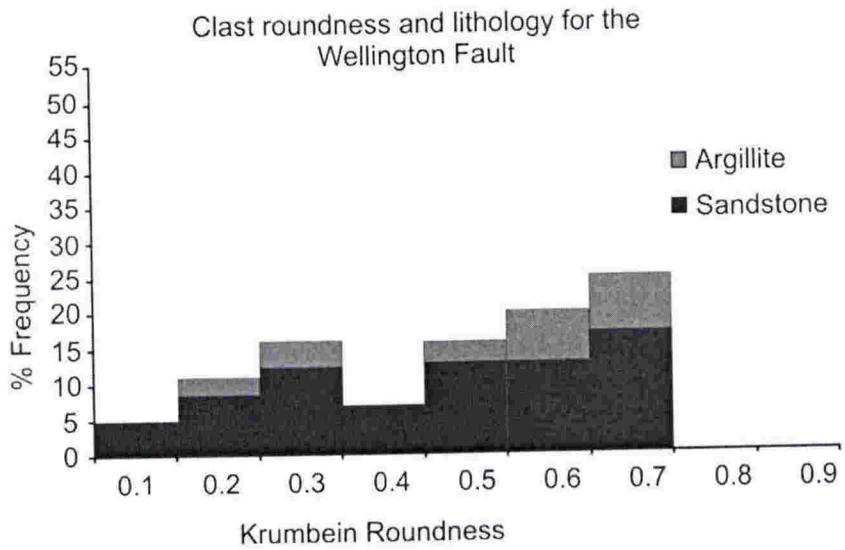

Figure 7.15 Roundness histogram for clasts from fault sheared fluvial conglomerate, Wellington Fault. The distribution is broad and bimodal, reflecting the combination of well-rounded fluvial clasts and the more angular component due to tectonic fracturing of some clasts. Average roundness is 0.47 and is the highest value for all environments studied.

The covariant plot of RA index versus C_{40} index (Figure 7.16) emphasises the low percentage of angular and very angular clasts (RA index of 16) and the high number of equidimensional clasts (low C_{40} index of 22), resulting in the Wellington Fault sample plotting in the lower left of the diagram.

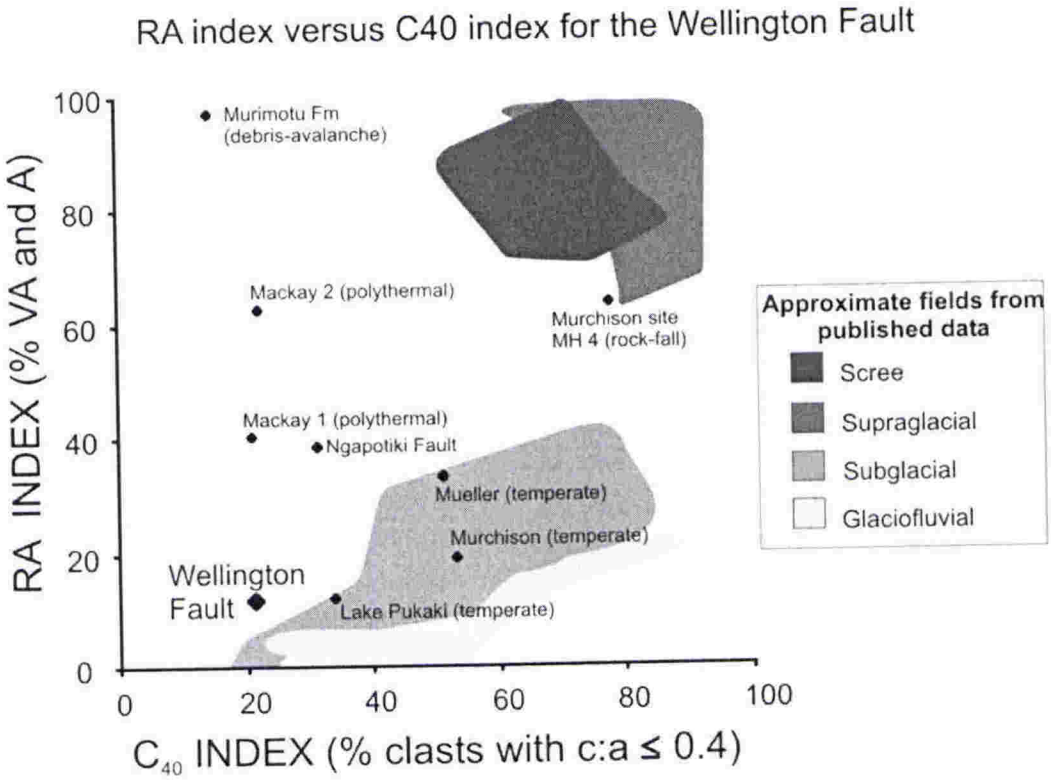

Figure 7.16 RA versus C_{40} index diagram for clasts from fault sheared fluvial conglomerate, Wellington Fault. Data from other environments is included for comparison. Shaded fields are from published data in Benn and Ballantyne (1994) and Bennett et al. (1997).

7.3.4 Clast striae

Forty three percent of the clasts from the fault sheared conglomerate display well-developed abrasional striae (asperity ploughing of Means, 1987). These occur in all roundness classes except the most angular (0.1) and are most prevalent on more rounded clasts (91 % of striated clasts are 0.5, 0.6 or 0.7 roundness). Striae occur on clasts of all shapes (Figure 7.14). Striae are more common on argillite clasts (65 % of all argillite

clasts) than sandstone clasts (35 % of all sandstone clasts). Striae from both the Wellington Fault and the Ngapotiki Fault are discussed in detail in 7.3.6.

7.3.5 Summary of Wellington Fault clasts

Clasts recovered from the Wellington Fault, Upper Hutt, represent a fluvial deposit that has been tectonically sheared by active faulting. Differential shearing within these zones has produced abrasional striae on the surfaces of many clasts.

Clast form and roundness distributions reflect the well-rounded (highest average roundness value for all environments studied) blocky shaped clasts of the fluvial conglomerate but also show a more angular component reflecting tectonically fractured clasts. The sample plots low on both axes of the RA-C_{40} diagram, distinct from other samples.

A remarkably high percentage of striated clasts (43 %) occur in this example (highest for all environments in this study). Striae preferentially occur on more rounded clasts and not at all on the most angular (0.1). Argillite clasts are twice as likely to carry striae than sandstone clasts.

7.3.6 Character of tectonic striae from the Ngapotiki and Wellington Faults

Characteristic features of striated clasts from the Ngapotiki and Wellington Faults are presented in Appendix 1, "Linear Abrasion Atlas - Tectonic striae". These features are discussed next, followed by detailed analyses of four clearly striated clasts.

Striae occasionally occur on the ends of clasts and Figure 7.17 shows an example from the Ngapotiki Fault. The striae are parallel and form a set 8 mm wide. Striae on clast ends are observed only on tectonic and debris-avalanche clasts.

Figure 7.17 An argillite clast from the Ngapotiki Fault shows parallel striae on the end of the clast. This is observed only in tectonic and debris avalanche clasts. This clast is also presented in appendix 1, Linear Abrasion Atlas, Tectonic striae, Image 3.

Larger clasts tend to show larger striae. For example, the sandstone cobble in Figure 7.18-A, from the Wellington Fault is the largest clast and has the largest striae measured in this study. The longest and widest striae are usually compound striae that consist of several smaller parallel striae. The clast shows striae sub-parallel to the long axis, which has been fractured by tectonic movement. Fractures are typically normal to the long axis of the clast. This clast is also shown in Figure 7.19, clast 1. The clast shown in (Figure 7.18-B) has a pervasively striated surface with remarkably straight striae, oblique to the long axis and continuous across the curved surface.

A feature peculiar to tectonically striated clasts is the concentration of striae on the margins of the clast, where the curvature increases toward the end. An example is shown in Figure 7.18-C, where abrasion has truncated part of a surface on a rounded clast. Individual striae are difficult to identify individually, but comprise a clearly abraded surface. The striae overlap and have a corrugated appearance akin to ridge and groove lineations, such as those described by Means (1987). Clast D, (Figure 7.18) displays multiple striae orientations. The clast is almost equidimentional and some striae are curved suggesting that the clast has rotated during the striation process.

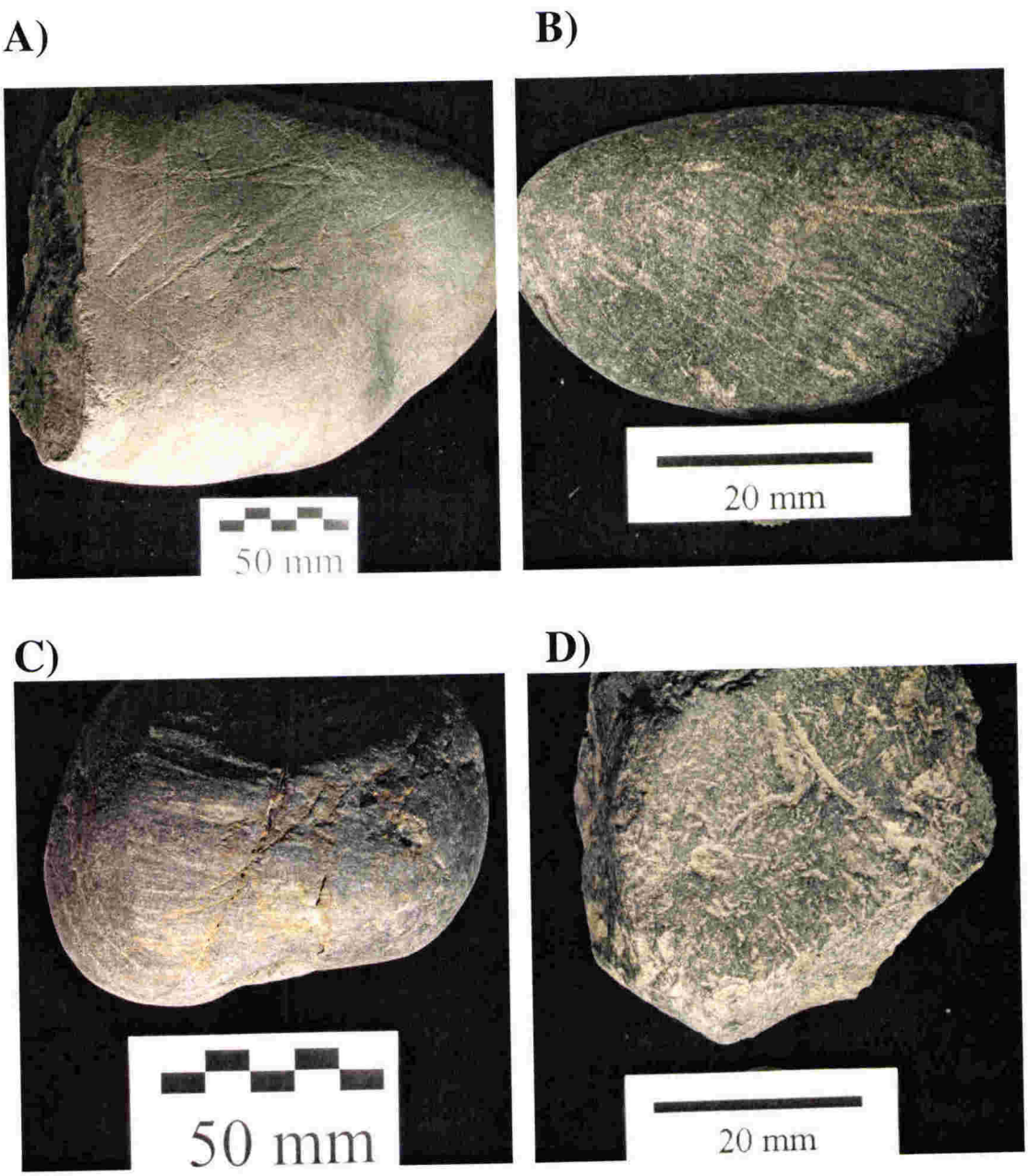

Figure 7.18 A) A large clast showing striae up to 5 mm wide and 86 mm long oriented sub-parallel to the long axis. The clast is fractured normal to the long axis (clast 1 in Figure 7.19). B) Parallel striae oriented oblique to the long axis on a curved surface. C) A rounded clast with a corrugated abrasion surface concentrated on the curved margin of the clast. D) A flat surface with striae showing multiple striae orientations and some curved striae (clast 3 in Figure 7.19). Larger images of these and other clasts with additional comments are presented in appendix 1, Linear abrasion Atlas – Tectonic striae.

Striae orientation

Striae orientation for the four clasts measured in detail show wide variation. These are displayed in Figure 7.19. Clast 1 is a moderately elongate sandstone clast (b:a ratio of 0.65). It is the largest and most rounded clast of the four. The striae show a moderate preferred orientation oblique to the clast long axis. There is however, a wide variation in other striae orientations, giving a range of 88° and high standard deviation of 45°. The clast displays 6 % curved striae. Clast 2, which is the second largest and most elongate clast (b:a axial ratio of 0.51), shows a weak mode perpendicular to the long axis, but overall shows variable orientations with a range of 88° and the highest standard deviation of all four clasts (49.8°). This clast has one curved striation.

Clast 3 is the smallest and most equidimensional clast of the collection (b:a axial ratio of 0.80). Only 15 striae were measured, but they nevertheless show two weak modes oblique to the long axis and 53 % of striae falling between 150° and 180°. The striae show a smaller range in orientations (70°) and lower standard deviation of 33°. Two of the fifteen striae are curved. Clast 4 is an argillite clast from the Ngapotiki Fault and is the least rounded of the 4 clasts. It is moderately elongate (b:a axial ratio of 0.74) but shows striae that are remarkably parallel to the long axis (63 % of striae within 10°). It has the smallest range (54°) and standard deviation (18°) of all four clasts. This clast has 6 % curved striae.

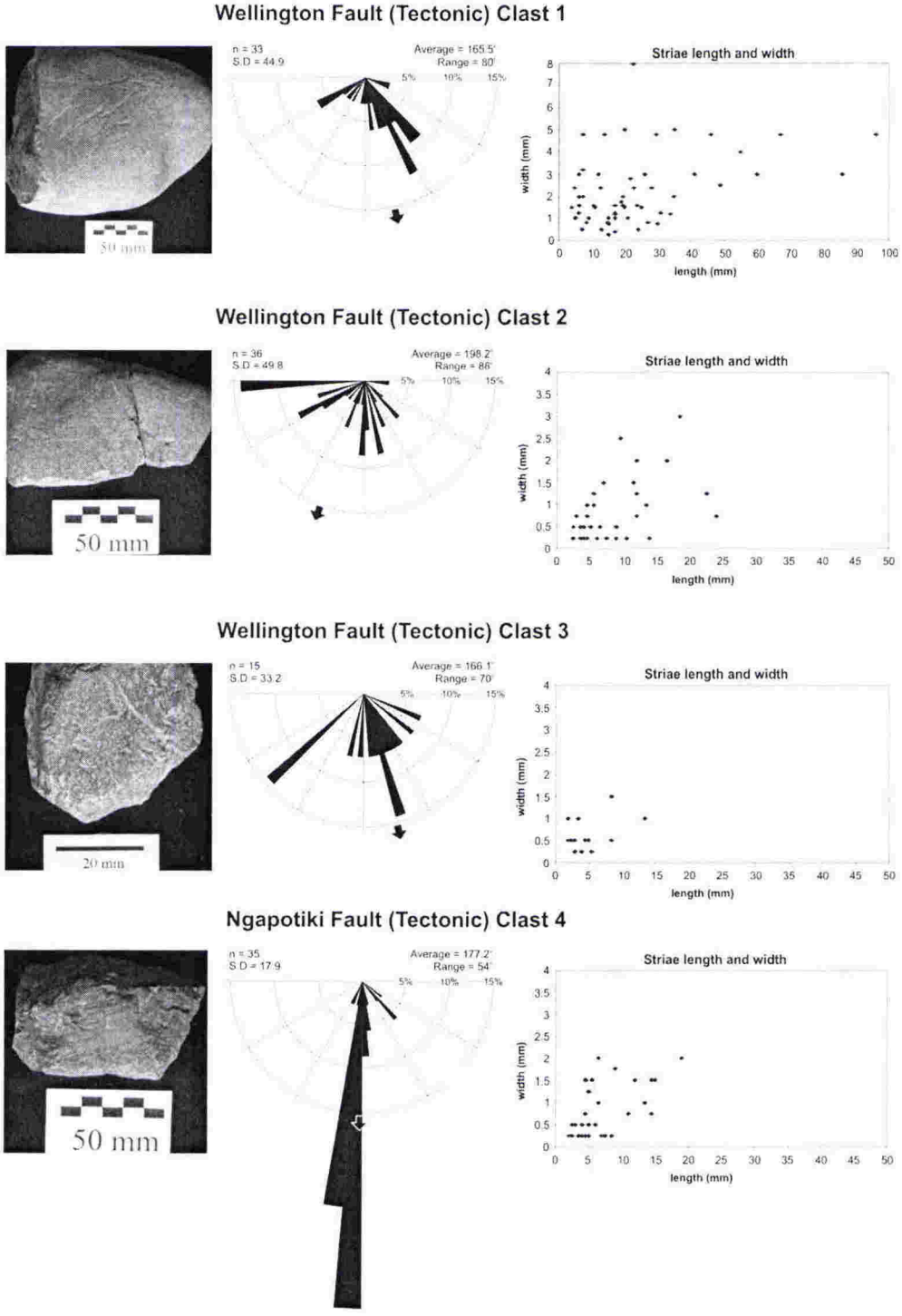

Figure 7.19 Striated clasts from the Wellington and Ngapotiki Faults. The half-rose diagrams represent orientation of striae relative to the long axis of the clast (azimuth of 180°). Striae are grouped into 5° segments. The black arrows indicate average striae orientation. Also shown is a plot of striae length versus width. Larger, colour images of these and other clasts are presented in appendix 1, Linear Abrasion Atlas – Tectonic striae.

Striae length

Striae length is related to clast size. The longest striae (86 mm) and highest average (17.4 mm) occur on the largest clast (clast 1 is 224 mm long) whereas the shortest maximum striae length (13.5 mm) and lowest average length (4.9 mm) occur on the smallest clast (clast 3 is 45 mm long). If the large clast is ignored, the range in striae lengths for the other 3 clasts is actually low and the averages are reasonably close (between 4.9 mm and 8.3 mm) (Figure 7.20).

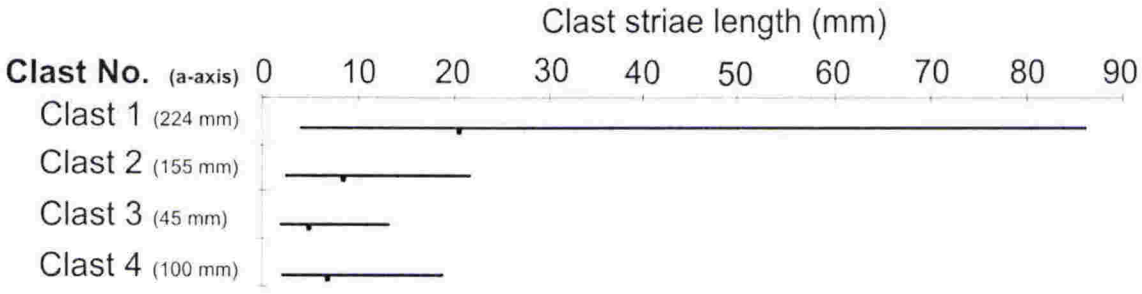

Figure 7.20 Striae length, ranges and averages for the four clasts from the Wellington Fault (clasts 1, 2 and 3) and Ngapotiki Fault. The longest striae, greatest range and highest average occur on the longest clast (clast 1) and the smallest range and lowest average occur on the smallest clast (clast 3).

Striae width

Striae width shows a similar relationship to size (Figure 7.21). The widest striae (5 mm) and highest average width (1.7 mm) occur on the largest clast (clast 1) and the smallest maximum width (1.5 mm) and lowest average width (0.6 mm) occur on the smallest clast (clast 3). Many of the widest striae are compound striae. Again, if the large clast is ignored, average striae width shown by the other 3 clasts is reasonably close (between 0.6 mm and 0.8 mm) despite significant clast size difference.

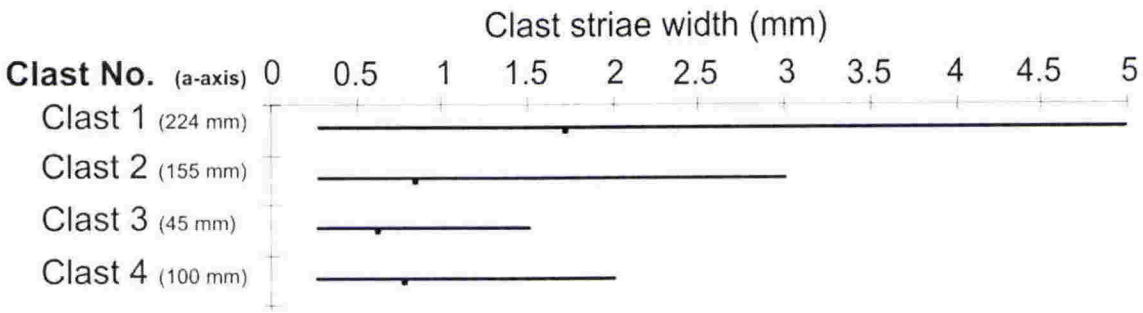

Figure 7.21 Striae width ranges and averages for the four tectonically striated clasts. Striae width is related to clast size with longer and wider striae occurring on larger clasts.

Striae width and length

Long striae are often the widest striae, but there are exceptions (Figure 7.19). The width/length ranges and averages for the largest sandstone clast (clast 1) and smallest clast (clast 3, argillite) are very similar, despite the large differences in actual striae width and length measurements, indicating they have similar shape. In fact, the smallest clast (clast 3) has a slightly higher average width/length ratio than the other three clasts, suggesting that relatively, it has shorter, wider striae. It is also the most equidimensional clast (Figure 7.22).

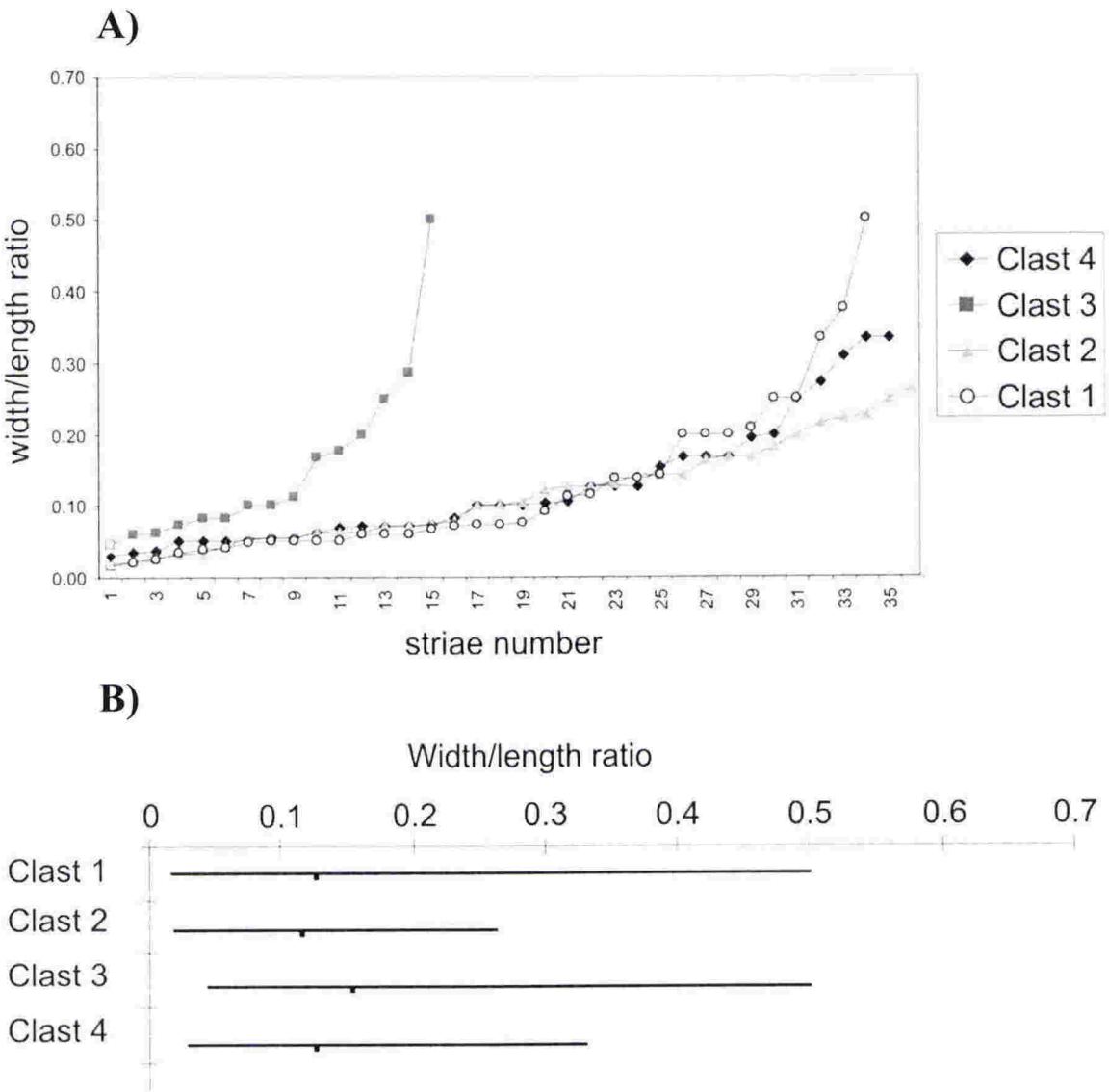

Figure 7.22 A) Width/length ratios ranked lowest to highest. B) Width/length ratio ranges and averages. Average ratios are similar, although the smallest and most equidimensional clast has the highest overall average.

Striae density

Striae density on the tectonic clasts varies widely and appears to be related to the size of the clast and lithology. The largest clast (sandstone) shows the lowest density per cm^2

(0.35) of all clasts in all environments studied whereas the smallest clast (argillite) has the highest density of 2.2 striae per cm^2. The percentage of background striae also shows this pattern with the largest clast showing the lowest percent background striae (40 %) and the smallest clast showing 100 % background striae. Clasts 2 and 3 have close background striae values of 56 % and 52 % respectively (Figure 7.23). The percentage of grid squares showing at least 1 striation varies from 45 % to 78 % indicating that striae are variably distributed across the clast surfaces.

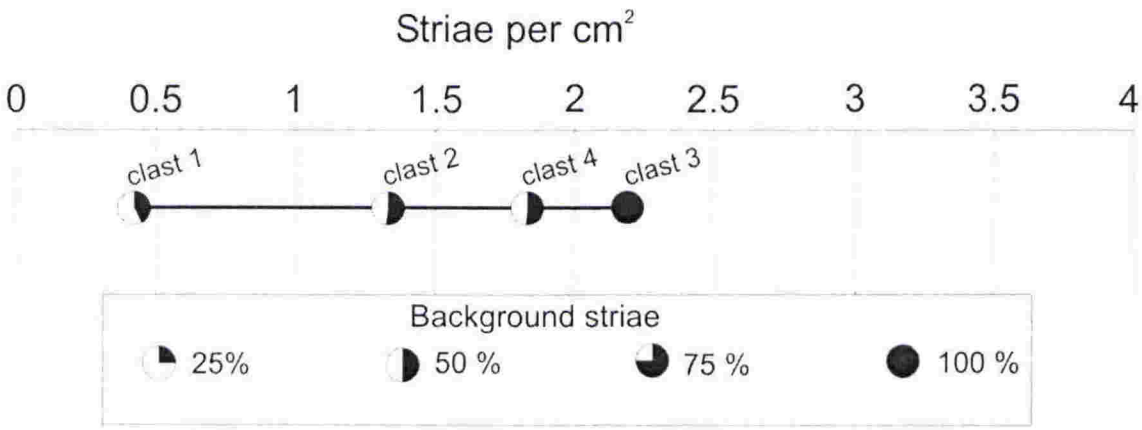

Figure 7.23 Striae density diagram showing the number of striae per cm^2 for each clast and the percentage of "background" striae. Striae density is related to clast size and lithology, with lower striae density occurring on larger clasts.

7.4 COMPARISON, DISCUSSION AND CONCLUSION

Clasts from both examples of tectonically sheared conglomerate have similar central clusters on the clast forms diagrams. Both samples also show bimodal roundness distributions, although the Ngapotiki Fault sample has more angular clasts (average roundness of 0.33), than the Wellington Fault sample (average roundness of 0.47). This is highlighted on the RA-C_{40} diagram and reflects the rounded character of the original beach or fluvial clasts as well as an angular component due to tectonic fracturing of some clasts, and in the case of the Ngapotiki Fault, possibly a few tectonically generated clasts.

Both samples show a similar percentage fractured clasts (Ngapotiki Fault has 21 % and Wellington Fault has 17 %) and these are usually oriented normal to the clast long axes.

There is a large difference in the percentage of striated clasts (Ngapotiki Fault has 22 % and the Wellington Fault has 43 % striated clasts (highest for all environments studied). This may reflect the focussed deformation along the narrow shear planes in the Wellington fault as opposed to the wider, pervasive shear zone of the Ngapotiki Fault. In both cases, striae preferentially occur on argillite clasts.

These results are difficult to compare with other studies of tectonically striated clasts. The striae described by Clifton (1965) were microscopic and parallel, typically less than 0.5 mm long and 0.05 mm wide forming a "polished" surface, similar in appearance to slickensides. However, a few were abrasional striae up to and several mm long and up to 1 mm wide. The striae were generally parallel to fracture planes in the pebbles and normal to the regional structural trend. This contrasts with the lack of tectonic polish and much larger striae described on the Wellington and Ngapotiki Fault clasts. In addition, the fractures described by Clifton (1965) were usually oriented normal to the long axis of the clast and to the striae, whereas the examples in this study show fracturing normal to the clast long axes.

CHAPTER EIGHT

SUMMARY AND CONCLUSIONS

8.1 INTRODUCTION

This chapter summarises the results of this new investigation of clast striae and clast shape from both glacial and non-glacial environments. The chapter concludes with an assessment of our understanding of linear abrasion features and possible avenues for future research.

8.2 CLAST SHAPE

8.2.1 Form and roundness

Summary form and roundness for all clast samples are presented in Figure 8.1. The clasts in samples from the Mueller and Murchison Glaciers show central clusters on the form diagrams with similar average c:a axial ratios of 0.40 and 0.39, roundness averages of 0.32 and 0.34 (subangular) and show 22 % and 28 % faceted clasts respectively. The Lake Pukaki sample has a slightly higher average c:a axial ratio (0.45) and is better rounded (0.43, subrounded) than the two glacier samples, reflecting the slightly blockier shapes and better-rounded character of the probable fluvial source of the moraine clasts. The moraine sample has a higher percentage of faceted clasts (40 %) indicating that these clasts were more intensely abraded than the clasts in the thin debris bands in the modern glaciers.

These results contrast strongly with clasts from the polythermal Mackay Glacier, which show distinctly blockier shapes with higher average c:a axial ratios of 0.5 and 0.53, lower average roundness values of 0.23 (angular) and 0.28 (subangular) and show lower percentages of faceted clasts (12 % and 22 %). The difference most likely reflects the isotropic lithologies (granite and dolerite) in contrast to the softer sandstone and argillite lithologies which could produce more tabular clasts. Alternatively, the shape characteristics may also reflect conditions beneath the glaciers with clasts in the polythermal glacier being less intensely abraded than those from the temperate glaciers.

The debris-avalanche sample from the Murimotu Formation is distinct because it has the highest c:a axial ratio (0.54), lowest average roundness of 0.16 (very-angular) and least range in roundness values of all samples in this study. Forty percent of clasts show flat or undulating fracture faces with distinctly sharp edges that are unrelated to the long axis. These features reflect both the massive crystalline volcanic source rock with no natural planes of weakness and the violent processes within the debris-avalanche that produce frequent clast fracturing but little rounding.

The Murchison rock-fall clast sample is also distinct as it has the lowest average c:a axial ratio (0.31) of all samples in this study, although it also has a low average roundness of 0.23 (angular) and 40 % of clasts show flat fracture faces. These results are also interpreted to be primarily the result of lithologic differences, with the argillite clasts in the rock-fall deposit preferentially breaking along bedding planes producing slabby-shaped clasts. However, the rock-fall process does appear to round clast edges better than the debris-avalanche.

Finally, the tectonically modified clasts from the Ngapotiki and Wellington Faults show intermediate values for average c:a axial ratios of 0.45 and 0.49 respectively. The samples both show broad, bimodal roundness distributions but with markedly different average roundness values (0.33, subangular for the Ngapotiki Fault and 0.48, subrounded for the Wellington Fault).

The tectonic clasts from the Ngapotiki and Wellington Faults do not generally show distinct flat surfaces. However, some clasts are fractured (22 % for the Ngapotiki Fault and 15 % for the Wellington Fault), usually perpendicular to the clast long axis. This results in some clasts becoming more angular than before fracturing, thus producing distinct bimodal roundness distributions. For the Ngapotiki Fault clasts, these features are interpreted to represent a combination of subrounded beach clasts but also more angular tectonically fractured or tectonically produced clasts. In the case of the Wellington Fault, the higher roundness values reflect the well-rounded fluvial clasts combined with a component of tectonically fractured angular clasts.

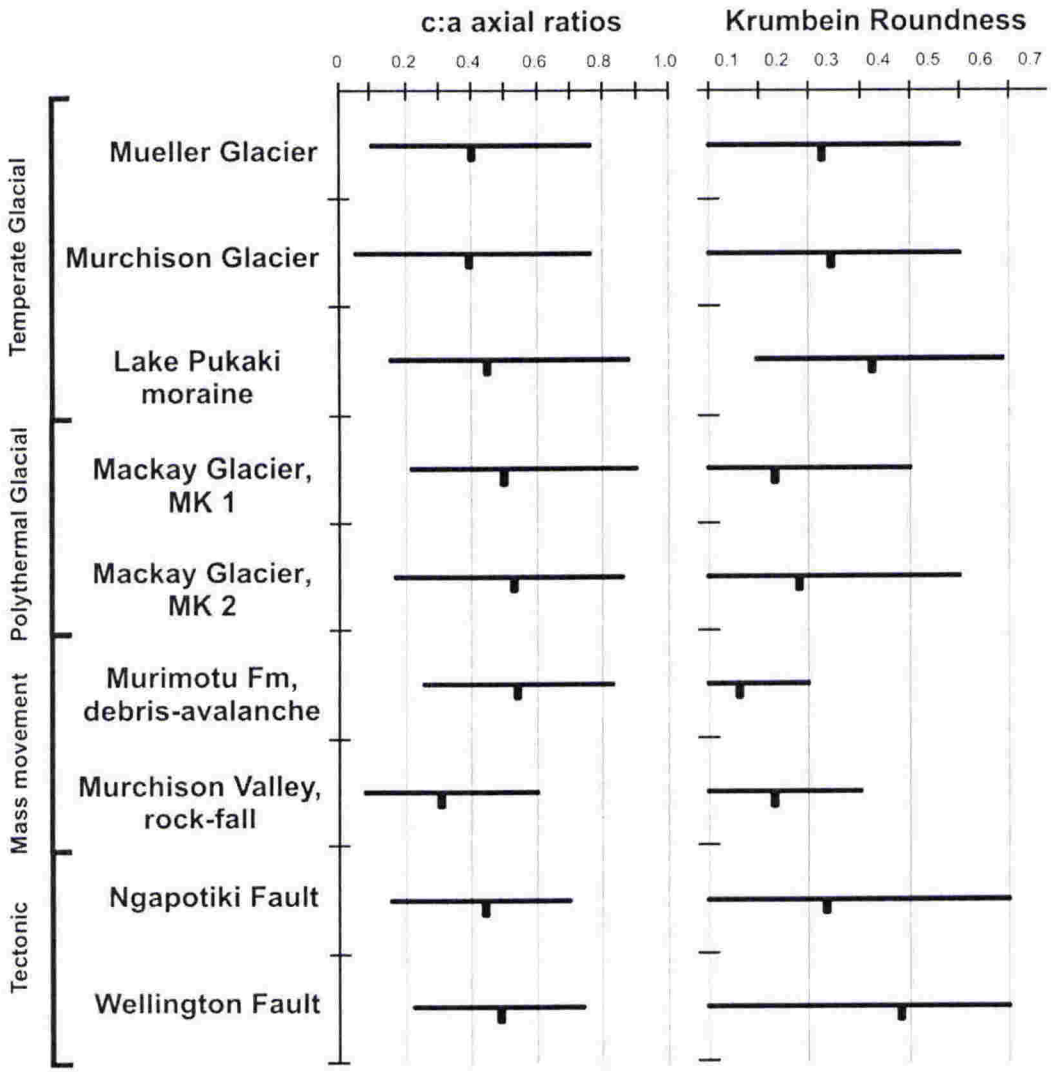

Figure 8.1 Summary ranges and averages for c:a axial ratios and roundness for all samples in this study.

The shape and roundness characteristics are also displayed on an RA-C_{40} diagram (Figure 8.2). The diagram is effective for distinguishing the different environments. The three temperate glacial samples all plot in the "subglacial" field, as defined from published data of glacial clasts from temperate and polythermal glaciers in the Arctic. The samples for the polythermal Mackay Glacier plot outside this field because of the blockier shape and lower roundness. The reason for this difference in shape is not clear, but probably relates either to the particular lithologies present in the Mackay Glacier samples or possibly a difference in the sub-glacial conditions beneath the Mackay Glacier from those beneath the polythermal glaciers studied by Bennett et al. (1997) which are used in the RA-C_{40} diagram.

The Murimotu debris-avalanche sample plots in a unique position on the RA-C_{40} diagram distinct from glacial, rock-fall and tectonic samples, reflecting its exceptionally blocky and angular character. The Murchison rock-fall sample also plots high on the diagram because of its high percentage of very-angular and angular clasts, but plots well to the right, close to the fields defined for supraglacial and scree, reflecting the unmodified slabby shape of the clasts. The tectonic sample from the Ngapotiki fault plots between the temperate and polythermal samples because it has intermediate shape and roundness values and the sample from the Wellington Fault plots lower and further to the left because of its lack of angular and blocky fluvially shaped clasts.

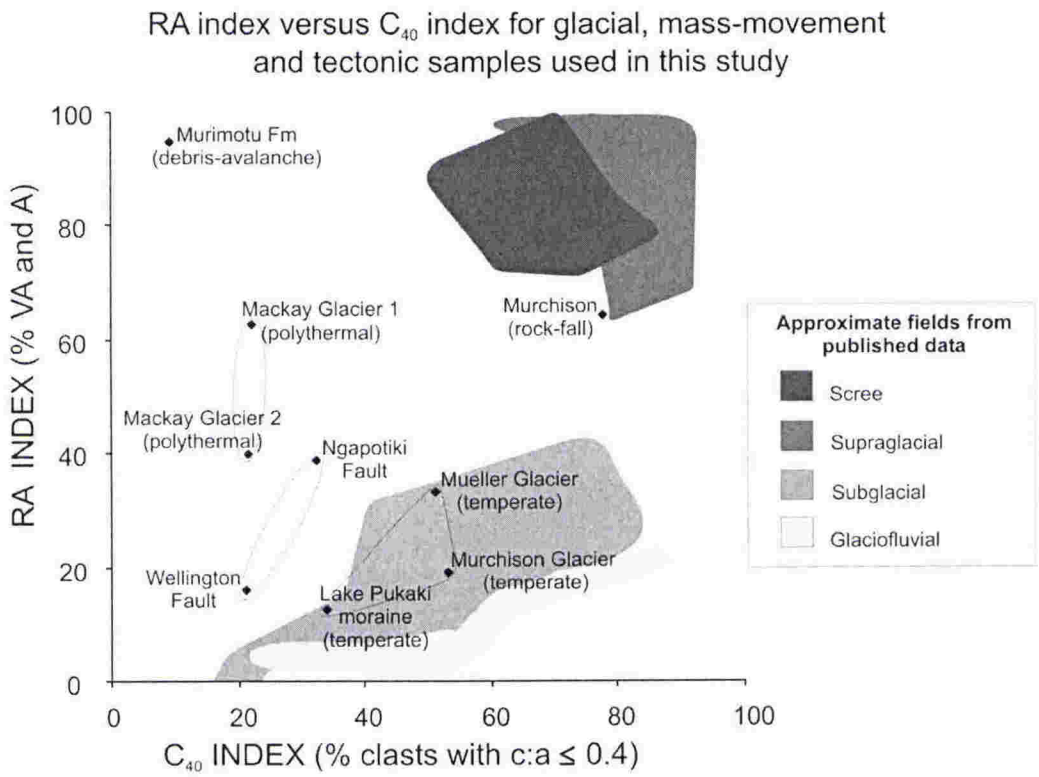

Figure 8.2 RA-C_{40} diagram of Benn and Ballantyne (1994), showing values from all samples in this study. Shaded fields are from published data in Benn and Ballantyne (1994) and Bennett et al. (1997).

8.3 STRIAE CHARACTERISTICS

Most environments show a wide range in striae characteristics. The percentages of striated clasts in the samples of modern temperate glaciers are 11 % and 16 %, while the percentage of striated clasts in temperate till is 33 %. In all examples, the striae preferentially occur on faceted argillite clasts, and on subangular to rounded clasts. The percentages support the inference from clast shape that abrasion intensity was significantly higher within the basal zone that produced the Lake Pukaki moraine than within discrete debris layers in the modern glaciers. However, these values are within the broad limits of percentage of striated clasts reported from other known glacial deposits.

The polythermal Mackay Glacier shows lower percentages of striated clasts (8 % and 5 %) that form preferentially on facets of subrounded and rounded mudstone and some dolerite clasts. The percentages contrast with the value of 51 % striated clasts from basal debris on an iceberg that showed basal grooving (Macpherson 1987), suggesting that abrasion at the glacier bed is more intense than in thin debris layers that have been elevated to an englacial position, as discussed in Chapter 4.

Ten percent of clasts in the Murimotu debris-avalanche clasts show striae and they commonly occur on flat fracture surfaces and only on very angular clasts. The rock-fall deposit shows a much higher percentage of striated clasts (26 %). They occur only on flat fracture faces of very-angular to subangular argillite clasts.

The tectonically deformed samples show generally high percentages of striated clasts (22 % for the Ngapotiki Fault and 43 % for the Wellington Fault). The latter is the highest percentage of all samples in this study. The striae occur on both whole and tectonically fractured clasts and preferentially on argillite clasts. They occur on subangular to well-rounded clasts and are often concentrated at the margins of clasts where the surface curvature increases around the clast end. Occasionally striae form on the ends of clasts. Abrasion features within the faulted conglomerates studied here are as common as those from temperate glaciers.

8.3.1 Striae orientation

Striae on clasts from the Lake Pukaki moraine (temperate glacial) show a strong tendency to be parallel to the long axis of the clast, consistent with observation from other known glacial deposits. However, there are exceptions, and some clasts show no preferred orientation particularly if they are nearly equidimensional. These clasts also show curved striae suggesting that they are more likely to rotate and receive striae of multiple orientations. The polythermal clasts from Cuff Cape, at the margin of the polythermal Mackay Glacier, also show a strong tendency to be sub-parallel to the long axes. Again, exceptions occur, with some clasts with defined long axis showing striae

with no preferred orientation, and one almost equidimensional clast showing long axis parallel striae but also occasional curved striae. Nevertheless, the overall orientation characteristics of striae on the temperate and polythermal clasts are similar, and consistent with previous observations of other know glacial striae on clasts.

The debris-avalanche clasts commonly show no preferred striae orientation, or weak clustering of striae that are usually not related to the clast long axis. Some clasts show curved striae. Rare examples display parallel striae on a single surface, but again, they are not related to the clast long axis. Striae occasionally occur on flat faces on the end of clasts. This is not observed on glacially striated clasts. The Murchison Valley rock-fall clasts typically show no preferred orientation or weakly clustered striae but they are unrelated to the clast long axis. These clasts sometimes show curved striae.

Finally, striated clasts from the Ngapotiki and Wellington Faults range from long axis parallel on some elongate clasts to no preferred orientation. However, other variably shaped clasts show moderately grouped striae oblique to the clast long axis. All the tectonically striated clasts show at least one curved striation, indicating some rotation occurred during the striating process.

8.3.2 Striae length and width

Striae length and width ranges and averages for all environments studied are presented in Figure 8.3 and width/length ratios presented in Figure 8.4. The striae on temperate striated clasts from the Lake Pukaki moraine are related to the size of the clast with the longest striae and widest striae (and higher average lengths and widths) occurring on longer clasts. However, striae length is not closely related to striae width. Some longer striae are wider than average, but this is not consistent. Width/length ratios show the highest average (relatively shorter and wider striae) occur on the smallest and most equidimensional clast. The clasts lack the wide compound striae seen in other environments and show that most striae are actually formed by relatively fine-grained matrix of the basal debris.

The clasts from the polythermal Mackay Glacier, show generally shorter and wider striae. On these clasts there is no clear relationship between striae length or width and the clast size. The widest striae represent compound striae on some clasts and this gives high maximum width/length ratios. However, average width/length ratios are close and only marginally higher than those for temperate striated clasts, indicating that most striae in both environments are similar except for the few larger compound striae on the polythermal clasts. The disparity in the relationship between striae size and clast size is confusing and may simply reflect the low number of clasts studied.

Debris-avalanche striae are generally shorter and wider than glacial striae with higher average width length ratios. The length has no obvious relationship with clast size or shape. The clasts all show some compound striae, and width appears to be related to clast size with the widest striation and highest average width occurring on the largest clast and smallest maximum width and lowest average on the smallest clast.

Rock-fall striae from the Murchison Valley are also generally shorter than glacial striae, with one clast showing the lowest average striae length (4.1 mm) of all clasts in all environments studied, but also showing large variation in width. Some clasts have compound striae with a maximum width up to 4 mm (on the smallest clast), although average widths are actually very close and lower than most other environments. Striae length and width are not related to clast size.

Tectonic striae show a strong relationship between striae length and width and clast size with the longest striation (86 mm) and widest striation (5 mm) (not the same striation) measured in this study occurring on the largest tectonic clast. This is also reflected in the average length and width values, with the highest averages on the largest clast and lowest average on the smallest clast. Even if the largest clast is excluded, average striae widths are generally greater than for temperate striae and rock-fall striae, but overlap with polythermal striae and debris-avalanche striae. Average width/length ratios are slightly higher than other environments, except debris-avalanche.

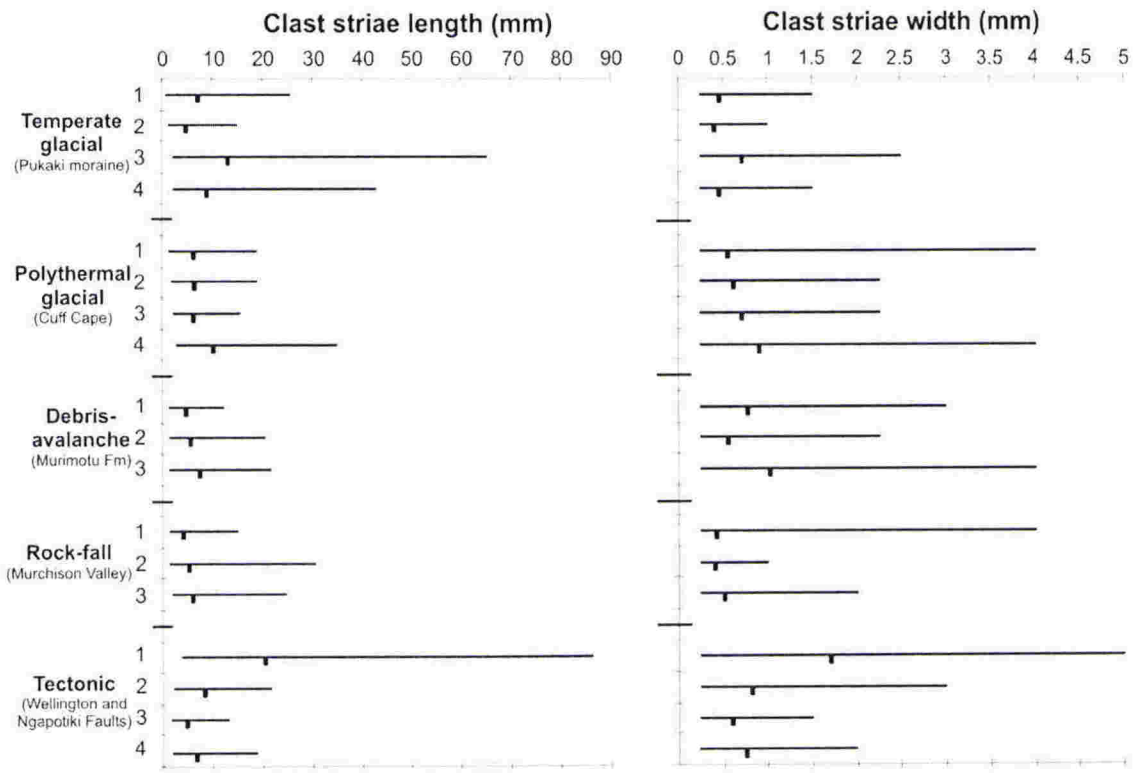

Figure 8.3 Summary range chart showing the maximum, minimum and average striae length and width for each clast in the various environments studied.

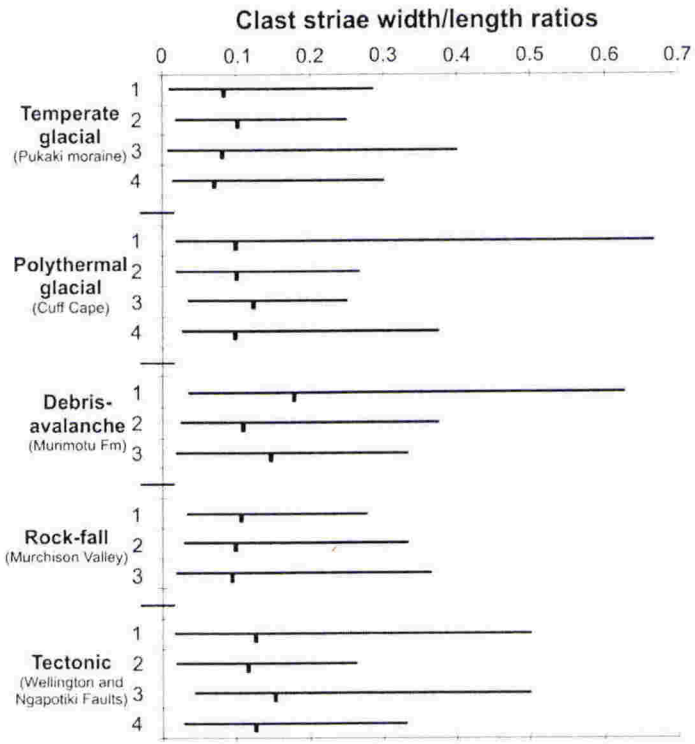

Figure 8.4 Summary range chart showing the maximum, minimum and average width/length ratios for each clast from the various environments studied.

8.3.3 Striae density

Striae density is measured as striae per cm^2 and percentage of "background" microstriae and these are summarised in Figure 8.5. The density of temperate glacial striae from clasts from the Lake Pukaki moraine are distinctive because they have the highest striae per cm^2 of all environments studied and all clasts examined in detail show 100 % background striae. This is closely matched by the polythermal-striated clasts from the Mackay Glacier, which also show at least 2 striae per cm^2 and at least 92 % background striae. Clasts from both environments show striae distributed widely across the surfaces. The general overlap of these two environments suggests that the striae density characteristics of temperate and polythermal striated clasts are essentially the same, and that basal glacial processes producing striae are similar.

The two mass movement examples have a generally lower striae density than the glacial clasts. However, there is considerable variability within these samples. The Murimotu debris-avalanche densities range from 1.2 to 1.7 striae per cm^2 and background striae shows the smallest range of all environments (28 % to 56 %). The striae are often patchy in their distribution. The Murchison rock-fall clasts show the greatest variability of all environments ranging from the lowest density of 1.4 to 2.8 striae per cm^2 and background striae ranging from a low of 20 % to 100 %. Striae distribution is irregular with some clasts showing intensely striated patches whereas others show a more even distribution.

Tectonic clasts also show striae variable densities from a low of 0.45 striae per cm^2 (lowest of all environments (40 % background), up to 2.2 striae cm^2 (100 % background). The striae density is related to the clast size, with larger clasts showing lower density. The striae distribution is often greatest around the margins of surfaces where the curvature increased at the clast end.

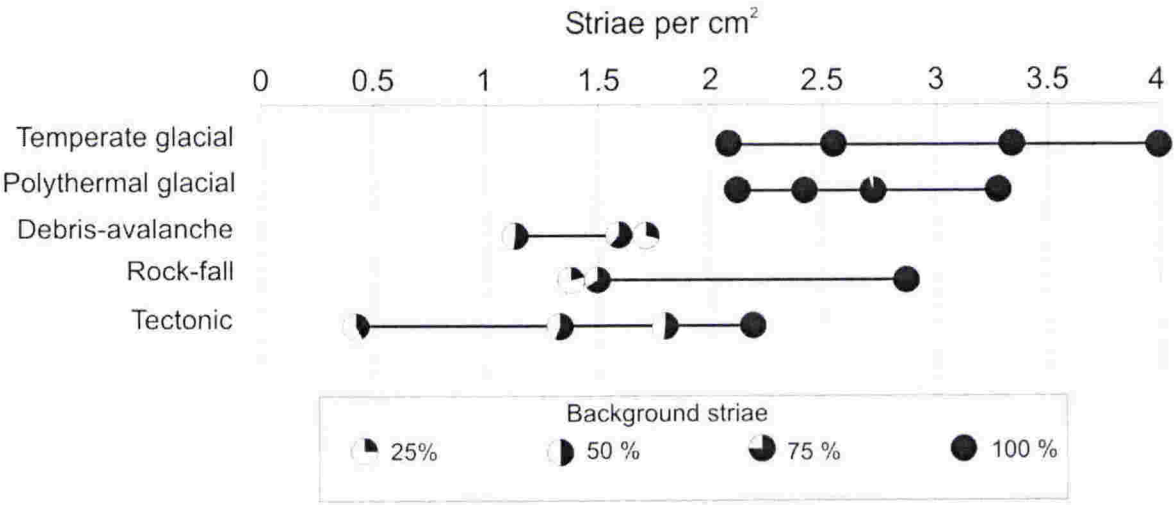

Figure 8.5 Density diagram showing the striae per cm^2 and also the percentage of background microstriae over the measured surface. The background striae are represented as a pie graph with the black portion representing the percentage of background striae.

The results indicate that there is a clear distinction in striae density between glacial and non-glacial clasts. Although some overlap occurs, glacial clasts generally show a distinctly greater density in striae. There is little distinction in striae density between the various non-glacial environments as there is a large overlap in both striae per cm^2 and background striae.

8.3.4 Conclusions

Striae occur in a wide range of environments from variety of processes. This is not widely appreciated by Earth scientists. Table 8.1 shows summary clast and striae characteristics from all the environments studied. The use of form indices and roundness is useful for characterising clasts and provides a basis for distinguishing deposits of different origins. However, there is common overlap in summary statistics between some environments and data are better visualised on covariant RA-C_{40} diagrams. Although these were designed by Benn and Ballantyne (1994) to discriminate between clasts in various glacial sediments, it has proved a useful tool for plotting clast

data from a range of non-glacial environments as well. Temperate glacial clasts plot predictably in the sub-glacial field, but the examples of polythermal glacial clasts do not. This may reflect both the difference in lithologies but may also indicate that these clasts have experienced less basal glacial abrasion. It is not clear whether this is because the sampled debris layers have been predominantly englacial rather than basal or whether there is actually a significant difference in the conditions beneath the Mackay Glacier from those beneath temperate glaciers.

Mass-movement clasts from the two deposits plot separately from each other and are distinct from all other samples, mainly because of their angularity. Tectonic clasts are more variable because of the character of the clasts in the deposits prior to being incorporated within the fault zone.

The percentage of striated clasts in a deposit is not in itself a good indicator of a glacial origin. The generation of striae is dependent on lithology in all environments. The relationship between striae, clast faces and roundness is a useful indicator of striae origin, with temperate and polythermal glacial striae preferentially occurring on glacially faceted surfaces of subrounded to rounded clasts, whereas mass-movement striae are found preferentially occurring on fracture faces of the most angular clasts and occasionally on clast ends. Striae are also found on clast ends in tectonically deformed deposits. Striae preferentially occur on subrounded and rounded clasts in the tectonic samples, but these clasts do not have distinctive facets or faces, and the shape depends largely on the character of the pre-existing conglomerate deposit.

Striae orientation is also a useful characteristic. Temperate and polythermal glacial clasts show a strong tendency for striae to be sub-parallel to the clast long axis, although rare exceptions occur. Mass-movement striae are generally less clustered or show no preferred orientation and are unrelated to the long axis of the clasts. Tectonic striae show a wide range but are commonly weakly clustered sub-parallel to the long axis and often concentrated on clast margins.

Striae size is not particularly diagnostic. On similar sized-clasts, average striae length is generally similar in all environments, although mass movement striae tend to be slightly shorter. Average striae width is also similar, with overlap in width measurements between most environments, although rock-fall striae are slightly narrower. Striae size is clearly related to clast size on the temperate and tectonic clasts, but on mass movement clasts, striae appear to be independent of clast size. Compound striae occur on clasts in all environments.

Striae density highlights the fact that temperate and polythermal-striated clasts have a high density of both striae per cm^2 and background striae. Other environments show extremely variable striae density characteristics that overlap with each other considerably.

Overall, there are some observable and measurable differences in striae formed in different environments, however striae alone have only limited use in reliably discriminating between environments. The combination of clast shape and striae analyses allows striated clasts to be adequately described and provides enough criteria to make a sound judgement as to whether they are glacial or non-glacial. Documentation of striae from more examples would be useful for improving the confidence in these criteria. However, a significant advance in describing striae from different environments is likely to require a refined approach utilising more sophisticated methods of analysis such as detailed shape analysis on high-resolution digital images.

Table 8.1 Summary table for clasts from all environments studied. A) Clast shape and roundness characteristics. B) Striae characteristics.

A) Clast shape and roundness

Environment	Temperate	Polythermal	Mass-movement		Tectonic	
Example	**NZ Glaciers and published data**	**Mackay Glacier (overturned bergs)**	**Debris avalanche (Murimotu Fm)**	**Rock-fall (Murchison Valley)**	**Ngapotiki Fault**	**Wellington Fault**
Shape	Triangular, flatiron or "bullet" shape, stoss-lee ends are common. Facets with rounded edges also common. Average c:a axial ratios: 0.39, Mueller Glacier 0.40, Murchison Glacier 0.45, Lake Pukaki moraine	Some "bullet" shapes, stoss-lee ends and facets with rounded edges are common. Generally more blocky than temperate glacial clasts. Average c:a axial ratio: 0.50, overturned berg MK 1 0.53, overturned berg MK 2	Dominated by very blocky clasts, common flattish fracture surfaces with sharp edges. Average c:a axial ratio: 0.54	Common slabby and elongate clasts from fracture along bedding planes. Average c:a axial ratio: 0.31	Central clustering on form diagram. Mix of blocky rounded beach clasts and more variably shaped tectonically fractured clasts. Average c:a axial ratio: 0.45	Central cluster on form diagram. Slightly more blocky than Ngapotiki Fault. Combination of fluvial clasts and tectonically fractured clasts. Average c:a axial ratio: 0.49
Roundness	Sub-angular to sub-rounded (published). Roundness range for this study: 0.1 to 0.7 (v. angular to well-rounded. Average roundness 0.32, Mueller (sub-angular) 0.34, Murchison (sub-angular) 0.43, Lake Pukaki (subrounded)	Roundness range: 0.1-0.6 (v. angular to rounded) (this study) Average roundness: 0.23, for MK 1 (angular) 0.28, for MK 2 (subangular)	Roundness range: 0.1-0.3 (v. angular to sub-angular) Average roundness: 0.16 (angular)	Roundness range: 0.1-0.4 (v. angular to sub-rounded) Average roundness: 0.23 (angular)	Roundness range: 0.1-0.7 (v. angular to well-rounded) Average roundness: 0.33 (sub-angular)	Roundness range: 0.1-0.7 (v. angular to well-rounded) Average roundness: 0.48 (sub rounded)

B) Striae characteristics

Striae characteristics

Environment	Temperate	Polythermal	Mass-movement		Tectonic	
Example	**NZ Glaciers and published data**	**Mackay Glacier (overturned bergs)**	**Debris avalanche (Murimotu Fm)**	**Rock-fall (Murchison Valley)**	**Ngapotiki Fault**	**Wellington Fault**
Striae % and lithology	0 to 65 % striated (published) 11% Mueller Glacier 16% Murchison Glacier 33% Lake Pukaki Moraine Striae preferentially on argillite	5 % striae for MK 1 8 % striae for MK 2 Striae preferentially on argillite	10 % striated clasts. Striae occur on andesite and andesite/dacite.	26 % striated clasts Striae occur exclusively on argillite clasts.	22 % striated clasts. Striae occur on both sandstone and argillite, slightly more common on argillite clasts.	43 % striated clasts. Highest number of striae on clasts from all environments studied. Striae preferentially occur on argillite clasts.
Facets/flat faces/ fractures	Up to 60 % facets (published) 22% Mueller Glacier 28% Murchison Glacier 41% Lake Pukaki moraine Striae usually occur on facets, but rarely on curved surfaces.	12.% facets for MK 1 22 % facets for MK 2 Striae occur only on facets	40% of clasts show flat or undulating fracture faces with very sharp edges. These are unrelated to clast long axis. Striae typically occur on fracture faces.	40 % of argillite clasts show fracture along bedding planes. Striae only occur on fresh flat fracture surfaces.	21% of clasts are fractured. Fractures occur normal to clast long axis. Striae occur on both whole and fractured clasts. Striae occasionally occur on clast ends	15% of clasts are fractured. Fractures occur normal to clast long axis. Striae occur on both broken and whole clasts.
Striae orientation	Commonly parallel to long axis on elongate clasts, less parallel on more rounded or equidimentional clasts.	Commonly parallel to long axis on elongate clasts, but some exceptions.	Striae commonly have no preferred orientation, but occasional weakly clustered striae and rare parallel striae.	Striae show either no preferred orientation or are weakly clustered, but unrelated to the long axis.	Striae orientation ranges from no preferred orientation to parallel. Some show long axis parallel striae, but many are weakly clustered and oblique to the long axis.	
Striae & clast size	Longer and wider striae occur on larger clasts. Average striae length ranges from 4.5 mm to 13.2 mm. Average width ranges from 0.39 mm to 0.74 mm. No wide compound striae seen.	Relationship between striae size and clast size is not obvious. Average length ranges from 6 mm to 10 mm. Average width ranges from 0.54 to 0.90. Some clasts have compound striae.	Average length ranges from 4.5 mm to 7.29 mm and is not related to clasts size. Average width ranges from 0.78 mm to 1 mm, with wider striae occurring on larger clasts. Frequent compound striae.	Length and width unrelated to clast size. Average length ranges from 4.1 mm to 5.7 mm and average width ranges from 0.4 to 0.5 mm. Occasional compound striae.	Larger clasts show longer and wider striae. Average length ranges from 4.9 mm to 20.5 mm. Average width ranges from 1.76 mm to 1.69 mm. Wide compound striae are common. Some striated surfaces from Ngapotiki Fault have a corrugated ridge and groove appearance.	
Striae & clast round-ness	Striae occur on clasts in roundness classes 0.2-0.7 (angular to well-rounded clasts). Most common on 0.5 (rounded)	Striae occur on clasts in the 0.2-0.5 roundness classes (angular to rounded clasts)	Striae only occur on clasts in the 0.1 roundness class (very-angular).	Striae occur on clasts in 0.1-0.4 roundness classes (v. angular to sub-rounded)	Striae occur on clasts in 0.2 – 0.6 roundness classes, (angular to rounded) but preferentially on 0.6 (rounded). Striae are often concentrated on margins of clasts where surface curved toward the clast end.	Striae occur on clasts in 0.2-0.7 roundness classes, (angular to well-rounded) but 91% occur on 0.5-0.7 (sub-rounded to rounded). Striae often concentrated on margins of clasts.
Striae density	High density. Striae per cm^2 ranges from 2 to 4. Background striae is 100 %. Striae are widely distributed.	High density. Striae per cm^2 ranges from 2.1 to 3.3. Background striae is at least 92 %. Striae are widely distributed.	Variable density. Striae per cm^2 ranges from 1.2 to 1.7. Background striae ranges from 28 % to 59 %. Striae distribution is patchy.	Variable density. Striae per cm^2 ranges from 1.4 to 2.8. Background striae rages from 20 % to 100%. Striae distribution is irregular.	Variable density. Striae per cm^2 ranges from 0.35 to 2.2. Background striae ranges from 40% to 100%. Larger clasts have lower striae density than smaller clasts.	
Other	Curved striae may indicate rotation and realignment of clast during transport. Many studies acknowledge lithology is important for striae generation.	Some clasts show curved striae. Striae are rare on granite, and occasional on dolerite clasts. Common on fine sedimentary clasts.	Some clasts show rare curved striae.	All clasts show rare curved striae	Some clasts show curved striae.	Some clasts show curved striae.

8.3.5 Striae survivability and fluvial transport distance

The study of the "survivability" of glacial features of clasts (shape, facets and striae) during fluvial transport downstream from the Murchison temperate glacier has shown that these features change progressively and predictably with increasing fluvial transport distance. This allows transport distance and the proximity to the glacier margin to be estimated for glaciofluvial deposits in glacial environment reconstructions. The data from this study indicate that on sandstone and argillite clasts, striae are removed within 1 to 2 km of fluvial transport. Therefore, glaciofluvial deposits with striated clasts are distinctly glacier proximal. Glacially produced facets survive longer, but most are removed within 4 to 6 km of fluvial transport. Glacial facets become increasingly difficult to distinguish from other flattish surfaces under increasing fluvial transport but some appear to survive at least 11 km. While it would be inappropriate to make too strong a claim from a single study of this sort, the results are considered to indicate at least the order of distance associated with the changes described here.

8.4 POLAR GLACIAL ABRASION FEATURES

Four types of linear abrasion marks produced by a cold-based glacier at Allan Hills, Antarctica, have been identified in this thesis. Measurements of abrasion mark shape, distribution and orientation has allowed the construction of a model of cold-based glacier abrasion processes and documented a previously unrecognised cold-based glacier advance 2 km into the present ice-free area of Allan Hills. Abrasions that occur on wind-polished dolerite clasts are formed by debris being dragged over the clast surface. However, the clasts were not transported beneath the glacier, but rather abraded *in situ*. Therefore the abrasion marks usually occur on the stoss side of the clasts and are oriented parallel to the direction of glacier movement rather than the long-axis of the clasts. In addition, the length and width of the abrasion marks is extremely variable and depends on the shape of the abrading fragment and the shape of the abraded clast.

Overall, the discovery of abrasion marks from a cold-based glacier is a significant advance in understanding polar glacial processes and has provided new criteria for recognising the passage of cold-based glaciers in polar areas or regions where cold-based ice may have existed in the past. These results are also presented in Atkins et al. (2002), included at the end of this thesis.

8.5 ACHIEVEMENTS AND FUTURE WORK

This study has provided the first systematic study of linear abrasion features from both glacial and non-glacial environments. The results have shown that non-glacial striae are more common than is generally acknowledged and that useful conclusions can be made on the basis of combined clast shape and striae analyses. The study has also identified several features of striae indicative of certain environments, which has indicated the potential for further work to establish better criteria for interpreting striated surfaces in the geological record. Although the numbers of striated clasts in this study is low, and therefore the conclusions must be treated as tentative, a new procedure has been established for the analysis of striae. In doing so, many difficulties were overcome, but some remain.

In addition, previously unrecognised features of erosion from cold-based glaciers have been described and criteria provided for recognising cold-based erosion in other locations. Finally, the survivability of glacial abrasion features of clasts once they have entered a fluvial system has been assessed, providing a basis for estimating the proximity of a glaciofluvial deposit to the glacier front.

To develop striae analysis as a more effective palaeoenvironmental tool, future research could concentrate on producing further systematic descriptions of striae from both glacial and non-glacial environments. This might involve recording further distinctive features of striae by extending the "atlas of linear abrasion features", but also is likely to require a more sophisticated approach, possibly employing computer-based digital image analysis to recognise more subtle differences in striae shape.

REFERENCES

Agassiz, J.L.R., 1838, On glaciers and the evidence of their having once existed in Scotland, Ireland an England. Proceedings of the Geological Society of London, v. 3, p. 327-332.

Aitchison, J.C., Bradshaw, M.A., and Newman, J., 1988, Lithofacies and origin of the Buckeye Formation: Late Paleozoic glacial and glaciomarine sediments, Ohio Range, Transantarctic Mountains, Antarctica. Palaeogeography, Palaeoclimatology, Palaeoecology, v. 64, p. 93-104.

Aitken, J.D., 1991, Two late Proterozoic glaciations, Mackenzie Mountains, northwest Canada. Geology, v. 19, p. 445-448.

Anderson, J.B., 1983, Ancient glacial-marine deposits: their spatial and temporal distribution. In: Glacial-marine sedimentation, B.F., Molnia, (ed), Plenum Press, New York, p. 3-92.

Atkins, C.B., and Barrett, P.J., 2000, Field report for 1997 on glacial deposits at Allan Hills, Antarctica. Victoria University Antarctic Data Series Report, no. 22, 36 p.

Atkins, C.B., 2001, Glacial influence from clast features in Oligocene and Miocene strata cored in CRP-2/2A and CRP-3, Victoria Land Basin, Antarctica. In: Studies from the Cape Roberts Project, Ross sea, Antarctica, Scientific Results of CRP-3. Terra Antarctica, v. 8, no. 3, p. 263-274.

Atkins, C.B., Barrett, P.J., and Hicock, S., 2002, Cold glaciers erode and deposit: Evidence from Allan Hills, Antarctica. Geology, v. 30, no. 7, p. 659-662.

Ballance, P.F., and Watters, W.A., 1971, The Mawson Diamictite and the Carapace Sandstone Formations of the Ferrar Group at Allan Hills and Carapace Nunatak, Victoria Land, Antarctica: New Zealand Journal of Geology and Geophysics, v. 14, p. 512-527.

Barnett, V.H., 1910, Striations in gravel bars of the Yukon and Porcupine Rivers, Alaska. Bulletin of the Geological Society of America, v. 20, p. 76-78.

Barrett, P.J., 1975b, Characteristics of pebbles from Cenozoic marine glacial sediments in the Ross Sea (DSDP sites 270-274) and the south Indian Ocean (site 268). In Hayes, D.E and Frakes, L.A, (eds) 1975, Initial reports of the Deep Sea Drilling Project, Washington. 28, p. 769-784.

Barrett, P.J., 1980, The shape of rock particles, a critical review. Sedimentology, v. 27, p. 291-303.

Barrett, P.J., Henrys, S., Bartek, L.R., Brancolini, G., Busetti, M., Davey, F.J., Hannah, M.J., and Pyne, A.R., 1995, Geology of the margin of the Victoria Land basin off Cape Roberts, southwest Ross Sea. In: Cooper, A.K., Barker, P.F., and Barncolini, G, (eds.), Geology and Seismic stratigraphy of the Antarctic margin, Antarctic Research Series, v. 69, AGU, Washington, p.183-208.

Bates, R.L., and Jackson, J.A., (eds), 1987, Glossary of Geology, third edition, American Geological Institute, Alexandria, Virginia.

Begg, J., Perrin, N., and Van Dissen, R., 1997, The Wellington-Hutt valley segment of the Wellington Fault. In: Geological Society of New Zealand Annual Conference Field Trip Guide, November, 1997.

Benn, D.I., 1994, Fabric shape and the interpretation of sedimentary fabric data. Journal of Sedimentary Research, v. 51, p. 63-71.

Benn, D.I., and Evans, D.J.A., 1998, Glaciers and Glaciation. London, Arnold, 734 p.

Benn, D.I., and Ballantyne, C.K., 1993, The description and representation of particle shape. Earth Surface Processes and Landforms, v. 18, p. 665-672.

Benn, D.I., and Ballantyne, C.K., 1994, Reconstructing the transport history of glacigenic sediments: a new approach based on the co-variance of clast form indices. Sedimentary Geology, v. 91, p. 215-227.

Bennett, M.R., Doyle, P., and Mather, A.E., 1996, Dropstones: Their origin and significance: a comment. Palaeogeography, Palaeoclimatology, Palaeoecology, v. 121, p. 331-339.

Bennett, M.R., Doyle, P., Mather, A.E., and Woodfin, J.L., 1994, Testing the significance of dropstones: an example from southeast Spain. Geological Magazine, v. 131, no.6, p. 845-848.

Bennett, M.R., Hambrey, M.J., and Huddart, D., 1997, Modification of clast shape in high-Arctic glacial environments. Journal of Sedimentary Research, v.67, no.3, p. 550-559.

Bennett M.R., Waller R.I., Glasser N.F., Hambrey M.J., and Huddart D., 1999, Glacigenic clast fabrics: genetic fingerprint or wishful thinking? Journal of Quaternary Science, v. 14, no. 2, p. 125-135.

Berryman, K. R., 1990, Late Quaternary movement on the Wellington Fault in the Upper Hutt area, New Zealand. New Zealand Journal of Geology and Geophysics, v. 33, p. 257-270.

Bishop, K.M., 1997, Miocene rock-avalanche deposits, Halloran/Silurian Hills area, Southeastern California. Environmental and Engineering Geoscience, v. 3, no. 4, p. 501-

512.

Blackwelder, E., 1930, Striated boulders as evidence of glacial action. Geological Society of America Bulletin, v. 41, p. 154.

Blatter, H., and Hutter, K., 1991, Polythermal conditions in Arctic glaciers. Journal of Glaciology, v. 37, p. 261-269.

Boulton, G.S., 1972, The role of thermal regime in glacial sedimentation, *in* Price, R. J., and Sugden, D. E., compilers, Polar geomorphology: London, Institute of British Geographers Special Publication, no. 4, p. 1-19.

Boulton G.S., 1978, Boulder shapes and grain-size distributions of debris as indicators of transport paths through a glacier and till genesis. Sedimentology, v. 25, p. 773-799.

Boulton, G.S., 1974, Processes and patterns of glacial erosion. In, Coates, D.R., (ed), Glacial Geomorphology. Binghampton, NY, State University of New York, p. 41-87.

Boulton, G. S., 1979, Processes of glacier erosion on different substrata. Journal of Glaciology, v. 23, no. 89, p. 15-37.

Calkin, P. E., 1974, Subglacial geomorphology surrounding the ice-free valleys of southern Victoria Land, Antarctica. Journal of Glaciology, v. 13, p. 415-431.

Cape Roberts Science Team, 1999. Studies from the Cape Roberts Project, Ross Sea, Antarctica, Initial Report on CRP-2/2A. Terra Antarctica, v. 6, nos. 1/2, p. 1-173. With Supplement, 245 p.

Cape Roberts Science Team, 2000. Studies from the Cape Roberts Project, Ross Sea, Antarctica, Initial report on CRP-3, Terra Antarctica, v. 7. nos. 1/2, p. 1-209. With Supplement, 305 p.

Chamberlain, T.C., 1888, Rock scourings of the great ice invasion. U.S Geological Survey annual report, v. 7, p. 147-248.

Chinn, T.J., 1996, New Zealand glacier responses to climate change of the past century. New Zealand Journal of Geology and Geophysics, v. 39, no.3, p. 415-428.

Chumakov, N.M., 1998, Stones scattered in Cretaceous deposits in South England. Lithology and Mineral Resources, v. 33, no. 4, p. 313-326.

Clifton, H.E., 1965, Tectonic polish of pebbles. Journal of Sedimentary Petrology, v. 35, p. 867-873.

Cuffey, K.M., Conway, H., Hallet, B., Gades, A.M., and Raymond, C.F., 1999, Interfacial water in polar glaciers and glacier sliding at –17 ^{0}C. Geophysical Research Letters, v. 26, p. 751-752.

Cuffey, K.M., Conway, H., Gades, A.M., Hallet, B., Lorrain, R., Severinghaus, J.P., Steig, E.J., Vaughn, B., and White, J.W.C., 2000, Entrainment at cold glacier bed. Geology, v. 28, p. 351-354.

Decker, E.R., and Bucher, G.J., 1982, Geothermal studies in the Ross Island-Dry Valley region. In: C., Craddock (ed). Antarctic Geosciences, University of Wisconsin Press, Madison, Wisconsin, 1982, p.887-895.

Denton, G.H., and Hughes, T.J., 2002, Reconstructing the Antarctic Ice Sheet at the Last Glacial Maximum. Quaternary Science Reviews, v. 21, p. 193-202.

Dionne, J., 1970, Aspects morpho-sedimenologiques du glacial, en particulier descotes du Saint-Laurent. Unpublished PhD thesis, University of Paris.

Dionne, J., 1973, Distiction entre stries glacielles et stries. Revue de geographie de la Montreal, v. 27, no. 2, p. 185-190.

Dionne, J., 1979, Ice action in the Lacustrine environment. A review with particular reference to subarctic Quebec, Canada. Earth Science Reviews, v. 15, p. 185-212.

Dionne, J., 1985, Drift-ice abrasion marks along rocky shores. Journal of Glaciology, v. 31, no. 109, p. 237-241.

Domack, E.W., Anderson, B., and Kurtz, D.D., 1980, Clast shape as an indicator of transport and depositional mechanisms in glacial marine sediments: George V Continental Shelf, Antarctica. Journal of Sedimentary Petrology, v. 50, no. 3, p. 813-820.

Domack, E.W., and Lawson, D.E., 1985, Pebble fabric in an ice-rafted diamicton. Journal of Geology, v. 93, p. 577-591.

Donovan, S.K., and Pickerill, R.K., 1997, Dropstones: Their origin and significance: a comment. Palaeogeography, Palaeoclimatology, Palaeoecology, v. 131, p. 175-178.

Dowdeswell, J.A., Hambrey, M.J., Wu Ruitang., 1985, A comparison of clast fabric and shape in late Precambrian and modern glacigenic sediments. Journal of Sedimentary Petrology, v. 55, no. 5, p. 691-704.

Dott, R.H., JR. 1961, Squantum "Tillite", Massachusetts- Evidence of glaciation or subaqueous mass movements? Geological Society of America Bulletin, v. 72, p. 1289-1306.

Drake, L.D., 1972, Mechanisms of clast attrition in basal till. Geological Society of America Bulletin, v. 83, p. 2159-2166.

Drewry, D.J., 1986, Glacial Geologic Processes. London: Edward Arnold, 276 p.

Dyson, J.L., 1937, Snowslide striations. Journal of Geology, v. 45, p. 549-557.

Echelmeyer, K., and Wang, Z., 1987, Direct observation of basal sliding and deformation of basal drift at sub-freezing temperatures. Journal of Glaciology, v. 33, no. 113, p. 83-98.

England, J., 1986, Glacial erosion of a high Arctic valley. Journal of Glaciology, v. 32. no. 110, p. 60-64.

Eyles, N., 1990, Marine debris-flows. Late Precambrian "tillites" of the Avalonian – Cadomian orogenic belt. Palaeogeography, Palaeoclimatology, Palaeoecology, v. 79, p. 73-98.

Eyles, N., 1993, Earth's glacial record and its tectonic setting. Earth Science Reviews, v. 35, p. 1-248.

Eyles, N., and Boyce, J.I., 1998, Kinematic indicators in fault gouge; tectonic analog for soft-bedded ice sheets. Sedimentary Geology, v. 116, no. 1-2, p. 1-12.

Eyles, C.H., and Eyles, N., 1989, The Upper Cenozoic White River "tillites" of southern Alaska: Subaerial slope and fan delta deposits in a strike-slip setting. Geological Society of America Bulletin, v. 101, p. 1091-1102.

Falconer, G., 1966, Preservation of vegetation and patterned ground under a thin ice body in Baffin Island, N.W.T, Geographical Bulletin, v. 8, no. 2, p. 194-200.

Faure, G., and Buchanan, D., 1987, Glaciology of the East Antarctic Ice Sheet at the Allan Hills: a preliminary interpretation. Antarctic Journal of the United States, v. 22, p. 74-75.

Fielding, C.R., Naish, T.R., and Woolfe, K.J., 2001. Facies architecture of the CRP-3 drillhole, Victoria Land Basin, Antarctica. Terra Antarctica, v. 8, no. 3, p. 217-224.

Fininger, T., 1978, The extraordinary striated outcrop at Saqsaywaman, Peru. Geological Society of America Bulletin, v. 89, p. 494-503.

Fininger, T., 1979, The extraordinary striated outcrop at Saqsaywaman, Peru: Discussion and reply. Geological Society of America Bulletin, Part 1, v. 90, p. 320.

Flemming, R.W., and Johnson, A.M., 1989, Structures associated with strike-slip faults that bound landslide elements. Engineering Geology, v. 27, p. 39-114.

Fleuty, M.J., 1975, Slickensides and slickenlines. Geological Magazine, v. 112, no. 3, p. 319-322.

Flint, R.F., 1971, Glacial and Quaternary Geology, New York.

Fowler, A.C., 1986, Sub-temperate basal sliding. Journal of Glaciology, v. 32, no. 110, p. 3-5.

Frakes, L.A., 1979, Climates throughout geologic time. Elsevier Scientific Publishing, 310p.

Fry, N., 1992, Stress ratio determinations from striated faults: a spherical plot for cases of near vertical principal stresses. Journal of Structural Geology, v. 14, p. 1121-1131.

Gair, H.S., 1967, Geological map of New Zealand 1:250000, Sheet 20, Mt Cook 1st Edition. Department of Scientific and Industrial Research, Wellington, New Zealand.

Gary, M., McAfee, R.Jr., and Wolf, C.L., (eds), 1977, Glossary of Geology. American Geological institute, Washington, DC.

Geikie, A., 1863, On the glacial drift of Scotland. Geological Society of Glasgow Transactions, I, pt. II, p. 1-190.

Gilbert, R., 1990, Rafting in glacimarine environments. In: Dowdeswell, J.A., and Scourse, J.D., (eds.) 1990, Glacimarine Environments: Processes and Sediments. Geological Society Special Publication no. 53, p.105-120.

Glasser, N.F., Crawford, K.R., Hambrey, M.J., Bennett, M.R. and Huddart, D., 1998, Lithological and structural controls on the surface wear characteristics of glaciated metamorphic bedrock surfaces: Ossian Sarsfjellet, Svalbard. Journal of Geology, v. 106. p. 319-329.

Goldthwait, R.P., 1960, Study of ice cliff in Nanatarssuag, Greenland, Technical Report of snow, ice and permafrost research establishment, v. 39, p. 1-103.

Grange, L.I., 1931, Conical hills on Egmont and Ruapehu volcanoes. New Zealand Journal of Science and Technology, v. 12, p. 376-384.

Grapes, R. H., Little, T.A., Browne, G.H., Rait, G.J., 1997, Ngapotiki Thrust, White Rock and Te Kaukau Point, Southeast Wairarapa: Active and Inactive structures of the Hikurangi Forearc. In: Geological Society of New Zealand Annual Conference Field Trip Guide, November, 1997.

Greely, R., and Iverson, J.D., 1985, Wind as a geological Process. Cambridge University Press, Cambridge, p. 333.

Gregg, D.R., 1960, The Geology of Tongariro subdivision. New Zealand Geological Survey Bulletin, no. 40, DSIR, Wellington.

Gregory, H.E., 1915, Notes on the shape of pebbles. American Journal of Science, 4th survey, v. 39, p.300-304.

Grey, J.M., 1982, Unweathered, glaciated bedrock on an exposed lakebed in Wales. Journal of Glaciology, v. 28, no. 10, p. 483-497.

Grunewald, U., Sparks, R.S.J., Kearns, S., and Komorowski, J C., 2000, Friction marks on blocks from pyroclastic flow on Soufriere Hills volcano, Montserrat: Implications for flow mechanisms. Geology, v. 28, no. 9, p. 827-830.

Hackett, W.R., and Houghton, B.F., 1989, A facies model for a Quaternary andesite composite volcano: Ruapehu, New Zealand. Bulletin of Volcanology, v. 51, p. 51-68.

Hall, K.J., 1989, Clast Shape. In: Barrett, P. J., (ed.), Antarctic Cenozoic History from the CIROS-1 Drillhole, McMurdo Sound, Antarctica. Wellington DSIR Bulletin, v. 245, p. 63-66.

Hallet, B., 1979, A theoretical model of glacial abrasion. Journal of Glaciology, v. 23, no. 89, p. 39-50.

Hallet, B., 1981, Glacial abrasion and sliding: their dependence on debris concentration in basal ice. Annals of Glaciology, v. 2, p. 23-28.

Hallet, B., 1996, Glacial quarrying: a simple theoretical model. Annals of Glaciology, v. 22, p. 1-8.

Hambrey, M.J., 1994, Glacial Environments. UCL Press. University College. London, 296 p.

Hambrey, M.J., 1989, Grain Fabric. In: Barrett, P.J., (ed), Antarctic Cenozoic History from the CIROS-1 drillhole, McMurdo Sound. DSIR Bulletin, v. 245, p. 59-62.

Hambrey, M.J., and Harland, W.B., 1981, (eds), Earths pre-Pleistocene glacial record. International Geological Correlation Programme, project 38: Cambridge University Press.

Hancock, P.L., and Barka, A.A., 1987, Kinematic indicators on active normal faults in western Turkey. Journal of Structural Geology, v. 9, no. 5/6, p. 573-584.

Hancox, G.T., Chinn, T.J., and McSaveney, M.J., 1991, Immediate report-Mt Cook rock avalanche, 14 December 1991. DSIR Geology and Geophysics, Lower Hutt, New Zealand, 15 p.

Harrington, H.J., 1971, Glacial-like "Striated floor" originated by Debris-laden torrential water flows. Journal of Sedimentary Petrology, v. 40, p. 1344-1347.

Hart, J.K., 1996, Proglacial glaciotectonic deformation associated with glaciolacustrine sedimentation, Lake Pukaki, New Zealand. Journal of Quaternary Science, v. 11, no. 2, p, 149-160.

Hewitt, K., 1999, Quaternary moraines vs catastrophic rock-avalanches in the Karakoram Himalaya, Northern Pakistan. Quaternary Research, v. 51, p. 220-237.

Hicock, S.R., 2000, Mesoscopic analysis of diamictite in semiconsolidated, non-oriented core. Journal of Sedimentary Research, Section B: Stratigraphy and Global Studies, v. 70, p. 967-969.

Hindmarsh, R.C.A., 1996, Sliding of till over bedrock: scratching, polishing, comminution and kinetic-wave theory. Annals of Glaciology, v. 22, p. 105-115.

Hochstein, M.P., Nobes, D.C., Leary, S.F., Claridge, D., Henrys, S.A., and Pyne, A., 1995, Downwasting of the Tasman Glacier, South Island, New Zealand: changes in the terminus region between 1971 and 1993. New Zealand Journal of Geology and Geophysics, v. 38, no. 1, p. 1-16.

Holdsworth, G., 1974, Meserve Glacier, Wright Valley, Antarctica: part 1. Basal processes: Ohio State University, Institute of Polar Studies Report, no. 37, 104 p.

Holmes, C.D., 1941, Till Fabric. Geological Society of America Bulletin, v. 52, p. 1299-1354.

Holmes, C.D., 1960, Evolution of till stone shapes, Central New York. Geological Society of America Bulletin, v. 71, p. 1645-1660.

Holmlund, P., and Näslund, J.O., 1994, The glacially sculptured landscape of Dronning Maud Land, Antarctica, formed by wet-based mountain glaciation and not by the present ice sheet, Boreas, v. 23, p. 139-148.

Homer, L., and Moore, P., 1989, Reading the Rocks, A guide to the geological features of the Wairarapa, New Zealand Geological Survey, DSIR, Landscape Publishing Limited, Wellington, New Zealand.

Hovey, E.O., 1909, Striations and U-shaped valleys produced by other than glacial action. Bulletin of the Geological Society of America, v. 20, p. 409-416.

Huddart, D., 1994, Rock-type controls on downstream changes in clast parameters in sandur systems in southesast Iceland. Journal of Sedimentary Research, Part A: Sedimentary Petrology and Processes, v. 64, no. 2, p. 215-225.

Huggett, Q.J., and Kidd, R.B., 1983, Identification of ice-rafted and other exotic material in deep-sea dredge hauls. Geo-Marine Letters, v. 3, p. 23-29.

Hughes, T.J., 1998, Ice sheets: Oxford, Oxford University Press, 343 p.

Humlum, O., 1985, Changes in texture and fabric of particles in glacial traction with distance from source, Myrdalsjokull, Iceland. Journal of Glaciology, v. 31, p. 150-156.

Iverson, N.R., 1988, Variables influencing the depth of glacial striations. Abstracts with programs - Geological Society of America, v. 20, no. 6, p. 422.

Iverson, N.R., 1990, Laboratory simulations of glacial abrasion: comparison with theory. Journal of Glaciology, v. 36, no. 124, p. 304-314.

Iverson, N.R., 1991, Morphology of glacial striae: Implications for abrasion of glacier beds and fault surfaces. Geological Society of America Bulletin, v. 103, p. 1308-1316.

Jensen, P.A., and Wulff-Pedersen, E., 1996, Glacial of non-glacial origin for the Bigganjargga Tillite, Finnmark, Northern Norway. Geological Magazine, v. 133, no. 2, p. 137-145.

Judson, S., and Barks, R.E., 1961, Microstriations on polished pebbles. American Journal of Science, v. 259, p. 371-381.

Klemen, J., 1990, On the use of glacial striae for reconstruction of paleo-ice sheet flow patterns. Geografiska Annaler, series A Pysical Geography, v. 72, no. 3-4, p. 217-236.

Kleman, J., and Borgstrom, I., 1994, Glacial land forms indicative of a partly frozen bed. Journal of Glaciology, v. 40, p. 255-264.

Kleman, J., Borgstrom, I., Hattestand, C., 1994, Evidence for a relict glacial landscape in Quebec-Labrador, Palaeogeography, Palaeoclimatology, Palaeoecology, v. 111, p. 217-228.

Kruger, J., 1984, Clasts with stoss-lee form in lodgement tills: a discussion. Journal of Glaciology, v. 30, no. 105, p.241-243.

Krumbein, W.C., 1941, Measurement and geological significance of shape and roundness of sedimentary particles. Journal of Sedimentary Petrology, v. 11, p. 64-72.

Kuenen, P.H., 1971, Unpublished, The longtitudinal striation of glacial erratics (with experiments). Courtesy, J. J.M. van der Meer, Department of Geography, Queen Mary, University of London.

Kuhn, G., Melles, M., Ehrmann, W.U., Hambrey, M.J., and Schmiedl, G., 1993, Character of clasts in glaciomarine sediments as indicator of transport and depositional processes, Weddell and Lazarev seas, Antarctica. Journal of Sedimentary Petrology, v. 63, no. 3, p. 477-487.

Laverdiere, C., Guimont, P., 1980, Terminologie, illustree des forms minures D'erosion glaciaire. In: Le vocabulaire de la Geomorphologie glaciaire, IX. Geogr. Phys. Quat., v. 34, no. 3, p. 363-377.

Laverdiere, C., Guimont, P., Dionne, J., 1985, Les forms et les marques de l'erosion glaciaire du plancher rocheux; signification, terminologie, illustration. Palaeogeography, Palaeoclimatology, Palaeoecology, v. 51, no. 1-4, p. 365-387.

Laverdiere, C., Guimont, P., Pharand, M., 1979, Marks and forms on glacier beds: Formation and classification. Journal of Glaciology, v. 23, p. 414-416.

Lewis, C.A., and Illgner, P.M., 2000, Late Quaternary glaciation in southern Africa: moraine ridges and glacial deposits at Mount Enterprise in the Drakensberg of Eastern Cape Province, South Africa. Journal of Quaternary Science, v. 16, no. 4, p. 365-374.

Lewis, K. B., and Pettinga, J. R. 1993. The emerging, imbricate frontal wedge of the Hikurangi margin. In South Pacific sedimentary basins. Sedimentary basins of the world 2. P.F. Balance (ed). p. 225-250. Elsevier Science Publications B. V., Amsterdam.

Lliboutry, L., 1973, Microstriated ground in the Andes. (Discussion.) Journal of Glaciology, v. 13, no. 68. p. 322.

Lundin, E.R., 1989, Thrusting of the Claron Formation, the Bryce Canyon region, Utah. Geological Society of America Bulletin, v. 101, p. 1038-1050.

Lundqvist, J., 1989, Till and glacial landforms in a dry, polar region. Zeitschrift Fur Geomorphologie NF, v. 33, no. 1, p. 27-41.

Macpherson, A.J., 1987, The Mackay glacier/Granite harbour system (Ross Dependency, Antarctica) -a study in nearshore glacial marine sedimentation. Unpublished PhD thesis, Victoria University of Wellington library.

Mathews, W.H., 1979, Simulated glacial abrasion. Journal of Glaciology, v. 23, no. 89. p. 51-56.

Mattsson, A., 1997, Glacial striae, glacigenous sediments and Weichselian ice movements in southernmost Sweden. Sedimentary Geology, v. 111, p. 285-311.

McCarroll, D., Matthews, J.A., and Shakesby, R.A., 1989, "Striations" produced by catastrophic subglacial drainage of a glacier-dammed lake, Mjolkedalsbreen, southern Norway. Journal of Glaciology, v. 35, no. 120, p. 193-196.

McLennan, A.G., 1971, Ambiguous "Glacial striae" formed near waterbodies. Canadian Journal of Earth Science, v. 8, p. 477-479.

Means, W. D. 1987. A newly recognized type of slickenside striation. Journal of Structural Geology, v. 9, no. 5/6, p. 585-590.

Menzies, J., (ed), 1995a, Modern glacial environments. Processes, dynamics and sediments. Butterworth-Heinemann Ltd. London.

Miller, H., 1850, On peculiar scratched pebbles, etc. in the boulder clay. Report of the British Association, p. 94.

Miller, H., 1884, On boulder glaciation: Royal Society Edinburgh Proceedings, v. 8, p 156-189.

Mills, H.H., 1979, Downstream rounding of pebbles: a quantitative review. Journal of Sedimentary Petrology, v. 49, p. 295-302.

Moncrieff, A.C.M., and Hambrey, M.J., 1988, Late Precambrian glacially-related grooved and striated surfaces in the Tillite Group of central east Greenland. Palaeogeography, Palaeoclimatology and Palaeoecology, v. 65, p. 183-200.

Näslund, J.O., 1997, Subglacial preservation of valley morphology at Amundsenisen, Western Dronning Maud Land, Antarctica: Earth Surface Processes and Landforms, v. 22, p. 441-455.

Naish, T.R., Barrett, P.J., Dunbar, G.B., Woolfe, K.J., Dunn, A.G., Henrys, S.A., Claps, M., Powell, R.D., Fielding, C.R., 2001a, Sedimentary cyclicity in CRP drillcore, Victoria Land Basin, Antarctica. Terra Antarctica, v. 8, no. 3, p.225-244.

Naish, T.R., Woolfe, K.J., Barrett, P.J., Wilson, G.S., **Atkins, C.B.,** and others. 2001b. Orbitally induced oscillations in the East Antarctic Ice Sheet: Direct evidence from the Cape Roberts Drilling Project. Nature, v. 413, p. 719-723.

Nicols, R.L., 1961, Characteristics of beaches formed in Polar climates. American Journal of Science, v. 259, p. 694-708.

Ocampo, A.C., Pope, K., Fisher, A.G., Morrison, J., Fisher, F., Alvarez, W., King, D., Rampino, M., Webster, C., 1996, Belize K/T boundary deposits; relation to Chicxulub impact. Abstracts with programs: Geological Society of America, 28th annual meeting, v. 28, no. 7, p. 182.

Palmer, B.A., and Neall, V.E., 1989, The Murimotu Formation – 9500 year old deposits of a debris avalanche and associated lahars, Mount Ruapehu, North Island, New Zealand. New Zealand Journal of Geology and Geophysics, v. 39, p. 477-486.

Park, J., 1926, Morainic mounds on the Waimarino Plain near Ruapehu. Transactions of the New Zealand Institute, v. 56, p. 382-383.

Petit, J.P., 1987, Criteria for the sense of movement on fault surfaces in brittle rocks. Journal of Structural Geology, v. 9, no. 5/6, p. 597-608.

Pettijohn, F.J., 1956, Sedimentary Rocks. 2nd edition. New York. Harper and Brothers. p. 718.

Porter, S.C, 1975, Equilibrium-line altitudes of late Quaternary glaciers in the Southern Alps, New Zealand. Quaternary Research, v. 5, p. 6-25.

Powell, R.D., Krissek, L.A., and van der Meer, J.J.M., 2000, Preliminary depositional environmental analysis of CRP-2/2A, Victoria Land Basin, Antarctica: Palaeoecological and palaeoclimatic inferences. Terra Antarctica, v. 7, no. 3, p. 313-322.

Powell, C.M., and Veevers, J.J., 1987, Namurian uplift in Australia and South America triggered the main Gondwanan glaciation. Nature, v. 326, no. 6109, p. 177-179.

Powers, M.C., 1953, A new roundness scale for sedimentary particles. Journal of Sedimentary Petrology, v. 23, p. 117-119.

Pyne, A.R., Barrett, P.J., Macpherson, A.J., Dunbar, R.B., 1991, Sedimentation around a polar marine glacier tongue, Mackay Glacier, South Victoria Land. Sixth International symposium on Antarctic Earth Sciences, International Symposium on Antarctic Earth Sciences, v. 6, p. 485-487.

Raine, J.I., and Askin, R.A., 2001, Terrestrial palynology of Cape Roberts Project drillcore CRP-3, Victoria Land Basin, Antarctica. Terra Antarctica, v. 8, no. 4, p. 389-400.

Rampino, M.R., Ernston, K., Fisher, A.G., King, D.T. Jr., Ocampo, A.C., Pope, K.O., 1996, Characteristics of clasts in K/T debris-flow diamictites in Belize compared with other known proximal ejecta deposits. Abstracts with programs - Geological Society of America, 28th annual meeting, v. 28, no. 7, p. 182.

Rastas, J., and Seppala, M., 1981, Rock jointing and abrasion on Roches moutonnees, SW Finland. Annals of Glaciology, v. 2, p. 159-163.

Rattenbury, M.S., and Sporli, K.B., 1985, Paleostress orientations from striations in Torlesse rocks, Otaki Forks, Tararua range, New Zealand. New Zealand Journal of Geology and Geophysics, v. 28, no. 3, p. 435-442.

Rea, B.R., Whalley, W.B., Rainey, M.M., and Gordon, J.E., 1996, Blockfields, old or new? Evidence and implications from some plateaus in northern Norway. Geomorphology, v. 15, p. 109-121.

Robertson, J.A., 1971, A long axis clast fabric comparison of the Squantum "Tillite", Massachusetts and the Gowganda Formation. Ontario. -Discussion. Journal of Sedimentary Petrology, v. 41, p. 606-608.

Robin, G. de Q., 1955, Ice movement and temperature distribution in glaciers and ice sheets: Journal of Glaciology, v. 2, p. 523-532.

Robin, G. de Q., 1983, General glaciology, *in* Robin, G. de Q., (ed), The climatic record in polar ice sheets: New York, Cambridge University Press, p. 212.

Savage, N.M., 1972, Soft-sediment glacial grooving of Dwyka age in South Africa. Journal of Sedimentary Petrology, v. 42, no. 2, p. 307- 308.

Schermerhorn, L.J.G., 1974a, Late Precambrian mixtites: glacial and/or nonglacial. American Journal of Science, v. 274, p. 673-824.

Schermerhorn, L.J.G., 1974b, No evidence for glacial origin of Late Precambrian tilliods in Angola. Nature, v. 252, p. 114-115.

Schopf, J.M., and Feininger, T., 1979, The extraordinary striated outcrop at Saqsaywaman, Peru: Discussion and reply. Geological Society of America Bulletin, v. 90, no. 3, p. 1390.

Schubert, C., 1973, Striated ground in the Venezuelan Andes. Journal of Glaciology, v. 12, no. 66, p. 461-468.

Schuster, R.L., and Crandell, D.R., 1984, Catastrophic debris avalanches from volcanoes. IV International Symposium on landslides proceedings, v. 1, p. 567-572.

Scott, K.M., 1988, Origins, behaviour, and sedimentology of lahars and lahar-runout flow in the Toutle-Cowlitz River system, Mount St. Helens, Washington. U.S. Geological Survey Professional Paper, 1447A, p. 76.

Scrivenor, J.B., 1929, The mudstream (lahars) of Gunong Keloel in Java. Geological Magazine, v. 66, p. 433-434.

Selby, M.J., 1993, Hillslope materials and processes. 2nd edition. Oxford University, 451 p.

Shakesby, R.A., and Matthews, J.A., 1996, Glacial activity and paraglacial landsliding in the Devensian late glacial: evidence from Craig Cerrig-gleisiad and Fan Dringarth, Fforest Fawr (Brecon Beacons), south Wales. Geological Journal, v.31, no. 2, p. 143-157.

Sharp, M., 1982, Modification of clasts in Lodgement tills by glacial erosion. Journal of Glaciology, v. 28, no. 100, p. 475-481.

Sharpe, D. R., and Shaw, J., 1989, Erosion of bedrock by subglacial meltwater, Cantley, Quebec. Geological Society of America Bulletin, v.101, p.1011-1020.

Shaw, J., 1987, Subglacial erosional marks, Wilton Creek, Ontario. Canadian Journal of Earth Science, v. 25, p. 1256-1267.

Shaw, J., 1994, Hairpin erosional marks, horseshoe vortices and subglacial erosion. Sedimentary Geology, v. 91, no. 1-4, p. 269-283.

Shoemaker, E.M., 1988, On the formation of basal drag for the case of sparse debris. Journal of Glaciology, v. 34, no. 118, p. 259-264.

Shreve, R. L., 1984, Glacier sliding at subfreezing temperatures. Journal of Glaciology, v. 30, p. 341-347.

Siegert, M.J., 2001, Ice sheets and late Quaternary environmental change: New York, Wiley, 231 p.

Sneed, E.D., and Folk, R.L., 1958, Pebbles in the lower Colorado River, Texas, a study on particle morphogenesis. Journal of Geology, v. 66, p 114-150.

Sparks, R. S. J., Gardeweg, M. C., Calder, E.S and Matthews, S. J., 1997, Erosion by pyroclastic flows on Lascar volcano, Chile. Bulletin of Volcanology, v. 58, p. 557-565.

Spenceley, A. P., 2001, Grooves and striations on the Stanthorpe Adamellite: evidence for a possible Late Middle- Late Triassic age glaciation. Australian Journal of Earth Sciences, v. 48, p. 777-784.

Splettstoesser, J. F., 1985, Unusual erosional feature in sandstone, Falkland Islands: striations caused by penguin feet. Abstracts with programs - Geological Society of America, v. 17, no. 5, p. 328.

Sugden, D.E., 1978. Glacial erosion by the Laurentide ice sheet. Journal of Glaciology, v. 20, no. 83, p. 367-391.

Sugden, D.E and John, B.S., 1976. Glaciers and Landscape. Edward Arnold, London.

Sugden, D.E., Denton, G.H., and Marchant, D.R., 1991, Subglacial meltwater channel systems and ice sheet overriding, Asgard Range, Antarctica: Geografiska Annaler, v. 73A, p. 109-121.

Summerfield, M.A., Sugden, D.E., Denton, G.H., Marchant, D.R., Cockburn, H.A.P., and Stuart, F.M., 1999, Cosmogenic isotope data support previous evidence of extremely low rates of denudation in the Dry Valleys region, southern Victoria Land, Antarctica, *in* Smith, B.J., et al., (eds), Uplift, erosion and stability: Geological Society [London], Special Publication 162, 255p.

Sundell, K. A., 1985, The Castle rocks chaos: A gigantic Eocene landslide-debris flow within the Southeastern Absaroka Range, Wyoming. PhD thesis, University of California, Santa Barbara.

Talarico, F., Sandroni, S., Fielding C., and **Atkins C.B.**, 2000. Variability, petrography and provenance of basement clasts from CRP-2/2A drillcore (Victoria Land Basin, Ross Sea, Antarctica). In Studies from the Cape Roberts Project, Ross sea, Antarctica, Scientific Results of CRP-2/2A, part 2. Terra Antarctica. v. 7, no. 4/5, p. 529-544.

The Concise Oxford Dictionary of current English, sixth edition, 1976, edited by J.B. Sykes. Oxford University Press, Ely House, London, 1368 p.

The New Penguin Dictionary of Geology, 1996, Kearey, P., Penguin Books, London, 366 p.

The Penguin Dictionary of Physical Geography, 1984, D.G.A., Whitten., Penguin Books, London, England, 591 p.

The Penguin Dictionary of Geology 1972, D.G.A., Whitten and J.R.V Brooks., Penguin Books, London, England, 495 p.

Tija, H.D., 1964, Slickensides and fault movements. Bulletin of the Geological Society of America, v. 75, p. 683-686.

Tija, H.D., 1971. Fault movement, reoriented stress field and subsidiary structures. Pacific Geology, v. .5, p. 49-70.

Todd, J. E., 1892, Striation of rocks by river ice. Economic Geology, p. 396-400.

Topping, W.W., 1973, Tephrostratigraphy and chronology of Late Quaternary eruptives from the Tongariro Volcanic Centre, New Zealand. New Zealand Journal of Geology and Geophysics, v. 16, p. 397-423.

Tremblay, M., 1961, Wind striations in northern Alberta and Saskatchewan, Canada. Geological Society of America Bulletin, v.72, p. 1561-1564.

Twiss, R.J., and Moores, E.M., 1992. Structural Geology. University of California at Davis. W. H. Freeman and company, New York, 532 p.

Varnes, D.J., 1958, Landslide types and processes. Highway research board, Special report (Washington, DC), v. 29, p. 20-47.

Virkkala, K., 1960, On striations and glacier movements in the Tampere region, southern Finland. Societe Geoloqique de Finlande, Comptes Renus, v. 32, p.159-176.

Van Houten, F.B., 1957, Appraisal of Ridgeway and Gunison "tillites" southwestern Colorado. Geological Society of America Bulletin, v. 68, p 383-388.

von Engeln, O.D., 1930, Type form of facetted and striated glacial pebbles. American Journal of Science, 5th series, v. 19. p. 9-16.

Wadell, H., 1932, Volume, shape and roundness of rock particles. Journal of Geology, v. 41, p. 310-331.

Wentworth, C.K., 1928, Striated cobbles in Southern States. Geological society of America Bulletin, v. 39, p. 941-954.

Wentworth, C.K., 1936a, An analysis of the shapes of glacial cobbles. Journal of Sedimentary Petrology, v. 6, p. 85-96.

Wentworth, C.K., 1936b, The shapes of glacial and ice jam cobbles. Journal of Sedimentary Petrology. v. 6, no.2, p. 97-108.

Weertman, J., 1961, Mechanism for the formation of inner moraines found near the edges of cold ice caps and ice sheets. Journal of Glaciology, v. 3, p. 965-978.

Whitney, M. I., 1978, The role of vorticity in developing lineation by wind erosion. Geological Society of America Bulletin, v. 89, p. 1-18.

Winterer, E.L., 1963, Late pre Cambrian pebbly mudstone in Normandy, France: tillite or tilliod? In Nairn, A.E.M., (ed), Problems in palaeoclimatology: London, Interscience, p. 159-178.

Winterer, E.L., and von der Borch, C.C., 1968, Striated pebbles in a mudflow deposit, South Australia. Palaeogeography, Palaeoclimatology, Palaeoecology, v. 5, no. 2, p.205-211.

Woodworth-Lynas, C.M.T., and Dowdeswell, J.A., 1994, Soft-sediment striated surfaces and massive diamicton facies produced by floating ice. In: Earths glacial record, 1994, M. Deynoux (ed), International Geological Correlation Project, 260, Cambridge.

Zamoruev, V.V., 1974, Striations on pebbles and boulders. Lithology and Mineral Resources, v. 9, no. 4, p. 475-479.

Zotov, V.D., 1940, Certain types of soil erosion and resultant relief features on the higher mountains of New Zealand. New Zealand Journal of Science and Technology, v. 21, p. 256-262.

APPENDIX 1

PHOTOGRAPHIC ATLAS OF LINEAR ABRASION FEATURES

Introduction

This photographic atlas provides images and notes on of linear abrasion features studied in this thesis. It is intended as a visual guide to the many characteristics of these features that are inherently difficult to describe numerically. It includes examples on scales from metres to millimetres.

Contents

The atlas comprises five parts representing three glacial and two non-glacial environments in which linear abrasions form.

Part One: **Temperate glacial striae**

Examples of striated clasts in debris layers from basal ice in the Mueller and Murchison Glaciers and from the Lake Pukaki moraine, Mt. Cook region, New Zealand.

Part Two: **Polythermal glacial striae**

Striated clast from overturned icebergs of the Mackay Glacier tongue and Cuff Cape, Granite Harbour, Victoria Land, Antarctica.

Part Three: **Cold-based linear abrasion features**

Examples of abraded bedrock and clasts from Allan Hills, Victoria Land, Antarctica.

Part Four: **Mass movement abrasion features**

Examples of striated clasts from a volcanic debris-avalanche, Mt Ruapehu, New Zealand and a rock-fall in the Murchison Valley, Mt. Cook region, New Zealand.

Part Five: **Tectonic striae**

Examples of striated clasts from a tectonically deformed fluvial deposit, Wellington Fault, New Zealand and tectonically deformed beach gravel, Ngapotiki Fault, New Zealand.

Methods

Field photographs of bedrock abrasion features were taken with a conventional 35mm camera using colour positive film.

Images of striated clasts presented in this Atlas were generated with a Canon G2 4.0 million pixel digital camera mounted vertically on a camera and lighting stand. The stand has an adjustable vertical camera mount and bi-directional lighting (Figure 1). Several removable close-up lenses were utilised depending on the scale of the clast.

Lighting direction and angles vary for each image and were designed to provide the clearest image of the striae. The lights used were four 75-watt fog lamps (two on each side on the base plate). These were usually set at 45° and the clast was illuminated from

one side only. A free-standing light box with two LED lights set in flexible arms was used for very low-angle lighting on some clasts.

Images were manipulated in Corel Photo-paint, Version 10 to enhance image intensity and contrast.

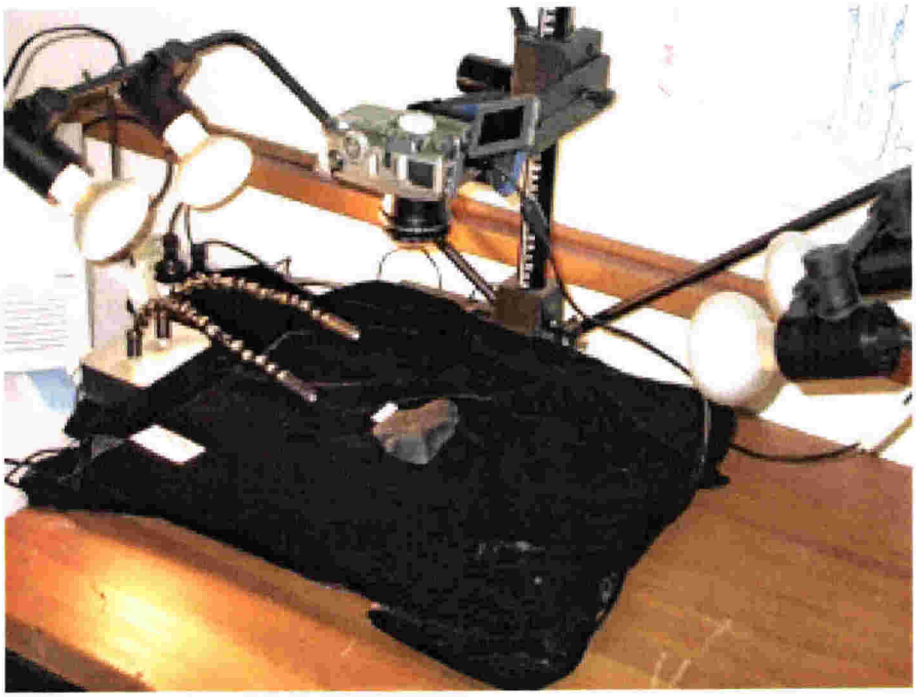

Figure 1. Camera and lighting stand used to take digital images of clasts. The camera is mounted vertically and the clast is illuminated from one side.

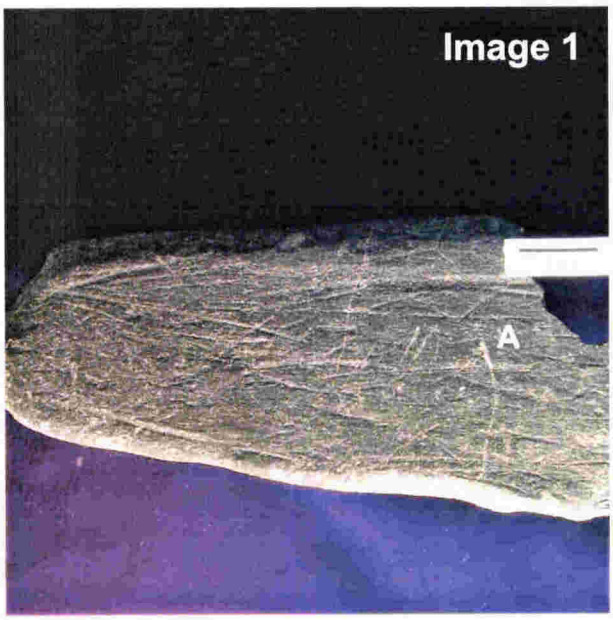

Parallel fine glacial striae

Image 1 shows a glacially faceted and striated argillite clast with a bullet shaped stoss end and a sharp, broken lee end.

Abundant fine striae occur on the facet, oriented predominantly parallel to the long axis of the clast. The surface has several larger striae up to 3 mm wide superimposed on a "background" of microstriae that are difficult to identify individually.

Striae orientation typically deviates by less than 15° from the clast long axis, although rare striae deviate up to 75° degrees (A).

Location: Lake Pukaki moraine, Mt. Cook region, New Zealand, 170°10'00"44°10'30"

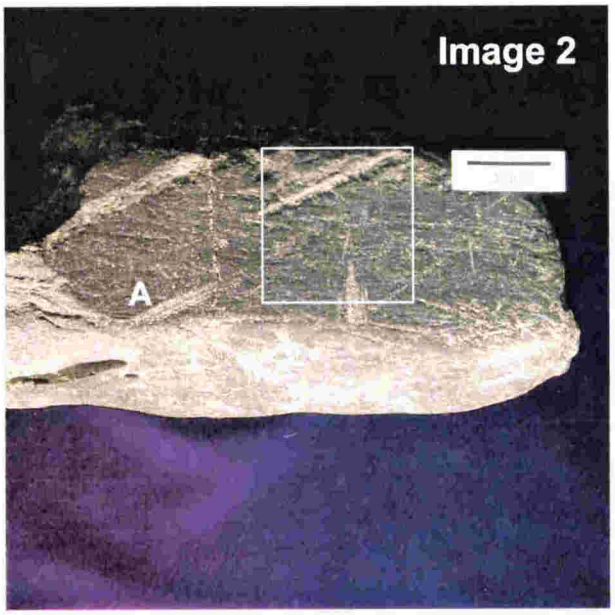

Large and small striae

Image 2 shows the obverse facet of the clast in Image 1.

On this surface, many long-axis parallel striae are clear, as well as larger striae oriented oblique to the long-axis. One of these large striae has smaller parallel striae on the surface (compound striation) (A).

Inset square is enlarged in Image 3.

Location: Lake Pukaki moraine, Mt. Cook region, New Zealand, 170°10'00"44°10'30"

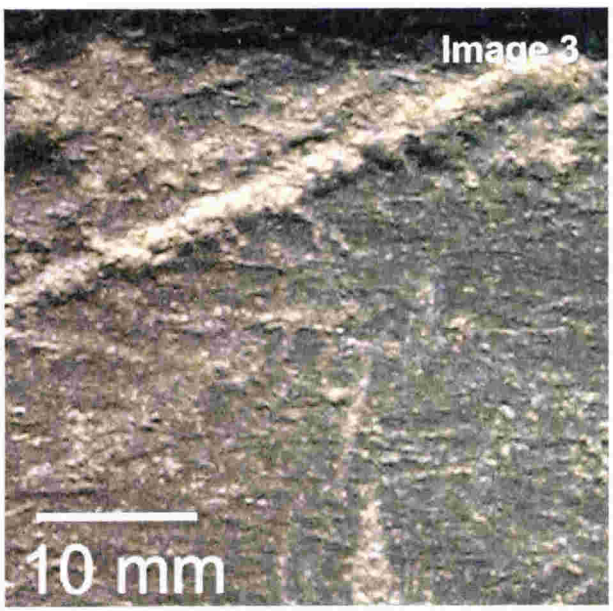

Closeup of large and small striae

Image 3 shows closeup detail of the surface of the clast in Image 2.

The large striation shown is 38 mm long and 6 mm wide with jagged sides and bottom. Some of these larger striae have several fine parallel striae on their surfaces.

Also visible is the "background" of microstriae (lower part of image).

Location: Lake Pukaki moraine, Mt. Cook region, New Zealand, 170°10'00"44°10'30"

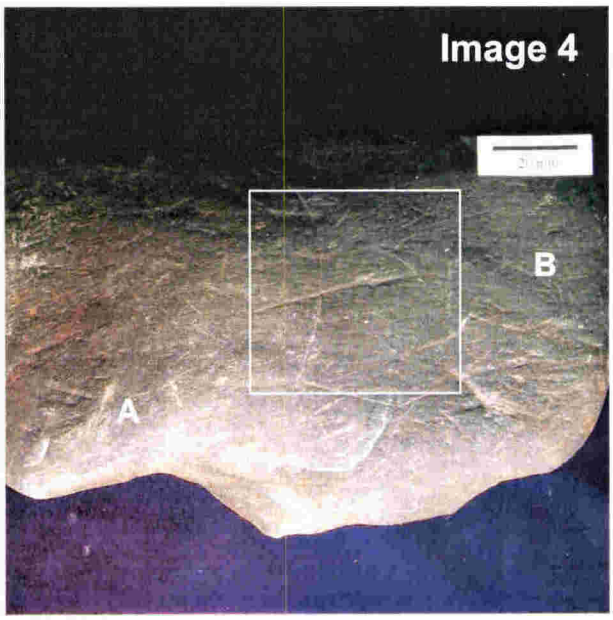

Parallel fine glacial striae

Image 4 is another example of parallel glacial striae on a glacially shaped argillite clast. Most striae are sub-parallel to the long axis of the clast.

The orientation of some larger striae deviate from the clast long axis by up to 65°(A).

A "background" of microstriae occurs over the entire surface of the clast.

Location: Lake Pukaki moraine, Mt. Cook region, New Zealand, 170°10'00"44°10'30'

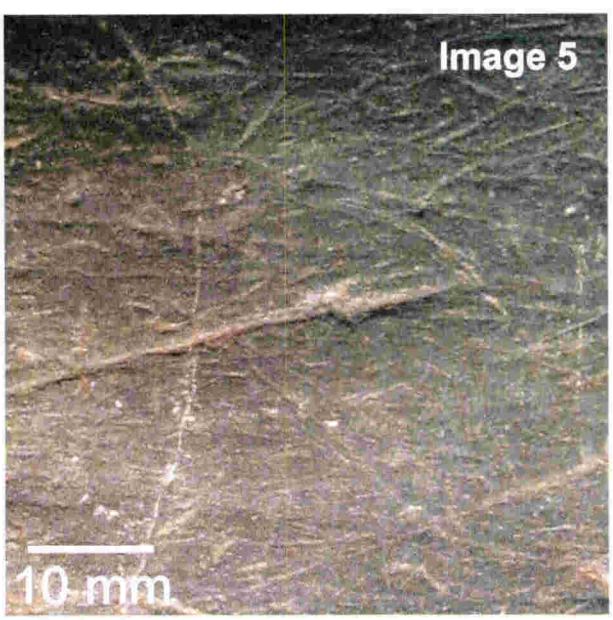

Closeup of parallel fine glacial striae

Image 5 shows a closeup of the surface of the clast in Image 4.

The large striation in the centre is 30 mm long and up to 1.5 mm wide and deviates by about 15° from the long axis of the clast.

The "background" microstriae are clearly visible at this scale.

Location: Lake Pukaki moraine, Mt. Cook region, New Zealand, 170°10'00"44°10'30'

Parallel fine glacial striae on a curved surface

Image 6 shows fine glacial striae oriented predominantly parallel to the clast long-axis but on a curved surface rather than a flat facet. This implies that the striating tools were held firmly against the clast as they were dragged over it.

Location: Lake Pukaki moraine, Mt. Cook region, New Zealand, 170°10'00"44°10'30"

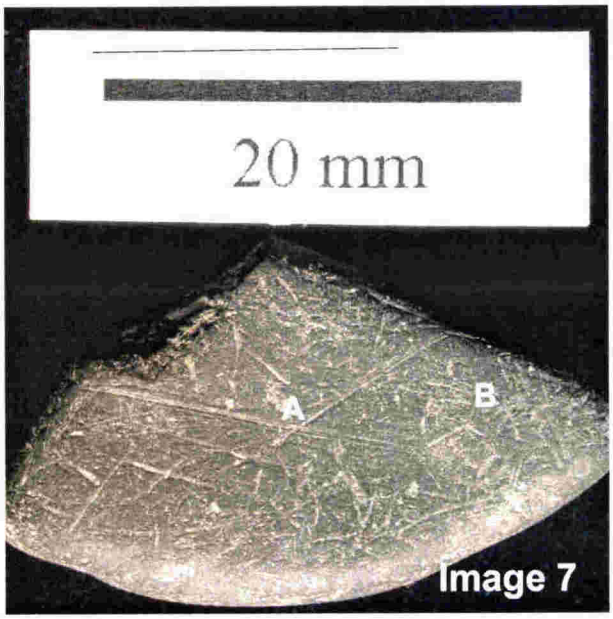

Variably oriented striae

Image 7 shows an argillite clast with a clearly faceted and striated surface that has variably oriented striae.

Two thin straight striae up to 15 mm long are oriented oblique to the long-axis of the clast and intersect (A).

A "background" of microstriae that have no preferred orientation is visible (B)

Location: Lake Pukaki moraine, Mt. Cook region, New Zealand, 170°10'00"44°10'30"

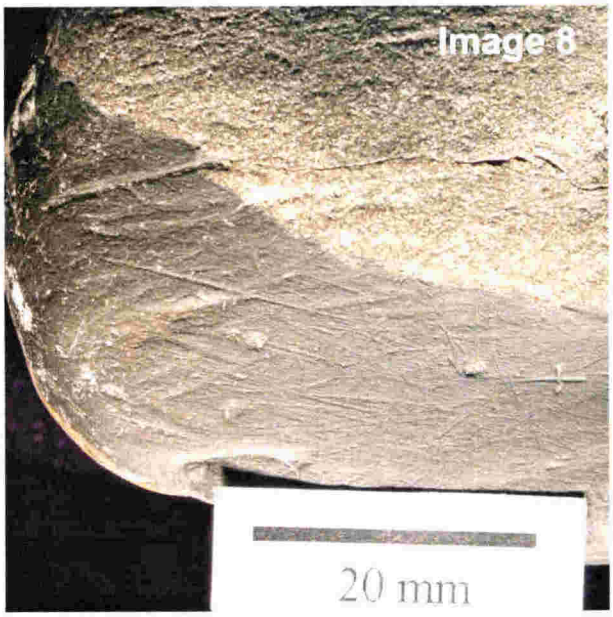

Lithologic influence on striae

The clast in Image 8 contains a contact between sandstone (light colour) and argillite (darker) on the same facet.

Fine glacial striae are obvious on the argillite portion, but less obvious on the sandstone.

This illustrates how lithology can affect striae preservation.

Location: Lake Pukaki moraine, Mt. Cook, New Zealand, 170°10'00"44°10'30"

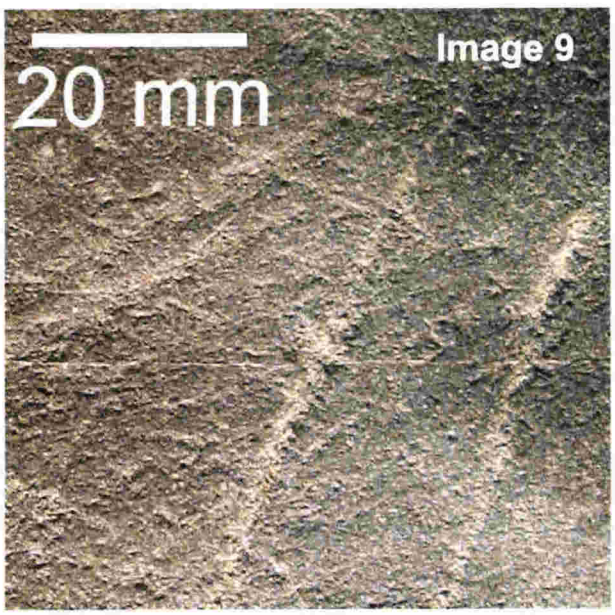

Lithologic influence on striae

Image 9 shows part of a sandstone clast from the Lake Pukaki moraine.

The recognisable striae are generally larger than those on argillite clasts (e.g. Image 8).

Small striae and background microstriae are not distinguishable on the rough surface texture due to the coarser grainsize.

Location: Lake Pukaki moraine, Mt. Cook, New Zealand, 170°10'00"44°10'30"

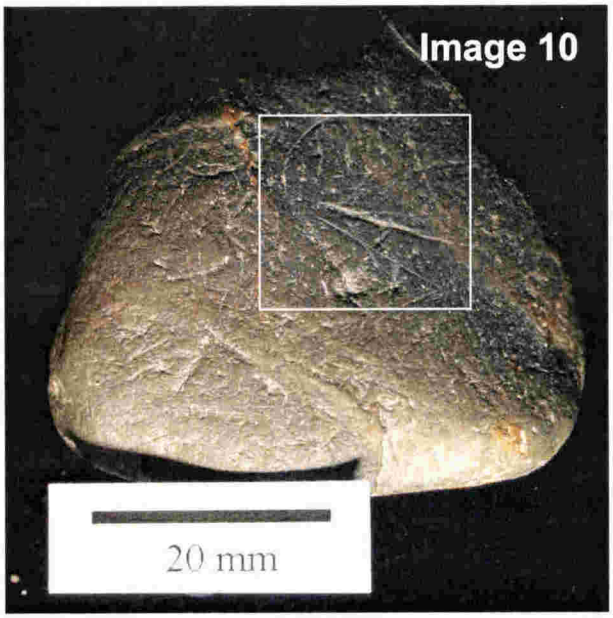

Random ly oriented striae

Image 10 shows a rounded and equidimensional (nearly equal long and intermediate axes) argillite clast.

Striae occur on both sides of the clast and have no preferred orientation, and some are curved. These individual large striae occur against a "background" of microstriae.

The inset square is enlarged in Image 11.

Location: Lake Pukaki moraine, Mt. Cook region, New Zealand, 170°10'00"44°10'30"

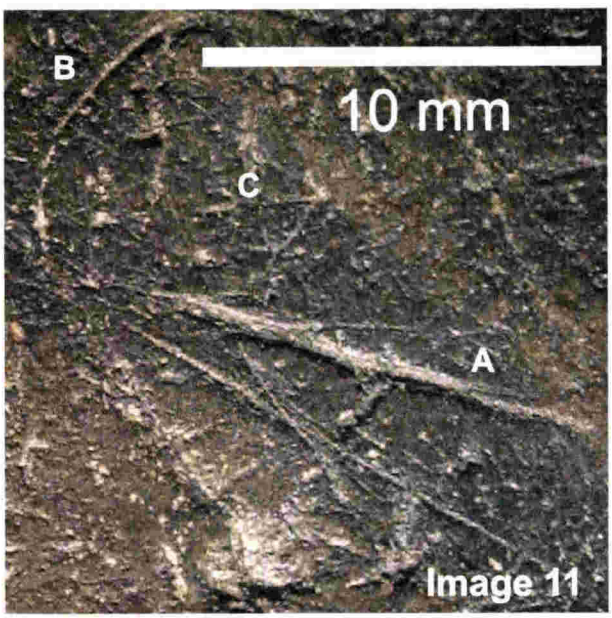

Closeup of randomly oriented striae

Image 11 shows a closeup of the clast in Image 10. Straie include:

A large straight striation, 12 mm long and up to 0.6 mm wide (A).

A curved striation indicating clast rotation during the striation process (B).

A "background" of randomly oriented microstriae (C).

Location: Lake Pukaki moraine, Mt. Cook region, New Zealand, 170°10'00"44°10'30"

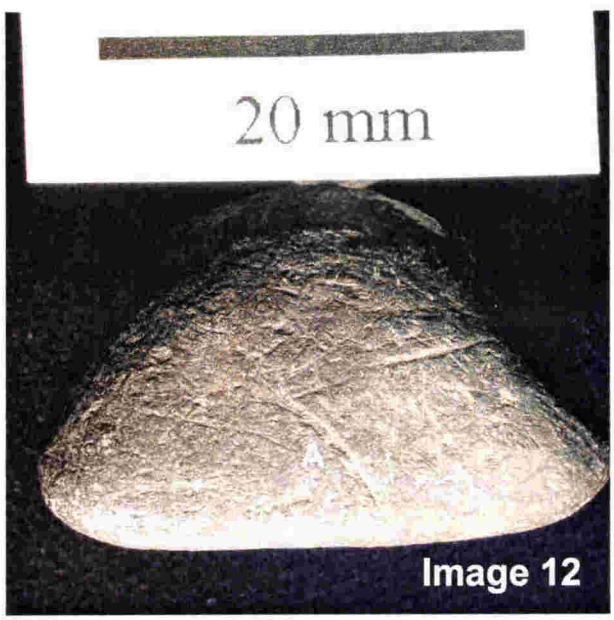

Randomly oriented striae

Image 12 shows an argillite clast with a more defined long axis than the clast is images 10 and 11. However, this clast also has random striae orientations.

Individual larger striae are set against a "background" of microstriae.

One of the larger striae is slightly curved, suggesting clast rotation during the striating process (A).

Location: Lake Pukaki moraine, Mt. Cook region, New Zealand, 170°10'00"44°10'30"

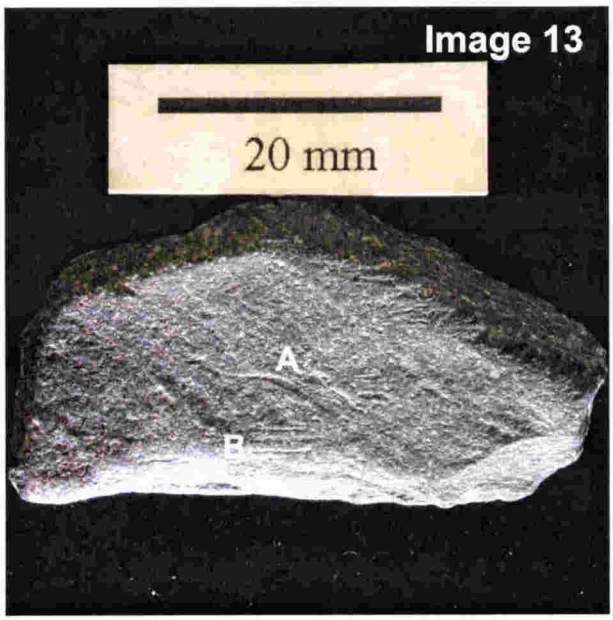

Sub-parallel striae with no background striae

Image 13 shows a small clast from the Mueller Glacier. It has a clear facet but sparse striae.

A slightly curved individual striation (A) is visible as well as a set of short parallel striae (B).

The clast does not have a background of microstriae that is common on the Lake Pukaki clasts.

Location: Murchison Glacier, Mt. Cook region, New Zealand, 170°20'08"43°36'07"

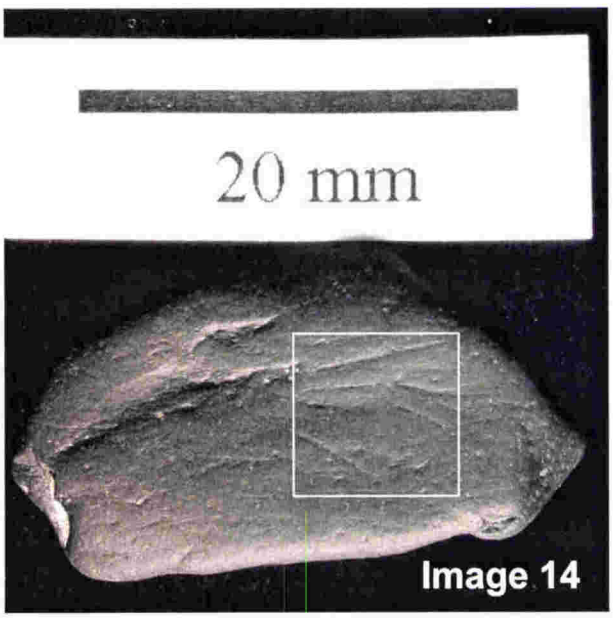

Sub-parallel striae with no background striae

The clast in Image 14 is an argillite clast from site MH 2 (50 m downstream from the Murchison Glacier). Several obvious striae are visible and these are oriented sub-parallel to the long axis of the clast.

Unlike other glacial examples, this clast has no "background" of microstriae, probably due to abrasion during fluvial transport.

The inset square is enlarged in Image 15.

Location: Murchison Glacier, Mt. Cook region, New Zealand, 170°20'08"43°36'07"

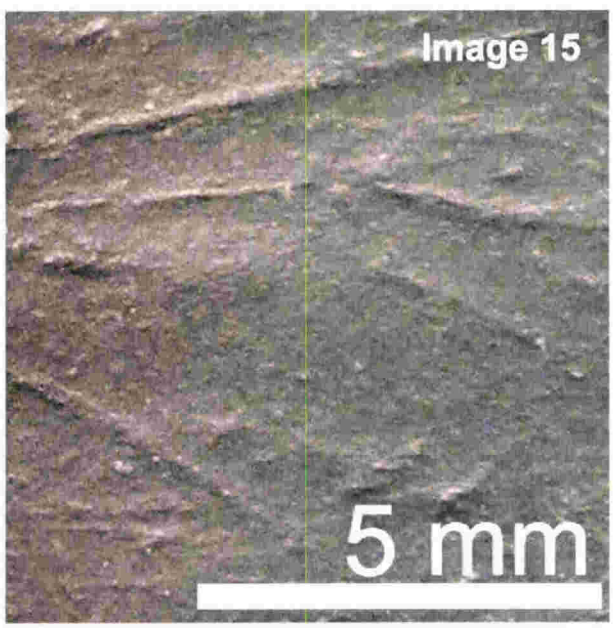

Closeup of sub-parallel striae with no background striae

This image clearly shows the distinct but smooth striae on the surface of the clast as well as the lack of "background" striae that are typically present on other glacial clasts.

Location: Murchison Glacier, Mt. Cook region, New Zealand, 170°20'08"43°36'07"

Large and small striae

Image 1 shows a faceted mudstone clast from Cuff Cape. The striae are oriented predominantly parallel to the long axis of the clast, but a few deviate up to 70° degrees from the long axis.

The clast shows a "background" of "microstriae" accompanied by several larger individual striae.

The inset square is enlarged in Image 2.

Location: Cuff Cape, Antarctica
162°30'00"76°59'00"

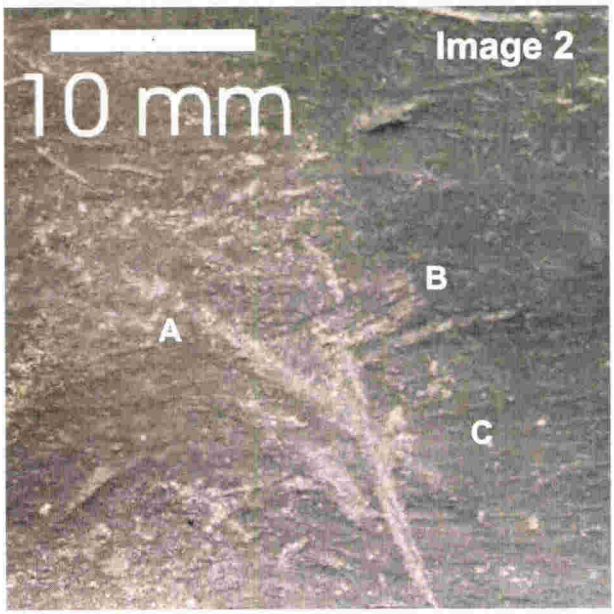

Closeup of large and small striae

This image shows a close up view of the clast in Image 1.

Several individual striae are oriented oblique to the long axis of the clast (A).

Compound striae consisting of several smaller parallel striae are also visible (B).

(A) and (B) are set against a "background" of microstriae that are parallel to the clast long axis of the clast (C).

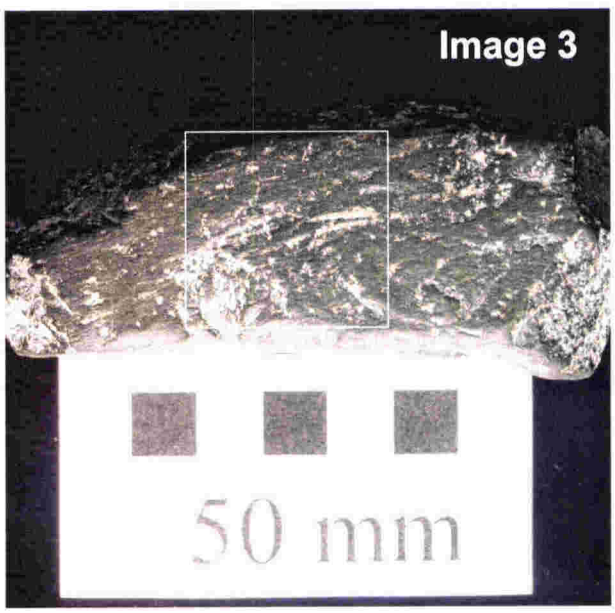

Long-axis parallel striae

Image 3 shows a striated mudstone clast from the Mackay Glacier. It has four facets that show striae. The striae are predominantly parallel to the long axis.

A "background" of microstriae covers the surface of the clast.

A few larger striae are also visible.

The inset square is enlarged in the Image 4.

Location: Mackay Glacier, Antarctica
162°30'00"76°57'00"

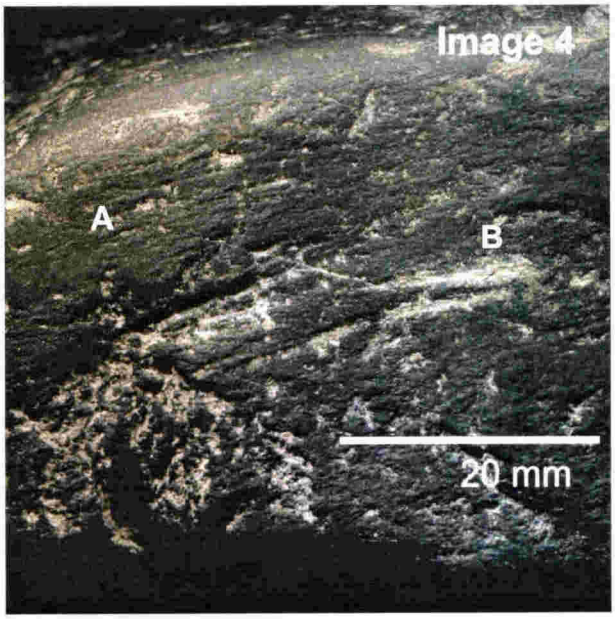

Mudstone clast closeup

Image 4 shows a close up of the mudstone clast in Image 3.

A "background" of microstriae covering almost the entire surface is visible at this scale (A).

Larger striae up to 4 mm wide are superimposed on this surface (B).

Location: Mackay Glacier, Antarctica 162°30'00"76°57'00"

Sparse large striae

The clast in Image 5 from the Mackay Glacier shows large individual striae (up to 27 mm long and 3 mm wide) oriented parallel to the long axis

Unlike most other clasts, this one does not display the characteristic "background" of microstriae.

Location: Mackay Glacier, Antarctica 162°30'00"76°57'00"

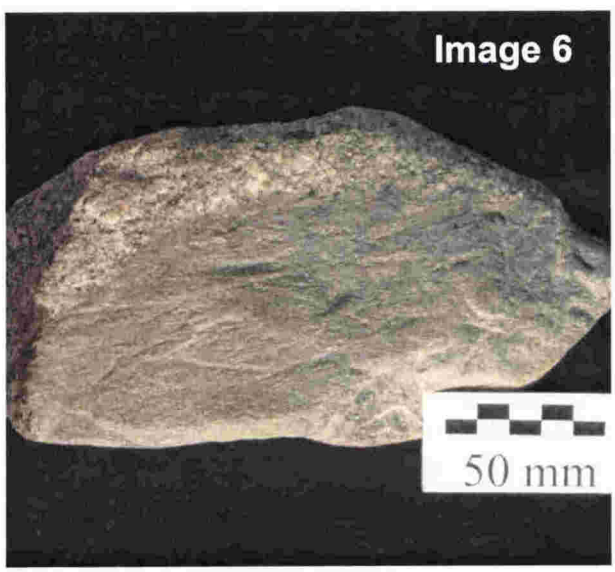

Cuff Cape dolerite/granite contact

Image 6 shows a glacially faceted clast that contains a contact between dolerite (grey area in lower part) and granite (lighter, speckled area).

Striae parallel to the long axis of the clast are clearly visible on the dolerite portion but not on the granite, even though the surface has been abraded. This illustrates the important influence has lithology striae generation.

Location: Cuff Cape, Antarctica 162°30'00"76°59'00"

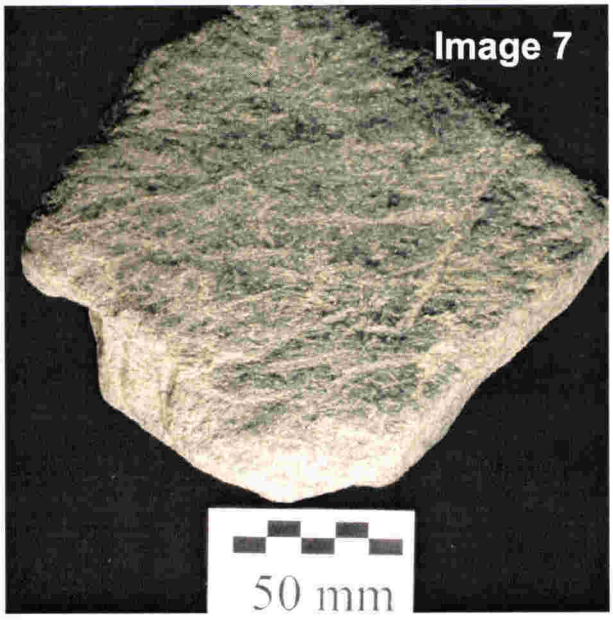

Indistinct striae on glacial facet

Image 7 shows a medium-fine grained granite clast from the Mackay Glacier. The clast shows a clear glacial facet, with abundant but poorly inscribed striae mostly parallel to the long axis, although the long axis is not distinct.

These striae are clearly visible on a facet of this size but are difficult to see on smaller clasts, illustrating that lithology and clast size influence striae character.

Location: Mackay Glacier, Antarctica 162°30'00"76°57'00"

Long axis parallel striae

Image 8 shows a well developed facet on an elongate dolerite clast. The surface is intensely striated with striae oriented almost exclusively parallel to the long axis of the clast.

Location: Cuff Cape, Antarctica 162°30'00"76°59'00"

Short striae with no preferred orientation

Image 9 shows a clear glacial facet on a dolerite clast, with striae that are mostly short and not oriented parallel to the long axis.

This indicates that clast shape does not necessarily influence the orientation of the striae.

Location: Cuff Cape, Antarctica 162°30'00"76°59'00"

Parallel striae on equidimensional clast

The clast in image 10 does not have a distinct long axis. Nevertheless, the striae are oriented predominantly parallel to the long axis, suggesting that clast form does not necessarily influence striae orientation.

Location: Cuff Cape, Antarctica
162°30'00"76°59'00"

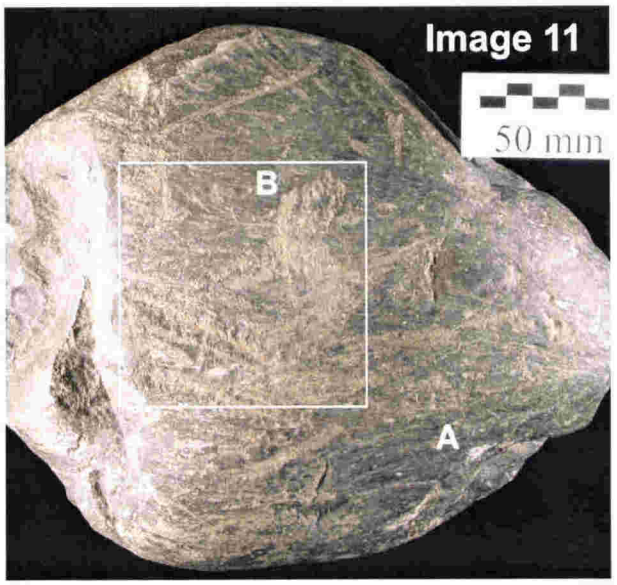

Large compound striae

Image 11 shows a large dolerite cobble showing a bullet nose (right) and a plucked lee end (left). It displays a densely striated surface, with striae predominantly parallel to long axis, although some diverge from the bullet nose (A).

Large compound striae (up to 20 mm wide and 60 mm long) occur with finer parallel striae on the surface (B).

A "background" of microstriae is also visible. Inset square is enlarged in image 12.

Location: Cuff Cape, Antarctica
162°30'00"76°59'00"

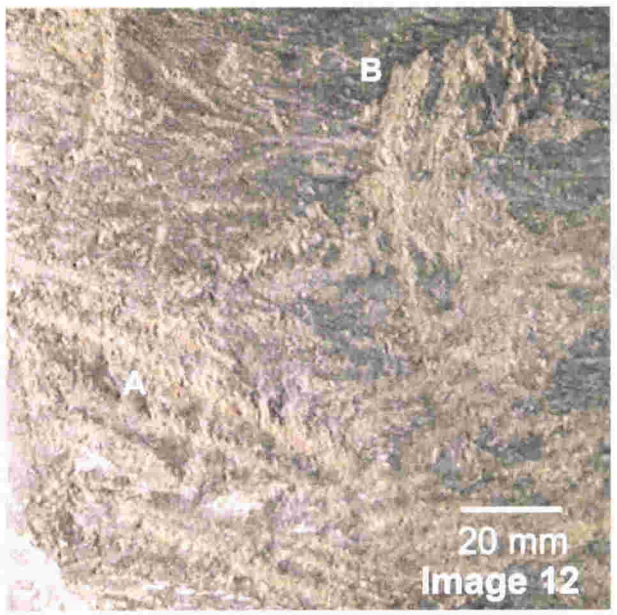

Closeup of large compound striae

Image 12 shows a close up of the clast surface. The large compound striae have irregular channel shapes and uneven channel surfaces with several striae making up the overall abrasion mark (A).

The upper righthand part of the image shows a broad compound striation that is curved and almost perpendicular to the long axis, suggesting clast rotation during the abrasion process (B).

Location: Cuff Cape, Antarctica
162°30'00"76°59'00"

Type 1: Broad scrapes

Broad (up to 500 mm width, 40 mm depth, 1200 mm length), unweathered scrapes typically consist of many smaller striae or grooves centimetres or millimetres in width. Some examples show progressive increase in depth and width, with an abrupt terminus. Typically, the abrasion mark has crushed sandstone remnants of the abrading tool smeared onto the surface, particularly at the deepest terminal wall. Occasionally, small cm-scale "levees" occur along the sides of the abrasion mark.

Location: Allan Hills, Antarctica, 159°42'20"76°41'51"

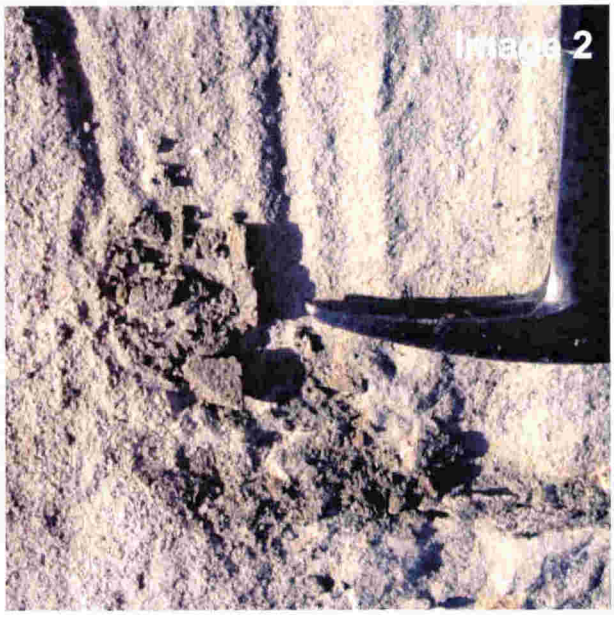

Broad scrapes-closeup

Image 2 shows a closeup of the end of the broad scrape in Image 1. The crushed remnants of the abrading tool are visible at the terminal wall.

Location: Allan Hills, Antarctica, 159°42'20"76°41'51"

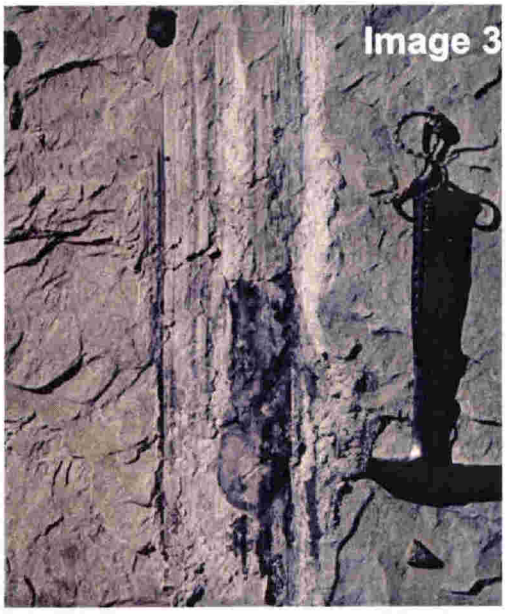

Type 1: Broad scrape

Image 3 shows an example of a type 1 abrasion that has a symmetrical shape. (i.e. does not become progressively deeper and wider. Here, the abrading tool has contacted the bedrock surface, and then lifted off again.

Location: Allan Hills, Antarctica, 159°43'50"76°41'43"

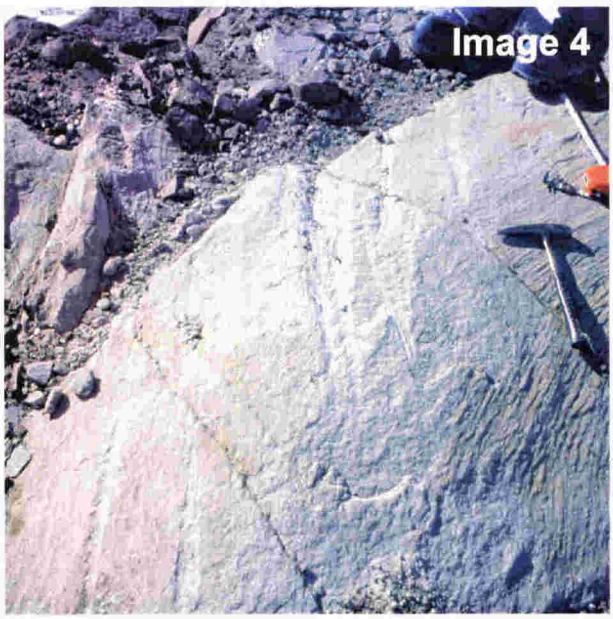

Type 2: Individual striae and grooves

Variably shaped, unweathered, individual linear abrasions (scrapes, striae, and grooves) make up a wide variety of discrete abrasion marks (typically cm in width and depth and decimetres long). Where several marks occur in one location, they are generally sub parallel. Some show a progressive increase in depth and width whereas others have more symmetrical, tapered ends. Occasionally, individual marks occur "in line" to form a trail of marks up to 2 m in length. Some marks have crushed sandstone remnants of the abrading tool smeared onto the surface and /or are bordered by small cm-scale "levees."
Location: Allan Hills, Antarctica, 159°40'00"76°41'54"

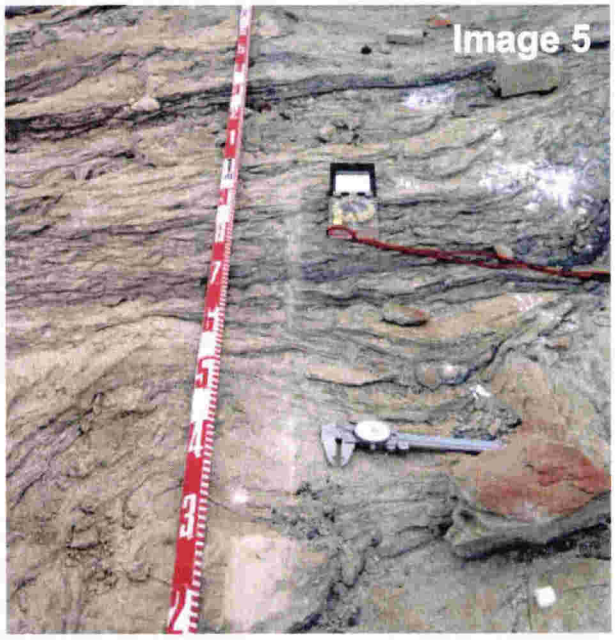

Individual striae and grooves

Image 5 shows an example of a type 2 abrasion where several abrasions occur "in line" over 2 m, indicating the abrading tool made contact several times as it progressed across the surface.

Location: Allan Hills, Antarctica, 159°38'30"76°41'25"

Individual striae and grooves

Image 6 shows a closeup of a typical type 2 abrasion. Width and depth are variable along the intermittent but distinct abrasion.

Location: Allan Hills, Antarctica, 159°45'30"76°42'58"

Type 3: Scraped boulders and cobbles

Type 3 abrasion marks are variably shaped, unweathered scrapes up to several cm wide (and related striae) that occur on the stoss side of some weathered dolerite boulders and cobbles. These are usually lodged within, or resting on, Sirius diamictite. Abrasion has removed the characteristic dark brown desert varnish from the surfaces of the boulders, making the marks clearly visible. Some boulders have been overturned, exposing the non-wind polished surface underneath.

Location: Allan Hills, Antarctica, 159°38'00"76°41'15"

Scraped boulders and cobbles

Image 8 shows scraped cobbles on a Beacon bedrock surface. These clasts have fresh abrasion marks on the stoss sides and often concentrated along prominent ridges on the clasts. The abrasion marks are commonly oriented sub-parallel to the long axis of the clast. Ice movement was from bottom to top in Image 8.

Location: Allan Hills, Antarctica, 159°38'00"76°41'15"

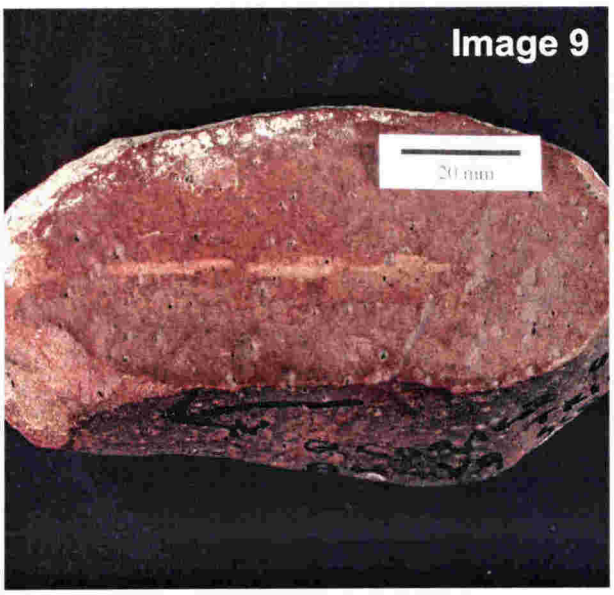

Scraped boulders and cobbles

Image 9 shows a type 3 abrasion on a desert varnished, wind polished dolerite cobble. The abrasion occurs on a distinct wind sculpted facet and has cut through the brown weathered surface leaving a distinct abrasion mark. It is oriented parallel to the long axis which also tends to be oriented north south. Ice flow was from left to right (north to south).

Location: Allan Hills, Antarctica, 159°40'40"76°42'25"

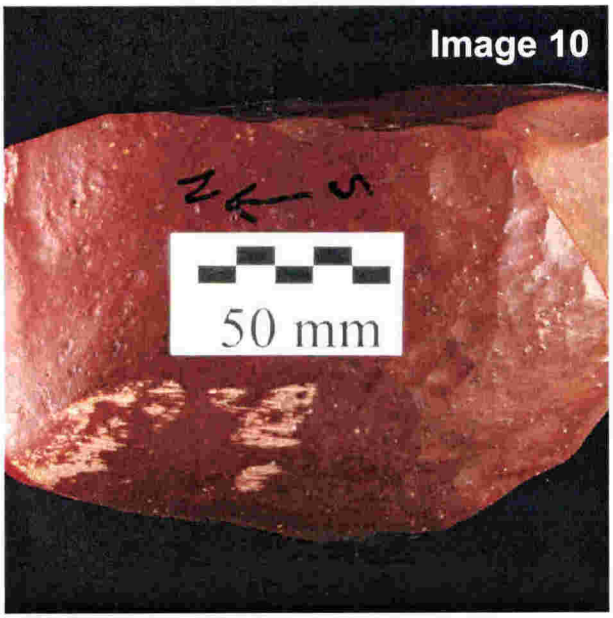

Type 3: Scraped boulders and cobbles

Image 10 shows another type 3 abrasion on a desert varnished, wind polished dolerite cobble. The abrasion begins on the stoss side and ends on the highest point of the broad top surface where the abrading tool has lifted off. Abrasion has cut through the brown weathered surface leaving a distinct mark. Ice flow was from left to right (north to south).

Location: Allan Hills, Antarctica, 159°37'00"76°42'12"

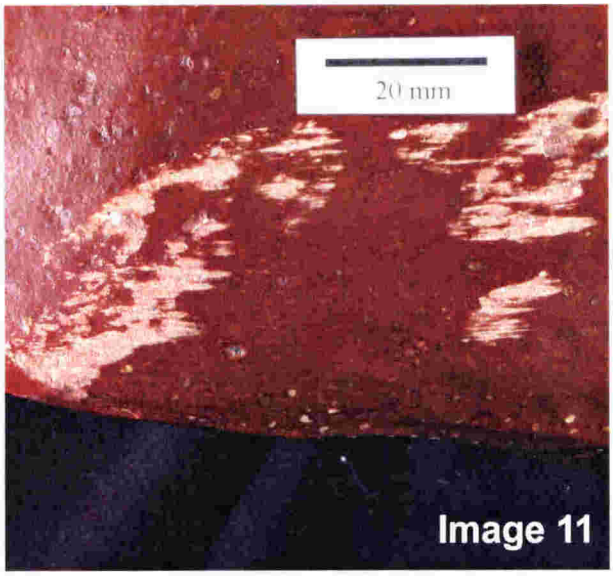

Scraped boulders and cobbles close up

A closeup of the type 3 abrasion in Image 10 shows that it consists of many linear abrasions created by the overridng tool. The tool is likely to have been another dolerite clast as all other local lithologies are softer than the dolerite.

Location: Allan Hills, Antarctica, 159°37'00"76°42'12"

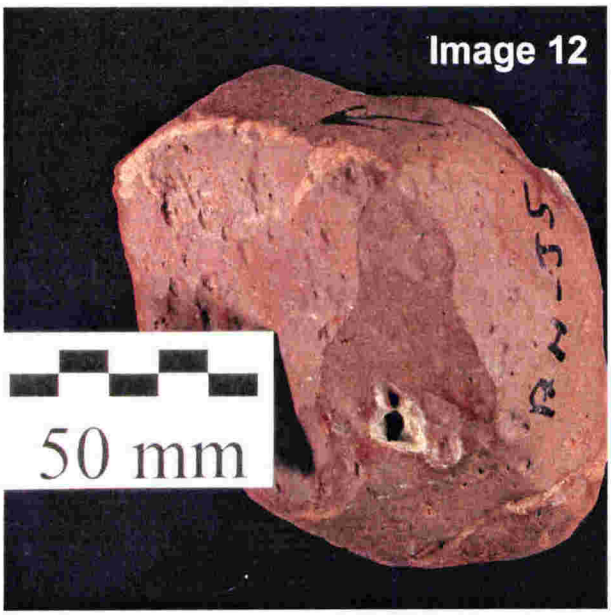

Scraped boulders and cobbles

Image 12 shows an example of type 3 abrasion where the stoss side of a prominent ridge on the clast has been abraded. The ridge in this case is oriented approximately north-south. The abrading rock has contacted the stoss side of this clast and has been dragged up the stoss side and lifted off at the highest point. Ice flow was from left to right (north to south).

Location: Allan Hills, Antarctica, 159°42'10"76°42'38"

Type 4: Ridge-and-groove lineations

Image 13 displays a surface with abraded patches consisting of many parallel lineations (mm scale width and depth), described here as ridge-and-groove lineations. The surfaces are typically dark and have a platy appearance with a sheen similar to slickensides. These abraded patches occur within thin carbonaceous layers beneath brecciated sandstone debris and indicate north to south glacier movement. These are produced by slip on the carbonaceous layers due to glaciotectonic ice loading.

Location: Allan Hills, Antarctica, 159°42'20"76°41'53"

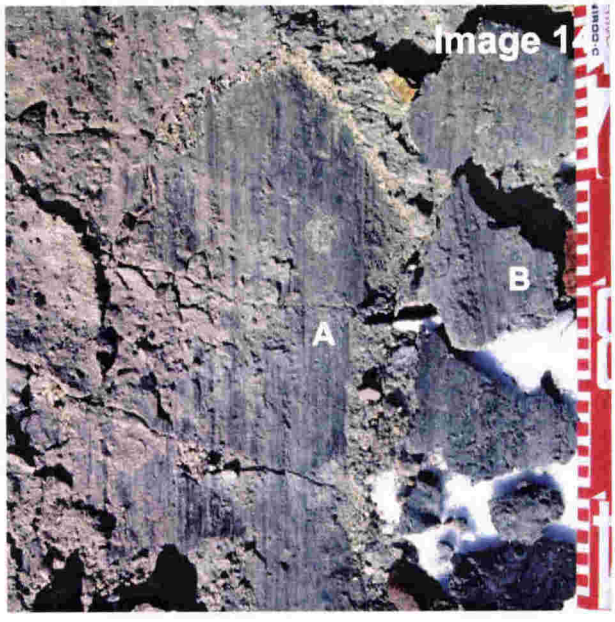

Ridge-and-groove lineations

Closeup of a slickensided surface showing mm scale ridges and grooves that are produced on the slip plane (A). On the right is the overlying layer that has been lifted from the abraded surface (B).

Location: Allan Hills, Antarctica, 159°42'20"76°41'53"

Ridge-and-groove lineations

Image 15 shows another closeup of a ridge-and-groove surface that has been partially weathered. In the upper centre of the image is part of the overlying layer still attached onto the abraded surface.

Location: Allan Hills, Antarctica, 159°42'20"76°41'53"

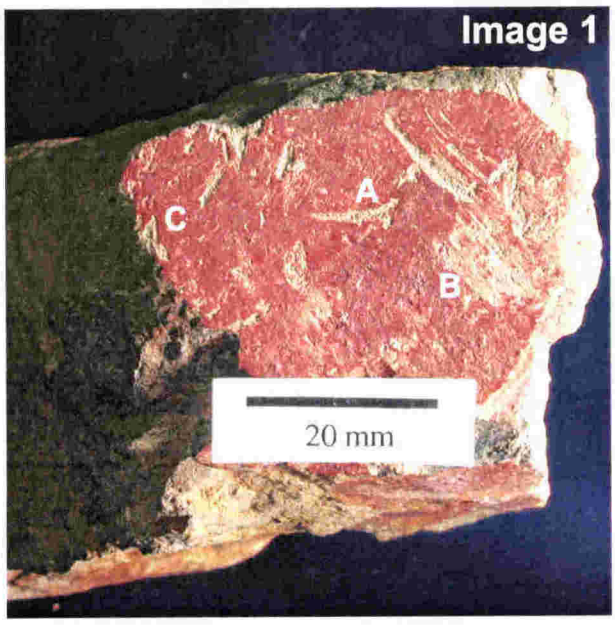

Individual randomly oriented striae

Image 1 shows a flat, weathered surface on the end of an andesite clast. The striae are weakly clustered and consist of:

Slightly curved striae up to 12 mm long and 2.5 mm wide (A).

Compound striae (up to 12 mm long, 6 mm wide) consisting of many smaller striae (B).

"Background" microstriae (barely visible) (<0.2 mm wide and <2 mm long) (C).

Striae on the ends of clasts only occurs in debris-avalanche and tectonic environments. Location: Murimotu Fm, Mt Ruapehu, New Zealand, 175°30'30"39°10'10"

Sets of sub-parallel striae

In contrast to Image 1, the clast in Image 2 shows a large uneven face of an andesite/dacite clast with frequent overlapping striae. The striae comprise:

Broad compound striae consisting of fine parallel striae oblique to the long axis (A).

Individual striae with multiple orientations are also present (B).

Inset square enlarged in Image 3.

Location: Murimotu Fm, Mt Ruapehu, New Zealand, 175°30'30"39°10'10"

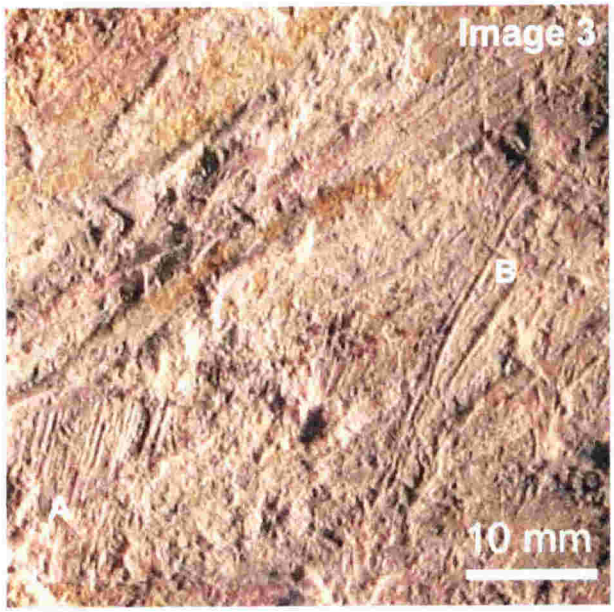

Closeup of Image 2

A closeup of the inset area in Image 2 shows:

Fine parallel striae (< 0.5 mm wide) forming compound striation 10 mm wide (A).

Several individual striae up to 20 mm long and up to 1 mm wide (B).

Location: Murimotu Fm, Mt Ruapehu, New Zealand, 175°30'30"39°10'10"

Parallel striae on an equidimensional clast

Image 4 shows a weathered flat surface of an equidimensional andesite clast. The striae are up to 25 mm long and have variable widths along a single striation (maximum width is 2 mm). These striae are parallel to each other, but not to the long axis (which is indistinct).

Location: Murimotu Fm, Mt Ruapehu 175°30'30"39°10'10"

Individual and splayed striae

Image 5 shows a large undulating surface of an andesite/dacite clast that displays:

Many individual striae with no preferred orientation and also compound striae (A).

Fine striae that splay out toward the clast margins. This area is enlarged in Image 6.

Location: Murimotu Fm, Mt Ruapehu, New Zealand, 175°30'30"39°10'10"

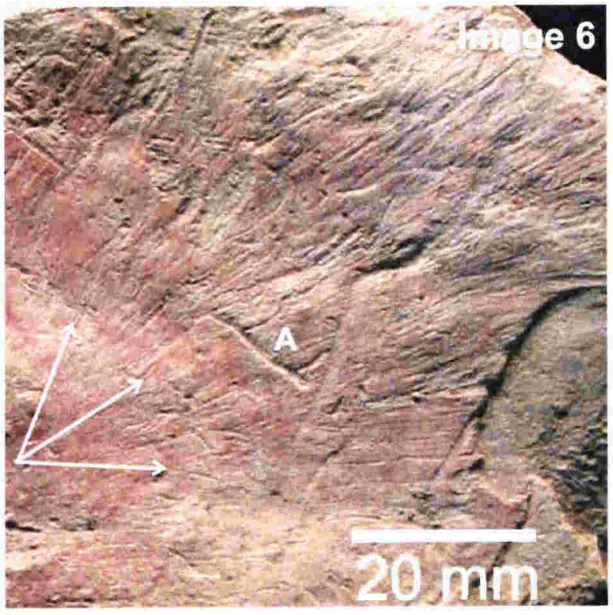

Closeup of splayed striae

This image shows the detail of the fine radiating striae (< 0.05 mm wide and up to 10 mm long. Arrows indicate the spread of striae orientations. The reason for this splayed pattern is not clear.

A larger striation cuts across the splayed striae (A).

Location: Murimotu Fm, Mt Ruapehu, New Zealand, 175°30'30"39°10'10"

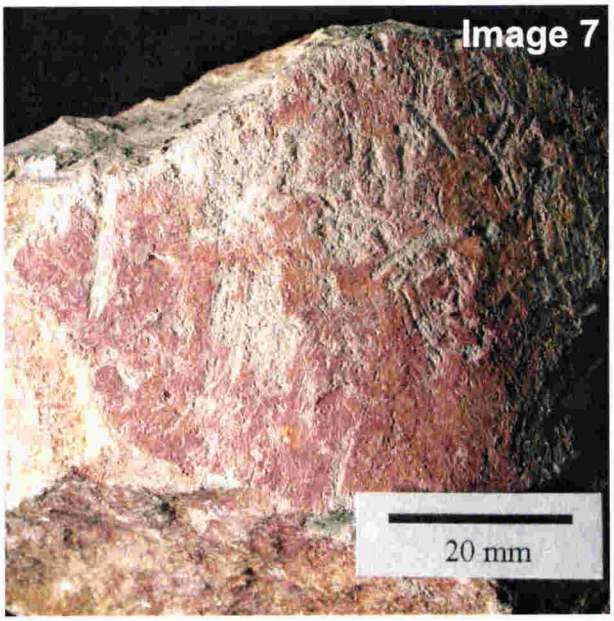

Striae on curved surfaces

Image 7 shows a weathered andesite clast with individual striae on a smooth curved surface. These show wide variation with no preferred orientation.

This illustates that striae do not form exclusively on flat surfaces.

Location: Murimotu Fm, Mt Ruapehu 175°30'30"39°10'10"

Small striae and variable orientation

Image 8 shows an andesite/dacite clast with a flat weathered surface. This surface contains abundant small striae with a wide variation in striae orientation and only a weak preferred orientation, oblique to the clast long axis.

Inset square is enlarged in Image 9.

Location: Murimotu Fm, Mt Ruapehu 175°30'30"39°10'10"

Closeup of Image 9

Image 9 shows a closeup of the inset square in Image 8.

Individual striae are generally less than 5 mm long and 0.5 mm wide although one is 2.5 mm wide (A).

Occasionally, many striae overlap forming completely abraded patches (B).

Location: Murimotu Fm, Mt Ruapehu 175°30'30"39°10'10"

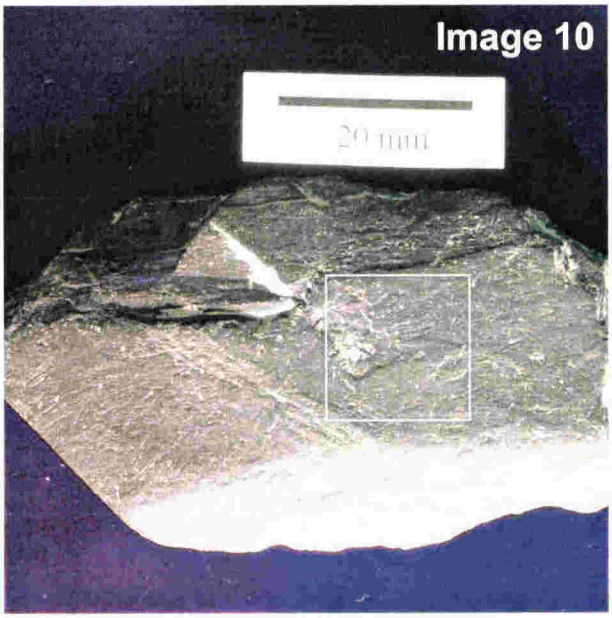

Small-scale striae, sub-parallel to the long axis

Image 10 shows an elongate argillite clast from a rock-fall scree deposit (MH 4). Most of the striated rock-fall clasts have flat surfaces produced by fracturing along bedding planes.

On this clast, a high density of small striae occur predominantly aligned parallel to the long axis of the clast. A "background" of microstriae occur over most of the clast surface.

Inset square is enlarged in Image 11.

Location: Site MH 4, Murchison Valley, Mt Cook, New Zealand, 170°19'45"43°36'30"'

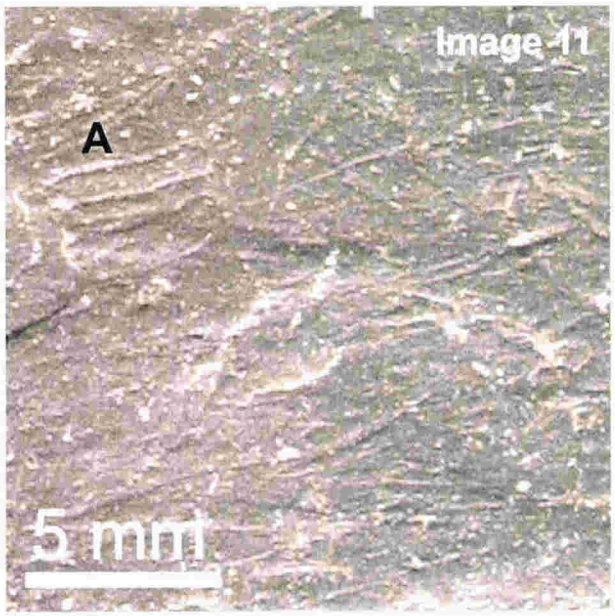

Closeup of Image 10

Image 11 shows a closeup of the clast surface.

Individual striae up to 5 mm long are visible (A) against the "background" microstriae.

Most striae are < 3 mm long, although some larger striae are up to 5 mm long (A).

Most striae are sub parallel to the long axis of the clast.

Location: Site MH 4, Murchison Valley, Mt Cook, New Zealand, 170°19'45"43°36'30"

Individual striae and compound striae

The clast in image 12 shows an angular argillite clast with a typical flat face and sharp edges.

Many small striae with no preferred orientation are visible (A).

Also present is a large compound striation that is 12 mm long and 4 mm wide. This has smaller parallel striae on the surface (not visible at this scale) (B).

Location: Site MH 4, Murchison Valley, Mt Cook, New Zealand, 170°19'45"43°36'30"

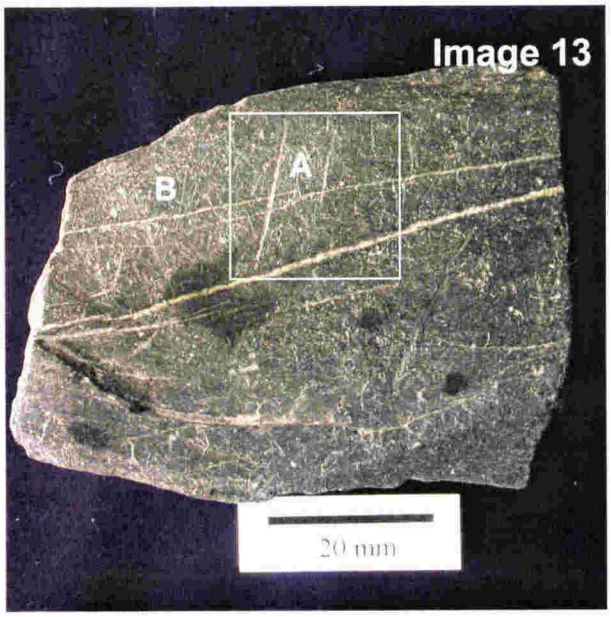

Parallel striae

Image 13 shows another striated argillite rock-fall clast.

It displays several well-defined parallel striae that are not related to the clast long axis (A).

Parts of the clast show a "background" of microstriae (B).

Inset square is enlarged in Image 16.

Location: Site MH 4, Murchison Valley, Mt Cook, New Zealand, 170°19'45"43°36'30"

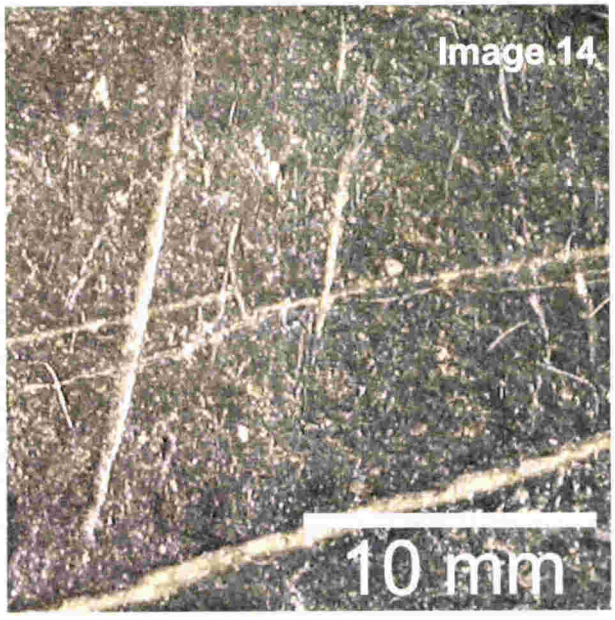

Closeup of Image 13

Image 14 shows a closeup view of part of the clast in Image 14. Two well-defined parallel striae are visible, the largest is 18 mm long and 0.5 mm wide. These are oblique to the long axis of the clast.

A "background" of much smaller striae is visible around the larger striae.

Location: Site MH 4, Murchison Valley, Mt Cook, New Zealand, 170°19'45"43°36'30"

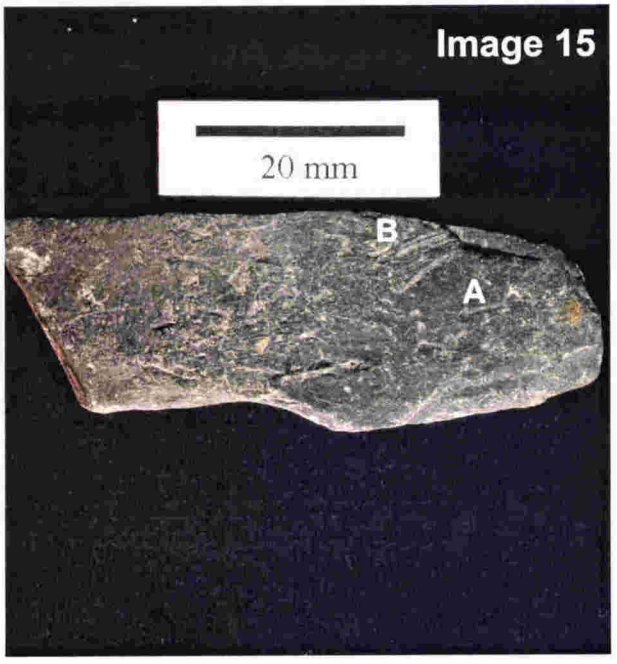

Rare small striae

The clast in Image 15 is an example angular argillite with a flat bedding surface showing only a few small striae oriented oblique to the clast long axis. These include:

Short (< 5 mm) individual striae (A).

A wider compound striation that has several smaller parallel striae (B).

Location: Site MH 4, Murchison Valley, Mt Cook, New Zealand, 170°19'45"43°36'30"

Long axis parallel striae

Image 1 shows an angular argillite clast from the Ngapotiki Fault with a flat planed and densely striated surface.

Individual striae are indistinct but together make up a clearly abraded surface with striae parallel to the long axis of the clast.

Location: Ngapotiki Fault, New Zealand 175°21'10"41°35'05"

Multiple striae orientations

Image 2 shows a small, almost equidimensional argillite clast. The surface has abundant, mostly short striae with no preferred orientation. The largest striae is 15 mm long, 1 mm wide and slightly curved (A).

The curved striae together with the lack of preferred striae orientation, indicates clast rotation during the striating process and suggests that equidimensional clasts have more variable striae orientations.

Location: Wellington Fault, New Zealand 175°05'00"41°07'00"

Striae on clast ends

Image 3 shows striae on the end of a sub-angular argillite clast (A).

Striae are up to 30 mm long and parallel forming a set 8 mm wide that is parallel to the long axis of the facet.

Also visible is an individual short, wide striation almost perpendicular to the main set of striae and long axis of the face (B).

Striae on clast ends are only observed on tectonic and debris-avalanche clasts

Location: Ngapotiki Fault, New Zealand 175°21'07"41°35'03"

Planed surface and parallel striae concentrated on clast margin

This sandstone clast is a well-rounded beach clast incorporated in the Ngapotiki Fault.

The surface displays indistinct parallel striae that form an obvious planed surface.

The abraded surface is curved across the clast (top to bottom of image) but terminates abruptly where the curvature of the surface increases.

Location: Ngapotiki Fault, New Zealand 175°21'07"41°35'03"

Parallel striae concentrated on clast margin

The clast in Image 5 displays faint striae sub-parallel to the long axis of the clast, but concentrated at the margin of the surface where the curvature of the clast increases (A).

Also visible is extensional open fractures oriented approximately perpendicular to the striae orientation and long axis of the clast (B).

Such fractures occur on 21% of clasts from this site.

Location: Ngapotiki Fault, New Zealand 175°21'07"41°35'03"

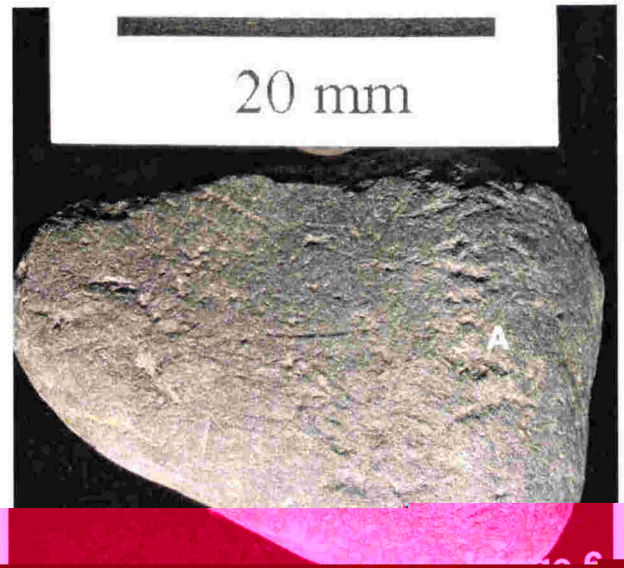

Striae concentrated on clast margin

This argillite clast from the Wellington Fault shows a flat surface with well-rounded ends.

A few striae occur on the flat surface at variable orientations. However, the concentration of striae occurs at the extreme end of the flat surface where the curvature of the clast increases (A).

This concentration of striae at the margins, occurs on tectonic clasts of all sizes.

Location: Wellington Fault, New Zealand 175°05'00"41°07'00"

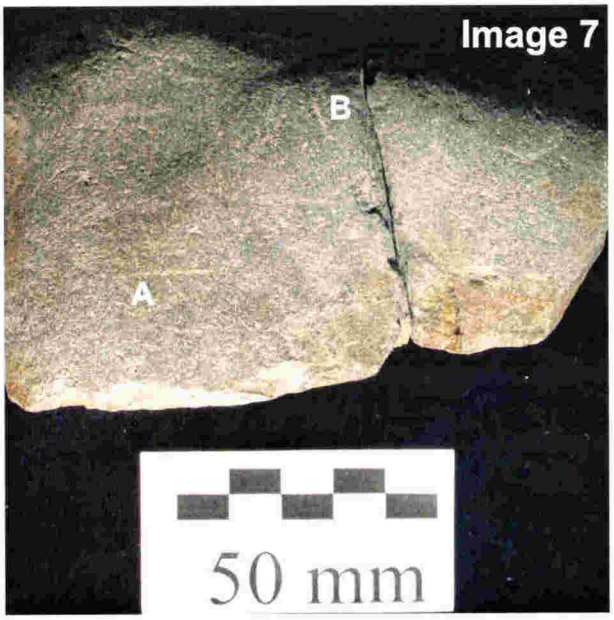

Broken and striated clast

Image 7 is a sandstone clast from a fluvial conglomerate that has been incorporated into the Wellington Fault. The surface shows striae, some oriented parallel to the long axis of the clast (A), but others at various orientations up to 90° from the long axis (B).

The clast has been fractured by tectonic movement and the break is oriented approximately perpendicular to the long axis of the clast. No striae occur on the fractured surface.

Location: Wellington Fault, New Zealand 175°05'00"41°07'00"

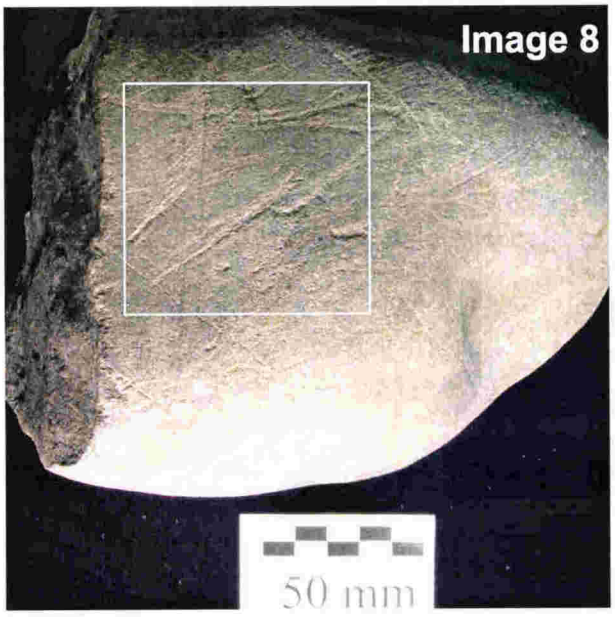

Large striae on cobble

The sandstone cobble in Image 8 is a well-rounded fluvial clast incorporated into the Wellington Fault. The clast was oriented with the long axis parallel to the slip plane in the outcrop.

Most striae are oblique to the long axis. Some are compound striae with smaller parallel striae on the surface. Parts of the surface show "background" microstriae. This clast has also been fractured perpendicular to the long axis.

Location: Wellington Fault, New Zealand 175°05'00"41°07'00"

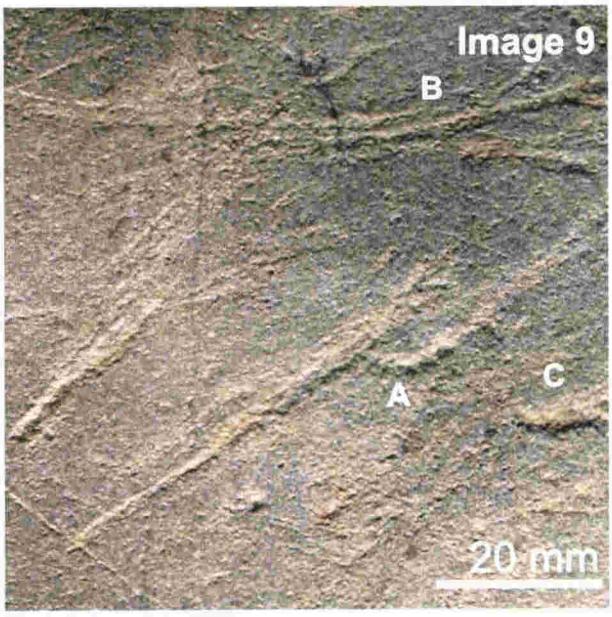

Closeup of large striae

Image 9 shows a closeup of the large striae in Image 8. The striae are up to 86 mm long and 5 mm wide (the largest measured in this study).

An individual striation that curves by about 60° at one end. This indicates the striating fragment rotated out of the striation track (A).

A curved compound (5 mm wide) with smaller parallel striae on the surface (B).

A short and wide striation (8 mm long and 4 mm wide) (C).
Location: Wellington Fault, New Zealand 175°05'00"41°07'00"

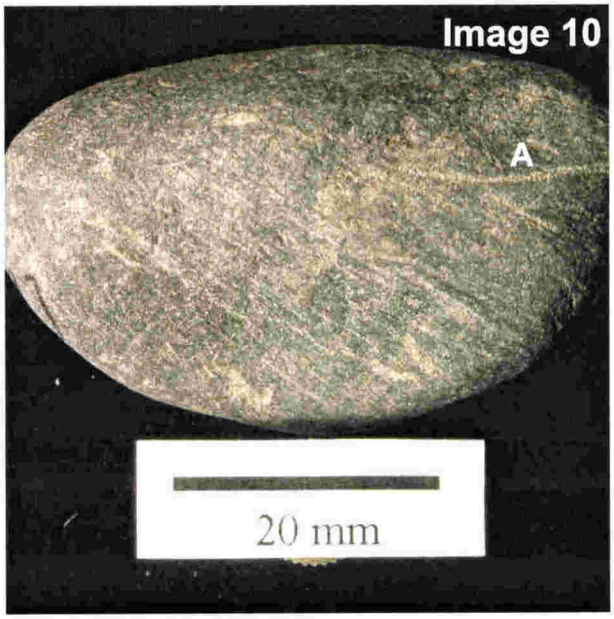

Parallel striae oblique to the long axis on a curved surface

The clast in image 10 has parallel, fine striae oblique to the long axis of the clast and are continuous over a curved surface.

Most striae are indistinct but overall make up a densely abraded surface.

One larger, clear striation is 17 mm long and 0.5 mm wide and oriented parallel to the long axis (A).

Location: Ngapotiki Fault, New Zealand 175°21'07"41°35'03"

Multiple striae orientations

This small argillite clast from the Wellington Fault has small striae with multiple orientations despite the clast having a well-defined long axis.

Location: Wellington Fault, New Zealand 175°05'00"41°07'00"

Sub-parallel striae on curved surface

This argillite clast from the Ngapotiki Fault clast that has no flat surfaces, but shows a few striae that are sub-parallel to the long axis of the clast (A).

The striae are straight and extend over the curved surface.

Location: Ngapotiki Fault, New Zealand 175°21'07"41°5'03"

LOCATION: MUELLER GLACIER, NEW ZEALAND **COLLECTION : 100 CLASTS FROM BASAL ICE**

NO.	LITHOLOGY	AXIS LENGTH			AVERAGE	AXIAL RATIOS		KRUMBEIN ROUNDNESS	FACETS	STRIAE	RA	C40
		A	B	C		C/A	B/A					
1	SANDSTONE	34	30	10	24.7	0.29	0.88	0.1	NO	NO	1	1
2	SANDSTONE	21	18	8	15.7	0.38	0.86	0.1	NO	NO	1	1
3	ARGILLITE	31	21	11	21.0	0.35	0.68	0.1	NO	NO	1	1
4	SANDSTONE	65	40	20	41.7	0.31	0.62	0.1	NO	NO	1	1
5	ARGILLITE	26	17	4	15.7	0.15	0.65	0.1	NO	NO	1	1
6	SANDSTONE	30	22	10	20.7	0.33	0.73	0.1	NO	NO	1	1
7	SANDSTONE	21	19	6	15.3	0.29	0.90	0.1	NO	NO	1	1
8	SANDSTONE	26	12	10	16.0	0.38	0.46	0.1	NO	NO	1	1
9	SANDSTONE	26	22	10	19.3	0.38	0.85	0.1	NO	NO	1	1
10	ARGILLITE	29	17	3	16.3	0.10	0.59	0.1	NO	NO	1	1
11	SANDSTONE	21	16	6	14.3	0.29	0.76	0.1	NO	NO	1	1
12	SANDSTONE	30	12	8	16.7	0.27	0.40	0.2	NO	NO	1	1
13	ARGILLITE	43	23	10	25.3	0.23	0.53	0.2	NO	YES	1	1
14	ARGILLITE	52	35	26	37.7	0.50	0.67	0.2	NO	NO	1	0
15	SANDSTONE	19	15	9	14.3	0.47	0.79	0.2	NO	NO	1	0
16	ARGILLITE	18	10	6	11.3	0.33	0.56	0.2	NO	NO	1	1
17	SANDSTONE	32	24	12	22.7	0.38	0.75	0.2	NO	NO	1	1
18	ARGILLITE	21	10	4	11.7	0.19	0.48	0.2	NO	NO	1	1
19	ARGILLITE	32	16	10	19.3	0.31	0.50	0.2	NO	NO	1	1
20	QUARTZ	22	15	9	15.3	0.41	0.68	0.2	NO	NO	1	0
21	SANDSTONE	22	21	11	18.0	0.50	0.95	0.2	NO	NO	1	0
22	QUARTZ	26	19	18	21.0	0.69	0.73	0.2	NO	NO	1	0
23	SANDSTONE	23	18	6	15.7	0.26	0.78	0.2	NO	NO	1	1
24	SANDSTONE	26	17	13	18.7	0.50	0.65	0.2	NO	NO	1	0
25	SANDSTONE	27	19	10	18.7	0.37	0.70	0.2	YES	NO	1	1
26	SANDSTONE	30	16	6	17.3	0.20	0.53	0.2	YES	NO	1	1
27	ARGILLITE	26	12	8	15.3	0.31	0.46	0.2	YES	NO	1	1
28	ARGILLITE	28	14	10	17.3	0.36	0.50	0.2	YES	NO	1	1
29	ARGILLITE	30	21	8	19.7	0.27	0.70	0.2	YES	NO	1	1
30	SANDSTONE	40	19	8	22.3	0.20	0.48	0.2	NO	NO	1	1
31	SANDSTONE	31	22	9	20.7	0.29	0.71	0.2	NO	NO	1	1
32	SANDSTONE	17	10	9	12.0	0.53	0.59	0.2	NO	NO	1	0
33	ARGILLITE	32	20	10	20.7	0.31	0.63	0.2	NO	NO	1	1
34	SANDSTONE	22	12	11	15.0	0.50	0.55	0.2	NO	NO	1	0
35	SANDSTONE	26	13	10	16.3	0.38	0.50	0.3	NO	NO	0	1
36	SANDSTONE	27	23	12	20.7	0.44	0.85	0.3	YES	NO	0	0
37	SANDSTONE	55	35	15	35.0	0.27	0.64	0.3	NO	NO	0	1
38	SANDSTONE	40	22	18	26.7	0.45	0.55	0.3	YES	NO	0	0
39	SANDSTONE	40	22	17	26.3	0.43	0.55	0.3	YES	NO	0	0
40	SANDSTONE	30	29	15	24.7	0.50	0.97	0.3	NO	NO	0	0
41	SANDSTONE	38	29	16	27.7	0.42	0.76	0.3	NO	NO	0	0
42	SANDSTONE	39	20	19	26.0	0.49	0.51	0.3	NO	NO	0	0
43	SANDSTONE	40	38	20	32.7	0.50	0.95	0.3	NO	NO	0	0
44	SANDSTONE	29	16	14	19.7	0.48	0.55	0.3	NO	NO	0	0
45	ARGILLITE	21	16	10	15.7	0.48	0.76	0.3	NO	NO	0	0
46	ARGILLITE	22	13	10	15.0	0.45	0.59	0.3	NO	YES	0	0
47	SANDSTONE	32	26	12	23.3	0.38	0.81	0.3	NO	NO	0	1
48	SANDSTONE	25	15	9	16.3	0.36	0.60	0.3	NO	NO	0	1
49	SANDSTONE	28	18	15	20.3	0.54	0.64	0.3	NO	NO	0	0
50	SANDSTONE	21	16	9	15.3	0.43	0.76	0.3	NO	NO	0	0
51	SANDSTONE	19	17	9	15.0	0.47	0.89	0.3	NO	NO	0	0
52	SANDSTONE	19	17	9	15.0	0.47	0.89	0.3	NO	NO	0	0
53	SANDSTONE	23	15	9	15.7	0.39	0.65	0.3	NO	NO	0	1
54	SANDSTONE	19	12	7	12.7	0.37	0.63	0.3	NO	NO	0	1
55	SANDSTONE	18	13	8	13.0	0.44	0.72	0.3	NO	NO	0	0
56	SANDSTONE	47	25	16	29.3	0.34	0.53	0.3	NO	NO	0	1
57	SANDSTONE	76	40	16	44.0	0.21	0.53	0.3	YES	NO	0	1
58	SANDSTONE	42	31	20	31.0	0.48	0.74	0.4	NO	NO	0	0
59	SANDSTONE	40	29	20	29.7	0.50	0.73	0.4	NO	NO	0	0
60	SANDSTONE	54	50	41	48.3	0.76	0.93	0.4	NO	NO	0	0
61	SANDSTONE	54	29	18	33.7	0.33	0.54	0.4	YES	NO	0	1
62	ARGILLITE	27	18	12	19.0	0.44	0.67	0.4	NO	NO	0	0
63	ARGILLITE	27	21	10	19.3	0.37	0.78	0.4	YES	YES	0	1
64	SANDSTONE	31	14	6	17.0	0.19	0.45	0.4	NO	NO	0	1
65	SANDSTONE	21	17	10	16.0	0.48	0.81	0.4	NO	NO	0	0
66	SANDSTONE	31	24	16	23.7	0.52	0.77	0.4	NO	NO	0	0
67	SANDSTONE	22	21	11	18.0	0.50	0.95	0.4	NO	NO	0	0
68	SANDSTONE	25	18	11	18.0	0.44	0.72	0.4	NO	NO	0	0
69	SANDSTONE	29	23	11	21.0	0.38	0.79	0.4	NO	NO	0	1
70	SANDSTONE	21	16	6	14.3	0.29	0.76	0.4	YES	NO	0	1
71	ARGILLITE	34	22	18	24.7	0.53	0.65	0.4	NO	NO	0	0
72	SANDSTONE	36	20	11	22.3	0.31	0.56	0.4	NO	NO	0	1
73	SANDSTONE	36	27	12	25.0	0.33	0.75	0.4	YES	NO	0	1
74	ARGILLITE	21	14	10	15.0	0.48	0.67	0.4	YES	YES	0	0
75	SANDSTONE	32	12	9	17.7	0.28	0.38	0.4	YES	NO	0	1
76	SANDSTONE	35	26	18	26.3	0.51	0.74	0.4	YES	NO	0	0
77	SANDSTONE	27	21	16	21.3	0.59	0.78	0.4	NO	NO	0	0
78	SANDSTONE	18	15	9	14.0	0.50	0.83	0.4	NO	NO	0	0
79	ARGILLITE	27	20	10	19.0	0.37	0.74	0.4	YES	NO	0	1
80	SANDSTONE	16	11	10	12.3	0.63	0.69	0.4	NO	NO	0	0
81	SANDSTONE	25	22	11	19.3	0.44	0.88	0.4	YES	NO	0	0
82	SANDSTONE	19	11	9	13.0	0.47	0.58	0.4	NO	NO	0	0
83	ARGILLITE	22	11	7	13.3	0.32	0.50	0.4	NO	NO	0	1
84	ARGILLITE	43	20	9	24.0	0.21	0.47	0.5	YES	YES	0	1
85	SANDSTONE	27	22	11	20.0	0.41	0.81	0.5	NO	NO	0	0
86	SANDSTONE	38	30	14	27.3	0.37	0.79	0.5	NO	NO	0	1
87	SANDSTONE	40	25	17	27.3	0.43	0.63	0.5	NO	NO	0	0
88	SANDSTONE	57	36	30	41.0	0.53	0.63	0.5	NO	NO	0	0
89	SANDSTONE	36	33	22	30.3	0.61	0.92	0.5	NO	NO	0	0
90	ARGILLITE	34	18	11	21.0	0.32	0.53	0.5	NO	YES	0	1
91	SANDSTONE	26	20	16	20.7	0.62	0.77	0.5	NO	NO	0	0
92	SANDSTONE	30	22	13	21.7	0.43	0.73	0.5	NO	NO	0	0
93	SANDSTONE	29	17	11	19.0	0.38	0.59	0.5	NO	NO	0	1
94	ARGILLITE	34	13	7	18.0	0.21	0.38	0.5	NO	NO	0	1
95	ARGILLITE	19	11	7	12.3	0.37	0.58	0.5	NO	YES	0	1
96	ARGILLITE	20	11	8	13.0	0.40	0.55	0.5	YES	YES	0	1
97	ARGILLITE	18	12	9	13.0	0.50	0.67	0.5	YES	YES	0	0
98	SANDSTONE	59	38	19	38.7	0.32	0.64	0.6	YES	NO	0	1
99	SANDSTONE	83	41	35	53.0	0.42	0.49	0.6	NO	YES	0	0
100	SANDSTONE	36	27	16	26.3	0.44	0.75	0.6	NO	NO	0	0
AVERAGE		**31.1**	**20.6**	**12.2**	**21.3**	**0.40**	**0.67**	**0.32**	NA	NA	NA	NA
TOTAL		NA	NA	NA	NA	NA	NA	NA	**22**	**11**	**34**	**52**

SUMMARY STATISTICS

LITHOLOGY	NO. CLASTS	STRIAE	% STRI	FACETS	% FAC
SANDSTONE	**72**	1	1.4	13	18.1
ARGILLITE	**26**	10	38.5	9	34.6
QUARTZ	**2**	0	0.0	0	0.0
TOTAL	**100**	11		22	

ROUNDNESS	TOTAL CLAST	FACETS	% FAC	STRIAE	% STRI	SANDSTONE	% SST	ARGILLITE	% ARG	QUARTZ	% QTZ
0.1	11	0	0	0	0.0	8	11.1	3	11.5	0	0.0
0.2	23	5	21.7	1	4.3	12	16.7	9	34.6	2	100.0
0.3	23	4	17.4	2	8.7	21	29.2	2	7.7	0	0
0.4	26	9	34.6	2	7.7	20	27.8	6	23.1	0	0
0.5	14	3	21.4	5	35.7	8	11.1	6	23.1	0	0
0.6	3	1	33.3	1	33.3	3	4.2	0	0	0	0
0.7	0	0	0	0	0.0	0	0	0	0	0	0
0.8	0	0	0	0	0.0	0	0	0	0	0	0
0.9	0	0	0	0	0.0	0	0	0	0	0	0

LOCATION: MURCHISON GLACIER, NEW ZEALAND **COLLECTION : 100 CLASTS FROM BASAL ICE**

NO.	LITHOLOGY	AXIS LENGTH			AVERAGE	AXIAL RATIOS		KRUMBEIN ROUNDNESS	FACETS	STRIAE	RA	C40
		A	B	C		C/A	B/A					
1	SANDSTONE	97	64	63	74.67	0.65	0.66	0.4	NO	NO	0	0
2	SANDSTONE	66	51	24	47.00	0.36	0.77	0.2	NO	NO	1	1
3	SANDSTONE	78	51	23	50.67	0.29	0.65	0.4	YES	NO	0	1
4	SANDSTONE	65	60	34	53.00	0.52	0.92	0.3	NO	NO	0	0
5	SANDSTONE	63	34	17	38.00	0.27	0.54	0.4	NO	NO	0	1
6	SANDSTONE	51	36	12	33.00	0.24	0.71	0.3	YES	NO	0	1
7	ARGILLITE	31	26	15	24.00	0.48	0.84	0.4	YES	YES	0	0
8	SANDSTONE	79	46	39	54.67	0.49	0.58	0.4	YES	NO	0	0
9	SANDSTONE	113	68	24	68.33	0.21	0.60	0.2	NO	NO	1	1
10	SANDSTONE	50	36	23	36.33	0.46	0.72	0.3	NO	NO	0	0
11	SANDSTONE	51	34	15	33.33	0.29	0.67	0.5	YES	NO	0	1
12	SANDSTONE	40	21	16	25.67	0.40	0.53	0.6	NO	NO	0	1
13	ARGILLITE	35	34	21	30.00	0.60	0.97	0.3	YES	NO	0	0
14	SANDSTONE	44	33	23	33.33	0.52	0.75	0.4	YES	NO	0	0
15	ARGILLITE	23	21	5	16.33	0.22	0.91	0.3	YES	NO	0	1
16	SANDSTONE	39	24	11	24.67	0.28	0.62	0.3	NO	NO	0	1
17	ARGILLITE	29	24	16	23.00	0.55	0.83	0.3	NO	NO	0	0
18	SANDSTONE	34	31	10	25.00	0.29	0.91	0.2	NO	NO	1	1
19	SANDSTONE	33	30	25	29.33	0.76	0.91	0.4	NO	NO	0	0
20	SANDSTONE	81	60	35	58.67	0.43	0.74	0.4	YES	NO	0	0
21	SANDSTONE	23	19	9	17.00	0.39	0.83	0.4	NO	NO	0	1
22	SANDSTONE	46	37	16	33.00	0.35	0.80	0.2	NO	NO	1	1
23	SANDSTONE	36	18	6	20.00	0.17	0.50	0.3	NO	NO	0	1
24	SANDSTONE	28	18	7	17.67	0.25	0.64	0.3	NO	NO	0	1
25	SANDSTONE	51	31	20	34.00	0.39	0.61	0.4	YES	NO	0	1
26	ARGILLITE	30	18	5	17.67	0.17	0.60	0.4	YES	YES	0	1
27	ARGILLITE	31	15	8	18.00	0.26	0.48	0.4	YES	YES	0	1
28	ARGILLITE	35	29	10	24.67	0.29	0.83	0.3	YES	YES	0	1
29	ARGILLITE	27	25	10	20.67	0.37	0.93	0.4	NO	NO	0	1
30	SANDSTONE	49	36	17	34.00	0.35	0.73	0.3	NO	NO	0	1
31	SANDSTONE	49	31	16	32.00	0.33	0.63	0.3	NO	NO	0	1
32	ARGILLITE	19	12	8	13.00	0.42	0.63	0.5	NO	YES	0	0
33	SANDSTONE	35	25	7	22.33	0.20	0.71	0.3	NO	NO	0	1
34	SANDSTONE	30	20	14	21.33	0.47	0.67	0.3	NO	NO	0	0
35	SANDSTONE	51	44	24	39.67	0.47	0.86	0.3	NO	NO	0	0
36	SANDSTONE	26	21	15	20.67	0.58	0.81	0.4	NO	NO	0	0
37	ARGILLITE	22	14	8	14.67	0.36	0.64	0.4	NO	NO	0	1
38	SANDSTONE	36	27	19	27.33	0.53	0.75	0.4	NO	NO	0	0
39	SANDSTONE	40	35	20	31.67	0.50	0.88	0.2	NO	NO	1	0
40	SANDSTONE	17	10	9	12.00	0.53	0.59	0.3	NO	NO	0	0
41	SANDSTONE	75	51	39	55.00	0.52	0.68	0.2	NO	NO	1	0
42	SANDSTONE	59	42	26	42.33	0.44	0.71	0.3	NO	NO	0	0
43	ARGILLITE	27	14	4	15.00	0.15	0.52	0.5	YES	YES	0	1
44	SANDSTONE	27	19	6	17.33	0.22	0.70	0.2	NO	NO	1	1
45	SANDSTONE	41	21	14	25.33	0.34	0.51	0.3	YES	NO	0	1
46	SANDSTONE	40	29	19	29.33	0.48	0.73	0.3	NO	NO	0	0
47	SANDSTONE	42	36	21	33.00	0.50	0.86	0.4	NO	NO	0	0
48	SANDSTONE	46	35	15	32.00	0.33	0.76	0.3	YES	NO	0	1
49	ARGILLITE	17	12	4	11.00	0.24	0.71	0.3	YES	YES	0	1
50	SANDSTONE	36	25	15	25.33	0.42	0.69	0.3	YES	NO	0	0
51	SANDSTONE	41	33	17	30.33	0.41	0.80	0.3	YES	NO	0	0
52	SANDSTONE	31	22	16	23.00	0.52	0.71	0.6	NO	NO	0	0
53	SANDSTONE	46	22	12	26.67	0.26	0.48	0.3	NO	NO	0	1
54	SANDSTONE	75	40	24	46.33	0.32	0.53	0.2	NO	NO	1	1
55	SANDSTONE	42	22	17	27.00	0.40	0.52	0.2	NO	NO	1	0
56	ARGILLITE	28	17	6	17.00	0.21	0.61	0.4	YES	YES	0	1
57	SANDSTONE	27	21	10	19.33	0.37	0.78	0.2	NO	NO	1	1
58	SANDSTONE	44	34	27	35.00	0.61	0.77	0.3	NO	NO	0	0
59	SANDSTONE	24	19	13	18.67	0.54	0.79	0.4	NO	NO	0	0
60	SANDSTONE	34	32	12	26.00	0.35	0.94	0.6	NO	NO	0	1
61	SANDSTONE	32	24	19	25.00	0.59	0.75	0.3	NO	NO	0	0
62	SANDSTONE	39	33	21	31.00	0.54	0.85	0.3	YES	YES	0	0
63	SANDSTONE	81	40	34	51.67	0.42	0.49	0.3	YES	YES	0	0
64	ARGILLITE	33	21	12	22.00	0.36	0.64	0.3	NO	NO	0	1
65	SANDSTONE	56	27	20	34.33	0.36	0.48	0.3	YES	NO	0	1
66	ARGILLITE	20	14	8	14.00	0.40	0.70	0.4	YES	NO	0	1
67	ARGILLITE	22	12	6	13.33	0.27	0.55	0.3	NO	NO	0	1
68	SANDSTONE	85	37	30	50.67	0.35	0.44	0.3	YES	YES	0	1
69	SANDSTONE	30	14	11	18.33	0.37	0.47	0.5	NO	NO	0	1
70	SANDSTONE	32	21	12	21.67	0.38	0.66	0.4	NO	NO	0	1
71	ARGILLITE	19	18	8	15.00	0.42	0.95	0.4	YES	YES	0	0
72	ARGILLITE	29	10	7	15.33	0.24	0.34	0.3	NO	NO	0	1
73	ARGILLITE	41	15	5	20.33	0.12	0.37	0.2	NO	NO	1	1
74	SANDSTONE	36	29	16	27.00	0.44	0.81	0.4	NO	NO	0	0
75	SANDSTONE	35	26	15	25.33	0.43	0.74	0.5	NO	NO	0	0
76	ARGILLITE	32	22	9	21.00	0.28	0.69	0.3	NO	YES	0	1
77	ARGILLITE	17	16	10	14.33	0.59	0.94	0.5	YES	YES	0	0
78	SANDSTONE	46	32	22	33.33	0.48	0.70	0.2	NO	NO	1	0
79	ARGILLITE	26	22	14	20.67	0.54	0.85	0.5	YES	YES	0	0
80	SANDSTONE	32	17	12	20.33	0.38	0.53	0.2	NO	NO	1	1
81	SANDSTONE	25	21	13	19.67	0.52	0.84	0.5	NO	NO	0	0
82	SANDSTONE	24	21	7	17.33	0.29	0.88	0.5	NO	NO	0	1
83	ARGILLITE	32	10	5	15.67	0.16	0.31	0.4	NO	YES	0	1
84	ARGILLITE	26	13	9	16.00	0.35	0.50	0.3	NO	NO	0	1
85	SANDSTONE	33	22	20	25.00	0.61	0.67	0.3	NO	NO	0	0
86	ARGILLITE	17	12	8	12.33	0.47	0.71	0.4	NO	NO	0	0
87	SANDSTONE	37	31	17	28.33	0.46	0.84	0.2	NO	NO	1	0
88	SANDSTONE	40	31	16	29.00	0.40	0.78	0.4	NO	NO	0	1
89	SANDSTONE	35	16	9	20.00	0.26	0.46	0.1	NO	NO	1	1
90	SANDSTONE	24	14	12	16.67	0.50	0.58	0.5	NO	NO	0	0
91	SANDSTONE	24	13	10	15.67	0.42	0.54	0.2	NO	NO	1	0
92	SANDSTONE	16	15	10	13.67	0.63	0.94	0.3	NO	NO	0	0
93	SANDSTONE	37	24	12	24.33	0.32	0.65	0.3	NO	NO	0	1
94	ARGILLITE	21	16	8	15.00	0.38	0.76	0.2	NO	NO	1	1
95	SANDSTONE	22	15	11	16.00	0.50	0.68	0.3	NO	NO	0	0
96	SANDSTONE	22	13	9	14.67	0.41	0.59	0.5	NO	NO	0	0
97	SANDSTONE	19	14	8	13.67	0.42	0.74	0.3	NO	NO	0	0
98	SANDSTONE	41	25	22	29.33	0.54	0.61	0.1	NO	NO	1	0
99	SANDSTONE	23	15	8	15.33	0.35	0.65	0.2	NO	NO	1	1
100	SANDSTONE	21	14	11	15.33	0.52	0.67	0.2	NO	NO	1	0
AVERAGE		**38.7**	**26.2**	**15.3**	**26.7**	**0.40**	**0.69**	**0.34**	NA	NA	NA	NA
TOTAL		NA	NA	NA	NA	NA	NA		**28**	**16**	**20**	**52**

SUMMARY STATISTICS

LITHOLOGY	NO. CLASTS	STRIAE	% STRI	FACETS	% FAC
SANDSTONE	**74**	3	4.1	15	20.3
ARGILLITE	**26**	13	50.0	13	50.0
TOTAL	**100**	16		28	

ROUNDNESS	TOTAL CLAST	FACETS	% FAC	STRIAE	% STRI	SANDSTONE	% SST	ARGILLITE	% ARG
0.1	2	0	0	0	0.0	2	2.7	0	0.0
0.2	18	0	0	0	0.0	16	21.6	2	7.7
0.3	40	13	32.5	6	15.0	30	40.5	10	38.5
0.4	26	11	42.3	6	23.1	16	21.6	10	38.5
0.5	11	4	36.4	4	36.4	7	9.5	4	15.4
0.6	3	0	0	0	0.0	3	4.1	0	0
0.7	0	0	0	0	0.0	0	0	0	0
0.8	0	0	0	0	0.0	0	0	0	0
0.9	0	0	0	0	0.0	0	0	0	0

LOCATION , MURCHISON VALLEY, MT COOK
COLLECTION : MH 2, 50 CLASTS (50 metres downstream from MH 1)

NO.	LITHOLOGY	AXIS LENGTH			AVR	AXIAL RATIOS		KRUMBEIN ROUNDNESS	FACETS	STRIAE	RA	C40
		A	B	C		C/A	B/A					
1	SANDSTONE	30	25	16	23.7	0.53	0.83	0.3	YES	NO	0	0
2	SANDSTONE	42	36	17	31.7	0.40	0.86	0.4	YES	NO	0	0
3	SANDSTONE	56	35	16	35.7	0.29	0.63	0.1	NO	NO	1	1
4	SANDSTONE	77	61	41	59.7	0.53	0.79	0.6	NO	NO	0	0
5	SANDSTONE	35	26	7	22.7	0.20	0.74	0.4	NO	NO	0	1
6	SANDSTONE	34	26	17	25.7	0.50	0.76	0.4	NO	NO	0	0
7	SANDSTONE	30	19	15	21.3	0.50	0.63	0.4	YES	NO	0	0
8	SANDSTONE	37	28	13	26.0	0.35	0.76	0.3	NO	NO	0	1
9	SANDSTONE	40	33	18	30.3	0.45	0.83	0.6	NO	NO	0	0
10	SANDSTONE	35	34	24	31.0	0.69	0.97	0.4	NO	NO	0	0
11	SANDSTONE	34	19	11	21.3	0.32	0.56	0.4	YES	YES	0	1
12	SANDSTONE	41	39	15	31.7	0.37	0.95	0.5	NO	NO	0	1
13	SANDSTONE	27	24	10	20.3	0.37	0.89	0.3	NO	NO	0	1
14	SANDSTONE	60	36	24	40.0	0.40	0.60	0.3	YES	YES	0	1
15	SANDSTONE	51	27	20	32.7	0.39	0.53	0.3	NO	NO	0	1
16	SANDSTONE	33	25	16	24.7	0.48	0.76	0.2	YES	NO	1	0
17	SANDSTONE	45	30	23	32.7	0.51	0.67	0.3	YES	NO	0	0
18	SANDSTONE	45	38	30	37.7	0.67	0.84	0.4	NO	NO	0	0
19	SANDSTONE	35	27	13	25.0	0.37	0.77	0.4	NO	NO	0	1
20	SANDSTONE	41	37	20	32.7	0.49	0.90	0.4	YES	NO	0	0
21	SANDSTONE	57	47	28	44.0	0.49	0.82	0.4	YES	NO	0	0
22	SANDSTONE	60	26	20	35.3	0.33	0.43	0.2	YES	YES	1	1
23	SANDSTONE	34	22	10	22.0	0.29	0.65	0.2	NO	YES	1	1
24	SANDSTONE	24	15	12	17.0	0.50	0.63	0.3	YES	NO	0	0
25	SANDSTONE	66	51	33	50.0	0.50	0.77	0.3	YES	NO	0	0
26	SANDSTONE	41	17	13	23.7	0.32	0.41	0.2	NO	NO	1	1
27	SANDSTONE	37	28	21	28.7	0.57	0.76	0.6	YES	NO	0	0
28	SANDSTONE	57	39	19	38.3	0.33	0.68	0.3	YES	NO	0	1
29	SANDSTONE	59	53	20	44.0	0.34	0.90	0.5	NO	NO	0	1
30	SANDSTONE	34	27	21	27.3	0.62	0.79	0.3	NO	NO	0	0
31	SANDSTONE	37	27	12	25.3	0.32	0.73	0.4	NO	NO	0	1
32	SANDSTONE	53	37	17	35.7	0.32	0.70	0.2	NO	NO	1	1
33	SANDSTONE	36	22	20	26.0	0.56	0.61	0.4	NO	NO	0	0
34	SANDSTONE	27	24	13	21.3	0.48	0.89	0.4	NO	NO	0	0
35	SANDSTONE	32	23	18	24.3	0.56	0.72	0.2	NO	NO	1	0
36	SANDSTONE	23	17	11	17.0	0.48	0.74	0.4	NO	NO	0	0
37	SANDSTONE	27	20	7	18.0	0.26	0.74	0.1	NO	NO	1	1
38	ARGILLITE	30	27	8	21.7	0.27	0.90	0.4	YES	YES	0	1
39	SANDSTONE	46	28	20	31.3	0.43	0.61	0.3	NO	NO	0	0
40	SANDSTONE	37	23	15	25.0	0.41	0.62	0.1	NO	NO	1	0
41	SANDSTONE	17	11	8	12.0	0.47	0.65	0.6	NO	NO	0	0
42	SANDSTONE	46	30	22	32.7	0.48	0.65	0.5	NO	NO	0	0
43	SANDSTONE	32	27	22	27.0	0.69	0.84	0.2	NO	NO	1	0
44	SANDSTONE	44	22	15	27.0	0.34	0.50	0.2	NO	NO	1	1
45	SANDSTONE	20	12	10	14.0	0.50	0.60	0.5	YES	NO	0	0
46	SANDSTONE	56	37	21	38.0	0.38	0.66	0.6	YES	NO	0	1
47	ARGILLITE	28	21	6	18.3	0.21	0.75	0.6	YES	NO	0	1
48	SANDSTONE	33	23	17	24.3	0.52	0.70	0.4	YES	NO	0	0
49	SANDSTONE	50	27	17	31.3	0.34	0.54	0.3	NO	NO	0	1
50	SANDSTONE	27	26	10	21.0	0.37	0.96	0.3	NO	NO	0	1
AVERAGE		**40.0**	**28.7**	**17.0**	**28.6**	**0.43**	**0.72**	**0.36**	NA	NA	NA	NA
TOTAL		NA	NA	NA	NA	NA	NA	NA	**19**	**4**	**11**	**23**
%									**38**	**8**	**22**	**46**

SUMMARY STATISTICS

LITHOLOGY	NO.	%	STRIAE	%	FACETS	%
SANDSTONE	**48**	96.0	3	6.3	17	35.4
ARGILLITE	**2**	4.0	1	50.0	2	100.0
TOTAL	**50**		4		19	

ROUNDNESS	TOTAL CLASTS	%	FACETS	% FAC	STRIAE	% STRI
0.1	3	6	0	0	0.0	0.0
0.2	8	16	2	25	2	25.0
0.3	13	26	6	46	2	15.4
0.4	16	32	7	44	0	0.0
0.5	4	8	1	25	0	0
0.6	6	12	3	50	0	0
0.7	0	0	0	0	0	0
0.8	0	0	0	0	0	0
0.9	0	0	0	0	0	0
	50		19		4	

ROUNDNESS	SANDSTONE	% SST	ARGILLITE	% ARG
0.1	3	6	0	0.0
0.2	8	17	0	0.0
0.3	13	27	0	0.0
0.4	15	31	1	50.0
0.5	4	8	0	0
0.6	5	10	1	0
0.7	0	0	0	0
0.8	0	0	0	0
0.9	0	0	0	0
	48		2	

LOCATION , MURCHISON VALLEY, MT COOK
COLLECTION : MH 3, 50 CLASTS (650 metres downstream from MH 1)

NO.	LITHOLOGY	AXIS LENGTH			AVR	AXIAL RATIOS		KRUMBEIN ROUNDNESS	FACETS	STRIAE	RA	C40
		A	B	C		C/A	B/A					
1	SANDSTONE	41	29	14	28.0	0.34	0.71	0.3	NO	NO	0	1
2	SANDSTONE	55	40	16	37.0	0.29	0.73	0.4	NO	NO	0	1
3	SANDSTONE	55	29	21	35.0	0.38	0.53	0.3	NO	NO	0	1
4	SANDSTONE	45	34	19	32.7	0.42	0.76	0.4	YES	NO	0	0
5	SANDSTONE	55	36	20	37.0	0.36	0.65	0.3	**YES**	NO	0	1
6	SANDSTONE	27	19	11	19.0	0.41	0.70	0.2	NO	NO	1	0
7	SANDSTONE	31	25	16	24.0	0.52	0.81	0.4	NO	NO	0	0
8	SANDSTONE	60	49	34	47.7	0.57	0.82	0.5	NO	NO	0	0
9	ARGILLITE	61	30	17	36.0	0.28	0.49	0.3	NO	NO	0	1
10	SANDSTONE	35	28	10	24.3	0.29	0.80	0.5	NO	NO	0	1
11	SANDSTONE	70	34	22	42.0	0.31	0.49	0.3	**YES**	NO	0	1
12	SANDSTONE	45	32	24	33.7	0.53	0.71	0.4	NO	NO	0	0
13	SANDSTONE	34	29	12	25.0	0.35	0.85	0.3	NO	NO	0	1
14	SANDSTONE	41	25	16	27.3	0.39	0.61	0.2	NO	NO	1	1
15	SANDSTONE	55	45	34	44.7	0.62	0.82	0.2	NO	NO	1	0
16	SANDSTONE	31	22	14	22.3	0.45	0.71	0.5	NO	NO	0	0
17	SANDSTONE	67	45	36	49.3	0.54	0.67	0.5	NO	NO	0	0
18	ARGILLITE	38	16	8	20.7	0.21	0.42	0.4	**YES**	**YES**	0	1
19	SANDSTONE	80	46	30	52.0	0.38	0.58	0.2	NO	NO	1	1
20	SANDSTONE	60	52	31	47.7	0.52	0.87	0.6	NO	NO	0	0
21	SANDSTONE	28	19	14	20.3	0.50	0.68	0.3	NO	NO	0	0
22	SANDSTONE	22	21	14	19.0	0.64	0.95	0.4	NO	NO	0	0
23	SANDSTONE	67	24	23	38.0	0.34	0.36	0.3	**YES**	NO	0	1
24	SANDSTONE	55	40	32	42.3	0.58	0.73	0.5	NO	NO	0	0
25	ARGILLITE	50	42	27	39.7	0.54	0.84	0.3	NO	NO	0	0
26	SANDSTONE	74	56	44	58.0	0.59	0.76	0.2	NO	NO	1	0
27	SANDSTONE	50	35	24	36.3	0.48	0.70	0.4	NO	NO	0	0
28	SANDSTONE	42	31	16	29.7	0.38	0.74	0.3	NO	NO	0	1
29	SANDSTONE	49	44	24	39.0	0.49	0.90	0.3	NO	NO	0	0
30	SANDSTONE	54	33	17	34.7	0.31	0.61	0.2	NO	NO	1	1
31	SANDSTONE	54	47	31	44.0	0.57	0.87	0.3	NO	NO	0	0
32	SANDSTONE	53	30	17	33.3	0.32	0.57	0.2	**YES**	NO	1	1
33	SANDSTONE	67	37	30	44.7	0.45	0.55	0.3	NO	NO	0	0
34	SANDSTONE	58	31	17	35.3	0.29	0.53	0.4	**YES**	NO	0	1
35	SANDSTONE	75	33	26	44.7	0.35	0.44	0.4	**YES**	NO	0	1
36	SANDSTONE	32	16	8	18.7	0.25	0.50	0.2	NO	NO	1	1
37	SANDSTONE	94	60	44	66.0	0.47	0.64	0.3	NO	NO	0	0
38	SANDSTONE	72	52	42	55.3	0.58	0.72	0.3	NO	NO	0	0
39	SANDSTONE	47	35	15	32.3	0.32	0.74	0.6	NO	NO	0	1
40	ARGILLITE	44	32	20	32.0	0.45	0.73	0.5	NO	NO	0	0
41	ARGILLITE	40	25	12	25.7	0.30	0.63	0.5	NO	NO	0	1
42	SANDSTONE	25	21	13	19.7	0.52	0.84	0.5	NO	NO	0	0
43	SANDSTONE	83	55	35	57.7	0.42	0.66	0.3	NO	NO	0	0
44	SANDSTONE	50	29	15	31.3	0.30	0.58	0.3	**YES**	NO	0	1
45	SANDSTONE	45	37	19	33.7	0.42	0.82	0.4	NO	NO	0	0
46	SANDSTONE	54	42	27	41.0	0.50	0.78	0.3	NO	NO	0	0
47	SANDSTONE	31	22	16	23.0	0.52	0.71	0.4	NO	NO	0	0
48	SANDSTONE	45	26	13	28.0	0.29	0.58	0.3	NO	NO	0	1
49	SANDSTONE	34	22	15	23.7	0.44	0.65	0.4	NO	NO	0	0
50	SANDSTONE	74	55	31	53.3	0.42	0.74	0.3	NO	NO	0	0
AVG		**51.1**	**34.3**	**21.7**	**35.7**	**0.42**	**0.69**	**0.35**	NA	NA	NA	NA
TOTAL		NA	NA	NA	NA	NA	NA	NA	**8**	**1**	**8**	**22**
%									**16**	**2**	**16**	**44**

SUMMARY STATISTICS

LITHOLOGY	NO.	%	STRIAE	%	FACETS	%
SANDSTONE	**45**	90.0	0	0.0	7	15.6
ARGILLITE	**5**	10.0	1	20.0	1	20.0
TOTAL	**50**		1		8	

ROUNDNESS	TOTAL CLASTS	%	FACETS	% FAC	STRIAE	% STRI
0.1	0	0	0	0	0	0
0.2	8	16	1	13	0	0
0.3	20	40	4	20	0	0
0.4	12	24	3	25	1	8
0.5	8	16	0	0	0	0
0.6	2	4	0	0	0	0
0.7	0	0	0	0	0	0
0.8	0	0	0	0	0	0
0.9	0	0	0	0	0	0
	50		8		1	

ROUNDNESS	SANDSTONE	% SST	ARGILLITE	% ARG
0.1	0	0	0	0
0.2	8	18	0	0
0.3	18	40	2	40
0.4	11	24	1	20
0.5	6	13	2	40
0.6	2	4	0	0
0.7	0	0	0	0
0.8	0	0	0	0
0.9	0	0	0	0
	45		5	

LOCATION , MURCHISON VALLEY SITE 4, MT. COOK
COLLECTION : MH 4, 50 CLASTS FROM ROCK-FALL/SCREE DEPOSIT

NO.	LITHOLOGY	AXIS LENGTH			AVR	AXIAL RATIOS		KRNESS	FLAT	STRIAE	RA	C40
		A	B	C		C/A	B/A		FACES			
1	SANDSTONE	53	44	18	38.3	0.34	0.83	0.2	NO	NO	1	1
2	SANDSTONE	45	27	7	26.3	0.16	0.60	0.2	NO	NO	1	1
3	SANDSTONE	50	35	20	35.0	0.40	0.70	0.3	NO	NO	0	1
4	SANDSTONE	90	45	22	52.3	0.24	0.50	0.2	YES	NO	1	1
5	SANDSTONE	56	23	10	29.7	0.18	0.41	0.3	NO	NO	0	1
6	ARGILLITE	92	56	18	55.3	0.20	0.61	0.4	YES	NO	0	1
7	ARGILLITE	30	20	6	18.7	0.20	0.67	0.2	YES	YES	1	1
8	SANDSTONE	80	32	26	46.0	0.33	0.40	0.2	NO	NO	1	1
9	SANDSTONE	40	30	15	28.3	0.38	0.75	0.3	NO	NO	0	1
10	ARGILLITE	38	22	8	22.7	0.21	0.58	0.2	NO	YES	1	1
11	ARGILLITE	37	20	17	24.7	0.46	0.54	0.2	YES	YES	1	0
12	SANDSTONE	55	20	8	27.7	0.15	0.36	0.2	NO	NO	1	1
13	ARGILLITE	37	22	12	23.7	0.32	0.59	0.4	YES	YES	0	1
14	ARGILLITE	35	15	6	18.7	0.17	0.43	0.3	YES	YES	0	1
15	ARGILLITE	65	40	5	36.7	0.08	0.62	0.1	YES	YES	1	1
16	SANDSTONE	50	27	15	30.7	0.30	0.54	0.3	YES	NO	0	1
17	ARGILLITE	25	17	10	17.3	0.40	0.68	0.3	NO	NO	0	1
18	ARGILLITE	26	20	6	17.3	0.23	0.77	0.2	NO	NO	1	1
19	SANDSTONE	42	30	25	32.3	0.60	0.71	0.2	YES	NO	1	0
20	ARGILLITE	68	49	15	44.0	0.22	0.72	0.1	NO	YES	1	1
21	SANDSTONE	60	24	12	32.0	0.20	0.40	0.1	NO	NO	1	1
22	ARGILLITE	59	51	7	39.0	0.12	0.86	0.1	NO	YES	1	1
23	SANDSTONE	47	36	24	35.7	0.51	0.77	0.3	NO	NO	0	0
24	ARGILLITE	60	20	5	28.3	0.08	0.33	0.1	YES	YES	1	1
25	SANDSTONE	36	25	21	27.3	0.58	0.69	0.2	YES	NO	1	0
26	SANDSTONE	44	30	7	27.0	0.16	0.68	0.2	NO	NO	1	1
27	SANDSTONE	43	32	19	31.3	0.44	0.74	0.3	NO	NO	0	0
28	SANDSTONE	60	51	22	44.3	0.37	0.85	0.2	YES	NO	1	1
29	ARGILLITE	49	29	12	30.0	0.24	0.59	0.2	YES	YES	1	1
30	ARGILLITE	27	14	6	15.7	0.22	0.52	0.3	YES	YES	0	1
31	ARGILLITE	39	19	10	22.7	0.26	0.49	0.3	YES	YES	0	1
32	SANDSTONE	30	22	12	21.3	0.40	0.73	0.3	NO	NO	0	1
33	SANDSTONE	34	20	11	21.7	0.32	0.59	0.2	NO	NO	1	1
34	SANDSTONE	37	27	10	24.7	0.27	0.73	0.2	YES	NO	1	1
35	SANDSTONE	26	18	12	18.7	0.46	0.69	0.3	NO	NO	0	0
36	SANDSTONE	52	30	14	32.0	0.27	0.58	0.2	NO	NO	1	1
37	SANDSTONE	40	33	24	32.3	0.60	0.83	0.2	YES	NO	1	0
38	SANDSTONE	39	20	10	23.0	0.26	0.51	0.2	NO	NO	1	1
39	ARGILLITE	105	87	27	73.0	0.26	0.83	0.3	YES	YES	0	1
40	SANDSTONE	40	16	15	23.7	0.38	0.40	0.3	NO	NO	0	1
41	SANDSTONE	46	24	12	27.3	0.26	0.52	0.2	NO	NO	1	1
42	SANDSTONE	56	38	22	38.7	0.39	0.68	0.2	NO	NO	1	1
43	SANDSTONE	46	35	21	34.0	0.46	0.76	0.3	NO	NO	0	0
44	SANDSTONE	39	26	17	27.3	0.44	0.67	0.2	NO	NO	1	0
45	SANDSTONE	39	24	17	26.7	0.44	0.62	0.2	YES	NO	1	0
46	SANDSTONE	23	12	11	15.3	0.48	0.52	0.2	NO	NO	1	0
47	ARGILLITE	30	22	8	20.0	0.27	0.73	0.2	YES	NO	1	1
48	SANDSTONE	30	26	9	21.7	0.30	0.87	0.2	NO	NO	1	1
49	SANDSTONE	45	26	10	27.0	0.22	0.58	0.2	NO	NO	1	1
50	SANDSTONE	28	16	10	18.0	0.36	0.57	0.3	NO	NO	0	1
AVERAGE		**46.5**	**28.9**	**13.7**	**29.7**	**0.31**	**0.63**	**0.23**	NA	NA	NA	NA
TOTAL		NA	NA	NA	NA	NA	NA	NA	**20**	**13**	**32**	**39**
%									**40**	**26**	**64**	**78**

SUMMARY STATISTICS

LITHOLOGY	NO.	%	STRIAE	%	FACES	%
SANDSTONE	**33**	66.0	0	0.0	8	24.2
ARGILLITE	**17**	34.0	13	76.5	12	70.6
TOTAL	**50**		13		20	

ROUNDNESS	TOTAL CLASTS	%	FACES	% FACES	STRIAE	% STRI
0.1	5	10	2	40	4	80
0.2	28	56	11	39	4	14
0.3	15	30	5	33	4	27
0.4	2	4	2	100	1	50
0.5	0	0	0	0	0	0
0.6	0	0	0	0	0	0
0.7	0	0	0	0	0	0
0.8	0	0	0	0	0	0
0.9	0	0	0	0	0	0
	50		20		13	

ROUNDNESS	SANDSTONE	% SST	ARGILLITE	% ARG
0.1	2	6.1	4	23.5
0.2	20	60.6	6	35.3
0.3	11	33.3	5	29.4
0.4	0	0	2	11.8
0.5	0	0	0	0
0.6	0	0	0	0
0.7	0	0	0	0
0.8	0	0	0	0
0.9	0	0	0	0
	33		17	

LOCATION , MURCHISON VALLEY, MT COOK
COLLECTION : MH 5, 50 CLASTS (2200 metres downstream from MH 1)

NO.	LITHOLOGY	AXIS LENGTH			AVR	AXIAL RATIOS		KRNESS	FACETS	STRIAE	RA	C40
		A	B	C		C/A	B/A					
1	SANDSTONE	57	27	20	34.7	0.35	0.47	0.7	NO	NO	0	1
2	SANDSTONE	55	34	26	38.3	0.47	0.62	0.4	YES	NO	0	0
3	SANDSTONE	52	31	21	34.7	0.40	0.60	0.6	NO	NO	0	0
4	SANDSTONE	86	76	49	70.3	0.57	0.88	0.3	NO	NO	0	0
5	SANDSTONE	66	41	28	45.0	0.42	0.62	0.4	NO	NO	0	0
6	SANDSTONE	50	31	14	31.7	0.28	0.62	0.5	NO	NO	0	1
7	SANDSTONE	46	39	24	36.3	0.52	0.85	0.4	NO	NO	0	0
8	ARGILLITE	27	11	4	14.0	0.15	0.41	0.7	NO	NO	0	1
9	SANDSTONE	30	19	10	19.7	0.33	0.63	0.5	NO	NO	0	1
10	SANDSTONE	32	19	11	20.7	0.34	0.59	0.5	NO	NO	0	1
11	SANDSTONE	53	29	15	32.3	0.28	0.55	0.4	YES	NO	0	1
12	SANDSTONE	84	58	41	61.0	0.49	0.69	0.7	NO	NO	0	0
13	SANDSTONE	56	46	36	46.0	0.64	0.82	0.4	NO	NO	0	0
14	SANDSTONE	32	24	15	23.7	0.47	0.75	0.8	NO	NO	0	0
15	SANDSTONE	43	37	18	32.7	0.42	0.86	0.4	NO	NO	0	0
16	SANDSTONE	110	90	46	82.0	0.42	0.82	0.5	NO	NO	0	0
17	SANDSTONE	41	21	19	27.0	0.46	0.51	0.7	NO	NO	0	0
18	SANDSTONE	36	20	17	24.3	0.47	0.56	0.3	NO	NO	0	0
19	SANDSTONE	37	26	19	27.3	0.51	0.70	0.3	NO	NO	0	0
20	SANDSTONE	45	32	23	33.3	0.51	0.71	0.4	YES	NO	0	0
21	SANDSTONE	66	52	28	48.7	0.42	0.79	0.5	YES	NO	0	0
22	SANDSTONE	95	77	56	76.0	0.59	0.81	0.7	NO	NO	0	0
23	SANDSTONE	30	28	11	23.0	0.37	0.93	0.5	NO	NO	0	1
24	SANDSTONE	55	41	30	42.0	0.55	0.75	0.5	NO	NO	0	0
25	SANDSTONE	41	36	22	33.0	0.54	0.88	0.4	NO	NO	0	0
26	SANDSTONE	70	52	35	52.3	0.50	0.74	0.3	NO	NO	0	0
27	SANDSTONE	50	22	13	28.3	0.26	0.44	0.6	NO	NO	0	1
28	SANDSTONE	82	81	40	67.7	0.49	0.99	0.3	NO	NO	0	0
29	SANDSTONE	53	28	25	35.3	0.47	0.53	0.3	NO	NO	0	0
30	SANDSTONE	62	36	25	41.0	0.40	0.58	0.3	YES	NO	0	0
31	ARGILLITE	42	23	10	25.0	0.24	0.55	0.5	YES	NO	0	1
32	SANDSTONE	64	35	27	42.0	0.42	0.55	0.4	NO	NO	0	0
33	SANDSTONE	73	32	27	44.0	0.37	0.44	0.3	NO	NO	0	1
34	SANDSTONE	96	56	41	64.3	0.43	0.58	0.4	YES	NO	0	0
35	SANDSTONE	47	35	28	36.7	0.60	0.74	0.3	NO	NO	0	0
36	SANDSTONE	73	56	34	54.3	0.47	0.77	0.7	NO	NO	0	0
37	ARGILLITE	41	23	19	27.7	0.46	0.56	0.6	NO	NO	0	0
38	SANDSTONE	75	47	18	46.7	0.24	0.63	0.5	NO	NO	0	1
39	SANDSTONE	57	45	17	39.7	0.30	0.79	0.5	NO	NO	0	1
40	ARGILLITE	54	27	22	34.3	0.41	0.50	0.3	YES	NO	0	0
41	SANDSTONE	52	40	31	41.0	0.60	0.77	0.5	NO	NO	0	0
42	ARGILLITE	83	57	33	57.7	0.40	0.69	0.5	YES	NO	0	1
43	SANDSTONE	73	30	15	39.3	0.21	0.41	0.3	NO	NO	0	1
44	SANDSTONE	48	45	29	40.7	0.60	0.94	0.3	NO	NO	0	0
45	ARGILLITE	37	25	19	27.0	0.51	0.68	0.6	NO	NO	0	0
46	SANDSTONE	45	35	19	33.0	0.42	0.78	0.3	NO	NO	0	0
47	SANDSTONE	56	42	29	42.3	0.52	0.75	0.6	NO	NO	0	0
48	SANDSTONE	80	36	19	45.0	0.24	0.45	0.2	NO	NO	1	1
49	SANDSTONE	44	23	21	29.3	0.48	0.52	0.7	NO	NO	0	0
50	SANDSTONE	54	47	27	42.7	0.50	0.87	0.5	NO	NO	0	0
AVERAGE		**56.7**	**38.5**	**24.5**	**39.9**	**0.43**	**0.67**	**0.47**	NA	NA	NA	NA
TOTAL		NA	NA	NA	NA	NA	NA	NA	**9**	**0**	**1**	**15**
%									**18**	**0**	**2**	**30**

SUMMARY STATISTICS

LITHOLOGY	NO.	%	STRIAE	%	FACETS	%
SANDSTONE	**44**	88.0	0	0.0	6	13.6
ARGILLITE	**6**	12.0	0	0.0	3	50.0
TOTAL	**50**		0		9	

ROUNDNESS	TOTAL CLASTS	%	FACETS	% FAC	STRIAE	% STRI
0.1	0	0	0	0	0	0
0.2	1	2	0	0	0	0
0.3	13	26	2	15	0	0
0.4	10	20	4	40	0	0
0.5	13	26	3	23	0	0
0.6	5	10	0	0	0	0
0.7	7	14	0	0	0	0
0.8	1	2	0	0	0	0
0.9	0	0	0	0	0	0
	50		9		0	

ROUNDNESS	SANDSTONE	% SST	ARGILLITI	% ARG
0.1	0	0	0	0
0.2	1	2	0	0
0.3	12	27	1	17
0.4	10	23	0	0
0.5	11	25	2	33
0.6	3	7	2	33
0.7	6	14	1	17
0.8	1	2	0	0
0.9	0	0	0	0
	44		6	

LOCATION , MURCHISON VALLEY, MT COOK
COLLECTION : MH 6, 50 CLASTS (2450 metres downstream from MH 1)

NO.	LITHOLOGY	AXIS LENGTH			AVR	AXIAL RATIOS		KRNESS	FACETS	STRIAE	RA	C40
		A	B	C		C/A	B/A					
1	SANDSTONE	89	70	39	66.0	0.44	0.79	0.7	NO	NO	0	0
2	SANDSTONE	43	26	16	28.3	0.37	0.60	0.6	NO	NO	0	1
3	ARGILLITE	64	25	8	32.3	0.13	0.39	0.3	NO	NO	0	1
4	SANDSTONE	45	40	33	39.3	0.73	0.89	0.4	YES	NO	0	0
5	SANDSTONE	39	25	15	26.3	0.38	0.64	0.4	NO	NO	0	1
6	SANDSTONE	35	34	12	27.0	0.34	0.97	0.5	NO	NO	0	1
7	SANDSTONE	33	21	16	23.3	0.48	0.64	0.6	NO	NO	0	0
8	SANDSTONE	44	26	22	30.7	0.50	0.59	0.4	YES	NO	0	0
9	SANDSTONE	52	26	20	32.7	0.38	0.50	0.3	NO	NO	0	1
10	SANDSTONE	90	74	47	70.3	0.52	0.82	0.3	NO	NO	0	0
11	SANDSTONE	84	60	46	63.3	0.55	0.71	0.6	NO	NO	0	0
12	SANDSTONE	39	36	27	34.0	0.69	0.92	0.5	NO	NO	0	0
13	SANDSTONE	38	22	18	26.0	0.47	0.58	0.6	NO	NO	0	0
14	ARGILLITE	60	48	25	44.3	0.42	0.80	0.4	NO	NO	0	0
15	SANDSTONE	42	30	22	31.3	0.52	0.71	0.4	NO	NO	0	0
16	ARGILLITE	36	35	10	27.0	0.28	0.97	0.4	NO	NO	0	1
17	SANDSTONE	60	53	40	51.0	0.67	0.88	0.6	NO	NO	0	0
18	SANDSTONE	39	37	15	30.3	0.38	0.95	0.5	YES	NO	0	1
19	SANDSTONE	61	27	22	36.7	0.36	0.44	0.2	NO	NO	1	1
20	SANDSTONE	40	33	30	34.3	0.75	0.83	0.5	NO	NO	0	0
21	SANDSTONE	40	35	20	31.7	0.50	0.88	0.5	NO	NO	0	0
22	ARGILLITE	47	24	12	27.7	0.26	0.51	0.7	NO	NO	0	1
23	SANDSTONE	42	25	16	27.7	0.38	0.60	0.5	NO	NO	0	1
24	SANDSTONE	45	35	23	34.3	0.51	0.78	0.3	YES	NO	0	0
25	SANDSTONE	72	45	23	46.7	0.32	0.63	0.5	NO	NO	0	1
26	SANDSTONE	90	58	46	64.7	0.51	0.64	0.5	NO	NO	0	0
27	SANDSTONE	42	26	4	24.0	0.10	0.62	0.3	YES	NO	0	1
28	SANDSTONE	33	27	16	25.3	0.48	0.82	0.2	NO	NO	1	0
29	ARGILLITE	44	30	15	29.7	0.34	0.68	0.4	NO	NO	0	1
30	SANDSTONE	36	20	16	24.0	0.44	0.56	0.6	NO	NO	0	0
31	SANDSTONE	42	38	16	32.0	0.38	0.90	0.2	NO	NO	1	1
32	SANDSTONE	36	25	14	25.0	0.39	0.69	0.4	YES	NO	0	1
33	SANDSTONE	54	45	23	40.7	0.43	0.83	0.2	NO	NO	1	0
34	SANDSTONE	40	29	17	28.7	0.43	0.73	0.5	NO	NO	0	0
35	SANDSTONE	33	29	12	24.7	0.36	0.88	0.1	NO	NO	1	1
36	SANDSTONE	22	14	13	16.3	0.59	0.64	0.6	NO	NO	0	0
37	SANDSTONE	60	51	36	49.0	0.60	0.85	0.1	NO	NO	1	0
38	ARGILLITE	27	25	13	21.7	0.48	0.93	0.3	NO	NO	0	0
39	SANDSTONE	35	21	20	25.3	0.57	0.60	0.5	NO	NO	0	0
40	SANDSTONE	70	44	22	45.3	0.31	0.63	0.1	NO	NO	1	1
41	SANDSTONE	35	29	17	27.0	0.49	0.83	0.3	NO	NO	0	0
42	SANDSTONE	35	20	17	24.0	0.49	0.57	0.4	NO	NO	0	0
43	SANDSTONE	48	41	26	38.3	0.54	0.85	0.6	NO	NO	0	0
44	SANDSTONE	77	67	50	64.7	0.65	0.87	0.6	NO	NO	0	0
45	SANDSTONE	32	25	15	24.0	0.47	0.78	0.4	NO	NO	0	0
46	SANDSTONE	81	65	37	61.0	0.46	0.80	0.8	NO	NO	0	0
47	SANDSTONE	31	22	15	22.7	0.48	0.71	0.5	YES	NO	0	0
48	SANDSTONE	44	25	20	29.7	0.45	0.57	0.2	NO	NO	1	0
49	SANDSTONE	31	21	16	22.7	0.52	0.68	0.4	NO	NO	0	0
50	SANDSTONE	31	19	18	22.7	0.58	0.61	0.4	NO	NO	0	0
AVERAGE		**47.8**	**34.6**	**21.8**	**34.7**	**0.46**	**0.73**	**0.43**	NA	NA	NA	NA
TOTAL		NA	NA	NA	NA	NA	NA	NA	**7**	**0**	**8**	**17**
%									**14**	**0**	**16**	**34**

SUMMARY STATISTICS

LITHOLOGY	NO.	%	STRIAE	%	FACETS	%
SANDSTONE	**44**	88.0	0	0.0	7	15.9
ARGILLITE	**6**	12.0	0	0.0	0	0.0
TOTAL	**50**				7	

ROUNDNESS	TOTAL CLASTS	%	FACETS	% FAC	STRIAE	% STRI
0.1	3	6	0	0	0	0
0.2	5	10	0	0	0	0
0.3	7	14	2	29	0	0
0.4	12	24	3	25	0	0
0.5	11	22	2	18	0	0
0.6	9	18	0	0	0	0
0.7	2	4	0	0	0	0
0.8	1	2	0	0	0	0
0.9	0	0	0	0	0	0
	50		7		0	

ROUNDNESS	SANDSTONE	% SST	ARGILLITE	% ARG
0.1	3	6.8	0	0
0.2	5	11.4	0	0
0.3	5	11.4	2	33
0.4	9	20.5	3	50
0.5	11	25.0	0	0
0.6	9	20.5	0	0
0.7	1	2.3	1	17
0.8	1	2.3	0	0
0.9	0	0	0	0
	44		6	

LOCATION , MURCHISON VALLEY, MT COOK
COLLECTION : MH 7, 50 CLASTS (3550 metres downstream from MH 1)

NO.	LITHOLOGY	AXIS LENGTH			AVR	AXIAL RATIOS		KRNESS	FACETS	STRIAE	RA	C40
		A	B	C		C/A	B/A					
1	SANDSTONE	27	22	12	20.3	0.44	0.81	0.6	NO	NO	0	0
2	SANDSTONE	75	72	30	59.0	0.40	0.96	0.3	NO	NO	0	1
3	SANDSTONE	67	56	42	55.0	0.63	0.84	0.4	NO	NO	0	0
4	SANDSTONE	97	66	42	68.3	0.43	0.68	0.4	NO	NO	0	0
5	SANDSTONE	45	34	22	33.7	0.49	0.76	0.3	NO	NO	0	0
6	SANDSTONE	63	43	34	46.7	0.54	0.68	0.6	NO	NO	0	0
7	SANDSTONE	37	24	10	23.7	0.27	0.65	0.3	NO	NO	0	1
8	SANDSTONE	44	35	21	33.3	0.48	0.80	0.3	NO	NO	0	0
9	SANDSTONE	62	34	27	41.0	0.44	0.55	0.4	NO	NO	0	0
10	SANDSTONE	110	62	35	69.0	0.32	0.56	0.4	NO	NO	0	1
11	SANDSTONE	50	45	43	46.0	0.86	0.90	0.7	NO	NO	0	0
12	SANDSTONE	34	27	20	27.0	0.59	0.79	0.6	NO	NO	0	0
13	SANDSTONE	40	26	14	26.7	0.35	0.65	0.5	YES	NO	0	1
14	SANDSTONE	75	40	29	48.0	0.39	0.53	0.6	NO	NO	0	1
15	SANDSTONE	37	35	15	29.0	0.41	0.95	0.3	NO	NO	0	0
16	SANDSTONE	70	51	34	51.7	0.49	0.73	0.3	NO	NO	0	0
17	SANDSTONE	46	40	16	34.0	0.35	0.87	0.4	NO	NO	0	1
18	SANDSTONE	59	44	39	47.3	0.66	0.75	0.8	NO	NO	0	0
19	SANDSTONE	76	48	46	56.7	0.61	0.63	0.6	NO	NO	0	0
20	SANDSTONE	85	42	30	52.3	0.35	0.49	0.3	YES	NO	0	1
21	SANDSTONE	70	48	36	51.3	0.51	0.69	0.8	NO	NO	0	0
22	ARGILLITE	42	30	14	28.7	0.33	0.71	0.4	NO	NO	0	1
23	SANDSTONE	60	43	22	41.7	0.37	0.72	0.3	NO	NO	0	1
24	SANDSTONE	69	57	40	55.3	0.58	0.83	0.4	NO	NO	0	0
25	ARGILLITE	48	22	8	26.0	0.17	0.46	0.3	NO	NO	0	1
26	SANDSTONE	36	22	19	25.7	0.53	0.61	0.5	NO	NO	0	0
27	SANDSTONE	86	65	51	67.3	0.59	0.76	0.4	NO	NO	0	0
28	SANDSTONE	64	41	32	45.7	0.50	0.64	0.5	NO	NO	0	0
29	SANDSTONE	35	20	19	24.7	0.54	0.57	0.3	NO	NO	0	0
30	SANDSTONE	41	25	20	28.7	0.49	0.61	0.5	NO	NO	0	0
31	SANDSTONE	56	39	29	41.3	0.52	0.70	0.4	NO	NO	0	0
32	SANDSTONE	83	27	17	42.3	0.20	0.33	0.2	NO	NO	1	1
33	SANDSTONE	83	80	20	61.0	0.24	0.96	0.2	NO	NO	1	1
34	SANDSTONE	67	46	26	46.3	0.39	0.69	0.5	NO	NO	0	1
35	SANDSTONE	63	44	16	41.0	0.25	0.70	0.4	NO	NO	0	1
36	SANDSTONE	46	43	31	40.0	0.67	0.93	0.5	NO	NO	0	0
37	SANDSTONE	62	32	16	36.7	0.26	0.52	0.3	NO	NO	0	1
38	SANDSTONE	60	41	33	44.7	0.55	0.68	0.3	NO	NO	0	0
39	SANDSTONE	51	47	25	41.0	0.49	0.92	0.3	NO	NO	0	0
40	SANDSTONE	120	77	57	84.7	0.48	0.64	0.5	NO	NO	0	0
41	SANDSTONE	31	27	16	24.7	0.52	0.87	0.6	NO	NO	0	0
42	SANDSTONE	37	27	21	28.3	0.57	0.73	0.5	NO	NO	0	0
43	SANDSTONE	36	29	22	29.0	0.61	0.81	0.4	NO	NO	0	0
44	SANDSTONE	79	53	45	59.0	0.57	0.67	0.6	NO	NO	0	0
45	SANDSTONE	40	24	21	28.3	0.53	0.60	0.3	NO	NO	0	0
46	SANDSTONE	27	26	16	23.0	0.59	0.96	0.3	NO	NO	0	0
47	SANDSTONE	85	61	43	63.0	0.51	0.72	0.5	NO	NO	0	0
48	SANDSTONE	97	56	44	65.7	0.45	0.58	0.6	NO	NO	0	0
49	SANDSTONE	92	81	54	75.7	0.59	0.88	0.4	NO	NO	0	0
50	SANDSTONE	130	60	49	79.7	0.38	0.46	0.4	YES	NO	0	1
AVERAGE		**61.9**	**42.8**	**28.5**	**44.4**	**0.47**	**0.71**	**0.43**	NA	NA	NA	NA
TOTAL		NA	NA	NA	NA	NA	NA	NA	**3**	**0**	**2**	**16**
%									**6**	**0**	**4**	**32**

SUMMARY STATISTICS

LITHOLOGY	NO.	%	STRIAE	%	FACETS	%
SANDSTONE	**48**	96.0	0	0.0	3	6.3
ARGILLITE	**2**	4.0	0	0.0	0	0.0
TOTAL	**50**		0		3	

ROUNDNESS	TOTAL CLASTS	%	FACETS	% FAC	STRIAE	% STRI
0.1	0	0	0	0	0	0
0.2	2	4	0	0	0	0
0.3	15	30	1	7	0	0
0.4	13	26	1	8	0	0
0.5	9	18	1	11	0	0
0.6	8	16	0	0	0	0
0.7	1	0	0	0	0	0
0.8	2	0	0	0	0	0
0.9	0	0	0	0	0	0
	50		3		0	

ROUNDNESS	SANDSTONE	% SST	ARGILLITE	% ARG
0.1	0	0	0	0
0.2	2	4	0	0
0.3	14	29	1	50
0.4	12	25	1	50
0.5	8	17	0	0
0.6	9	19	0	0
0.7	1	2	0	0
0.8	2	4	0	0
0.9	0	0	0	0
	48		2	

LOCATION , MURCHISON VALLEY, MT COOK
COLLECTION : MH 8, 50 CLASTS (3800 metres downstream from MH 1)

NO.	LITHOLOGY	AXIS LENGTH			AVR	AXIAL RATIOS		KRNESS	FACETS	STRIAE	RA	C40
		A	B	C		C/A	B/A					
1	SANDSTONE	50	29	17	32.0	0.34	0.58	0.7	NO	NO	0	1
2	SANDSTONE	54	21	20	31.7	0.37	0.39	0.6	NO	NO	0	1
3	SANDSTONE	36	27	20	27.7	0.56	0.75	0.7	NO	NO	0	0
4	SANDSTONE	31	27	20	26.0	0.65	0.87	0.6	NO	NO	0	0
5	SANDSTONE	41	30	24	31.7	0.59	0.73	0.5	NO	NO	0	0
6	SANDSTONE	41	31	21	31.0	0.51	0.76	0.4	NO	NO	0	0
7	SANDSTONE	41	36	27	34.7	0.66	0.88	0.5	NO	NO	0	0
8	SANDSTONE	36	21	11	22.7	0.31	0.58	0.8	NO	NO	0	1
9	SANDSTONE	39	22	17	26.0	0.44	0.56	0.6	**YES**	NO	0	0
10	SANDSTONE	35	27	16	26.0	0.46	0.77	0.6	NO	NO	0	0
11	SANDSTONE	45	35	22	34.0	0.49	0.78	0.5	NO	NO	0	0
12	SANDSTONE	42	37	22	33.7	0.52	0.88	0.6	NO	NO	0	0
13	SANDSTONE	34	26	19	26.3	0.56	0.76	0.7	NO	NO	0	0
14	SANDSTONE	42	24	8	24.7	0.19	0.57	0.5	**YES**	NO	0	1
15	ARGILLITE	37	35	25	32.3	0.68	0.95	0.5	NO	NO	0	0
16	SANDSTONE	36	30	8	24.7	0.22	0.83	0.5	NO	NO	0	1
17	SANDSTONE	92	50	40	60.7	0.43	0.54	0.4	NO	NO	0	0
18	SANDSTONE	35	22	12	23.0	0.34	0.63	0.7	NO	NO	0	1
19	SANDSTONE	52	43	27	40.7	0.52	0.83	0.6	NO	NO	0	0
20	SANDSTONE	50	35	33	39.3	0.66	0.70	0.4	NO	NO	0	0
21	SANDSTONE	63	62	44	56.3	0.70	0.98	0.5	NO	NO	0	0
22	SANDSTONE	75	62	55	64.0	0.73	0.83	0.4	NO	NO	0	0
23	SANDSTONE	35	24	14	24.3	0.40	0.69	0.7	NO	NO	0	1
24	ARGILLITE	36	25	11	24.0	0.31	0.69	0.7	NO	NO	0	1
25	SANDSTONE	31	24	19	24.7	0.61	0.77	0.5	NO	NO	0	0
26	SANDSTONE	37	34	12	27.7	0.32	0.92	0.5	NO	NO	0	1
27	SANDSTONE	26	22	17	21.7	0.65	0.85	0.4	NO	NO	0	0
28	SANDSTONE	36	20	14	23.3	0.39	0.56	0.5	**YES**	NO	0	1
29	SANDSTONE	39	25	15	26.3	0.38	0.64	0.6	NO	NO	0	1
30	SANDSTONE	30	22	15	22.3	0.50	0.73	0.6	NO	NO	0	0
31	SANDSTONE	29	19	13	20.3	0.45	0.66	0.6	NO	NO	0	0
32	SANDSTONE	24	19	14	19.0	0.58	0.79	0.5	NO	NO	0	0
33	SANDSTONE	17	15	9	13.7	0.53	0.88	0.5	NO	NO	0	0
34	SANDSTONE	48	35	21	34.7	0.44	0.73	0.7	NO	NO	0	0
35	SANDSTONE	45	38	29	37.3	0.64	0.84	0.4	**YES**	NO	0	0
36	SANDSTONE	48	19	13	26.7	0.27	0.40	0.7	NO	NO	0	1
37	SANDSTONE	41	28	15	28.0	0.37	0.68	0.4	**YES**	NO	0	1
38	SANDSTONE	35	26	13	24.7	0.37	0.74	0.7	NO	NO	0	1
39	SANDSTONE	29	19	13	20.3	0.45	0.66	0.6	NO	NO	0	0
40	SANDSTONE	45	22	16	27.7	0.36	0.49	0.4	NO	NO	0	1
41	SANDSTONE	27	17	12	18.7	0.44	0.63	0.7	NO	NO	0	0
42	SANDSTONE	35	24	20	26.3	0.57	0.69	0.4	NO	NO	0	0
43	SANDSTONE	23	19	8	16.7	0.35	0.83	0.7	NO	NO	0	1
44	ARGILLITE	26	14	8	16.0	0.31	0.54	0.4	NO	NO	0	1
45	SANDSTONE	31	21	19	23.7	0.61	0.68	0.4	NO	NO	0	0
46	SANDSTONE	22	20	12	18.0	0.55	0.91	0.4	NO	NO	0	0
47	SANDSTONE	31	23	11	21.7	0.35	0.74	0.3	NO	NO	0	1
48	SANDSTONE	32	19	15	22.0	0.47	0.59	0.7	NO	NO	0	0
49	SANDSTONE	35	26	14	25.0	0.40	0.74	0.5	NO	NO	0	1
50	ARGILLITE	30	19	13	20.7	0.43	0.63	0.6	NO	NO	0	0
AVERAGE		**38.6**	**27.4**	**18.3**	**28.1**	**0.47**	**0.72**	**0.55**	NA	NA	NA	NA
TOTAL		NA	NA	NA	NA	NA	NA	NA	**5**	**0**	**0**	**19**
%									**10**	**0**	**0**	**38**

SUMMARY STATISTICS

LITHOLOGY	NO.	%	STRIAE	%	FACETS	%
SANDSTONE	**46**	92.0	0	0.0	5	10.9
ARGILLITE	**4**	8.0	0	0.0	0	0.0
TOTAL	**50**		0		5	

ROUNDNESS	TOTAL CLASTS	%	FACETS	% FAC	STRIAE	% STRI
0.1	0	0	0	0	0.0	0.0
0.2	0	0	0	0	0	0.0
0.3	1	2	0	0	0	0.0
0.4	12	24	2	17	0	0.0
0.5	13	26	2	15	0	0
0.6	11	22	1	9	0	0
0.7	12	24	0	0	0	0
0.8	1	2	0	0	0	0
0.9	0	0	0	0	0	0
	50		5		0	

ROUNDNESS	SANDSTONE	% SST	ARGILLITE	% ARG
0.1	0	0	0	0
0.2	0	0	0	0
0.3	1	2	0	0
0.4	11	24	1	25
0.5	12	26	1	25
0.6	10	22	1	25
0.7	11	24	1	25
0.8	1	2	0	0
0.9	0	0	0	0
	46		4	

LOCATION , MURCHISON VALLEY, MT COOK
COLLECTION : MH 9, 50 CLASTS (6200 metres downstream from MH 1)

NO.	LITHOLOGY	AXIS LENGTH			AVR	AXIAL RATIOS		KRNESS	FACETS	STRIAE	RA	C40
		A	B	C		C/A	B/A					
1	SANDSTONE	56	41	35	44.0	0.63	0.73	0.3	NO	NO	0	0
2	SANDSTONE	42	34	21	32.3	0.50	0.81	0.5	NO	NO	0	0
3	SANDSTONE	52	36	24	37.3	0.46	0.69	0.6	NO	NO	0	0
4	SANDSTONE	40	36	24	33.3	0.60	0.90	0.4	NO	NO	0	0
5	SANDSTONE	48	46	32	42.0	0.67	0.96	0.7	NO	NO	0	0
6	SANDSTONE	45	37	24	35.3	0.53	0.82	0.4	YES	NO	0	0
7	SANDSTONE	47	32	22	33.7	0.47	0.68	0.7	NO	NO	0	0
8	SANDSTONE	45	30	25	33.3	0.56	0.67	0.7	NO	NO	0	0
9	SANDSTONE	44	29	23	32.0	0.52	0.66	0.7	NO	NO	0	0
10	SANDSTONE	36	35	27	32.7	0.75	0.97	0.7	NO	NO	0	0
11	SANDSTONE	42	24	20	28.7	0.48	0.57	0.6	NO	NO	0	0
12	SANDSTONE	34	27	17	26.0	0.50	0.79	0.7	NO	NO	0	0
13	SANDSTONE	52	38	24	38.0	0.46	0.73	0.5	NO	NO	0	0
14	SANDSTONE	30	23	7	20.0	0.23	0.77	0.8	NO	NO	0	1
15	SANDSTONE	45	30	24	33.0	0.53	0.67	0.5	NO	NO	0	0
16	SANDSTONE	37	17	15	23.0	0.41	0.46	0.5	NO	NO	0	0
17	SANDSTONE	54	36	29	39.7	0.54	0.67	0.6	NO	NO	0	0
18	SANDSTONE	49	30	22	33.7	0.45	0.61	0.8	NO	NO	0	0
19	SANDSTONE	59	29	20	36.0	0.34	0.49	0.5	YES	NO	0	1
20	SANDSTONE	40	20	18	26.0	0.45	0.50	0.5	YES	NO	0	0
21	SANDSTONE	30	25	15	23.3	0.50	0.83	0.7	NO	NO	0	0
22	SANDSTONE	40	30	19	29.7	0.48	0.75	0.4	NO	NO	0	0
23	SANDSTONE	31	30	17	26.0	0.55	0.97	0.4	NO	NO	0	0
24	SANDSTONE	46	22	20	29.3	0.43	0.48	0.5	NO	NO	0	0
25	SANDSTONE	55	39	22	38.7	0.40	0.71	0.5	NO	NO	0	1
26	SANDSTONE	44	25	20	29.7	0.45	0.57	0.5	NO	NO	0	0
27	SANDSTONE	52	42	26	40.0	0.50	0.81	0.5	NO	NO	0	0
28	SANDSTONE	35	29	22	28.7	0.63	0.83	0.6	NO	NO	0	0
29	SANDSTONE	44	30	21	31.7	0.48	0.68	0.6	NO	NO	0	0
30	SANDSTONE	40	38	17	31.7	0.43	0.95	0.4	NO	NO	0	0
31	SANDSTONE	39	22	11	24.0	0.28	0.56	0.5	NO	NO	0	1
32	SANDSTONE	42	36	27	35.0	0.64	0.86	0.5	NO	NO	0	0
33	SANDSTONE	40	21	15	25.3	0.38	0.53	0.5	NO	NO	0	1
34	SANDSTONE	44	31	26	33.7	0.59	0.70	0.5	NO	NO	0	0
35	SANDSTONE	44	31	18	31.0	0.41	0.70	0.6	NO	NO	0	0
36	SANDSTONE	37	25	20	27.3	0.54	0.68	0.5	NO	NO	0	0
37	SANDSTONE	49	32	29	36.7	0.59	0.65	0.6	NO	NO	0	0
38	SANDSTONE	36	30	17	27.7	0.47	0.83	0.6	NO	NO	0	0
39	SANDSTONE	38	32	19	29.7	0.50	0.84	0.5	NO	NO	0	0
40	SANDSTONE	38	30	19	29.0	0.50	0.79	0.6	NO	NO	0	0
41	SANDSTONE	45	32	14	30.3	0.31	0.71	0.7	NO	NO	0	1
42	SANDSTONE	55	36	26	39.0	0.47	0.65	0.5	NO	NO	0	0
43	SANDSTONE	40	26	22	29.3	0.55	0.65	0.6	NO	NO	0	0
44	SANDSTONE	34	25	21	26.7	0.62	0.74	0.7	NO	NO	0	0
45	SANDSTONE	35	27	22	28.0	0.63	0.77	0.7	NO	NO	0	0
46	SANDSTONE	37	22	15	24.7	0.41	0.59	0.7	NO	NO	0	0
47	SANDSTONE	30	20	18	22.7	0.60	0.67	0.6	NO	NO	0	0
48	SANDSTONE	30	16	12	19.3	0.40	0.53	0.6	NO	NO	0	1
49	SANDSTONE	39	22	19	26.7	0.49	0.56	0.6	NO	NO	0	0
50	SANDSTONE	45	29	16	30.0	0.36	0.64	0.4	NO	NO	0	1
AVERAGE		**42.2**	**29.7**	**20.8**	**30.9**	**0.49**	**0.71**	**0.57**	NA	NA	NA	NA
TOTAL		NA	NA	NA	NA	NA	NA	NA	**3**	**0**	**0**	**8**
%									**6**	**0**	**0**	**16**

SUMMARY STATISTICS

LITHOLOGY	NO.	%	STRIAE	%	FACETS	%
SANDSTONE	**50**	100.0	0	0.0	3	6.0
ARGILLITE	**0**	0.0	0	0.0	0	0.0
TOTAL	**50**		0		3	

ROUNDNESS	TOTAL CLASTS	%	FACETS	% FAC	STRIAE	% STRI
0.1	0	0	0	0	0	0
0.2	0	0	0	0	0	0
0.3	1	2	0	0	0	0
0.4	6	12	1	17	0	0
0.5	17	34	2	12	0	0
0.6	13	26	0	0	0	0
0.7	11	22	0	0	0	0
0.8	2	4	0	0	0	0
0.9	0	0	0	0	0	0
	50		3		0	

ROUNDNESS	SANDSTONE	% SST	ARGILLITE	% ARG
0.1	0	0	0	0
0.2	0	0	0	0
0.3	1	2	0	0
0.4	6	12	0	0
0.5	17	34	0	0
0.6	13	26	0	0
0.7	11	22	0	0
0.8	2	4	0	0
0.9	0	0	0	0
	50		0	

LOCATION , MURCHISON VALLEY, MT COOK
COLLECTION : MH 10, 50 CLASTS (11000 metres downstream from MH 1)

NO.	LITHOLOGY	AXIS LENGTH			AVR	AXIAL RATIOS		KRNESS	FACETS	STRIAE	RA	C40
		A	B	C		C/A	B/A					
1	SANDSTONE	37	20	15	24.0	0.41	0.54	0.6	NO	NO	0	0
2	SANDSTONE	37	32	27	32.0	0.73	0.86	0.7	NO	NO	0	0
3	SANDSTONE	39	35	27	33.7	0.69	0.90	0.7	NO	NO	0	0
4	SANDSTONE	48	27	24	33.0	0.50	0.56	0.6	NO	NO	0	0
5	SANDSTONE	30	27	20	25.7	0.67	0.90	0.7	NO	NO	0	0
6	SANDSTONE	63	40	24	42.3	0.38	0.63	0.7	NO	NO	0	1
7	SANDSTONE	42	36	25	34.3	0.60	0.86	0.6	YES	NO	0	0
8	SANDSTONE	65	45	38	49.3	0.58	0.69	0.7	NO	NO	0	0
9	SANDSTONE	35	25	22	27.3	0.63	0.71	0.7	NO	NO	0	0
10	SANDSTONE	48	36	15	33.0	0.31	0.75	0.6	NO	NO	0	1
11	SANDSTONE	32	26	24	27.3	0.75	0.81	0.5	NO	NO	0	0
12	SANDSTONE	44	41	20	35.0	0.45	0.93	0.7	NO	NO	0	0
13	SANDSTONE	33	19	13	21.7	0.39	0.58	0.6	YES	NO	0	1
14	SANDSTONE	30	19	12	20.3	0.40	0.63	0.5	NO	NO	0	1
15	SANDSTONE	43	25	18	28.7	0.42	0.58	0.7	NO	NO	0	0
16	SANDSTONE	46	39	21	35.3	0.46	0.85	0.5	NO	NO	0	0
17	SANDSTONE	34	31	17	27.3	0.50	0.91	0.5	NO	NO	0	0
18	SANDSTONE	43	20	16	26.3	0.37	0.47	0.4	NO	NO	0	1
19	SANDSTONE	45	43	27	38.3	0.60	0.96	0.6	NO	NO	0	0
20	SANDSTONE	52	44	29	41.7	0.56	0.85	0.4	NO	NO	0	0
21	SANDSTONE	40	29	23	30.7	0.58	0.73	0.4	NO	NO	0	0
22	SANDSTONE	37	27	14	26.0	0.38	0.73	0.7	NO	NO	0	1
23	SANDSTONE	49	34	20	34.3	0.41	0.69	0.5	NO	NO	0	0
24	SANDSTONE	25	22	19	22.0	0.76	0.88	0.5	NO	NO	0	0
25	SANDSTONE	35	26	14	25.0	0.40	0.74	0.5	NO	NO	0	1
26	SANDSTONE	42	32	22	32.0	0.52	0.76	0.8	NO	NO	0	0
27	SANDSTONE	38	26	22	28.7	0.58	0.68	0.5	NO	NO	0	0
28	SANDSTONE	24	18	14	18.7	0.58	0.75	0.7	NO	NO	0	0
29	SANDSTONE	36	25	17	26.0	0.47	0.69	0.6	YES	NO	0	0
30	SANDSTONE	40	26	15	27.0	0.38	0.65	0.6	NO	NO	0	1
31	SANDSTONE	37	22	18	25.7	0.49	0.59	0.5	NO	NO	0	0
32	SANDSTONE	37	27	15	26.3	0.41	0.73	0.6	YES	NO	0	0
33	SANDSTONE	38	23	15	25.3	0.39	0.61	0.5	NO	NO	0	1
34	SANDSTONE	27	24	20	23.7	0.74	0.89	0.6	NO	NO	0	0
35	SANDSTONE	42	24	16	27.3	0.38	0.57	0.6	NO	NO	0	1
36	SANDSTONE	46	40	20	35.3	0.43	0.87	0.6	NO	NO	0	0
37	SANDSTONE	38	23	13	24.7	0.34	0.61	0.6	NO	NO	0	1
38	SANDSTONE	42	39	19	33.3	0.45	0.93	0.6	NO	NO	0	0
39	SANDSTONE	34	19	14	22.3	0.41	0.56	0.4	NO	NO	0	0
40	SANDSTONE	33	25	16	24.7	0.48	0.76	0.7	NO	NO	0	0
41	SANDSTONE	40	30	24	31.3	0.60	0.75	0.6	NO	NO	0	0
42	SANDSTONE	50	23	15	29.3	0.30	0.46	0.5	NO	NO	0	1
43	SANDSTONE	31	16	12	19.7	0.39	0.52	0.5	NO	NO	0	1
44	SANDSTONE	35	30	20	28.3	0.57	0.86	0.5	NO	NO	0	0
45	SANDSTONE	21	20	8	16.3	0.38	0.95	0.6	NO	NO	0	1
46	SANDSTONE	40	22	19	27.0	0.48	0.55	0.6	NO	NO	0	0
47	SANDSTONE	34	16	10	20.0	0.29	0.47	0.7	NO	NO	0	1
48	SANDSTONE	30	26	15	23.7	0.50	0.87	0.5	NO	NO	0	0
49	SANDSTONE	51	37	27	38.3	0.53	0.73	0.6	NO	NO	0	0
50	SANDSTONE	37	20	17	24.7	0.46	0.54	0.4	NO	NO	0	0
AVERAGE		**39.1**	**28.0**	**18.9**	**28.7**	**0.49**	**0.72**	**0.58**	NA	NA	NA	NA
TOTAL		NA	NA	NA	NA	NA	NA	NA	**4**	**0**	**0**	**15**
%									**8**	**0**	**0**	**30**

SUMMARY STATISTICS

LITHOLOGY	NO.	%	STRIAE	%	FACETS	%
SANDSTONE	**50**	100.0	0	0.0	4	8.0
ARGILLITE	**0**	0.0	0	0.0	0	0.0
TOTAL	**50**		0		4	

ROUNDNESS	TOTAL CLASTS	%	FACETS	% FAC	STRIAE	% STRI
0.1	0	0	0	0	0	0.0
0.2	0	0	0	0	0	0.0
0.3	0	0	0	0	0	0.0
0.4	5	10	0	0	0	0.0
0.5	14	28	0	0	0	0.0
0.6	18	36	4	22	0	0.0
0.7	12	24	0	0	0	0.0
0.8	1	2	0	0	0	0.0
0.9	0	0	0	0	0	0.0
	50		4		0	

ROUNDNESS	SANDSTONE	% SST	ARGILLITE	% ARG
0.1	0	0	0	0
0.2	0	0	0	0
0.3	0	0	0	0
0.4	5	0	0	0
0.5	14	0	0	0
0.6	18	0	0	0
0.7	12	0	0	0
0.8	1	0	0	0
0.9	0	0	0	0
	50		0	0

LOCATION: LAKE PUKAKI MORAINE, NEW ZEALAND

COLLECTION : 100 CLASTS FROM TILL

NO.	LITHOLOGY	AXIS LENGTH			AVERAGE	AXIAL RATIOS		KRUMBEIN ROUNDNESS	FACETS	STRIAE	RA	C40
		A	B	C		C/A	B/A					
1	ARGILLITE	2.4	2.1	0.8	1.77	0.33	0.88	0.2	YES	YES	1	1
2	SANDSTONE	2.7	1.5	1.4	1.87	0.52	0.56	0.2	YES	NO	1	0
3	SANDSTONE	5.1	3.1	1.7	3.30	0.33	0.61	0.2	NO	NO	1	1
4	SANDSTONE	5.6	3.4	2.6	3.87	0.46	0.61	0.2	NO	NO	1	0
5	SANDSTONE	4.1	2.6	1.6	2.77	0.39	0.63	0.2	NO	NO	1	1
6	ARGILLITE	2.6	1.1	1	1.57	0.38	0.42	0.2	YES	YES	1	1
7	ARGILLITE	2.7	2.1	0.6	1.80	0.22	0.78	0.2	YES	YES	1	1
8	SANDSTONE	1.8	1.5	1.2	1.50	0.67	0.83	0.2	NO	NO	1	0
9	SANDSTONE	2.4	1.1	1	1.50	0.42	0.46	0.2	YES	NO	1	0
10	SANDSTONE	1.6	1.5	1.4	1.50	0.88	0.94	0.2	NO	NO	1	0
11	SANDSTONE	3.5	2.5	1.5	2.50	0.43	0.71	0.2	NO	NO	1	0
12	ARGILLITE	3.6	3.1	1	2.57	0.28	0.86	0.2	YES	YES	1	1
13	SANDSTONE	3.9	2	1.1	2.33	0.28	0.51	0.2	NO	YES	1	1
14	ARGILLITE	3.1	2.1	0.5	1.90	0.16	0.68	0.3	YES	YES	0	1
15	SANDSTONE	2.9	1.7	1.3	1.97	0.45	0.59	0.3	NO	NO	0	0
16	SANDSTONE	4.5	2.5	2	3.00	0.44	0.56	0.3	NO	NO	0	0
17	SANDSTONE	3.6	2.7	1.1	2.47	0.31	0.75	0.3	NO	NO	0	1
18	SANDSTONE	5	3	2.1	3.37	0.42	0.60	0.3	YES	NO	0	0
19	SANDSTONE	8	6	3.5	5.83	0.44	0.75	0.3	YES	YES	0	0
20	SANDSTONE	2.2	1.6	1	1.60	0.45	0.73	0.3	NO	NO	0	0
21	ARGILLITE	3	2.9	1.2	2.37	0.40	0.97	0.3	YES	YES	0	1
22	SANDSTONE	3.5	2.5	2.1	2.70	0.60	0.71	0.3	YES	YES	0	0
23	ARGILLITE	5.5	3	1.1	3.20	0.20	0.55	0.3	YES	YES	0	1
24	SANDSTONE	4	3.2	1.9	3.03	0.48	0.80	0.3	NO	NO	0	0
25	ARGILLITE	2.8	1.5	0.6	1.63	0.21	0.54	0.3	YES	YES	0	1
26	ARGILLITE	4.1	2.9	2.1	3.03	0.51	0.71	0.3	YES	YES	0	0
27	SANDSTONE	4	3.1	2	3.03	0.50	0.78	0.3	NO	NO	0	0
28	ARGILLITE	3.5	3.1	0.7	2.43	0.20	0.89	0.3	YES	YES	0	1
29	SANDSTONE	3.7	3	1.8	2.83	0.49	0.81	0.3	NO	NO	0	0
30	SANDSTONE	5	4.2	1.5	3.57	0.30	0.84	0.3	YES	YES	0	1
31	SANDSTONE	2.9	2.6	1.1	2.20	0.38	0.90	0.3	NO	NO	0	1
32	SANDSTONE	3.9	2	1.6	2.50	0.41	0.51	0.3	NO	NO	0	0
33	SANDSTONE	5.2	2.6	2	3.27	0.38	0.50	0.3	YES	NO	0	1
34	SANDSTONE	2.5	1.6	1.2	1.77	0.48	0.64	0.3	NO	NO	0	0
35	SANDSTONE	2.1	1.6	1	1.57	0.48	0.76	0.3	NO	NO	0	0
36	SANDSTONE	2	1.6	1	1.53	0.50	0.80	0.3	NO	NO	0	0
37	SANDSTONE	2.6	2.1	1.1	1.93	0.42	0.81	0.3	YES	NO	0	0
38	SANDSTONE	2.5	1.6	1.3	1.80	0.52	0.64	0.3	NO	NO	0	0
39	SANDSTONE	4.5	3	1.7	3.07	0.38	0.67	0.3	YES	NO	0	1
40	SANDSTONE	3.8	2.2	1.5	2.50	0.39	0.58	0.3	YES	YES	0	1
41	SANDSTONE	3.9	3	2	2.97	0.51	0.77	0.4	YES	NO	0	0
42	SANDSTONE	3.8	3	2	2.93	0.53	0.79	0.4	NO	NO	0	0
43	SANDSTONE	2.7	1.5	1	1.73	0.37	0.56	0.4	NO	NO	0	1
44	SANDSTONE	2.6	1.6	1.1	1.77	0.42	0.62	0.4	NO	NO	0	0
45	SANDSTONE	3	2.3	1.1	2.13	0.37	0.77	0.3	NO	NO	0	1
46	SANDSTONE	3.6	2.8	2.5	2.97	0.69	0.78	0.4	YES	NO	0	0
47	ARGILLITE	2.9	2	0.9	1.93	0.31	0.69	0.4	NO	NO	0	1
48	SANDSTONE	4.5	3.2	2.4	3.37	0.53	0.71	0.4	NO	NO	0	0
49	ARGILLITE	2.5	1.9	0.9	1.77	0.36	0.76	0.4	YES	YES	0	1
50	SANDSTONE	4.6	3	1.9	3.17	0.41	0.65	0.4	NO	NO	0	0
51	SANDSTONE	2.6	1.5	1.1	1.73	0.42	0.58	0.4	YES	NO	0	0
52	SANDSTONE	2.2	1.7	1.5	1.80	0.68	0.77	0.4	NO	NO	0	0
53	SANDSTONE	3.8	3	1.5	2.77	0.39	0.79	0.4	NO	YES	0	1
54	ARGILLITE	7	5	1.9	4.63	0.27	0.71	0.4	YES	YES	0	1
55	SANDSTONE	9.5	8.5	2.4	6.80	0.25	0.89	0.5	YES	YES	0	1
56	SANDSTONE	3.5	1.9	1.4	2.27	0.40	0.54	0.5	YES	NO	0	1
57	SANDSTONE	2.6	2	1	1.87	0.38	0.77	0.5	NO	NO	0	1
58	SANDSTONE	5.5	3	2.6	3.70	0.47	0.55	0.5	NO	YES	0	0
59	SANDSTONE	2.5	1.7	1.4	1.87	0.56	0.68	0.5	YES	NO	0	0
60	SANDSTONE	3.5	2.1	1.6	2.40	0.46	0.60	0.5	NO	NO	0	0
61	SANDSTONE	4.1	3	2.5	3.20	0.61	0.73	0.5	YES	NO	0	0
62	ARGILLITE	4	2.2	1.6	2.60	0.40	0.55	0.5	YES	YES	0	1
63	SANDSTONE	2	1.7	1	1.57	0.50	0.85	0.5	NO	NO	0	0
64	SANDSTONE	4.1	2.5	2.1	2.90	0.51	0.61	0.5	YES	YES	0	0
65	SANDSTONE	4.5	3.5	2	3.33	0.44	0.78	0.5	YES	YES	0	0
66	SANDSTONE	2.1	2	1.1	1.73	0.52	0.95	0.5	YES	NO	0	0
67	SANDSTONE	2.1	1.5	1	1.53	0.48	0.71	0.5	NO	NO	0	0
68	SANDSTONE	2.5	1.5	1	1.67	0.40	0.60	0.5	NO	NO	0	1
69	SANDSTONE	11	9.5	7	9.17	0.64	0.86	0.5	NO	YES	0	0
70	SANDSTONE	7	5.3	5.2	5.83	0.74	0.76	0.6	NO	NO	0	0
71	SANDSTONE	11.6	6.3	5.5	7.80	0.47	0.54	0.6	NO	YES	0	0
72	SANDSTONE	7.1	6	4	5.70	0.56	0.85	0.6	NO	NO	0	0
73	SANDSTONE	4.5	3.2	2	3.23	0.44	0.71	0.6	YES	YES	0	0
74	SANDSTONE	2.1	2	1	1.70	0.48	0.95	0.6	NO	NO	0	0
75	SANDSTONE	3.9	2.7	2	2.87	0.51	0.69	0.6	NO	NO	0	0
76	SANDSTONE	4	2.5	2	2.83	0.50	0.63	0.6	YES	NO	0	0
77	SANDSTONE	3.9	3	1.7	2.87	0.44	0.77	0.6	NO	NO	0	0
78	ARGILLITE	4.2	2.9	1.7	2.93	0.40	0.69	0.6	YES	YES	0	0
79	ARGILLITE	2.6	2	0.8	1.80	0.31	0.77	0.6	YES	YES	0	1
80	SANDSTONE	5.3	4	2.9	4.07	0.55	0.75	0.6	NO	NO	0	0
81	SANDSTONE	4	3.5	1.6	3.03	0.40	0.88	0.6	YES	YES	0	1
82	SANDSTONE	2.9	2.1	1.6	2.20	0.55	0.72	0.6	NO	YES	0	0
83	ARGILLITE	3.4	1.8	1.7	2.30	0.50	0.53	0.6	NO	YES	0	0
84	SANDSTONE	2.4	1.6	1.5	1.83	0.63	0.67	0.6	NO	NO	0	0
85	SANDSTONE	4.9	2.9	2.1	3.30	0.43	0.59	0.6	NO	NO	0	0
86	SANDSTONE	3	2.5	1.8	2.43	0.60	0.83	0.6	NO	NO	0	0
87	SANDSTONE	2.1	2	1.1	1.73	0.52	0.95	0.6	NO	NO	0	0
88	SANDSTONE	4.2	3.3	1.4	2.97	0.33	0.79	0.6	YES	NO	0	1
89	SANDSTONE	2.6	2.1	1.4	2.03	0.54	0.81	0.6	NO	NO	0	0
90	SANDSTONE	4.3	3.5	2.5	3.43	0.58	0.81	0.6	NO	NO	0	0
91	ARGILLITE	4	2.5	1.5	2.67	0.38	0.63	0.6	YES	YES	0	1
92	SANDSTONE	5	4.5	2.6	4.03	0.52	0.90	0.6	YES	YES	0	0
93	SANDSTONE	2.8	2	1.8	2.20	0.64	0.71	0.6	NO	NO	0	0
94	SANDSTONE	2.4	2	1.5	1.97	0.63	0.83	0.6	NO	NO	0	0
95	SANDSTONE	3.8	2.7	1.7	2.73	0.45	0.71	0.6	NO	NO	0	0
96	SANDSTONE	2.5	1.8	1.5	1.93	0.60	0.72	0.6	NO	NO	0	0
97	SANDSTONE	3.1	1.7	1.5	2.10	0.48	0.55	0.6	NO	NO	0	0
98	SANDSTONE	1.9	1.8	0.9	1.53	0.47	0.95	0.7	NO	NO	0	0
99	SANDSTONE	2.5	2.1	1.5	2.03	0.60	0.84	0.7	NO	NO	0	0
100	SANDSTONE	2.9	2.7	1.1	2.23	0.38	0.93	0.7	NO	NO	0	1
AVERAGE		**3.8**	**2.7**	**1.7**	**2.7**	**0.45**	**0.72**	NA	NA	NA	NA	NA
TOTAL		NA	NA	NA	NA	NA	NA	**0.43**	**40**	**33**	**13**	**34**

SUMMARY STATISTICS

LITHOLOGY	NO. CLASTS	STRIAE	% STRI	FACETS	% FAC
SANDSTONE	**82**	16	19.5	25	30.5
ARGILLITE	**18**	17	94.4	16	88.9
TOTAL	**100**	33		41	

ROUNDNESS	TOTAL CLAST	FACETS	% FAC	STRIAE	% STRI	SANDSTONE	% SST	ARGILLITE	% ARG
0.1	0	0	0	0	0.0	0	0.0	0	0.0
0.2	13	6	46.2	5	38.5	9	11.0	4	22.2
0.3	28	14	50.0	10	35.7	22	26.8	6	33.3
0.4	13	5	38.5	3	23.1	10	12.2	3	16.7
0.5	15	8	53.3	6	40.0	14	17.1	1	5.6
0.6	28	8	0.0	9	32.1	24	29.3	4	22.2
0.7	3	0	0	0	0.0	3	3.7	0	0.0
0.8	0	0	0	0	0.0	0	0.0	0	0.0
0.9	0	0	0	0	0.0	0	0.0	0	0.0

LOCATION, LAKE PUKAKI MORAINE, NEW ZEALAND
COLLECTION : SELECTED STRIATED CLAST 1

LITHOLOGY:	FINE SANDSTONE
LENGTH OF LONG (A) AXIS:	125 mm
LENGTH OF INTERMEDIATE (B) AXIS:	50 mm
B/A AXIAL RATIO:	0.40
KRUMBEIN ROUNDNESS:	0.6

SQUARE No.	STRIAE DENSITY	
	STRIAE PER SQ	BACKGROUND STRIAE
1	0	YES
2	2	YES
3	2	YES
4	1	YES
5	1	YES
6	2	YES
7	2	YES
8	2	YES
9	2	YES
10	0	YES
11	0	YES
12	0	YES
13	0	YES
14	0	YES
15	0	YES
16	0	YES
17	0	YES
18	0	YES
19	2	YES
20	1	YES
21	0	YES
22	1	YES
23	2	YES
24	3	YES
25	4	YES
26	3	YES
27	2	YES
28	1	YES
29	0	YES
30	1	YES
31	2	YES
32	2	YES
33	3	YES
34	2	YES
35	1	YES
36	1	YES
37	2	YES
38	2	YES
39	3	YES
40	1	YES
41	1	YES
42	1	YES
43	1	YES
44	3	YES
45	3	YES
46	3	YES
47	1	YES
48	0	YES
49	2	YES
50	0	YES
51	1	YES
52	2	YES
53	3	YES
54	2	YES
55	2	YES
56	3	YES
57	2	YES
58	1	YES
59	1	YES
60	2	YES
61	2	YES
62	0	YES
63	0	YES
64	0	YES
65	0	YES
66	1	YES
67	1	YES
68	1	YES
69	2	YES
70	1	YES
71	3	YES
72	1	YES
73	1	YES
74	2	YES
75	1	YES
76	1	YES
77	1	YES
78	3	YES
79	2	YES
80	4	YES
81	3	YES
82	0	YES
83	2	YES
84	3	YES
85	0	YES
86	1	YES
87	0	YES
88	0	YES
89	1	YES
90	1	YES
91	0	YES
92	0	YES
93	1	YES
94	3	YES
95	1	YES
96	1	YES
97	2	YES
98	0	YES
99	2	YES
100	0	YES
%		**100**
MIN	**0**	
AVERAGE	**1.4**	
MAX	**4**	
% ≥ 1 STRIAE	**74**	

STRIAE No.	ORIENTATION FROM A-AXIS	CURVED STRIAE	LENGTH (MM)	WIDTH (MM)	WIDTH/ LENGTH RATIO	COMPOUND STRIATION
1	188	NO	3.5	1	0.29	NO
2	135	NO	4.5	0.5	0.11	NO
3	162	NO	6	0.75	0.13	NO
4	180	NO	7	0.25	0.04	NO
5	180	NO	10	1.5	0.15	NO
6	204	NO	15	1	0.07	NO
7	180	NO	23.5	0.5	0.02	NO
8	150	NO	4.5	0.25	0.06	NO
9	187	NO	15	1	0.07	NO
10	180	NO	7	0.25	0.04	NO
11	180	NO	4.5	0.25	0.06	NO
12	140	NO	7.5	0.25	0.03	NO
13	161	NO	2.5	0.25	0.10	NO
14	205	NO	4.5	0.25	0.06	NO
15	210	NO	10	1	0.10	NO
16	230	NO	5.5	0.25	0.05	NO
17	250	NO	3	0.5	0.17	NO
18	180	NO	1	0.25	0.25	NO
19	180	NO	11	0.5	0.05	NO
20	180	NO	6	0.5	0.08	NO
21	160	NO	5	0.5	0.10	NO
22	200	NO	25.5	0.25	0.01	NO
23	185	NO	22.5	1	0.04	NO
24	185	NO	9	1	0.11	NO
25	172	NO	5	0.5	0.10	NO
26	180	NO	3	0.25	0.08	NO
27	199	NO	6	0.25	0.04	NO
28	180	NO	5.5	0.25	0.05	NO
29	147	NO	5	0.25	0.05	NO
30	157	NO	2	0.25	0.13	NO
31	210	NO	3.5	0.5	0.14	NO
32	152	NO	4	0.5	0.13	NO
33	194	NO	8.5	0.25	0.03	NO
34	180	NO	13.5	0.5	0.04	NO
35	203	NO	4.5	0.25	0.06	NO
36	160	NO	5	0.25	0.05	NO
37	200	NO	6.5	0.25	0.04	NO
38	152	NO	2.5	0.25	0.10	NO
39	180	NO	3	0.25	0.08	NO
40	130	NO	4	0.5	0.13	NO
41	156	NO	4.5	0.25	0.06	NO
42	180	NO	5	0.25	0.05	NO
43	215	NO	4.5	0.5	0.11	NO
44	180	NO	9	0.25	0.03	NO
45	212	NO	5.5	0.5	0.09	NO
46	180	NO	5	0.5	0.10	NO
47	152	NO	6	0.25	0.04	NO
48	180	NO	4	0.25	0.06	NO
49	200	NO	3	0.5	0.17	NO
50	180	NO	3.5	0.25	0.07	NO
TOTAL		**0**				**0**
MIN	**130.0**		**1.0**	**0.25**	**0.01**	
AVERAGE	**180.5**		**6.9**	**0.45**	**0.08**	
MAX	**250.0**		**25.5**	**1.50**	**0.29**	
RANGE	**70.0**		**24.5**	**1.25**	**0.28**	
S.DEV	**24.0**		**5.3**	**0.29**	**0.05**	

TOTAL MEASURED AREA:	**25 sq cm**
TOTAL STRIAE FOR MEASURED AREA:	**64**
AVERAGE STRIAE PER SQ CM:	**2.6**

STRIAE ORIENTATION HALF ROSE DIAGRAM

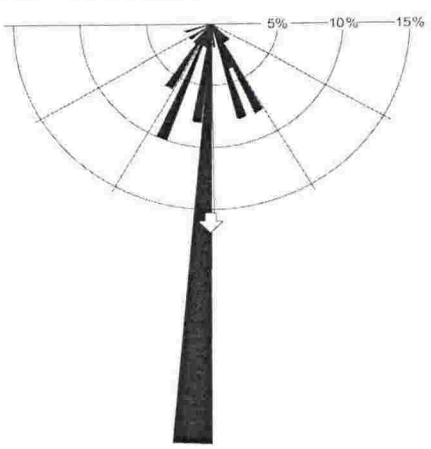

LOCATION, LAKE PUKAKI MORAINE, NEW ZEALAND
COLLECTION : SELECTED STRIATED CLAST 2

LITHOLOGY:	ARGILLITE
LENGTH OF LONG (A) AXIS:	46 mm
LENGTH OF INTERMEDIATE (B) AXIS:	45 mm
B/A AXIAL RATIO:	0.98
KRUMBEIN ROUNDNESS:	0.6

SQUARE No.	STRIAE DENSITY	
	STRIAE PER SQ	BACKGROUND STRIAE
1	1	YES
2	4	YES
3	1	YES
4	1	YES
5	2	YES
6	2	YES
7	2	YES
8	3	YES
9	2	YES
10	1	YES
11	2	YES
12	2	YES
13	3	YES
14	5	YES
15	2	YES
16	3	YES
17	2	YES
18	2	YES
19	2	YES
20	2	YES
21	5	YES
22	2	YES
23	3	YES
24	1	YES
25	2	YES
26	2	YES
27	2	YES
28	1	YES
29	0	YES
30	2	YES
31	2	YES
32	4	YES
33	0	YES
34	3	YES
35	3	YES
36	1	YES
37	0	YES
38	2	YES
39	2	YES
40	2	YES
41	2	YES
42	1	YES
43	1	YES
44	1	YES
45	1	YES
46	1	YES
47	4	YES
48	3	YES
49	3	YES
50	1	YES
TOTAL		50
MIN	0	100%
AVERAGE	2.0	
MAX	5	
% ≥ 1 STRIAE	94	

STRIAE No.	ORIENTATION FROM A-AXIS	CURVED STRIAE	LENGTH (MM)	WIDTH (MM)	WIDTH/ LENGTH RATIO	COMPOUND STRIATION
1	236	NO	2.5	0.25	0.10	NO
2	110	NO	2.5	0.25	0.10	NO
3	210	NO	3	0.25	0.08	NO
4	247	NO	2.5	0.25	0.10	NO
5	244	NO	3.5	0.25	0.07	NO
6	245	NO	2.5	0.25	0.10	NO
7	135	NO	3	0.25	0.08	NO
8		YES(> 5°)	3	0.25	0.08	NO
9	255	NO	1.5	0.25	0.17	NO
10	130	NO	3	0.75	0.25	NO
11	180	NO	4.5	0.25	0.06	NO
12	158	YES	5.5	0.5	0.09	NO
13	215	NO	2	0.25	0.13	NO
14	217	NO	5	0.75	0.15	NO
15	129	NO	5	0.75	0.15	NO
16	234	NO	6	0.5	0.08	NO
17	156	NO	5	0.25	0.05	NO
18	239	NO	5	0.5	0.10	NO
19		YES(> 5°)	8.5	0.25	0.03	NO
20	269	NO	3.5	0.5	0.14	NO
21	197	NO	15	1	0.07	NO
22	168	NO	13.5	0.25	0.02	NO
23	132	NO	2	0.5	0.25	NO
24	153	NO	5.5	0.25	0.05	NO
25	129	NO	3.5	0.25	0.07	NO
26	250	NO	13	0.25	0.02	NO
27	98	NO	3	0.25	0.08	NO
28	211	NO	8.5	0.25	0.03	NO
29	223	NO	4.5	0.5	0.11	NO
30	216	NO	5.5	0.75	0.14	NO
31	239	NO	9	1	0.11	NO
32	150	NO	2	0.25	0.13	NO
33	250	NO	2	0.25	0.13	NO
34	251	NO	4	0.25	0.06	NO
35	165	NO	4.5	0.5	0.11	NO
36	173	NO	3.5	0.25	0.07	NO
37	238	NO	5.5	0.5	0.09	NO
38	251	NO	5	0.5	0.10	NO
39	166	NO	2.5	0.25	0.10	NO
40	196	NO	2.5	0.5	0.20	NO
41	183	NO	6.5	0.5	0.08	NO
42	209	NO	3	0.25	0.08	NO
43	151	NO	5	0.25	0.05	NO
44	148	NO	3	0.5	0.17	NO
45	232	NO	3	0.25	0.08	NO
46	241	NO	3	0.5	0.17	NO
47	178	NO	2	0.25	0.13	NO
48	126	NO	3	0.25	0.08	NO
49	116	NO	2	0.25	0.13	NO
50	130	NO	3	0.25	0.08	NO
TOTAL		1				0
MIN	98.0		1.5	0.25	0.02	
AVERAGE	191.2		4.5	0.39	0.10	
MAX	269.0		15.0	1.00	0.25	
RANGE	89.0		13.5	0.75	0.23	
S.DEV	48.4		3.0	0.20	0.05	

TOTAL MEASURED AREA:	12.5 sq cm
TOTAL STRIAE FOR MEASURED AREA:	50
AVERAGE STRIAE PER SQ CM:	4

STRIAE ORIENTATION HALF ROSE DIAGRAM

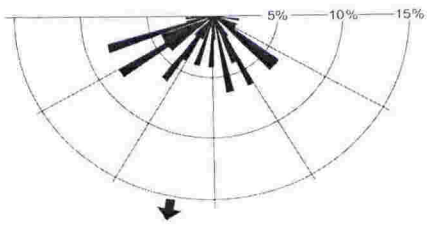

LOCATION, LAKE PUKAKI MORAINE, NEW ZEALAND
COLLECTION : SELECTED STRIATED CLAST 3

LITHOLOGY:	FINE SANDSTONE
LENGTH OF LONG (A) AXIS:	196 mm
LENGTH OF INTERMEDIATE (B) AXIS:	80 mm
B/A AXIAL RATIO:	0.41
KRUMBEIN ROUNDNESS:	0.3

SQUARE No.	STRIAE DENSITY	
	STRIAE PER SQ	BACKGROUND STRIAE
1	3	YES
2	2	YES
3	2	YES
4	1	YES
5	2	YES
6	2	YES
7	1	YES
8	1	YES
9	0	YES
10	2	YES
11	3	YES
12	3	YES
13	0	YES
14	2	YES
15	3	YES
16	3	YES
17	0	YES
18	1	YES
19	3	YES
20	2	YES
21	2	YES
22	3	YES
23	2	YES
24	2	YES
25	0	YES
26	1	YES
27	2	YES
28	2	YES
29	1	YES
30	1	YES
31	1	YES
32	2	YES
33	2	YES
34	1	YES
35	2	YES
36	1	YES
37	0	YES
38	3	YES
39	2	YES
40	1	YES
41	1	YES
42	1	YES
43	2	YES
44	1	YES
45	1	YES
46	1	YES
47	1	YES
48	2	YES
49	1	YES
50	1	YES
51	2	YES
52	1	YES
53	2	YES
54	1	YES
55	1	YES
56	1	YES
57	3	YES
58	2	YES
59	2	YES
60	1	YES
61	0	YES
62	0	YES
63	0	YES
64	2	YES
65	2	YES
66	2	YES
67	3	YES
68	2	YES
69	3	YES
70	4	YES
71	3	YES
72	3	YES
73	2	YES
74	1	YES
75	0	YES
76	0	YES
77	1	YES
78	2	YES
79	3	YES
80	3	YES
81	4	YES
82	2	YES
83	1	YES
84	3	YES
85	2	YES
86	2	YES
87	0	YES
88	0	YES
89	1	YES
90	1	YES
91	4	YES
92	1	YES
93	2	YES
94	3	YES
95	2	YES
96	2	YES
97	1	YES
98	3	YES
99	1	YES
100	1	YES
TOTAL		**100**
MIN	**0**	
AVERAGE	**1.7**	
MAX	**4**	
% ≥ 1 STRIAE	**89**	

STRIAE No.	ORIENTATION FROM A-AXIS	CURVED STRIAE	LENGTH (MM)	WIDTH (MM)	WIDTH/ LENGTH RATIO	COMPOUND STRIATION
1	187	NO	7.5	0.25	0.03	NO
2	186	NO	17	0.25	0.01	NO
3	163	NO	4.5	1	0.22	NO
4	170	NO	20	0.75	0.04	NO
5	126	NO	11.5	0.75	0.07	NO
6	173	NO	15	2	0.13	NO
7		YES(> 5°)	12.5	0.5	0.04	NO
8	151	NO	4.5	0.25	0.06	NO
9	180	NO	10	2.5	0.25	NO
10	179	NO	30	0.25	0.01	NO
11	156	NO	20	1	0.05	NO
12	145	NO	13.5	1	0.07	NO
13	167	NO	5	0.75	0.15	NO
14	168	NO	25.5	2	0.08	NO
15	165	NO	30	1	0.03	NO
16	143	NO	3	0.25	0.08	NO
17	216	NO	5	1	0.20	NO
18	191	NO	17	1.5	0.09	NO
19	171	NO	5	0.5	0.10	NO
20	151	NO	8.5	1	0.12	NO
21	141	NO	8	1	0.13	NO
22	175	NO	7.5	0.25	0.03	NO
23	188	NO	65	1	0.02	NO
24	183	YES	53.5	1	0.02	NO
25	143	NO	2.5	1	0.40	NO
26	179	NO	16	0.5	0.03	NO
27	178	NO	13	0.25	0.02	NO
28	186	NO	9.5	0.25	0.03	NO
29	180	NO	13.5	0.25	0.02	NO
30	171	NO	21	0.5	0.02	NO
31	167	NO	11	1.75	0.16	NO
32	223	NO	15	0.75	0.05	NO
33	167	NO	40	2.25	0.06	NO
34	170	NO	15.5	1	0.06	NO
35	141	NO	4.5	0.25	0.06	NO
36	168	NO	5.5	1	0.18	NO
37	182	NO	12	0.25	0.02	NO
38	151	NO	6	0.25	0.04	NO
39	196	NO	10.5	2	0.19	NO
40	151	NO	3	0.5	0.17	NO
41	165	NO	6	0.25	0.04	NO
42	209	NO	8.5	0.25	0.03	NO
43	202	NO	5.5	0.25	0.05	NO
44	172	NO	3	0.25	0.08	NO
45	188	NO	6.5	0.25	0.04	NO
46	167	NO	12	0.25	0.02	NO
47	180	NO	7	0.25	0.04	NO
48	188	NO	9	0.25	0.03	NO
49	190	NO	3.5	0.25	0.07	NO
50	143	NO	3.5	0.25	0.07	NO
TOTAL		**1**				**0**
MIN	**126.0**		**2.5**	**0.25**	**0.01**	
AVERAGE	**172.1**		**13.2**	**0.74**	**0.08**	
MAX	**223.0**		**65.0**	**2.50**	**0.40**	
RANGE	**54.0**		**62.5**	**2.25**	**0.39**	
S.DEV	**20.2**		**12.4**	**0.61**	**0.08**	

TOTAL MEASURED AREA:	**25 sq cm**
TOTAL STRIAE FOR MEASURED AREA:	**52**
AVERAGE STRIAE PER SQ CM:	**2.1**

STRIAE ORIENTATION HALF ROSE DIAGRAM

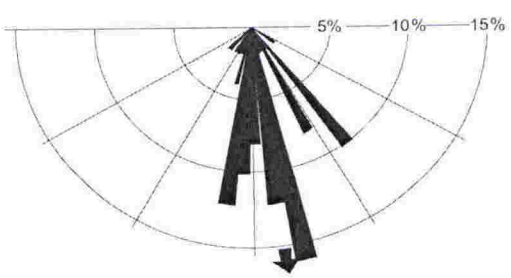

LOCATION, LAKE PUKAKI MORAINE, NEW ZEALAND
COLLECTION : SELECTED STRIATED CLAST 4

LITHOLOGY:	ARGILLITE
LENGTH OF LONG (A) AXIS:	165 mm
LENGTH OF INTERMEDIATE (B) AXIS:	104 mm
B/A AXIAL RATIO:	0.63
KRUMBEIN ROUNDNESS:	0.5

SQUARE No.	STRIAE DENSITY	
	STRIAE PER SQ	BACKGROUND STRIAE
1	2	YES
2	1	YES
3	1	YES
4	2	YES
5	3	YES
6	3	YES
7	4	YES
8	2	YES
9	3	YES
10	3	YES
11	4	YES
12	6	YES
13	1	YES
14	1	YES
15	0	YES
16	1	YES
17	1	YES
18	1	YES
19	4	YES
20	3	YES
21	4	YES
22	3	YES
23	2	YES
24	1	YES
25	2	YES
26	4	YES
27	4	YES
28	6	YES
29	5	YES
30	5	YES
31	5	YES
32	4	YES
33	4	YES
34	6	YES
35	5	YES
36	6	YES
37	8	YES
38	3	YES
39	1	YES
40	2	YES
41	4	YES
42	1	YES
43	2	YES
44	4	YES
45	2	YES
46	2	YES
47	3	YES
48	4	YES
49	3	YES
50	5	YES
51	5	YES
52	3	YES
53	2	YES
54	1	YES
55	1	YES
56	2	YES
57	1	YES
58	0	YES
59	2	YES
60	1	YES
61	2	YES
62	1	YES
63	2	YES
64	2	YES
65	1	YES
66	0	YES
67	3	YES
68	2	YES
69	3	YES
70	1	YES
71	1	YES
72	1	YES
73	1	YES
74	1	YES
75	2	YES
76	2	YES
77	2	YES
78	1	YES
79	1	YES
80	3	YES
81	2	YES
82	1	YES
83	3	YES
84	1	YES
85	0	YES
86	2	YES
87	1	YES
88	1	YES
89	1	YES
90	0	YES
91	0	YES
92	0	YES
93	0	YES
94	0	YES
95	2	YES
96	1	YES
97	1	YES
98	0	YES
99	1	YES
100	1	YES
TOTAL		100
MIN	0	
AVERAGE	2.2	
MAX	8	
% ≥ 1 STRIAE	90	

STRIAE No.	ORIENTATION FROM A-AXIS	CURVED STRIAE	LENGTH (MM)	WIDTH (MM)	WIDTH/ LENGTH RATIO	COMPOUND STRIATION
1	227	NO	43	1	0.02	NO
2	230	NO	10	1	0.10	NO
3	191	NO	10	0.5	0.05	NO
4	191	NO	4.5	0.25	0.06	NO
5	180	NO	3.5	0.25	0.07	NO
6	158	NO	13	0.5	0.04	NO
7	156	NO	4	0.25	0.06	NO
8	131	NO	5.5	0.25	0.05	NO
9	176	NO	35	0.5	0.01	NO
10	179	NO	4	0.25	0.06	NO
11	170	NO	10	0.25	0.03	NO
12	215	NO	8	0.75	0.09	NO
13	176	NO	18	0.5	0.03	NO
14	166	NO	11	0.25	0.02	NO
15	195	YES	10.5	0.75	0.07	NO
16	196	NO	15	0.5	0.03	NO
17	196	NO	5	0.25	0.05	NO
18	165	NO	2.5	0.25	0.10	NO
19	205	NO	6.5	0.75	0.12	NO
20	143	NO	23	0.5	0.02	NO
21	125	NO	7.5	1	0.13	YES
22	151	NO	8	0.75	0.09	NO
23	154	NO	4.5	0.25	0.06	NO
24	151	NO	7	0.5	0.07	NO
25	179	NO	4.5	0.25	0.06	NO
26	140	NO	15	0.5	0.03	NO
27	202	NO	6	0.25	0.04	NO
28	179	NO	8.5	0.75	0.09	NO
29	130	NO	3.5	0.25	0.07	NO
30	122	NO	13.5	0.25	0.02	NO
31	187	NO	12.5	0.25	0.02	NO
32	212	NO	4	0.25	0.06	NO
33	165	NO	4.5	0.25	0.06	NO
34	209	NO	6	0.5	0.08	NO
35	165	NO	7.5	0.25	0.03	NO
36	158	NO	4.5	0.25	0.06	NO
37	156	NO	2.5	0.75	0.30	NO
38	180	NO	5.5	0.5	0.09	NO
39	155	NO	7	0.5	0.07	NO
40	170	NO	8.5	0.25	0.03	NO
41	170	NO	4.5	0.5	0.11	NO
42	155	NO	7.5	1.5	0.20	YES
43		YES(> 5°)	7.5	0.75	0.10	NO
44	215	NO	5.5	0.25	0.05	NO
45	171	NO	5	0.25	0.05	NO
46	172	NO	7.5	0.25	0.03	NO
47	180	NO	3.5	0.25	0.07	NO
48	194	NO	17	0.25	0.01	NO
49	183	NO	3	0.5	0.17	NO
50	145	NO	4	0.5	0.13	NO
TOTAL		1				2
MIN	122.0		2.5	0.25	0.01	
AVERAGE	173.9		9.0	0.46	0.07	
MAX	230.0		43.0	1.50	0.30	
RANGE	58.0		40.5	1.25	0.29	
S.DEV	25.9		7.6	0.27	0.05	

TOTAL MEASURED AREA:	25 sq cm
TOTAL STRIAE FOR MEASURED AREA:	84
AVERAGE STRIAE PER SQ CM:	3.4

STRIAE ORIENTATION HALF ROSE DIAGRAM

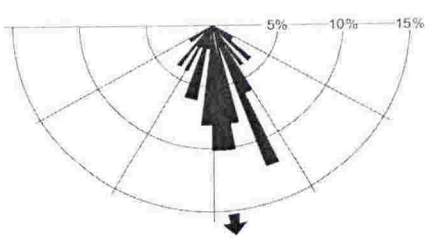

LOCATION: MACKAY GLACIER, ANTARCTICA

COLLECTION : 100 CLASTS FROM BASAL ICE (MK 1, INNER BERG)

NO.	LITHOLOGY	AXIS LENGTH			AVERAGE	AXIAL RATIOS		SPHERICITY	KRUMBEIN ROUNDNESS	FACETS	STRIAE	RA	C40
		A	B	C		C/A	B/A						
1	DOLERITE	2.6	2	1.1	1.90	0.42	0.77	0.62	0.1	NO	NO	1	0
2	DOLERITE	3.2	2.5	1.8	2.50	0.56	0.78	0.74	0.1	NO	NO	1	0
3	DOLERITE	2.2	1.6	1.1	1.63	0.50	0.73	0.70	0.1	NO	NO	1	0
4	DOLERITE	3.8	2.8	1.2	2.60	0.32	0.74	0.52	0.1	NO	NO	1	1
5	GRANITE	2	1.5	1.1	1.53	0.55	0.75	0.74	0.1	NO	NO	1	0
6	DOLERITE	2.9	2.2	1	2.03	0.34	0.76	0.54	0.1	NO	NO	1	1
7	GRANITE	3.1	1.5	1.4	2.00	0.45	0.48	0.75	0.1	NO	NO	1	0
8	GRANITE	1.8	1.7	0.6	1.37	0.33	0.94	0.49	0.1	NO	NO	1	1
9	GRANITE	3.7	2.5	2.3	2.83	0.62	0.68	0.83	0.1	NO	NO	1	0
10	DOLERITE	2.5	1.5	1.1	1.70	0.44	0.60	0.69	0.1	NO	NO	1	0
11	DOLERITE	2.4	1.9	0.6	1.63	0.25	0.79	0.43	0.1	NO	NO	1	1
12	DOLERITE	2.5	1.6	0.9	1.67	0.36	0.64	0.59	0.1	NO	NO	1	1
13	DOLERITE	2.5	2.2	1.6	2.10	0.64	0.88	0.78	0.1	NO	NO	1	0
14	GRANITE	2	1.8	1.1	1.63	0.55	0.90	0.70	0.1	NO	NO	1	0
15	GRANITE	2.2	1.6	1.2	1.67	0.55	0.73	0.74	0.1	NO	NO	1	0
16	GRANITE	2.1	1.7	1.5	1.77	0.71	0.81	0.86	0.1	NO	NO	1	0
17	GRANITE	2.3	1.8	0.9	1.67	0.39	0.78	0.58	0.1	NO	NO	1	1
18	DOLERITE	3	1.8	1	1.93	0.33	0.60	0.57	0.1	NO	NO	1	1
19	DOLERITE	2.1	1.8	1.4	1.77	0.67	0.86	0.81	0.1	NO	NO	1	0
20	GRANITE	1.9	1.5	1.3	1.57	0.68	0.79	0.84	0.1	NO	NO	1	0
21	GRANITE	2.1	1.9	1	1.67	0.48	0.90	0.63	0.1	NO	NO	1	0
22	DOLERITE	3.1	2.2	1.1	2.13	0.35	0.71	0.57	0.1	NO	NO	1	1
23	OTHER	1.8	1	0.9	1.23	0.50	0.56	0.77	0.1	NO	NO	1	0
24	GRANITE	4.1	2.5	2	2.87	0.49	0.61	0.73	0.2	NO	NO	1	0
25	DOLERITE	6	4.6	4.1	4.90	0.68	0.77	0.85	0.2	YES	YES	1	0
26	GRANITE	3.1	2.4	2.1	2.53	0.68	0.77	0.84	0.2	NO	NO	1	0
27	DOLERITE	5.4	3.1	2.1	3.53	0.39	0.57	0.64	0.2	NO	NO	1	1
28	DOLERITE	3.4	2	1.6	2.33	0.47	0.59	0.72	0.2	NO	NO	1	0
29	DOLERITE	4.4	3.1	1.6	3.03	0.36	0.70	0.58	0.2	NO	NO	1	1
30	DOLERITE	5.8	4.9	2.2	4.30	0.38	0.84	0.56	0.2	NO	NO	1	1
31	DOLERITE	3.8	2	1.6	2.47	0.42	0.53	0.70	0.2	NO	NO	1	0
32	GRANITE	3.1	2	1.4	2.17	0.45	0.65	0.68	0.2	NO	NO	1	0
33	DOLERITE	2.5	2.1	1.8	2.13	0.72	0.84	0.85	0.2	NO	NO	1	0
34	DOLERITE	2.8	1.5	1.4	1.90	0.50	0.54	0.78	0.2	YES	NO	1	0
35	DOLERITE	3.4	2.9	1.9	2.73	0.56	0.85	0.72	0.2	NO	NO	1	0
36	GRANITE	1.6	1.5	1.2	1.43	0.75	0.94	0.84	0.2	NO	NO	1	0
37	DOLERITE	2.8	2.2	1.2	2.07	0.43	0.79	0.62	0.2	NO	NO	1	0
38	DOLERITE	3.6	2.5	1.5	2.53	0.42	0.69	0.63	0.2	NO	NO	1	0
39	GRANITE	3.1	2	1.2	2.10	0.39	0.65	0.62	0.2	NO	NO	1	1
40	DOLERITE	4.2	4	3.8	4.00	0.90	0.95	0.95	0.2	NO	NO	1	0
41	DOLERITE	5.6	5	3	4.53	0.54	0.89	0.69	0.2	NO	NO	1	0
42	DOLERITE	2.3	1.5	1	1.60	0.43	0.65	0.66	0.2	NO	NO	1	0
43	DOLERITE	2.1	1.4	1	1.50	0.48	0.67	0.70	0.2	NO	NO	1	0
44	DOLERITE	2	1.5	1.4	1.63	0.70	0.75	0.87	0.2	NO	NO	1	0
45	DOLERITE	4	3	1.7	2.90	0.43	0.75	0.63	0.2	NO	NO	1	0
46	DOLERITE	2.7	1.4	1	1.70	0.37	0.52	0.64	0.2	YES	NO	1	1
47	DOLERITE	3	2	1.1	2.03	0.37	0.67	0.59	0.2	NO	NO	1	1
48	DOLERITE	3.2	2.4	1.6	2.40	0.50	0.75	0.70	0.2	NO	NO	1	0
49	DOLERITE	3.5	3.4	2.5	3.13	0.71	0.97	0.81	0.2	NO	NO	1	0
50	DOLERITE	2.5	1.5	1.4	1.80	0.56	0.60	0.81	0.2	NO	NO	1	0
51	GRANITE	2.1	2	1.5	1.87	0.71	0.95	0.81	0.2	NO	NO	1	0
52	GRANITE	2	1.6	1.2	1.60	0.60	0.80	0.77	0.2	NO	NO	1	0
53	GRANITE	2	1.2	1	1.40	0.50	0.60	0.75	0.2	NO	NO	1	0
54	DOLERITE	2.5	2.3	1.2	2.00	0.48	0.92	0.63	0.2	NO	NO	1	0
55	DOLERITE	2.8	2	1.6	2.13	0.57	0.71	0.77	0.2	NO	NO	1	0
56	DOLERITE	2	1.5	1	1.50	0.50	0.75	0.70	0.2	NO	NO	1	0
57	DOLERITE	3.8	2.5	1.1	2.47	0.29	0.66	0.51	0.2	YES	NO	1	1
58	GRANITE	2.5	2	1.1	1.87	0.44	0.80	0.63	0.2	NO	NO	1	0
59	OTHER	3.2	2.7	1.5	2.47	0.47	0.84	0.64	0.2	NO	NO	1	0
60	GRANITE	3.3	2.5	1	2.27	0.30	0.76	0.50	0.2	NO	NO	1	1
61	DOLERITE	1.9	1.6	1.2	1.57	0.63	0.84	0.78	0.2	NO	NO	1	0
62	DOLERITE	2	1.5	0.9	1.47	0.45	0.75	0.65	0.2	NO	NO	1	0
63	DOLERITE	2.4	1.3	1	1.57	0.42	0.54	0.69	0.2	NO	NO	1	0
64	DOLERITE	2.8	2	1.2	2.00	0.43	0.71	0.64	0.3	YES	NO	0	0
65	DOLERITE	2.9	1.9	1.4	2.07	0.48	0.66	0.71	0.3	NO	NO	0	0
66	DOLERITE	2.9	1.5	1.1	1.83	0.38	0.52	0.66	0.3	YES	NO	0	1
67	GRANITE	3.8	2.5	2	2.77	0.53	0.66	0.75	0.3	YES	NO	0	0
68	GRANITE	2.2	1.5	1.1	1.60	0.50	0.68	0.72	0.3	NO	NO	0	0
69	OTHER	3.4	2.9	2	2.77	0.59	0.85	0.74	0.3	NO	NO	0	0
70	DOLERITE	7	5.5	4.6	5.70	0.66	0.79	0.82	0.3	NO	NO	0	0
71	GRANITE	5.2	4.1	2.9	4.07	0.56	0.79	0.74	0.3	NO	NO	0	0
72	DOLERITE	3.1	2	1.1	2.07	0.35	0.65	0.58	0.3	YES	YES	0	1
73	DOLERITE	5.1	4.2	2.6	3.97	0.51	0.82	0.68	0.3	YES	NO	0	0
74	GRANITE	2.5	1.6	1.5	1.87	0.60	0.64	0.83	0.3	NO	NO	0	0
75	GRANITE	1.9	1.5	1.2	1.53	0.63	0.79	0.80	0.3	NO	NO	0	0
76	DOLERITE	2.9	1.9	1.2	2.00	0.41	0.66	0.64	0.3	NO	NO	0	0
77	DOLERITE	2.9	1.6	1.5	2.00	0.52	0.55	0.79	0.3	YES	NO	0	0
78	GRANITE	2.5	1.5	1.4	1.80	0.56	0.60	0.81	0.3	NO	NO	0	0
79	DOLERITE	3.3	2	1.5	2.27	0.45	0.61	0.70	0.3	NO	NO	0	0
80	DOLERITE	2.1	1.9	1.1	1.70	0.52	0.90	0.67	0.3	NO	NO	0	0
81	DOLERITE	2	1.7	1.1	1.60	0.55	0.85	0.71	0.3	YES	NO	0	0
82	DOLERITE	3.9	3.2	2.5	3.20	0.64	0.82	0.80	0.3	YES	NO	0	0
83	DOLERITE	3.5	2	0.9	2.13	0.26	0.57	0.49	0.3	YES	YES	0	1
84	GRANITE	3.6	2.5	1.9	2.67	0.53	0.69	0.74	0.3	NO	NO	0	0
85	DOLERITE	3.6	3.1	2	2.90	0.56	0.86	0.71	0.3	NO	NO	0	0
86	DOLERITE	2	1.5	1.3	1.60	0.65	0.75	0.83	0.3	NO	NO	0	0
87	DOLERITE	13	6.5	4.2	7.90	0.32	0.50	0.60	0.3	YES	YES	0	1
88	DOLERITE	11.5	3.9	2.5	5.97	0.22	0.34	0.52	0.3	YES	YES	0	1
89	GRANITE	10.3	6.6	4.7	7.20	0.46	0.64	0.69	0.3	YES	NO	0	0
90	DOLERITE	9.2	7.5	4	6.90	0.43	0.82	0.62	0.3	YES	YES	0	0
91	DOLERITE	3.3	2.2	2	2.50	0.61	0.67	0.82	0.4	NO	NO	0	0
92	DOLERITE	4.5	3.9	2	3.47	0.44	0.87	0.61	0.4	NO	NO	0	0
93	GRANITE	4.7	3.4	2.8	3.63	0.60	0.72	0.79	0.4	NO	NO	0	0
94	GRANITE	6.6	5	3.5	5.03	0.53	0.76	0.72	0.4	NO	NO	0	0
95	DOLERITE	4.5	3.5	2	3.33	0.44	0.78	0.64	0.4	YES	NO	0	0
96	DOLERITE	5	4.5	3	4.17	0.60	0.90	0.74	0.4	YES	NO	0	0
97	OTHER	9.2	3.5	3.1	5.27	0.34	0.38	0.67	0.4	YES	YES	0	1
98	OTHER	4.1	3.7	3	3.60	0.73	0.90	0.84	0.5	YES	NO	0	0
99	DOLERITE	2.6	2.1	1.5	2.07	0.58	0.81	0.75	0.5	NO	NO	0	0
100	SILTSTONE	1.5	1.4	0.7	1.20	0.47	0.93	0.62	0.5	YES	YES	0	0
AVERAGE		**3.5**	**2.5**	**1.7**	**2.6**	**0.50**	**0.73**	**0.70**	**0.23**	NA	NA	NA	NA
TOTAL		NA	NA	NA	NA	NA	NA	NA	NA	**22**	**8**	**63**	**22**

SUMMARY STATISTICS

LITHOLOGY	NO. CLASTS	STRIAE	% STRI	FACET	% FACET
DOLERITE	**64**	6	9	17	27
GRANITE	**30**	0	0	2	7
SILTSTONE	**1**	1	100	1	100
OTHER	**5**	1	20	2	40
TOTAL	**100**	8		22	

ROUNDNESS	TOTAL CLAST	FACETS	% FAC	STRIAE	% STRI	DOLERITE	% DOL	GRANITE	% GRAN	SILTSTONE	% SILT	OTHER	% OTH
0.1	23	0	0	0	0	12	19	10	33	0	0	1	20
0.2	40	4	10	1	3	29	45	10	33	0	0	1	20
0.3	27	13	48	5	19	18	28	8	27	0	0	1	20
0.4	7	3	43	1	14	4	6	2	7	0	0	1	20
0.5	3	2	67	1	33	1	2	0	0	1	100	1	20
0.6	0	0	0	0	0	0	0	0	0	0	0	0	0
0.7	0	0	0	0	0	0	0	0	0	0	0	0	0
0.8	0	0	0	0	0	0	0	0	0	0	0	0	0
0.9	0	0	0	0	0	0	0	0	0	0	0	0	0

LOCATION: MACKAY GLACIER, ANTARCTICA

COLLECTION : 100 CLASTS FROM BASAL ICE (MK 2, OUTER BERG)

NO.	LITHOLOGY	AXIS LENGTH			AVERAGE	AXIAL RATIOS		SPHERICITY	KRUMBEIN ROUNDNESS	FACETS	STRIAE	RA	C40
		A	B	C		C/A	B/A						
1	GRANITE	7.2	5.5	2	4.90	0.28	0.76	0.47	0.1	NO	NO	1	1
2	GRANITE	2.8	1.7	0.9	1.80	0.32	0.61	0.56	0.1	NO	NO	1	1
3	GRANITE	2.1	1.7	0.8	1.53	0.38	0.81	0.57	0.1	NO	NO	1	1
4	GRANITE	2.2	1.8	1.2	1.73	0.55	0.82	0.72	0.1	NO	NO	1	0
5	GRANITE	2	1.8	1.1	1.63	0.55	0.90	0.70	0.1	NO	NO	1	0
6	DOLERITE	2.9	1.2	1	1.70	0.34	0.41	0.66	0.1	NO	NO	1	1
7	GRANITE	2.2	1.8	1.1	1.70	0.50	0.82	0.68	0.1	NO	NO	1	0
8	GRANITE	2.2	1.2	0.8	1.40	0.36	0.55	0.63	0.1	NO	NO	1	1
9	GRANITE	1.3	1.1	1	1.13	0.77	0.85	0.89	0.1	NO	NO	1	0
10	GRANITE	5.8	4.6	3.5	4.63	0.60	0.79	0.77	0.1	NO	NO	1	0
11	GRANITE	2.5	2.2	1.8	2.17	0.72	0.88	0.84	0.2	NO	NO	1	0
12	GRANITE	2.5	1.9	1.8	2.07	0.72	0.76	0.88	0.2	NO	NO	1	0
13	GRANITE	3	2.4	1.6	2.33	0.53	0.80	0.71	0.2	NO	NO	1	0
14	GRANITE	2	1.8	1.2	1.67	0.60	0.90	0.74	0.2	NO	NO	1	0
15	GRANITE	3.5	2	1.6	2.37	0.46	0.57	0.72	0.2	NO	NO	1	0
16	DOLERITE	3.4	1.9	1.3	2.20	0.38	0.56	0.64	0.2	NO	NO	1	1
17	GRANITE	2.3	1.4	1.1	1.60	0.48	0.61	0.72	0.2	NO	NO	1	0
18	GRANITE	3	1.7	1.1	1.93	0.37	0.57	0.62	0.2	NO	NO	1	1
19	GRANITE	2.4	1.7	1	1.70	0.42	0.71	0.63	0.2	NO	NO	1	0
20	GRANITE	2.3	2	1.1	1.80	0.48	0.87	0.64	0.2	NO	NO	1	0
21	GRANITE	3.2	2	1.1	2.10	0.34	0.63	0.58	0.2	NO	NO	1	1
22	GRANITE	3.1	1.8	1.7	2.20	0.55	0.58	0.80	0.2	NO	NO	1	0
23	GRANITE	2.5	1.8	1.3	1.87	0.52	0.72	0.72	0.2	NO	NO	1	0
24	GRANITE	2.1	1.8	1.7	1.87	0.81	0.86	0.92	0.2	NO	NO	1	0
25	GRANITE	2.2	1.8	1.3	1.77	0.59	0.82	0.76	0.2	NO	NO	1	0
26	GRANITE	4	2.2	1.6	2.60	0.40	0.55	0.67	0.2	YES	NO	1	1
27	GRANITE	3.9	2.7	1.8	2.80	0.46	0.69	0.68	0.2	NO	NO	1	0
28	GRANITE	3.9	2	1.6	2.50	0.41	0.51	0.69	0.2	NO	NO	1	0
29	GRANITE	4	2.8	1.4	2.73	0.35	0.70	0.56	0.2	NO	NO	1	1
30	GRANITE	3.1	2	1.1	2.07	0.35	0.65	0.58	0.2	NO	NO	1	1
31	GRANITE	2.4	1.7	1.5	1.87	0.63	0.71	0.82	0.2	NO	NO	1	0
32	GRANITE	2.5	1.9	1.5	1.97	0.60	0.76	0.78	0.2	NO	NO	1	0
33	GRANITE	2.1	1.6	1.5	1.73	0.71	0.76	0.88	0.2	NO	NO	1	0
34	GRANITE	2.4	1.7	1.5	1.87	0.63	0.71	0.82	0.2	NO	NO	1	0
35	DOLERITE	2.5	2.3	1.7	2.17	0.68	0.92	0.80	0.2	NO	NO	1	0
36	DOLERITE	2.9	1.6	0.5	1.67	0.17	0.55	0.38	0.2	NO	NO	1	1
37	OTHER	2.1	1.9	1.1	1.70	0.52	0.90	0.67	0.2	NO	NO	1	0
38	DOLERITE	1.8	1.3	0.6	1.23	0.33	0.72	0.54	0.2	NO	NO	1	1
39	DOLERITE	6.8	4.6	3.1	4.83	0.46	0.68	0.68	0.2	NO	NO	1	0
40	GRANITE	3.1	2.7	1.8	2.53	0.58	0.87	0.73	0.3	NO	NO	0	0
41	GRANITE	2.1	1.8	1.3	1.73	0.62	0.86	0.77	0.3	NO	NO	0	0
42	DOLERITE	2	1.6	0.8	1.47	0.40	0.80	0.59	0.3	YES	NO	0	1
43	DOLERITE	3.1	2.1	1.9	2.37	0.61	0.68	0.82	0.3	NO	NO	0	0
44	GRANITE	3	2.7	2.4	2.70	0.80	0.90	0.89	0.3	NO	NO	0	0
45	GRANITE	2.3	1.8	0.7	1.60	0.30	0.78	0.49	0.3	NO	NO	0	1
46	DOLERITE	2.8	1.6	1.5	1.97	0.54	0.57	0.80	0.3	NO	NO	0	0
47	DOLERITE	3	2.3	2	2.43	0.67	0.77	0.84	0.3	NO	NO	0	0
48	GRANITE	2.2	1.1	1	1.43	0.45	0.50	0.75	0.3	NO	NO	0	0
49	GRANITE	4.1	3	2	3.03	0.49	0.73	0.69	0.3	NO	NO	0	0
50	DOLERITE	2.4	1.5	1	1.63	0.42	0.63	0.66	0.3	NO	NO	0	0
51	GRANITE	3.4	2.4	1.4	2.40	0.41	0.71	0.62	0.3	NO	NO	0	0
52	GRANITE	2.6	1.2	1	1.60	0.38	0.46	0.69	0.3	NO	NO	0	1
53	DOLERITE	3.8	2.5	1.8	2.70	0.47	0.66	0.70	0.3	YES	NO	0	0
54	DOLERITE	2.4	1.4	1	1.60	0.42	0.58	0.67	0.3	YES	YES	0	0
55	GRANITE	2.7	1.8	1.1	1.87	0.41	0.67	0.63	0.3	NO	NO	0	0
56	GRANITE	2.1	1.8	1.5	1.80	0.71	0.86	0.84	0.3	NO	NO	0	0
57	GRANITE	2.3	1.8	1.3	1.80	0.57	0.78	0.74	0.3	NO	NO	0	0
58	GRANITE	2.1	1.5	1.1	1.57	0.52	0.71	0.73	0.3	NO	NO	0	0
59	GRANITE	3.7	3.2	2.4	3.10	0.65	0.86	0.79	0.3	NO	NO	0	0
60	GRANITE	2.5	2.2	1.5	2.07	0.60	0.88	0.74	0.3	NO	NO	0	0
61	GRANITE	2.4	2	1.2	1.87	0.50	0.83	0.67	0.3	NO	NO	0	0
62	DOLERITE	3.6	2.5	2.2	2.77	0.61	0.69	0.81	0.3	NO	NO	0	0
63	GRANITE	2	1.2	1	1.40	0.50	0.60	0.75	0.3	YES	YES	0	0
64	OTHER	2	1.5	1.1	1.53	0.55	0.75	0.74	0.3	NO	NO	0	0
65	GRANITE	2.9	2.1	1.8	2.27	0.62	0.72	0.81	0.3	NO	NO	0	0
66	GRANITE	2.8	2.1	1.2	2.03	0.43	0.75	0.63	0.3	NO	NO	0	0
67	GRANITE	1.6	1.5	1.3	1.47	0.81	0.94	0.89	0.3	NO	NO	0	0
68	GRANITE	2.2	1.6	1.1	1.63	0.50	0.73	0.70	0.3	NO	NO	0	0
69	GRANITE	1.9	1.4	1.1	1.47	0.58	0.74	0.77	0.3	NO	NO	0	0
70	DOLERITE	3.6	2.7	2.1	2.80	0.58	0.75	0.77	0.3	NO	NO	0	0
71	GRANITE	5.3	4	2.9	4.07	0.55	0.75	0.74	0.3	NO	NO	0	0
72	DOLERITE	3.7	3.5	3.2	3.47	0.86	0.95	0.93	0.3	NO	NO	0	1
73	GRANITE	2.7	2.5	1	2.07	0.37	0.93	0.53	0.3	NO	NO	0	0
74	GRANITE	2.9	2.4	2.1	2.47	0.72	0.83	0.86	0.4	NO	NO	0	0
75	GRANITE	4	3.9	2.6	3.50	0.65	0.98	0.76	0.4	NO	NO	0	0
76	DOLERITE	4	2.8	1.7	2.83	0.43	0.70	0.64	0.4	YES	NO	0	0
77	DOLERITE	2.9	2.6	2.5	2.67	0.86	0.90	0.94	0.4	NO	NO	0	0
78	DOLERITE	2.1	1.2	1.1	1.47	0.52	0.57	0.78	0.4	YES	NO	0	0
79	GRANITE	2.1	1.7	0.9	1.57	0.43	0.81	0.61	0.4	NO	NO	0	0
80	GRANITE	2.4	2.1	1.9	2.13	0.79	0.88	0.90	0.4	NO	NO	0	0
81	GRANITE	5	4.2	3.6	4.27	0.72	0.84	0.85	0.4	NO	NO	0	0
82	DOLERITE	4	3.6	2.2	3.27	0.55	0.90	0.70	0.4	YES	NO	0	0
83	GRANITE	6.1	4.8	4.1	5.00	0.67	0.79	0.83	0.4	NO	NO	0	0
84	GRANITE	6	5.3	4.1	5.13	0.68	0.88	0.81	0.4	NO	NO	0	0
85	GRANITE	3.4	1.9	1.8	2.37	0.53	0.56	0.80	0.4	NO	NO	0	0
86	DOLERITE	3	1.7	1.1	1.93	0.37	0.57	0.62	0.4	YES	YES	0	1
87	DOLERITE	7.8	6.7	5	6.50	0.64	0.86	0.78	0.4	YES	YES	0	0
88	GRANITE	6	5.5	3.8	5.10	0.63	0.92	0.76	0.4	NO	NO	0	0
89	GRANITE	2.2	1.1	0.8	1.37	0.36	0.50	0.64	0.4	NO	NO	0	1
90	OTHER	2.1	1.1	0.7	1.30	0.33	0.52	0.60	0.4	NO	NO	0	1
91	DOLERITE	4.2	3.1	3	3.43	0.71	0.74	0.89	0.5	NO	NO	0	0
92	DOLERITE	3.7	2.8	2.1	2.87	0.57	0.76	0.75	0.5	NO	NO	0	0
93	GRANITE	2.6	1.7	1.1	1.80	0.42	0.65	0.65	0.5	YES	NO	0	0
94	GRANITE	5	3	2.2	3.40	0.44	0.60	0.69	0.5	NO	NO	0	0
95	GRANITE	3	2.1	2	2.37	0.67	0.70	0.86	0.5	NO	NO	0	0
96	GRANITE	2	1.8	1	1.60	0.50	0.90	0.66	0.5	NO	NO	0	0
97	SILTSTONE	2.1	1.5	1	1.53	0.48	0.71	0.68	0.5	YES	YES	0	0
98	GRANITE	3.1	2.5	2.4	2.67	0.77	0.81	0.91	0.6	NO	NO	0	0
99	GRANITE	2.1	1.5	1	1.53	0.48	0.71	0.68	0.3	NO	NO	0	0
100	GRANITE	8.5	7.7	3	6.40	0.35	0.91	0.52	0.2	NO	NO	1	1
AVERAGE		3.1	2.3	1.7	2.4	0.53	0.74	0.72	0.28	NA	NA	NA	NA
TOTAL		NA	NA	NA	NA	NA	NA	NA	NA	12	5	40	21

SUMMARY STATISTICS

LITHOLOGY	NO. CLASTS	STRIAE	% STRI	FACET	% FACET
DOLERITE	24	3	13	8	33
GRANITE	72	0	0	2	3
SILSTONE	1	1	100	1	100
OTHER	3	1	33	1	33
TOTAL	100	5		12	

ROUNDNESS	TOTAL CLAST	FACETS	% FAC	STRIAE	% STRI	DOLERITE	% DOL	GRANITE	% GRAN	SILTSTONE	% SILT	OTHER	% OTH
0.1	10	0	0	0	0	1	4	9	13	0	0	0	0
0.2	30	1	3	0	0	5	21	24	33	0	0	1	33
0.3	35	4	11	2	6	10	42	24	33	0	0	1	33
0.4	17	5	29	2	12	6	25	10	14	0	0	1	33
0.5	7	2	29	1	14	2	8	4	6	1	100	0	0
0.6	1	0	0	0	0	0	0	1	1	0	0	0	0
0.7	0	0	0	0	0	0	0	0	0	0	0	0	0
0.8	0	0	0	0	0	0	0	0	0	0	0	0	0
0.9	0	0	0	0	0	0	0	0	0	0	0	0	0

LOCATION: CUFF CAPE, ANTARCTICA
COLLECTION : SELECTED STRIATED CLAST 1

LITHOLOGY:	MUDSTONE
LENGTH OF LONG (A) AXIS:	93 mm
LENGTH OF INTERMEDIATE (B) AXIS:	64 mm
B/A AXIAL RATIO:	0.69
KRUMBEIN ROUNDNESS:	0.4

SQUARE No.	STRIAE DENSITY	
	STRIAE PER SQ	BACKGROUND STRIAE
1	1	YES
2	1	YES
3	1	YES
4	2	YES
5	2	YES
6	3	YES
7	3	YES
8	3	YES
9	3	YES
10	2	YES
11	1	YES
12	0	YES
13	1	YES
14	1	NO
15	3	YES
16	3	YES
17	0	YES
18	1	YES
19	0	YES
20	2	YES
21	2	YES
22	3	YES
23	1	YES
24	1	YES
25	1	YES
26	1	YES
27	2	YES
28	2	YES
29	1	YES
30	0	YES
31	1	YES
32	1	YES
33	2	YES
34	1	YES
35	1	YES
36	1	YES
37	2	YES
38	3	YES
39	2	YES
40	0	NO
41	1	YES
42	1	YES
43	1	YES
44	1	YES
45	0	YES
46	0	YES
47	0	YES
48	0	YES
49	0	YES
50	1	YES
51	2	YES
52	3	YES
53	1	YES
54	0	YES
55	1	YES
56	1	NO
57	0	NO
58	1	YES
59	1	YES
60	1	YES
61	1	YES
62	2	YES
63	1	YES
64	2	YES
65	0	NO
66	0	NO
67	0	YES
68	0	YES
69	3	YES
70	3	YES
71	3	YES
72	1	YES
73	0	YES
74	2	YES
75	3	YES
76	3	YES
77	2	YES
78	1	NO
79	1	NO
80	2	YES
81	1	YES
82	0	YES
83	0	YES
84	0	YES
85	0	YES
86	0	YES
87	1	YES
88	1	YES
89	1	YES
90	2	YES
91	0	YES
92	0	YES
93	2	YES
94	4	YES
95	1	YES
96	1	YES
97	1	YES
98	1	YES
99	4	YES
100	2	YES
%		92
MIN	0	
AVERAGE	1.3	
MAX	4	
% ≥ 1 STRIAE	76	

STRIAE No.	ORIENTATION FROM A-AXIS	CURVED STRIAE	LENGTH (MM)	WIDTH (MM)	WIDTH/ LENGTH RATIO	COMPOUND STRIATION
1	180	YES	12.5	0.75	0.06	NO
2	224	NO	2.5	0.25	0.10	NO
3	194	NO	4	0.25	0.06	NO
4	225	NO	7.5	0.25	0.03	NO
5	160	NO	7.5	0.25	0.03	NO
6	160	NO	4.5	0.25	0.06	NO
7	234	NO	12.5	0.25	0.02	NO
8	193	NO	9	0.25	0.03	NO
9	180	NO	5	0.25	0.05	NO
10	130	NO	5.5	0.5	0.09	NO
11	183	NO	12.5	0.5	0.04	NO
12	179	NO	4.5	0.25	0.06	NO
13	126	NO	9.5	0.75	0.08	NO
14	156	NO	2.5	0.5	0.20	NO
15	176	NO	4.5	0.25	0.06	NO
16	166	NO	3	0.25	0.08	NO
17	198	NO	6	1	0.17	NO
18	214	NO	11.5	0.25	0.02	NO
19	175	NO	8	0.25	0.03	NO
20	200	NO	3.5	0.25	0.07	NO
21	167	NO	8	0.25	0.03	NO
22	180	NO	4	0.25	0.06	NO
23	167	NO	2.5	0.25	0.10	NO
24	187	NO	5.5	0.5	0.09	NO
25	157	NO	3	0.25	0.08	NO
26	270	NO	5	1	0.20	NO
27	159	NO	6	4	0.67	YES
28	156	NO	6.5	1	0.15	NO
29	255	NO	19	1.25	0.07	NO
30	220	NO	17.5	2	0.11	NO
31	164	NO	5	0.25	0.05	NO
32	235	NO	10	2	0.20	NO
33	160	YES	8	0.25	0.03	NO
34	184	NO	9.5	0.25	0.03	NO
35	180	NO	2.5	0.25	0.10	NO
36	157	NO	3.5	0.25	0.07	NO
37	140	NO	5	1	0.20	NO
38	140	NO	5	0.25	0.05	NO
39	180	NO	1.5	0.25	0.17	NO
40	180	NO	1.5	0.25	0.17	NO
41	202	NO	2	0.5	0.25	NO
42	175	NO	5.5	0.75	0.14	NO
43	236	NO	4.5	0.5	0.11	NO
44	166	NO	4.5	0.25	0.06	NO
45	220	NO	4.5	0.5	0.11	NO
46	190	NO	5	0.25	0.05	NO
47	220	NO	3	0.25	0.08	NO
48	212	NO	3.5	0.25	0.07	NO
49	202	NO	2.5	0.25	0.10	NO
50	180	NO	4.5	0.25	0.06	NO
TOTAL		2				1
MIN	126.0		1.5	0.25	0.02	
AVERAGE	185.9		6.1	0.54	0.10	
MAX	270.0		19.0	4.00	0.67	
RANGE	90.0		17.5	3.75	0.65	
S.DEV	31.2		3.8	0.65	0.10	

TOTAL MEASURED AREA:	25 sq cm
TOTAL STRIAE FOR MEASURED AREA:	68
AVERAGE STRIAE PER SQ CM:	2.7

STRIAE ORIENTATION HALF ROSE DIAGRAM

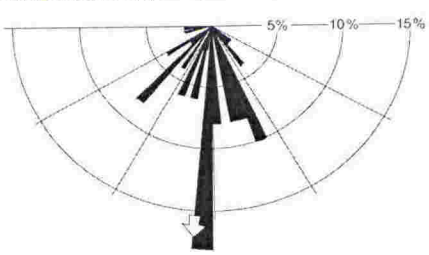

LOCATION: CUFF CAPE, ANTARCTICA
COLLECTION : SELECTED STRIATED CLAST 2

LITHOLOGY:	DOLERITE
LENGTH OF LONG (A) AXIS:	250 mm
LENGTH OF INTERMEDIATE (B) AXIS:	125 mm
B/A AXIAL RATIO:	0.50
KRUMBEIN ROUNDNESS:	0.3

SQUARE No.	STRIAE DENSITY	
	STRIAE PER SQ	BACKGROUND STRIAE
1	3	YES
2	2	YES
3	3	YES
4	2	YES
5	3	YES
6	1	YES
7	2	YES
8	3	YES
9	2	YES
10	1	YES
11	2	YES
12	1	YES
13	1	YES
14	1	YES
15	1	YES
16	1	YES
17	3	YES
18	2	YES
19	0	YES
20	1	YES
21	2	YES
22	2	YES
23	2	YES
24	1	YES
25	1	YES
26	2	YES
27	1	YES
28	2	YES
29	1	YES
30	0	YES
31	2	YES
32	2	YES
33	1	YES
34	1	YES
35	1	YES
36	2	YES
37	1	YES
38	1	YES
39	0	YES
40	1	YES
41	1	YES
42	3	YES
43	3	YES
44	1	YES
45	0	YES
46	1	YES
47	1	YES
48	0	YES
49	2	YES
50	3	YES
51	2	YES
52	3	YES
53	1	YES
54	0	YES
55	2	YES
56	2	YES
57	0	YES
58	0	YES
59	1	YES
60	1	YES
61	1	YES
62	1	YES
63	2	YES
64	1	YES
65	1	YES
66	1	YES
67	3	YES
68	2	YES
69	1	YES
70	1	YES
71	2	YES
72	4	YES
73	1	YES
74	3	YES
75	1	YES
76	0	YES
77	2	YES
78	1	YES
79	0	YES
80	0	YES
81	0	YES
82	1	YES
83	2	YES
84	0	YES
85	1	YES
86	1	YES
87	1	YES
88	2	YES
89	1	YES
90	0	YES
91	2	YES
92	2	YES
93	2	YES
94	1	YES
95	0	YES
96	0	YES
97	0	YES
98	0	YES
99	0	YES
100	1	YES
%		**100**
MIN	**0**	
AVERAGE	**1.3**	
MAX	**4**	
% ≥ 1 STRIAE	**81**	

STRIAE No.	ORIENTATION FROM A-AXIS	CURVED STRIAE	LENGTH (MM)	WIDTH (MM)	WIDTH/ LENGTH RATIO	COMPOUND STRIATION
1	172	NO	5	0.25	0.05	NO
2	176	NO	4	0.25	0.06	NO
3	183	NO	3.5	0.5	0.14	NO
4	157	NO	5	0.25	0.05	NO
5	186	NO	13.5	0.25	0.02	NO
6	186	NO	4	0.25	0.06	NO
7	189	NO	4.5	0.5	0.11	NO
8	188	NO	4	0.5	0.13	NO
9	180	NO	8.5	1	0.12	NO
10	151	NO	5	0.25	0.05	NO
11	161	NO	3	0.25	0.08	NO
12	191	NO	3	0.25	0.08	NO
13	180	NO	2	0.25	0.13	NO
14	181	NO	4	0.75	0.19	NO
15	180	NO	7	0.25	0.04	NO
16	174	NO	8.5	1.5	0.18	NO
17	204	NO	5.5	1.25	0.23	NO
18	185	NO	9	1.75	0.19	NO
19	175	NO	3.5	0.25	0.07	NO
20	161	NO	7	0.25	0.04	NO
21	203	NO	5.5	0.25	0.05	NO
22	120	NO	3	0.5	0.17	NO
23	181	NO	3	0.25	0.08	NO
24	181	NO	8.5	1.75	0.21	NO
25	155	NO	4.5	0.5	0.11	NO
26	178	NO	11	0.5	0.05	NO
27	180	NO	4.5	0.25	0.06	NO
28	156	NO	9.5	0.25	0.03	NO
29	180	NO	13	0.25	0.02	NO
30	164	NO	8	0.5	0.06	NO
31	165	NO	7	0.75	0.11	NO
32	181	NO	3	0.5	0.17	NO
33	192	NO	7	0.5	0.07	NO
34	191	NO	4	0.25	0.06	NO
35	167	NO	16	2.25	0.14	NO
36	178	NO	7.5	2	0.27	NO
37	188	NO	19	2	0.11	NO
38	141	NO	3.5	0.25	0.07	NO
39	160	NO	7.5	1.25	0.17	NO
40	185	NO	3.5	0.5	0.14	NO
41	161	NO	6	0.25	0.04	NO
42	186	NO	6	0.25	0.04	NO
43	162	NO	12.5	0.25	0.02	NO
44	180	NO	4.5	0.75	0.17	NO
45	166	NO	5.5	0.25	0.05	NO
46	162	NO	4.5	0.25	0.06	NO
47	180	NO	5	1	0.20	NO
48	181	NO	4.5	0.5	0.11	NO
49	155	NO	8	0.75	0.09	NO
50	180	NO	5.5	0.5	0.09	NO
TOTAL		**0**				**0**
MIN	**120.0**		**2.0**	**0.25**	**0.02**	
AVERAGE	**174.4**		**6.4**	**0.62**	**0.10**	
MAX	**204.0**		**19.0**	**2.25**	**0.27**	
RANGE	**60.0**		**17.0**	**2.00**	**0.25**	
S.DEV	**15.5**		**3.5**	**0.54**	**0.06**	

TOTAL MEASURED AREA:	**25 sq cm**
TOTAL STRIAE FOR MEASURED AREA:	**83**
AVERAGE STRIAE PER SQ CM:	**3.3**

STRIAE ORIENTATION HALF ROSE DIAGRAM

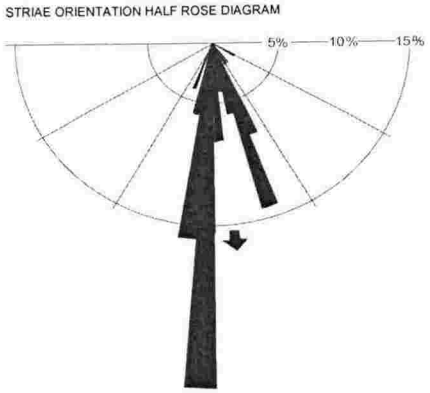

LOCATION: CUFF CAPE, ANTARCTICA
COLLECTION : SELECTED STRIATED CLAST 3

LITHOLOGY:	DOLERITE
LENGTH OF LONG (A) AXIS:	153 mm
LENGTH OF INTERMEDIATE (B) AXIS:	115 mm
B/A AXIAL RATIO:	0.75
KRUMBEIN ROUNDNESS:	0.3

SQUARE No.	STRIAE DENSITY	
	STRIAE PER SQ	BACKGROUND STRIAE
1	1	YES
2	2	YES
3	0	YES
4	0	YES
5	0	YES
6	1	YES
7	4	YES
8	0	YES
9	1	YES
10	0	YES
11	1	YES
12	1	YES
13	0	YES
14	2	YES
15	1	YES
16	0	YES
17	1	YES
18	2	YES
19	3	YES
20	1	YES
21	1	YES
22	1	YES
23	1	YES
24	3	YES
25	1	YES
26	0	YES
27	0	YES
28	1	YES
29	1	YES
30	0	YES
31	0	YES
32	1	YES
33	2	YES
34	2	YES
35	2	YES
36	1	YES
37	2	YES
38	3	YES
39	2	YES
40	2	YES
41	1	YES
42	0	YES
43	0	YES
44	1	YES
45	2	YES
46	3	YES
47	1	YES
48	0	YES
49	2	YES
50	1	YES
51	1	YES
52	0	YES
53	0	YES
54	1	YES
55	1	YES
56	2	YES
57	0	YES
58	2	YES
59	1	YES
60	0	YES
61	1	YES
62	0	YES
63	1	YES
64	2	YES
65	1	YES
66	0	YES
67	0	YES
68	1	YES
69	0	YES
70	2	YES
71	2	YES
72	1	YES
73	2	YES
74	3	YES
75	2	YES
76	1	YES
77	0	YES
78	0	YES
79	1	YES
80	2	YES
81	2	YES
82	0	YES
83	0	YES
84	0	YES
85	0	YES
86	0	YES
87	0	YES
88	0	YES
89	0	YES
90	0	YES
91	0	YES
92	1	YES
93	0	YES
94	1	YES
95	3	YES
96	2	YES
97	1	YES
98	1	YES
99	2	YES
100	2	YES
%		100
MIN	0	
AVERAGE	1.0	
MAX	4	
% ≥ 1 STRIAE	65	

STRIAE No.	ORIENTATION FROM A-AXIS	CURVED STRIAE	LENGTH (MM)	WIDTH (MM)	WIDTH/ LENGTH RATIO	COMPOUND STRIATION
1	210	NO	5.5	1	0.18	NO
2	205	NO	6	1	0.17	NO
3	162	NO	3.5	0.5	0.14	NO
4	166	NO	3	0.75	0.25	NO
5	224	NO	9.5	0.75	0.08	NO
6	205	NO	4.5	0.5	0.11	NO
7	235	NO	7.5	1	0.13	NO
8	235	NO	10	1	0.10	NO
9	167	NO	3.5	0.25	0.07	NO
10	175	NO	7	0.25	0.04	NO
11	212	NO	6.5	0.25	0.04	NO
12	180	NO	10	1.25	0.13	NO
13	213	NO	2.5	0.5	0.20	NO
14	179	NO	15.5	1	0.06	NO
15	185	NO	5	0.5	0.10	NO
16	242	NO	8	0.5	0.06	NO
17	226	NO	5	1	0.20	NO
18	215	NO	5	0.5	0.10	NO
19	104	NO	7	1	0.14	NO
20	221	NO	3.5	0.5	0.14	NO
21	225	NO	8	1	0.13	NO
22	136	NO	8.5	1	0.12	NO
23	178	NO	5	1.25	0.25	NO
24	131	NO	7	1	0.14	NO
25	110	NO	7	1.25	0.18	NO
26	154	NO	3	0.25	0.08	NO
27	159	NO	6	1	0.17	NO
28	208	NO	4	1	0.25	NO
29	211	NO	4.5	0.25	0.06	NO
30	171	NO	6	0.5	0.08	NO
31	175	NO	4	0.25	0.06	NO
32	130	NO	6	0.75	0.13	NO
33	220	NO	4	0.25	0.06	NO
34	151	NO	3	0.25	0.08	NO
35	169	NO	4.5	0.75	0.17	NO
36	220	NO	11.5	2.25	0.20	NO
37	216	NO	4	0.25	0.06	NO
38	181	NO	3.5	0.75	0.21	NO
39	203	NO	6	0.25	0.04	NO
40	134	NO	5.5	0.25	0.05	NO
41	172	NO	5.5	0.25	0.05	NO
TOTAL		0				0
MIN	104.0		2.5	0.25	0.04	
AVERAGE	185.7		6.0	0.70	0.12	
MAX	242.0		15.5	2.25	0.25	
RANGE	76.0		13.0	2.00	0.21	
S.DEV	35.8		2.6	0.42	0.06	

TOTAL MEASURED AREA:	25 sq cm
TOTAL STRIAE FOR MEASURED AREA:	60
AVERAGE STRIAE PER SQ CM:	2.4

STRIAE ORIENTATION HALF ROSE DIAGRAM

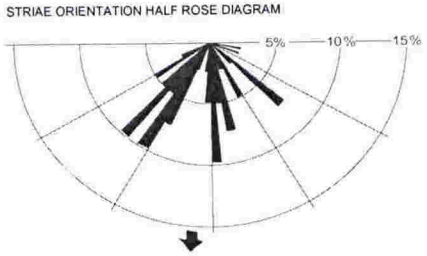

LOCATION: CUFF CAPE, ANTARCTICA
COLLECTION : SELECTED STRIATED CLAST 4

LITHOLOGY:	DOLERITE
LENGTH OF LONG (A) AXIS:	133 mm
LENGTH OF INTERMEDIATE (B) AXIS:	120 mm
B/A AXIAL RATIO:	0.90
KRUMBEIN ROUNDNESS:	0.4

SQUARE No.	STRIAE DENSITY	
	STRIAE PER SQ	BACKGROUND STRIAE
1	0	YES
2	0	YES
3	0	YES
4	2	YES
5	2	YES
6	2	YES
7	0	YES
8	0	YES
9	1	YES
10	1	YES
11	2	YES
12	0	YES
13	1	YES
14	0	YES
15	0	YES
16	2	YES
17	1	YES
18	0	YES
19	1	YES
20	1	YES
21	1	YES
22	1	YES
23	0	YES
24	0	YES
25	0	YES
26	0	YES
27	1	YES
28	0	YES
29	0	YES
30	1	YES
31	2	YES
32	2	YES
33	1	YES
34	2	YES
35	3	YES
36	3	YES
37	1	YES
38	1	YES
39	0	YES
40	2	YES
41	3	YES
42	1	YES
43	2	YES
44	3	YES
45	2	YES
46	1	YES
47	2	YES
48	2	YES
49	1	YES
50	0	YES
51	1	YES
52	0	YES
53	0	YES
54	1	YES
55	0	YES
56	2	YES
57	1	YES
58	1	YES
59	2	YES
60	1	YES
61	2	YES
62	2	YES
63	2	YES
64	2	YES
65	2	YES
66	4	YES
67	2	YES
68	2	YES
69	0	YES
70	0	YES
71	0	YES
72	1	YES
73	2	YES
74	3	YES
75	1	YES
76	0	YES
77	1	YES
78	4	YES
79	2	YES
80	0	YES
81	2	YES
82	1	YES
83	1	YES
84	1	YES
85	1	YES
86	0	YES
87	1	YES
88	1	YES
89	2	YES
90	1	YES
91	1	YES
92	2	YES
93	2	YES
94	2	YES
95	1	YES
96	3	YES
97	2	YES
98	3	YES
99	1	YES
100	1	YES
%		100
MIN	0	
AVERAGE	1.2	
MAX	4	
% ≥ 1 STRIAE	75	

STRIAE No.	ORIENTATION FROM A-AXIS	CURVED STRIAE	LENGTH (MM)	WIDTH (MM)	WIDTH/ LENGTH RATIO	COMPOUND STRIATION
1	264	NO	18.5	1	0.05	NO
2	125	NO	8	3	0.38	YES
3	167	NO	20	3	0.15	NO
4	194	NO	5.5	0.25	0.05	NO
5	133	NO	5	0.25	0.05	NO
6	191	NO	8	0.5	0.06	NO
7	161	NO	32.5	2.25	0.07	NO
8	200	NO	13	4	0.31	YES
9	164	NO	25.5	1.5	0.06	NO
10	184	NO	8	0.75	0.09	NO
11	183	NO	7.5	0.5	0.07	NO
12	161	NO	10	1	0.10	NO
13	123	NO	7.5	0.5	0.07	NO
14	161	NO	3.5	0.25	0.07	NO
15	266	NO	7	0.25	0.04	NO
16	180	NO	18.5	0.5	0.03	NO
17	172	NO	13	1.25	0.10	NO
18	164	NO	10.5	0.5	0.05	NO
19	130	NO	4.5	0.5	0.11	NO
20	120	NO	4	1	0.25	NO
21	175	NO	12.5	0.5	0.04	NO
22	163	NO	3.5	0.75	0.21	NO
23	196	NO	8	1	0.13	NO
24	150	NO	3.5	0.5	0.14	NO
25	171	NO	7	1.5	0.21	NO
26	170	NO	8	0.75	0.09	NO
27	161	NO	12.5	0.75	0.06	NO
28	211	NO	11	1	0.09	NO
29	209	NO	13.5	1.5	0.11	NO
30	189	NO	6.5	1	0.15	NO
31		YES(> 5°)	12.5	0.5	0.04	NO
32	180	NO	6	0.5	0.08	NO
33	212	NO	6	0.5	0.08	NO
34	186	NO	5	0.25	0.05	NO
35	180	NO	10	0.75	0.08	NO
36	141	NO	6	0.25	0.04	NO
37	241	NO	11	0.5	0.05	NO
38	205	NO	9	1	0.11	NO
39	167	NO	35	2	0.06	NO
40	137	NO	13	1	0.08	NO
41	181	NO	3.5	0.25	0.07	NO
42	189	NO	3	0.5	0.17	NO
43	172	NO	5	0.25	0.05	NO
44	195	NO	6	1	0.17	NO
45	180	NO	6	0.25	0.04	NO
46	196	NO	8	0.25	0.03	NO
47	180	NO	10.5	0.5	0.05	NO
48	126	NO	7	1	0.14	NO
49	144	NO	6.5	0.25	0.04	NO
50	182	NO	13.5	1.25	0.09	NO
TOTAL		0				2
MIN	120.0		3.0	0.25	0.03	
AVERAGE	176.2		10.0	0.90	0.10	
MAX	266.0		35.0	4.00	0.38	
RANGE	86.0		32.0	3.75	0.35	
S.DEV	31.8		6.8	0.78	0.07	

TOTAL MEASURED AREA:	25 sq cm
TOTAL STRIAE FOR MEASURED AREA:	53
AVERAGE STRIAE PER SQ CM:	2.1

STRIAE ORIENTATION HALF ROSE DIAGRAM

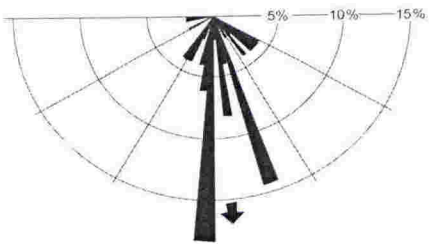

LOCATION, CENTRAL ALLAN HILLS, ANTARCTICA
COLLECTION : 10 WEATHERED, WIND POLISHED DOLERITE CLASTS WITH FRESH ABRASION MARKS

Clast No.	A -AXIS LENGTH	STRIAE DIMENSIONS (MAX) LENGTH	WIDTH	DEPTH	STRIAE ORIENT'N FROM "A" AXIS	STRIAE DEVI'N FROM "A" AXIS	STRIAE ORIENT'N FROM NORTH	STRIAE DEVI'N FROM NORTH	CURVATURE DEGREES	COMMENT
1	243	80	30	<1	198	18	180	0	Nil	Broad scrape consisting of multiple small striae on top flat surface
2	124	17	5	<1	255	75	180	0	Nil	Scrape limited by surface area of top flat surface, also, stoss (northern) side breakage
3	109	45	3	<1	190	10	214	34	Nil	Intermittent scratch on stoss (northern) surface, Intermittant due to irregular surface
4	143	45	5	<1	170	10	170	10	Nil	Intermittent irregular scrape along top flat surface edge (abraded edge)
5	124	70	5	<1	164	16	196	16	30	Striae on stoss (northern) ridge edge, curves by 30 degees due to ridge curvature
6	125	45	6	<1	175	25	170	10	Nil	Intermittant scrape on stoss (northern) side on surface edge, also top ridge lee side breakage
7	123	79	4	<1	180	0	180	0	Nil	Clear intermittent scratch on surface parallel to a-axis and ridge of clast. Length governed by clast length
8a	120	23	13	<1	219	39	180	0	Nil	Wide irregular scrape on top flat surface
8b	"	39	7	<1	219	39	180	0	Nil	Intermittant scape along raised ridge
9	166	60	4	<1	238	58	200	20	15	Scrape on stoss (northern) side from top ridge, trails off and curves 15 degrees toward north
10	150	58	17	<1	141	39	150	30	Nil	Several wide scratches on stoss side
Average	**142.7**	**51**	**9**		**195.4**	**29.9**	**181.8**			

LOCATION , MANHAUL BAY AND ODELL GLACIER MARGINS, ALLAN HILLS, ANTARCTICA
DATA FROM COLD-BASED LINEAR ABRASIONS ON BEDROCK

LOCATION	NO.	TYPE	AZIMUTH	LENGTH	WIDTH	DEPTH	W/L RATIO
MHG 1	1	TYPE 2	194	170	27	1.5	0.16
	2	TYPE 2	191	470	20	5	0.04
	3	TYPE 2	195	350	34	7	0.10
	4	TYPE 2	196	220	14	5	0.06
	5	TYPE 2	185	220	48	NIL	0.22
MHG 2	1	TYPE 2	205	290	20	5	0.07
	2	TYPE 2	190	230	30	7	0.13
	3	TYPE 2	201	90	10	2	0.11
	4	TYPE 2	180	230	35	5	0.15
	5	TYPE 2	189	660	10	2	0.02
MHG 3	1	TYPE 2	200	90	12	1	0.13
	2	TYPE 2	178	40	10	10	0.25
	3	TYPE 2	197	530	70	5	0.13
	4	TYPE 2	184	70	26	3	0.37
	5	TYPE 2	213	240	40	5	0.17
	6	TYPE 1	194	450	80	26.5	0.18
	7	TYPE 2	192	360	28	5.8	0.08
	8	TYPE 2	204	120	35	NIL	0.29
	9	TYPE 2	191	1680	65	5.6	0.04
	10	TYPE 2	197	470	60	7	0.13
MHG 4	1	TYPE 2	223	100	26	9	0.26
	2	TYPE 2	204	40	11	0.5	0.28
	3	TYPE 2	211	80	30	1	0.38
	4	TYPE 2	195	420	20	2	0.05
	5	TYPE 2	192	50	8	3	0.16
	6	TYPE 2	184	50	15	1	0.30
	7	TYPE 2	216	150	4.6	0.9	0.03
	8	TYPE 2	228	52	4	0.9	0.08
	9	TYPE 2	216	74	2.9	0.7	0.04
	10	TYPE 2	222	30	3.6	1.4	0.12
	11	TYPE 2	226	22	9.5	2.2	0.43
MHG 5	1	TYPE 2	184	250	20	5	0.08
	2	TYPE 2	209	280	35	8	0.13
	3	TYPE 2	211	220	55	6	0.25
	4	TYPE 2	171	420	15	1	0.04
	5	TYPE 2	196	160	8	0.5	0.05
MHG 6	1	TYPE 2	221	370	25	4	0.07
	2	TYPE 2	200	430	8	1	0.02
	3	TYPE 2	205	430	66	5	0.15
	4	TYPE 2	212	200	26	3	0.13
	5	TYPE 2	201	230	23	3	0.10
	6	TYPE 2	212	800	25	2	0.03
	7	TYPE 2	220	120	50	3	0.42
	8	TYPE 2	206	100	30	1	0.30
	9	TYPE 2	202	90	17	3	0.19
	10	TYPE 2	218	1250	160	7	0.13
	11	TYPE 2	200	60	4	1	0.07
	12	TYPE 2	222	640	11	2	0.02
	13	TYPE 2	167	430	20	1	0.05
	14	TYPE 2	196	230	17	0.5	0.07
	15	TYPE 2	213	150	16	2	0.11

LOCATION , MANHAUL BAY AND ODELL GLACIER MARGINS, ALLAN HILLS, ANTARCTICA
DATA FROM COLD-BASED LINEAR ABRASIONS ON BEDROCK

LOCATION	NO.	TYPE	AZIMUTH	LENGTH	WIDTH	DEPTH	W/L RATIO
MHG 7	1	TYPE 2	212	200	20	2	0.10
	2	TYPE 2	191	130	4	2	0.03
	3	TYPE 2	171	270	22	1	0.08
	4	TYPE 2	192	350	30	3	0.09
	5	TYPE 2	196	580	28	3	0.05
	6	TYPE 1	185	800	75	18	0.09
	7	TYPE 2	194	370	40	6	0.11
	8	TYPE 2	190	1780	46	7	0.03
MHG 8	1	TYPE 2	190	110	3	1	0.03
	2	TYPE 2	177	140	65	5	0.46
	3	TYPE 2	183	180	14	2	0.08
	4	TYPE 2	181	130	10	1	0.08
	5	TYPE 2	173	70	6	2	0.09
MHG 9	1	TYPE 2	173	170	30	2	0.18
	2	TYPE 2	173	420	90	8	0.21
	3	TYPE 2	162	400	30	3	0.08
	4	TYPE 2	179	NA	NA	NA	NA
	5	TYPE 2	167	NA	NA	NA	NA
	6	TYPE 2	176	NA	NA	NA	NA
	7	TYPE 2	176	NA	NA	NA	NA
	8	TYPE 2	167	NA	NA	NA	NA
MHG 10	1	TYPE 2	178	420	20	3	0.05
	2	TYPE 2	166	400	30	6	0.08
	3	TYPE 1	173	800	470	25	0.59
	4	TYPE 1	189	340	120	20	0.35
	5	TYPE 2	172	230	28	15	0.12
MHG 11	1	TYPE 1	185	800	220	30	0.28
	2	TYPE 1	157	720	210	21.5	0.29
	3	TYPE 2	157	350	45	3	0.13
	4	TYPE 1	169	420	130	30	0.31
	5	TYPE 1	169	1130	300	40	0.27
MHG 12	1	TYPE 2	158	NA	NA	NA	NA
	2	TYPE 2	156	NA	NA	NA	NA
	3	TYPE 2	170	NA	NA	NA	NA
ODELL	1	TYPE 2		370	32	1.9	0.09
	2	TYPE 2	284	480	48	3.5	0.10
	3	TYPE 2	279	1050	94	NIL	0.09
	5	TYPE 2	281	200	60	6.5	0.30
	6	TYPE 2	262	1300	29	4.5	0.02
	7	TYPE 2	262	130	17	1.5	0.13
	8	TYPE 2	277	200	23	6.5	0.12
	9	TYPE 2	266	270	21	6	0.08
	10	TYPE 2	284	130	37	12	0.28
	11	TYPE 2	269	NA	NA	NA	NA
	12	TYPE 2	269	NA	NA	NA	NA
	13	TYPE 2	250	NA	NA	NA	NA

SUMMARY STATISTICS

TYPE 1 ABRASIONS	LENGTH	WIDTH	W/L RATIO
MAXIMUM	1130	470	0.29
AVERAGE	682	200	0.6
MINIMUM	340	75	0.09
TYPE 2 ABRASIONS	**LENGTH**	**WIDTH**	**W/L RATIO**
MAXIMUM	1780	160	0.46
AVERAGE	324	29	0.13
MINIMUM	22	3	0.02

LOCATION, MURIMOTU FORMATION, NEW ZEALAND

COLLECTION : 100 CLASTS FROM DEBRIS-AVALANCHE DEPOSIT

NO.	LITHOLOGY	AXIS LENGTH			AVERAGE	AXIAL RATIOS		SPHERICITY	KRUMBEIN ROUNDNESS	FACETS	STRIAE	RA	C40
		A	B	C		C/A	B/A						
1	ANDESITE	65	47	40	50.7	0.62	0.72	0.81	0.1	YES	YES	1	0
2	ANDESITE	90	70	56	72.0	0.62	0.78	0.79	0.1	YES	YES	1	0
3	ANDESITE/DACITE	57	53	31	47.0	0.54	0.93	0.69	0.1	NO	NO	1	0
4	ANDESITE	77	55	27	53.0	0.35	0.71	0.56	0.1	YES	NO	1	1
5	ANDESITE	66	46	17	43.0	0.26	0.70	0.46	0.1	YES	YES	1	1
6	ANDESITE	69	63	40	57.3	0.58	0.91	0.72	0.1	YES	YES	1	0
7	ANDESITE	63	61	47	57.0	0.75	0.97	0.83	0.1	YES	YES	1	0
8	ANDESITE	68	52	42	54.0	0.62	0.76	0.79	0.1	YES	YES	1	0
9	ANDESITE	87	77	36	66.7	0.41	0.89	0.58	0.1	YES	YES	1	0
10	ANDESITE/DACITE	71	44	25	46.7	0.35	0.62	0.59	0.1	NO	NO	1	1
11	ANDESITE/DACITE	45	34	33	37.3	0.73	0.76	0.89	0.1	NO	NO	1	0
12	ANDESITE/DACITE	47	36	17	33.3	0.36	0.77	0.56	0.1	YES	NO	1	1
13	ANDESITE/DACITE	63	55	41	53.0	0.65	0.87	0.79	0.1	NO	NO	1	0
14	ANDESITE	65	60	46	57.0	0.71	0.92	0.82	0.1	YES	YES	1	0
15	ANDESITE	76	34	24	44.7	0.32	0.45	0.61	0.1	YES	NO	1	1
16	ANDESITE/DACITE	42	29	23	31.3	0.55	0.69	0.76	0.1	YES	NO	1	0
17	ANDESITE	55	36	25	38.7	0.45	0.65	0.68	0.1	YES	YES	1	0
18	ANDESITE	54	34	24	37.3	0.44	0.63	0.68	0.1	YES	NO	1	0
19	ANDESITE/DACITE	52	31	17	33.3	0.33	0.60	0.57	0.1	NO	NO	1	1
20	ANDESITE	46	37	15	32.7	0.33	0.80	0.51	0.1	YES	NO	1	1
21	ANDESITE	47	35	28	36.7	0.60	0.74	0.78	0.1	NO	NO	1	0
22	ANDESITE	39	25	15	26.3	0.38	0.64	0.62	0.1	YES	YES	1	1
23	ANDESITE	41	25	17	27.7	0.41	0.61	0.66	0.1	NO	NO	1	0
24	ANDESITE	55	40	23	39.3	0.42	0.73	0.62	0.1	NO	NO	1	0
25	ANDESITE	37	35	25	32.3	0.68	0.95	0.79	0.1	NO	NO	1	0
26	ANDESITE/DACITE	42	23	15	26.7	0.36	0.55	0.62	0.1	YES	NO	1	1
27	ANDESITE	30	25	24	26.3	0.80	0.83	0.92	0.1	NO	NO	1	0
28	ANDESITE/DACITE	54	31	22	35.7	0.41	0.57	0.66	0.1	NO	NO	1	0
29	ANDESITE	59	40	17	38.7	0.29	0.68	0.50	0.1	YES	NO	1	1
30	ANDESITE	55	49	30	44.7	0.55	0.89	0.70	0.1	YES	NO	1	0
31	ANDESITE	39	31	22	30.7	0.56	0.79	0.74	0.1	YES	NO	1	0
32	ANDESITE	61	42	23	42.0	0.38	0.69	0.59	0.1	YES	NO	1	1
33	ANDESITE	55	42	17	38.0	0.31	0.76	0.50	0.1	YES	NO	1	1
34	ANDESITE	45	36	25	35.3	0.56	0.80	0.73	0.1	YES	NO	1	0
35	ANDESITE/DACITE	33	20	17	23.3	0.52	0.61	0.76	0.1	NO	NO	1	0
36	ANDESITE	29	26	21	25.3	0.72	0.90	0.84	0.1	NO	NO	1	0
37	ANDESITE/DACITE	46	40	20	35.3	0.43	0.87	0.60	0.1	YES	NO	1	0
38	ANDESITE/DACITE	47	38	25	36.7	0.53	0.81	0.71	0.1	YES	NO	1	0
39	ANDESITE/DACITE	47	43	32	40.7	0.68	0.91	0.80	0.1	NO	NO	1	0
40	ANDESITE/DACITE	29	19	17	21.7	0.59	0.66	0.81	0.1	YES	NO	1	0
41	ANDESITE/DACITE	45	30	26	33.7	0.58	0.67	0.80	0.1	YES	NO	1	0
42	ANDESITE	40	35	19	31.3	0.48	0.88	0.64	0.1	YES	NO	1	0
43	ANDESITE/DACITE	119	66	43	76.0	0.36	0.55	0.62	0.2	YES	NO	1	1
44	ALTERED	85	57	40	60.7	0.47	0.67	0.69	0.2	NO	NO	1	0
45	ALTERED	70	49	48	55.7	0.69	0.70	0.88	0.2	YES	NO	1	0
46	ANDESITE	61	51	41	51.0	0.67	0.84	0.82	0.2	YES	NO	1	0
47	ANDESITE/DACITE	65	49	34	49.3	0.52	0.75	0.72	0.2	NO	NO	1	0
48	ANDESITE	77	63	47	62.3	0.61	0.82	0.77	0.2	NO	NO	1	0
49	ANDESITE/DACITE	70	42	41	51.0	0.59	0.60	0.83	0.2	YES	NO	1	0
50	ANDESITE/DACITE	69	52	42	54.3	0.61	0.75	0.79	0.2	NO	NO	1	0
51	ANDESITE	84	47	45	58.7	0.54	0.56	0.80	0.1	NO	NO	1	0
52	ANDESITE/DACITE	56	42	29	42.3	0.52	0.75	0.71	0.2	NO	NO	1	0
53	ANDESITE/DACITE	54	36	25	38.3	0.46	0.67	0.69	0.2	NO	NO	1	0
54	ANDESITE/DACITE	45	32	29	35.3	0.64	0.71	0.84	0.2	NO	NO	1	0
55	ANDESITE/DACITE	72	48	46	55.3	0.64	0.67	0.85	0.2	NO	NO	1	0
56	ANDESITE/DACITE	33	24	21	26.0	0.64	0.73	0.82	0.2	NO	NO	1	0
57	ANDESITE/DACITE	22	19	16	19.0	0.73	0.86	0.85	0.2	NO	NO	1	0
58	ANDESITE/DACITE	43	36	25	34.7	0.58	0.84	0.74	0.2	YES	NO	1	0
59	ANDESITE/DACITE	38	29	17	28.0	0.45	0.76	0.64	0.2	NO	NO	1	0
60	ANDESITE	29	26	16	23.7	0.55	0.90	0.70	0.2	NO	NO	1	0
61	ANDESITE/DACITE	51	29	23	34.3	0.45	0.57	0.71	0.2	NO	NO	1	0
62	ALTERED	50	35	22	35.7	0.44	0.70	0.65	0.2	NO	NO	1	0
63	ANDESITE/DACITE	49	37	31	39.0	0.63	0.76	0.81	0.2	NO	NO	1	0
64	ANDESITE/DACITE	43	26	25	31.3	0.58	0.60	0.83	0.2	YES	NO	1	0
65	ANDESITE/DACITE	62	38	27	42.3	0.44	0.61	0.68	0.1	NO	NO	1	0
66	ALTERED	84	53	37	58.0	0.44	0.63	0.68	0.2	NO	NO	1	0
67	ANDESITE/DACITE	68	50	34	50.7	0.50	0.74	0.70	0.2	NO	NO	1	0
68	ANDESITE/DACITE	45	44	30	39.7	0.67	0.98	0.77	0.2	YES	NO	1	0
69	ALTERED	42	26	15	27.7	0.36	0.62	0.59	0.2	NO	NO	1	1
70	ANDESITE/DACITE	25	22	15	20.7	0.60	0.88	0.74	0.2	YES	NO	1	0
71	ALTERED	37	36	22	31.7	0.59	0.97	0.72	0.2	NO	NO	1	0
72	ANDESITE/DACITE	52	33	21	35.3	0.40	0.63	0.64	0.2	YES	NO	1	0
73	ANDESITE/DACITE	45	29	21	31.7	0.47	0.64	0.70	0.2	NO	NO	1	0
74	ANDESITE/DACITE	31	26	20	25.7	0.65	0.84	0.79	0.2	YES	NO	1	0
75	ALTERED	49	39	29	39.0	0.59	0.80	0.76	0.2	NO	NO	1	0
76	ALTERED	89	47	40	58.7	0.45	0.53	0.73	0.2	NO	NO	1	0
77	ANDESITE/DACITE	62	51	36	49.7	0.58	0.82	0.75	0.1	YES	NO	1	0
78	ANDESITE/DACITE	61	53	37	50.3	0.61	0.87	0.75	0.2	NO	NO	1	0
79	ANDESITE/DACITE	57	44	29	43.3	0.51	0.77	0.70	0.2	NO	NO	1	0
80	ANDESITE/DACITE	44	33	22	33.0	0.50	0.75	0.70	0.2	NO	NO	1	0
81	ALTERED	44	28	24	32.0	0.55	0.64	0.78	0.1	NO	NO	1	0
82	ANDESITE/DACITE	40	30	24	31.3	0.60	0.75	0.78	0.2	NO	NO	1	0
83	ANDESITE/DACITE	42	37	23	34.0	0.55	0.88	0.70	0.2	NO	NO	1	0
84	ALTERED	39	36	31	35.3	0.79	0.92	0.88	0.2	NO	NO	1	0
85	ANDESITE/DACITE	35	31	29	31.7	0.83	0.89	0.92	0.2	NO	NO	1	0
86	ANDESITE	35	30	20	28.3	0.57	0.86	0.73	0.1	NO	NO	1	0
87	ALTERED	22	16	15	17.7	0.68	0.73	0.86	0.2	NO	NO	1	0
88	ANDESITE/DACITE	32	26	17	25.0	0.53	0.81	0.71	0.2	NO	NO	1	0
89	ANDESITE/DACITE	52	30	28	36.7	0.54	0.58	0.80	0.2	NO	NO	1	0
90	ANDESITE	59	45	31	45.0	0.53	0.76	0.72	0.2	NO	NO	1	0
91	ANDESITE/DACITE	55	32	26	37.7	0.47	0.58	0.73	0.2	NO	NO	1	0
92	ANDESITE	61	45	35	47.0	0.57	0.74	0.77	0.2	NO	NO	1	0
93	ANDESITE/DACITE	32	27	20	26.3	0.63	0.84	0.78	0.2	NO	NO	1	0
94	ANDESITE/DACITE	32	20	16	22.7	0.50	0.63	0.74	0.2	YES	NO	1	0
95	ANDESITE/DACITE	33	26	16	25.0	0.48	0.79	0.67	0.2	NO	NO	1	0
96	ALTERED	43	30	19	30.7	0.44	0.70	0.66	0.2	NO	NO	1	0
97	ANDESITE/DACITE	23	19	16	19.3	0.70	0.83	0.84	0.2	NO	NO	1	0
98	ANDESITE/DACITE	34	25	20	26.3	0.59	0.74	0.78	0.3	NO	NO	0	0
99	ANDESITE/DACITE	28	25	22	25.0	0.79	0.89	0.89	0.3	NO	NO	0	0
100	ANDESITE/DACITE	41	32	19	30.7	0.46	0.78	0.65	0.3	NO	NO	0	0
AVERAGE		**51.5**	**37.9**	**27.0**	**38.8**	**0.54**	**0.75**	**0.73**	**0.16**	NA	NA	NA	NA
TOTAL		NA	NA	NA	NA	NA	NA	NA	NA	**40**	**10**	**97**	**14**

SUMMARY STATISTICS

LITHOLOGY	NO. CLASTS	STRIAE	% STRI	FACES	% FACES
ANDESITE	**34**	10	29.4	22	64.7
ANDESITE/DACITE	**54**	0	0	17	31.5
ALTERERD	**12**	0	0	1	8.3
TOTAL	**100**	10		40	

ROUNDNESS	TOTAL CLAST	FRAC	%	STRIAE	% STRI	ANDESITE	% ANDESITE	ANDESITE/DACITE	%ANDESITE/DACITE	ALTERED	% ALTERED
0.1	47	29	61.7	10.0	21.3	29	85.3	17	31.5	1	8.3
0.2	50	11	22.0	0	0.0	5	14.7	34	63.0	11	91.7
0.3	3	0	0.0	0	0.0	0	0.0	3	5.6	0	0.0
0.4	0	0	0.0	0	0.0	0	0.0	0	0.0	0	0.0
0.5	0	0	0.0	0	0.0	0	0.0	0	0.0	0	0.0
0.6	0	0	0.0	0	0.0	0	0.0	0	0.0	0	0.0
0.7	0	0	0.0	0	0	0	0.0	0	0.0	0	0.0
0.8	0	0	0.0	0	0	0	0.0	0	0.0	0	0.0
0.9	0	0	0.0	0	0	0	0.0	0	0.0	0	0.0

LOCATION: MURIMOTU FORMATION, NEW ZEALAND
COLLECTION : SELECTED DEBRIS-AVALANCHE STRIATED CLAST 1

LITHOLOGY:	ANDESITE
LENGTH OF LONG (A) AXIS:	170 mm
LENGTH OF INTERMEDIATE (B) AXIS:	110 mm
B/A AXIAL RATIO:	0.65
KRUMBEIN ROUNDNESS:	0.1

SQUARE No.	STRIAE DENSITY	
	STRIAE PER SQ	BACKGROUND STRIAE
1	0	YES
2	4	YES
3	2	YES
4	3	YES
5	2	YES
6	0	YES
7	0	YES
8	3	YES
9	2	YES
10	3	YES
11	3	YES
12	1	NO
13	2	NO
14	2	NO
15	2	NO
16	4	NO
17	2	NO
18	2	NO
19	1	NO
20	0	NO
21	0	NO
22	1	NO
23	2	NO
24	2	YES
25	1	YES
26	2	YES
27	1	YES
28	2	YES
29	1	YES
30	2	YES
31	2	YES
32	3	YES
33	3	NO
34	2	NO
35	2	NO
36	3	YES
37	4	NO
38	3	NO
39	0	NO
40	0	NO
41	1	NO
42	0	NO
43	0	YES
44	1	NO
45	0	NO
46	1	NO
47	1	NO
48	2	NO
49	1	YES
50	4	NO
51	2	YES
52	0	YES
53	2	YES
54	2	YES
55	1	NO
56	2	NO
57	1	YES
58	2	YES
59	2	YES
60	2	YES
61	2	YES
62	0	YES
63	0	YES
64	1	YES
65	3	YES
66	0	YES
67	2	YES
68	2	YES
69	0	YES
70	1	YES
71	1	YES
72	0	YES
73	2	YES
74	2	YES
75	2	YES
76	1	NO
77	2	NO
78	3	YES
79	2	YES
80	2	NO
81	0	NO
82	3	NO
83	3	NO
84	3	YES
85	0	NO
86	0	YES
87	2	YES
88	3	YES
TOTAL		52
MIN	0	59%
AVERAGE	1.6	
MAX	4	
% ≥ 1 STRIAE	78.4	

STRIAE No.	ORIENTATION FROM A-AXIS	CURVED STRIAE (> 5°)	LENGTH (MM)	WIDTH (MM)	WIDTH/ LENGTH RATIO	COMPOUND STRIATION
1	106	NO	2	0.25	0.13	NO
2	107	NO	1.5	0.25	0.17	NO
3	108	NO	1.5	0.25	0.17	NO
4	164	NO	7.5	2	0.27	NO
5	206	NO	2.5	1	0.40	NO
6	108	NO	6	0.25	0.04	NO
7	110	NO	3	0.5	0.17	NO
8		YES(> 5°)	8.5	1.5	0.18	NO
9		YES(> 5°)	6	1.5	0.25	NO
10	180	NO	4	1.5	0.38	NO
11	170	NO	9	2	0.22	NO
12	124	NO	6	0.25	0.04	NO
13	117	NO	7	3	0.43	YES
14	94	NO	2.5	1	0.40	NO
15	134	NO	7	0.25	0.04	NO
16		YES(> 5°)	4	0.25	0.06	NO
17	142	NO	3	0.25	0.08	NO
18	185	NO	3.5	1	0.29	NO
19	114	NO	3	0.25	0.08	NO
20	240	NO	2.5	0.25	0.10	NO
21	105	NO	4.5	1	0.22	NO
22	144	NO	3.5	0.25	0.07	NO
23	192	NO	4	1	0.25	NO
24	145	YES	3.5	0.25	0.07	NO
25	125	NO	6.5	0.25	0.04	NO
26	182	NO	5.5	0.25	0.05	NO
27	197	NO	2.5	0.25	0.10	NO
28	147	NO	12.5	1.25	0.10	NO
29	169	NO	8.5	1.25	0.15	NO
30	163	NO	8	2	0.25	YES
31	190	NO	5	0.25	0.05	NO
32	260	NO	5.5	1.5	0.27	NO
33	195	NO	3	0.25	0.08	NO
34	201	NO	3.5	0.25	0.07	NO
35	260	NO	3.5	1	0.29	NO
36	210	NO	9	2.25	0.25	NO
37	110	NO	2	0.25	0.13	NO
38	202	NO	4.5	1	0.22	NO
39	131	NO	3.5	1	0.29	NO
40	251	NO	5.5	0.25	0.05	NO
41	156	NO	6	1	0.17	NO
42	233	NO	3.5	0.25	0.07	NO
43	146	NO	3.5	1	0.29	NO
44	145	NO	5	0.25	0.05	NO
45	155	NO	2	0.25	0.13	NO
46	255	NO	2	1.25	0.63	NO
47	230	NO	2	0.25	0.13	NO
48	135	NO	2	0.25	0.13	NO
49	154	NO	3	1	0.33	NO
50	136	NO	3	0.25	0.08	NO
TOTAL		1				2
MIN	94.0		1.5	0.25	0.04	
AVERAGE	164.5		4.5	0.78	0.18	
MAX	260.0		12.5	3.00	0.63	
RANGE	86.0		11.0	2.75	0.59	
S.DEV	47.0		2.4	0.67	0.13	

TOTAL MEASURED AREA:	88 sq cm
TOTAL STRIAE FOR MEASURED AREA:	108
AVERAGE STRIAE PER SQ CM:	1.2

STRIAE ORIENTATION HALF ROSE DIAGRAM

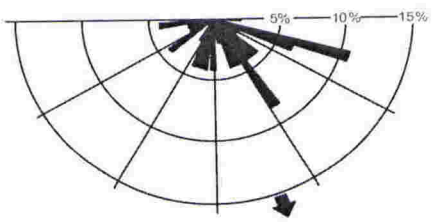

LOCATION: MURIMOTU FORMATION, NEW ZEALAND
COLLECTION : SELECTED DEBRIS-AVALANCHE STRIATED CLAST 2

LITHOLOGY:	ANDESITE
LENGTH OF LONG (A) AXIS:	110 mm
LENGTH OF INTERMEDIATE (B) AXIS:	95 mm
B/A AXIAL RATIO:	0.86
KRUMBEIN ROUNDNESS:	0.1

SQUARE No.	STRIAE DENSITY	
	STRIAE PER SQ	BACKGROUND STRIAE
1	0	NO
2	0	NO
3	1	NO
4	1	YES
5	0	YES
6	0	NO
7	1	YES
8	0	NO
9	0	NO
10	0	NO
11	2	YES
12	1	YES
13	0	NO
14	0	NO
15	0	NO
16	2	NO
17	2	YES
18	0	YES
19	0	NO
20	0	NO
21	0	YES
22	2	YES
23	0	YES
24	1	NO
25	1	NO
26	2	NO
27	1	NO
28	0	NO
29	0	NO
30	0	NO
31	3	YES
32	4	NO
33	1	NO
34	2	YES
35	3	NO
36	1	NO
37	1	YES
38	0	YES
39	0	NO
40	0	NO
41	3	NO
42	1	NO
43	2	NO
44	2	NO
45	0	NO
46	2	NO
47	2	NO
48	2	NO
49	0	NO
50	0	NO
51	1	NO
52	0	NO
53	1	NO
54	0	NO
55	2	NO
56	2	NO
57	0	YES
58	0	YES
59	1	YES
60	1	YES
61	0	NO
62	2	NO
63	2	NO
64	1	NO
65	0	YES
66	0	YES
67	0	NO
68	1	NO
69	0	NO
70	2	NO
71	0	YES
72	2	NO
73	0	NO
74	0	NO
75	1	YES
76	0	YES
77	0	NO
78	2	YES
79	0	NO
80	3	NO
81	0	NO
82	0	NO
83	1	YES
84	1	YES
85	1	NO
86	1	NO
87	0	NO
88	0	NO
89	0	NO
90	0	NO
91	0	YES
92	2	NO
93	1	NO
94	0	NO
95	0	NO
96	0	NO
97	0	NO
98	0	NO
99	0	NO
100	1	YES
%		**28**
MIN	**0**	
AVERAGE	**0.8**	
MAX	**4**	
% ≥ 1 STRIAE	**48**	

STRIAE No.	ORIENTATION FROM A-AXIS	CURVED STRIAE	LENGTH (MM)	WIDTH (MM)	WIDTH/ LENGTH RATIO	COMPOUND STRIATION
1	123	NO	3.5	0.25	0.07	NO
2	122	NO	1.5	0.25	0.17	NO
3	180	NO	4.5	0.25	0.06	NO
4	185	NO	3	0.25	0.08	NO
5	180	NO	5.5	0.25	0.05	NO
6	185	NO	4	1	0.25	NO
7	176	NO	1.5	0.25	0.17	NO
8	122	NO	2	0.75	0.38	NO
9	187	**YES**	14	1	0.07	NO
10	187	**YES**	11.5	1	0.09	**YES**
11	193	NO	5	0.5	0.10	NO
12	170	NO	1.5	0.5	0.33	NO
13	184	NO	2.5	0.25	0.10	NO
14	194	NO	3.5	0.25	0.07	NO
15	183	NO	9.5	0.25	0.03	NO
16	175	NO	11.5	1.5	0.13	**YES**
17	166	NO	7	0.25	0.04	NO
18	172	NO	3.5	0.25	0.07	NO
19	170	NO	3.5	0.25	0.07	NO
20	174	NO	3	0.25	0.08	NO
21	175	NO	16	2.25	0.14	**YES**
22	174	NO	20.5	2	0.10	**YES**
23	190	NO	3	0.25	0.08	NO
24	180	NO	8.5	0.25	0.03	NO
25	180	NO	4.5	0.25	0.06	NO
26	205	NO	2.5	0.25	0.10	NO
27	175	NO	5.5	1	0.18	**YES**
28	184	NO	9	1.5	0.17	**YES**
29	176	NO	10	1	0.10	NO
30	167	NO	11.5	0.75	0.07	NO
31	130	NO	4.5	0.25	0.06	NO
32	130	NO	2	0.25	0.13	NO
33	130	NO	5	0.25	0.05	NO
34	166	NO	2.5	0.25	0.10	NO
35	185	NO	4	0.25	0.06	NO
36	182	NO	2	0.25	0.13	NO
37	170	NO	3	0.25	0.08	NO
38	172	NO	2	0.25	0.13	NO
39	163	NO	3	0.25	0.08	NO
40	201	NO	3	0.25	0.08	NO
TOTAL		**2**				**5**
MIN	**122.0**		**1.5**	**0.25**	**0.03**	
AVERAGE	**171.6**		**5.6**	**0.54**	**0.11**	
MAX	**205.0**		**20.5**	**2.25**	**0.38**	
RANGE	**58.0**		**19.0**	**2.00**	**0.35**	
S.DEV	**21.4**		**4.4**	**0.51**	**0.07**	

TOTAL MEASURED AREA:	**25 sq cm**
TOTAL STRIAE FOR MEASURED AREA:	**43**
AVERAGE STRIAE PER SQ CM:	**1.7**

STRIAE ORIENTATION HALF ROSE DIAGRAM

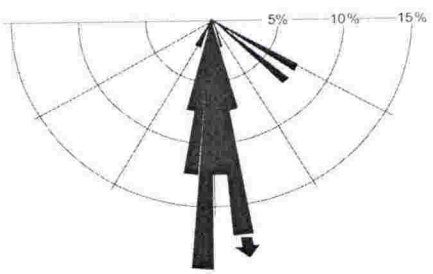

LOCATION: MURIMOTU FORMATION, NEW ZEALAND
COLLECTION : SELECTED DEBRIS-AVALANCHE STRIATED CLAST 3

LITHOLOGY:	ANDESITE
LENGTH OF LONG (A) AXIS:	190 mm
LENGTH OF INTERMEDIATE (B) AXIS:	115 mm
B/A AXIAL RATIO:	0.61
KRUMBEIN ROUNDNESS:	0.1

SQUARE No.	STRIAE DENSITY	
	STRIAE PER SQ	BACKGROUND STRIAE
1	3	NO
2	0	YES
3	1	YES
4	2	NO
5	1	YES
6	2	YES
7	2	YES
8	1	YES
9	2	NO
10	0	NO
11	0	NO
12	4	NO
13	1	YES
14	2	YES
15	2	YES
16	0	YES
17	2	YES
18	2	YES
19	0	NO
20	1	NO
21	2	NO
22	2	YES
23	1	YES
24	0	YES
25	0	NO
26	2	YES
27	1	NO
28	2	NO
29	1	NO
30	1	NO
31	3	NO
32	1	NO
33	2	NO
34	4	YES
35	3	YES
36	1	NO
37	0	NO
38	1	NO
39	2	YES
40	1	YES
41	1	NO
42	1	YES
43	1	YES
44	2	NO
45	2	NO
46	1	NO
47	3	NO
48	3	NO
49	3	NO
50	4	NO
51	3	NO
52	4	NO
53	2	NO
54	2	YES
55	2	NO
56	2	NO
57	1	YES
58	0	YES
59	0	YES
60	2	YES
61	6	YES
62	1	YES
63	1	YES
64	1	YES
65	1	NO
66	1	NO
67	1	YES
68	0	NO
69	1	NO
70	1	NO
71	1	NO
72	1	YES
73	0	YES
74	1	YES
75	0	YES
76	1	YES
77	3	YES
78	2	YES
79	4	YES
80	3	YES
81	1	YES
82	1	YES
83	3	YES
84	2	NO
85	2	YES
86	0	YES
87	1	YES
88	0	YES
89	0	NO
90	1	NO
91	1	NO
92	0	NO
93	2	YES
94	0	YES
95	0	YES
96	1	YES
97	2	YES
98	0	YES
99	1	YES
100	0	YES
%		**56**
MIN	**0**	
AVERAGE	**1.5**	
MAX	**6**	
% ≥ 1 STRIAE	**79**	

STRIAE No.	ORIENTATION FROM A-AXIS	CURVED STRIAE	LENGTH (MM)	WIDTH (MM)	WIDTH/ LENGTH RATIO	COMPOUND STRIATION
1	244	NO	8	1	0.13	NO
2	143	NO	10	1	0.10	NO
3	129	NO	6	0.25	0.04	NO
4	130	NO	7.5	1.5	0.20	NO
5	155	NO	9.5	1	0.11	NO
6	126	NO	5	0.25	0.05	NO
7	207	NO	2	0.5	0.25	NO
8	210	NO	1.5	0.5	0.33	NO
9	139	NO	3	0.25	0.08	NO
10	196	NO	4	0.75	0.19	NO
11	152	NO	11	2.25	0.20	NO
12	145	NO	7	1.25	0.18	**YES**
13	225	NO	10.5	0.25	0.02	NO
14	246	NO	6.5	1.25	0.19	NO
15	142	NO	6.5	0.75	0.12	NO
16	137	NO	13	1.25	0.10	NO
17	216	NO	4.5	0.5	0.11	NO
18	145	NO	16	**4**	0.25	**YES**
19	214	NO	2	0.5	0.25	NO
20	136	NO	4.5	0.75	0.17	NO
21	123	NO	15.5	4	0.26	**YES**
22	140	NO	3	0.75	0.25	NO
23	125	NO	13	0.25	0.02	NO
24	186	NO	8.5	0.5	0.06	NO
25	172	NO	21.5	4	0.19	**YES**
26	135	NO	7.5	2	0.27	NO
27	136	NO	3.5	0.75	0.21	NO
28	210	NO	2.5	0.5	0.20	NO
29	151	NO	3.5	0.5	0.14	NO
30		**YES(> 5°)**	17	2	0.12	NO
31	128	NO	10	0.75	0.08	NO
32	191	NO	3	0.25	0.08	NO
33	134	NO	3	0.5	0.17	NO
34	201	NO	5.5	0.5	0.09	NO
35	156	NO	7	1	0.14	NO
36	156	NO	5	0.25	0.05	NO
37	149	NO	7.5	0.25	0.03	NO
38	140	NO	2.5	0.25	0.10	NO
39	189	NO	2.5	0.5	0.20	NO
40	182	NO	12	1.25	0.10	NO
TOTAL		**0**				**4**
MIN	**123.0**		**1.5**	**0.25**	**0.02**	
AVERAGE	**165.2**		**7.3**	**1.01**	**0.15**	
MAX	**246.0**		**21.5**	**4.00**	**0.33**	
RANGE	**66.0**		**20.0**	**3.75**	**0.31**	
S.DEV	**36.0**		**4.7**	**1.00**	**0.08**	

TOTAL MEASURED AREA:	**25 sq cm**
TOTAL STRIAE FOR MEASURED AREA:	**40**
AVERAGE STRIAE PER SQ CM:	**1.6**

STRIAE ORIENTATION HALF ROSE DIAGRAM

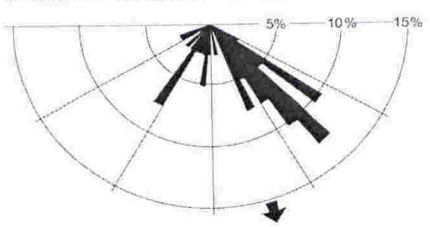

LOCATION , MURCHISON VALLEY SITE 4, NEW ZEALAND **COLLECTION : 50 CLASTS FROM ROCK FALL/SCREE DEPOSIT**

NO.	LITHOLOGY	AXIS LENGTH			AVERAGE	AXIAL RATIOS		SPHERICITY	KRUMBEIN ROUNDNESS	FACES	STRIAE	RA	C40
		A	B	C		C/A	B/A						
1	SANDSTONE	53	44	18	38.3	0.34	0.83	0.52	0.2	NO	NO	1	1
2	SANDSTONE	45	27	7	26.3	0.16	0.60	0.35	0.2	NO	NO	1	1
3	SANDSTONE	50	35	20	35.0	0.40	0.70	0.61	0.3	NO	NO	0	1
4	SANDSTONE	90	45	22	52.3	0.24	0.50	0.50	0.2	YES	NO	1	1
5	SANDSTONE	56	23	10	29.7	0.18	0.41	0.43	0.3	NO	NO	0	1
6	ARGILLITE	92	56	18	55.3	0.20	0.61	0.40	0.4	YES	NO	0	1
7	ARGILLITE	30	20	6	18.7	0.20	0.67	0.40	0.2	YES	YES	1	1
8	SANDSTONE	80	32	26	46.0	0.33	0.40	0.64	0.2	NO	NO	1	1
9	SANDSTONE	40	30	15	28.3	0.38	0.75	0.58	0.3	NO	NO	0	1
10	ARGILLITE	38	22	8	22.7	0.21	0.58	0.43	0.2	NO	YES	1	1
11	ARGILLITE	37	20	17	24.7	0.46	0.54	0.73	0.2	YES	YES	1	0
12	SANDSTONE	55	20	8	27.7	0.15	0.36	0.39	0.2	NO	NO	1	1
13	ARGILLITE	37	22	12	23.7	0.32	0.59	0.56	0.4	YES	YES	0	1
14	ARGILLITE	35	15	6	18.7	0.17	0.43	0.41	0.3	YES	YES	0	1
15	ARGILLITE	65	40	5	36.7	0.08	0.62	0.22	0.1	YES	YES	1	1
16	SANDSTONE	50	27	15	30.7	0.30	0.54	0.55	0.3	YES	NO	0	1
17	ARGILLITE	25	17	10	17.3	0.40	0.68	0.62	0.3	NO	NO	0	1
18	ARGILLITE	26	20	6	17.3	0.23	0.77	0.41	0.2	NO	NO	1	1
19	SANDSTONE	42	30	25	32.3	0.60	0.71	0.79	0.2	YES	NO	1	0
20	ARGILLITE	68	49	15	44.0	0.22	0.72	0.41	0.1	NO	YES	1	1
21	SANDSTONE	60	24	12	32.0	0.20	0.40	0.47	0.1	NO	NO	1	1
22	ARGILLITE	59	51	7	39.0	0.12	0.86	0.26	0.1	NO	YES	1	1
23	SANDSTONE	47	36	24	35.7	0.51	0.77	0.70	0.3	NO	NO	0	0
24	ARGILLITE	60	20	5	28.3	0.08	0.33	0.28	0.1	YES	YES	1	1
25	SANDSTONE	36	25	21	27.3	0.58	0.69	0.79	0.2	YES	NO	1	0
26	SANDSTONE	44	30	7	27.0	0.16	0.68	0.34	0.2	NO	NO	1	1
27	SANDSTONE	43	32	19	31.3	0.44	0.74	0.64	0.3	NO	NO	0	0
28	SANDSTONE	60	51	22	44.3	0.37	0.85	0.54	0.2	YES	NO	1	1
29	ARGILLITE	49	29	12	30.0	0.24	0.59	0.47	0.2	YES	YES	1	1
30	ARGILLITE	27	14	6	15.7	0.22	0.52	0.46	0.3	YES	YES	0	1
31	ARGILLITE	39	19	10	22.7	0.26	0.49	0.52	0.3	YES	YES	0	1
32	SANDSTONE	30	22	12	21.3	0.40	0.73	0.61	0.3	NO	NO	0	1
33	SANDSTONE	34	20	11	21.7	0.32	0.59	0.57	0.2	NO	NO	1	1
34	SANDSTONE	37	27	10	24.7	0.27	0.73	0.47	0.2	YES	NO	1	1
35	SANDSTONE	26	18	12	18.7	0.46	0.69	0.68	0.3	NO	NO	0	0
36	SANDSTONE	52	30	14	32.0	0.27	0.58	0.50	0.2	NO	NO	1	1
37	SANDSTONE	40	33	24	32.3	0.60	0.83	0.76	0.2	YES	NO	1	0
38	SANDSTONE	39	20	10	23.0	0.26	0.51	0.51	0.2	NO	NO	1	1
39	ARGILLITE	105	87	27	73.0	0.26	0.83	0.43	0.3	YES	YES	0	1
40	SANDSTONE	40	16	15	23.7	0.38	0.40	0.71	0.3	NO	NO	0	1
41	SANDSTONE	46	24	12	27.3	0.26	0.52	0.51	0.2	NO	NO	1	1
42	SANDSTONE	56	38	22	38.7	0.39	0.68	0.61	0.2	NO	NO	1	1
43	SANDSTONE	46	35	21	34.0	0.46	0.76	0.65	0.3	NO	NO	0	0
44	SANDSTONE	39	26	17	27.3	0.44	0.67	0.66	0.2	NO	NO	1	0
45	SANDSTONE	39	24	17	26.7	0.44	0.62	0.68	0.2	YES	NO	1	0
46	SANDSTONE	23	12	11	15.3	0.48	0.52	0.76	0.2	NO	NO	1	0
47	ARGILLITE	30	22	8	20.0	0.27	0.73	0.46	0.2	YES	NO	1	1
48	SANDSTONE	30	26	9	21.7	0.30	0.87	0.47	0.2	NO	NO	1	1
49	SANDSTONE	45	26	10	27.0	0.22	0.58	0.44	0.2	NO	NO	1	1
50	SANDSTONE	28	16	10	18.0	0.36	0.57	0.61	0.3	NO	NO	0	1
AVERAGE		**46.5**	**28.9**	**13.7**	**29.7**	**0.31**	**0.63**	**0.53**	**0.23**	NA	NA	NA	NA
TOTAL		NA	NA	NA	NA	NA	NA	NA	NA	**20**	**13**	**32**	**39**
%										**40**	**26**	**64**	**78**

SUMMARY STATISTICS

LITHOLOGY	NO. CLASTS	%	STRIAE	% STRI	FACES	% FACES
SANDSTONE	**33**	66.0	0	0.0	8	24.2
ARGILLITE	**17**	34.0	13	76.5	12	70.6
TOTAL	**50**	100.0	13		20	

ROUNDNESS	TOTAL CLAST	%	FACES	% FACES	STRIAE	% STRIAE	SANDSTONE	% SST	ARGILLITE	% ARG
0.1	5	10	2	40	4.0	80	2	6.1	4	23.5
0.2	28	56	11	39	4	14	20	60.6	6	35.3
0.3	15	30	5	33	4	27	11	33.3	5	29.4
0.4	2	4	2	0	1	50	0	0	2	11.8
0.5	0	0	0	0	0	0	0	0	0	0
0.6	0	0	0	0	0	0	0	0	0	0
0.7	0	0	0	0	0	0	0	0	0	0
0.8	0	0	0	0	0	0	0	0	0	0
0.9	0	0	0	0	0	0	0	0	0	0
TOTAL			20		13.0		33		17	

LOCATION: SITE MH4, MURCHISON VALLEY, NEW ZEALAND
COLLECTION : SELECTED ROCK-FALL STRIATED CLAST 1

LITHOLOGY:	ARGILLITE
LENGTH OF LONG (A) AXIS:	62 mm
LENGTH OF INTERMEDIATE (B) AXIS:	40 mm
B/A AXIAL RATIO:	0.65
KRUMBEIN ROUNDNESS:	0.1

SQUARE No.	STRIAE DENSITY	
	STRIAE PER SQ	BACKGROUND STRIAE
1	3	YES
2	3	YES
3	1	YES
4	2	YES
5	1	YES
6	1	YES
7	2	YES
8	1	YES
9	0	YES
10	0	YES
11	0	YES
12	0	YES
13	0	YES
14	1	YES
15	0	YES
16	0	YES
17	0	YES
18	1	YES
19	2	YES
20	2	YES
21	3	YES
22	1	YES
23	1	YES
24	1	YES
25	1	YES
26	1	YES
27	2	YES
28	1	YES
29	1	YES
30	3	YES
31	1	YES
32	0	YES
33	0	YES
34	0	YES
35	0	YES
36	2	YES
37	1	YES
38	5	YES
39	3	YES
40	1	YES
41	0	YES
42	1	YES
43	2	YES
44	3	YES
45	1	YES
46	0	YES
47	3	YES
48	1	YES
49	1	YES
50	1	YES
%		50
MIN	0	100%
AVERAGE	1.2	
MAX	5	
% ≥ 1 STRIAE	72	

STRIAE No.	ORIENTATION FROM A-AXIS	CURVED STRIAE	LENGTH (MM)	WIDTH (MM)	WIDTH/ LENGTH RATIO	COMPOUND STRIATION
1	200	NO	5.5	0.25	0.05	NO
2	213	NO	4	0.25	0.06	NO
3	148	NO	5	0.25	0.05	NO
4	270	NO	1.5	0.25	0.17	NO
5	270	NO	2.5	0.25	0.10	NO
6	185	YES	15	0.5	0.03	NO
7	275	NO	2.5	0.25	0.10	NO
8	270	NO	1.5	0.25	0.17	NO
9	227	YES	6.5	0.5	0.08	NO
10	157	NO	1.5	0.25	0.17	NO
11	160	NO	3	0.25	0.08	NO
12	271	NO	5	0.5	0.10	NO
13	252	NO	1.5	0.25	0.17	NO
14	255	NO	1.5	0.25	0.17	NO
15	253	NO	1.5	0.25	0.17	NO
16	216	NO	3	0.25	0.08	NO
17	258	NO	5	0.25	0.05	NO
18	262	NO	1.5	0.25	0.17	NO
19	134	NO	4.5	0.25	0.06	NO
20	271	NO	1.5	0.25	0.17	NO
21	153	NO	14.5	4	0.28	YES
22	150	NO	5	0.5	0.10	NO
23	145	NO	2.5	0.5	0.20	NO
24	245	NO	2	0.25	0.13	NO
25	242	NO	5	0.75	0.15	NO
26	115	YES	5	0.25	0.05	NO
27	160	NO	3	0.25	0.08	NO
28	110	NO	3	0.25	0.08	NO
29	230	NO	6	0.25	0.04	NO
30	205	NO	4	0.25	0.06	NO
31	200	NO	5.5	0.25	0.05	NO
32	153	NO	7	0.25	0.04	NO
33	130	NO	4	0.25	0.06	NO
34	132	NO	3.5	0.25	0.07	NO
35	210	NO	1.5	0.25	0.17	NO
TOTAL		3				1
MIN	110.0		1.5	0.25	0.03	
AVERAGE	203.6		4.1	0.41	0.11	
MAX	275.0		15.0	4.00	0.28	
RANGE	90.0		13.5	3.75	0.24	
S.DEV	53.9		3.1	0.64	0.06	

TOTAL MEASURED AREA:	12.5 sq cm
TOTAL STRIAE FOR MEASURED AREA:	35
AVERAGE STRIAE PER SQ CM:	2.8

STRIAE ORIENTATION HALF ROSE DIAGRAM

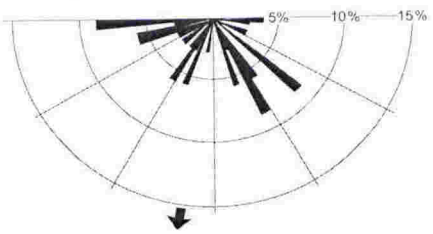

LOCATION: SITE MH4, MURCHISON VALLEY, NEW ZEALAND
COLLECTION : SELECTED ROCKFALL STRIATED CLAST 2

LITHOLOGY:	ARGILLITE
LENGTH OF LONG (A) AXIS:	77 mm
LENGTH OF INTERMEDIATE (B) AXIS:	56 mm
B/A AXIAL RATIO:	0.73
KRUMBEIN ROUNDNESS:	0.2

SQUARE No.	STRIAE DENSITY	
	STRIAE PER SQ	BACKGROUND STRIAE
1	0	YES
2	1	YES

STRIAE No.	ORIENTATION FROM A-AXIS	CURVED STRIAE	LENGTH (MM)	WIDTH (MM)	WIDTH/ LENGTH RATIO	COMPOUND STRIATION
1	120	NO	30.5	1	0.03	NO
2	197	NO	4	1	0.25	NO

LOCATION: SITE MH 4, MURCHISON VALLEY, NEW ZEALAND
COLLECTION : SELECTED ROCK-FALL STRIATED CLAST 3

LITHOLOGY:	ARGILLITE
LENGTH OF LONG (A) AXIS:	104 mm
LENGTH OF INTERMEDIATE (B) AXIS:	84 mm
B/A AXIAL RATIO:	0.81
KRUMBEIN ROUNDNESS:	0.2

SQUARE No.	STRIAE DENSITY	
	STRIAE PER SQ	BACKGROUND STRIAE
1	0	NO
2	0	NO
3	0	NO
4	0	NO
5	0	NO
6	1	NO
7	0	NO
8	1	NO
9	0	NO
10	2	YES
11	3	YES
12	0	NO
13	1	NO
14	0	NO
15	1	NO
16	0	NO
17	0	NO
18	1	NO
19	1	NO
20	0	NO
21	1	NO
22	0	NO
23	0	NO
24	0	NO
25	0	NO
26	1	NO
27	1	NO
28	1	NO
29	0	NO
30	1	YES
31	1	NO
32	0	NO
33	1	NO
34	2	NO
35	1	NO
36	0	NO
37	0	NO
38	0	NO
39	0	NO
40	1	NO
41	1	NO
42	0	NO
43	2	NO
44	0	NO
45	0	NO
46	0	NO
47	1	NO
48	0	NO
49	0	NO
50	0	NO
51	0	NO
52	0	YES
53	0	YES
54	2	YES
55	2	YES
56	2	YES
57	3	YES
58	3	YES
59	1	YES
60	1	NO
61	1	NO
62	1	NO
63	2	YES
64	3	YES
65	1	YES
66	4	YES
67	3	YES
68	0	YES
69	2	YES
70	1	NO
71	0	NO
72	1	NO
73	0	NO
74	1	NO
75	3	NO
76	1	NO
77	0	NO
78	1	NO
79	2	NO
80	2	NO
81	0	NO
82	0	NO
83	0	YES
84	1	YES
85	0	NO
86	0	NO
87	0	NO
88	1	NO
89	0	NO
90	0	NO
91	0	NO
92	1	NO
93	1	NO
94	2	NO
95	0	NO
96	0	NO
97	0	NO
98	0	NO
99	0	NO
100	0	NO
%		**20**
MIN	**0**	
AVERAGE	**0.8**	
MAX	**4**	
% ≥ 1 STRIAE	**49**	

STRIAE No.	ORIENTATION FROM A-AXIS	CURVED STRIAE	LENGTH (MM)	WIDTH (MM)	WIDTH/ LENGTH RATIO	COMPOUND STRIATION
1	198	NO	3.5	0.75	0.21	NO
2	241	NO	4.5	0.25	0.06	NO
3	248	NO	5	0.25	0.05	NO
4	251	NO	5.5	0.25	0.05	NO
5	242	**YES**	24.5	1.25	0.05	NO
6	97	NO	11.5	1	0.09	NO
7	142	NO	7.5	1.25	0.17	NO
8	185	NO	6	0.25	0.04	NO
9	246	NO	6.5	0.25	0.04	NO
10	269	NO	3.5	0.25	0.07	NO
11	250	NO	12.5	0.25	0.02	NO
12	197	NO	8.5	0.25	0.03	NO
13	239	NO	4.5	0.25	0.06	NO
14	237	NO	4	0.25	0.06	NO
15	237	NO	6.5	0.25	0.04	NO
16	165	NO	6	1.75	0.29	NO
17	185	NO	5.5	2	0.36	**YES**
18	214	NO	3.5	0.5	0.14	NO
19	246	NO	6	0.25	0.04	NO
20	185	NO	4.5	0.25	0.06	NO
21	230	NO	2	0.25	0.13	NO
22	241	NO	2.5	0.25	0.10	NO
23	245	NO	2.5	0.25	0.10	NO
24	153	NO	4.5	0.25	0.06	NO
25	107	NO	4.5	0.5	0.11	NO
26	233	NO	4.5	0.25	0.06	NO
27	174	NO	3.5	0.25	0.07	NO
28	127	NO	6	0.25	0.04	NO
29	136	NO	6.5	0.25	0.04	NO
30	117	NO	3	0.25	0.08	NO
31	260	NO	3	0.5	0.17	NO
32	259	NO	4	0.25	0.06	NO
33	91	NO	6.5	0.25	0.04	NO
34	117	NO	2.5	0.5	0.20	NO
TOTAL		1				1
MIN	**91.0**		**2.0**	**0.25**	**0.02**	
AVERAGE	**198.9**		**5.7**	**0.47**	**0.09**	
MAX	**269.0**		**24.5**	**2.00**	**0.36**	
RANGE	**89.0**		**22.5**	**1.75**	**0.34**	
S.DEV	**54.9**		**4.0**	**0.45**	**0.08**	

TOTAL MEASURED AREA:	**25 sq cm**
TOTAL STRIAE FOR MEASURED AREA:	**34**
AVERAGE STRIAE PER SQ CM:	**1.4**

STRIAE ORIENTATION HALF ROSE DIAGRAM

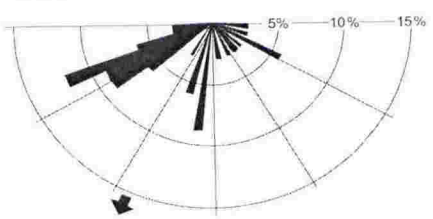

LOCATION: NGAPOTIKI THRUST, NEW ZEALAND **COLLECTION : 100 CLASTS FROM FAULT PLANE ABOVE BEACH BOULDERS**

NO.	LITHOLOGY	AXIS LENGTH			AVERAGE	AXIAL RATIOS		SPHERICITY	KRUMBEIN ROUNDNESS	FRACTURE	STRIAE	RA	C40
		A	B	C		C/A	B/A						
1	SANDSTONE	4.5	1.9	1.1	2.5	0.24	0.42	0.52	0.1	YES	NO	1	1
2	SANDSTONE	3.2	2.6	2.2	2.7	0.69	0.81	0.84	0.1	YES	NO	1	0
3	SANDSTONE	5.6	3.4	2.5	3.8	0.45	0.61	0.69	0.1	YES	NO	1	0
4	ARGILLITE	3.0	2.5	1.6	2.4	0.53	0.83	0.70	0.1	NO	NO	1	0
5	ARGILLITE	3.0	1.2	1.0	1.7	0.33	0.40	0.66	0.1	NO	NO	1	1
6	SANDSTONE	3.6	2.6	1.6	2.6	0.44	0.72	0.65	0.1	NO	NO	1	0
7	SANDSTONE	5.6	2.6	2.5	3.6	0.45	0.46	0.76	0.1	NO	NO	1	0
8	SANDSTONE	2.2	1.5	1.3	1.7	0.59	0.68	0.80	0.1	NO	NO	1	0
9	ARGILLITE	2.2	1.6	1.3	1.7	0.59	0.73	0.78	0.1	NO	NO	1	0
10	SANDSTONE	3.0	2.5	2.1	2.5	0.70	0.83	0.84	0.1	NO	NO	1	0
11	ARGILLITE	10.0	5.5	5.0	6.8	0.50	0.55	0.77	0.2	YES	YES	1	0
12	ARGILLITE	12.0	11.0	8.0	10.3	0.67	0.92	0.79	0.2	YES	YES	1	0
13	ARGILLITE	5.6	4.2	3.4	4.4	0.61	0.75	0.79	0.2	YES	NO	1	0
14	ARGILLITE	5.5	3.0	2.1	3.5	0.38	0.55	0.65	0.2	YES	NO	1	1
15	SANDSTONE	5.2	4.9	2.9	4.3	0.56	0.94	0.69	0.2	NO	NO	1	0
16	SANDSTONE	3.3	2.2	1.6	2.4	0.48	0.67	0.71	0.2	NO	YES	1	0
17	ARGILLITE	5.1	3.1	2.1	3.4	0.41	0.61	0.66	0.2	NO	NO	1	0
18	SANDSTONE	2.3	2.1	1.6	2.0	0.70	0.91	0.81	0.2	NO	NO	1	0
19	SANDSTONE	3.3	1.4	1.0	1.9	0.30	0.42	0.60	0.2	NO	NO	1	1
20	ARGILLITE	2.4	1.5	1.4	1.8	0.58	0.63	0.82	0.2	NO	NO	1	0
21	SANDSTONE	5.5	3.7	2.4	3.9	0.44	0.67	0.66	0.2	YES	NO	1	0
22	SANDSTONE	5.1	3.4	2.1	3.5	0.41	0.67	0.64	0.2	NO	YES	1	0
23	ARGILLITE	6.1	5.3	3.1	4.8	0.51	0.87	0.67	0.2	NO	NO	1	0
24	SANDSTONE	3.2	2.6	1.5	2.4	0.47	0.81	0.65	0.2	NO	NO	1	0
25	ARGILLITE	6.9	4.7	2.5	4.7	0.36	0.68	0.58	0.2	NO	NO	1	1
26	ARGILLITE	4.2	3.2	2.0	3.1	0.48	0.76	0.67	0.2	YES	NO	1	0
27	ARGILLITE	3.4	2.1	2.0	2.5	0.59	0.62	0.83	0.2	NO	NO	1	0
28	SANDSTONE	3.1	2.5	0.9	2.2	0.29	0.81	0.47	0.2	NO	NO	1	1
29	ARGILLITE	2.5	1.9	1.1	1.8	0.44	0.76	0.64	0.2	NO	YES	1	0
30	SANDSTONE	3.0	1.6	1.1	1.9	0.37	0.53	0.63	0.2	NO	NO	1	1
31	ARGILLITE	2.9	2.2	1.5	2.2	0.52	0.76	0.71	0.2	NO	NO	1	0
32	ARGILLITE	2.6	1.5	1.1	1.7	0.42	0.58	0.68	0.2	YES	NO	1	0
33	ARGILLITE	2.4	2.0	0.9	1.8	0.38	0.83	0.56	0.2	NO	YES	1	1
34	SANDSTONE	2.4	1.8	1.0	1.7	0.42	0.75	0.62	0.2	NO	NO	1	0
35	ARGILLITE	2.6	1.7	0.9	1.7	0.35	0.65	0.57	0.2	NO	NO	1	1
36	ARGILLITE	2.4	2.0	1.3	1.9	0.54	0.83	0.71	0.2	YES	NO	1	0
37	ARGILLITE	2.1	1.4	1.1	1.5	0.52	0.67	0.75	0.2	NO	NO	1	0
38	ARGILLITE	2.4	1.4	0.7	1.5	0.29	0.58	0.53	0.2	NO	NO	1	1
39	ARGILLITE	12.4	11.3	5.0	9.6	0.40	0.91	0.57	0.2	NO	YES	1	0
40	SANDSTONE	9.3	7.3	3.5	6.7	0.38	0.78	0.57	0.3	NO	YES	0	1
41	SANDSTONE	7.6	4.9	3.5	5.3	0.46	0.64	0.69	0.3	YES	YES	0	0
42	SANDSTONE	4.6	3.4	2.5	3.5	0.54	0.74	0.74	0.3	YES	YES	0	0
43	SANDSTONE	4.4	3.3	0.7	2.8	0.16	0.75	0.33	0.3	NO	NO	0	1
44	SANDSTONE	4.0	2.3	1.6	2.6	0.40	0.58	0.66	0.3	NO	NO	0	1
45	SANDSTONE	4.2	3.1	2.6	3.3	0.62	0.74	0.81	0.3	NO	NO	0	0
46	SANDSTONE	5.6	2.5	2.3	3.5	0.41	0.45	0.73	0.3	NO	NO	0	0
47	SANDSTONE	5.3	3.1	2.9	3.8	0.55	0.58	0.80	0.3	NO	NO	0	0
48	SANDSTONE	4.7	2.3	2.1	3.0	0.45	0.49	0.74	0.3	NO	NO	0	0
49	SANDSTONE	6.7	3.2	2.2	4.0	0.33	0.48	0.61	0.3	NO	YES	0	1
50	ARGILLITE	4.6	2.0	1.7	2.8	0.37	0.43	0.68	0.3	YES	YES	0	1
51	SANDSTONE	3.7	2.8	1.4	2.6	0.38	0.76	0.58	0.3	NO	NO	0	1
52	SANDSTONE	3.2	2.2	1.5	2.3	0.47	0.69	0.69	0.3	NO	NO	0	0
53	ARGILLITE	2.2	2.0	0.8	1.7	0.36	0.91	0.53	0.3	NO	NO	0	1
54	SANDSTONE	3.0	1.8	1.5	2.1	0.50	0.60	0.75	0.3	NO	NO	0	0
55	SANDSTONE	2.7	1.7	0.9	1.8	0.33	0.63	0.56	0.3	NO	NO	0	1
56	ARGILLITE	3.5	2.4	0.7	2.2	0.20	0.69	0.39	0.3	NO	YES	0	1
57	SANDSTONE	2.4	2.0	1.5	2.0	0.63	0.83	0.78	0.3	NO	NO	0	0
58	ARGILLITE	2.3	1.7	1.0	1.7	0.43	0.74	0.64	0.3	NO	NO	0	0
59	ARGILLITE	3.2	2.2	1.2	2.2	0.38	0.69	0.59	0.3	NO	NO	0	1
60	ARGILLITE	2.5	2.1	1.3	2.0	0.52	0.84	0.69	0.3	NO	NO	0	0
61	SANDSTONE	2.4	1.7	1.3	1.8	0.54	0.71	0.75	0.3	NO	NO	0	0
62	ARGILLITE	3.4	2.3	1.4	2.4	0.41	0.68	0.63	0.3	NO	NO	0	0
63	SANDSTONE	2.3	1.5	1.2	1.7	0.52	0.65	0.75	0.3	NO	NO	0	0
64	SANDSTONE	6.3	6.2	3.2	5.2	0.51	0.98	0.64	0.3	NO	NO	0	0
65	SANDSTONE	13.5	9.3	5.7	9.5	0.42	0.69	0.64	0.4	NO	YES	0	0
66	SANDSTONE	14.1	10.6	4.9	9.9	0.35	0.75	0.55	0.4	YES	YES	0	1
67	SANDSTONE	5.1	3.5	2.7	3.8	0.53	0.69	0.74	0.4	NO	NO	0	0
68	SANDSTONE	6.5	5.3	3.2	5.0	0.49	0.82	0.67	0.4	NO	NO	0	0
69	ARGILLITE	2.7	1.5	1.2	1.8	0.44	0.56	0.71	0.4	NO	NO	0	0
70	ARGILLITE	2.5	2.4	1.1	2.0	0.44	0.96	0.59	0.4	NO	NO	0	0
71	SANDSTONE	3.3	1.4	0.7	1.8	0.21	0.42	0.48	0.4	NO	NO	0	1
72	ARGILLITE	3.0	2.3	1.7	2.3	0.57	0.77	0.75	0.4	NO	NO	0	0
73	SANDSTONE	4.5	3.1	2.1	3.2	0.47	0.69	0.68	0.4	YES	NO	0	0
74	ARGILLITE	3.0	1.7	1.0	1.9	0.33	0.57	0.58	0.4	NO	NO	0	1
75	SANDSTONE	4.6	2.4	2.0	3.0	0.43	0.52	0.72	0.4	NO	NO	0	0
76	SANDSTONE	6.4	4.7	2.6	4.6	0.41	0.73	0.61	0.4	NO	NO	0	0
77	SANDSTONE	8.4	5.4	4.2	6.0	0.50	0.64	0.73	0.5	NO	NO	0	0
78	SANDSTONE	5.1	3.5	2.4	3.7	0.47	0.69	0.69	0.5	NO	NO	0	0
79	SANDSTONE	3.6	3.1	1.4	2.7	0.39	0.86	0.56	0.5	NO	NO	0	1
80	ARGILLITE	5.0	3.3	2.2	3.5	0.44	0.66	0.67	0.5	NO	YES	0	0
81	ARGILLITE	3.7	1.6	1.5	2.3	0.41	0.43	0.73	0.5	YES	YES	0	0
82	ARGILLITE	2.5	1.6	1.1	1.7	0.44	0.64	0.67	0.5	YES	NO	0	0
83	SANDSTONE	2.5	2.0	1.2	1.9	0.48	0.80	0.66	0.5	NO	NO	0	0
84	SANDSTONE	2.3	1.5	1.4	1.7	0.61	0.65	0.83	0.5	NO	NO	0	0
85	ARGILLITE	2.2	1.5	1.3	1.7	0.59	0.68	0.80	0.5	NO	NO	0	0
86	SANDSTONE	11.0	7.8	5.9	8.2	0.54	0.71	0.74	0.6	NO	YES	0	0
87	ARGILLITE	4.5	3.7	2.6	3.6	0.58	0.82	0.74	0.6	YES	NO	0	0
88	SANDSTONE	4.5	2.7	1.6	2.9	0.36	0.60	0.60	0.6	YES	NO	0	1
89	ARGILLITE	2.8	1.0	0.9	1.6	0.32	0.36	0.66	0.6	NO	NO	0	1
90	ARGILLITE	3.4	2.4	1.5	2.4	0.44	0.71	0.65	0.6	NO	NO	0	0
91	SANDSTONE	2.7	2.2	0.7	1.9	0.26	0.81	0.44	0.6	NO	NO	0	1
92	ARGILLITE	4.8	3.0	1.9	3.2	0.40	0.63	0.63	0.6	NO	YES	0	1
93	ARGILLITE	4.2	2.7	1.6	2.8	0.38	0.64	0.61	0.6	YES	YES	0	1
94	SANDSTONE	4.1	1.7	1.1	2.3	0.27	0.41	0.56	0.6	NO	YES	0	1
95	SANDSTONE	3.9	2.6	2.0	2.8	0.51	0.67	0.74	0.6	NO	YES	0	0
96	ARGILLITE	2.1	1.2	0.7	1.3	0.33	0.57	0.58	0.6	NO	NO	0	1
97	ARGILLITE	2.2	1.0	0.8	1.3	0.36	0.45	0.67	0.6	NO	NO	0	1
98	ARGILLITE	2.1	1.1	1.0	1.4	0.48	0.52	0.76	0.7	NO	NO	0	0
99	SANDSTONE	2.7	1.6	1.3	1.9	0.48	0.59	0.73	0.7	NO	NO	0	0
100	ARGILLITE	1.8	1.4	0.8	1.3	0.44	0.78	0.64	0.3	NO	NO	0	0
AVERAGE		**4.3**	**3.0**	**1.9**	**3.1**	**0.45**	**0.68**	**0.67**	**0.33**	NA	NA	NA	NA
TOTAL		NA	NA	NA	NA	NA	NA	NA	NA	**21**	**22**	**39**	**32**

SUMMARY STATISTICS

LITHOLOGY	NO.CLASTS	STRIAE	% STRI	FRAC	% FRAC
SANDSTONE	**54**	11	20	13	24
ARGILLITE	**46**	11	24	8	17
TOTAL	**100**	22		21	

ROUNDNESS	TOTAL CLAST	FRAC	% FRAC	STRIAE	% STRIAE	SANDSTONE	% SST	ARGILLITE	% ARG
0.1	10	3	30	0	0	7	13	3	7
0.2	29	8	28	7	24	10	19	19	41
0.3	26	3	12	6	23	18	33	8	17
0.4	12	2	17	2	17	8	15	4	9
0.5	9	2	22	2	22	5	9	4	9
0.6	12	3	25	5	42	5	9	7	15
0.7	2	0	0	0	0	1	2	1	2
0.8	0	0	0	0	0	0	0	0	0
0.9	0	0	0	0	0	0	0	0	0

LOCATION: WELLINGTON FAULT, NEW ZEALAND

COLLECTION : 100 CLASTS FROM FAULT PLANE

NO.	LITHOLOGY	AXIS LENGTH			AVERAGE	AXIAL RATIOS		SPHERICITY	KRUMBEIN ROUNDNESS	FRACTURE	STRIAE	RA	C40
		A	B	C		C/A	B/A						
1	SANDSTONE	3.2	1.6	1.4	2.1	0.44	0.50	0.73	0.1	NO	NO	1	0
2	SANDSTONE	5.3	4.7	3.1	4.4	0.58	0.89	0.73	0.1	YES	NO	1	0
3	SANDSTONE	3.4	2.4	2.2	2.7	0.65	0.71	0.84	0.1	YES	NO	1	0
4	SANDSTONE	4.5	2.7	2.5	3.2	0.56	0.60	0.80	0.1	NO	NO	1	0
5	SANDSTONE	3	2	1.8	2.3	0.60	0.67	0.82	0.1	NO	NO	1	0
6	SANDSTONE	3.6	3.2	1.9	2.9	0.53	0.89	0.68	0.2	NO	NO	1	0
7	SANDSTONE	3	2.8	1.4	2.4	0.47	0.93	0.62	0.2	NO	YES	1	0
8	SANDSTONE	3	2.2	1.7	2.3	0.57	0.73	0.76	0.2	NO	NO	1	0
9	SANDSTONE	2.8	2.5	1.5	2.3	0.54	0.89	0.69	0.2	YES	NO	1	0
10	SANDSTONE	5.2	4	2.2	3.8	0.42	0.77	0.62	0.2	YES	NO	1	0
11	ARGILLITE	6	4.7	3.3	4.7	0.55	0.78	0.73	0.2	NO	NO	1	0
12	SANDSTONE	2.7	2.1	1.6	2.1	0.59	0.78	0.77	0.2	YES	NO	1	0
13	SANDSTONE	3.5	3.3	1.7	2.8	0.49	0.94	0.63	0.2	NO	NO	1	0
14	ARGILLITE	3	1.8	1.6	2.1	0.53	0.60	0.78	0.2	NO	NO	1	0
15	SANDSTONE	3.3	2.1	1.6	2.3	0.48	0.64	0.72	0.2	YES	NO	1	0
16	ARGILLITE	3.1	2.7	1.6	2.5	0.52	0.87	0.68	0.2	NO	NO	1	0
17	SANDSTONE	4.3	3.3	3.2	3.6	0.74	0.77	0.90	0.3	NO	NO	0	0
18	ARGILLITE	2.1	2	1.1	1.7	0.52	0.95	0.66	0.3	NO	NO	0	0
19	ARGILLITE	2.5	1.7	1.2	1.8	0.48	0.68	0.70	0.3	NO	NO	0	0
20	SANDSTONE	3.2	2.1	2	2.4	0.63	0.66	0.84	0.3	NO	NO	0	0
21	ARGILLITE	2.8	2	1.5	2.1	0.54	0.71	0.74	0.3	NO	NO	0	0
22	SANDSTONE	7.2	3.6	3.4	4.7	0.47	0.50	0.77	0.3	NO	NO	0	0
23	SANDSTONE	3.8	2.9	1.6	2.8	0.42	0.76	0.62	0.3	YES	NO	0	0
24	SANDSTONE	5	3.5	3.1	3.9	0.62	0.70	0.82	0.3	NO	NO	0	0
25	SANDSTONE	2.4	1.6	1.3	1.8	0.54	0.67	0.76	0.3	NO	NO	0	0
26	SANDSTONE	2.2	1.6	1.4	1.7	0.64	0.73	0.82	0.3	NO	NO	0	0
27	SANDSTONE	2.8	2	1.3	2.0	0.46	0.71	0.67	0.3	NO	NO	0	0
28	SANDSTONE	3.8	2.3	1.4	2.5	0.37	0.61	0.61	0.3	NO	NO	0	1
29	SANDSTONE	2.2	1.5	1.3	1.7	0.59	0.68	0.80	0.3	NO	NO	0	0
30	SANDSTONE	5	3.9	2.5	3.8	0.50	0.78	0.69	0.3	NO	NO	0	0
31	SANDSTONE	6.4	5.8	3.5	5.2	0.55	0.91	0.69	0.3	NO	NO	0	0
32	ARGILLITE	4.4	3.4	2.5	3.4	0.57	0.77	0.75	0.3	NO	YES	0	0
33	SANDSTONE	4.6	3.2	2.3	3.4	0.50	0.70	0.71	0.4	NO	NO	0	0
34	SANDSTONE	4.7	2.5	1.6	2.9	0.34	0.53	0.60	0.4	YES	NO	0	1
35	SANDSTONE	6	4.6	3.1	4.6	0.52	0.77	0.71	0.4	NO	NO	0	0
36	SANDSTONE	4.4	3.3	2.1	3.3	0.48	0.75	0.67	0.4	NO	YES	0	0
37	SANDSTONE	3.6	2.7	2.5	2.9	0.69	0.75	0.86	0.4	NO	NO	0	0
38	SANDSTONE	4	3.3	2.9	3.4	0.73	0.83	0.86	0.4	NO	NO	0	0
39	SANDSTONE	5.2	3.1	3	3.8	0.58	0.60	0.83	0.4	YES	YES	0	0
40	ARGILLITE	2.8	2.4	1.6	2.3	0.57	0.86	0.73	0.5	YES	NO	0	0
41	SANDSTONE	3.6	2	1.4	2.3	0.39	0.56	0.65	0.5	NO	YES	0	1
42	SANDSTONE	3.8	2	1.8	2.5	0.47	0.53	0.75	0.5	YES	YES	0	0
43	SANDSTONE	3.7	2.2	1.5	2.5	0.41	0.59	0.65	0.5	NO	YES	0	0
44	SANDSTONE	4.6	3.5	2.2	3.4	0.48	0.76	0.67	0.5	NO	YES	0	0
45	SANDSTONE	3.8	2.6	1.6	2.7	0.42	0.68	0.64	0.5	NO	NO	0	0
46	SANDSTONE	3.6	2.4	2	2.7	0.56	0.67	0.78	0.5	NO	NO	0	0
47	SANDSTONE	2.8	2.1	1.5	2.1	0.54	0.75	0.73	0.5	NO	NO	0	0
48	SANDSTONE	4.8	3.5	2.1	3.5	0.44	0.73	0.64	0.5	NO	YES	0	0
49	ARGILLITE	3.9	3	1.8	2.9	0.46	0.77	0.65	0.5	NO	YES	0	0
50	SANDSTONE	3.2	2.6	1.3	2.4	0.41	0.81	0.59	0.5	NO	NO	0	0
51	SANDSTONE	3.2	2.2	1.6	2.3	0.50	0.69	0.72	0.5	NO	YES	0	0
52	SANDSTONE	3.2	2.7	1.8	2.6	0.56	0.84	0.72	0.5	NO	NO	0	0
53	SANDSTONE	5	3.6	3.4	4.0	0.68	0.72	0.86	0.5	NO	YES	0	0
54	SANDSTONE	8.6	6.7	4.6	6.6	0.53	0.78	0.72	0.5	NO	NO	0	0
55	ARGILLITE	6.2	4.5	3	4.6	0.48	0.73	0.69	0.5	YES	YES	0	0
56	SANDSTONE	7.8	7	3.1	6.0	0.40	0.90	0.56	0.6	NO	YES	0	1
57	ARGILLITE	7	4.5	3	4.8	0.43	0.64	0.66	0.6	NO	YES	0	0
58	SANDSTONE	4.2	3.1	1.6	3.0	0.38	0.74	0.58	0.6	NO	NO	0	1
59	SANDSTONE	3.8	3.4	2	3.1	0.53	0.89	0.68	0.6	NO	YES	0	0
60	ARGILLITE	4.7	3.3	2.1	3.4	0.45	0.70	0.66	0.6	NO	YES	0	0
61	SANDSTONE	3.1	2.4	2.3	2.6	0.74	0.77	0.89	0.6	NO	NO	0	0
62	SANDSTONE	4.8	3.1	1.6	3.2	0.33	0.65	0.56	0.6	NO	NO	0	1
63	SANDSTONE	3.2	2	1.1	2.1	0.34	0.63	0.58	0.6	NO	YES	0	1
64	SANDSTONE	4.1	3	2.5	3.2	0.61	0.73	0.80	0.6	NO	NO	0	0
65	ARGILLITE	2.6	1.8	1	1.8	0.38	0.69	0.60	0.6	NO	YES	0	1
66	SANDSTONE	5.1	4.1	2.2	3.8	0.43	0.80	0.62	0.6	YES	YES	0	0
67	SANDSTONE	2.1	1.8	1	1.6	0.48	0.86	0.64	0.6	NO	NO	0	0
68	ARGILLITE	3.8	2.5	2	2.8	0.53	0.66	0.75	0.6	NO	YES	0	0
69	SANDSTONE	3.1	2	1.5	2.2	0.48	0.65	0.72	0.6	NO	YES	0	0
70	SANDSTONE	4	3.7	2.1	3.3	0.53	0.93	0.67	0.6	NO	NO	0	0
71	SANDSTONE	4.6	3.5	2.8	3.6	0.61	0.76	0.79	0.6	NO	YES	0	0
72	ARGILLITE	6	4.6	3	4.5	0.50	0.77	0.69	0.6	NO	YES	0	0
73	ARGILLITE	5.2	3.5	2.4	3.7	0.46	0.67	0.68	0.6	NO	NO	0	0
74	SANDSTONE	2.8	2	1.8	2.2	0.64	0.71	0.83	0.6	NO	YES	0	0
75	ARGILLITE	9.2	7.6	4.4	7.1	0.48	0.83	0.65	0.6	NO	YES	0	0
76	ARGILLITE	5.6	3.5	3.1	4.1	0.55	0.63	0.79	0.7	NO	YES	0	0
77	SANDSTONE	4.2	3.2	1.6	3.0	0.38	0.76	0.58	0.7	NO	YES	0	1
78	SANDSTONE	3.5	2.5	1	2.3	0.29	0.71	0.49	0.7	NO	NO	0	1
79	SANDSTONE	8	7	3	6.0	0.38	0.88	0.55	0.7	NO	YES	0	1
80	ARGILLITE	3.1	2.4	1.2	2.2	0.39	0.77	0.58	0.7	NO	YES	0	1
81	ARGILLITE	3.3	2.9	1.5	2.6	0.45	0.88	0.62	0.7	NO	YES	0	0
82	SANDSTONE	3.5	1.7	1.5	2.2	0.43	0.49	0.73	0.7	NO	NO	0	0
83	ARGILLITE	3	1.3	1	1.8	0.33	0.43	0.64	0.7	NO	YES	0	1
84	SANDSTONE	6	5.5	2.5	4.7	0.42	0.92	0.58	0.7	NO	NO	0	0
85	SANDSTONE	3.2	3	1.2	2.5	0.38	0.94	0.53	0.7	NO	YES	0	1
86	ARGILLITE	4.4	2.8	1.8	3.0	0.41	0.64	0.64	0.7	NO	YES	0	0
87	SANDSTONE	3.1	2.7	1.1	2.3	0.35	0.87	0.53	0.7	YES	YES	0	1
88	SANDSTONE	3.9	2.9	2.8	3.2	0.72	0.74	0.89	0.7	YES	YES	0	0
89	ARGILLITE	3.5	2.1	1.8	2.5	0.51	0.60	0.76	0.7	NO	YES	0	0
90	ARGILLITE	4.4	1.8	1	2.4	0.23	0.41	0.51	0.7	NO	NO	0	1
91	SANDSTONE	3.3	1.8	1.5	2.2	0.45	0.55	0.73	0.7	NO	NO	0	0
92	ARGILLITE	3.1	2	1	2.0	0.32	0.65	0.55	0.7	NO	YES	0	1
93	SANDSTONE	2.7	2.1	1	1.9	0.37	0.78	0.56	0.7	NO	YES	0	1
94	SANDSTONE	2.7	1.5	1.3	1.8	0.48	0.56	0.75	0.7	NO	NO	0	0
95	SANDSTONE	2.8	2.5	1	2.1	0.36	0.89	0.53	0.7	NO	YES	0	1
96	SANDSTONE	3.4	2	1.2	2.2	0.35	0.59	0.60	0.7	NO	YES	0	1
97	SANDSTONE	2.9	1.7	1.5	2.0	0.52	0.59	0.77	0.7	NO	YES	0	0
98	SANDSTONE	3.2	2.7	1	2.3	0.31	0.84	0.49	0.7	NO	NO	0	1
99	SANDSTONE	3.1	2.1	1.5	2.2	0.48	0.68	0.70	0.7	NO	NO	0	0
100	ARGILLITE	3	2.4	1	2.1	0.33	0.80	0.52	0.7	NO	YES	0	1
AVERAGE		4.0	2.9	2.0	3.0	0.49	0.73	0.69	0.48	NA	NA	NA	NA
TOTAL		NA	NA	NA	NA	NA	NA	NA	NA	15	43	16	22

SUMMARY STATISTICS

LITHOLOGY	NO.CLASTS	STRIAE	% STRI	FRAC	% FRAC
SANDSTONE	74	26	35	12	16
ARGILLITE	26	17	65	3	12
TOTAL	100	43		15	

ROUNDNESS	TOTAL CLAST	FRAC	% FRAC	STRIAE	% STRIAE	SANDSTONE	% SST	ARGILLITE	% ARG
0.1	5	2	40	0	0	5	7	0	0.0
0.2	11	4	36	1	9	8	11	3	12
0.3	16	1	6	1	6	12	16	4	15
0.4	7	2	29	2	29	7	9	0	0
0.5	16	3	19	9	56	13	18	3	12
0.6	20	1	5	13	65	13	18	7	27
0.7	25	2	8	17	68	16	22	9	35
0.8	0	0	0	0	0	0	0	0	0
0.9	0	0	0	0	0	0	0	0	0

LOCATION: WELLINGTON FAULT, NEW ZEALAND
COLLECTION : SELECTED STRIATED CLAST 1

LITHOLOGY:	SANDSTONE
LENGTH OF LONG (A) AXIS:	224 mm
LENGTH OF INTERMEDIATE (B) AXIS:	146 mm
B/A AXIAL RATIO:	0.65
KRUMBEIN ROUNDNESS:	0.5

SQUARE No.	STRIAE DENSITY	
	STRIAE PER SQ	BACKGROUND STRIAE
1	1	YES
2	1	YES
3	2	YES
4	2	YES
5	2	YES
6	1	NO
7	1	YES
8	1	YES
9	2	YES
10	1	YES
11	3	YES
12	2	NO
13	2	NO
14	2	NO
15	2	NO
16	0	NO
17	2	YES
18	3	YES
19	3	YES
20	3	YES
21	1	YES
22	2	YES
23	1	YES
24	1	YES
25	1	NO
26	2	NO
27	3	NO
28	2	YES
29	2	YES
30	0	YES
31	0	YES
32	1	YES
33	1	NO
34	3	NO
35	2	YES
36	2	NO
37	1	NO
38	2	NO
39	2	NO
40	2	NO
41	1	NO
42	1	NO
43	0	NO
44	1	NO
45	2	NO
46	1	YES
47	1	NO
48	2	NO
49	1	NO
50	0	YES
51	1	NO
52	1	NO
53	0	NO
54	1	NO
55	2	YES
56	1	NO
57	2	NO
58	2	NO
59	2	NO
60	0	NO
61	0	NO
62	2	NO
63	1	NO
64	0	YES
65	1	YES
66	1	YES
67	1	NO
68	1	NO
69	1	NO
70	0	NO
71	1	NO
72	1	NO
73	1	NO
74	1	NO
75	0	YES
76	0	YES
77	0	YES
78	0	NO
79	1	NO
80	1	NO
81	1	NO
82	0	NO
83	2	NO
84	1	NO
85	0	NO
86	2	YES
87	3	NO
88	1	NO
89	0	YES
90	0	YES
91	0	YES
92	0	YES
93	2	YES
94	3	YES
95	1	NO
96	1	NO
97	1	NO
98	1	NO
99	0	NO
100	0	NO
%		40
MIN	0	
AVERAGE	1.2	
MAX	3	
% ≥ 1 STRIAE	78	

STRIAE No.	ORIENTATION FROM A-AXIS	CURVED STRIAE	LENGTH (MM)	WIDTH (MM)	WIDTH/ LENGTH RATIO	COMPOUND STRIATION
1	236	NO	5	1	0.200	NO
2	236	NO	5	1	0.200	NO
3	221	NO	41	3	0.073	NO
4	218	NO	30	0.75	0.025	NO
5	161	NO	9	1	0.111	NO
6	152	NO	11	1.5	0.136	NO
7	135	NO	35	5	0.143	YES
8	156	NO	24	0.5	0.021	NO
9	110	NO	13	0.5	0.038	NO
10		YES(> 5°)	86	3	0.035	YES
11	136	NO	26	3	0.115	NO
12	169	NO	15	0.75	0.050	NO
13	180	NO	25	1.5	0.060	NO
14	140	NO	49	2.5	0.051	NO
15	173	NO	19	1.75	0.092	NO
16	107	NO	17	1.25	0.074	NO
17	100	NO	17	1	0.059	NO
18	175	NO	20	5	0.250	NO
19	150	NO	17	1	0.059	NO
20	155	NO	31	1.25	0.040	NO
21	232	NO	11	1.5	0.136	NO
22	145	NO	60	3	0.050	YES
23	160	NO	21	1	0.048	NO
24	141	NO	5	1	0.200	NO
25	136	NO	6	3	0.500	YES
26	243	NO	15	0.75	0.050	NO
27	240	NO	7	0.5	0.071	NO
28	150	NO	6	2	0.333	NO
29	141	NO	4	1.5	0.375	NO
30	205	NO	15	1	0.067	NO
31	147	YES	15	0.25	0.017	NO
32	154	NO	6	1.25	0.208	NO
33	171	NO	12	3	0.250	NO
34	187	NO	20	1.5	0.075	NO
TOTAL		1				4
MIN	100.00		4.00	0.25	0.017	
AVERAGE	168.55		20.53	1.69	0.124	
MAX	243.00		86.00	5.00	0.500	
RANGE	80.00		82.00	4.75	0.483	
S.DEV	39.92		17.38	1.19	0.112	

TOTAL MEASURED AREA:	100 sq cm
TOTAL STRIAE FOR MEASURED AREA:	45
AVERAGE STRIAE PER SQ CM:	0.45

STRIAE ORIENTATION HALF ROSE DIAGRAM

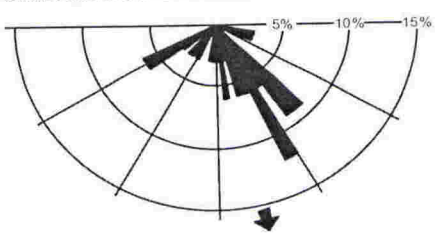

LOCATION: WELLINGTON FAULT, NEW ZEALAND
COLLECTION : SELECTED STRIATED CLAST 2

LITHOLOGY:	SANDSTONE
LENGTH OF LONG (A) AXIS:	155 mm
LENGTH OF INTERMEDIATE (B) AXIS:	79 mm
B/A AXIAL RATIO:	0.51
KRUMBEIN ROUNDNESS:	0.3

SQUARE No.	STRIAE DENSITY	
	STRIAE PER SQ	BACKGROUND STRIAE
1	0	YES
2	2	YES
3	0	NO
4	0	NO
5	0	NO
6	1	NO
7	0	NO
8	1	NO
9	1	NO
10	1	NO
11	0	YES
12	1	YES
13	1	YES
14	2	YES
15	1	NO
16	0	NO
17	3	YES
18	0	NO
19	1	YES
20	1	YES
21	1	YES
22	1	NO
23	1	NO
24	2	NO
25	1	YES
26	1	YES
27	0	YES
28	2	NO
29	0	NO
30	0	NO
31	0	NO
32	0	NO
33	0	NO
34	0	NO
35	0	NO
36	0	NO
37	0	NO
38	0	YES
39	2	YES
40	0	YES
41	0	YES
42	0	NO
43	2	NO
44	0	NO
45	2	YES
46	3	YES
47	2	YES
48	1	YES
49	0	YES
50	3	YES
51	1	YES
52	1	YES
53	1	YES
54	1	YES
55	2	YES
56	1	YES
57	1	YES
58	2	YES
59	1	YES
60	0	YES
61	0	YES
62	0	YES
63	0	YES
64	0	YES
65	1	YES
66	1	YES
67	1	YES
68	0	YES
69	0	YES
70	0	YES
71	0	YES
72	0	YES
73	1	NO
74	0	NO
75	1	YES
76	0	YES
77	1	NO
78	2	NO
79	2	YES
80	2	YES
81	1	YES
82	0	NO
83	0	NO
84	0	NO
85	1	NO
86	1	NO
87	0	NO
88	1	NO
89	1	NO
90	0	NO
91	2	NO
92	1	NO
93	1	NO
94	0	YES
95	1	YES
96	0	YES
97	1	YES
98	1	YES
99	1	YES
100	0	NO
%		56
MIN	0	
AVERAGE	0.8	
MAX	3	
% ≥ 1 STRIAE	56	

STRIAE No.	ORIENTATION FROM A-AXIS	CURVED STRIAE	LENGTH (MM)	WIDTH (MM)	WIDTH/ LENGTH RATIO	COMPOUND STRIATION
1	244	NO	5.5	1.25	0.227	NO
2	240	NO	11.5	1.5	0.130	NO
3	95	NO	9.5	2.5	0.263	NO
4	265	NO	16.5	2	0.121	NO
5	266	NO	13.5	1	0.074	NO
6	267	NO	14	0.25	0.018	NO
7	93	NO	9	0.5	0.056	NO
8	165	NO	18.5	3	0.162	YES
9	239	NO	5	0.5	0.100	NO
10	253	NO	3.5	0.5	0.143	NO
11	268	NO	2.5	0.5	0.200	NO
12	178	NO	22.5	1.25	0.056	NO
13	252	NO	3.5	0.5	0.143	NO
14	234	NO	6.5	0.5	0.077	NO
15	265	NO	12	0.75	0.063	NO
16	183	NO	12	1.25	0.104	NO
17	186	NO	6	0.25	0.042	NO
18	133	NO	24	0.75	0.031	NO
19	180	NO	4	0.5	0.125	NO
20	195	NO	3	0.75	0.250	NO
21		YES(> 5°)	9	0.25	0.028	NO
22	222	NO	10.5	0.25	0.024	NO
23	179	NO	3.5	0.5	0.143	NO
24	155	NO	4.5	0.75	0.167	NO
25	237	NO	4.5	1	0.222	NO
26	165	NO	3.5	0.25	0.071	NO
27	166	NO	12	2	0.167	NO
28	152	NO	7	1.5	0.214	NO
29	180	NO	4	0.25	0.063	NO
30	200	NO	3.5	0.25	0.071	NO
31	209	NO	4.5	0.25	0.056	NO
32	202	NO	5.5	1	0.182	NO
33	137	NO	4	0.5	0.125	NO
34	240	NO	2.5	0.25	0.100	NO
35	156	NO	7.5	0.25	0.033	NO
36	135	NO	4	0.25	0.063	NO
TOTAL		0				1
MIN	93.00		2.50	0.25	0.018	
AVERAGE	198.17		8.13	0.82	0.114	
MAX	268.00		24.00	3.00	0.263	
RANGE	88.00		21.50	2.75	0.245	
S.DEV	49.80		5.61	0.69	0.069	

TOTAL MEASURED AREA:	25 sq cm
TOTAL STRIAE FOR MEASURED AREA:	33
AVERAGE STRIAE PER SQ CM:	1.3

STRIAE ORIENTATION HALF ROSE DIAGRAM

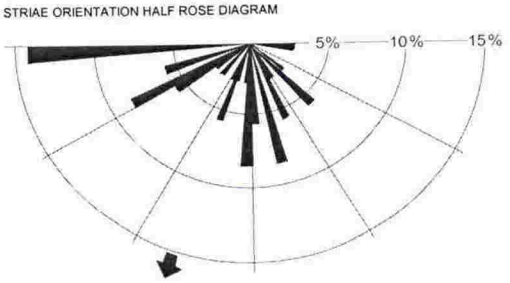

LOCATION: WELLINGTON FAULT, NEW ZEALAND
COLLECTION : SELECTED STRIATED CLAST 3

LITHOLOGY:	ARGILLITE
LENGTH OF LONG (A) AXIS:	45 mm
LENGTH OF INTERMEDIATE (B) AXIS:	36 mm
B/A AXIAL RATIO:	0.80
KRUMBEIN ROUNDNESS:	0.3

SQUARE No.	STRIAE DENSITY	
	STRIAE PER SQ	BACKGROUND STRIAE
1	1	YES
2	1	YES
3	0	YES
4	1	YES
5	1	YES
6	0	YES
7	1	YES
8	1	YES
9	3	YES
10	2	YES
11	0	YES
12	0	YES
13	1	YES
14	3	YES
15	1	YES
16	3	YES
17	2	YES
18	1	YES
19	0	YES
20	1	YES
21	1	YES
22	1	YES
23	0	YES
24	0	YES
25	0	YES
26	1	YES
27	4	YES
28	1	YES
29	1	YES
30	0	YES
31	0	YES
32	0	YES
33	1	YES
34	3	YES
35	1	YES
36	0	YES
TOTAL		36
MIN	0	100%
AVERAGE	1.0	
MAX	4	
% ≥ 1 STRIAE	67	

STRIAE No.	ORIENTATION FROM A-AXIS	CURVED STRIAE	LENGTH (MM)	WIDTH (MM)	WIDTH/ LENGTH RATIO	COMPOUND STRIATION
1	180	NO	3	0.25	0.083	NO
2	163	NO	3	0.25	0.083	NO
3	110	NO	2	0.5	0.250	NO
4	149	NO	3.5	1	0.286	NO
5	151	NO	5	0.5	0.100	NO
6	141	YES	13.5	1	0.074	NO
7	229	NO	5.5	0.25	0.045	NO
8	227	NO	2	1	0.500	YES
9		YES(> 5°)	8.5	0.5	0.059	NO
10	161	NO	8.5	1.5	0.176	NO
11	168	NO	4	0.25	0.063	NO
12	129	NO	5	0.5	0.100	NO
13	156	NO	4.5	0.5	0.111	NO
14	191	NO	3	0.5	0.167	NO
15	171	NO	2.5	0.5	0.200	NO
TOTAL		1				1
MIN	110.00		2.00	0.25	0.045	
AVERAGE	166.14		4.90	0.60	0.153	
MAX	229.00		13.50	1.50	0.500	
RANGE	70.00		11.50	1.25	0.455	
S.DEV	33.19		3.12	0.36	0.120	

TOTAL MEASURED AREA:	9 sq cm
TOTAL STRIAE FOR MEASURED AREA:	20
AVERAGE STRIAE PER SQ CM:	2.2

STRIAE ORIENTATION HALF ROSE DIAGRAM

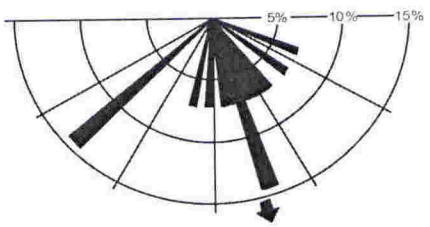

LOCATION: NGAPOTIKI FAULT, NEW ZEALAND
COLLECTION : SELECTED STRIATED CLAST 4

LITHOLOGY:	ARGILLITE
LENGTH OF LONG (A) AXIS:	100 mm
LENGTH OF INTERMEDIATE (B) AXIS:	74 mm
B/A AXIAL RATIO:	0.74
KRUMBEIN ROUNDNESS:	0.2

SQUARE No.	STRIAE DENSITY	
	STRIAE PER SQ	BACKGROUND STRIAE
1	0	NO
2	1	NO
3	1	YES
4	2	YES
5	3	YES
6	3	YES
7	1	YES
8	1	YES
9	0	NO
10	1	NO
11	0	NO
12	0	NO
13	0	NO
14	3	YES
15	1	YES
16	2	YES
17	0	YES
18	0	YES
19	0	YES
20	1	YES
21	0	YES
22	2	YES
23	0	NO
24	0	NO
25	1	NO
26	2	YES
27	4	YES
28	2	YES
29	1	YES
30	1	YES
31	2	YES
32	2	YES
33	4	YES
34	3	YES
35	0	NO
36	0	NO
37	1	YES
38	0	NO
39	0	NO
40	0	NO
41	0	NO
42	0	NO
43	2	YES
44	2	YES
45	1	YES
46	2	YES
47	1	YES
48	1	YES
49	0	YES
50	0	NO
51	0	NO
52	0	NO
53	0	NO
54	1	NO
55	2	NO
56	2	YES
57	2	YES
58	2	YES
59	1	YES
60	0	YES
61	0	YES
62	0	NO
63	0	NO
64	0	NO
65	0	NO
66	0	NO
67	0	NO
68	0	NN
69	0	NO
70	2	NO
71	1	NO
72	2	YES
73	0	YES
74	0	YES
75	0	YES
76	0	YES
77	0	YES
78	0	NO
79	0	NO
80	0	NO
81	0	NO
82	0	NO
83	2	NO
84	2	NO
85	2	YES
86	1	YES
87	1	YES
88	0	YES
89	0	YES
90	0	NO
91	0	NO
92	0	NO
93	0	NO
94	0	NO
95	0	NO
96	0	NO
97	0	NO
98	0	YES
99	2	YES
100	0	YES
%		**52**
MIN	**0**	
AVERAGE	**0.8**	
MAX	**4**	
% ≥ 1 STRIAE	**45**	

STRIAE No.	ORIENTATION FROM A-AXIS	CURVED STRIAE	LENGTH (MM)	WIDTH (MM)	WIDTH/ LENGTH RATIO	COMPOUND STRIATION
1	185	NO	12	1.5	0.125	NO
2	136	NO	4.5	0.25	0.056	NO
3	135	NO	2.5	0.25	0.100	NO
4	200	NO	5	0.25	0.050	NO
5	189	NO	15	1.5	0.100	NO
6	180	NO	4	0.5	0.125	NO
7	180	NO	14.5	0.75	0.052	NO
8	181	NO	3.5	0.25	0.071	NO
9	181	NO	2.5	0.5	0.200	NO
10	180	NO	5.5	1.5	0.273	NO
11	171	YES	8.5	0.25	0.029	NO
12	194	NO	4	0.25	0.063	NO
13	181	NO	2	0.25	0.125	NO
14	186	YES	7.5	0.25	0.033	NO
15	167	NO	3.5	0.25	0.071	NO
16	205	NO	6	0.5	0.083	NO
17	180	NO	4.5	1.5	0.333	NO
18	179	NO	9	1.75	0.194	NO
19	188	NO	19	2	0.105	NO
20	185	NO	13.5	1	0.074	NO
21	186	NO	11	0.75	0.068	NO
22	180	NO	3.5	0.25	0.071	NO
23	142	NO	5	0.5	0.100	NO
24	126	NO	4.5	0.25	0.056	NO
25	185	NO	6.5	2	0.308	NO
26	180	NO	4.5	1.5	0.333	NO
27	185	NO	3	0.5	0.167	NO
28	181	NO	6.5	1	0.154	NO
29	186	NO	14.5	1.5	0.103	NO
30	181	NO	4.5	0.75	0.167	NO
31	170	NO	3	0.5	0.167	NO
32	176	NO	5	1.25	0.250	NO
33	180	NO	7	0.25	0.036	NO
34	178	NO	5	0.25	0.050	NO
35	182	NO	5	0.25	0.050	NO
TOTAL		**2**				**0**
MIN	**126.00**		**2.00**	**0.25**	**0.029**	
AVERAGE	**177.17**		**6.71**	**0.76**	**0.124**	
MAX	**205.00**		**19.00**	**2.00**	**0.333**	
RANGE	**54.00**		**17.00**	**1.75**	**0.304**	
S.DEV	**17.15**		**4.25**	**0.59**	**0.086**	

TOTAL MEASURED AREA:	**25 sq cm**
TOTAL STRIAE FOR MEASURED AREA:	**45**
AVERAGE STRIAE PER SQ CM:	**1.8**

STRIAE ORIENTATION HALF ROSE DIAGRAM

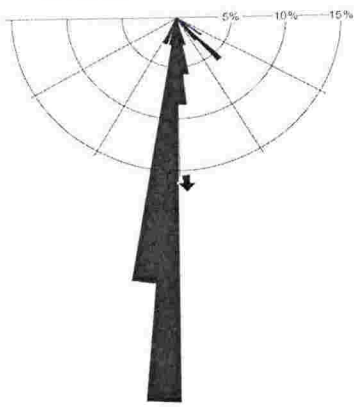

APPENDIX 7

CAPE ROBERTS PROJECT, ANTARCTICA

Introduction

The Cape Roberts Project (CRP) was a multinational co-operative drilling programme that recovered almost 1500 m of Cenozoic strata from three drillholes (CRP-1, CRP-2/2A and CRP-3) on the western margin of the Victoria Land Basin, Antarctica. One of the primary goals of the project was to obtain a palaeoclimatic record of the Ross Sea region to better understand ice sheet history. The recovered strata represent sediments from 34 Ma to 17 Ma, overlain by a thin Pleistocene sequence. The lower 300 m of the CRP-3 core shows mostly shallow marine sandstone deposition, with little indication of a glacial influence. However, a repeated glacial advance and retreat signal is increasingly clear higher in the core, with the onset of direct glacial deposition becoming well-developed in the upper part of CRP-3 and the overlying CRP-2/2A core (Cape Roberts Science Team, 1999; 2000). These cycles are thought to represent the sedimentary response to orbitally induced oscillations in the East Antarctic Ice Sheet (Naish et al., 2001b). Overall the core documents climatic deterioration from cool temperate conditions and the initiation of glaciation in the earliest Oligocene, to increasingly colder conditions through the early Miocene (Raine and Askin, 2001) and a subsequent change to permanent polar conditions seen today.

The cores were divided into several recurrent lithofacies from which process and palaeoenvironmental interpretations were made and depositional models developed. This provided the basis for recognising the depositional cyclicity and a sequence stratigraphy interpretation, which divided the cores into unconformity–bound depositional sequences. These are thought to represent the accumulation of sediment

during cycles of glacier advance and retreat (Fielding et al., 2001, Naish et al., 2001a). The sequences are typically bounded by sharp erosional surfaces that represent glacial erosion surfaces, either from glacier movement across the seafloor during glacial lowstand or the more distal effects of glacier advance. Coarse-grained units such as diamictite or conglomerate reflecting ice contact or glacier proximal deposition, usually overlie the erosional surfaces. These in turn are usually overlain by generally upward fining successions of various finer grained facies representing marine deposition during sea level transgression/ highstand and glacial retreat. Understanding the origin of the coarse-grained units is critical to the overall interpretation. The origin of abrasion features on the clasts was considered to be of particular value in estimating proximity to glacier ice.

Clast studies

Clast shape and fabric studies were carried out on whole-round core samples from the coarse-grained units from the Cape Roberts cores using the method outlined in Chapter 2. In addition, an apparatus and method of measuring three-dimensional fabric from drillcore was devised (see Chapter 2). The results were combined with the distribution of striated clast and out-sized clasts from finer-grained facies to assess the contribution and character of glacially derived sediment. The results are documented in Talarico et al. (2000) and Atkins (2001) and are not repeated here. However, a brief comparison with the clast shape and striae data from the modern Mackay Glacier is presented here because the Mackay Valley and Glacier have existed throughout most of the Cenozoic and therefore is likely to have been the primary sediment source for the strata at Cape Roberts (Powell et al., 2000)

The coarse-grained facies were divided into diamictite, conglomerate and pebbly sandstone facies. The diamictites were interpreted as representing either subglacial deposits or debris flows with iceberg rainout. Conglomerates were interpreted to represent fluvial discharges or mass flows that had redeposited fluvial gravels. Pebbly

sandstones were interpreted as marine-deposited sands with iceberg rainout introducing clasts (Cape Roberts Science Team, 2000).

Shape and roundness data for CRP-2/2A and the modern Mackay Glacier samples from overturned icebergs are summarised on RA-C_{40} diagram in Figure 1. There is poor distinction between the different facies on the basis of clast form and roundness (Atkins, 2001). Samples described as diamictites do not consistently fall within the subglacial field and conglomerates do not plot near the glaciofluvial field. Most of the samples from CRP-2/2A show less blockiness and angularity than the modern Mackay Glacier clasts suggesting that the modern samples have experienced less basal glacial transport than clasts in the cores.

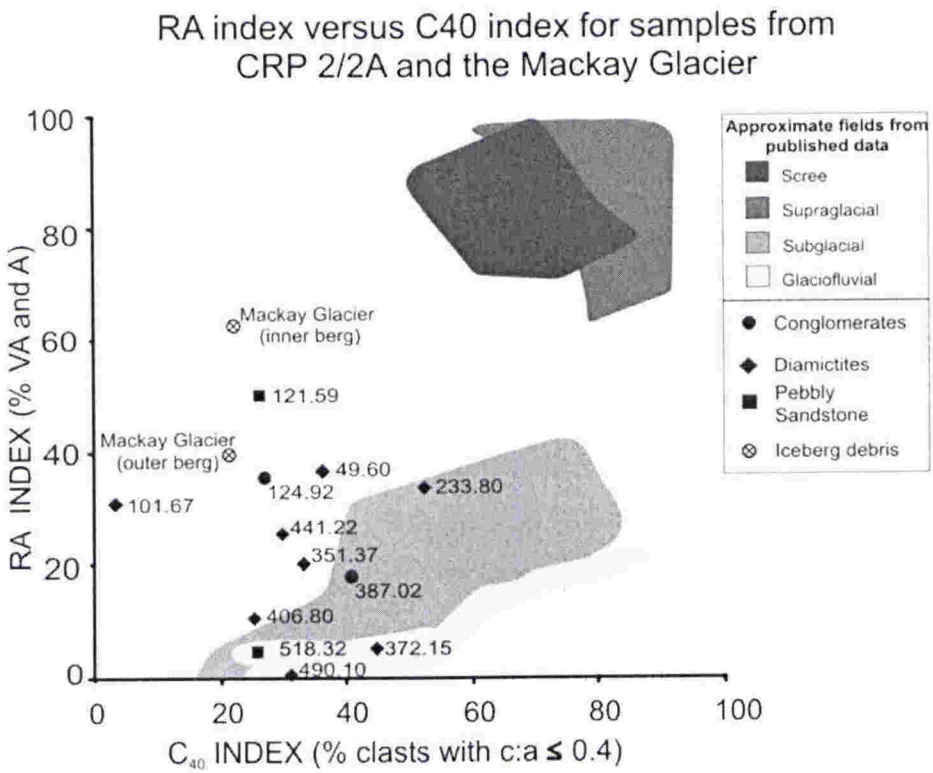

Figure 1 RA-C_{40} diagram of Benn and Ballantyne (1994), showing values from all CRP-2/2A and the Mackay Glacier. CRP-2/2A sample numbers refer to depth below sea floor. RA index is the percentage of angular and very angular clasts and C_{40} index is the percentage of clasts with a c:a axial ratio of ≤ 0.4. Shaded fields are from published data in Benn and Ballantyne (1994) and Bennett et al. (1997).

The CRP-2/2A samples that plot closest to the modern samples are all from above 125 metres below sea-floor (mbsf) within the Miocene strata. This possibly indicates there was a change toward blockier, less modified clast shapes as the climate became increasingly cooler and the Mackay Glacier changed from temperate to polythermal. This is a tentative interpretation because there are only a small number of samples considered and it may simply indicate that the upper few samples were sourced from debris that was transported higher in the glacier and received only limited basal abrasion.

Nine of the ten samples from CRP-3 were classified as conglomerates and all plot much lower on the diagram. This reflects the overall slightly higher roundness and lack of angular clasts in these samples. Several samples plot within the subglacial field, with others plotting lower in the glaciofluvial field. The only diamictite sample (94.96) plots higher on the RA axis but is still outside the subglacial field and is well below clasts from the modern Mackay Glacier. These data show there are a variety of shapes in the conglomerate facies, but all are quite unlike modern debris from the Mackay Glacier.

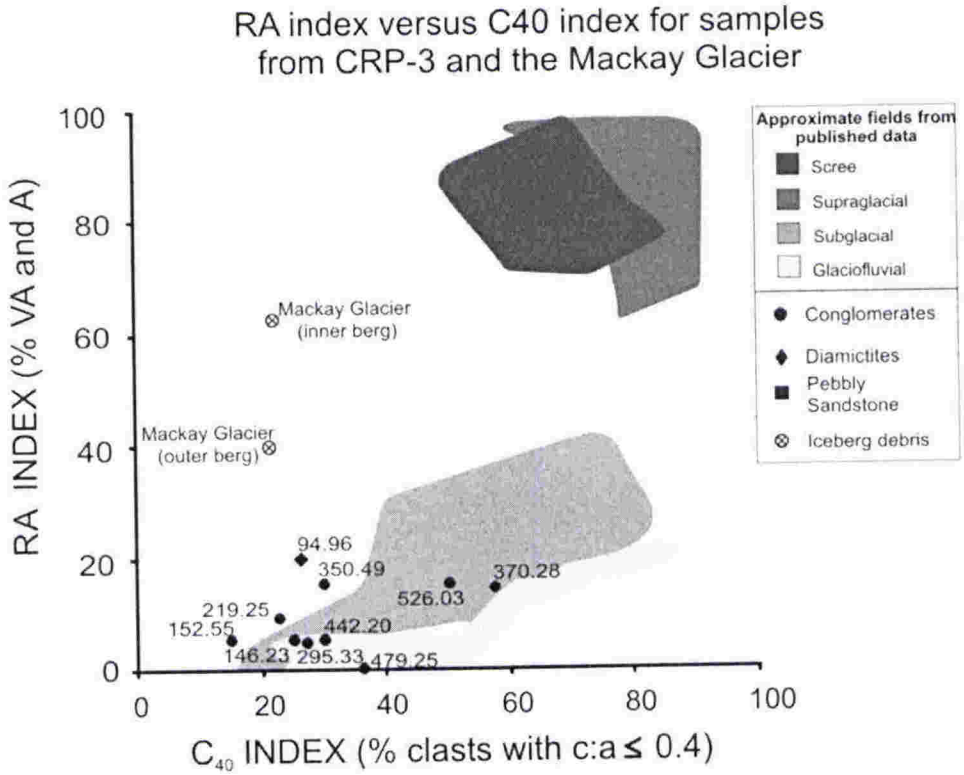

Figure 2 RA-C_{40} diagram of Benn and Ballantyne (1994), showing values from all CRP-3 and the Mackay Glacier. CRP-3 sample numbers refer to depth below sea floor RA index is the percentage of angular and very angular clasts and C_{40} index is the percentage of clasts with a c:a axial ratio of ≤ 0.4. Shaded fields are from published data in Benn and Ballantyne (1994) and Bennett et al. (1997).

Facets were recorded on at least 30 % of clasts in the CRP-2/2A clast samples (except one). Slightly fewer but still usually more than 25 % were recorded on the CRP-3 samples. This is generally higher than the number of faceted clasts found in the modern Mackay Glacier samples (12 % and 22 %). This is consistent with the modern glacier clasts being less rounded and slightly blockier than the Cape Roberts clasts, and suggests that the modern samples have experienced less basal transport than the Cape Roberts clasts, even those in the lower part of CRP-3.

Striated clasts

Only 32 striated clasts were recovered from the Cape Roberts cores. These were mostly fine-grained sedimentary and occasionally dolerite clasts from both the whole-round clast samples and from finer-grained facies from throughout the core. Striated clasts were considered to represent clasts that had undergone basal glacial transport and were deposited at the drillsite either by direct glacial deposition (in the diamictite facies) or by ice-rafting and vertical rainout from icebergs into finer-grained facies. Striation from non-glacial processes was considered unlikely. Despite the very low number of striated clasts, the distribution is sporadic, but persistent throughout much of the cores and this was used to infer a persistent glacial influence during most of the time represented by the cores (Atkins, 2001).

The striae vary greatly in character but most are faintly inscribed and often solitary (Figure 3-A). Occasionally, many striae occur on a single facet and these may vary between multiple orientations (Figure 3-B), and parallel orientation (Figure 3-C). One clast from the top few metres of the core shows long axis parallel striae on curved surfaces and displays a pervasive background of microstriae (Figure 3-D). While the numbers of striae were too few to allow detailed striae analysis, these general characteristics are consistent with those on striated clasts from modern overturned icebergs on the Mackay Glacier. The exception is clast D in Figure 3, which shows striae that are likely to have been created within a deforming fine-grained matrix.

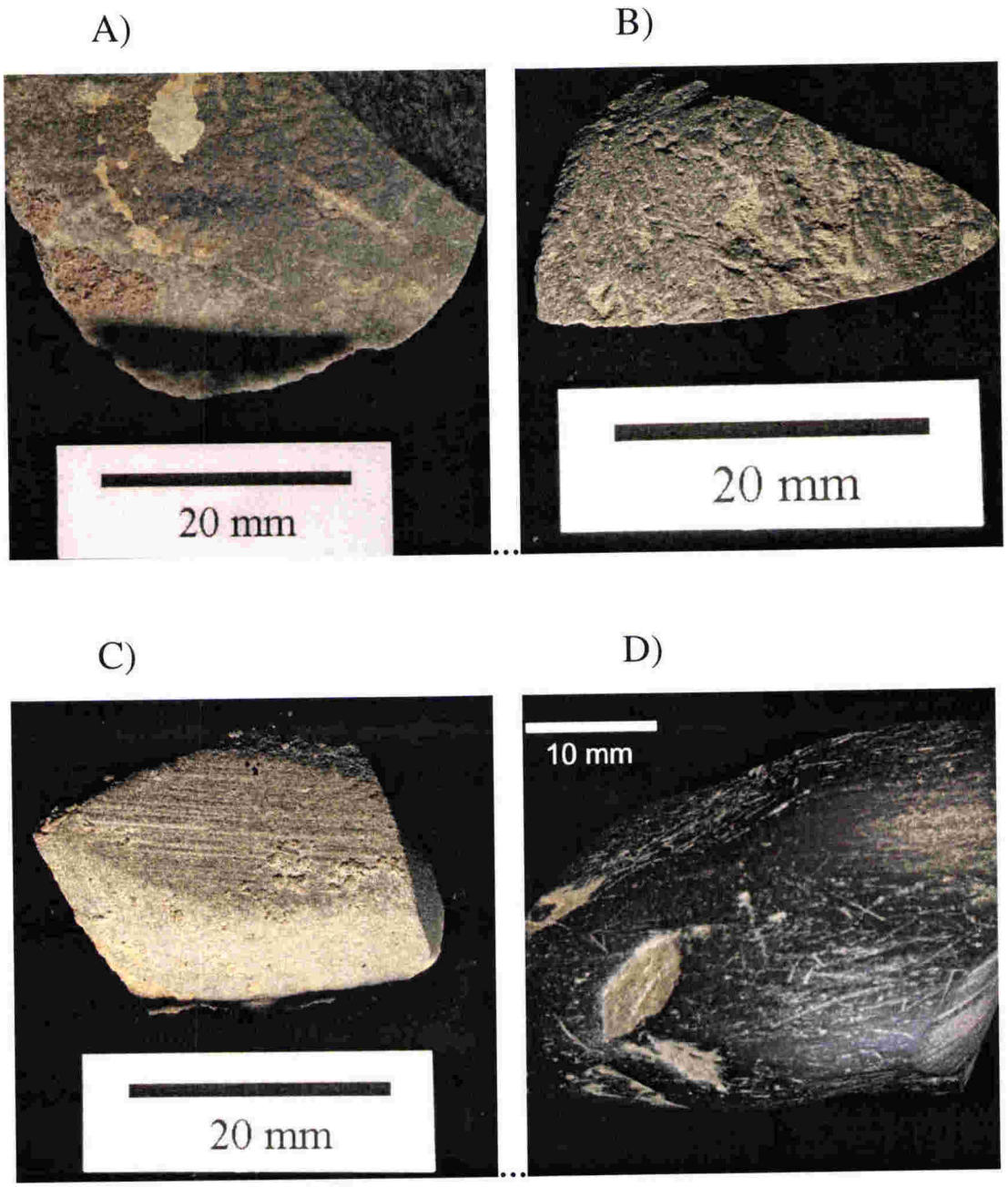

Figure 3 Examples of striated clasts from the Cape Roberts cores. A) A solitary large striation on a dolerite clast from a conglomerate unit (387.7 mbsf, CRP-2/2A). B) Striae with multiple orientations on a mudstone clast within a mudstone unit (199.6 mbsf, CRP-3). C) Parallel striae on a dolerite clast from a pebbly sandstone unit (595.45 mbsf, CRP-2/2A). D) A striated mudstone clast showing long axis parallel striae superimposed on a background of "microstriae" from a diamictite unit (11.0 mbsf, CRP-2).

Several of the conglomerate samples from both CRP-2/2A and CRP-3 displayed faceted and striated clasts. This, combined with the shape characteristics suggests that the clasts within the conglomerates have not experienced significant fluvial transport. Based on the results of the striae survivability study in the Murchison Valley, New Zealand, it is suggested that the striated clasts travelled no more than 2 km from the glacier margin. The conglomerates without striated clasts, but with faceted clasts were probably transported less than 5 km.

Conclusion

Although the Mackay Glacier is the most likely source of sediment for the strata cored at Cape Roberts, the clast shape characteristics from the cores differ from the modern clasts within debris layers of the Mackay Glacier. The clasts from conglomerate beds in CRP-3 show much greater rounding, but all of these deposits display faceted clasts and some show striae. This indicates that the clasts were glacially sourced and did not experience significant fluvial transport, supporting their interpretation as glacier proximal mass flows or short transport fluvial discharges. The clasts in CRP-2/2A show more variable shape characteristics with little distinction between diamictite, conglomerate and pebbly sandstone facies. The samples above 125 mbsf plot the closest to the modern glacier samples, tentively suggesting a possible change toward blockier and more angular clasts during the Miocene as the Mackay Glacier likely changed from temperate to polythermal conditions. Striae alone are too few to allow confident interpretation of their origin. However, in the context of high latitude deposition and abundance of other indicators such as out-sized clasts, the striae are interpreted to be glacial.

Terra Antartica
2001, **8**(3), 263-274

TERRA ANTARTICA

Glacial Influence from Clast Features in Oligocene and Miocene Strata Cored in CRP-2/2A and CRP-3, Victoria Land Basin, Antarctica

C.B. ATKINS

School of Earth Sciences, Victoria University of Wellington, P O Box 600, Wellington - New Zealand (Cliff.Atkins@vuw.ac.nz)

Received 6 November 2000; *accepted in revised form* 10 October 2001

Abstract - Clasts from the Cape Roberts Project cores CRP-2/2A and CRP-3 provide indications of glacially influenced depositional environments in Oligocene and Miocene strata in the western Victoria Land Basin, Antarctica. CRP-2/2A is interpreted to represent strongly glacially influenced, unconformity bound depositional sequences produced by repeated advance and retreat of floating and grounded ice across the shelf. A similar interpretation is extended to the upper 330 meters of the CRP-3 core, but the lower part of the core records shallow marine deposition with significantly less glacial influence. Clast shape analysis from selected coarse-grained facies throughout the cored interval indicates that most clasts are glacially sourced, with little distinction between diamictite and conglomeratic facies. Three dimensional clast fabric analysis from units immediately above sequence boundaries generally display weak or random fabrics and do not suggest that grounded ice actually reached the drillsite at these intervals. Striated and outsized clasts present in fine-grained lithofacies throughout the cores provide further evidence of sub-glacially transported sediment and iceberg rafting. The distribution of these striated and out-sized clasts indicate that a significant glacial influence persisted through most of the time represented by the cores with glaciers actively calving at sea-level introducing ice-berg rafted glacial debris even in the earliest Oligocene.

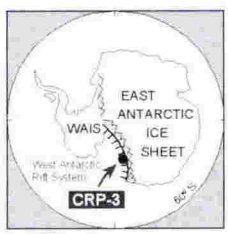

BACKGROUND

The Cape Roberts Project (CRP) is an international drilling effort, with one of the primary objectives being to obtain a palaeoclimatic history of the Ross Sea region to better understand ice sheet history. The background and details of the project goals are outlined in the Initial report of CRP-2/2A (Cape Roberts Science Team, 1999). Almost 1500 m of strata was recovered on the western margin of the Victoria Land Basin from three drill holes. This paper reports on the features of clasts from two of these, CRP-2/2A and CRP-3, representing strata deposited in the Oligocene and Early Miocene (34-19 Ma). CRP-3 cored 820 metres (m) of the oldest Cenozoic strata in this part of the basin (34-31 Ma). The core records mostly shallow marine deposition with only minor indications of glacially influenced sediment in the lower 300 m, but a repeated glacial advance and retreat signal becoming increasingly clear in the upper part indicating the onset of direct glacial deposition. The glacial fluctuations are evident throughout the 600 m of overlying strata of CRP-2/2A recording the period for 31-19 Ma (Cape Roberts Science Team, 1999). The strata in CRP-2/2 and CRP-3 are divided into lithostratigraphic units and sub-units on the basis of lithological changes. Facies analysis of the sequence identified a number of recurrent lithofacies on the basis of lithology, bed contacts and thickness, sedimentary structures and colour. Twelve such lithofacies are recognised in CRP-2/2A and ten in CRP-3. From these, process and palaeo-environmental interpretations of the sediments were made and preliminary depositional models developed. This lithostratigraphic and facies analysis provided the basis for recognising depositional cyclicity and was used to construct a sequence stratigraphic interpretation of each drillcore. This followed the approach adopted by Fielding et al., (1998) and divides the drillcores into unconformity-bound depositional sequences. CRP-2/2A was divided into 25 sequences, and CRP-3 was divided into 23 sequences down to 480.27 metres below sea floor (mbsf) (Cape Roberts Science Team, 1999). These are thought to represent the accumulation of sediment during cycles of glacier advance and retreat and may also occur in concert with relative sea-level changes. These sequences are typically bounded by sharp erosion surfaces that mark abrupt facies dislocations and represent glacial surfaces of erosion either by movement of grounded ice across the sea floor or more distal effects of glacier advance. These are

disaggregated using chisels to expose individual whole clasts (uncut by coring) in a manner similar to that outlined by Hicock (2000). Three dimensional clast fabric data was collected by recording the trend of the a-axis (long axis) of each clast with a protractor. The plunge was measured with a standard geological compass inclinometer. None of the samples was oriented with respect to north because no azimuth could be determined at the drill site. The lithology of each whole clast greater than 0.5 centimetres in diameter was determined. Lengths of the three orthogonal axes (a, b and c) were measured using standard metric callipers to investigate clast shape. Clast roundness was examined using the visual roundness chart of Krumbein (1941). Krumbein roundness values correspond to Powers (1953) roundness classes as follows: very angular 0.0–0.17; angular 0.17–0.25; subangular 0.25–0.35; subrounded 0.35–0.49; rounded 0.49–0.7; well rounded 0.7–1.0. Clasts were also examined for surface features such as facets and striae. In addition to the whole round core samples, the distribution of striated clasts and out-sized clasts throughout the entire cores were obtained from core examination and core box images. Out-sized clasts are defined as clasts 0.1 m or more in diameter and at least 100 times the diameter of the enclosing sediment. Definitions of siliciclastic sediments in the CRP cores are outlined in Hambrey et al., (1997). Diamictite is defined as a poorly sorted terrigenous sediment with between 10 and 90 percent sand and between 1 and 30 percent clasts. Conglomerate contains greater than 30 percent clasts.

In the study of clast morphology it is useful to view clast shape as the summation of three independent properties: form, roundness and surface texture (Barrett, 1980). These have commonly been regarded as good indicators of transport mechanisms (Kuhn et al., 1993), and widely used in the analysis of conglomerates and diamictites to help distinguish those of glacial origin from those of non-glacial origin and to differentiate between different glacial facies (Hall, 1989). Form is the gross overall shape of a clast and is displayed on ternary particle-form diagrams following Benn and Ballantyne (1994). This plots the b/a and c/a axial ratios of clasts and divides them into three basic shapes: 1) Blocks (spheres), 2) Slabs (discs) and 3) Elongate (rods). Clast morphology is further explored using covariant plots of clast form and roundness following the method of Benn and Ballantyne (1994). This plots the C_{40} index (percentage of clasts with c/a axial ratio of ≤ 0.4) against the RA index (percentage of angular and very angular clasts) and provides superior data visualisation than the more traditional sphericity and roundness plots (Bennett et al., 1997). Clasts that have experienced "active" glacial transport often have high c/a axial ratios and rounded edges and "passively" transported clasts are more angular and have low c/a axial ratios.

Clast fabric has been used by many workers to assist in the interpretation of clast-rich sediments, particularly those of glacial origin, specifically to infer the mode of deposition and to define glacial flow directions (*e.g.* Domack & Lawson, 1985; Dowdeswell et al., 1985; Dowdeswell & Sharp, 1986). Fabric data are normally displayed on lower hemisphere, equal area (Schmidt) stereonet plot that allows a visual analysis of data clustering or modality. In addition, the orientation tensor or eigenvalue method is widely used to analyse fabric data and essentially summarise fabric strength. Benn (1994b) introduced the powerful "eigenvalue ratios" ternary diagram for analysing fabric data and is superior to other types of eigenvalue plot because it focuses attention on fabric shape, thereby facilitating interpretation (Bennett et al., 1999). This method is employed here.

Tab. 2 - List of whole round core sample numbers and depth in meters below sea floor (mbsf), with facies number for each sample.

Sample No.	Sample depth (mbsf)	Facies number
CRP 2/2A Sample 1	49.60-49.80	7
CRP 2/2A Sample 2	101.67-101.85	7
CRP 2/2A Sample 3	121.59-121.79	5
CRP 2/2A Sample 4	124.92-125.92	9,10
CRP 2/2A Sample 5	233.80-234.04	7
CRP 2/2A Sample 6	351.37-351.67	7
CRP 2/2A Sample 7	372.15-372.46	6
CRP 2/2A Sample 8	387.02-387.32	10
CRP 2/2A Sample 9	406.80-407.09	7
CRP 2/2A Sample 10	441.22-441.52	7
CRP 2/2A Sample 11	490.10-490.39	7
CRP 2/2A Sample 12	518.32-518.62	3
CRP 3 Sample 1	94.96-95.16	7
CRP 3 Sample 2	146.23-146.47	10
CRP 3 Sample 3	152.55-152.80	10
CRP 3 Sample 4	219.25-219.47	10
CRP 3 Sample 5	295.33-295.53	10
CRP 3 Sample 6	350.49-350.83	9
CRP 3 Sample 7	370.28-370.55	10
CRP 3 Sample 8	442.20-442.45	10
CRP 3 Sample 9	479.25-479.45	9
CRP 3 Sample 10	526.03-526.33	10

RESULTS

Several lithologies are represented by the clasts. Granitoid and dolerite clasts are dominant in all samples with minor sedimentary, volcanic and metamorphic clasts present also. Lithologies of the types in the CRP cores have little influence on clast shape or roundness (Bennett et al., 1997; Dowdeswell et al., 1985; Kuhn et al., 1993) and therefore results from different lithologies are not treated separately here. However, surface features are strongly influenced by lithology and given particular attention below.

Form

Form is displayed on ternary particle diagrams in figure 1. The results show that all samples contain a

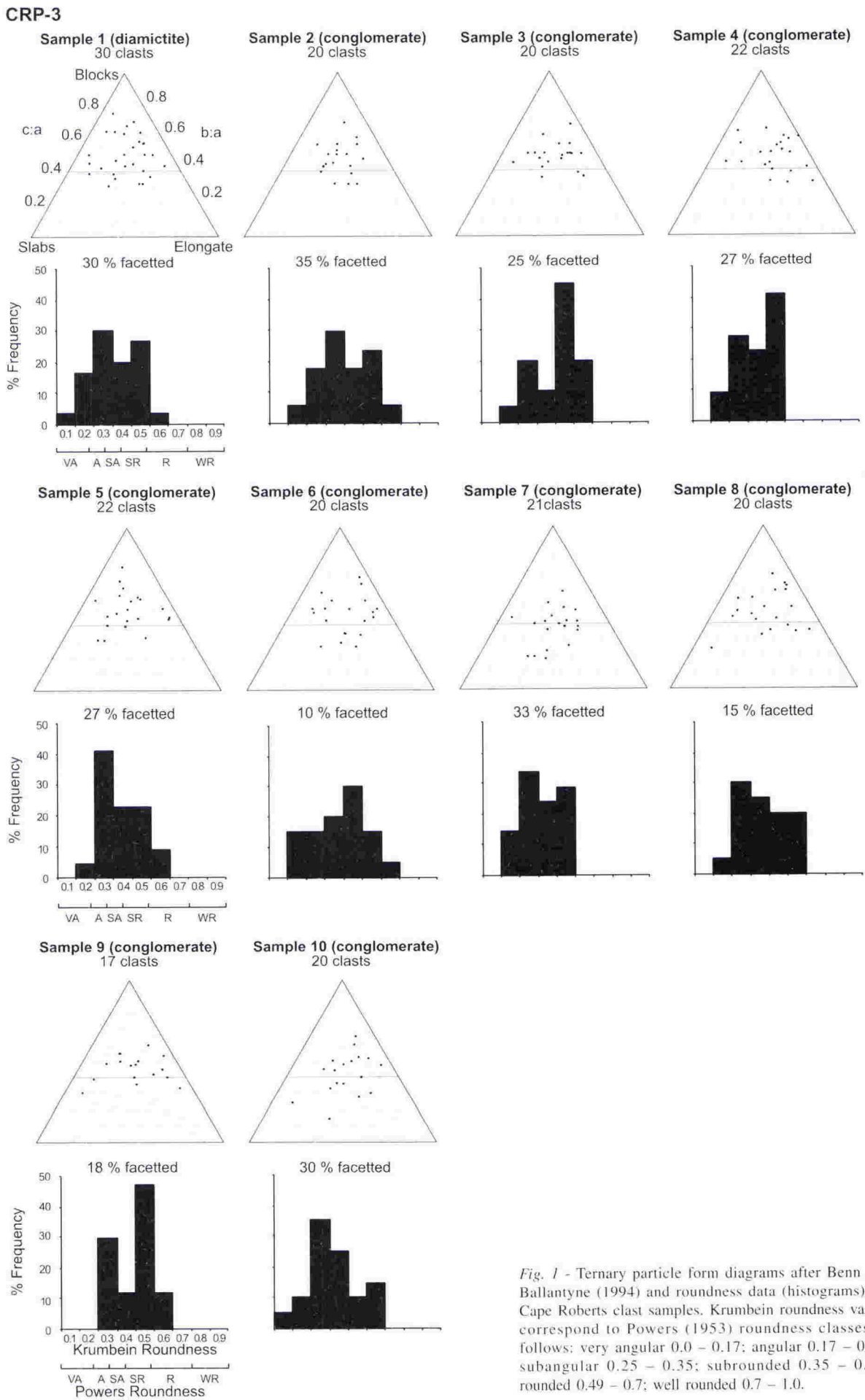

Fig. 1 - Ternary particle form diagrams after Benn and Ballantyne (1994) and roundness data (histograms) for Cape Roberts clast samples. Krumbein roundness values correspond to Powers (1953) roundness classes as follows: very angular 0.0 – 0.17; angular 0.17 – 0.25; subangular 0.25 – 0.35; subrounded 0.35 – 0.49; rounded 0.49 – 0.7; well rounded 0.7 – 1.0.

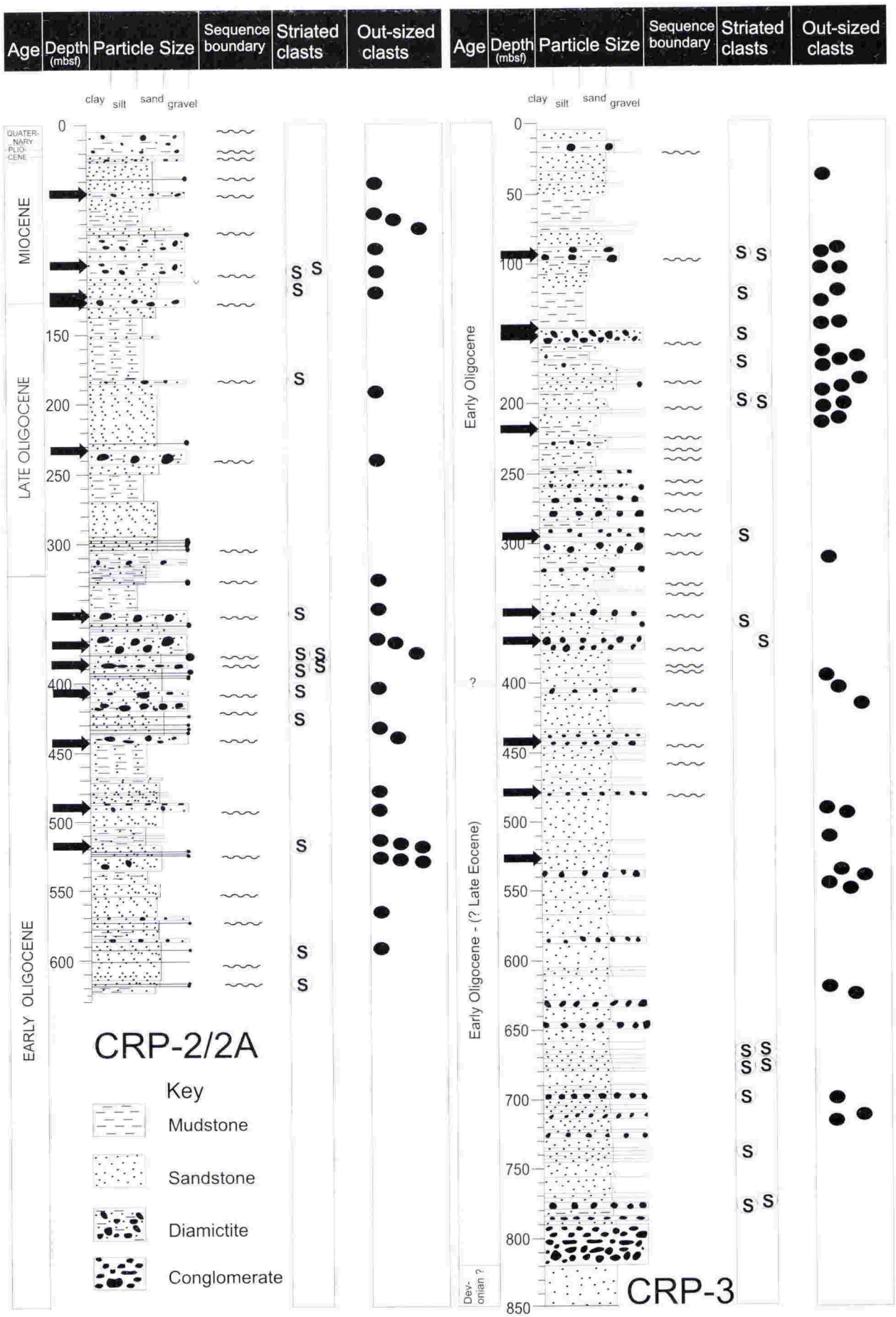

Fig. 3 - Stratigraphic columns for CRP-2/2A and CRP-3, with distribution of out-sized clasts (diameter greater than 0.1m) and striated clasts. Out-sized clasts are not plotted in conglomeratic facies 9 or 10. Dark arrows indicate whole-round core sample locations.

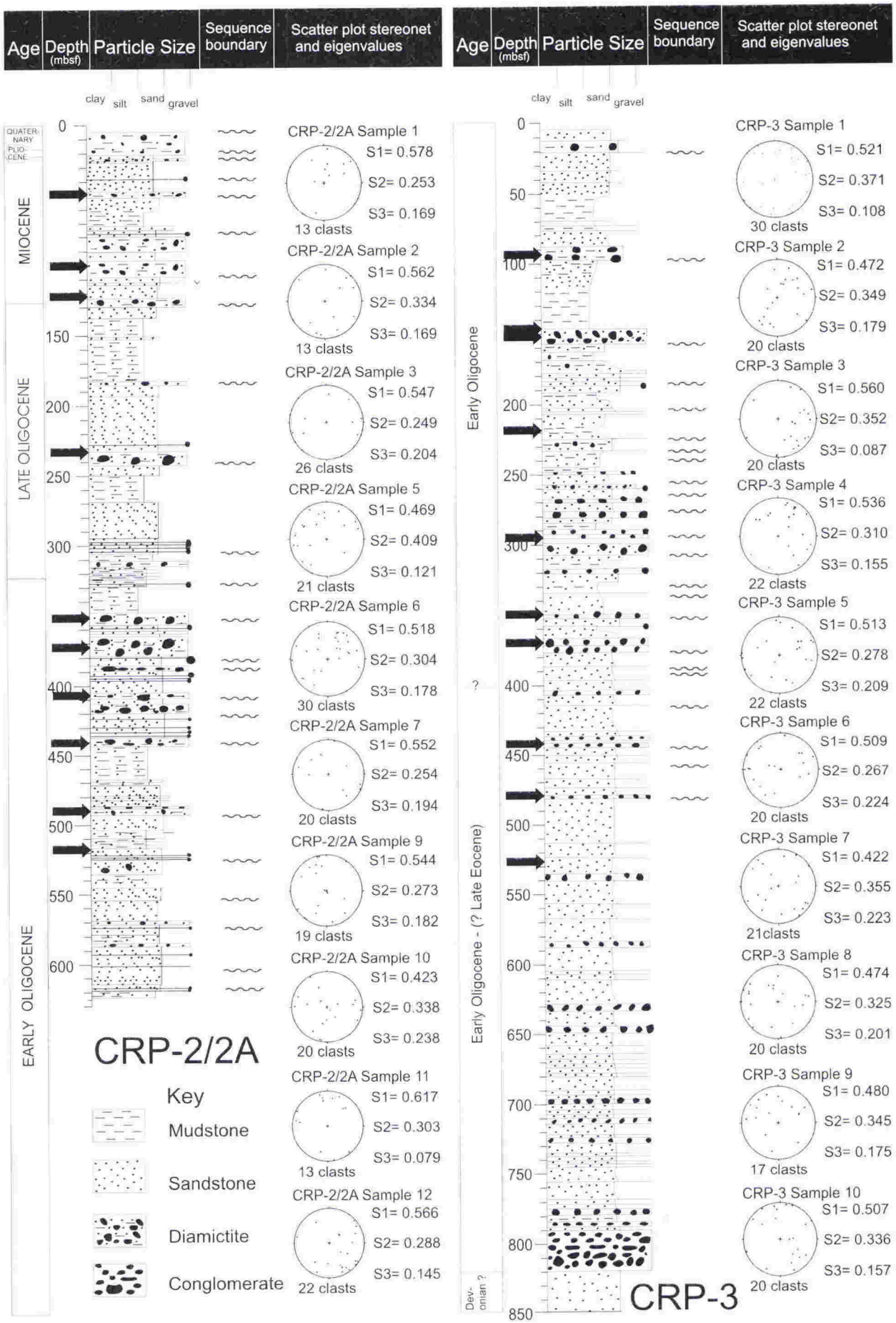

Fig. 5 - Stratigraphic columns for CRP-2/2A and CRP-3, with fabric data displayed as lower hemisphere, equal area Schmidt stereoplots. Principle eigenvalues are presented also. Dark arrows indicate whole-round core sample locations.

rafted debris. In diamictite units (facies 6 and 7) out-sized clasts may represent ice-contact deposition such as subglacial till or by rainout of iceberg rafted debris, particularly in the stratified diamictites (facies 6). As these are glacially related processes, out-sized clasts in these facies have been included in the distribution. The distribution of out-sized clasts indicates that significant ice-rafting occurred throughout most of the time represented by the cores.

Three dimensional clast fabric analysis from coarse grained facies is a useful method of investigating clast orientation that may indicate whether or not grounded ice extended out to the drillsite during eustatic lowstand. However, many researchers have commented on the problems involved with interpreting fabric data (*e.g.* Dowdeswell and Sharp, 1986; Benn, 1994b; Hicock et al., 1996; Bennett et al., 1999). For example, Hicock et al., (1996) advocated the use of Schmidt plots in conjunction with eigenvalue analysis. They stress that multiple criteria must be considered when drawing conclusions on till genesis and that clast fabric alone is not able to discriminate between different glacigenic facies. Problems are compounded when attempting clast fabric analysis in drillcores. Often, very low numbers of whole clasts are availabie and other criteria such as glaciotectonic structures are not visible on core scale. In addition, only split core faces are usually available, prompting some to attempt two dimensional fabric studies (*e.g.* Hambrey, 1989). For the CRP cores, three dimensional clast fabric analysis was possible from the whole round core samples, but many of the other limitations apply, meaning that the fabric data, in particular eigenvalues, must be viewed cautiously. Although the data are simply too limited to infer specific genesis of coarse-grained facies and eigenvalues only provide a basic guide to fabric strength, stereoplots and eigenvalues are considered here to provide a indication (or lack of) of ice grounding at any of these intervals. Analysis of stereoplots show that none of the three dimensional clast fabrics have tightly clustered data and eigenvalue ratios highlight the absence of highly elongate, low isotropy fabrics indicative of subglacial tills or grounded ice at the drillsite.

CONCLUSIONS

Clasts from selected coarse-grained intervals in the Miocene/Oligocene strata in the Cape Roberts cores show features indicating subglacial transport histories and confirm that most clast-rich sediments are glacially derived. There is little real difference in clast shape between diamictites and conglomerates and the presence of subglacially derived facetts and striae on some clasts within conglomerates (facies 9 and 10), indicates the clasts have not experienced significant fluvial transport and that conglomerates are glacier proximal high-density mass flows or very short transport subglacial discharges.

Three dimensional clast fabrics from the drillcores must be treated cautiously, but weak to random orientations do not suggest ice grounded at the drillsite, although other evidence (van der Meer, 2000) indicate periods of grounded ice in the Late Oligocene and Early Miocene.

Out-sized clasts and striated clasts in fine-grained lithofacies represent dropstones sourced from ice-bergs. The distribution of these striated and out-sized clasts indicate that a glacial influence was significant and persistent during most of the time represented by the cores with glaciers actively calving at sea-level introducing ice-berg rafted glacial debris into the Ross sea region even in the very earliest Oligocene.

ACKNOWLEDGEMENTS - The Cape Roberts drilling team are acknowledged for their superb efforts in recovery and Science team are thanked for initial interpretation of the cores. Additional core sampling at the Alfred-Wegener Institute in Bremerhaven, Germany was partly funded by a Trans Antarctic Association grant. Constructive reviews provided by Steve Hicock, Matthew Bennett and Kurt Kjaer and editorial handling by Jaap van der Meer substantially improved the manuscript.

REFERENCES

Barrett P.J., 1980. The shape of rock particles, a critical review. *Sedimentology*, **27**, 291-303.

Benn D.I., 1994b. Fabric shape and the interpretation of sedimentary fabric data. *Journal of Sedimentary Research*, **A64**, 910-915.

Benn D.I. & Ballantyne C.K., 1994. Reconstructing the transport history of glacigenic sediments: a new approach based on the co-variance of clast form indices. *Sedimentary Geology*, **91**, 215-227.

Bennett M.R., Doyle P., Mather A.E. & Woodfin J.L., 1994. Testing the climatic significance of dropstones: an example from southeast Spain. *Geol. Magazine*, **131**, 845-848.

Bennett M.R., Hambrey M.J. & Huddart D., 1997. Modification of clast shape in High-Arctic glacial environments. *Journal of Sedimentary Research*, **67**, 550-559.

Bennett M.R., Waller R.I., Glasser N.F., Hambrey M.J., & Huddart D., 1999. Glacigenic clast fabrics: genetic fingerprint or wishful thinking? *Journal of Quaternary Science*, **14**, 125-135.

Cape Roberts Science Team, 1999. Studies from the Cape Roberts Project, Ross Sea, Antarctica. Initial Report on CRP-2/2A. *Terra Antartica*, **6**, 1-173. With Supplement, 228 p.

Cape Roberts Science Team., 2000. Studies from the Cape Roberts Project, Ross Sea, Antarctica. Initial Report on CRP-3. *Terra Antartica*, **7**, 1-209. With Supplement, 305 p.

Dionne J. 1985., Drift-ice abrasion marks along rocky shores. *Journal of Glaciology*, **31**, 237-241.

Domack E.W. & Lawson D.E., 1985. Pebble fabric in an ice-rafted diamicton. *Journal of Geology*, **93**, 577-591.

Dowdeswell J.A., Hambrey M.J. & Ruitang Wu., 1985. A comparison of clast fabric and shape in Late Precambrian and modern glacigenic sediments. *Journal of Sedimentary Petrology*, **55**, 691-704.

Dowdeswell J.A. & Sharp M.J., 1986. Characterization of pebble fabrics in modern terrestrial glacigenic sediments. *Sedimentology*, **33**, 699-710.

Fielding C.F., Woolfe K.J., Howe J.A & Lavelle M., 1998.

Cold glaciers erode and deposit: Evidence from Allan Hills, Antarctica

C.B. Atkins
P.J. Barrett
Antarctic Research Centre and School of Earth Sciences, Victoria University, Wellington, New Zealand
S.R. Hicock
Department of Earth Sciences, University of Western Ontario, London, Ontario N6A 5B7, Canada

ABSTRACT

Here we report previously undescribed features of erosion and deposition by a cold (polar) glacier. A recent study challenged the assumption that cold glaciers neither slide nor abrade their beds, but no geological evidence was offered. The features we describe include abrasion marks, subglacial deposits, glaciotectonically deformed substrate, isolated blocks, ice-cored debris mounds, and boulder trains, all products of a recent cold ice advance and retreat. Mapping these features elsewhere in Antarctica will document recent shifts in the East Antarctic Ice Sheet margin, providing new insight on regional mass-balance changes.

Keywords: cold-based glaciers, abrasion, Allan Hills, Antarctic ice sheet, glacial deposition.

INTRODUCTION

It is commonly assumed that basal sliding and abrasion take place only beneath glaciers that are warm based, whether temperate or subpolar (e.g., Jackson, 1997; Benn and Evans, 1998; Siegert, 2001), and that significant erosion and deposition do not occur beneath cold-based glaciers, which are frozen to their beds. This has even led to the view that landscapes are actually protected beneath cold ice (e.g., Sugden et al., 1991; Naslund, 1997; Stroeven and Kleman, 1999).

The possibility of erosion, entrainment, and deposition by cold glaciers was proposed by Boulton's (1972) theoretical work; by Holdsworth (1974) on the basis of field observations beneath Meserve Glacier, Antarctica; by Shreve (1984) on the basis of theoretical work; and by others on the basis of theoretical and experimental work (Fowler, 1986; Cuffey et al., 2000; Martini et al., 2001). Direct observation of basal sliding and debris entrainment at subfreezing temperatures of −5 °C was claimed by Echelmeyer and Wang (1987). Cuffey et al. (1999, 2000) found evidence of active entrainment and sliding at −17 °C beneath Meserve Glacier, Antarctica, and suggested that it is time to abandon the assumption that cold-based glaciers do not slide and abrade. None of these studies has reported ancient cold-based glacial features that have survived to the present day. In this paper we describe and interpret the geological evidence of erosion and deposition exposed by the retreat of a cold-based glacier in the Allan Hills, Antarctica.

ALLAN HILLS ENVIRONMENT

The Allan Hills (76°42′S, 159°40′E) form a wishbone-shaped nunatak located high (1600–2100 m above sea level) in the Transantarctic Mountains in south Victoria Land near the edge of the present East Antarctic Ice Sheet (Fig. 1). The center of the wishbone is occupied by the Manhaul Bay Glacier (informal name), ~3 km across, 6 km long, and 200 m thick. The glacier is fed by ice flowing north on either side of Allan Hills, turning south around the tips of the wishbone. The ice between the arms of the wishbone is wind-sculpted "blue ice" typical of ablation that has been measured as 5 cm/yr in ice fields several kilometers west (Faure and Buchanan, 1987). The mean annual temperature (MAT) is −30 °C (Robin, 1983). Ice movement at the southern margin has not been measured, but is presumed to be close to zero because the sigmoidal cross section of the ice front reveals that the ice front is retreating. This inference is confirmed by the preservation of soft, crushed sandstone smeared on a bedrock ridge that protrudes from the ice and by the presence of bedrock striae within a few meters of the present margin.

The bedrock of Allan Hills comprises flat-lying Permian and Triassic sandstones, shales, and coal measures of the Beacon Supergroup,

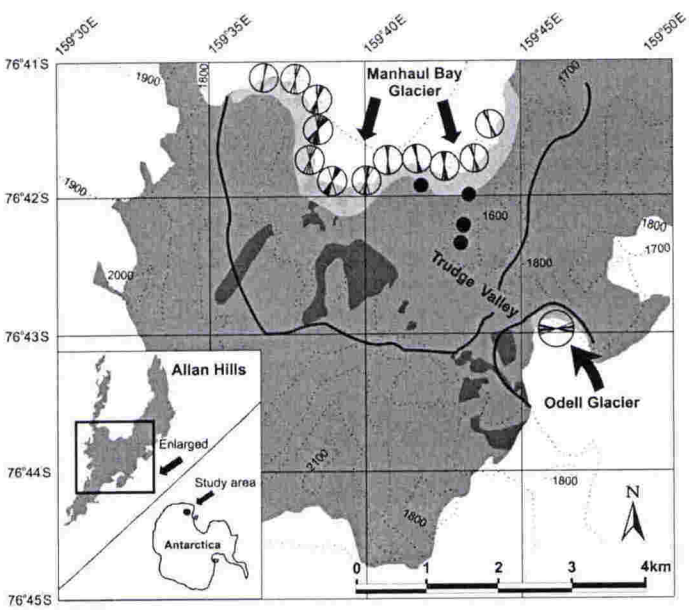

Figure 1. Map of central Allan Hills, Antarctica, showing distribution of features recording former extent of Manhaul Bay and Odell Glaciers. Ice-cored debris cones are plotted as solid dots. Dark shading shows distribution of much older Sirius diamictite. Light, transparent shading and rose diagrams display distribution and orientation of abrasion marks and breccia-debris trails around ice margins. Large dark arrows indicate ice advance direction of Manhaul Bay and Odell Glaciers into present ice-free areas. Contours in meters above sea level.

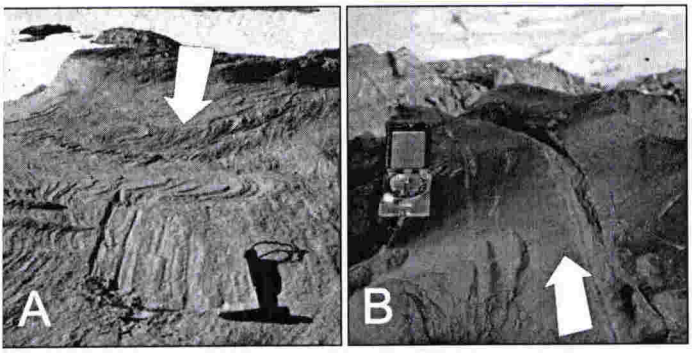

Figure 2. Examples of erosional features around margin of Manhaul Bay Glacier. A: Type 1 abrasion. Large broad scrape consisting of multiple grooves on Beacon sandstone. Example becomes deeper and wider with abrupt terminus and has remnants of abrading tool on surface. Arrow indicates ice-movement direction. Hammer is 33 cm long. B: Type 3 abrasion. Unweathered scrapes on weathered, wind-polished dolerite boulder in Sirius diamictite. Many of these boulders have been overturned. Arrows indicate direction of ice movement.

intruded by sills and thin dikes of Jurassic Ferrar Dolerite (Ballance and Watters, 1971). Patches of Sirius Group diamictite mantle the Beacon strata in the central area. Although these deposits have not been dated directly, other Sirius deposits and rock surfaces in the Dry Valleys region south of Allan Hills have yielded ages as old as 10 Ma, with volcanic-ash deposits as old as 15 Ma (Summerfield et al., 1999). The nature of the surfaces and the preservation of the ashes indicate that the landscape has undergone persistent polar desert conditions dominated by wind erosion since those times.

The present Manhaul Bay Glacier is estimated as ~200 m thick in the middle, with basal temperatures of ~−24 °C (estimated from the MAT of −30 °C and the graph of Robin, 1955, Fig. 3). The features that we describe next occur on rock platforms and ridges beyond the margin of the glacier, and have been exposed by glacial retreat. These features formed beneath ice that we estimate to be of similar thickness and low basal temperature.

COLD-BASED EROSIONAL FEATURES AT ALLAN HILLS

Erosional features are represented principally by abrasion marks, which occur on Beacon sandstone surfaces and on the upper surface of Sirius diamictite, close to the margins of the Manhaul Bay and Odell Glaciers (Fig. 1). Abrasion marks are most common within several meters of the ice edge and rare beyond 50 m. The marks are variable in shape, size, and grouping, and are unlike the more consistent, uniform sets of parallel striae and grooves found commonly on bedrock abraded by warm-based sliding ice. Abrasion marks at Allan Hills can be divided into four types as described next.

Type 1: Broad Scrapes

Broad (to 500 mm width, 40 mm depth, 1200 mm length), unweathered scrapes typically consist of many smaller striae or grooves centimeters or millimeters in width. Some examples (Fig. 2A) show progressive increase in depth and width with an abrupt terminus. Typically the abrasion mark has crushed sandstone remnants of the abrading tool smeared onto the surface, particularly at the deepest terminal wall. Occasionally, small centimeter-scale "levees" occur along the sides of the abrasion mark. These marks are close to the present margin of the Manhaul Bay Glacier and indicate ice movement from north to south.

Type 2: Individual Striae and Grooves

Variably shaped, unweathered individual linear abrasions (scrapes, striae, and grooves) make up a wide variety of discrete abrasion marks (typically centimeters in width and depth and decimeters long). Where several marks occur in one location, they are generally subparallel. Some show a progressive increase in depth and width (nailhead), whereas others have more symmetrical, tapered ends. Occasionally, individual marks occur in line to form a trail of marks to 2 m in length. Some marks have crushed sandstone remnants of the abrading tool smeared onto the surface and/or are bordered by small centimeter-scale levees. These abrasions are common near the present margins of Manhaul Bay and Odell Glaciers and rarely farther inland from the ice, protected beneath brecciated sandstone debris.

Type 3: Scraped Boulders

Variably shaped, unweathered scrapes to several centimeters wide (and related striae) occur on the stoss side of some weathered dolerite boulders lodged within, or resting on, Sirius diamictite. Abrasion has removed the characteristic dark brown desert varnish from the surfaces of the boulders, making the marks clearly visible (Fig. 2B). Some boulders have been overturned, exposing the non-wind-polished surface underneath. These distinctive overturned and abraded boulders were found over a wide area in the central Allan Hills, and to 1800 m south (inland) of the present Manhaul Bay Glacier margin (Fig. 1).

Type 4: Ridge and Groove Lineations

Localized surfaces display abraded patches with many parallel fine lineations (millimeter scale width and depth), described here as ridge and groove lineations. The surfaces are typically dark and have a platy appearance and a sheen similar to slickensides. These abraded patches occur within thin carbonaceous layers beneath brecciated sandstone debris and indicate north to south glacier movement. These patches occur over a wide area in the central Allan Hills within the Manhaul Bay Glacier advance limit shown in Figure 1.

COLD-BASED DEPOSITIONAL FEATURES AT ALLAN HILLS

In addition to erosional features, four depositional features attributed to cold-based ice are recognized at Allan Hills.

Type 1: Sandstone and Siltstone Breccia

The sandstone and siltstone breccias are unlithified, poorly compacted deposits, typically <30 cm thick and <3 m across, consisting of variably crushed or brecciated Beacon sandstone and siltstone. Some deposits have been extensively crushed, but often contain blocks to 40 cm in diameter. Deposits are commonly attached to vertical walls of Beacon escarpments that face the present Manhaul Bay and Odell Glaciers. Breccia deposits are typically elongated and taper inland from glacier margins (Fig. 3A[1]). In places Beacon rocks have been partially brecciated and thrust onto the adjacent bedrock immediately inland. The breccia extends 2.5 km south of, and at least 100 m higher in elevation than, the present ice margin of the Manhaul Bay Glacier.

Type 2: Isolated Boulders

Sandstone boulders to 3 m in diameter are scattered widely over Beacon platforms of the central Allan Hills and as far south as Trudge Valley. Some boulders form poorly defined boulder trains indicating ice movement to the south. Several boulder trains are visible trailing

[1]GSA Data Repository item 2002070, Additional images of erosion and deposition by cold ice at Allan Hills, Antarctica, is available on request from Documents Secretary, GSA, P.O. Box 9140, Boulder, CO 80301-9140, USA, editing@geosociety.org, or at www.geosociety.org/pubs/ft2002.htm.

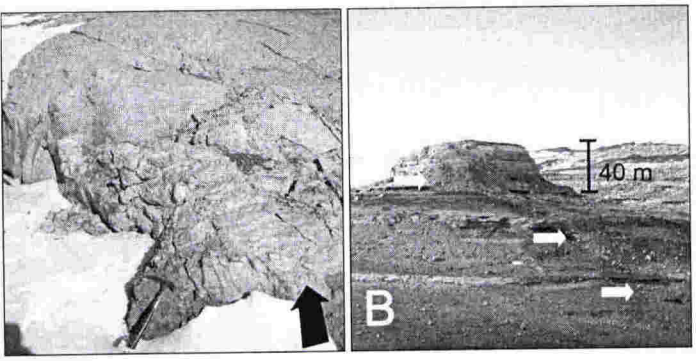

Figure 3. Examples of depositional features (see text footnote 1). A: Type 1 deposition. Brecciated sandstone plastered onto bedrock escarpment. Breccia is smeared into debris trails in direction of ice advance (arrow). Hammer is 33 cm long. View looking south from Manhaul Bay Glacier. B: Type 4 deposition. View of southern end of bedrock ridge (middle distance) from southwest. Manhaul Bay Glacier (middle left) overtopped ridge from north. Large volume of crushed sandstone debris occurs on lee side of ridge and faint boulder trains trail south into Trudge Valley (arrows).

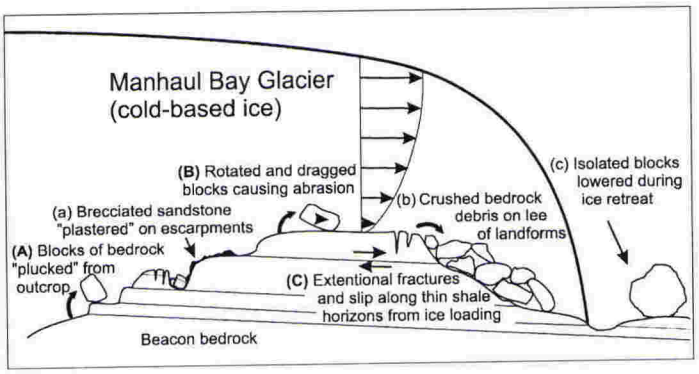

Figure 4. Schematic model of processes beneath cold-based ice at Allan Hills. Vertical profile indicates assumed ice velocity within glacier. Erosion followed by entrainment occur by (A) plucking stoss sides of outcrops, (B) dragging blocks along bedrock surface either by sliding or rotation of clast by velocity gradient above bed, and (C) glaciotectonic extension producing fractures and differential slip along weak layers producing abraded, slickenside surfaces. Deposition occurs by (a) in situ brecciation of bedrock or plastering entrained substrate onto bedrock escarpments projecting into ice mass, (b) accumulation of glaciotectonically brecciated substrate on lee sides of bedrock ridges and escarpments, and (c) formation of ice-cored debris cones and lowering of plucked blocks onto bedrock platforms during ice retreat.

southward from an area of rubble on the southern (lee) side of a prominent ridge, and extend into Trudge Valley ~2250 m south of Manhaul Bay Glacier.

Type 3: Ice-Cored Debris Cones

Ice-cored debris cones to 3 m high and 7 m in diameter occur on bedrock platforms and in a low valley south of Manhaul Bay Glacier. In each case the ice-cored cone is completely covered by loose Beacon debris ranging from sand to boulders. The cones occur as much as 1000 m inland from the present margin of Manhaul Bay Glacier.

Type 4: Sandstone Debris on Lee Slopes

Crushed bedrock debris ranging in size from sand to boulders occurs on the southern sides of bedrock ridges and escarpments or on the northern walls of bedrock depressions. The debris has a chaotic appearance and thins away from the landform. The scale of the debris piles varies from several tens of meters (Fig. 3B) to <1 m. Debris piles are widespread within the advance limit of Manhaul Bay Glacier and consistently rest against the lee sides of bedrock highs. Extensional fractures in the southern edges of bedrock ridges or in the northern edges of escarpments are associated with these sandstone debris deposits. Fractures are typically oriented subparallel to the ice margin and vary in length and width depending on the scale of the outcrop. In places, it is possible to see where blocks of bedrock have been fractured and tilted south, then added to the debris piles.

INTERPRETATION OF EROSIONAL AND DEPOSITIONAL FEATURES

Broad scrapes (type 1 abrasion marks) and individual striae and grooves (type 2 abrasion marks) are interpreted to be the result of debris within the ice being dragged along the bedrock by either basal slip or forward rotational movement (created by the striator projecting into the deforming ice mass). This principle was suggested by Drewry (1986). Because the abrading particles were most likely to be the same lithology as the bedrock, there was little hardness contrast, and abrasions tend to be broad and shallow and commonly have remnants of the sandstone striator on the abraded surface or as low levees on the sides. This is particularly noticeable on abrasions that progressively deepen and then terminate abruptly, indicating that the striator disintegrated under dry simple shear with no meltwater to wash away the levees (Fig. 2A). Examples that have more symmetrical tapered ends suggest that the striator contacted the bed briefly, but lifted off again. Occasionally, several of these abrasions occur in line over 1–2 m where the striator touched the bedrock surface several times on its journey. A similar process is inferred for the short irregular abrasional markings on wind-polished boulders (type 3 abrasion marks) (Fig. 2B). Differential ice movement close to the glacier bed initially dragged the striating tool over the boulders and then overturned them. Type 4 abrasion is interpreted as a glaciotectonic structure formed by differential slip on thin, weak carbonaceous shale layers within the Beacon strata in response to increased shear stress from loading as cold ice moved over bedrock promontories.

Sandstone and siltstone breccia (type 1 deposition) appears to be the result of in situ brecciation of bedrock escarpments where shear stress from overriding ice is focused on an upglacier edge, causing failure and crushing of the rock, or where already entrained debris is trapped by the edge and plastered on, some debris being deposited farther as debris trails in the direction of ice movement (Fig. 3A). We suggest that this type of deposit constitutes a simple form of glaciotectonite (Pedersen, 1989; Benn and Evans, 1998) or a cold-based deformation till (Dreimanis, 1989). The orientation of these trails is consistent with abrasion features at the same location. Isolated blocks (type 2 deposition) were plucked from bedrock escarpments, transported passively within the ice, and lowered onto bedrock surfaces during ice retreat. We found no abrasion marks on these scattered blocks or on the surrounding substrate, as might be expected if the boulder were dragged by basal glacial ice. Ice-cored debris cones (type 3 deposition) are interpreted as remnant features from loose debris that fell or was pushed onto the surface of the Manhaul Bay Glacier, thermally protecting the ice as the glacier ablated back to the present margin. Type 4 deposition is inferred to have taken place on the lee slopes of ridges and escarpments, with glaciotectonic tensional fracturing facilitating erosion of the unsupported lee sides of the landforms (Fig. 3B). The accumulation of rock debris there may have formed by sandstone blocks falling off, or being toppled over by, the retreating glacier margin. Figure 4 is a simple schematic model that we have developed to explain these observations.

RECENT GLACIAL HISTORY OF ALLAN HILLS

Orientations of abrasion marks (types 1 and 2) and debris trails (type 1 depositional feature) were measured within 50–100 m of the ice margin of Manhaul Bay Glacier. The measurements are displayed as mirror-image rose diagrams in Figure 1 and show a splayed pattern radiating from beneath the glacier. All indicate movement from north to south (inland). The solid lines in Figure 1 represent the maximum advance positions for the margins of the Manhaul Bay and Odell Glaciers, delineated by the most inland positions of overturned and abraded boulders and sandstone breccia (type 1 deposition). A reconstruction of the longitudinal profile of the Manhaul Bay Glacier, following the modern profile to the limit shown, indicates that a maximum ice thickness of ~200 m was attained at the present southern ice margin.

On the basis of fresh striae cutting through desert varnish on rotated boulders, the unweathered appearance of glacial scrapes, grooves, and striae on rock ledges close to the ice margins, and piles of fresh, angular sandstone blocks (type 4 deposition) covering empty glacitectonic fractures, we suggest that the features described here formed during the Last Glacial Maximum. This was the last time the East Antarctic Ice Sheet was more extensive in this region (Hughes, 1998; Siegert, 2001; Denton and Hughes, 2002). We assume that a more extensive Manhaul Bay Glacier produced many abrasion features over the extensive bedrock platforms it once covered, but that nearly all of these have been destroyed by wind erosion, apart from those most recently exposed by ice ablation or protected by debris.

CONCLUSIONS

The recent advance of the Manhaul Bay Glacier, the limit and thickness of which have been reasonably well defined, must have been entirely cold based. This has produced a range of glacial erosional and depositional features that differ significantly from those made by warm-based glaciers.

These features have been used to define the limit of the southward advance of cold ice 2 km into the present ice-free area of the central Allan Hills during the Last Glacial Maximum. This advance overtopped landforms to 100 m above the present ice limit. Such an ice advance requires that the adjacent outlet glaciers flowing north past Allan Hills (Fig. 1) were higher by a similar amount. These newly recognized cold glacier features provide criteria for mapping the former Last Glacial Maximum extent of ice throughout the Transantarctic Mountains and elsewhere in Antarctica.

ACKNOWLEDGMENTS

This work was funded partially by a Victoria University of Wellington Postgraduate Scholarship (to Atkins), by Swiss National Science Foundation grants 21-043469.95 and 21-053942.98, and by University of Western Ontario Academic Development Fund grants (to Hicock). Antarctica New Zealand provided logistical support. Jeremy Mitchell and Vanessa Thorn assisted in the field. Discussions with Phil Holme, Mark Lloyd Davies, Jaap van der Meer, and Christian Schlüchter are gratefully acknowledged. Constructive reviews were provided by Kurt Cuffey and Matthew Roberts.

REFERENCES CITED

Ballance, P.F., and Watters, W.A., 1971, The Mawson Diamictite and the Carapace Sandstone Formations of the Ferrar Group at Allan Hills and Carapace Nunatak, Victoria Land, Antarctica: New Zealand Journal of Geology and Geophysics, v. 14, p. 512–527.

Benn, D.I., and Evans, D.J.A., 1998, Glaciers and glaciation: London, Arnold, 734 p.

Boulton, G.S., 1972, The role of thermal regime in glacial sedimentation, *in* Price, R.J., and Sugden, D.E., compilers, Polar geomorphology: Institute of British Geographers Special Publication 4, p. 1–19.

Cuffey, K.M., Conway, H., Hallet, B., Gades, A.M., and Raymond, C.F., 1999, Interfacial water in polar glaciers and glacier sliding at −17 °C: Geophysical Research Letters, v. 26, p. 751–752.

Cuffey, K.M., Conway, H., Gades, A.M., Hallet, B., Lorrain, R., Severinghaus, J.P., Steig, E.J., Vaughn, B., and White, J.W.C., 2000, Entrainment at cold glacier bed: Geology, v. 28, p. 351–354.

Denton, G.H., and Hughes, T.J., 2002, Reconstructing the Antarctic Ice Sheet at the Last Glacial Maximum: Quaternary Science Reviews, v. 21, p. 193–202.

Dreimanis, A., 1989, Tills: Their genetic terminology and classification, *in* Goldthwait, R.P., and Matsch, C.L., eds., Genetic classification of glacigenic deposits: Rotterdam, Balkema, p. 17–83.

Drewry, D.J., 1986, Glacial geologic processes: London, Edward Arnold, 276 p.

Echelmeyer, K., and Wang, Z., 1987, Direct observation of basal sliding and deformation of basal drift at sub-freezing temperatures: Journal of Glaciology, v. 33, p. 83–98.

Faure, G., and Buchanan, D., 1987, Glaciology of the East Antarctic Ice Sheet at the Allan Hills: A preliminary interpretation: Antarctic Journal of the United States, v. 22, p. 74–75.

Fowler, A.C., 1986, Sub-temperate basal sliding: Journal of Glaciology, v. 32, p. 3–5.

Holdsworth, G., 1974, Meserve Glacier, Wright Valley, Antarctica: Part 1. Basal processes: Ohio State University, Institute of Polar Studies Report 37, 104 p.

Hughes, T.J., 1998, Ice sheets: Oxford, Oxford University Press, 343 p.

Jackson, J.A., ed., 1997, Glossary of geology (Fourth edition): Alexandria, Virginia, American Geological Institute, 769 p.

Martini, I.P., Brookfield, M.E., and Sadura, S., 2001, Principles of glacial geomorphology and geology: Upper Saddle River, New Jersey, Prentice-Hall, 381 p.

Naslund, J.O., 1997, Subglacial preservation of valley morphology at Amundsenisen, Western Dronning Maud Land, Antarctica: Earth Surface Processes and Landforms, v. 22, p. 441–455.

Pedersen, S.A.S., 1989, Glacitectonite: Brecciated sediments and cataclastic sedimentary rocks formed subglacially, *in* Goldthwait, R.P., and Matsch, C.L., eds., Genetic classification of glacigenic deposits: Rotterdam, Balkema, p. 89–91.

Robin, G.de Q., 1955, Ice movement and temperature distribution in glaciers and ice sheets: Journal of Glaciology, v. 2, p. 523–532.

Robin, G.de Q., 1983, General glaciology, *in* Robin, G.de Q., ed., The climatic record in polar ice sheets: New York, Cambridge University Press, p. 212.

Shreve, R.L., 1984, Glacier sliding at subfreezing temperatures: Journal of Glaciology, v. 30, p. 341–347.

Siegert, M.J., 2001, Ice sheets and late Quaternary environmental change: New York, Wiley, 231 p.

Stroeven, A.P., and Kleman, J., 1999, Age of Sirius Group on Mount Feather, McMurdo Dry Valleys, Antarctica, based on glaciological inferences from the overridden mountain range of Scandinavia: Global and Planetary Change, v. 23, p. 231–247.

Sugden, D.E., Denton, G.H., and Marchant, D.R., 1991, Subglacial meltwater channel systems and ice sheet overriding, Asgard Range, Antarctica: Geografiska Annaler, v. 73A, p. 109–121.

Summerfield, M.A., Sugden, D.E., Denton, G.H., Marchant, D.R., Cockburn, H.A.P., and Stuart, F.M., 1999, Cosmogenic isotope data support previous evidence of extremely low rates of denudation in the Dry Valleys region, southern Victoria Land, Antarctica, *in* Smith, B.J., et al., eds., Uplift, erosion and stability: Geological Society [London] Special Publication 162, 255 p.

Manuscript received February 1, 2002
Revised manuscript received April 1, 2002
Manuscript accepted April 2, 2002

Printed in USA